Effector Functions of Mucosal Associated Invariant T cells in Response to Viral Infections and Vaccines



Ali Amini
St John's College
University of Oxford

Thesis submitted for the degree Doctor of Philosophy in Biomedical and Clinical Sciences
Michaelmas, 2022

Supervisors: Paul Klenerman, Nuffield Department of Medicine

Nicholas Provine, Nuffield Department of Medicine

Holm Uhlig, Nuffield Department of Medicine

For My Family

از دی که گذشت هیچ ازو یاد مکن
فردا که نیامده ست فریاد مکن
برنامده و گذشته بنیاد مکن
حالی خوش باش و عمر بر باد مکن

من ظاهرِ نیستی و هستی دان
من باطنِ هر فراز و پستی دانم؛
با این‌همه از دانشِ خود شَرْمَم باد
گر مرتبه‌ای وَرایِ مستی دانم

Abstract

Effector Functions of Mucosal Associated Invariant T cells in Response to Viral Infections and Vaccines

Ali Amini
St John's College, University of Oxford
A thesis submitted for the degree of Doctor of Philosophy
Michaelmas Term, 2022

The rapid propagation of host immune responses following nucleic-acid sensing is necessary for protection against viruses and vaccines. Cytokines, such as type I interferon (IFN), play a key role. Mucosal Associated Invariant T (MAIT) cells and related CD161+ innate-like lymphocytes are exquisitely sensitive to anti-viral cytokines and can trigger rapid effector functions such as IFN-γ production, which is important for protection. The aim of this thesis is to investigate whether human MAIT cells and related CD161+ lymphocytes respond to novel nucleic-acid based Adenoviral vectored (AdV) and mRNA vaccines, and understand how this might occur.

First, I show that CD161+ lymphocytes, which include MAIT cells, Vδ2+ γδ T cells, and NK cells, are the main producers of early IFN-γ in response to ChAdOx1-GFP infection of human peripheral blood mononuclear cells (PBMC*) in vitro*. These cells are activated by AdV-derived type I IFN, IL-18, and TNF. Although innate-like lymphocytes rapidly upregulate CD69 expression in response to type I IFN produced by plasmacytoid dendritic cells (pDCs), IFN-γ production requires monocyte-derived IL-18 and TNF.

Next, a longitudinal cohort study of healthcare workers (HCW) was used to understand the early immune response following SARS-CoV-2 AdV and mRNA vaccines. I show that early IFN-γ production after ChAdOx1-S prime is mainly due to cytokine-mediated innate-like lymphocyte activation, and is less prominent after boost. In contrast, enhanced IFN-γ production after BNT162b2 boost is associated with adaptive immune measures at the time of immunisation, and is reduced with extended dosing intervals. In vitro experiments show that IFN-γ dependent IFN-γR1 signalling can amplify early innate-like lymphocyte-derived IFN-γ production, which may influence the reactogenicity and immunogenicity of vaccine schedules.

Finally, I examine the early immune response in Inflammatory Bowel Disease (IBD) patients on biologic therapy targeting TNF, a key cytokine for type I IFN-dependent IFN-γ production. The baseline circulating innate-like lymphocytes of IBD patients are distinct from healthy controls, with higher frequencies of Vδ2+ γδ T cells in patients receiving anti-TNF compared to those receiving anti-integrin therapy. Similarly, early IFN-γ generated after ChAdOx1-S prime is lower in IBD patients on anti-TNF, with no difference in type I IFN production. In vitro experiments show that anti-TNF reduces Ad-V induced pDC maturation, maintaining type I IFN production, but reduces monocyte-derived IL-18.

Overall, this thesis provides an insight into the early immune response to SARS-CoV-2 vaccines and highlights the role of cytokines, especially IFNs, and adaptive immunity in amplifying MAIT cell responses to novel vaccines. These findings raise questions about how environmental factors, like prior infections and the tissue cytokine milieu, may regulate immune responses, and the significance of innate-like lymphocytes to the variability of human immune responses.

Acknowledgements

First and foremost, I genuinely want to thank my supervisor, Paul Klenerman, for his unwavering guidance, intellectual, emotional, and financial support, as well as endless patience in the final protracted stretch – I can't imagine anyone who would have done the same. I also would like to acknowledge and thank my co-supervisors, Holm Uhlig and in particular Nicholas Provine who got me hooked in the lab, indulging endless wide-ranging and fun (for me at least!) discussions about immunology, vaccines, viruses, and their harbingers.

I would like to thank the following members of the Klenerman lab, Translational Gastroenterology Unit (TGU), and Peter Medawar Building for helpful suggestions, general technical advice, moral support, or lab-based fun: Lucy Garner, Michael FitzPatrick, Carl-Philipp Hackstein, Claire Hutchings, Narayan Ramamurthy, Ollie Sampson, Sarah Sasson, Stephanie Slevin, Chantal Hargreaves, Hebe Chen, Hannah Chen, Tharini Askumar, Dominik Aschenbrenner, Sumeet Pandey, Liam Hardy, and Helen Ferry. I'm also grateful to Pawel Swietach and Johanna Michl for welcoming me into DPAG.

For the patient cohort studies there are numerous people to thank, but in particular I'd like to thank Susanna Dunachie, Ellie Barnes, and Donal Skelly, as well as the volunteers, colleagues and patients who went out of their way to donate pints of blood.

I'm very grateful for support from the Wellcome Trust, and both Helen McShane and Louise Sampson for navigating the extra challenges of funding through the COVID pandemic.

None of this work would have been possible without my family. My parents, for actively encouraging curiosity and drive, and my extended family who have all in some way been a frequent source of support at times of desperation. My boys, Elias and Danial, who unbeknown to them made completion of this thesis so much more challenging but immeasurably more enjoyable.

Finally, most importantly, this work is dedicated to my wife Faezeh, whose sacrifice and tolerance were the only reason it was ever completed. Her (literal!) blood, sweat and tears kept me going when I was close to giving up at the most desperate moments. Thank you.

Thesis Contributions

Chapter 3

Nicholas Provine

Performed and analysed all data for Fig3.11|M. Also performed one repeat of pDC depletion experiment.

Chapter 4

Nicholas Provine

Assisted in sample processing and whole blood Tempus RNA extraction.

Lucy Garner

Assisted in whole blood Tempus RNA extraction, single-cell RNA sequencing experiments, library preparation and data analysis – including all data in Fig4.5 K-L.

Donal Skelly, Sile Johnson, Alex Deeks

Assisted in patient recruitment, cohort stratification, and database management.

Sophie Irwin

Assisted in sample processing.

Sandra Adele, Eloise Philipps,Tom Malone (**Susie Dunachie Lab)**

Performed all T cell IFN-γ ELISpots.

Wanwisa Dejnirattisai **(Gavin Screaton Lab)**

Performed all live virus neutralisation assays.

David Eyre, Stewart Cook,Tim James

Provided Abbott staff serology data, or kindly ran extra assays on serum banked separately.

Alex Mentzer

Provided a number of whole-blood RNA samples from donors banked pre-vaccination.

Michelle Taylor-Siddons

Kindly provided BNT162b2, mRNA-1273, and ChAdOx1-S vaccines used in vitro.

Robin Shattock, Paul McKay

Kindly provided saRNA vaccine stocks used in vitro.

Chapter 5

Jack Satsangi, Michael Lim, Thomas Marjot

Recruitment and consent of patients.

Nicholas Provine, Sophie Irwin, and Georgina Meacham

Collectively assisted in sample processing from baseline and day 1 cohort (all performed as a team on trial vaccination days).

Appendix

Nicholas Provine

Data from experiments published (Provine et al., 2021).

Helen Ferry, Liam Hardy

Sorted MAIT cells and CD8+ T cell populations for bicarbonate experiments.

Johanna Michls

Provided pre-prepared media for one experiment.

Pawel Swietach

Performed ImageJ analysis using a custom MATLAB script.

Declaration

I declare that this D.Phil thesis is my own work, other than where indicated clearly in the text.

No part of this work has been submitted for a research degree at this or any other University.

Covid Impact Statement

This thesis was both disrupted and aided by the COVID-19 pandemic, which began one month after my transfer of status. Our laboratories were closed from March until August 2020. During this time I was either seconded back to the NHS (until June 2020), home looking after our children, or contributing to the COVID research effort (e.g., processing blood samples as part of the Medawar response team). The main thesis disruption was the ability to perform wet lab experiments using healthy human blood, which persisted after the labs partially opened so some experiments in this thesis are preliminary and other data has not been included.

However, the pandemic did subsequently provide the opportunity to investigate early immune responses to vaccination and collaborate with brilliant people across Oxford, for which I am grateful.

List of Publications

Publications arising from Chapter 3

- Provine NM, **Amini A,** Garner LC, Spencer AJ, Dold C, Hutchings C, Silva Reyes L, FitzPatrick MEB, Chinnakannan S, Oguti B, Raymond M, Ulaszewska M, Troise F, Sharpe H, Morgan SB, Hinks TSC, Lambe T, Capone S, Folgori A, Barnes E, Rollier CS, Pollard AJ, Klenerman P. MAIT cell activation augments adenovirus vector vaccine immunogenicity. Science. 2021 Jan 29;371(6528):521-526.

- Provine NM*, **Amini A*,** Garner LC, FitzPatrick MEB, Dold C, Silva Reyes L, Chinnakannan S, Oguti B, Raymond M, Troise F, Capone S, Folgori A, Barnes E, Rollier CS, Pollard AJ, Klenerman P. Adenovirus vectors activate Vδ2+ γδT cells in a type I interferon-, TNF-, and IL-18-dependent manner. Eur J Immunol. 2021 Dec 27. (co-first author)

Publications arising from Appendix Chapter

- **Amini A**, Pang D, Hackstein C-P, Klenerman P. MAIT Cells in Barrier Tissues: Lessons from Immediate Neighbors. Front Immunol. 2020;11:584521.

Publications from associated work not described in the thesis

- Youngs J*, Provine NM*, Lim N*, Sharpe HR+, **Amini A+,** Chen YL+, Luo J, Edmans MD, Zacharopoulou P, Chen W, Sampson O, Paton R, Hurt WJ, Duncan DA, McNaughton AL, Miao VN, Leaver S, Wyncoll DLA, Ball J, Hopkins P, Skelly DT, Barnes E, Dunachie S, Ogg G, Lambe T, Pavord I, Shalek AK, Thompson CP, Xue L, Macallan DC, Goulder P, Klenerman P, Bicanic T. Identification of immune correlates of fatal outcomes in critically ill COVID-19 patients. PLoS Pathog. 2021 Sep 16;17(9):e1009804. (co-second author)

- FitzPatrick MEB*, Provine NM*, Garner LC*, Powell K, **Amini A,** Irwin SL, Ferry H, Ambrose T, Friend P, Vrakas G, Reddy S, Soilleux E, Klenerman P, Allan PJ. Human intestinal tissue-resident memory T cells comprise transcriptionally and functionally distinct subsets. Cell Rep. 2021 Jan 19;34(3):108661.

- Hagel JP, Garner LC, Bilton M, Mehta H, Leng T, Hackstein CP, Phalora P, **Amini A,** Akther HD, Provine NM, Edmans M, Willberg CB, Klenerman P. Human MAIT Cell Activation In Vitro. Methods Mol Biol. 2020;2098:97-124.

Publications arising from patient samples I recruited and banked in Chapter 4:

- Tuekprakhon A*, Nutalai R*, Dijokaite-Guraliuc A*, Zhou D*, Ginn HM, Selvaraj M, Liu C, Mentzer AJ, Supasa P, Duyvesteyn HME, Das R, Skelly D, Ritter TG, **Amini A**, Bibi S, Adele S, Johnson SA, Constantinides B, Webster H, Temperton N, Klenerman P, Barnes E, Dunachie SJ, Crook D, Pollard AJ, Lambe T, Goulder P, Paterson NG, Williams MA, Hall DR; OPTIC Consortium; ISARIC4C Consortium, Fry EE, Huo J, Mongkolsapaya J, Ren J, Stuart DI, Screaton GR. Antibody escape of SARS-CoV-2 Omicron BA.4 and BA.5 from vaccine and BA.1 serum. Cell. 2022 Jul 7;185(14):2422-2433.e13.

- Nutalai R*, Zhou D*, Tuekprakhon A*, Ginn HM*, Supasa P*, Liu C*, Huo J*, Mentzer AJ*, Duyvesteyn HME, Dijokaite-Guraliuc A, Skelly D, Ritter TG, **Amini A**, Bibi S, Adele S, Johnson SA, Constantinides B, Webster H, Temperton N, Klenerman P, Barnes E, Dunachie SJ, Crook D, Pollard AJ, Lambe T, Goulder P; OPTIC consortium, ISARIC4C consortium, Paterson NG, Williams MA, Hall DR, Mongkolsapaya J, Fry EE, Dejnirattisai W, Ren J, Stuart DI, Screaton GR. Potent cross-reactive antibodies following Omicron breakthrough in vaccinees. Cell. 2022 Jun 9;185(12):2116-2131.e18.

- Murray SM, Barbanti M, Campbell C, Brown A, Chen L, Dhanapal J, Tseu B, Pervaiz O, Peters L, Springett S, Danby R, Adele S, Phillips E, Malone T, **Amini A**, Stafford L, Deeks AS, Dunachie S, Klenerman P, Peniket A, Barnes E, Kesavan M. Impaired humoral and cellular response to primary COVID-19 vaccination in patients less than 2 years after allogeneic bone marrow transplant. Br J Haematol. 2022 Aug;198(4):668-679.

- Phillips E, Adele S, Malone T, Deeks A, Stafford L, Dobson SL, **Amini A**, Skelly D, Eyre D, Jeffery K, Conlon CP, Dold C, Otter A, D'Arcangelo S, Turtle L; PITCH Consortium, Klenerman P, Barnes E, Dunachie SJ. Comparison of two T-cell assays to evaluate T-cell responses to SARS-CoV-2 following vaccination in naïve and convalescent healthcare workers. Clin Exp Immunol. 2022 Jul 22;209(1):90-98.

- Dejnirattisai W*, Huo J*, Zhou D*, Zahradník J*, Supasa P*, Liu C*, Duyvesteyn HME, Ginn HM, Mentzer AJ, Tuekprakhon A, Nutalai R, Wang B, Dijokaite A, Khan S, Avinoam O, Bahar M, Skelly D, Adele S, Johnson SA, **Amini A**, Ritter TG, Mason C, Dold C, Pan D, Assadi S, Bellass A, Omo-Dare N, Koeckerling D, Flaxman A, Jenkin D, Aley PK, Voysey M, Costa Clemens SA, Naveca FG, Nascimento V, Nascimento F, Fernandes da Costa C, Resende PC, Pauvolid-Correa A, Siqueira MM, Baillie V, Serafin N, Kwatra G, Da Silva K, Madhi SA, Nunes MC, Malik T, Openshaw PJM, Baillie JK, Semple MG, Townsend AR, Huang KA, Tan TK, Carroll MW, Klenerman P, Barnes E, Dunachie SJ, Constantinides B, Webster H, Crook D, Pollard AJ, Lambe T; OPTIC Consortium; ISARIC4C Consortium, Paterson NG, Williams MA, Hall DR, Fry EE, Mongkolsapaya J, Ren J, Schreiber G, Stuart DI, Screaton GR. SARS-CoV-2 Omicron-B.1.1.529 leads to widespread escape from neutralizing antibody responses. Cell. 2022 Jan 4:S0092-8674(21)01578-6.

- Payne RP*, Longet S*, Austin JA*, Skelly DT*, Dejnirattisai W, Adele S, Meardon N, Faustini S, Al-Taei S, Moore SC, Tipton T, Hering LM, Angyal A, Brown R, Nicols AR, Gillson N, Dobson SL, **Amini A**, Supasa P, Cross A, Bridges-Webb A, Reyes LS, Linder A, Sandhar G, Kilby JA, Tyerman JK, Altmann T, Hornsby H, Whitham R, Phillips E, Malone T, Hargreaves A, Shields A, Saei A, Foulkes S, Stafford L, Johnson S, Wootton DG, Conlon CP, Jeffery K, Matthews PC, Frater J, Deeks AS, Pollard AJ, Brown A, Rowland-Jones SL, Mongkolsapaya J, Barnes E, Hopkins S, Hall V, Dold C, Duncan CJA, Richter A, Carroll M, Screaton G, de Silva TI, Turtle L, Klenerman P, Dunachie S; PITCH Consortium. Immunogenicity of standard and extended dosing intervals of BNT162b2 mRNA vaccine. Cell. 2021 Nov 11;184(23):5699-5714.e11.

- Skelly DT*, Harding AC*, Gilbert-Jaramillo J, Knight ML, Longet S, Brown A, Adele S, Adland E, Brown H; Tipton T, Stafford L, Mentzer AJ, Johnson SA, **Amini A**, Tan TK, Schimanski L, Huang KA, Rijal P, Frater J, Goulder P, Conlon CP, Jeffery K, Dold C, Pollard AJ, Sigal A, de Oliveira T, Townsend AR, Klenerman P, Dunachie SJ, Barnes E, Carroll MW, James WS. Two doses of SARS-CoV-2 vaccination induce robust immune responses to emerging SARS-CoV-2 variants of concern. Nat Commun. 2021 Aug 17;12(1):5061.

Table of Contents

List of Figures *14*
List of Tables *21*
List of Abbreviations *22*
1. Introduction *25*

1.1 Antiviral response **25**
1.1.1 Innate sensing of viruses 25
1.1.2 Consequences of innate sensing 28

1.2 Innate antiviral cytokines **30**
1.2.1 Type I IFN 30
1.2.2 TNF 34
1.2.3 Inflammasome and IL-1 family cytokines 35
1.2.4 IFN-γ 36

1.3 Vaccines **40**
1.3.1 Viral vector vaccines 41
1.3.2 RNA vaccines 46

1.4 Innate and Innate-like IFN-γ producing lymphocytes **49**
1.4.1 Group 1 Innate Lymphoid Cells: NK cells, ILC1 49
1.4.2 Innate-like 'unconventional' T cells 50
1.4.3 CD1 restricted NKT cells 51
1.4.4 MAIT Cells 52
1.4.5 Gamma-delta (γδ) T cells: Vδ2+ and non-Vδ2+ 53
1.4.6 Shared features of innate-like lymphocytes 54
1.4.7 IFN-γ and innate-like lymphocytes 59
1.4.8 Tissue specific functions of innate-like lymphocytes 61

1.5 Knowledge gaps **65**

1.6 Aims of the Thesis **66**
2 Methods *67*

2.1 Media and buffers **67**

2.2 Viral vectors and vaccines **68**

2.3 Cells **69**

2.4 Isolation of cells **69**
2.4.1 PBMC isolation from blood 69
2.4.2 Cell isolation using magnetic bead enrichment 70

2.5 Collection of plasma, serum **71**

2.6 Functional assays **71**
2.6.1 Stimulation assays 72
2.6.2 TCR stimulation 72
2.6.3 Blocking assays 73

2.7 Cytokine and chemokine quantification **74**

2.8 MR1 tetramer generation and staining **74**

2.9 Flow Cytometry **75**
2.9.1 Viability staining 75
2.9.2 Surface staining 75
2.9.3 Intracellular cytokine staining (ICS) 75
2.9.4 Proliferation assays and labelling 76

2.9.5 Transcription factor staining 76
2.9.6 Data acquisition and analysis 76

2.10 Statistical analysis 76

3 MAIT cell and CD161+ lymphocyte responses to ChAdOx1 79

3.1 Introduction 79

3.2 Aims 82

3.3 Results 83
3.3.1 MAIT cells and CD161+ lymphocytes are the dominant sources of early IFN-γ in response to ChAdOx1-GFP in vitro 83
3.3.2 Interferons and antiviral cytokines are potently induced by ChAdOx1-GFP 91
3.3.3 Innate immune cells are transduced and activated to produce inflammatory cytokines in response to ChAdOx1-GFP 95
3.3.4 pDC-derived type I IFN is necessary but insufficient for robust sustained ChAdOx1-induced IFN-γ production 102
3.3.5 APC-derived factor is sufficient to sustain type I IFN-induced MAIT cell IFN-γ 113
3.3.6 TNF augments type I IFN-dependent MAIT cell IFN-γ 122
3.3.7 TNF is necessary for ChAdOx1-induced early IFN-γ 135
3.3.8 Exosome inhibitors reduce TNF-dependent MAIT cell activation 138

3.4 Discussion 141
3.4.1 Type I IFN-induced MAIT cell activation: sensitive but controlled 142
3.4.2 Control of antiviral inflammation and TNF 144
3.4.3 ChAdOx1 innate sensing: type I IFN and pDC 145
3.4.4 Limitations 146

3.5 Conclusion and summary 147

4 Human early immune responses to SARS-CoV-2 vaccines 148

4.1 Introduction 148

4.2 Aims 151

4.3 Chapter specific materials and methods 152
4.3.1 Study design, and sample collection 152
4.3.2 Isolation of PBMCs, plasma and serum 154
4.3.3 Whole blood total RNA extraction and RNA-seq 155
4.3.4 Focus Reduction Neutralization Assay (FRNT) 155
4.3.5 IFN-γ T cell ELISpot assays 155
4.3.6 Antibody assays Abbott 156
4.3.7 Spike-specific T cell ICS 156
4.3.8 Spike protein detection in supernatants 156
4.3.9 Quantification and statistical analysis 157

4.4 Results 158
4.4.1 Study design and cohort characteristics 158
4.4.2 Differential immune activation post-prime and boost 159
4.4.3 Interferons dominate early SARS-CoV-2 vaccine-induced responses 166
4.4.4 Immune correlates of early ChAdOx1-S vaccine response 170
4.4.5 Immune correlates of early BNT162b2 vaccine response 174
4.4.6 SARS-CoV-2 vaccines produce spike protein, activate innate immune cells, and induce IFNs in vitro 182
4.4.7 Adaptive immune cells produce IFN-γ in response to SARS-CoV-2 vaccines in vitro 195
4.4.8 Innate-like lymphocytes amplify early IFN-γ in an IFN-γR-dependent manner 201
4.4.9 MHC-dependent MAIT cell activation 212
4.4.10 Functions of IFN-γ in vitro 216
4.4.11 Early immune correlates of adaptive responses to vaccines 218

4.5 Discussion 221
4.5.1 Early post-prime vaccine responses are dominated by innate immunity and type I IFN 222
4.5.2 Early boost responses are regulated by immune memory 225
4.5.3 IFN-γ as a regulator of innate and adaptive immunity 228
4.5.4 Relevance of findings to vaccinology 232
4.5.5 Limitations 236

4.6 Conclusion and Summary 237

5 Anti-TNF and human early immune responses to ChAdOx1-S 239

5.1 Introduction 239

5.2 Aims 242

5.3 Chapter specific materials and methods 243
5.3.1 OCTAVE Trial - design, and sample collection 243
5.3.2 Isolation of PBMCs, plasma and serum 247

5.4 Results 248
5.4.1 Characteristics of OCTAVE study cohort 248
5.4.2 Baseline immune profile of patients with IBD on immunomodulatory therapy 250
5.4.3 Early immune responses in IBD patients on immunomodulatory therapy 253
5.4.4 Anti-TNF increases pDC-derived type I IFN, but reduces monocyte-derived inflammasome-dependent cytokines in vitro 256

5.5 Discussion 262
5.5.1 Anti-TNF and baseline innate-like lymphocyte frequency 263
5.5.2 Anti-TNF reduces early ChAdOx1-S induced IFN-γ but not IFN-α 264
5.5.3 Relevance of findings to vaccinology and immunology 265
5.5.4 Limitations 267

5.6 Conclusions and summary 268

6 Work during COVID-19 pandemic 269

6.1 List of work published as part of a COVID-19 response team 269

6.2 List of papers published 269

7 Conclusions 270

7.1 MAIT cells and interferons 270

7.2 TNF regulates innate-like lymphocytes 272

7.3 Redundant and unique features of innate-like lymphocytes 273

7.4 Non-heritable regulation of innate-like lymphocyte responses 274

7.5 Future directions 277

8 References 280

9 Appendices 308

9.1 Supplementary Chapter: Tissue regulation of MAIT cells: sodium, bicarbonate, and SLC4A10 309
9.1.1 Introduction 309
9.1.2 Aims 317
9.1.3 Chapter specific materials and methods 318
9.1.4 Results 322
9.1.5 Discussion 331
9.1.6 Conclusions and summary 334

9.2 Supplemental figures 335

List of Figures

Figure 1.1 | Mucosal environmental factors which could influence immune responses directly and indirectly. (From Amini et al., Frontiers in Immunology, 2020) 61

Figure 1.2 Possible environmental factors capable of regulating MAIT cell transcriptional and effector responses (From Amini et al., Frontiers in Immunology 2020). 64

Figure 1.3| Innate sensing of nucleic acid vaccines and effector cytokines 65

Figure 3.1 | ChAdOx1-GFP induced MAIT cell activation in vitro peaking at 24h..... 85

Figure 3.2 | ChAdOx1-GFP induces MAIT cell activation in an MR1-independent manner. 86

Figure 3.3 | CD161+ innate-like lymphocytes are the dominant source of early IFN-γ after ChAdOx1-GFP..... 88

Figure 3.4 | Effector memory conventional T cells respond to ChAdOx1-GFP in vitro. 90

Figure 3.5 | Interferons dominate early cytokines at 24h after ChAdOx1-GFP stimulation *in vitro*. 92

Figure 3.6 | ChAdOx1 induced MAIT cell IFN-γ correlates with type I IFN and IL-12 in vitro. 94

Figure 3.7 | Heat-inactivation reduces ChAdOx1-GFP transduction and IFN-γ from innate-like lymphocytes in vitro. 96

Figure 3.8 | ChAdOx1-GFP transduces monocytes earlier than dendritic cells in vitro. ... 98

Figure 3.9 | Activation of antigen presenting cells in response to ChAdOx1-GFP in vitro. 100

Figure 3.10 | Type I IFN is necessary for maximal innate-like lymphocyte IFN-γ. 104

Figure 3.11 | Plasmacytoid dendritic cells produce IFN-α necessary for maximal innate-like lymphocyte IFN-γ. 107

Figure 3.12 | Type I and not type II/ II IFNs robustly induce early CD69 in innate-like lymphocytes. 109

Figure 3.13 | Type I induced MAIT cell IFN-γ at 24h requires accessory cells found in PBMC. 111
Figure 3.14 | Type I interferon induced MAIT cell IFN-γ at 6h in the absence of accessory cells..... 112
Figure 3.15 | A monocyte derived factor is specifically required for IFN-α-dependent MAIT cell activation in the absence of APC at 24h. 115
Figure 3.16 | Type I interferon alters the composition of PBMC, with a reduction in CD14+ cells..... 117
Figure 3.17 | Type I interferon induces cell death and reduced CD14 expression in enriched monocytes. 118
Figure 3.18 | Type I interferon induces cytokines, in particular TNF, from enriched monocytes 120
Figure 3.19 | Interferons induce TNF at early timepoints only in PBMC from monocytes. 121
Figure 3.20 | MAIT cells express TNFR2, which is potently up-regulated by antiviral cytokines..... 124
Figure 3.21 | Anti-TNF inhibits late but not early IFN-dependent MAIT cell activation in unfractionated PBMC..... 127
Figure 3.22 | Anti-TNF inhibits IFN-α and E.coli induced MAIT cell activation in fresh PBMC. 129
Figure 3.23 | TNFR2 agonism increases type I IFN-dependent MAIT IFN-γ in PBMC at 24h. 130
Figure 3.24 | TNFR2 agonism increases type I IFN-dependent MAIT cell IFN-γ in enriched CD8 at 24h..... 132
Figure 3.25 | TNF signalling is required for APC-independent MAIT cell IFN-γ in response to monocyte supernatant. 134
Figure 3.26 | TNF blockade and TNFR signalling is crucial for ChAdOx1 induced innate-like lymphocyte activation in vitro. 137

Figure 3.27 | Neutral-sphingomyelinase inhibitors reduce ChAdOx1 and IFN-dependent MAIT cell activation..... 140
Figure 4.1 | Schematic of healthcare worker study..... 152
Figure 4.2 | Innate-like lymphocytes show dynamic dichotomous CD69 expression in response to BNT162b2 and ChAdOx1-S..... 161
Figure 4.3 | Kinetics of innate-like lymphocyte CD69 expression in response to BNT162b2 and ChAdOx1-S peaks between 24-48h after immunisation in vivo..... 162
Figure 4.4 | BNT162b2 and ChAdOx1 display inverse patterns of changes in the frequency of MAIT cells, monocytes, and the activation of conventional T cells..... 164
Figure 4.5 | BNT162b2 and ChAdOx1-S induce an inverse pattern of interferon responses, with unique inflammasome induced cytokines after ChAdOx1-S prime. 168
Figure 4.6 | Early IFN-γ after ChAdOx1-S is highest in young females..... 171
Figure 4.7 | Early IFN-γ after ChAdOx1-S correlates with changes in IFN-α, innate-like lymphocyte activation and lymphopenia one day after immunisation..... 173
Figure 4.8 | Early IFN-γ after BNT162b2 boost correlates with innate-like lymphocyte activation and degree of lymphopenia one day after immunisation..... 175
Figure 4.9| BNT162b2 boost induced IFN-γ and innate-like T cell activation higher after shorter boosting intervals..... 176
Figure 4.10 | Comparison of spike-specific adaptive immunity at the time of boost in healthcare workers boosted with longer boosting intervals. 178
Figure 4.11 | Early post-boost IFN-γ and innate-like lymphocyte activation correlates with spike-specific adaptive immune responses prior to boost. 180
Figure 4.12 | Prior infection is specifically associated with increased early IFN-γ and immune activation after BNT162b2 prime. 181
Figure 4.13 | SARS-CoV-2 vaccines secrete spike RBD protein in PBMC in vitro..... 183
Figure 4.14 | ChAdOx1-S and mRNA-1273 express SARS-CoV-2 S1 protein in vitro - with pDC expression unique to ChAdOx1-S. 185

Figure 4.15 | ChAdOx1-S and mRNA-1273 kinetics of SARS-CoV-2 S1 protein differ - with very early expression in monocytes after ChAdOx1-S, followed by later expression in pDC. 186
Figure 4.16 | Plasmacytoid dendritic cells produce IFN-α in response to ChAdOx1-S but not mRNA vaccines in vitro..... 188
Figure 4.17 | SARS-CoV-2 vaccines induce distinct patterns and kinetics of MHC-I, MHC-II and CD80 expression in antigen presenting cells..... 190
Figure 4.18 | RNA vaccine induced interferons: comparison of self-amplifying and nucleoside-modified vaccines in vitro. 192
Figure 4.19 | SARS-CoV-2 mRNA vaccines induce CD69 not potent innate-like lymphocyte IFN-γ or TNF secretion in vitro..... 194
Figure 4.20 | Conventional but not unconventional T cells produce IFN-γ after BNT162b2 stimulation in vitro. 196
Figure 4.21 | Differences in conventional and unconventional IFN-γ responsive cells to SARS-CoV-2 vaccines in vitro. 198
Figure 4.22 | Very early IFN-γ production is absent after mRNA vaccine stimulation, and dominated by CD4+ conventional T cells after ChAdOx1-S and spike-peptide stimulation. 200
Figure 4.23 | Autologous serum increases mRNA vaccine-induced IFN-γ in vitro. 202
Figure 4.24 | Patterns of cytokine secretion in response to vaccines in vitro. 203
Figure 4.25 | MAIT cell IFN-γR signalling can modulate MAIT cell IFN-γ production in response to type I IFN and TNF mediated activation. 206
Figure 4.26 | IFN-γ increases total IFN-γ in response to spike peptide and SARS-CoV-2 mRNA vaccines through augmented innate-like lymphocyte activation. 208
Figure 4.27| IFN-γR1 (CD119) blockade reduces innate-like lymphocyte activation and total IFN-γ in response to spike peptide and SARS-CoV-2 mRNA vaccines. 210
Figure 4.28 | IFN-γR1 (CD119) blockade reduces total IFN-γ in response to spike peptide and SARS-CoV-2 mRNA vaccines. 211

Figure 4.29 | Conventional T cell correlates of vaccine-induced innate-like lymphocyte IFN-γ in vitro. 213
Figure 4.30 | Classical MHC mediated innate-like lymphocyte IFN-γ in vitro in response to SARS-CoV-2 spike protein and vaccines. 215
Figure 4.31 | IFN-γ reduces cell-associated SARS-CoV-2 S1 protein but increases secreted SARS-CoV-2 RBD in response to mRNA vaccines. 217
Figure 4.32 | Early MAIT cell activation after ChAdOx1-S prime correlates with subsequent spike-specific T-cell responses. 219
Figure 4.33 | Early IFN-γ after BNT162b2 anti-correlates with spike-specific antibody responses post boost. 220
Figure 4.34 Summary of potential causes and consequences of BNT162b2 induced IFN-γ. 238
Figure 5.1 | Schematic of OCTAVE study. 249
Figure 5.2 | IBD patients have reduced frequencies of MAIT cells compared to healthy controls pre-vaccination. 251
Figure 5.3 | IBD patients on anti-TNF have increased frequencies of Vδ2+ γδ T cells pre-vaccination. 252
Figure 5.4 | Innate-like lymphocytes are activated after ChAdOx1-S in IBD patients. 254
Figure 5.5 | IBD patients on anti-TNF have reduced induction of IFN-γ and IL-6 one day after ChAdOx1-S prime. 255
Figure 5.6 | Anti-TNF reduces ChAdOx1-GFP induced inflammasome-derived cytokines but not IFN-α. 257
Figure 5.7 | Anti-TNF increases pDC IFN-α and TNF production but reduces GFP transduction and activation in response to ChAdOx1-GFP in vitro. 259
Figure 5.8 | Anti-TNF reduces inflammasome-derived cytokines and monocyte cell death in response to ChAdOx1-GFP. 261
Figure 7.1 | Model for immune memory and differential regulation of vaccine-induced IFN-γ. 275

Figure 7.2 | Hypothesis for reciprocal control of innate, adaptive, and tissue immunity. 279
Appendix Figure 9.1 | Calibration of intracellular pH using cSNARF1. 321
Appendix Figure 9.2 | Sodium chloride alters MAIT cell cytokine responses in vitro. 323
Appendix Figure 9.3 | Sodium chloride alters MAIT cell cytokine responses in vitro after 72hr PBMC stimulation. 324
Appendix Figure 9.4 | Salt prevents type I IFN induced reduction in MAIT cell frequency. 325
Appendix Figure 9.5 | Salt prevents type I interferon induced caspase activation and cell-death. 326
Appendix Figure 9.6 | Method to assess impact of bicarbonate on intracellular pH of sorted human T cell populations. 327
Appendix Figure 9.7 | Bicarbonate is necessary to maintain optimum intracellular pH in MAIT cells but not naive CD8 T cells. 329
Appendix Figure 9.8 | Bicarbonate channel blocker, S0859, inhibits MAIT cell intracellular pH regulation. 330
Appendix Figure 9.9 | Bicarbonate transport may impact on MAIT cell antiviral responses. 331
Appendix Figure 9.10 |Working Model for the effects of Na and HCO3. 332
Appendix Figure 9.11 SF3.1 | Human MAIT cells are activated by Adenovirus vectors in vitro. 335
Appendix Figure 9.12 SF3.2 | Monocyte-derived IL-18 is necessary for potent innate-like lymphocyte induced IFN-γ in response to AdV. 335
Appendix Figure 9.13 SF3.3 | IL-12, IL-23 and IL-18 blockade reduce MAIT cell IFN-γ in response to ChAdOx1-GFP. 336
Appendix Figure 9.14 SF3.4 | A monocyte-derived factor is required for IFN-dependent MAIT cell IFN-γ. 336
Appendix Figure 9.15 SF4.1 | Gating strategies for cellular phenotyping. 337

Appendix Figure 9.16 SF4.2 | Persistently increased monocyte frequency 8 weeks after ChAdOx1-S prime..... 338
Appendix Figure 9.17 SF4.3 | Spike-specific T-cell ELISpot after BNT162b2 prime in data reanalysed from Payne et., al. 339
Appendix Figure 9.18 SF4.4 | Representative gating and plot after BNT162b2 in vitro. 340
Appendix Figure 9.19 SF4.5 | Cytokines induced by PBMC in response to SARS-CoV-2 vaccines, ChAdOx1-GFP, or spike protein in conventional media (R10). 341
Appendix Figure 9.20 SF4.6 | BNT162b2 cytokine secretion in the presence of absence of additional human serum 342
Appendix Figure 9.21 SF4.7 | IFN-γ induces monocyte TNF. 343
Appendix Figure 9.22 SF4.8 | Classical MHC blockade reduces early innate-like lymphocyte IFN-γ in response to ChAdOx1-GFP *in vitro*..... 344
Appendix Figure 9.23 SF4.9 | Classical MHC blockade reduces early MAIT cell IFN-γ in response to ChAdOx1-GFP *in vitro*. 345
Appendix Figure 9.24 SF9.1 | Gating strategy for identification of live single T cells among unfractionated fresh PBMC stimulated with plate bound aCD3/28 and cytokines. 346
Appendix Figure 9.25 SF9.2 | Identification and sorting of MAIT cells, naïve and effector memory CD8+ T cells. 347

List of Tables

Table 1.1 | MAIT cells in healthy human barrier tissues. 62

Table 2.1 | List of blocking antibodies 73

Table 2.2 | List of antibodies used for flow cytometry. 77

Table 4.1 | HCW cohort characteristics. 153

Table 4.2 | HCW cohort: summary of interval between sampling and vaccination. 154

Table 5.1 | OCTAVE – Baseline phenotype cohort characteristics. 244

Table 5.2 | OCTAVE - Baseline phenotype cohort (IBD patients) 245

Table 5.3 | OCTAVE – Day 1 cohort characteristics 246

Appendix Table 9.1 | Bicarbonate solutions 319

List of Abbreviations

ADA	Adalimumab
ADCC	Antibody-dependent cell mediated cytotoxicity
AdV	Adenovirus Vector
AIM	Activation-induced marker
APC	Antigen-presenting cell
ATP	Adenosine triphosphate
BAL	Bronchoalveolar lavage
BCG	Bacillus Calmette–Guérin
BCL	B cell lymphoma
BCR	B-cell receptor
BSA	Bovine serum albumin
CAR	Coxsackievirus and adenovirus receptor (CAR)
CAR-T	Chimeric antigen receptor T
CD	Crohn's Disease
CERT	Certolizumab
CFU	Colony forming units
ChAd	Chimpanzee-derived Adenovirus
CMV	Cytomegalovirus
CRP	C-reactive protein
DMSO	Dimethylsulphoxide
DN	Double negative (CD4-CD8-)
DNA	deoxyribonucleic acid
EDTA	ethylenediaminetetraacetic acid
ELISA	Enzyme-linked immunosorbent assay
EOMES	Eomesdermin
ER	Endoplasmic reticulum
ETN	Etanercept
FCS	Foetal calf serum
FDR	False discovery rate
FRNT	Fractional reduction neutralisation titre
GC	Germinal centre
GEM	Germline-encoded mycolyl lipid-reactive
GF	Germ free
GFP	Green fluorescent protein
GI	Gastrointestinal
GMFI	Geometric MFI
GPCR	G-protein coupled receptor
HCV	Hepatitis C Virus
HCW	Healthcare worker

HLA	Human leucocyte antigen
HMBPP	(E)-4-hydroxy-3-methyl-but-2-enyl pyrophosphate
IAV	Influenza A virus
IBD	Inflammatory Bowel Disease
ICAM	Intercellular adhesion molecule
ICS	Intracellular cytokine stain
IEL	Intraepithelial lymphocyte
IFN	Interferon
IFNAR	Interferon alpha-receptor
IFNGR	Interferon gamma-receptor
IL	Interleukin
ILC	Innate lymphoid cell
ILTC	Innate-like T cell
IM	Intramuscular
iNKT	Invariant natural killer T
IQR	Interquartile range
ISG	Interferon stimulated genes
ISRE	Interferon stimulated response element
IU	International Units
JAK	Janus kinase
LLOQ	Lower limit of quantitation
LN	Lymph node
LNP	Lipid nanoparticle
LPS	Lipopolysaccharide
MACS	Magnetic-activated cell sorting
MAIT	Mucosal associated invariant T
MAPK	Mitogen-activated protein kinases
MHC	Major Histocompatibility complex
MMR	Mumps Measles and Rubella
MOI	Multiplicity of Infection
MSMD	Mendelian susceptibility to mycobacterial disease
NBC	Na (sodium)-Bicarbonate Cotransporters
NCBE	Na (sodium)-driven Chloride-Bicarbonate Exchanger
NF-κB	Nuclear Factor kappa B
NHP	Non-human primate
NK	Natural killer
NLR	Nod-like receptors
PBMC	Peripheral blood mononuclear cells
PCR	Polymerase Chain Reaction
pDC	Plasmacytoid Dendritic Cell
PFU	Plaque forming units

PKR	Protein Kinase R
PLZF	Promyelocytic leukaemia zinc finger protein
PMA	Phytohemagglutinin
PRR	Pattern Recognition Receptor
RAG	Recombination activating gene
RBD	Receptor Binding Domain
RIG	Retinoic acid-inducible gene I
RLR	RIG-I like receptors
RNA	Ribonucleic acid
RPMI	Roswell Park Memorial Institute
RT	Room temperature
SARS	Severe Acute Respiratory Syndrome
SFU	Spot Forming Units
SLC	SoLute Carrier
SST	Serum separator tubes
STAT	Signal Transducer and Activator of Transcription (STAT)
STING	Stimulator of Interferon Genes
Tcm	T central memory
Tem	T effector memory
Temra	T effector memory RA
TF	Transcription factor
Tn	T naïve
TCR	T-cell receptor
TNF	Tumour necrosis factor
TNFR	TNF receptor
UC	Ulcerative colitis
VED	Vedolizumab
VITT	Vaccine-Induced Immune Thrombotic Thryombocytopenia
VP	Viral particle
WT	Wild type

1. Introduction

Anti-viral vaccines, like the pathogens they are designed to protect against, must evoke a host immune response. However, humans display remarkable variability in the magnitude and quality of both acute and lasting immune responses elicited to the same inoculum. To appreciate why this variability occurs, I will first discuss how immune responses are generated, applying these to novel vaccine platforms, then focussing on highly variable bridging innate-like lymphocytes which could amplify responses and are regulated by non-heritable factors, thus a potential source of heterogeneity. The focus of this thesis is on new vaccine technologies based on nucleic acids - therefore the antiviral immune response is most relevant to understanding how these vaccines engage the immune system.

1.1 Antiviral response

1.1.1 Innate sensing of viruses

Innate Immunity and cellular pattern recognition

The innate-immune system is the first to encounter foreign antigens and critical for both immediate protection and shaping long term adaptive immunity [1]. An immediate response to previously unencountered antigens relies on germline-encoded pattern recognition receptors (PRR), capable of recognising a finite number of pathogen-associated molecular patterns (PAMPs) shared between pathogens. This early form of immune recognition evolved in both animal and plant kingdoms and is a pre-requisite to multicellular life.

Structural pattern recognition

The first described and most widely studied PRR were Toll-like receptors (TLRs). First hypothesised by Charles Janeway [2], experimental evidence that germline-encoded proteins could induce immune responses to ancestrally encountered antigens came with the identification of the *Toll* gene in Drosophila which recognises hyphae to induce an antifungal

response via NF-κB signalling [3]. A human *Toll* homologue in Jurkat cells could induce inflammatory cytokines, interleukin 1 (IL-1), IL-6 and IL-8, together with co-stimulatory molecules for activation of adaptive immune cells [4]. The receptor for bacterial LPS, *Tlr4*, was then identified as the first mammalian PRR in mice [5], with nine TLRs since described in humans [6], primarily detecting extracellular or endosomal PAMPs.

TLRs recognise a wide range of PAMPs, including proteins, lipoproteins, and sugars. Although structurally viruses derive from host cells, TLR-mediated recognition of their nucleic acids can occur. The first described nucleic-acid sensor was TLR9 [7] - an endosomal sensor of double-stranded deoxyribonucleic acid (dsDNA), which preferentially binds unmethylated CpG DNA found in bacterial and viral genomes. TLR compartmentalisation minimises self-DNA induced aberrant immune activation; endosomal TLR-mediated recognition of virus nucleic acids is required to trigger TLR3 (dsRNA), TLR7, and TLR8. However, as exogenous naked DNA also induces potent cytokine production, cytosolic DNA sensors must also exist [8,9].

Cytosolic nucleic acid sensing

It soon became apparent that numerous proteins recognise cytosolic dsDNA[10]. First described as a property of Z-DNA-binding protein 1 (ZBP1)[11], the endoplasmic reticulum resident stimulator of interferon genes (STING) was identified as a major indirect dsDNA sensor[12,13]; STING recognises cyclic dinucleotide products of the DNA-sensing enzyme, cyclic GMP-AMP (cGAMP) synthase (cGAS), to induce type I interferon (IFN) [10]. Cytosolic DNA recognition also induces type I IFN-independent responses, exemplified by Absent in melanoma 2 (AIM2) which binds both DNA and an adaptor protein, apoptosis-related speck-like protein containing a C-terminal caspase recruitment domain (ASC), triggering caspase-1 mediated cell-death and production of cytokines IL-1β and IL-18[14].

Intracellular RNA can also trigger innate immune sensing in a manner which avoids recognition of ubiquitous host RNA. Retinoic-acid inducible gene I (RIG-I) like receptors

(RLR) recognise RNA conformations preferentially found in pathogens rather than self-RNA. The main RLRs capable of dsRNA recognition are RIG-I and melanoma differentiation associated gene 5 (MDA5). RIG-I is also triggered by ssRNA lacking the 5'-triphosphate caps of host mRNA [15].

Although both RNA and DNA sensors evolved to preferentially sense foreign (pathogenic) nucleic acids, self-RNA and self-DNA triggering can occur after release from damaged tissues which is of relevance when considering the impact of viruses (and vaccines) in the induction of immune responses [16].

Functional innate sensing

TLR sensors make no distinction between living and dead PAMPs, which the innate immune system achieves through recognition of the shared functional consequences of virulent pathogens[17]; tissue damage and disruption of homeostasis trigger damage associated molecular patterns (DAMPs) and homeostasis associated molecular patterns (HAMPS) respectively[18].

The intracellular nucleotide-binding and oligomerization domain (NOD)-like receptor (NLR) family make up a well described DAMP recognising family[19]. The best characterised is Cryopyrin, NLR family pyrin domain containing 3 (NLRP3), which detects diverse functional consequences of host cell membrane disruption - including cytosolic electrolyte imbalances, uric acid crystals, and ATP. Similar to AIM2 inflammasome activation the outcome is ASC engagement and caspase-1 activation to induce cell-death and cytokine production [20,21].

Another means of functional pathogen recognition is through detection of 'missing self'[22], a frequent virus-induced host modification, with natural killer (NK) cells particularly adept at detecting infected and stressed cells [22]. NK cell inhibitory receptors bind major

histocompatibility complex class (MHC) I present on the cell surface of all healthy cells; disinhibition by virus-induced downregulation of surface MHCI expression makes infected cells a target for NK-cell mediated killing [23].

In summary, the innate-immune system as the first tier of the immune response engages structural or functional features shared amongst pathogens, with the latter including host-cell modification, damage, or homeostatic disruption.

1.1.2 Consequences of innate sensing

Innate triggering ultimately attempts to clear insults either directly by sensor cells or through recruitment of other cells. The most important outcome for both virus and vaccine induced responses is induction of durable 'immune memory' for long term protection. Although immune memory is traditionally synonymous with adaptive immunity, generated through genetic recombination and clonal expansion, I will briefly touch on the emerging concept of 'trained immunity', which occurs through epigenetic reprogramming of innate immune cells.

Adaptive Immune memory

Adaptive immunity required for durable antigen-specific protection is only observed in vertebrates, mediated by B cells and T cells present as naïve cells with diverse repertoires of receptor specificities. The frequency of individual B and T cell clones with unique receptor specificities is extremely low, with durable protective immunity reliant on effective priming, clonal expansion, and long-term maintenance of specific cells after an initial antigen encounter.

Innate antigen-presenting cells (APC), and in particular dendritic cells (DCs), are adept at providing necessary factors for engaging and activating specific naïve (and memory) B and T cells. Broadly speaking activation of adaptive immune cells requires antigen presentation

by dendritic cells to an antigen-specific receptor, cell-surface co-stimulatory molecules, and cytokines.

The cytokine milieu determines the nature of adaptive immune response after T-cell receptor (TCR) and B-cell receptor (BCR) engagement, influencing the activation, proliferation, differentiation, and longevity of antigen-specific cells. For example, type I IFN skews CD4 T helper (Th) cells to a Th1 biased phenotype, and acts as a third signal to induce potent memory CD8+ T cell cytotoxicity, cytokine production, proliferation, and differentiation into long lived effector progeny. In B cells, type I IFN in combination with BCR signalling increases T-cell independent follicular B- cell antibody responses [24] and regulates BCR signalling itself[25]. A single innate immune effector from a relatively small population of infected cells can therefore induce broad and far-reaching responses, with unique interactions for different cell types during this amplification inherently capable of producing variability in final responses.

Innate Immune memory

Surprisingly, both plants and invertebrates, which lack adaptive immunity, can resist reinfection suggesting possible 'innate immune memory'. Some of this may not be true memory, as non-specific cross-protection could occur through generic innate immune activation. For example, TLR5 agonist (flagellin) protects against subsequent rotavirus infection through IL-22 and IL-18 induction [26]. However, in humans some vaccines do induce T and B cell-independent protection through long term functional changes in innate immune cells[27]. Mechanistically this 'trained immunity' occurs through epigenetic reprogramming of new inflammatory programs, which similar to adaptive memory responses can be both beneficial and harmful [27]. The duration of trained immunity is however shorter than adaptive immunity, lasting only for the lifespan of the cells involved rather than the individual, and generally less than a year, although non-specific protection after live-attenuated vaccination has been observed after 5 years [28–30].

Of relevance to human immune variation, diverse trained immune responses can be induced by both heritable and non-heritable factors. The non-specific protection afforded by Bacillus Calmette–Guérin (BCG)-vaccination is associated with monocyte gene modules [31], and varies based on environmental factors such as sex[32], age[33], circadian response [34], and the microbiome.

1.2 Innate antiviral cytokines

To understand how the innate immune system generates optimal adaptive immune responses, and how these might vary, we need to understand the cytokines of an immune response. Cytokines are small protein intermediates important for cellular communication. Key cytokines discussed in this thesis relevant to antiviral and vaccine-induced immune responses are outlined, including: (a) early primary cytokines directly induced after triggering of PAMPs or DAMPS, such as type I, TNF, and inflammasome-derived cytokines; (b) cytokines often induced by other (primary) cytokines, which in response to viruses (and vaccines) includes IFN-γ.

1.2.1 Type I IFN

Type I IFN is the oldest cytokine, discovered over 50 years ago by Isaacs and Lindenmann[35], which similar to type II IFN (IFN-γ) and type III IFN (IFN-λ), has functions relevant to infectious and non-infectious diseases[36]. The first identified function of type I IFN was however as an early soluble factor released by cells in response to virus infection capable of interfering (inhibiting) the further propagation of virus.

Type I IFN is however not a single cytokine, with humans possessing 17 genes for type I IFN which all bind the same receptor to induce shared downstream responses. The most common are IFN-α, which has 13 subtypes, and IFN-β, with other subtypes such as IFN-κ, IFN-ω, IFN-ε not discussed in this thesis [37]. Different type I IFNs have varying tissue specificity and kinetics, with some such as IFNε only expressed in the female reproductive

tract[38]. All nucleated cells can secrete IFN-α and IFN-β after PRR engagement, either in response to viruses or soluble nucleic acids released from tissue damage [37], and all cells can respond through interferon-α/β receptors (IFNAR).

The production of type I IFN downstream of endosomal TLR and intracellular nucleic acid sensors is primarily governed by expression of the interferon regulatory factor (IRF) family of transcription factors. IRF3 homodimers bind to the IFNB1 promoter to induce IFN-β, with NF-kB enhancing transcription [39]. IFN-α induction however also requires IRF7 expression which, unlike IRF3, is not constitutively expressed in all cells but induced downstream of type I IFN itself via IFN-stimulated gene response elements (ISRE). IFNAR-dependent IRF7 expression creates a positive feedback loop capable of rapidly generating large quantities of IFN-α, a phenomenon best observed in plasmacytoid dendritic cells (pDC)[40].

PDC represent a very small fraction (0.3%) of specialised circulating PBMCs with a distinctive morphology due to high rough endoplasmic reticulum (ER) content (reviewed [41]). Human pDC lack lineage markers (CD3, CD19, CD14, CD16, CD11c), and are identified by expression of CD303 (BDCA-2, CLEC4C; C-type lectin) and CD123 (IL-3 receptor) – with IL-3 important for survival in vitro - as well as unusually high expression of CD4 and Granzyme B (GzmB). As specialised IFN-α producing anti-viral sensors, pDC express high levels of IRF7 and endosomal nucleic acid sensors, TLR7 (ssRNA) and TLR9 (unmethylated CpG sequences of DNA). Innate triggering also induces upregulation of CD62L and migration to secondary lymphoid organs where pDCs mature - increasing expression of MHCII, CD80 and CD86 - to function more akin to conventional antigen-presenting DC.

Type I IFN signalling

The receptor for all type I IFN is a heterodimer of subunits (IFNAR1, IFNAR2) with different affinities[37,42], which ultimately signals expression of a vast range of IFN-stimulated genes

(ISGs). Intracellularly both IFNAR1 and IFNAR2 are constitutively bound to tyrosine receptor kinases, Janus Kinase 1 (JAK1) and Tyrosine kinase 2 (TYK2) respectively, with ligand induced IFNAR transphosphorylation recruiting cytosolic Signal Transducers and Activators of Transcription (STATs). Uniquely, type I IFN can activate all seven known STATs through canonical and non-canonical JAK-STAT signalling [43]. Canonical type I IFN signalling involves STAT1 and STAT2 phosphorylation, heterodimerisation, and recruitment of IRF9 to form the ISGF3 complex [37], which translocates to the nucleus and binds specific ISRE to initiate ISG transcription [44]. Non-canonical signalling through phosphorylation of STAT3-6 often occurs in specific cells with unique functions which are discussed later[37].

Type I IFN function

Type I IFN functions span innate and adaptive immunity, co-ordinating direct inhibition of virus replication and stimulation of adaptive antiviral responses.

ISGs directly impact all aspects of virus lifecycles [44]. Many restrict virus nucleic acid replication [45], with examples including protein kinase R (PKR) which inhibits translation, and 2'5 OAS RNAse L which degrades RNA. Other IFN-induced restriction factors include IFITM proteins which divert viruses to lysosomes for degradation[46]. Type I IFN also induces cell death of infected cells by inducing intrinsic and extrinsic pro-apoptotic molecules and death receptors with the aim to prevent paracellular live virus dissemination.

The central importance of type I IFN to the antiviral response is best highlighted by the proportion of virus genomes which have evolved to evade interferon signalling [47]. Large poxviruses in particular secrete numerous soluble decoy receptors to type I and type II IFN. IFN-α/β binding proteins (IFN-α/βBP) include B18R, a competitive inhibitor of IFNAR1 and IFNAR2 with homology to IL-1R2, which inhibits both IFN-α and IFN-β signalling; this property is used in laboratory research to probe the importance of type I IFN in vitro.

Indirect antiviral functions of type I IFN include its immunomodulation of innate and adaptive cells: dendritic cells, monocytes and macrophages, NK cells, T cells and B cells are all directly regulated by type I IFN.

Dendritic cell (DC) IFNAR signalling promotes maturation and antigen presenting functionality, through upregulation of cell surface MHC and co-stimulatory molecules (e.g,CD80, CD86) [48–50]. Similarly, pDC may differentiate into more potent activators of T cells [51], while monocytes also undergo type I IFN-mediated differentiation and tissue migration.

The effects of type I IFN on APC also modulate T cell function; increased DC maturation, migration, and MHC expression promotes antigen-presentation to T-cells. Furthermore, IFNAR signalling in CD8+ T cells is a third signal for their activation, survival and differentiation[52,53], inducing CD69 expression which may promote migration and tissue residency [54]. Some functions vary depending on the kinetics and duration of triggering, with chronic stimulation for example paradoxically dampening DC responses through induction of IL-10 and PD-L1.

Further evidence for the importance of type I IFN in antiviral responses comes from human primary immunodeficiencies involving key signalling components downstream of IFNAR; severe and often lethal virus infections have been described for TYK2 [55], STAT1[56], STAT2[57], IRF7[58], and IRF9 deficiency[59], although importantly other IFN signalling pathways share these mediators. Reports of individuals with unique type I IFN deficiency are rarer, with the best examples demonstrating importance to live-virus vaccine responses. An otherwise well infant with homozygous IFNAR2 loss-of-function mutations unfortunately suffered fatal MMR-induced encephalitis [60]. IFNAR1 deficiency has also been associated with adverse reactions to MMR and yellow fever vaccination[61]. Similarly, homozygous STAT2 loss-of-function resulted in disseminated measles after MMR vaccination in an

otherwise healthy 5-year-old, with cells displaying defective type I IFN responses in vitro[62]. Taken together, although some functions of type I IFN overlap with other IFNs, specific protection from unusual live-virus vaccine complications may suggest unique functions in response to large inoculums bypassing normal mucosal entry.

1.2.2 TNF

Tumour necrosis factor (TNF) is a heterotrimeric cytokine induced early during immune responses with pleotropic effects ranging from the control of cell growth, acute and chronic inflammation, as well as tissue homeostasis(reviewed [63]). Sources of TNF are diverse, with immune cells (macrophages, T cells, B cells, neutrophils) and stromal cells such as keratinocytes and fibroblasts all capable of TNF secretion.

The cell surface receptors for TNF are TNFR1 (p55) and TNFR2 (p75), which have differential expression, ligand specificity, and signalling. TNFR1 is constitutively expressed on most immune and non-immune cells, acting as the primary receptor for soluble TNF which has a short half-life. TNFR2 expression is inducible on immune and endothelial cells, binding membrane TNF. Both receptors are also secreted as soluble receptors, after cleavage by ADAM (a disintegrin and metalloproteinase) family enzymes.

Ultimately surface TNFR receptor ligation induces NF-kB signalling which co-operates with other cytokine and transcription factor pathways (MAPK, AP-1) to promote many of the immunomodulatory functions. The TNFR complex also recruits death domains important for effector functions such as apoptosis.

The effects of TNF vary depending on the cell triggered[63]. Monocyte TNF signalling induces activation, maturation, and chemotaxis, whereas the impact on T cells is often regulatory, tuning T cell function and TCR signalling. Other downstream functions include cell

trafficking to sites of inflammation, through increased chemokine production, migration and adhesion via ICAM-1 and LFA-1. Important pro-inflammatory functions are supported by observations of spontaneous inflammation in transgenic mice over-expressing TNF, with human inflammatory diseases such as IBD and Rheumatoid Arthritis often amenable to therapy with anti-TNF monoclonal antibodies.

1.2.3 Inflammasome and IL-1 family cytokines

As alluded to previously, DAMP recognition can trigger inflammasome activation and caspase-1 mediated maturation of IL-1 family cytokines, IL-1β and IL-18; both cytokines share structural similarity, are generally pro-inflammatory, and their release through gasdermin pores is usually accompanied by cell death (reviewed [64,65]).

IL-1α and IL-1β are initially synthesised as pro-molecules requiring caspase-1 mediated cleavage. IL-1R1 and IL-1 receptor accessory protein (IL-1RAP) are heterodimeric receptors which share signalling homology to the TLR superfamily, triggering NF-kB activation and inflammatory gene expression - all shared features amongst IL-1 family cytokine receptors. Proinflammatory functions of IL-1 include increased monocyte activation, adhesion, and cytokine production. Excessive IL-1 production occurs in many chronic inflammatory diseases, including autoinflammatory disorders associated with fevers and recurrent tissue inflammation, and biologic therapies targeting IL-1 are clinically used to reduce inflammation.

Similarly pro-IL-18 cleavage by caspase-1 allows IL-18 release from myeloid and tissue cells[66], with IL-18 receptor (IL-18R1 and IL-18Rap) signalling via MAPK and NF-kB. A key function relevant to this thesis is potent IFN-γ induction from NK and T cells when combined with other cytokines, exemplified clinically by macrophage activation syndromes where extremely high systemic IL-18 concentrations are associated with pathogenic IFN-γ.

1.2.4 IFN-γ

IFN-γ was first identified as an acid-labile antiviral interferon[67], and subsequently coined as 'macrophage activating factor' accompanied by profound early effects on innate immunity. Both human and murine IFN-γ only have a single gene producing a single 1.2kb mRNA-species [68], which codes for a polypeptide of 166 amino-acids. After a hydrophobic signal sequence (23 amino acids) is cleaved[69], non-covalent dimerization forms the 34kDa biologically active form[70]. Circulating IFN-γ only has a 2-minute half-life, and IFN-γR expressing cells such as platelets can increase systemic bioavailability, prolonged signalling generally requires continued secretion.

IFN-γ signalling and receptor expression

IFN-γ receptor expression and responsiveness is widespread among immune and non-immune cells, albeit more modest and less ubiquitous than IFNAR expression[70,71], with highest expression in non-lymphoid organs[71,72] The IFN-γR is a heterodimeric membrane protein of IFN-γR1 and IFN-γR2 encoded on chromosomes 8 and 21 respectively. IFN-γR1 is the higher affinity (Ka = 100-1000 M^{-1}) subunit primarily responsible for ligand binding, with both subunits required for signal transduction through constitutively associated JAK1 and JAK2[73]. After IFN-γR1:IFN-γ ligand binding, IFN-γR2 recruitment allows JAK1/JAK2-mediated receptor cross phosphorylation to reveal STAT binding sites. Canonical IFN-γR signalling occurs via phosphorylated STAT1 homodimers [74], which translocate to the nucleus and bind DNA promoters termed γ-activating sites (GAS). Promoters of IFN-γ target genes include transcription factors such as IRF1 and IRF5 that further amplify the breadth and magnitude of the IFN-γ transcriptional response [75]. Signalling is however regulated and terminated actively, through rapid internalisation of the IFN-γR [71], and STAT1 proteasomal degradation [76].

Intriguingly, IFN-γR expression is not restricted to classic effector cells but also high on many cells typically important as sources of IFN-γ, endowing feedback and feedforward regulation. Further regulation occurs from stimuli which specifically modulate basal IFN-γR expression.

IFN-γ producing cells

The very rapid production of IFN-γ implicates a role in the very early response to infections and potentially vaccines. However unlike type I IFN, lymphocytes are the main sources of IFN-γ; these include conventional CD8+ effector T cells[77,78], CD4+ Th1 T cells, NK cells and unconventional T cells, which will be discussed in detail (**Section 1.4**). IFN-γ production has to a lesser extent been described in APCs, including B cells [78].

IFN-γ functions

The importance of IFN-γ was only apparent in mice after challenge experiments. Both *Ifng*$^{-/-}$ [79] and *Ifngr*$^{-/-}$ mice[80] only have mild immune defects but are lethally susceptible to a range of pathogens including Listeria monocytogenes [81], and Mycobacteria[80]. In humans, mendelian susceptibility to mycobacterial disease (MSMD) is most apparent in the absence of IFN-γ signalling [82], with germline mutations affecting the IFN-γR (e.g., IFNGR1, IFNGR2), cytokines important for IFN-γ induction (IL-12B, IL-12RB1), or downstream IFN-γ signalling (STAT1, IRF8)[83] all contributing to reduced protection against mycobacteria.

The role of IFN-γ in virus infection is less clear. Many viruses express IFN-γR1 binding proteins as part of their lifecycle[84], with IFN-γ capable of inducing effectors such PKR which inhibits virus protein synthesis. However, although *Ifng*$^{-/-}$ mice have clear abnormalities in response to Vaccinia [85], this does not apply to all infections [86]. Some key functions of IFN-γ include the regulation of host-mediated pathology[87], with local tissue damage observed in IFN-γ transgenic with aberrant tissue-specific expression.

Further functions of IFN-γ include regulation of the innate response to infection. ISGs such as IRF1 and IRF5 can polarise inflammatory (M1) macrophages, promoting pathogen phagocytosis and killing through induction of nitric oxide synthase (NOS) and secretion of antimicrobial peptides[10,88]. Increased cell migration is also observed, through induction of CXC receptor 3 (CXCR3) binding chemokines, with increased adhesion molecule expression supporting cell-cell interactions required to amplify immune responses and cytokine production. When combined with upregulation of factors on innate cells important for antigen-presentation, such as MHC-I, MHC-II, and co-stimulatory molecule (CD80/86) expression[87], the innate functions of IFN-γ clearly also regulate adaptive immunity.

Early adaptive immune responses are also directly regulated by IFN-γ signalling in lymphocytes. IFN-γ upregulates T-bet expression in CD4+ T cells, which promotes feedforward Th1 differentiation and sensitises cells to Th1 lineage commitment, in part by inducing IL-12R [89]. IFN-γ signalling also plays a role in CD8+ T cells, promoting proliferation and cytotoxicity in response to viruses[90].

IFN-γ also has a protective role in enhancing humoral responses, in part through signalling in T follicular helper cells (Tfh). IFN-γ promotes Tfh maturation and accumulation, leading to increased germinal centre (GC) formation for necessary to support B cell proliferation, differentiation, affinity maturation and selection[91,92]. Tfh cells also acquire the capacity to secrete IFN-γ through transient IFN-γ-induced T-bet expression [93], and T-bet+Tfh cells can promote feedforward loops and pathogenic GC formation in high IFN-γ states[91].

Finally, IFN-γ has a direct effect on B cells that shapes humoral immunity. Recombinant IFN-γ induces IgM secretion from both mice [94], and human B cells [95], and mimics CD4 T cell help for antibody induction in vitro[96]. Furthermore, IFN-γ induced T-bet expression in B cells increases the expression of B cell lymphoma-6 (BCL-6), a key orchestrator of GC

reactions, which further promotes Tfh differentiation[97], and immunoglobulin class switching[98].

In sum, the initial cytokines induced in response to viruses have a wide range of effector functions, including impacts on lymphocytes of the adaptive immune system. As the immune response progresses, these early cytokines can trigger further cytokine production from lymphocytes, depending on the nature of the original antigen encounter[1]. For example, nucleic acids induce the cytokines discussed in this Chapter, as well as IL-12, which then promotes the production of additional cytokines from lymphocytes like IFN-γ. These bridging cells and cytokines occupy an intermediate stage between the earliest, predictable germline effectors and later adaptive immunity, which creates a window of opportunity for host-specific factors to potentially introduce variability in the final immune response.

1.3 Vaccines

Vaccines and adjuvants

An understanding of the mechanisms above can be leveraged to induce protection against pathogens through vaccination. Vaccines have been a cost-effective tool for global health optimisation for a long time, with targets expanding to include a range of viral, bacterial, and more-recently non-infectious diseases. Traditionally, vaccines were developed to target whole pathogens or specific antigenic components[99]. The former approach required attenuation of pathogenicity to generate the complete immune response from innate sensing to adaptive immunity, without the complications resulting from uncontrolled replication. This has been achieved through live-attenuated, replication-defective, or inactivated pathogens. Live-attenuated vaccines induce potent long-lived immune responses, as seen with the original small-pox vaccine, yellow-fever, and measles-mumps-rubella (MMR) vaccines. However, these vaccines can be fatal, particularly in individuals with a compromised IFN system. Vaccines composed of pathogen subunits are safer, but typically require additional adjuvants [16].

Adjuvants are often required to enhance vaccine responses. Many vaccines have inherent adjuvant capacity from non-antigenic targets that trigger innate immunity. For example, nucleic acids, lipids, and lectins in live-attenuated pathogens are all effective PAMPS. Some effective vaccines contain non-biologic components that act as DAMPs. For example, aluminium salts were classic adjuvants later identified as potent inflammasome activators. Adjuvants can also induce the release of cell-intrinsic DAMPs by promoting cell-death, and some are designed primarily as effective delivery vehicles to induce optimal antigen production and signals for adaptive immunity[16]. Ultimately all adjuvants engage innate immunity and enhance adaptive responses to vaccines, but less is known about novel vaccine technologies (viral vector, mRNA) deployed during the SARS-CoV-2 pandemic and how they are sensed by the innate immune system.

1.3.1 Viral vector vaccines

Recombinant viral vector vaccines were first utilized 40 years ago, using modified vaccinia virus with a transgene specific for hepatitis B surface antigen [100]. However, prior to the COVID-19 pandemic, only five such vaccines were licensed for use in humans against Japanese Encephalitis, Dengue, and Ebola. Currently, most licensed viral vector vaccines are Adenovirus vectors (AdV), which will be discussed in this thesis. Other prominent viral vector vaccines currently in use or development include vesicular stomatitis virus (VSV), Poxvirus, and Flavivirus vector vaccines.

Adenoviruses and Adenovirus vectors

Adenoviruses are family of non-enveloped linear double-stranded DNA viruses found in vertebrates. Over 100 serotypes have been described in humans, classified into species A-G based on their HA and phylogeny[101]. The most common circulating Adenoviruses are Ad5 and Ad2, belonging to the species C clade, with a significant proportion of the population seropositive to these from childhood infection.

As dsDNA viruses which do not form latency, Adenoviruses can rapidly enter cells and generate large quantities of antigen quickly without DNA integration. Their thermostability, aided by the absence of a viral envelope, makes them suitable for long term storage. Their diverse cellular tropism was a key consideration behind initial development as therapeutic gene expression delivery systems for conditions like alpha-1-antitrypsin and cystic fibrosis[102,103]. Although the potent immune response they elicit can be a barrier to long term transgene expression [104], it paved the way for their development as AdV vaccine platforms[105], as they induce high antibody and CTL responses against both the Adenovirus and the transgene antigen.

The current AdV vaccines are non-replicating due to deletion of E1 and E3 cassettes, which not only increase the transgene size possible, but also make them safe for use in immunocompromised individuals. To maintain potent transgene transcription, an exogenous Cytomegalovirus (CMV) promoter is used to sustain antigen production in vivo[106]. The licensed COVID-19 vaccines developed during the pandemic are based on either Ad5, Ad26 or the chimpanzee-derived AdV, ChAdOx1. However, the work discussed in this thesis began prior to the pandemic and specifically focuses on ChAdOx1.

Innate sensing of Adenovirus vectors

AdV offer a significant advantage as vaccine platforms, as they are inherently self-adjuvant and can be sensed by the innate immune system due to their capsid and dsDNA. Once taken up by innate immune cells via clathrin-mediated endocytosis, AdV trigger both TLR-dependent and independent PRR at multiple stages in the virus life cycle before gene expression [107,108]. The escape of AdV from the endo-lysosomal compartment is a particularly potent trigger for numerous signalling cascades, including type I IFN production[109].

AdV can be detected by several cell surface and endosomal PRRs, including TLR2 [110], TLR4[111], and endosomal TLR9 [104,110]. These PRRs can activate antiviral inflammatory pathways such as NF-κB, MAPK and IRFs, which ultimately lead to the generation of antigen-specific T-cell responses. AdV potency may be due to their capacity to trigger multiple MyD88-dependent pathways, with differences in AdV intracellular trafficking and engagement of late endosomal TLR9 possibly accounting for variable potency. However, potent CD8+ T cell responses can still occur in mice even in the absence of TLR and NOD (thus MyD88)-signalling, suggesting some redundancy [112].

Cytosolic sensing of AdV dsDNA can induce innate responses through various pathways. One such pathway involves binding of AdV DNA to cGAS after escape from endosomes,

triggering STING and TBK1-IRF3 mediated type I IFN induction[113–115]. However, the true importance of this pathway to transgene-specific adaptive immune responses is not clear, as although innate responses and type I IFN production are reduced after intravenous AdV immunisation in *cGAS* and *Sting*-deficient mice, preserved anti-vector immunity is generated [113]. It is possible the durability of transgene-expression, which is negatively regulated by IFN-signalling, is more important for transgene-specific CD8+ T cell responses. This could explain why *Ifnar* and *Sting*-deficient mice have altered kinetics of early CD8+ T cell responses, but ultimately develop equivalent total responses to wild-type mice at later timepoints[106]. Interestingly, the importance of STING-dependent acceleration of cellular immunity appears to be vector-specific, as it is crucial for ChAd63 but not Ad5. These findings suggest that a combination of innate triggers shape the early response to AdV, with some evidence of differential cytosolic sensing of vectors [106].

The cytosolic sensing of AdV can also induce type I IFN-independent inflammatory responses [116]. Ad5, for example, can activate the NLRP3 inflammasome in macrophages, leading to caspase-1 dependent IL-1β secretion in a transgene and replication independent manner [115,116]. Additionally, Ad-penton interactions with macrophage integrins can directly induce IL-1α in a NLRP3-independent manner [117]. However, the effects of other IL-1 family inflammasome-derived cytokines, such as IL-18, have yet to be studied extensively.

Overall, the relative importance of individual pathways downstream of AdV sensing is not clear and further complicated by the methodology of studies. There may be overlap or redundancy in inflammatory pathways in vivo, making it difficult to observe a phenotype when any single pathway is abrogated.

Pre-existing anti-vector immunity

The early response to AdV incorporates both innate and adaptive immunity, with a high seroprevalence of anti-Ad immunity in humans from prior Ad exposure which may impact

subsequent AdV-induced immunogenicity[118]. The inverse correlation between seroprevalence of anti-vector neutralising antibodies and subsequent immunogenicity has been appreciated for some time[119,120], particularly with Ad5-based vectors [121]. However, recent studies have found effective boosting in homologous AdV prime-boost regimens, despite the high neutralising antibodies post-prime[122]. In particular, anti-ChAdOx1 neutralising antibodies did not correlate with subsequent spike-specific adaptive immunity after ChAdOx1-S [123].

Higher vaccine doses may theoretically overcome any neutralising anti-vector immunity, but such regimens used for Ad5 were unacceptably reactogenic with little improvement in immunogenicity[119]. The preferred solution has been to use AdV serotypes that are rare in humans, such as Ad26, or found in other species, such as chimpanzee-derived vectors like ChAdOx1. However, these solutions do not necessarily overcome the issue of cross-reactive Ad-specific T cells that recognise epitopes conserved across many serotypes, including rarer species [124]. Indeed Ad-specific T cell responses are present in unvaccinated, Ad5-seronegative individuals[124], although their relevance to immune responses is unclear.

Consequences of Adenovirus vector sensing

Vector specific immune activation, including co-stimulatory molecule expression on DC and pDC[125], is a common immediate consequence of AdV sensing. This occurs in conjunction with type I IFN induction, which can both promote or inhibit optimal immunogenicity. For example, excessive type I IFN can dampen sustained transgene expression and durable transgene-specific antibody and CD8+ T cell responses [106,126]. Early ISG expression in draining lymph nodes (LN) 24h post-vaccination inversely correlates with protective transgene specific CD8+ T cell responses, potentially explaining why Ad5, which induces muted type I IFN in vivo, may result in more persistent antigen expression compared to more inflammatory ChAdOx1[127]. Mechanistically persistent antigen promotes early maintenance of CD8+ T cell effector memory cells by extending the contraction phase of

post-prime memory[128,129]. It remains unclear whether IFN-γ has similar effects on antigen persistence, and whether vaccine antigen persistence plays a role in immunogenicity in humans.

Low levels of type I IFN are required as 'signal 3' for optimal adaptive immunity[126,130,131]. Differences in AdV efficacy may depend on the exact timing and duration of IFN signalling[132], with short term type I IFN blockade at prime improving Ad5 induced immune memory[133].

Although clinically these early responses are crudely measured as reactogenicity, in-depth studies of the human early immune response are lacking. Increased understanding of how AdV induce early immune responses could help elucidate the key steps in generating durable adaptive responses.

1.3.2 RNA vaccines

The advent of mRNA vaccines has been a major breakthrough during the pandemic as newly licenced vaccines were trialled and taken forward with remarkable efficacy into humans (reviewed[134]). The two primary types of mRNA vaccines are nucleoside-modified and self-amplifying vaccines**.** mRNA vaccination offers several advantages, including intracellular antigen expression and cross-presentation, which stimulate robust T-cell responses similar to those observed after AdV vaccination. Unlike viral-vector vaccines, mRNA vaccines do not induce anti-vector immunity. Moreover, a more consistent manufacturing process, regardless of the antigen, speeds up vaccine development timelines.

RNA vaccines require alternative methods of delivery into target cells, and lipid nanoparticles (LNP) are the most widely used with substantially improved nucleic acid delivery, in vitro protein expression, and potency of adaptive immune responses[134]. LNP are similar in size to apolipoproteins (~100nm), with four major components: (1) cholesterol; (2) polyethylene-glycol (PEG); (3) ionisable lipid; and (4) helper lipids. After in vivo injection, LNP are opsonised by circulating proteins and delivered to cells expressing lipid scavenger receptors. Myocytes and local APCs endocytose LNP after intramuscular immunisation, triggering endosomal and cytosolic PRR while still allowing RNA translation into the antigen of interest to engage adaptive immune cells. RNA sensing has been finely optimised to increase tolerability, antigen production, and adaptive immunity.

Self-amplifying RNA vaccine sensing

Self-amplifying RNA (saRNA) mRNA vaccines contain the desired antigen and an alphavirus replicase which increases the required LNP size. After entering the cell, mRNA is rapidly amplified, similar to the increased antigen expression during natural virus infection[135]. While a saRNA vaccine for SARS-CoV-2 was developed and demonstrated

high immunogenicity in animal models[136], it was less effective in humans. Despite the lower dose required for saRNA vaccines, they trigger strong RNA sensing and type I IFN responses that could potentially impair immunogenicity.

Nucleoside-modified RNA vaccine sensing

Nucleoside-modified mRNA vaccines, which contain 1-methylpseudouridine (m1Ψ), were initially developed to enhance mRNA antigen production upon intracellular delivery while minimising the activation of nucleic-acid sensors. The primary sensors of synthetic mRNA are: (1) uridine-dependent RNA sensing; (2) dsRNA sensing; (3) uncapped 5' mRNA sensing. In humans, TLR7 and TLR8 are potent sensors of unmodified ssRNA, binding to guanosine and UUU ribonucleotide, or uridine and UG, respectively (reviewed [137]).

Kariko, Weissman et. al, observed that modifying RNA to make mRNA vaccines more similar to ribosomal RNA reduced innate stimulation and increased protein translation. Pseudo-uridine modification of uridine decreased binding to TLR7 and type I IFN production[138], without compromising adaptive immune responses. In vivo data from mice also confirmed a reduction in type I IFN at early time points after vaccination with nucleoside-modified vaccines[139].

Despite these modifications, nucleoside-modified vaccines still elicit an innate response, and local and systemic reactions have been observed in humans. While TLR7 binds to ssRNA[140], it is conceivable that not all RNA sensing is inhibited in response to vaccination, or that the release of endogenous unmodified RNA from vaccine-induced cell-death induces type I IFN, which may play a role in adaptive responses [141].

LNP sensing

Early responses to mRNA vaccines could also be attributed to the sensing of the mRNA LNP. LNP are designed to protect the cargo vaccine mRNA, promote lymphatic delivery,

and uptake by LN DC for antigen production [134]. However, empty LNP have previously been employed as adjuvants for protein vaccines[142], and when combined with the SARS-CoV-2 spike protein elicit strong immune responses in mice [143]. Mechanistically, IL-6 is rapidly induced, regulating Tfh function and GC development[143,144], and is likely responsible for the early vaccine-induced C-reactive protein (CRP) observed in trials[145].

Consequences of mRNA-LNP sensing

Issues with tolerability of mRNA vaccines may stem from innate sensing [146]. While some type I IFN production may be beneficial in response to mRNA vaccines due to their impact on DC maturation and migration to draining LN, this effect must be optimised to minimise inhibition of mRNA translation and unacceptable reactogenicity.

Another potential effect of mRNA-LNP sensing is the regulation of antigen kinetics, including durability and distribution. In humans, sustained antigen production in response to BNT162b2 has been associated with stronger GC B-cell responses and antibody titres[147], consistent with other vaccine data [148,149]. Increasing antigen also enhances T follicular helper cell responses and correlates with improved humoral immune responses [150]. The capacity for the early innate response to clear the antigen depot, either directly or indirectly, is an area of potential interest for optimising immune responses.

Overall, healthy adults mount an innate immune response to vaccines, which is likely to apply to novel vaccine platforms. However, the specific mechanisms remain unclear. Studies on the systems biology of human vaccine responses suggest that effective vaccines tend to induce robust ISG signatures[151,152], which may serve as important mechanistic determinants and biomarkers of effective vaccination[153].

1.4 Innate and Innate-like IFN-γ producing lymphocytes

Similar to NK cells, innate-like lymphocytes can respond in an antigen-independent manner during the course of an immune response[154,155]. This feature enables early sensing and amplification of innate signals, without necessarily being limited by the quantity, quality, and location of antigen. Innate-like lymphocytes possess a range of effector functions, and include unconventional T cells and innate-like B cells which bridge the innate and adaptive continuum between NK cells and conventional T cells [156]. While NK cells are strictly innate due to their lack of VDJ recombination, the term "innate-like lymphocyte" used in this thesis encompasses both NK cells and innate-like unconventional T cells. These cells share the capacity for rapid effector functions, particularly IFN-γ induction, which is relevant to vaccine-induced immune responses.

1.4.1 Group 1 Innate Lymphoid Cells: NK cells, ILC1

Innate lymphoid cells (ILCs) are defined as lymphocytes that develop independently of recombinant activating genes (RAG)-dependent antigen-receptor recombination[157]. NK cells were the first ILC to be discovered and were initially identified as cells mediating non-specific anti-tumour cytotoxicity[158]. Other similar cells with unusual functions, including the ability to secrete IL-22 [159], were later classified as a separate lineage derived from an Id2+ progenitor based on their cytokine secretion profiles [157].

NK cells and group 1 ILC1 both express the T-box transcription factor T-bet, require IL-15 for their development, and can produce IFN-γ and TNF [157]. However, NK cells express high levels of Eomesodermin (EOMES) which endows them with the capacity for strong granzyme-perforin mediated cytotoxicity and provides some redundancy to T-bet functions, allowing for the development of NK cells in the absence of T-bet. In humans, ILC1 are mainly resident in mucosal barrier tissues and express CD161 consistently, whereas NK cells mainly circulate between blood and lymphoid organs.

Some of the markers used to classify NK cells in this thesis vary during development. In human PBMC, NK cells are commonly divided into CD56bright and CD56dim populations, which are dominant in secondary lymphoid organs and blood, respectively[160]. CD56dim cells typically have higher cytotoxicity with greater expression of GzmB and perforin at rest, while CD56bright NK cells are more immunoregulatory with greater cytokine production. CD161 expression is also found in variable frequencies, similar to innate-like T cell populations.

1.4.2 Innate-like 'unconventional' T cells

Innate-like T cells (ILTC) refers to a group of T cells that share the capacity to induce rapid effector functions, develop in the thymus, like conventional adaptive αβ T cells, and express TCRs derived from RAG-mediated recombination. However, ILTC differ from conventional T cells as they have a limited TCR repertoire, with antigen specificities for non-peptide antigens, and are restricted by more evolutionarily ancient monomorphic non-MHC restriction elements. As such they are sometimes referred to as ‘unconventional T cells’ and include: MHC class I-related molecule (MR1)-restricted mucosal-associated invariant T (MAIT) cells, CD1d-restriceted invariant natural killer T (iNKT) cells, gamma-delta (γδ) T cells, and CD1b-restricted germline-encoded mycolyl lipid-reactive (GEM) T cells[161]. These cells undergo pre-programmed developmental maturation in the thymus[162], emerging with an effector memory phenotype prior to any peripheral antigen exposure, then preferentially migrate to and seed peripheral tissues[163].

The frequencies of ILTC vary widely between and within species. In humans, MAIT cells are the dominant αβ ILTC population, with iNKT and GEM T-cells much rarer[164], whereas in mice iNKT are much more abundant than MAIT cells. As ILTCs are variable and lack MHC-restricted recognition, they could potentially contribute to the heterogeneity of human antiviral responses and may be amenable to donor-agnostic therapies.

1.4.3 CD1 restricted NKT cells

Invariant NKT (iNKT) cells are the least common ILTC in humans but have been extensively studied in mice since their discovery in 1987 as a population of T cells with a Vβ8 biased TCR among double negative thymocytes [165,166]. They received their name because they express NK cell markers (NK1.1 or CD161 in mice and humans, respectively[167–169]) and an invariant TCRα chain (Vα14-Jα18 in mice, or Vα24-Jα18 in humans [170,171]).

In mice, the ligands for iNKT were identified as lipid antigens presented by CD1d, a monomorphic MHC-I-like restriction element. The first lipid antigen described was the glycosphingolipid, α-galactosylceramide (αGalCer)[172,173], which was subsequently loaded onto CD1d tetramers to enable recognition of 'type I' iNKT. Other CD1d-restricted NKT cells, termed 'type II' NKT, have less restricted TCRα repertoires recognising hydrophobic antigens, such as sulphatides[161]. These won't be discussed in this thesis.

Humans have an even more diverse family of CD1 restricted NKT cells in addition to CD1d-restricted iNKT expressing Vα24-Jα18[161]. These include CD1a-restricted T cells that recognise skin-derived lipid antigens, CD1b-restricted GEM T cells expressing TCR-Vα7.2, and CD1c-restricted T cells that recognise mycobacterial lipid phosphomycoketide. The frequency of these cells in circulation is extremely rare in humans, with the most prevalent CD1d-restricted iNKT comprising less than 1% of T cells in peripheral blood, although they are more abundant in tissues such as the lung and liver[174].

1.4.4 MAIT Cells

Mucosal-associated invariant T (MAIT) cells were coined as such after discovery of a population with invariant TCRα use enriched among double negative T cells in human blood and mouse intestine [171,175]. MAIT cells are an abundant innate-like effector memory T cell population in human blood, comprising up to 10% of peripheral T cells, and are also enriched in tissues [175–177]. They are defined as TRAV1-2+ (TCR Vα7.2+) T cells restricted by MR1 which recognizes non-peptide riboflavin biosynthesis intermediates conserved among bacteria and fungi [178–183]. All mammalian barrier surfaces are colonised by riboflavin-synthesizing commensals, and MR1 has co-evolved with MAIT cells through most mammalian evolution [184], thus being an example of barrier surfaces shaping human immunity.

Although MAIT cells are the dominant MR1-reactive T cell population in humans, there are other MR1-reactive T cells (MR1T) which bind the MR1-tetramer loaded with the riboflavin metabolite 5-(2-oxopropylideneamino)-6-D- ribitylaminouracil (5-OP-RU). However, only TRAV1-2+, MR1-reactive T cells acquire promyelocytic leukaemia zinc finger protein (PLZF) expression during thymic development to endow an effector memory phenotype. Other MR1T include riboflavin-reactive (TRAV1-2-) T cells, folate-reactive and MR1-autoreactive T cells[185]. Some of these MR1T can recognise endogenous or cancer associated antigens, which raises interesting questions about the evolution and non-MAIT cell dependent functions of MR1.

MAIT cells and iNKT have unique thymic development compared to conventional T cells, with selection on double-positive thymocytes rather than MHC-expressing thymic epithelial cells [186]. MAIT cells undergo a three-stage MR1-dependent development process. The first stage requires thymic development, but full maturation into PLZF+ effector memory cells

occurs in both the thymus and periphery in humans, with maturation required for CD161 expression [187].

In humans, peripheral MAIT cell frequency increases with age, peaking before 30 years, and then rapidly declines in adults over 60 years old to <1% of all T cells[188]. The majority of peripheral MAIT cells are CD8+ or double negative (CD4-CD8-), with a small fraction being CD4+ MAIT cells [183]. Roughly half of MAIT cells express CD56, which is associated with enhanced cytokine responsiveness[189].

The effector functions of MAIT cells are regulated by transcription factors, many of which are shared with other innate-like lymphocytes. In humans, these include expression of the type 1 transcription factor T-bet, and the type-17 transcription factor, retinoic-acid-receptor-related orphan gamma (RORγt), which are co-expressed; in mice, distinct expression defines separate MAIT1 and MAIT17 subsets [190,191]. As in NK cells, the cytotoxic function of MAIT cells is determined by EOMES, which together with PLZF and T-bet endows MAIT cells with the ability to rapidly execute effector functions and cytotoxicity in response to cytokines during an antiviral response.

1.4.5 Gamma-delta (γδ) T cells: Vδ2+ and non-Vδ2+

Gamma-delta (γδ) T cells were discovered in 1984 [192,193], and identified by their usage of γ and δ TCR chains that are restricted by non-classical MHC molecules. While present in all jawed vertebrates, there are species-specific biases in TCR. Embryologically, γδ T cells appear before αβ T cells and dominate the early foetal T cell repertoire before eventually being replaced by expanding αβ T cells.

In humans, γδ T cells make up ~5% of circulating T cells[194], with the majority (up to 75%) possessing the Vδ2/Vγ9 TCR pairing, referred to as Vδ2+ γδ T cells throughout this thesis.

The remaining non-Vδ2+ γδ T cells in PBMC are predominantly Vδ1+, which differ in terms of TCR specificity and functionality compared to Vδ2+ counterparts[164,195]. In humans and animals, γδ T cells of different TCR specificities migrate in waves into different tissues during development, resulting in tissue-biased TCR usage. Full functionality is established after TCR ligation in the thymus, which induces PLZF expression and distinct effector cytokine profiles, including the capacity for IFN-γ production[196].

This thesis focuses on immune responses in blood, with the primary distinction between Vδ2+ and Vδ2- γδ T cells. Vδ2+γδ T cells are thought to be restricted by the butyrophilin-like family of proteins (BTN2A/3A), which recognise self or microbially derived phosphoantigen metabolites [197]. Examples of metabolites include the isoprenoid pathway intermediate (E)-4-hydroxy-3-methyl-but-2-enyl pyrophosphate (HMBPP), produced by mycobacteria, and tumour metabolites such as isopentenyl pyrophosphate (IPP). The dominance of Vδ2+ γδ T cells in blood is likely due to polyclonal expansion, as observed in mycobacterial disease, where their ability to induce target cell lysis may play a protective role [198]. However, the function and phenotype of Vδ2+ γδ T cells are heterogeneous. CD26, a marker found on MAIT cells, can be used to distinguish CD26++CD94lo Vδ2+ γδ T cells, which display remarkable functional similarities to MAIT cells[199]. Moreover, both CD26 and CD94 can regulate Vδ2+ T cell cytokine responsiveness.

1.4.6 Shared features of innate-like lymphocytes

1.4.6.1 Rapid TCR-independent activation

The innate-like lymphocytes discussed exhibit both shared and distinct characteristics important for their identification and function in humans[164,186]. Their hallmark feature is rapid effector function, including cytokine production, mediated by the transcription factor PLZF, which supports TCR-independent activation through induction of cytokine receptors [200,201]. PLZF is induced early after positive thymic selection, and mice deficient in PLZF show

reduced frequencies of iNKT and MAIT cells, which display impaired cytokine secretion, tissue homing, and lack conventional markers of effector memory T cells[202]. Shared cytokine responsiveness to type I IFN, IL-18, and IL-12 has been reported for iNKT [203], MAIT cells [201], and γδ T cells[204], particularly the Vδ2+ subset[164]. This shared feature could enable these cells to respond to both viruses and vaccines.

1.4.6.2 Expression of CD161

CD161 expression, although not present in all innate-like lymphocytes, is associated with transcriptional profiles of innate responsiveness and expression of cytokines receptors such as IL-12R and IL-18R [200,201]. This characteristic has been confirmed in CD161+CD4 [205], CD161+NK cells [206], and CD161+γδ T cells, where higher CD161 expression is observed in the more cytokine responsive Vδ2+ subset[164]. However, CD161 is not a reliable marker for cytokine-responsive γδ T cells as many CD161-Vδ2+ are also capable of TCR-independent IFN-γ production.

Initially described as an NK marker similar to CD56 [207], CD161 (KLRB1) was soon found to be expressed among CD4+ and CD8+ T cells subsets that were enriched for IL-17 production[208]. The magnitude of CD161 expression varies among T cells, with intermediate and high expression identifying functionally distinct populations [209].

The exact function of CD161 in humans remains unresolved. Its ligand, lectin-like transcript 1 (LLT1) [210,211], is found on various immune cells including B cells, other activated APCs, and even T and NK cells[212]. In NK cells, ligation of CD161 is generally inhibitory [210,211], while in αβ T cells, the function is less clear, with reports of both inhibitory [213,214], and stimulatory effects [210,215]; CD161 ligation on subsets of γδ T cells was found to induce IFN-γ release[216,217]. Whether the impact of ligation is context dependent remains unclear, particularly in viral infections.

1.4.6.3 Activation in response to viruses

There is a growing body of evidence suggesting that innate-like lymphocytes share sensitivity to viruses and antiviral effectors during both acute and chronic infections. The antiviral functions of NK cells are well recognised, with severe herpesvirus infection in humans with NK cell deficiency, and increased mortality in mice with NK cell depletion after infection with IAV or murine cytomegalovirus (MCMV) [218]. Mechanistically, NK cells can recognise and kill infected cells through a combination of inhibitory and activating natural cytotoxicity receptors (NCRs) [219], with other functions, such as IFN-γ production, also linked to protection in chronic virus infections [220].

Other innate-like lymphocytes may also play a role in virus infection, with evidence that both iNKT and MAIT cells are activated early and protect against severe influenza. Mice deficient in iNKT cell (*CD1d*$^{-/-}$ or *Jα18*$^{-/-}$) die within the first 10 days of infection [221], and there is in vitro evidence that iNKT cells can kill IAV-infected monocytes. Additionally, CD40-CD40L mediated inhibition of suppressive MDSCs, which in turn limit IAV-specific responses[222], could explain why the administration of the iNKT ligand αGalCer is an effective adjuvant for mucosal antibody and CD8+ memory responses after IAV vaccination in mice [223].

MAIT cell deficiency (in *Mr1*$^{-/-}$ mice) is also linked to severe disease after PR8 IAV challenge, with reduced early effector recruitment in the absence of MAIT cell derived IFN-γ[224]. These findings may have implications for humans, as it has been observed that circulating MAIT cells are activated and reduced in frequency early after acute influenza, which correlates with improved survival and outcomes. This suggests that changes in the MAIT cell compartment may accompany effective antiviral responses.

During the COVID-19 pandemic, high dimensional immunology data has provided undeniable evidence that innate-like lymphocytes, particularly MAIT cells, are activated

during the early antiviral response[225,226,342,343]. In COVID-19 patients, unsupervised analysis of MAIT cells has identified CD69 and CD56 expression as key correlates of disease severity[225]. Interestingly, the expression of CD69 on MAIT cells is strongly associated with adverse or fatal outcomes, more so than other cytokine responsive cells; this finding was replicated in multiple studies[225,342,343], although one early study reported an inverse correlation between MAIT cell activation and good outcomes[226].

Overall, these findings suggest that MAIT cells and other innate-like lymphocytes may have an emerging role in shaping optimal responses to viruses, which could be leveraged to improve responses to vaccines.

1.4.6.4 Activation in response to vaccination

The early anti-viral immune response which activates innate-like lymphocytes may also contribute to their activation and relevant effector functions in response to vaccines, offering potential new avenues for enhancing subsequent vaccine-induced adaptive immunity.

There is evidence that vaccines can activate innate-like lymphocytes. For instance, after BCG-vaccination, MAIT cells make up a significant proportion of IFN-γ+CD8+ T cells through predominantly MR1-independent activation, even though replicating BCG generates MAIT cell TCR ligands [227]. In NHP given intravenous BCG, MAIT cells and Vγ9+ (but not Vγ9-) γδ T cells expanded over 200-fold from <5% to >50% of all T cells in bronchoalveolar lavage (BAL) fluid after 2 weeks[228]. MAIT cell and Vδ2+γ9+ γδ T cells can both be triggered via their TCR by BCG-derived ligands, in addition to sharing cytokine responsiveness.

Vaccines may also indirectly trigger innate-like lymphocyte activation through adaptive immune effectors. For example, NK cells can be stimulated by conventional CD4+ T cell

derived IL-2 [229], or through CD16 triggering dependent on antigen-antibody complexes[230,231]. As evidence, heightened secondary NK responses occur in vitro following vaccination with DTP (diphtheria, tetanus, and pertussis)[231], BCG and IAV[231].

Activated innate-like lymphocytes would make appealing targets as vaccine adjuvants due to their diverse range of effector functions, including both cell-to-cell interactions and cytokine production, which can potentially prime antigen-specific T cells[232]. Studies have shown that DC activation through cell surface CD40L:CD40 interactions can occur with iNKT cells [233], γδ T cells[234] and MAIT cells[235]. Additionally, cytokines produced by innate-like lymphocytes, such as IFN-γ, can potently activate APCs, leading to increased co-stimulation and antigen presentation, as well as (indirectly) promoting the recruitment of adaptive immune cells. For example, NK cell IFN-γ can improve the priming of IAV-specific CD8+ T cells, partly by enhancing the migration of naïve CD8+ T cells [236]. Similarly, iNKT cells and early IFN-γ dependent chemokines such as MCP-1 can increase antigen-specific CD8+ T cell responses to DNA vaccines in mice[237].

Innate-like lymphocytes may also play a role in regulating B cell responses. In the context of autoimmunity, infection, and vaccination, MAIT cells, iNKT cells, Vδ2+ T cells and NK cells can provide CD40-CD40L dependent B-cell help[238,239]. Additionally, the cytokines produced by innate-like lymphocytes can support B cell differentiation and proliferation, either directly[238,239], or indirectly by promoting APC activation [240], or CD4+ Tfh differentiation in the case of murine CXCR5+γδ T cells[241]. Moreover, some innate-like lymphocytes may have ‘Tfh-like’ functions; Tfh-like MAIT cells in human tonsils, which express CXCR5, BCL-6, ICOS and PD-1, can promote humoral responses in vitro[242]. Similar populations of iNKT[243–246], and Vδ2+γδ T cells[247,248], have also been identified with the capacity to provide B cell help and promote antibody production.

1.4.7 IFN-γ and innate-like lymphocytes

Many types of innate-like lymphocytes share the capacity for rapid IFN-γ production from pre-formed IFN-γ mRNA, which is of relevance to responses against viruses, vaccines, and intracellular pathogens[249]. Although not all innate-like lymphocyte subsets in all species produce IFN-γ, it is a hallmark of innate-like lymphocytes in humans and is linked to T-bet expression. T-bet induces chromatin remodelling of the IFNG locus[250], with the best evidence for its importance from humans with T-bet deficiency who have impaired development of NK cells, Vδ2+ γδ T cells, iNKT, and MAIT cells, but functionally maintain IFN-γ producing conventional CD4 (Th1) and CD8+ T cells[251].

IFN-γ production in naïve T cells is triggered by TCR crosslinking, whereas effector memory T cells and innate-like lymphocytes can also be triggered by APC-derived cytokines such as IL-12 and IL-18[252,253]. This cytokine combination activates STAT4, which is crucial for IFN-γ production in effector memory T cells and NK cells during viral infections[254]. Additionally, type I IFN can non-canonically signal transiently via STAT4, which explains the early (within 1hr) transient expression of IFN-γ after NK stimulation[255]. However, sustaining IFN-γ production requires other cytokines.

Interestingly, IFN-γ-mediated IFN-γ signalling between IFN-γ producers can lead to feedforward amplification, which can sustain the production of (protective) IFN-γ. Upon T-cell stimulation, IFN-γR is recruited to immune synapses, facilitating both autocrine and paracrine IFN-γ feedback loops that accelerate CD4+ Th1 polarisation for antiviral responses[256]. In a murine model of tissue HSV-1 infection, two waves of IFN-γ are observed: an early, smaller wave followed by a larger, T-cell dependent wave after a few days [257]. Notably, the late IFN-γ is absent in mice with *Ifngr*$^{-/-}$ CD4, with evidence that IFN-γ acts in an autocrine manner to promote CD4 T-cell mucosal entry, and a paracrine manner to induce CTL tissue migration.

IFN-γ can signal not only to conventional T cells via IFN-γR, but also to innate-like lymphocytes. In response to Listeria monocytogenes secondary challenge, IFN-γ accelerates NK and iNKT cell activation, resulting in more efficient recruitment and activation of effectors[258]. CD8+ T cells are the major source of early IFN-γ in this model, and their depletion prior to boost delays early NK-cell IFN-γ, which suggests that memory T cells may co-ordinate early innate-like lymphocyte responses via IFN-γ. Similarly, early IFN-γ and iNKT cells are required for αGal-Cer induced NK cell proliferation and cytotoxicity[259,260]. It is not yet clear whether these mechanisms apply more broadly to other innate-like lymphocytes.

Clinical data using recombinant IFN-γ reinforces the idea that IFN-γ producers are responsive to IFN-γ. IFN-γ administration in patients with relapsing remitting multiple sclerosis leads to increased exacerbations and increased NK cell activation after 24-72hrs, before the induction of inflammatory (CD16 expressing) monocytes and spontaneous conventional T cell proliferation[261]. In mice, administering recombinant IFN-γ at the time of malaria vaccination improves protective antigen-specific antibody responses [262,263], suggesting that increasing early vaccine-induced IFN-γ may enhance later adaptive vaccine responses.

Ultimately, early IFN-γ may act both upstream and downstream of innate immunity to regulate protective responses [264–266]. As innate-like lymphocytes are major IFN-γ producers, and IFN-γ is important for vaccine-induced protection [267], these cells may represent promising vaccine adjuvants.

1.4.8 Tissue specific functions of innate-like lymphocytes

Innate-like lymphocytes are not only present in circulation but are also prominent in tissues with unique tissue-specific functions. Many tissue-specific innate-like lymphocytes express CD161 in addition to the transcription factor RORγt (RORC) [186,268], which is crucial for barrier protective IL-17 production [269,270]. For example, MAIT cells in tissues are more activated than their circulating counterparts in homeostasis, and capable of increased cytokine production on activation[271–273] [**Table 1.1**]. It is now recognised that resident immune cells are in constant communication with their surrounding tissue environment, integrating cues from the local microbiome, cellular, environmental, and metabolic milieus for their development and function [270,274–277]. MAIT cells and innate-like lymphocytes occupy a similar niche and engage in similar crosstalk, allowing them to sense similar factors. Therefore, tissue-specific factors could modulate innate-like lymphocyte function at mucosal surfaces, which would be relevant to understanding how early immune responses are induced, particularly for novel mucosal vaccines (**Figure** 1.1**, Figure** 1.2).

Figure 1.1 | Mucosal environmental factors which could influence immune responses directly and indirectly. (From Amini et al., Frontiers in Immunology, 2020)

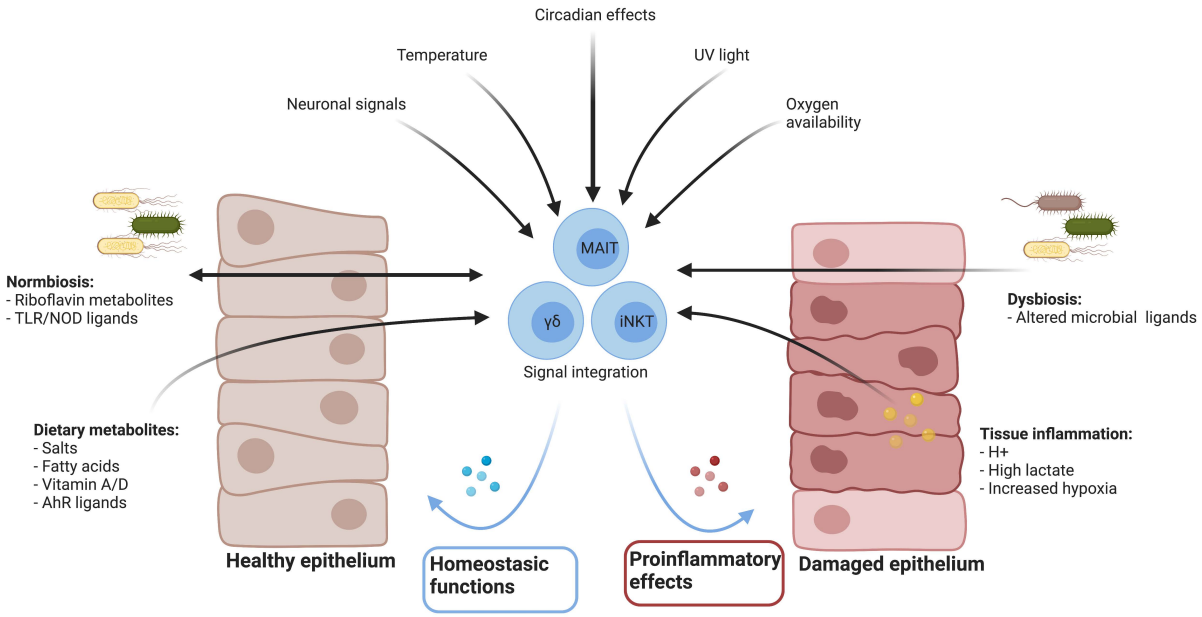

Table 1.1 | MAIT cells in healthy human barrier tissues.

Barrier tissue MAIT location	Frequency	Phenotype and activation	Ref
Oral			
Buccal mucosa *close to basement membrane, both within the epithelial layer and connective tissue.*	No enrichment compared to blood (50% of oral CD8αα T cells)	↑CD103$^+$ (20-80%) – most are CD8+ ↑HLA-DR, CD69, PD-1, CTLA-4 ↓CD38, perforin PMA/ionomycin stim: ↑IL-17A, GzmB (esp. CD103$^+$MAIT) ↓TNF, IFN-γ	278,279
Gut			
Gastric mucosa *Lamina propria*	LPMC 2% (0-12%) Gastric 1% (0.4-2.39)	↑CD103$^+$CD69$^+$(80%)	280 *281
Duodenum *Lamina propria and epithelium*	1.7% IEL 3% (0.1-5%) LPL 2% (0.5-4%)	↓IL-18Ra IL-12+IL-18 stim: ↓IFN-γ	164
Jejunum *Lamina propria and epithelium*	IEL: *60% (n=1*) (Va7.2+ T cells)		179
Colon *Lamina propria and epithelium*	No data in healthy Cancer: IEL 1%; LPL 2% Inactive UC 12% (30% of CD8$^+$ are MR1++)	Most CD8+, CD103+ *(n=1)* ↑CD69 (>90%), HLA-DR, CD25, TIGIT, PD-1, CTLA-4, LAG-3 ↑GzmB (baseline) ↑Tbet, RORγt PMA/ionomycin stim: ↑TNF, IFN-γ, IL-17A, IL-22 E coli stim: ↓IFN-γ	* 273 282,283
Rectum	2% (0.5-8%)	CD8$^+$ > DN MAIT ↑IL-23R, CSF-1, TNF, CD40LG, CRTAM ↓GzmK	272,284
Small intestine Foetal 2nd trimester	0.5% (0.2-1%)	CD8aa (30%), Ki67 (20%) PMA/ionomycin stim:↑IL-22 E coli stim: ↑IL-22, ↓IFN-γ	285
Lung			
Bronchial tree *Epithelium > lamina propria*	5% (Endobronchial biopsy) *TRAV1-2$^+$%CD8:* Trachea (42%) > proximal (35%) > distal bronchus (22%) (*n=1)*		286 287
Lung parenchyma	6% [TRAV1-2$^+$%CD8]		287
Lung parenchyma	0.8% (range 0.6-2)	CD127$^+$IL-18Ra$^+$ (>90%) CD8aa (20%), Ki67 (15%)	285

Foetal 2nd trimester		E coli stim: ↑IL-22, ↓IFN-γ	
Sputum	2%		286
BAL adult	2% *4% [TRAV1-2+%CD8]*	↑CD103+(75%), PMA/ionomycin stim: ↑IL-17A (esp. CD103+)	286,288 CD8+Va7.2 287
BAL children	1% 3% (in CAP)	Most CD103- – in CAP >50% CD103+ Plasma: ↑IL-12p70 ↓IFN-γ IL-22 IL-23 MIP-1a MIP-1b CAP: ↑IL-17A, IL-22, IL-23, IL-1b, IL-6, IL-12p70, MCP-1, MIP-1a, MIP-1b ↑ IL-17A: IFN-γ ratio ↑ *HIF1A, AHR, BATF, PLZF* ↓*TCF7*	*289
Skin			
Epidermis and dermis, *especially papillary dermis and adjacent to the superior vascular plexus*	3.8+/-0.32% (by IF) Epidermis: 1.5±0.5% (11.6±11.0% of CD8+) Dermis: 0.5±0.1% (4.6±4.0% of CD8+)	↑CLA+ (80%) ↑CD103+(80% epidermis, 40% dermis)	290 *120
Female Genital Tract			
Endometrium *Lamina propria close to and within glandular epithelium*	1% (range 0-3%)	↓PLZF (DN vs CD8+ MAIT ↓Tbet; ↑PLZF, RORγt, Helios) E coli stim: ↑polyfunctional, IL-17A, IL-22; ↓IFN-γ TNF GzmB	291,292
Cervix *Endocervix, adjacent to simple columnar epithelium; Transformation zone lamina propria; Ectocervix both sides of basement membrane, predominantly in epithelial clusters*	2% (range 0-6%)	↓Eomes	292
Placenta *Decidua parietalis*	2% (IVB 4%)	↑CD69 (80%), CD25 (25%), HLA-DR (35%), PD-1 (70%), Ki67 (15%) ↓CD127 (50%) E coli stim: ↑GzmB, Perforin	293

Location, frequency, phenotype, and function of MAIT cells in healthy human tissue compiled from studies to date. Frequency is expressed as a % of total CD3+ unless otherwise specified. Studies highlighted (*) defined MAIT cells using MR1-tetramer. All

other studies used proxy measures of variable stringency to identify MAIT cells, predominantly CD161+Va7.2+. Enrichment and comparisons of phenotype or function are compared to blood. BAL = bronchoalveolar lavage; Ca = cancer; CAP = community acquired pneumonia; DN = double negative; GzmB = granzyme B; DP = decidua parietalis; DN = double negative; IEL = intraepithelial lymphocytes; IF = immunofluorescence; IVB = intervillous blood; LPL = lamina propria lymphocytes.

Figure 1.2 Possible environmental factors capable of regulating MAIT cell transcriptional and effector responses (From Amini et al., Frontiers in Immunology 2020).

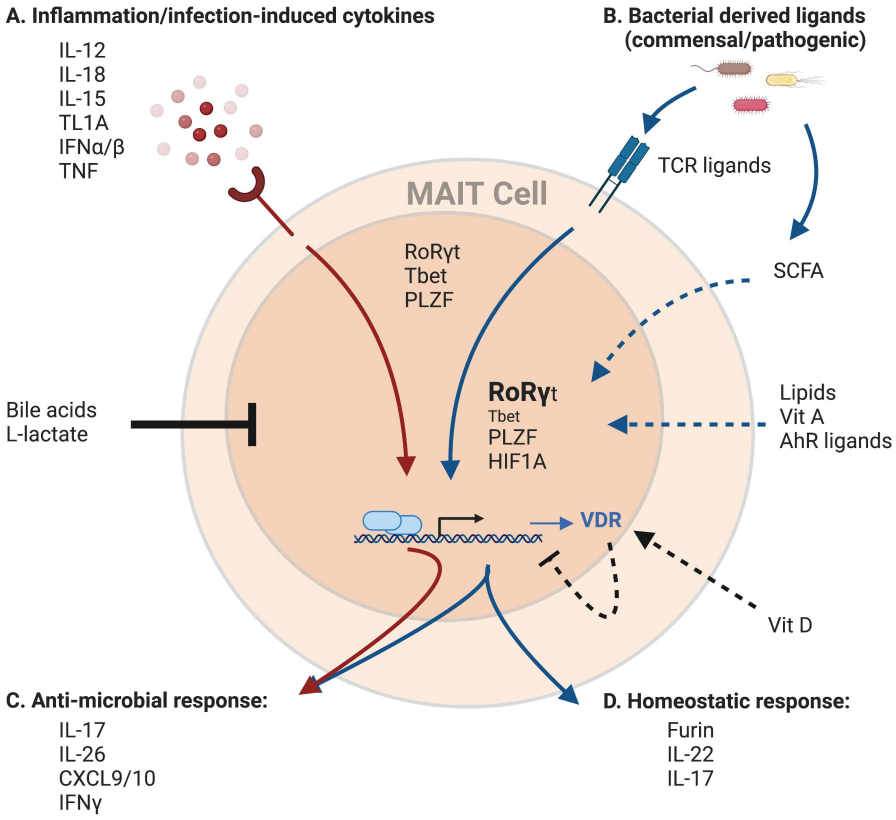

1.5 Knowledge gaps

The early immune response to vaccines can shape both reactogenicity and adaptive immunity, but our understanding of the response to novel nucleic acid vaccine platforms is limited. The innate immune system is responsible for mounting and orchestrating the initial response to nucleic acids, which involves the induction of cytokines such as type I IFN. Subsequently, the secondary cytokine IFN-γ is induced by innate-like bridging cells that integrate early innate signals, particularly at barrier tissues where the immune response is often initiated [161,294]. This thesis will focus on exploring how these signals are integrated and regulated (**Figure** 1.3).

Figure 1.3| Innate sensing of nucleic acid vaccines and effector cytokines

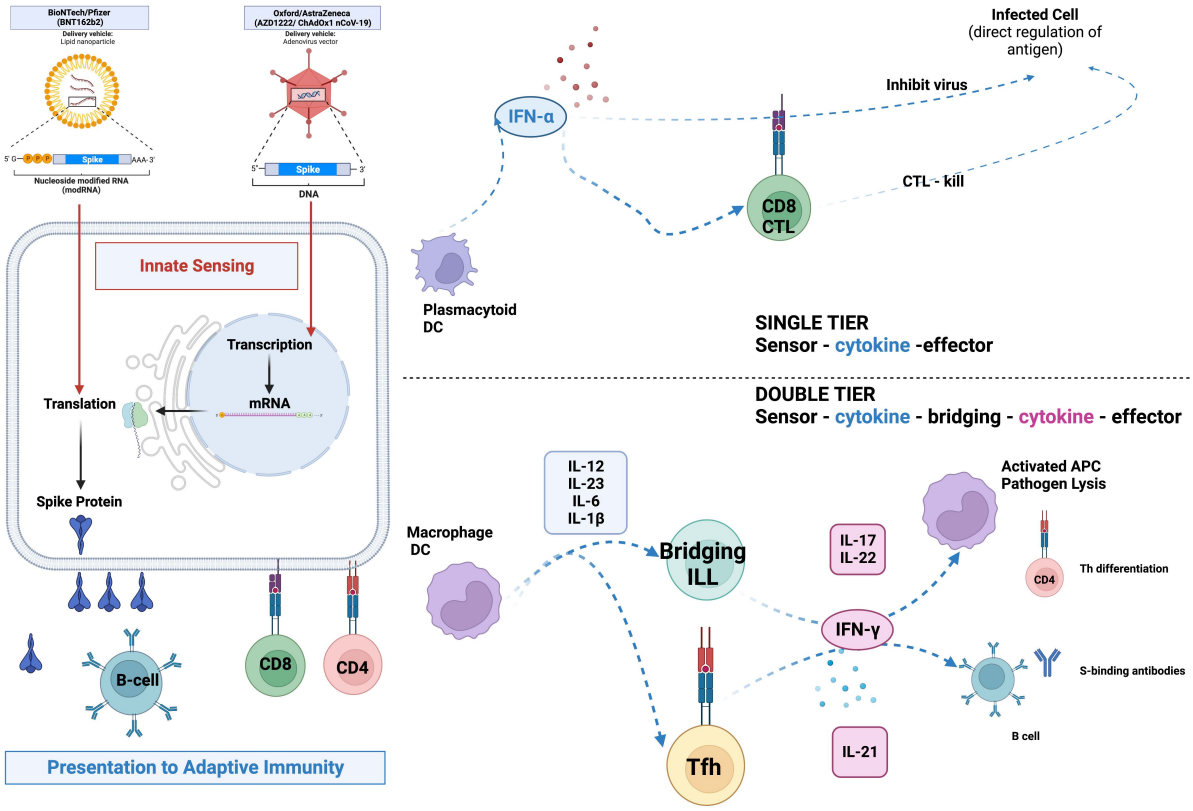

Figure adapted from Iwasaki & Medzhitov, 2015. In a single-tiered effector response, innate sensing (e.g., by pDC TLR7) induces an effector cytokine (e.g., IFN-α) which needs no further amplification. In a double-tiered effector response, innate cytokine signals are synthesised and amplified by bridging secondary lymphocyte populations which can then co-ordinate and tailor effector responses using secondary effector cytokines, such as IFN-γ. Bridging lymphocyte populations include those biased to generating type 1 (e.g., NK, iNKT, MAIT, CD8em), type 17 (Th17, iNKT, MAIT, ILC3) and type 2 cytokines (ILC3, Th2, iNKT).

1.6 Aims of the Thesis

This thesis is based on these assumptions:

1. An effective immune response to novel vaccines should resemble the response to natural viral infections.
2. MAIT cells and other CD161+ innate-like lymphocytes are abundant effectors and can contribute to early antiviral responses through cytokine-mediated activation.
3. Early immune responses to novel vaccines should recruit effectors rapidly to amplify responses and induce organism-wide adaptive immunity.
4. MAIT cells and innate-like lymphocytes occupy diverse tissue niches and are likely subject to regulation by tissue environmental factors, leading to heterogeneity in human responses.
5. Despite differences in effector functions, human blood MAIT cells are abundant and are an excellent tool for studying cytokine-dependent early immune responses.

Based on these assumptions, I hypothesise that MAIT cells will play a significant role in the response to SARS-CoV-2 nucleic acid vaccines. The thesis will address the following broad objectives:

1. Investigate whether MAIT cells and functionally similar innate-like lymphocytes are activated early in response to vaccines.
2. Determine the mechanisms regulating MAIT cell activation, comparing AdV and mRNA vaccine platforms.
3. Examine the role of factors that contribute to variability in human immune responses, such as underlying diseases and cytokine immunomodulatory therapies.

2 Methods

Methods relevant across multiple chapters are described below. Specific materials and methods are found in the relevant Chapter.

2.1 Media and buffers

R10: RPMI1640 with L-glutamine and sodium bicarbonate (Sigma-Aldrich), 10% foetal-calf serum (FCS; Sigma-Aldrich), 1xPenicllin-Streptomycin (Thermo Fisher Scientific).

Rh10: RPMI1640 with L-glutamine and sodium bicarbonate (Sigma-Aldrich), 10% human AB serum (pooled from 20 donors), 1xPenicillin-Streptomycin (Thermo Fisher Scientific).

Virus media: 10mM Tris, 7.5% sucrose, 150mM sodium chloride (NaCl), 1.5% Tween80 (all Sigma-Aldrich). Adjusted to pH7.8.

Freezing media: 90% FCS, 10% dimethylsulphoxide (DMSO; Sigma-Aldrich).

MACS buffer: Phosphate buffered saline (PBS; Sigma-Aldrich), 0.5% bovine-serum albumin (BSA; Sigma-Aldrich), 2mM ethylenediaminetetraacetic acid (EDTA; Sigma-Aldrich). Buffer sterile filtered.

FACS buffer: PBS, 0.5% BSA, 2mM EDTA.

Other media: X-VIVO15 (Lonza)

Sorting buffer: PBS, 2% FCS, 20mM N-2-hydroxyethylpiperazine-N'-2-ethanesulfonic acid (HEPES; Sigma-Aldrich), 50μM 2-β-mercaptoethanol (BME; Thermo Fisher Scientific), 1mM sodium pyruvate (Sigma-Aldrich), 1mM non-essential amino acids (Sigma-Aldrich), 5mM D-Glucose (Sigma-Aldrich).

Post-sort collection media: PBS, 20% FCS, 20mM HEPES

2.2 Viral vectors and vaccines

Viral vectors

All E1/E3-deleted replication incompetent adenovirus vectors were produced in HEK293 cells by the Jenner Institute Viral Vector Core Facility [295]. Preclinical recombinant vectors used in this thesis include: Ad5-GFP (VP:PFU ratio, 34), ChAdOx1-GFP (VP:PFU ratio, 73). Vectors were purified by CsCl2 gradient ultracentrifugation and QC tested in batches. Stocks were diluted and aliquoted to 10^{11} vp/ml in viral vector buffer (10mM Tris, 7.5% sucrose, 150mM NaCl, 0.1% Tween80, pH7.8) and stored at -80ºC.

Heat inactivation was performed as previously described [296]. Briefly, undiluted vectors were added in Eppendorf tubes to a heat block at 70˚C for 10 minutes. At the end, vectors were immersed in ice, before either use in cultures or storage at -80˚C.

SARS-CoV-2 Vaccines

LNP-nCoVsaRNA suspensions stored at -80˚C (*kindly provided by Robin Shattock and Paul McKay*) were diluted to 100µg/ml in PBS and used immediately.

BNT162b2 (Pfizer/BioNTech) was pooled from multiple vials of remnant material (*kindly provided by Michelle Taylor Siddons*), all reconstituted according to manufacturer's guidelines at 100µg/ml in 0.9% sodium chloride. BNT162b2 was either used immediately (fresh) or frozen at -80˚C at 100µg/ml for subsequent use, with equivalence demonstrated between fresh and frozen batches.

mRNA-1273 (Moderna) batches were diluted to 200µg/ml in 0.9% sodium chloride and immediately frozen.

ChAdOx1-S (AstraZeneca) was collected from OUH pharmacy as prediluted vials containing at least 10^{11} vp/ml ($5x10^8$ IU/ml), which was aliquoted and stored at -80˚C.

2.3 Cells

Primary cells

Adult peripheral blood mononuclear cells (PBMCs) were either separated from EDTA whole blood, or leucocyte cones (NHS Blood and Transplant, UK). In vitro assays used healthy donors from the laboratory. All healthy human samples were collected with informed consent under the Oxford GI Biobank Ethics (Ref:11/YH/0020).

2.4 Isolation of cells

2.4.1 PBMC isolation from blood

Fresh blood was collected from healthy volunteers in EDTA-coated Vacutainer tubes (BD Biosciences) or leucocyte cones from the NHS Blood and Transplant Service. PBMCs were isolated using density gradient centrifugation. Briefly, blood was diluted in PBS (1:1), layered over Lymphoprep (Axis-Shield), then centrifuged (2000rpm, 973g, 30min, 20˚C, without deceleration). The collected PBMC layer was washed in R10 media. Red blood cells were lysed in an ammonium-chloride-potassium solution (ACK) for 2min at room temperature, then washed in R10 prior to staining with Trypan Blue and counting manually on a haemocytometer. After a final wash in R10, cells were either used immediately or cryopreserved in freezing media in liquid nitrogen.

For vaccine cohort samples (Chapter 4, 5), blood was not diluted, instead layered directly onto Lymphoprep.

Cryopreservation and thawing of PBMCs

For cryopreservation, PBMCs were resuspended in freezing media and aliquoted in 1ml into cryovials. Cells were first frozen at -80˚C short term in cell freezing containers, before transferring to liquid nitrogen for long term storage.

Cryopreserved PBMCs were thawed quickly to 37˚C by transferring to pre-warmed R10 media. Cells were then washed in R10 prior to downstream use. **For vaccine cohort samples** (Chapter 4, 5), thawing was performed in R10 media with additional Benzonase (2µl; ≥25 U/µl; Sigma-Aldrich).

2.4.2 Cell isolation using magnetic bead enrichment

Enrichment of cell populations was performed using Miltenyi MicroBeads (Miltenyi Biotec) in conjunction with relevant columns for positive (LS) or negative (LD) selection. CD8, CD14, and CD123 MicroBeads were used to enrich or deplete CD8+ T cells, monocytes and pDC, respectively according to manufacturer's instructions. Briefly, cells were washed in RPMI, resuspended in 80µl of MACS buffer and 20µl of relevant microbeads per 10^7 PBMCs, then incubated at 4˚C for 15 minutes. Subsequent magnetically labelled cells were washed once in 2ml MACS buffer, centrifuged at 500g for 5min, then resuspended in 500µl of ice-cold MACS buffer ready for magnetic bead enrichment.

For positive selection, labelled cells were added to LS columns. After elution of the negative fraction, the magnet was removed and positively selected cells flushed using 10ml of MACS buffer, added in two sequential steps.

For negative selection, labelled cells were added to LD columns kept in the magnet throughout. The desired negative fraction was collected after additional washes with 10ml MACS buffer.

For co-culture experiments, CD14 enrichment was performed prior to CD8 enrichment. Purity for all positively selected populations was consistently >90% by flow cytometry.

2.5 Collection of plasma, serum

For collection of plasma, whole blood collected in EDTA tubes was centrifuged (2000rpm, 10min, room temperature), and supernatants (plasma) aspirated using a pipette without disturbing the cell layer. Plasma was stored at -80˚C.

Serum was collected in serum separator tubes (SST; BD Biosciences) then incubated at room temperature for between 30-60min in an upright position. SST tubes were then centrifuged (1800g, 15min), with serum transferred to cryovials and frozen at -80˚C.

2.6 Functional assays

Human PBMCs were stimulated in vitro using either fresh or freeze thawed PBMCs. For Adenovirus vector and SARS-CoV-2 vaccine stimulation, fresh cells were always used. For cytokine stimulation either fresh or freeze-thawed cells were used.

Cells were always incubated at 37˚C, 5% CO_2, in a total 200µl cell culture medium. Cell concentrations used were: 5x10^6/ml (total 10^6) for stimulations of unfractionated PBMC with AdV, SARS-CoV-2 vaccines, and cytokines; 1x10^6/ml (2x10^5) for stimulations of unfractionated PBMC with plate bound TCR stimulation (72hr), and stimulations with enriched cell populations.

For measurements of T cell cytokine production, stimulation times were either 24h or 72h, with Brefeldin A and Monensin (5 µg/ml; BioLegend) added for the final 4h incubation prior to staining in all cases. This step was omitted in cases where secreted cytokines were assayed, or only surface markers were being measured.

2.6.1 Stimulation assays

Cytokines used were at a final concentration 50ng/ml unless otherwise stated: IFN-α2A (Sigma-Aldrich), IFN-β (R&D Systems), IFN-γ (StemCell Technologies), IFN-λ3 (R&D Systems), IFN-λ4p70 (*kindly provided by Narayan Ramamurthy*), IL-12p40 (R&D Systems), IL-12p70 (R&D Systems), IL-18 (R&D Systems), TNF (R&D Systems).

TNF receptor agonist antibodies were both used at 2.5µg/ml: anti-TNFR1 (clone:MR1-2; Hycult Biotec), anti-TNFR2 agonist (clone: MR2-1, Hycult Biotec).

Adenovirus vectors were used at an MOI of 1000 (ie., 10^9 vp/ml) unless otherwise stated.

Vaccine vectors were used at 10µg/ml unless otherwise stated.

2.6.2 TCR stimulation

For **plate bound αCD3/28** MAIT cell activation, 96-well NUNC-MaxiSorp plates were coated and incubated with anti-CD3 (OKT3; 2.5µg/ml) for 2hrs (37˚C, 5% CO_2), then washed twice with PBS prior to plating 200,000 cells. Soluble anti-CD28 (CD28.2; 1µg/ml) was diluted with R10 and added together with other relevant stimuli at a final volume of 200µl (i.e.., 10^6 cells/ml).

For **Escherichia coli (E.coli) activation**, fixed E.coli (DH5α) were added to PBMC (10^6 cells at 10^7 cells/ml) in 96-well u-bottom plates at a ratio of 25 bacteria per cell (25BpC). Stocks of fixed E.coli (stored at 4˚C, 10^7 CFU/ml) were kindly provided by Joachim Hagel, after fixing for 20min in 2% paraformaldehyde and washing in PBS.

Phorbol 12-myristate 13-acetate **(PMA) and ionomycin** activation was performed in 96 well u-bottom plates using Biolegend cell stimulation cocktail. Either 2x10^5 CD8+ cells, or 1x10^6 PBMC were added per well.

2.6.3 Blocking assays

Inhibitory compounds were added immediately prior to stimulations where relevant, and samples mixed before incubation (37˚C, 5% CO_2). The pox-derived inhibitor, B18R (eBioScience), was used at 10µg/ml for most assays. The following blocking and inhibitory reagents were used at the indicated concentrations unless otherwise stated in the text (Table 2.1).

Exosome blockade was performed with GW4869 (Sigma-Aldrich), or Spiroepoxide (Insight Biotechnology Ltd) at 10µM.

Table 2.1 | List of blocking antibodies

Antibody	Target	Company	Clone
Adalimumab	TNF	AbbVie	N/A
Etanercept	TNF	Amgen	N/A
Vedolizumab	α4b7-integrin	Millennium	N/A
Certolizumab	TNF	UCB	N/A
Ustekinumab	IL-12/23p40	Janssen	N/A
Guselkumab	IL-23p19	Janssen	N/A
Anti-TNFR1	CD120a (TNFR1)	R&D	16805
Anti-TNFR2	CD120b (TNFR2)	R&D	22210
Anti-IFN-γR1	CD119 (IFN-γR1)	R&D	MAB6731
Anti-IFN-γ	IFN-γ	R&D	25718
Anti-IL-12p40	IL-12/23p40	BioLegend	C11.5
Anti-IL-12p70	IL-12p70	R&D	24910
Anti-IL-18	IL-18	R&D	125-2H
Anti-IFNAR2	Type I IFN	Millipore	MMHAR-2
Anti-MR1	MR1	BioLegend	26.5
Anti-MHC-I	HLA-A, B, C	BioLegend	W6/32
Anti-MHC-II	HLA-DR, DP, DQ	BioLegend	TÜ39
Anti-IgG1	IgG1	BioLegend	MOPC-21
Anti-IgG2	IgG2a	BioLegend	MOPC-173

2.7 Cytokine and chemokine quantification

Quantification of cytokines from both cell culture supernatants, human plasma or serum was performed using the LEGENDplex Human Inflammation Panel (13-plex, v-bottom) (BioLegend #740808) , or Human Antivirus Response Panel (BioLegend #740349) following manufacturer's instructions.

Briefly, all supernatants were thawed at room temperature (RT), centrifuged (2000g, 10 min), then incubated with standards and capture beads in a polypropylene 96-well V-bottom plate on a shaker (2hrs, RT). Plates were washed twice, incubated with biotinylated detection antibodies (2hrs, shaker, RT), after which Streptavidin-phycoerythrin (PE) was added (30min, shaker, RT). Finally, samples were washed twice, resuspended in Legendplex buffer, and acquired using a BD LSRII Cytometer and FACSDiva (v. 9.0). All data analysis was performed using the provided software.

Samples were diluted to ensure with the appropriate dynamic range of the assay and run in duplicate, with a maximum of one freeze-thaw cycle. The list of assayed cytokines for Human Inflammation Panel 1 were: IL-1β, IFN-α2, IFN-γ, TNF, MCP-1, IL-6, IL-8, IL-10, IL-12p70, IL-17A, IL-18, IL-23, and IL-33. Cytokines for Human antivirus response were: IL-1β, IL-6, IL-8, IL-10, IL-12p70, IFN-α, IFN-β, IFN-λ1, IL-29, IFN-λ2/3, IL-28, IFN-γ, TNF-α, IP-10, GM-CSF.

2.8 MR1 tetramer generation and staining

Human MR1/5-OP-RU and MR1/6-FP tetramers were generated using NIH Tetramer Core Facility biotinylated monomers and guidelines. Conjugation was performed to Streptavidin-Brilliant Violet 421 (BioLegend, Cat#405225).

2.9 Flow Cytometry

2.9.1 Viability staining

For flow cytometry assays, dead cells were stained using fixable live/dead near-IR (Life Technologies) for 15 minutes at 4˚C.

For cell sorting, SytoxGreen was diluted 1:60 in sterile filtered buffer FACS buffer, then further diluted 1:100 before adding to cells immediately prior to sorting.

MAIT cell caspase activation was assessed using FLICA (fluorescent inhibitor of cascade activation) assay (Vibrant FAM Polycaspase Kit, Thermo Fisher Scientific) according to manufacturer's protocols.

MAIT cell apoptosis was detected using Annexin/PI kit (BioLegend) staining with Annexin V in Annexin binding buffer for 15min according to manufacturer's protocols.

2.9.2 Surface staining

MR1 tetramer and CCR7 staining where used were performed in 50µl FACS buffer (40min, room temperature) prior to surface staining. For other surface staining, cells were stained with antibody cocktails in 50µl FACS buffer for 30 minutes at 4˚C. Antibody cocktails are listed (**Table 2.2**)

2.9.3 Intracellular cytokine staining (ICS)

For intracellular cytokine staining, Brefeldin A and Monensin were added at 1:1000 dilution for the last 4h of stimulation. Cells were fixed and permeabilised in 100µl BD Cytofix/Cytoperm solution (BD Biosciences) for 20min at 4˚C, washed twice in FACS buffer, then stained in 50µl BD Perm/Wash buffer (BD Biosciences) for 30 minutes at 4˚C.

2.9.4 Proliferation assays and labelling

Samples were labelled with 5μM CellTraceTM Violet (CTV; Invitrogen) according to the manufacturer's protocol, with a minor modification. Briefly, cells were washed twice then resuspended in PBS, before adding 5mM stock concentration of CTV (1:1000) in 15ml Falcon tubes. Cells were mixed and kept at RT in the dark for 10min, before adding ice cold R10 for 5min and washing three times in R10, changing Falcon tubes each time.

2.9.5 Transcription factor staining

Transcription factor and AIM2 staining was performed after surface staining, fixing cells using FoxP3 Fixation/Perm Buffer (eBioScience; 1hr, room temperature), washing, then staining with relevant antibodies for a further 1hr at room temperature.

2.9.6 Data acquisition and analysis

Flow cytometry data was acquired on a BD Fortessa or LSRII (BD Biosciences), and analysed using in FlowJo v10 (FlowJo, LLC). For phenotypic analysis, rare cell populations with fewer than 10 cells were excluded.

2.10 Statistical analysis

Statistical analysis was either performed in R Studio or GraphPad PRISM (v9). In all cases two-tailed p values are reported. Statistical significance was considered where $P<0.05$, with a trend and exact P value reported if $P<0.1$. Details of specific tests used are found within the relevant figure legends. Dose-response curves were analysed with tests for linear trend. Spearman's R correlation coefficient was used for all descriptive correlations.

Table 2.2 | List of antibodies used for flow cytometry.

Marker	Flurochrome	Clone	Dilution	Company
Live/Dead	Near-IR	--	1:400	Thermofisher
CCR6	BV605	G034E3	1:100 @ 37C	BioLegend
CCR7	APC	G043H7	1:100 @ 37C	BioLegend
CCR7	APC-Fire 750	G043H7	1:100 @ 37C	BioLegend
CD103	BV421	Ber-ACT8	1:200	BioLegend
CD11c	PE-CF594	B-Ly6	1:100	BD
CD120a	PE	16803	1:100	R&D
CD120b	FITC	22235	1:100	R&D
CD123	BV510	6H6	1:100	BioLegend
CD123	BV785	7G3	1:100	BioLegend
CD123	PE-Cy7	6H6	1:100	BioLegend
CD14	BV421	M5E2	1:100	BioLegend
CD14	BV650	M5E2	1:100	BioLegend
CD14	BV785	M5E2	1:200	BioLegend
CD141	BV786	1A4	1:100	BD
CD154	BV785	24-31	1:100	BioLegend
CD16	AF700	3G8	1:100	BD
CD16	BV650	3G8	1:100	BioLegend
CD161	APC	191B8	1:150	Miltenyi
CD161	PE	191B8	1:150	Miltenyi
CD19	BV510	HIB19	1:100	BioLegend
CD19	BV650	HIB19	1:100	BioLegend
CD19	PE-Cy7	HIB19	1:200	BioLegend
CD1c	APC	L161	1:100	BioLegend
CD25	BV650	BC96	1:100	BioLegend
CD25	BV786	M-A251	1:100	BD
CD303	APC	201A	1:100	BioLegend
CD3e	BV711	UCHT1	1:100	BD
CD3e	BV785	OKT3	1:100	BioLegend
CD3e	BV785	UCHT1	1:100	BioLegend
CD4	BV650	OKT4	1:100	BioLegend
CD4	BV711	OKT4	1:50	BioLegend
CD45RA	BV510	HI100	1:100	BioLegend
CD56	BV421	HCD56	1:100	BioLegend
CD56	BV480	NCAM16.2	1:50	BD
CD69	AF700	FN50	1:100	BioLegend

CD69	PE-Dazzle594	FN50	1:100	BioLegend
CD80	BV421	2D10	1:100	BioLegend
CD86	BV650	IT2.2	1:100	BioLegend
CD8a	AF700	SK1	1:150	BD
CD8a	BV650	RPA-T8	1:100	BioLegend
CD8a	BV650	SK1	1:100	BioLegend
CXCR6	BV421	K041E5	1:100	BioLegend
HLA-DR	AF700	L243	1:100	BioLegend
HLA-DR	BV421	G46-6	1:100	BD
IFNAR1	FITC	85228	1:50	R&D
IFNAR1	PE	85228	1:50	R&D
IFNAR2	FITC	7	1:50	Sino Biological
IFNAR2	PE	7	1:50	Sino Biological
IFNAR2	PE	REA124	1:50	Miltenyi
IL-18Ra	AF488	70625	1:25	R&D
PD-1	BV421	EH12.2H7	1:50	BioLegend
PD-L1	PE-Cy7	2D10	1:100	BioLegend
TCR gd	FITC	11F2	1:100	Miltenyi
TCR gd	FITC	B1	1:50	BioLegend
TCR Va24/Ja18	PE-Cy7	6B11	1:50	BioLegend
TCR Va7.2	BV605	3C10	1:50	BioLegend
TCR Vd2	BV711	B6	1:50	BioLegend
INTRACELLULAR CYTOKINES				
GzmB	AF647	GB11	1:200	BioLegend
IFNg	AF700	B27	1:100	BioLegend
IFNg	Pacific blue	B27	1:100	BioLegend
IL-17A	BV421	BL168	1:50	BioLegend
IL-17F	PE	SHLR17	1:100	eBioscience
TNFa	APC	mAb11	1:100	BioLegend
TNFa	BV605	mAb11	1:100	BioLegend
TNFa	FITC	mAb11	1:100	BioLegend
RORgt	BV421	Q21-559	1:25	BD

3 MAIT cell and CD161+ lymphocyte responses to ChAdOx1

3.1 Introduction

Adenovirus vectors (AdV) have grained traction over the last decade as vaccine candidates capable of inducing particularly potent antigen-specific T-cell responses to an immunogen of interest[131,297]. Two of the most promising candidates prior to the SARS-CoV-2 pandemic were based on the chimpanzee-derived adenovirus vector (ChAdOx1)[298,299], and the rare human adenovirus (Ad26)[300,301]. This promise was fulfilled as they became the earliest AdV to prove efficacy in robust trials[298,299,302]. Both vaccines were keenly developed given superior immunogenicity compared to the common circulating human Ad5, which is thought to be attributable to more prevalent Ad5-specific anti-vector immunity [119,303]; in adults, Ad5-neutralising antibodies are found in over 60%, with Ad5-reactive T-cells more frequent and found in over 80%, some of which are cross-reactive[303]. Curiously, Ad5 also generates distinct innate immune responses compared to the rarer Ad-serotypes which have superior immunogenicity in humans[106], although they have been relatively unexplored in terms of innate immune responses engendered. Early immune responses to AdV may dictate the duration and magnitude of transgene expression, relevant to the quality of adaptive responses[106,126]. Understanding how these innate responses are induced in response to the rare Ad-serotypes now commonly used for vaccines could therefore provide important clues to optimising vaccine potency.

Innate immune cells induce antiviral cytokines in response to AdV, including interferons and inflammasome-derived cytokines[304]. Cytokine and chemokine secretion peaks occur after 24h, both in vitro and in vivo, returning to baseline within 96h, with rare serotypes (Ad26, Ad35) inducing higher concentrations compared to Ad5 in both humans and NHP [304]; in particular, high IFN-α2, IL-6, TNF, and IFN-dependent MIP1-α and MIP1-β, are induced by these rare Coxsackievirus and adenovirus receptor (CAR)-independent human adenovirus

serotypes. No data exists however on early cytokine responses to chimpanzee-derived vectors.

Intriguingly, the induction of early IFN-γ - a potent cytokine for promoting adaptive immunity - is dependent entirely on T cells[304]. In vitro depletion of T cells - but not NK or myeloid cells - abolishes IFN-γ induced in response to Ad35 and Ad26 after 24h. This is surprising as Ad-26 and Ad-35 specific T cells are rare, therefore unlikely to be the dominant early source of IFN-γ. This is supported by the observation that transient early IFN-γ (as well as CXCL10, MCP-1, TNF) in volunteers vaccinated with Ad26.HIV-EnvA is highest in those with no evidence of prior Ad26 exposure. Plasmacytoid dendritic cells are also required for maximal early IFN-γ induction as depletion prior to stimulation with AdV in vitro modestly reduces IFN-γ at 24h, in addition to the expected reduction in IFN-α [304]. Therefore, both type I IFN and non-vector specific T cells likely drive high early IFN-γ after prime with rare AdV.

MAIT cells are unconventional T cells, with an effector memory phenotype, abundant in human blood, and capable of producing early IFN-γ. Like other unconventional T cells- including the highly overlapping Vδ2+ γδ cells, and iNKT cells - MAIT cells can rapidly respond to cytokines in the absence of TCR triggering[201]. This cytokine responsiveness is shared amongst CD161+ innate-like lymphocytes, including NK cells[200,305]. Importantly antiviral cytokines can potently activate these abundant cells to produce IFN-γ[249,306]; type I IFN can induce abundant IFN-γ from MAIT cells [306], Vδ2+ γδ T cells[307], iNKT[308], and NK cells[255,309,310]. Importantly, this early innate-like lymphocyte derived IFN-γ is critical for maximal protection in mice, both in response to influenza [306], and influenza vaccination[309].

However, it is unclear to what extent type I IFN is sufficient for robust (protective) IFN-γ responses, and what other signals are required. MAIT cells only robustly produce IFN-γ in response to combinations of cytokines[306]; in response to viruses such as influenza and hepatitis C, MAIT cell IFN-γ is dependent on both type I IFN and inflammasome-derived IL-

18 in combination. Type I IFN alone can directly signal via STAT4 to induce NK cell IFN-γ transiently, but again IL-18 is required for potent activation[255]. The exact combination of cellular and soluble signals required for robust MAIT cell and innate-like lymphocyte IFN-γ in response to antiviral cytokines is unknown.

3.2 Aims

The early response to chimpanzee-derived adenovirus vectors, including ChAdOx1, has thus far been unexplored but vitally important, given implications for ChAdOx1-S induced efficacy. Based on the above we **hypothesised** that:

1. ChAdOx1, similar to other AdV without pre-existing anti-vector immunity, will induce robust early innate immune activation and the production of antiviral cytokines – especially type I IFN and IFN-γ.
2. In the absence of ChAdOx1-specific conventional T cells, early IFN-γ in response to ChAdOx1 would be produced by unconventional T cells, including MAIT cells, which are more abundant and capable of sensing antiviral cytokines.
3. MAIT cells and unconventional T cells would need to sense multiple innate signals to induce robust IFN-γ, as well as other effector functions.

The work reported in this chapter was performed in close collaboration with Nicholas Provine, who originally confirmed robust MAIT cell IFN-γ production in vitro in response to ChAdOx1-GFP but not Ad5-GFP, in an IL-18 dependent manner, when work began (**Appendix SF3.1**).

The primary aims of this chapter were therefore to:

1. Identify the innate-like lymphocytes that are involved in early IFN-γ production in response to ChAdOx1-GFP in vitro.
2. Investigate the mechanisms of MAIT cell activation, including the need for additional accessory cell types, given the importance of MAIT cell IFN-γ in protective antiviral responses[224].

3.3 Results

Much of the work in this Chapter has been published in the following two papers:

- Provine NM, **Amini A**, Garner LC, Spencer AJ, Dold C, Hutchings C, Silva Reyes L, FitzPatrick MEB, Chinnakannan S, Oguti B, Raymond M, Ulaszewska M, Troise F, Sharpe H, Morgan SB, Hinks TSC, Lambe T, Capone S, Folgori A, Barnes E, Rollier CS, Pollard AJ, Klenerman P. MAIT cell activation augments adenovirus vector vaccine immunogenicity. Science. 2021 Jan 29;371(6528):521-526.
- Provine NM*, **Amini A***, Garner LC, FitzPatrick MEB, Dold C, Silva Reyes L, Chinnakannan S, Oguti B, Raymond M, Troise F, Capone S, Folgori A, Barnes E, Rollier CS, Pollard AJ, Klenerman P. Adenovirus vectors activate Vδ2+ γδT cells in a type I interferon-, TNF-, and IL-18-dependent manner. Eur J Immunol. 2022 May;52(5):835-837.

Data shown in this chapter are from experiments performed by me unless explicitly stated.

3.3.1 MAIT cells and CD161+ lymphocytes are the dominant sources of early IFN-γ in response to ChAdOx1-GFP in vitro

To test and track the early response to AdV in vitro we used two clinically manufactured AdV expressing a GFP transgene: ChAdOx1-GFP and Ad5-GFP. These experiments were initially performed by Nicholas Provine (**Appendix SF3.1**).

We first tested whether AdV were able to activate MAIT cells by stimulating human peripheral blood mononuclear cells (PBMC) with an increasing multiplicity of infection (MOI) of ChAdOx1-GFP, and measured MAIT cell activation (CD69, GzmB, IFN-γ expression) after 24h (**Fig3.1**).

MAIT cells were activated in a dose-dependent manner in response to ChAdOx1-GFP, with maximal IFN-γ at an MOI of 10^3 viral particles (vp) (53.9±8.0%; **Fig3.1 B**), together with robust induction of CD69 (99.2±0.4%; **Fig3.1 C**), and GzmB (22.7±5.3%; **Fig3.1 D**). Although MAIT cells were defined as CD161hiVα7.2+ T cells for most experiments, equivalent results were obtained using stringent MR1/5-OP-RU tetramer staining (**Appendix SF3.1 A**). In contrast, Ad5-GFP induced minimal MAIT activation, despite similar transduction, suggesting differential innate responses to Ad V (**Appendix SF3.1 B, C**).

At an optimal MOI of 10^3 vp, MAIT cell IFN-γ in response to ChAdOx1-GFP was first detectable at 16h (7.1±2.4%; $p<0.0001$ compared to no vector) and peaked at 24h (53.9±8.0%; **Fig3.1 E,F**). MAIT cell CD69 induction was more potent but similarly first detectable at 16h (93±2%; $p<0.0001$ compared to no vector; **Fig3.1 G**), and plateaued with near total CD69 expression at 24h (99.2±0.4%; **Fig3.1 G**). By comparison, Ad5-GFP induced lower CD69 at 16h (42.1±1.4%; **Fig3.1 G**) and no significant IFN-γ even at 24h compared to no vector controls (**Fig3.1 F**). These data implied that time-dependent signals are required to induce robust MAIT cell IFN-γ in response to ChAdOx1.

We confirmed no TCR signals were responsible as blocking MAIT cell TCR engagement with an anti-MR1 blocking antibody (10μg/ml; clone 26.5) prior to stimulation did not inhibit ChAdOx1-GFP induced IFN-γ production relative to isotype controls (**Fig3.2 B**), in line with previous robust TCR-independent antiviral IFN-γ production [306].

Figure 3.1 | ChAdOx1-GFP induced MAIT cell activation in vitro peaking at 24h.

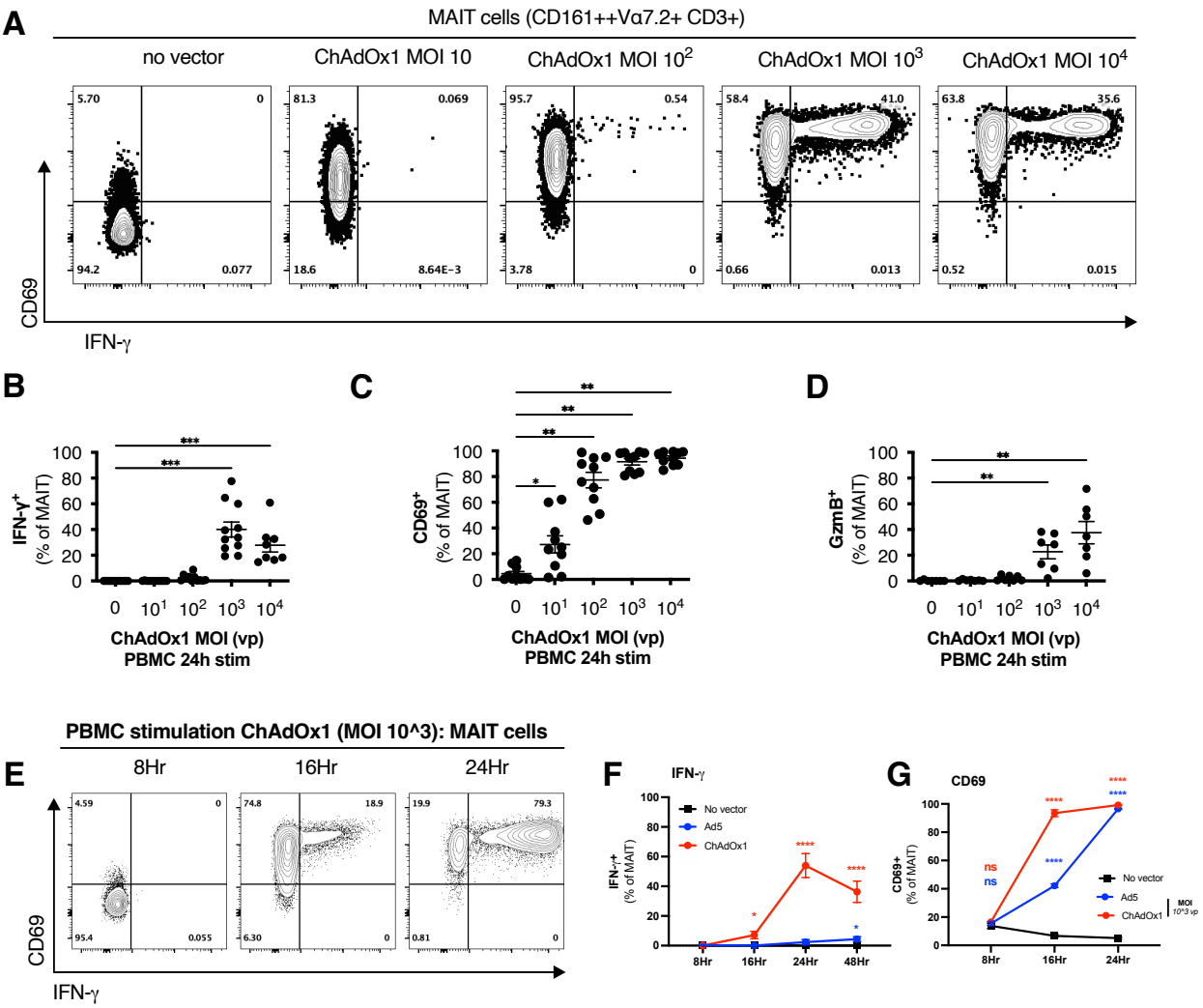

Fig3.1 | ChAdOx1-GFP induces MAIT cell activation in vitro peaking at 24h.
Fresh PBMCs were stimulated with ChAdOx1-GFP (or Ad5-GFP) at increasing multiplicity of infection (MOI). MAIT cell activation was measured (CD69, IFNγ, GzmB) at indicated times.
(A) Representative plot gated on MAIT cells (CD161++Vα7.2+) after 24h.
(B-D) Summary of MAIT cell activation at 24h, measuring IFN-γ (B), CD69 (C), and GzmB (D).
(E) Representative plot gated on MAIT cells (CD161++Vα7.2+) after 8h, 16h, or 24h stimulation with no vector, or AdV at MOI 10^3 vp.
(F,G) Summary of MAIT cell activation kinetics for IFN-γ (F), and CD69 (G). Statistical comparisons with no vector control.
Symbols indicate individual donors.
*p < 0.05; **p < 0.01; ***p < 0.001; ****p < 0.0001; ns, not significant.
Mean ± SEM is shown.
Statistical significance was determined using a two-way ANOVA with Dunnett's multiple comparison test (B-D), and unpaired student t-test (F,G).

Figure 3.2 | ChAdOx1-GFP induces MAIT cell activation in an MR1-independent manner.

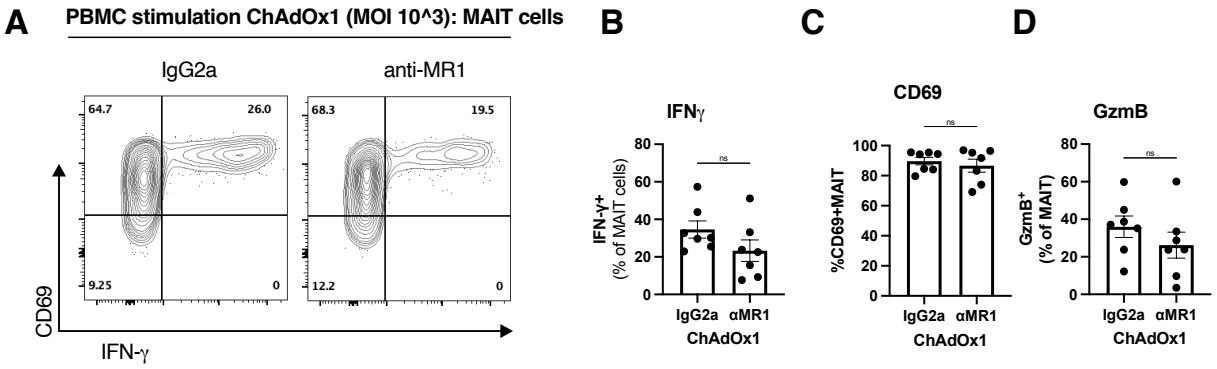

Fig3.2 | ChAdOx1-GFP induces MAIT cell activation in an MR1-independent manner.
Fresh PBMCs were treated with anti-MR1 antibody (10μg/ml) or isotype control (IgG2a; 10μg/ml), then stimulated with ChAdOx1-GFP (MOI 103 vp). MAIT cell activation was measured at 24h.
(A) Representative plot gated on MAIT cells (CD161++Vα7.2+) after 24h.
(B-D) Summary of MAIT cell activation at 24h, measuring IFN-γ (B), CD69 (C), and GzmB (D). (n=7 donors)
Symbols indicate individual donors. Mean ± SEM is show.
ns, not significant.
Statistical significance was determined using unpaired student t-tests (B-D).

The absence of TCR engagement implied that non-specific cytokine mediated activation, shared with other innate-like lymphocytes, might be responsible. We therefore next explored whether other cells in PBMC were also capable of IFN-γ production in response to ChAdOx1-GFP. At 24h IFN-γ production was indeed not unique to MAIT cells and found in 8% of PBMC (**Fig3.3 B**). Although ChAdOx1 induced IFN-γ was almost all limited to lymphocytes (**Fig3.3 C**), the majority (>95%) of IFN-γ+ cells were CD161+, either CD161+ non-B/T lymphocytes (66.1± 1.9%) or CD161+ T cells (29.4±2.3%)(**Fig3.3 D**), and therefore cell types capable of cytokine mediated, antigen-independent activation [200,201].

NK cells made up the bulk of IFN-γ producing non-B/T lymphocytes, in particular the more abundant CD161+ subset (94.9±0.1%). Some CD161-NK cells did contribute to total IFN-γ (4.3±0.7%) (**Fig3.3 E**), the majority of which were CD161-CD56bright (data not shown). Amongst T cells, the majority of IFN-γ+ cells in response to ChAdOx1-GFP were unconventional (~70%)(**Fig3.3 F**): MAIT cells (49.1±2.8%) and Vδ2+ γδT cells (21.3±3.1%) share innate-like responsiveness and dominated the early IFN-γ producing T cell compartment, unlike functionally distinct non-Vδ2+ γδ T cells (2.8±0.8%)(**Fig3.3 F**)[164,199]. The fraction of Vδ2+ γδ T cells expressing IFN-γ was similar to MAIT cells and CD161+ NK cells (29.2±3.7%, Vδ2; 41±6.3%, MAIT cells; 51.7±3.8%, NK cells; **Fig3.3 G**), and much higher than non-Vδ2+ γδ T cells (4.5±2.5%; **Fig3.3 G**). Dose responses curves for ChAdOx1-GFP induced IFN-γ (**Fig3.3 H**), and CD69 expression (**Fig3.3 I**) were also comparable for MAIT cells, Vδ2+ γδ T cells and CD161+ NK cells, supporting a shared mechanism of activation independent of TCR-recognition.

Figure 3.3 | CD161+ innate-like lymphocytes are the dominant source of early IFN-γ after ChAdOx1-GFP.

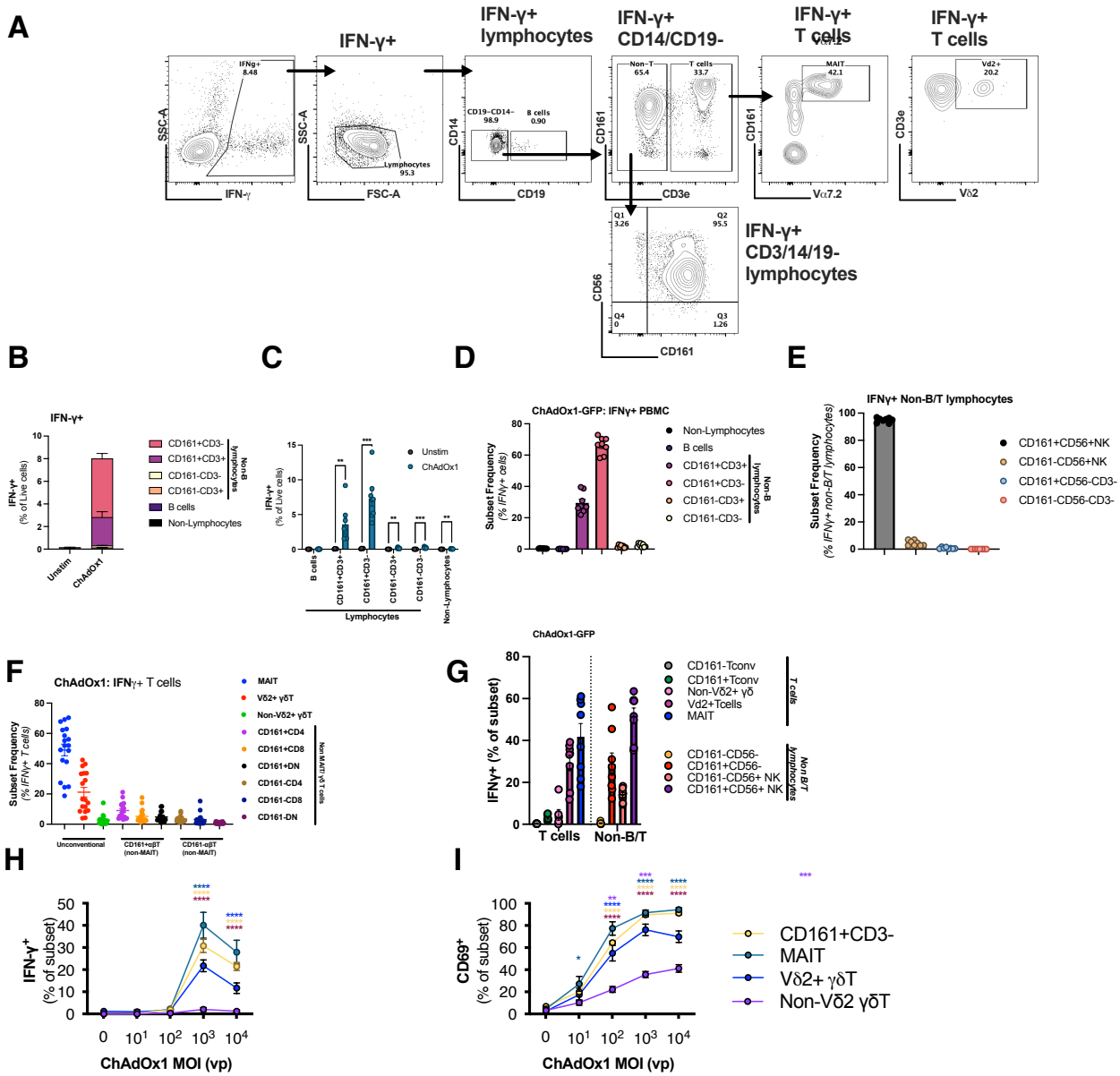

Fig3.3 | CD161+ innate-like lymphocytes are the dominant source of early IFNγ after ChAdOx1-GFP.
Fresh PBMCs were treated with ChAdOx1-GFP (MOI 10^3 vp), or no vector control (unstim), with all IFN-γ+ cells measured after 24h profiled.
(A) Representative gating to identify IFN-γ+ cells among PBMC.
(B-C) Frequency of IFN-γ+ cells among PBMC after ChAdOx1, including the contribution of indicated cell types. Summary histogram (B), and barplot (C) (n=8 donors).
(D-F) Frequency of each indicated cell type among IFN-γ+ PBMC (D), non-B/T lymphocytes (E), and T cells.
(G) IFN-γ expression as a fraction of T and non-B/T lymphocytes.
(H, I) Summary dose response curves of MAIT, Vδ2+ γδ, and CD161+ non-B/T lymphocyte IFNγ (H), and CD69 (I), in response to ChAdOx1-GFP at 24h (n=6 donors).
Symbols indicate individual donors and are pooled from 3 separate experiments.
Mean ± SEM is show.
*p < 0.05; **p < 0.01; ***p < 0.001; ****p < 0.0001; ns, not significant.
Statistical significance was determined using unpaired student t-tests (C), and two-way ANOVA with Dunnett's multiple comparison test (H-I)

A small population of non-MAIT αβT cells did however also contribute to early IFN-γ, with CD161+CD4+ T cells in particular making up 9.1±1.3% of the IFN-γ producing T cell compartment (**Fig3.3 F**). Almost all IFN-γ producing non-MAIT αβT cells were, similar to MAIT cells, effector memory (CCR7-CD45RA-)(**Fig3.4 A**), thus in addition to TCR triggering capable of cytokine-mediated bystander activation [154,311]. CD4 effector memory T cells were the most abundant non-MAIT αβT cells producing IFN-γ (58±7% of total IFN-γ+ non-MAIT αβT cells; **Fig3.4 B**). Although some of these could be iNKT cells, we found similar frequencies after excluding Vα24-Jα18 TCR expressing cells (*data not shown*), so any contribution is likely negligible.

Therefore, innate-like cytokine responsive cells, in particular CD161+ T and NK cells, are the dominant sources of IFN-γ in response to ChAdOx1-GFP in a manner independent of TCR-recognition.

Figure 3.4 | Effector memory conventional T cells respond to ChAdOx1-GFP in vitro.

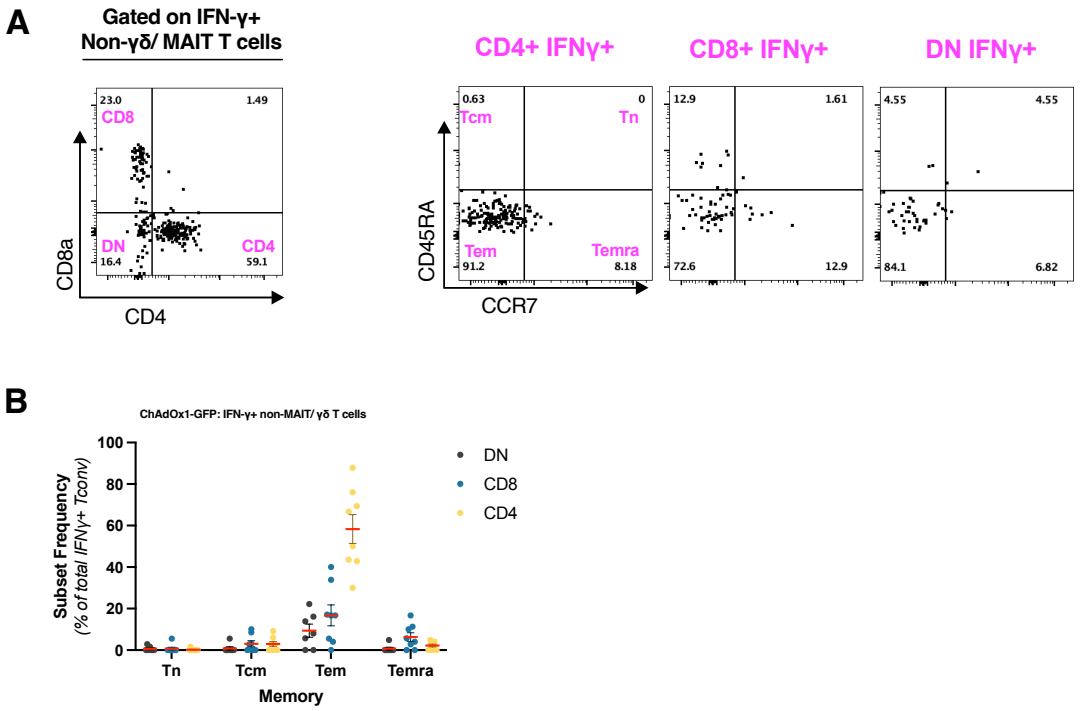

Fig3.4 | Effector memory conventional T cells respond to ChAdOx1-GFP in vitro.
Fresh PBMCs were treated with ChAdOx1-GFP (MOI 10^3 vp) and cytokine production by non-MAIT (CD161++Vα7.2+), non-γδ T cells measured after 24h (n= 7 donors).
(A) Representative plot of IFN-γ+ conventional T-cells after ChAdOx1, including frequency of memory subtypes among CD4, CD8 and DN T cells.
(B) Proportion of total IFNγ+ non-MAIT/ γδ T cells in response to ChAdOx1 which are naïve (Tn), central memory (Tcm), effector memory (Tem), or CD45RA-effector memory (Temra).
Symbols indicate individual donors.
Mean ± SEM is show. DN = double negative.

3.3.2 Interferons and antiviral cytokines are potently induced by ChAdOx1-GFP

To confirm that appreciable total IFN-γ is secreted in response to ChAdOx1, and identify cytokines which could activate cytokine-responsive CD161+ innate-like lymphocytes, we measured the concentration of inflammatory cytokines in cell culture supernatants after ChAdOx1-GFP stimulation (**Fig3.5**).

At very early (8h) timepoints, no cytokines were significantly induced compared to unstimulated controls (**Fig3.5 A**). As innate-like lymphocyte activation was also not observed at this time point, this implied that triggers for their activation are products of earlier cellular processes and not direct antiviral nucleic acid sensing. Clearly by 24h however a broad range of inflammatory mediators were induced, dominated by interferons and interferon-induced cytokines and chemokines (**Fig3.5 B**). Compared to unstimulated controls, there was a significant induction of IFN-α2 (median 9.4ng/ml; **Fig3.5 C**), IFN-β (median 1ng/ml; **Fig3.5 O**), IFN-γ (median 23ng/ml; **Fig3.5 D**), IFNλ1 (median 5.8ng/ml; **Fig3.5 P**) and IFNλ2/3 (median 0.3ng/ml; **Fig3.5 Q**). Furthermore, IFN-stimulated chemokines CCL2/MCP-1 (median 7.4ng/ml; **Fig3.5 E**), and CXCL10/IP10 (median 1.3ng/ml; **Fig3.5 R**). were also induced. Overall, the data supported the notion that ChAdOx1-GFP induces a strong antiviral response.

IL-1 family cytokines IL-1β (median 2500pg/ml; **Fig3.5 I**), IL-18 (median 120pg/ml, control 22pg/ml; **Fig3.5 J**) and IL-33 (median 22 pg/ml, control 6pg/ml; **Fig3.5 K**) were also potently induced, implying inflammasome activation could be induced by ChAdOx1, similar to previous observations for other AdV[304]. Potent induction of IL-12 family cytokines IL-12p70 (median 6pg/ml; **Fig3.5 L**) and IL-23 (median 20pg/ml; **Fig3.5 M**) would suggest potent TLR triggering, with both cytokines important for IFN-γ production by MAIT cells [312,313], Vδ2[199], and NK cells[314].

Figure 3.5 | Interferons dominate early cytokines at 24h after ChAdOx1-GFP stimulation *in vitro*.

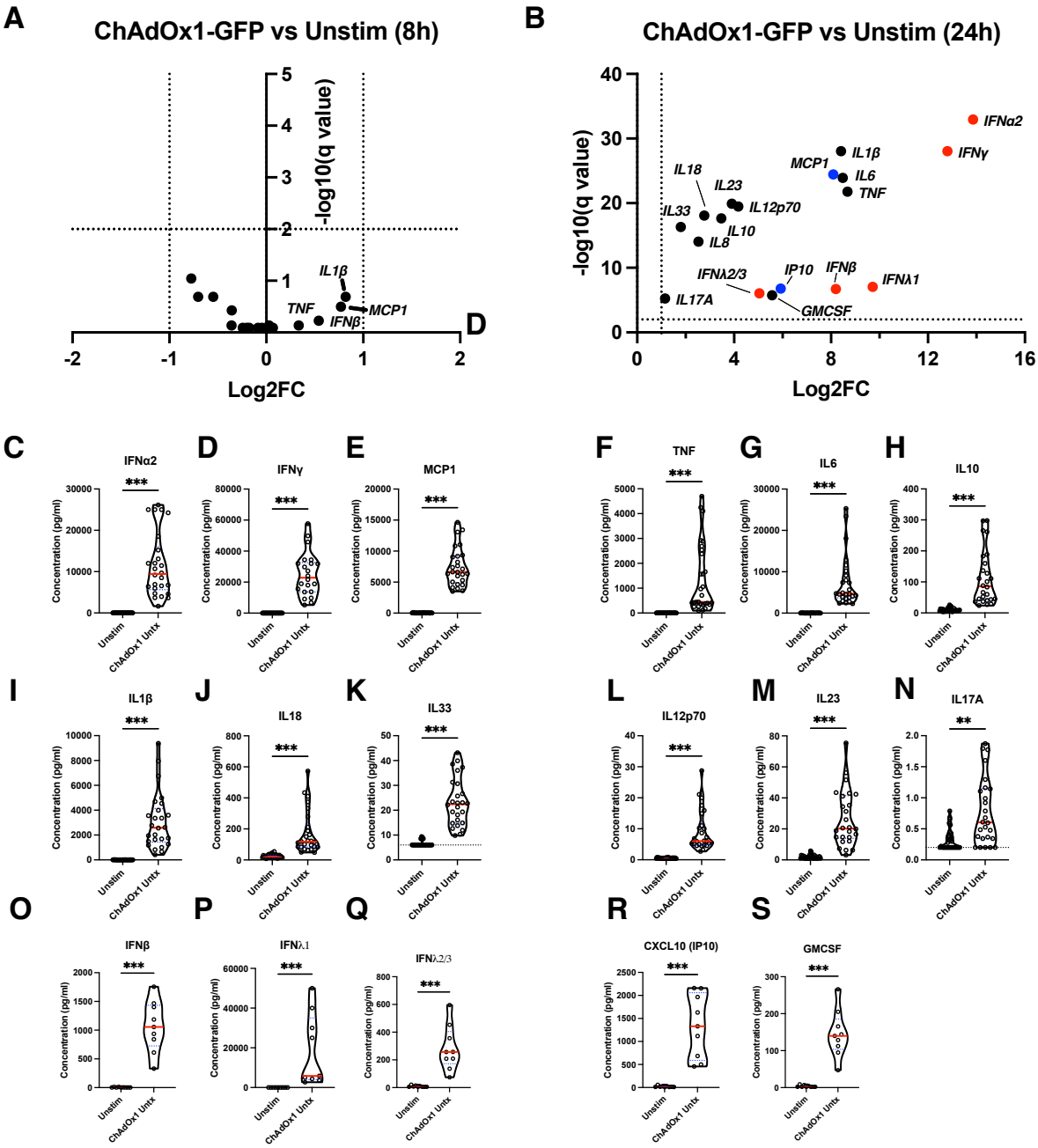

Fig3.5 | Interferons dominate early cytokines at 24h after ChAdOx1-GFP stimulation *in vitro*.
Fresh PBMCs were stimulated with ChAdOx1-GFP (MOI 10^3 vp), and cell culture supernatants were assayed for inflammatory cytokines at 8h (A, n=4), or 24h (B, O-S, n = 9; C-I, n=24).
(A,B) Volcano plots of log2FC in cytokines induced by ChAdOx1-GFP at 8h (A), or 24h (B). Interferons (red) and IFN-stimulated chemokines (blue).
(C-Q) Violin plots of cytokines secreted at 24h: IFNα2 (C), IFNγ (D); MCP1 (E); TNF (F), IL6 (G), IL10 (H), IL1β (I), IL18 (J), IL33 (K); IL12p70 (L), IL23 (M), and IL17A (N); IFNβ (O), IFNλ1 (P), IFNλ2/3 (Q), CXCL10 (R), GMCSF (S). Symbols indicate individual donors, with median (red). Dashed line indicates limit of detection (LOD) where visible.
*p < 0.05; **p < 0.01; ***p < 0.001; ****p < 0.0001; ns, not significant.
Statistical significance was determined using multiple paired t-tests of log2 transformed values, with Benjamini, Krieger, & Yekutieli correction for multiple comparisons (A, B); and unpaired non-parametric Mann-Whitney test (C-S).

To assess which cytokines might control innate-like lymphocyte IFN-γ production we focused on correlations between total secreted cytokines, total IFN-γ, and the frequency of IFN-γ-producing MAIT cells at 24h (**Fig3.6**).

There was a strong positive correlation between the frequency of IFN-γ+ MAIT cells and total IFN-γ concentration in supernatants (r =0.72, p = 0.0003; **Fig3.6 A**), supporting the in vitro data that activation of MAIT cells and similar CD161+ innate-like lymphocytes are a major contributor to the early IFN-γ response to ChAdOx1. There were also weak positive associations between the frequency of IFN-γ+ MAIT cells and secreted IFN-α2 (r =0.45, p = 0.0469; **Fig3.6 B**) and IL-12p70 (r = 0.445, p = 0.0491; **Fig3.6 C**), both cytokines capable of activating MAIT cell IFN-γ in combination[306]. Furthermore, the concentrations of IFN-α2, IL-12p70, and TNF showed a positive associated with total IFN-γ concentrations (**Fig3.6 D-E**), suggesting that cytokine dependent activation may drive maximal abundant early IFN-γ in response to ChAdOx1.

Figure 3.6 | ChAdOx1 induced MAIT cell IFN-γ correlates with type I IFN and IL-12 in vitro.

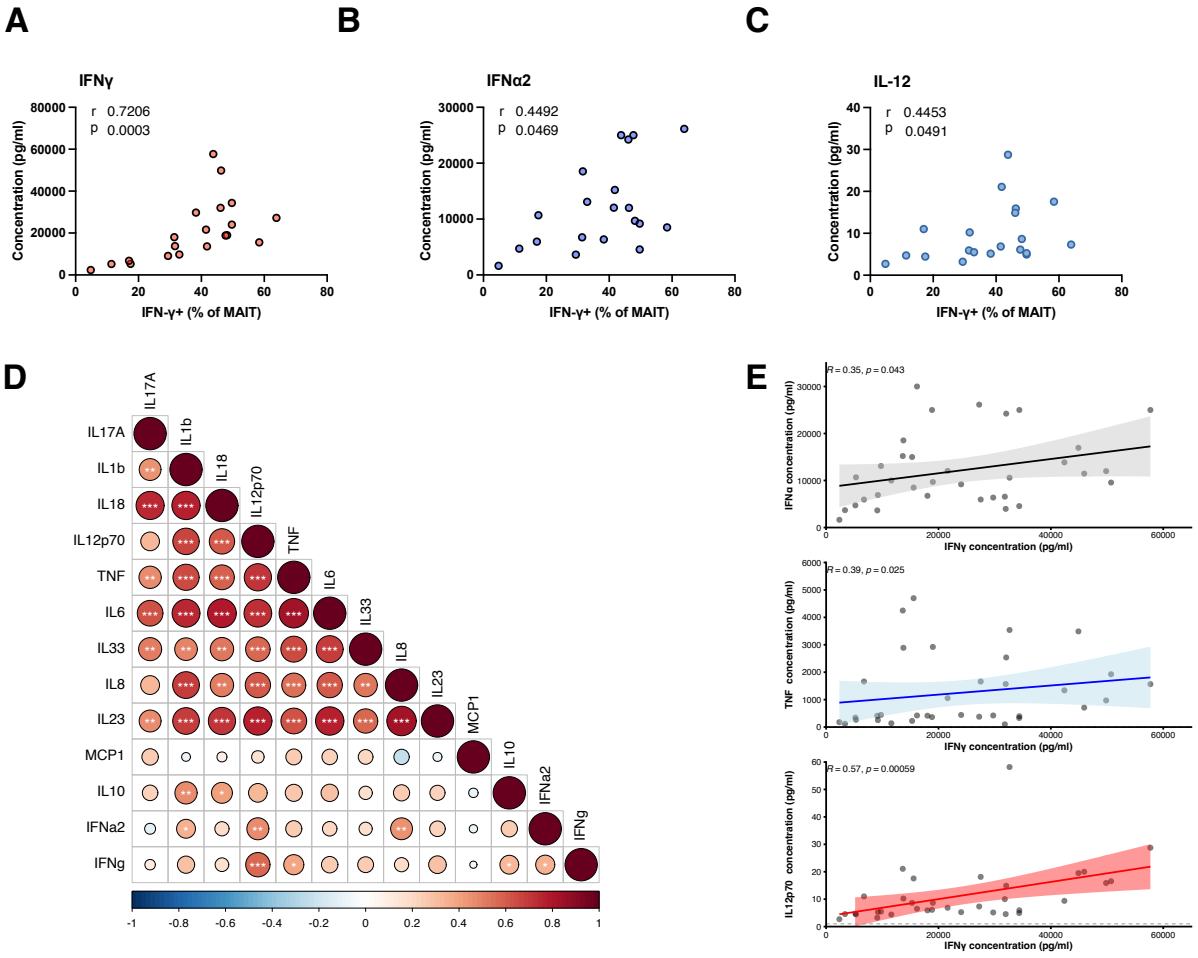

Fig3.6 | ChAdOx1 induced MAIT cell IFNγ correlates with type I IFN and IL12 in vitro.
Fresh PBMCs were stimulated with ChAdOx1-GFP (MOI 10^3 vp). MAIT cell IFNγ expression and cell culture supernatant concentrations of cytokines were assayed after 24h (n=20, pooled from separate experiments).
(A-C) Spearman's correlation of IFNγ+MAIT with supernatant IFNγ (A), IFNα2 (B), and IL12p70 (C).
(D) Correlation plot of supernatant cytokine concentrations induced in response to ChAdOx1-GFP.
(E) Spearman's correlation of supernatant IFNγ in response to ChAdOx1 with IFNα, TNF, and IL12p70.
Symbols indicate individual donors.
*p < 0.05; **p < 0.01; ***p < 0.001; ****p < 0.0001; ns, not significant.
Statistical significance was determined using spearman's correlation (A-E).

3.3.3 Innate immune cells are transduced and activated to produce inflammatory cytokines in response to ChAdOx1-GFP

Next, we sought to understand how ChAdOx1-induced cytokines important for MAIT cell activation are produced. Antiviral responses to AdV, including type I IFN secretion, require viral transduction and either TLR or nucleic acid sensing in innate cells[108], with subsequent activation and cytokine production. Nucleic acids sensors are triggered either in cytosolic or endosomal compartments after virus transduction, rather than non-specific uptake of vector proteins. To measure the importance of transduction to innate cytokine production, AdV were heat-inactivated using protocols which inhibit infectivity by denaturing proteins required for cell entry[296]. Heat-inactivation abolished PBMC GFP transgene expression in response to ChAdOx1-GFP (2.766±0.290% vs 0.003±0.001%; **Fig3.7 A-B**). Inhibition of productive cell entry with heat inactivation reduced total cytokines secreted (**Fig3.7 C-D**), in particular IFN-α2 (median 9439 vs 13 pg/ml), IL-12p70 (median 6.1 vs 1.8 pg/ml), and IFN-γ (median 18919 vs 462 pg/ml) (**Fig3.7 D**). The substantial reduction in total IFN-γ after heat-inactivation was associated with over 99.9% reduction in innate-like lymphocyte IFN-γ production (**Fig3.7 F**), and CD69 expression (**Fig3.7 G**), confirming that AdV transduction is required for robust innate-like lymphocyte activation.

We next compared the impact of heat-inactivation on conventional non-MAIT/ γδ T cell responses. Heat-inactivation again potently inhibited ChAdOx1-induced IFN-γ derived from conventional CD8+ T cells (0.125±0.03% to 0.004±0.002%, p <0.01; **Fig3.7 H**), with less potent inhibition of conventional CD4+ T cell IFN-γ (0.41 ±0.11% to 0.25±0.06%; p<0.01; **Fig3.7 H**), such that CD4+ T cells made up the dominant IFN-γ+ fraction in response to heat-inactivated ChAdOx1-GFP (**Fig3.7 H**). This suggested that even in ChAdOx-1 naïve donors, and in the absence of cytokines from virus transduction, conventional CD4+ T cells are triggered by AdV proteins. These could represent AdV hexon-specific CD4+ T cells cross-reactive to rare AdV serotypes.

Figure 3.7 | Heat-inactivation reduces ChAdOx1-GFP transduction and IFN-γ from innate-like lymphocytes in vitro.

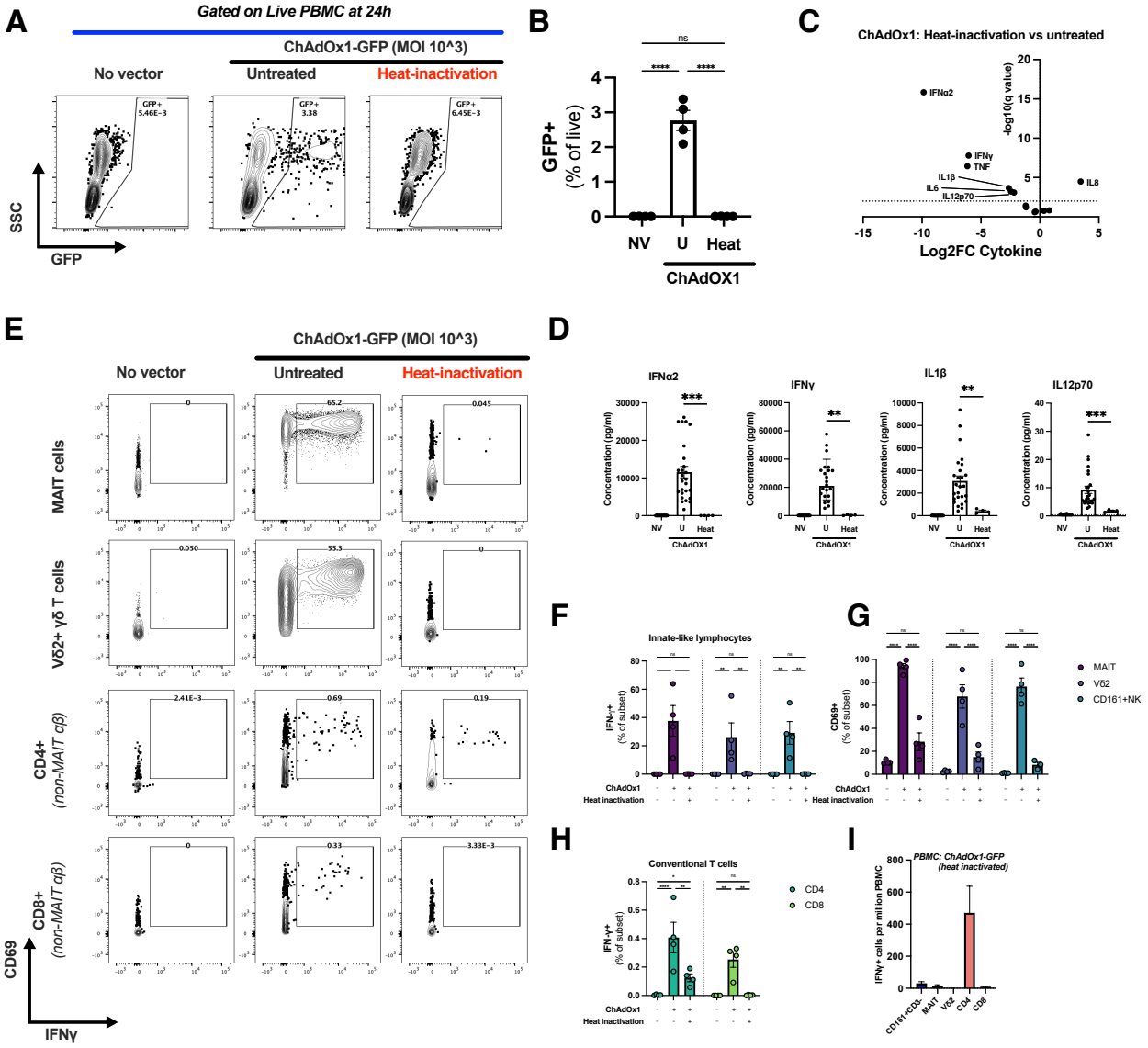

Fig3.7 | Heat-inactivation reduces ChAdOx1-GFP transduction and IFNγ from innate-like lymphocytes in vitro.

Fresh PBMCs from ChAdOx1 naïve donors were either untreated (no vector, NV) or treated with ChAdOx1-GFP (10^3 vp) which was heat-inactivated for 20min at 70˚C (Heat) or sham treated (U). After 24h, GFP transduction (A,B), secreted cytokines in supernatants (C,D) and activation of both innate-like lymphocytes and conventional (non-MAIT/ γδ) T cells was assessed (E-I). (n=4 donors)

(A-B) Representative plots (A), and summary data (B) of GFP expression in live PBMC at 24h.
(C) Volcano plots of log2FC in cytokines induced by ChAdOx1-GFP with and without heat inactivation.
(D) Summary of secreted IFNα, IFN-γ, IL-1β, and IL-12 in cell culture supernatants.
(E) Representative plots of IFN-γ production from MAIT, Vδ2, and conventional CD4+ and CD8+ T cells.
(F,G) Summary of MAIT, Vδ2, and non-B/T CD161+ lymphocyte IFN-γ (F) and CD69 (G) expression.
(H) Summary of non-MAIT/non-γδ T 'conventional' CD4+ and CD8+ IFNγ.
(I) Frequency of IFNγ+ cells (per million PBMC) after treatment with heat-inactivated ChAdOx1.
Symbols indicate individual donors. Mean ±SEM shown.
*p < 0.05; **p < 0.01; ***p < 0.001; ****p < 0.0001; ns, not significant.
Statistical significance was determined using: one-way ANOVA with Tukey's multiple comparison's test (B); multiple unpaired t-tests of log2 transformed cytokine concentrations, with Benjamini, Krieger, & Yekutieli correction for multiple comparisons (C); unpaired non-parametric Mann-Whitney test (D); and two-way ANOVA with Tukey's multiple comparison's test (F-H).

Next to assess which cells were transduced and activated, thus important for ChAdOx1-GFP mediated innate-like lymphocyte activation, we quantified GFP transgene expression in major PBMC populations at different time points (**Fig3.8 A, B**).

GFP expression in PBMC after ChAdOx1-GFP or Ad5-GFP was dose dependent (**Fig3.8 A**; **Appendix SF3.1**). At 24h, GFP was observed predominantly in monocytes, conventional and plasmacytoid dendritic cells (**Fig3.8**). T cells, NK cells and B cells were not appreciably transduced, although surprisingly basophils (HLADR+, CD123+, CD11c lo) also expressed GFP after 24h (**Fig3.8**). Curiously, at very early time points (8h) GFP expression is only observed in CD14+ monocytes after stimulation with ChAdOx1-GFP 10^3 vp/ml (9.9±0.3%; **Fig3.8 B, D, E**), with no GFP detectable in dendritic cells (**Fig3.8 D, E**). The fraction of live monocytes transduced increases with time and peaks between 24 and 48h (30% 24h; **Fig3.8 B**), at which point with dendritic cells including plasmacytoid dendritic cells also transgene positive (**Fig3.8 D, E**).

Figure 3.8 | ChAdOx1-GFP transduces monocytes earlier than dendritic cells in vitro.

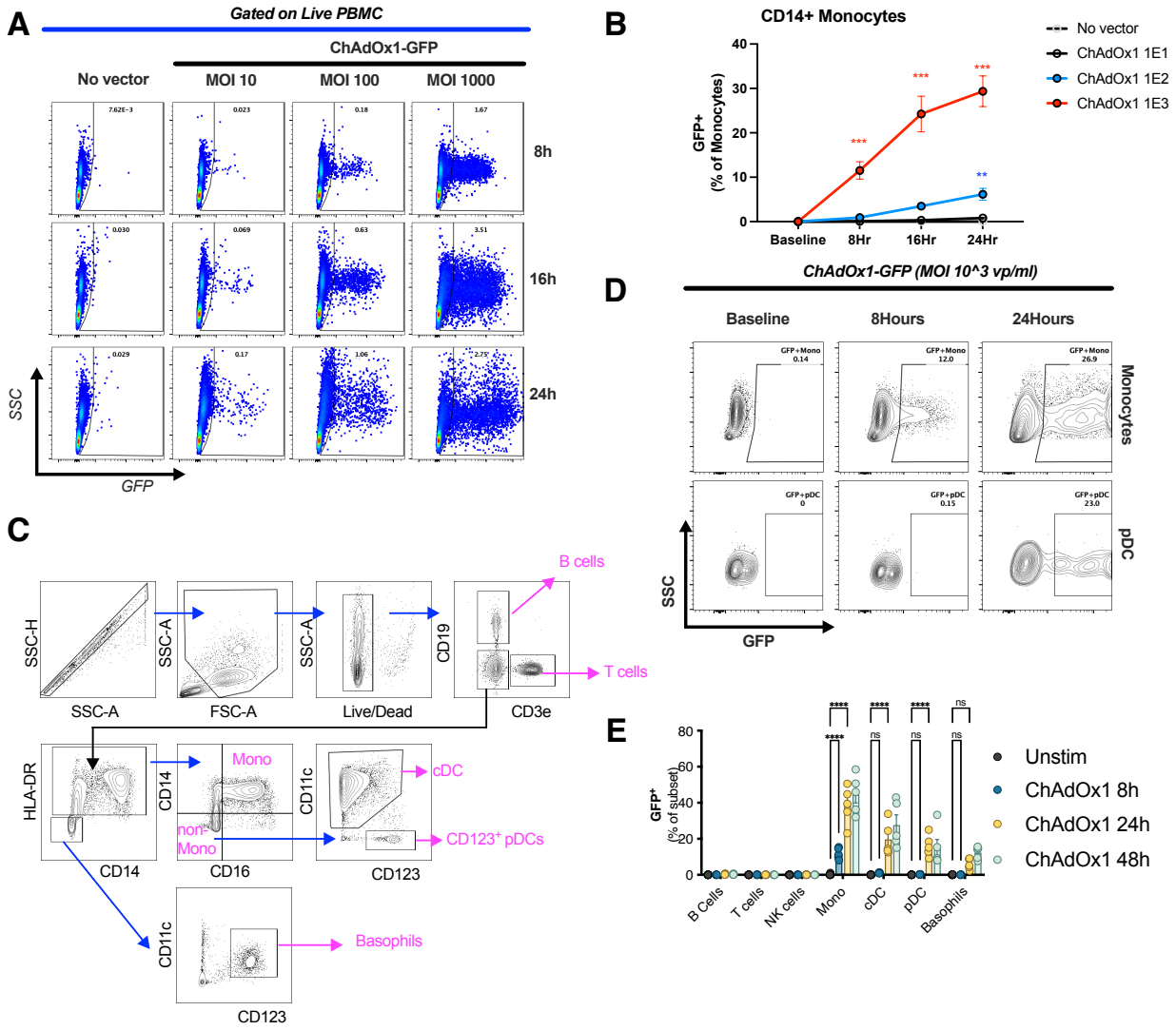

Fig3.8 | ChAdOx1-GFP transduces monocytes earlier than dendritic cells in vitro.
Fresh PBMCs were stimulated with ChAdOx1-GFP at increasing multiplicity of infection (MOI) for time indicated. The fraction of PBMC populations expressing GFP were quantified.
(A) Representative plots gated on live PBMC with increasing titration of ChAdOx1-GFP, highlighting GFP+ cells at 8h, 16h, and 24h.
(B) Gating scheme for identification of major PBMC immune cell subsets.
(C) Fraction of CD14+ monocytes expressing GFP at indicated time points with increasing ChAdOx1-GFP.
(D) Representative plots of monocyte (top) and pDC (bottom) GFP expression at 8h and 24h.
(E) Fraction of indicated immune subsets that are GFP+ at indicated times after transduction with ChAdOx1-GFP (10^3 vp).
Symbols indicate individual donors.
*p < 0.05; **p < 0.01; ***p < 0.001; ****p < 0.0001; ns, not significant.
Statistical significance was determined using two-way ANOVA with Dunnett's multiple comparison's test (B, E).
cDC = conventional dendritic cells; Mono = monocytes; pDC = plasmacytoid dendritic cells.

We next measured activation of transgene-induced APC to gauge their capacity to prime innate-like and adaptive immune cells, measuring MHC-I (pan HLA-A,B,C), MHC-II (HLA-DR) and CD80 as surrogate markers to reflect their capacity for antigen presentation and co-stimulation (**Fig3.9**). ChAdOx1-GFP induced HLA-DR expression in all APCs tested (**Fig3.9 B**). Upregulation of surface MHC-I expression was not however observed at 24h in cDC, despite up-regulation of CD80 similar to myeloid cells (**Fig3.9 B**). The kinetics of activation confirmed that APC CD80 expression, unlike HLA-DR, remains elevated at 48h (**Fig3.9 C, D**); HLA-DR expression fell after a peak at 24h in dendritic cells, B cells and classical monocytes.

We next asked whether GFP transduction was required for potent activation, comparing expression of activation markers in GFP+ and GFP- immune cells (**Fig3.9 E-G**). Classical monocytes in particular show higher activation (HLA-ABC, HLA-DR, CD80) in GFP+ cells at 24h (**Fig3.9 F**). Plasmacytoid dendritic cells had transduction-augmented HLA-DR expression at 24h only, with CD80 expression additionally increased in GFP+ cells at 48h (**Fig3.9 F, G**).

Therefore, in summary, APCs are activated in response to ChAdOx1-GFP in vitro, including many in the absence of GFP expression, suggesting that innate immune activation spreads quickly via secondary signals from initial cells encountering viral vectors.

Figure 3.9 | Activation of antigen presenting cells in response to ChAdOx1-GFP in vitro.

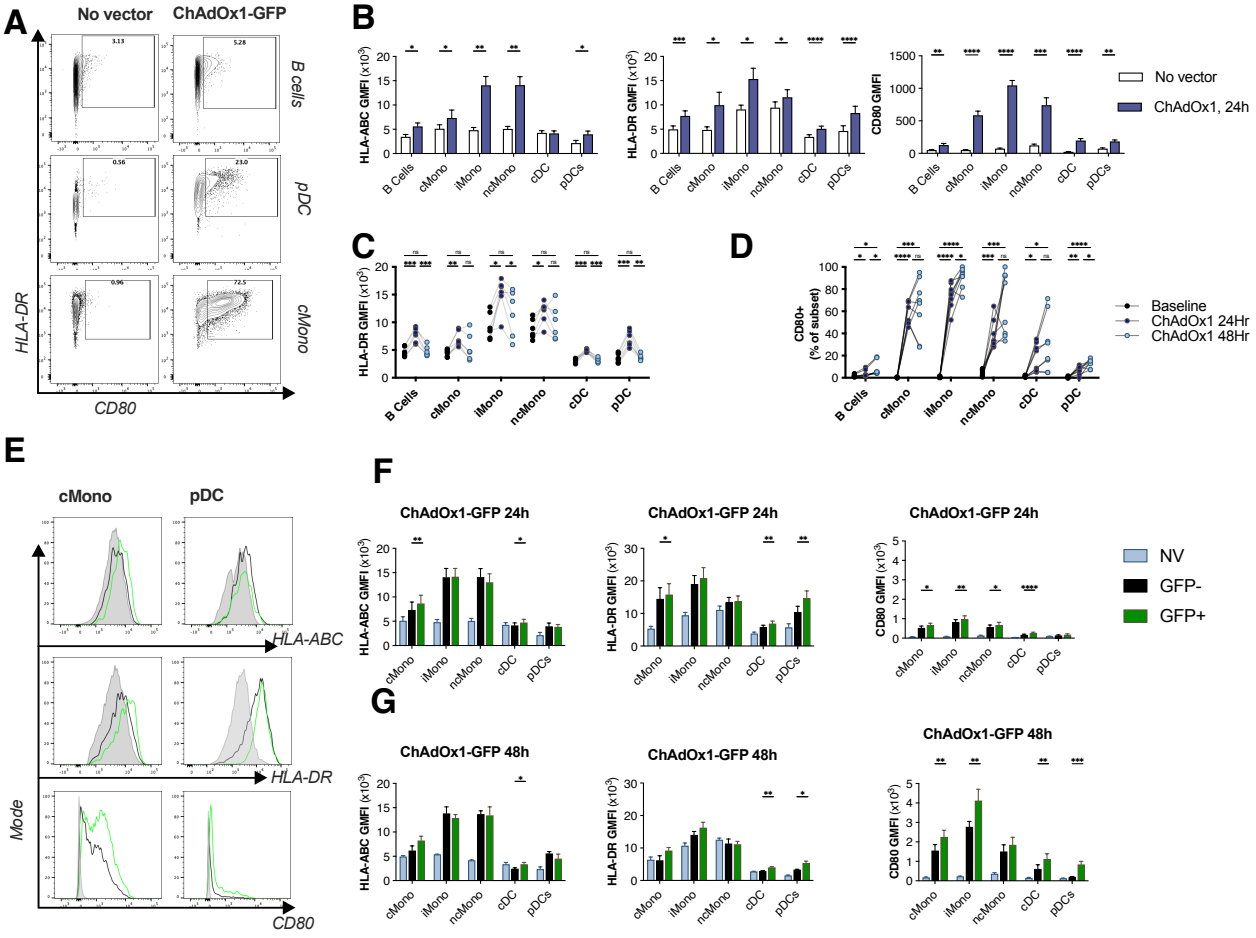

Fig3.9 | Activation of antigen presenting cells in response to ChAdOx1-GFP in vitro.
Fresh PBMCs were stimulated with ChAdOx1-GFP at 10^3 vp for the time indicated. Surface expression of activation markers (HLA-ABC, HLA-DR, CD80) was measured on major PBMC immune populations (data not shown for T cell and NK cells).
(A) Representative plots gated on live B cells (top), pDC (middle), and classical monocytes (bottom) 24h after ChAdOx1-GFP measuring HLA-DR and CD80 expression.
(B) Expression of HLA-ABC, HLA-DR, and CD80 on PBMC populations 24h after stimulation with ChAdOx1-GFP or no vector control (n=8).
(C, D) Expression kinetics of HLA-DR (C), and CD80 (D) at baseline, 24h and 48h after ChAdOx1-GFP stimulation (n=6).
(E) Representative plots gated on classical monocytes (left), or pDC (right) with expression of HLA-ABC, HLA-DR, and CD80 on GFP+ and GFP- cells at 24h.
(F, G) Summary of HLA-ABC, HLA-DR, and CD80 expression (GMFI) on GFP+ (black), and GFP- (green) PBMC populations 24h (F), or 48h (G) after stimulation with ChAdOx1-GFP or no vector (NV, blue) (n=6).
Symbols indicate individual donors. Mean ± SEM show.
*p < 0.05; **p < 0.01; ***p < 0.001; ****p < 0.0001; ns, not significant.
Statistical significance was determined using two-way ANOVA with Dunnett's multiple comparison's test (C, D), and multiple paired t tests (B, F, G).
pDC = plasmacytoid dendritic cell; cMono = classical monocyte; iMono = intermediate monocyte; ncMono = non-classical monocyte. GMFI = geometric mean.

Given that cell transduction was necessary for innate-like lymphocyte activation, we next sought to identify the necessary cell types. Numerically, monocytes and cDC were the dominant transduced cell population (**Fig3.8**), with monocyte cell death and appreciable IL-18 induction observed uniquely after ChAdOx1-GFP but not Ad5-GFP stimulation in vitro (Nicholas Provine; **Appendix SF3.2 A**). Given that only ChAdOx1-GFP potently induces innate-like lymphocyte IFN-γ, and IL-18 can activate MAIT cells in response to virus infections [306], we tested the impact of monocyte depletion on MAIT cell activation (Nicholas Provine, **Appendix SF3.2**). Monocyte depletion reduced ChAdOx1-induced IL-18, and concordantly reduced MAIT IFN-γ in vitro (Nicholas Provine, **Appendix SF3.2 B**). Furthermore, IL-18 and IL-18R blockade immediately prior to stimulation both potently inhibited MAIT cell and Vδ2+ γδ T cell IFN-γ in vitro (Nicholas Provine, **Appendix SF3.2 C**). Therefore, monocytes and inflammatory cell death derived IL-18 were required for AdV induced innate-like lymphocyte activation.

IL-18 is however insufficient to induce MAIT cell IFN-γ alone in PBMC, with combinations of other cytokines required[306]. We tested blockade of other cytokines induced by ChAdOx1-GFP in vitro (**Fig3.5**). Blockade of IL-12p40 (Guselkumab), and IL-23p19 (Ustekinumab) prior to ChAdOx1 stimulation inhibited MAIT cell IFN-γ (Guselkumab, 13.3±4.8%; Ustekinumab, 8.1±2.9%, control, 31.9±6.2%; **Appendix SF3.3 A**). Although statistically significant, mouse anti-human IL-12p70 inhibition resulted in only very modest reduction in IFN-γ (19.3±3.1% vs 34.6±4.8% IgG1 isotype), with IL-18 the most potent inhibitor of IFN-γ (2.8±0.9%; **Appendix SF3.3 A**). Intriguingly, inhibition of IL-23 dependent subunits (IL-12p40 and IL-23p19), but not IL-12p70 reduced ChAdOx1-induced MAIT cell GzmB (**Appendix SF3.3 B**). IL-23 can augment Vγ9Vδ2+ γδ T cell IFN-γ and GzmB expression[315], therefore a potential shared mediator of innate-like lymphocyte activation.

In summary, these data clearly implicated cytokines in the induction of robust early unconventional sources of IFN-γ in response to ChAdOx1.

3.3.4 pDC-derived type I IFN is necessary but insufficient for robust sustained ChAdOx1-induced IFN-γ production

To understand how early innate-like lymphocyte IFN-γ is produced in response to ChAdOx1, we focussed on the role of type I. This was primarily because IFN-α2 exhibited the highest induction by fold change in vitro at 24h (), was abolished by heat inactivation which profoundly reduced all unconventional sources of IFN-γ (**Fig3.7)** and correlated with total and MAIT IFN-γ production in vitro **(Fig3.6**). Given that intracellular nucleic acid sensing of AdV is a driver for IFN-α production[106], and type I IFN can potently activate MAIT cell IFN-γ in combination with other cytokines [306], we hypothesised that type I IFN contributes to MAIT cell and innate-like lymphocyte IFN-γ.

To test this hypothesis, we inhibited type I IFN signalling - either using a pox-derived soluble decoy type I IFN receptor (B18R) [316], or a blocking antibody against the IFNAR subunit (αIFNAR2) (**Fig3.10 A**). Both B18R and αIFNAR2 antibody inhibited IFN-γ produced by MAIT cells (nearly 3-fold; **Fig3.10 B**), Vδ2+ T cells (**Fig3.10 B**), and CD161+ NK cells in a dose-dependent manner (**Fig3.10 B**). Inhibition required high concentrations - with B18R more potent than αIFNAR2 antagonism (**Fig3.10 B**) - with specificity for IFN-γ as GzmB expression was not reduced (**Fig3.10 C**). CD69 expression was inhibited by B18R but not IFNAR blockade (**Fig3.10 D**). Furthermore, inhibition of type I IFN signalling only had a modest impact on conventional CD4+ T cell IFN-γ (0.417±0.106± vs 0.261±0.07%; ns), but was more important for conventional CD8+ T cell derived IFN-γ (0.243±0.054% vs 0.075±0.036%) (**Fig3.10 E,F**).

Examining cytokines secreted by PBMC in response to ChAdOx1, maximal inhibition with B18R reduced IFN-α2 over 600-fold (**Fig3.10 G**), with a corresponding 8-fold reduction in total IFN-γ (**Fig3.10 G,H**). Remarkably, IFN-γ was the only other cytokine of the inflammation panel tested inhibited in the absence of type I IFN signalling – with many such

as IL-1β , TNF, IL-6, IL-17A and IL-23 increased with B18R blockade prior to ChAdOx1-GFP stimulation (**Fig3.10 G, H-I**). Unsurprisingly, given the importance of IFNs to the antiviral response, type I IFN blockade increased the frequency of GFP+ cells at 24h (**Fig3.10 J**). Given the increase in IL-17A – a T-cell derived cytokine – the impact of type I IFN on available antigen could skew early conventional (and unconventional) TCR-mediated type 17 responses.

Figure 3.10 | Type I IFN is necessary for maximal innate-like lymphocyte IFN-γ.

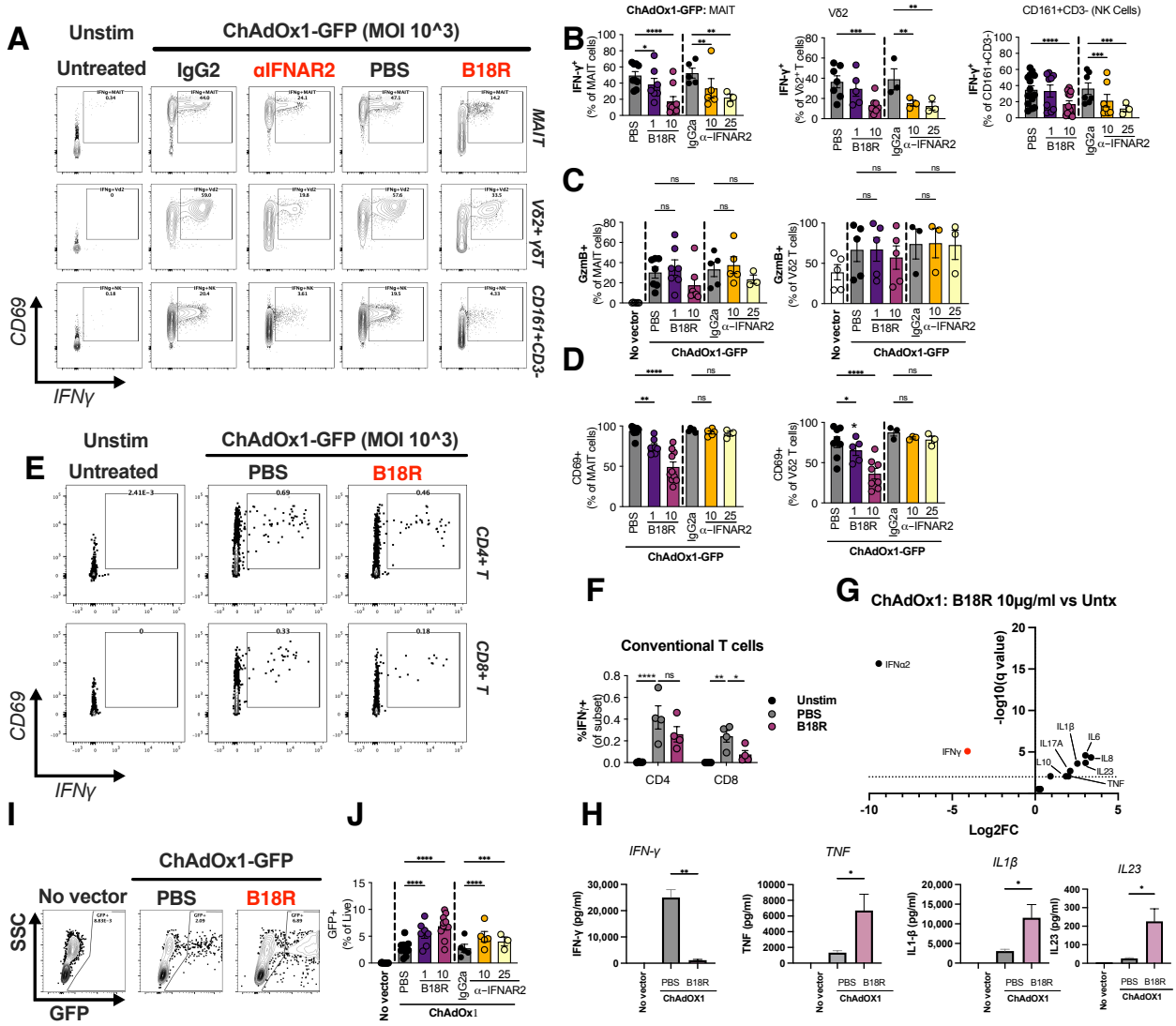

Fig3.10 | Type I IFN is necessary for maximal innate-like lymphocyte IFNγ.
Fresh PBMCs were stimulated with inhibitors of type I IFN (B18R, 1 or 10µg/ml; αIFNAR2, 10 or 25µg/ml) prior to stimulation with ChAdOx1-GFP (MOI 10^3 vp). Activation (CD69, GzmB, IFN-γ) in MAIT cells, Vδ2+ γδ T cells, and CD161+ non-B/T lymphocytes was measured after 24hrs.
(A) Representative plots of MAIT cells, Vδ2+ γδT cells and CD161+CD3- (NK) cells with or without ChAdOx1-GFP, in the presence of control (αIgG2, PBS) or type IFN blockade (αIFNAR2, 10µg/ml; B18R, 10µg/ml).
(B-D) Expression of IFN-γ (B), GzmB (C), and CD69 (D) on MAIT, Vδ2+ γδ T or CD161+CD3- (NK) cells.
(E,F) Representative plots of IFNγ from non-MAIT/γδ T cell conventional CD4+ (top) and CD8+ T cell (bottom) after ChAdOx1-GFP in the presence of B18R (10µg/ml) or PBS control.
(F) IFN-γ expression in conventional CD4+ and CD8+ T cells with and blockade with B18R (n=4).
(G) Volcano plots of log2FC in cytokines induced by ChAdOx1-GFP at 24h with and without blockade of type I IFN signalling with B18R.
(H) Concentration of IFN-γ, TNF, IL-1β, and IL-23 in cell culture supernatants at 24h (n=4).
(I) Representative plots of GFP expression gated on live PBMC with and without B18R.
(J) GFP expression among live PBMCs in the presence of indicated type I IFN blockers (n=3-8)
Symbols indicate individual donors, with median (red).
Dashed line indicates limit of detection (LOD) where visible.
*p < 0.05; **p < 0.01; ***p < 0.001; ****p < 0.0001; ns, not significant
Statistical significance was determined using repeated-measures one-way ANOVA with Dunnett correction (B-D; F, J); unpaired t-tests of log2 transformed values, with Benjamini, Krieger, & Yekutieli correction for multiple comparisons (G); and unpaired non-parametric Mann-Whitney test (H).

Next, we wanted to confirm the source of type I IFN in response to ChAdOx1. Plasmacytoid dendritic cells are the primary producers of IFN-α in PBMC [41], which are both transduced and activated by ChAdOx1-GFP (**Fig3.8**; **Fig3.9**), thus an obvious candidate. Although pDC were only transduced at 24h, we tested earlier, and later time points given that triggering of IFN-α production could precede transgene expression. In PBMC, IFN-α was only detectable by flow cytometry in pDC after 24h but not earlier (8h) or later (48h), indicating transient production in response to replication incompetent AdV (**Fig3.11 A,B**).

GFP+ pDC were more activated - with higher expression of CD80 and HLA-DR - compared to their GFP- counterparts (**Fig3.9**), but the expression of IFN-α did not differ appreciably based on pDC GFP expression (**Fig3.11 C, D**). The majority of IFN-α+pDC were however GFP negative (**Fig3.11 E**), with lower HLA-DR expression compared to GFP+IFN-α+ cells. Mechanisms could include transduction independent type I IFN induction, increased transduction induced cell-death, or substantial cytosolic or endosomal innate sensing in the absence of nuclear translocation after vector entry necessary for transgene expression. The presence of GFP+ pDC at 48h (**Fig3.9**), in the absence of appreciable IFN-α production (**Fig3.11 B**) would argue somewhat against cell death as the sole explanation.

Finally, to specifically confirm the importance of pDC-derived IFN-α in AdV-induced IFN-γ, we sought to deplete pDC prior to ChAdOx1-GFP stimulation. Depletion of CD123+ cells effectively reduces pDC in vitro [317], although we also found a reduction in CD123+ basophils which could also be transduced by ChAdOx1-GFP (**Fig3.8**). However, only CD123- depletion using LD (lymphocyte depletion) columns completely abolished pDC frequency in fresh PBMC, while basophils were also effectively depleted using LS (lymphocyte selection) columns (**Fig3.11 G, H**). Importantly it was only CD123+LD depletion which inhibited MAIT cell IFN-γ production in response to ChAdOx1-GFP (**Fig3.11 I, J**); CD123+ depletion using LS columns which reliably reduced basophils had no impact on MAIT IFN-γ, suggesting that pDC and not basophils were required. IFN-γ production from all innate-

like lymphocytes was reduced but not abolished in the absence of pDC (**Fig3.11 J-L**). As expected, pDC depletion resulted in reduced IFN-α in response to ChAdOx1 (**Fig3.11 M**, **data Nicholas Provine**), suggesting that pDC-derived IFN-α is important for robust innate-like lymphocyte IFN-γ production.

Figure 3.11 | Plasmacytoid dendritic cells produce IFN-α necessary for maximal innate-like lymphocyte IFN-γ.

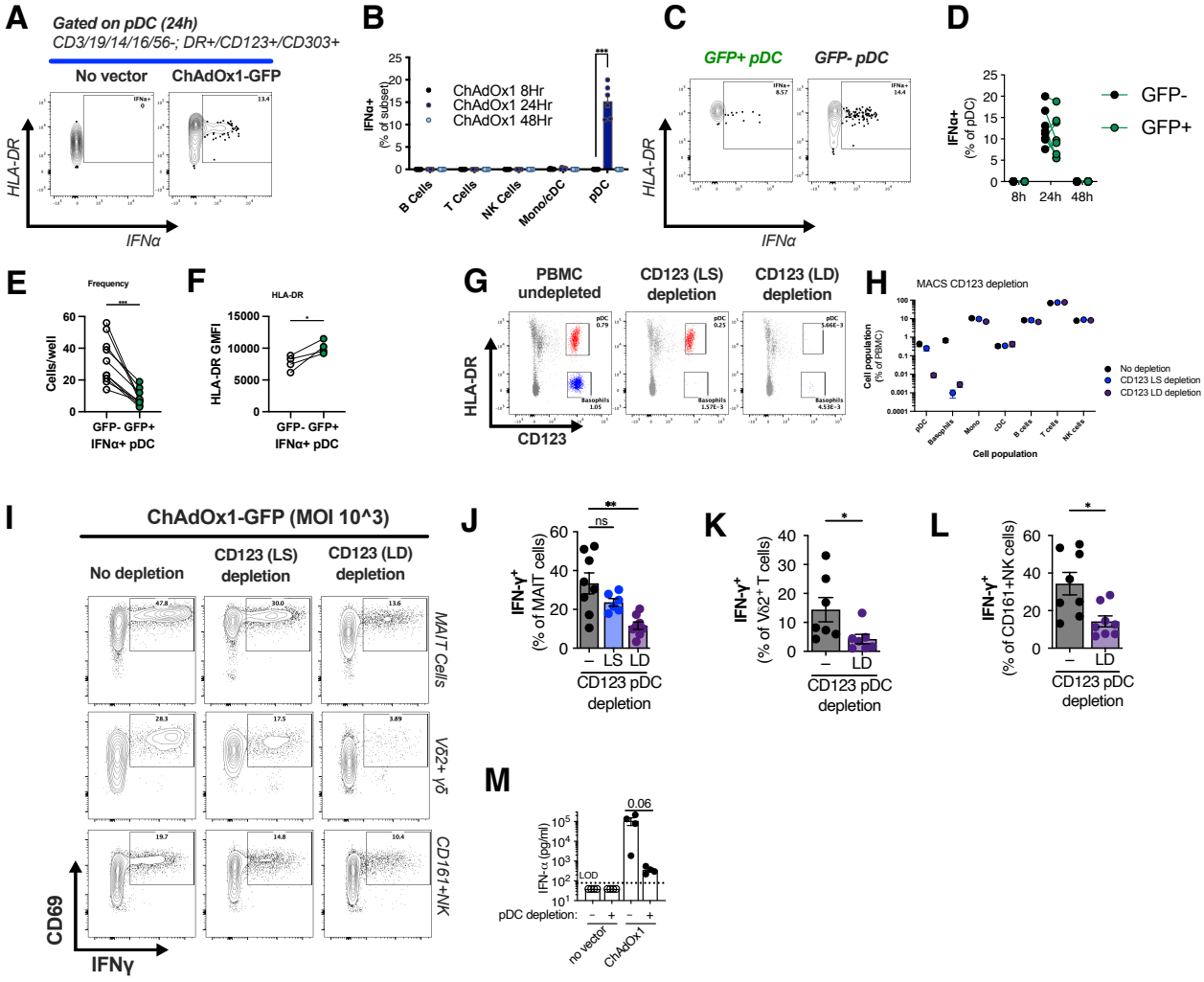

Fig3.11 | Plasmacytoid dendritic cells produce IFNα necessary for maximal innate-like lymphocyte IFNγ.
(A-F) Fresh PBMCs were stimulated with ChAdOx1-GFP (MOI 10^3 vp) and IFNα production in pDC measured at indicated timepoints.
(A) Representative plots of pDC IFNα expression after 24h.
(B) IFNα2 expression in PBMC populations at 8h, 24h, and 48h.
(C, D) Representative plots (C), and summary IFNα expression (D), in GFP+ and GFP- pDC.
(E, F) Frequency (E), and HLA-DR expression (F) of IFNα+ pDC which are GFP+ and GFP-.
(G) Representative plot of PBMC populations after CD123 magnetic bead depletion using LS or LD columns. Basophils (Lin-, HLADR-CD123+CD11clo, blue) and pDC (Lin-/HLADR+/CD123+/CD11c-/CD303+; red).
(H) Frequency of major cell populations in fresh PBMC after depletion using LS and LD columns.

(I-M) Fresh PBMC unfractionated or CD123-depleted PBMC were treated with ChAdOx1-GFP and innate-like lymphocyte activation measured at 24h.
(I) Representative plot of MAIT, Vδ2 γδ T, or NK cell (CD161+CD3-GzmB+) activation.
(J-L) IFNγ expression in MAIT cells (J), Vδ2+ T cells (K), and CD161+ NK cells (L), after stimulation of unfractionated or CD123-depleted PBMC with ChAdOx1-GFP.
(M) IFNα concentration in cell culture supernatants 24h after ChAdOx1-GFP with or without pDC depletion (LD columns).
Symbols indicate individual donors. Mean ±SEM shown. *
p < 0.05; **p < 0.01; ***p < 0.001; ****p < 0.0001; ns, not significant. Statistical significance was determined using two-way ANOVA with Dunnett's multiple comparison's test (B); paired t test (D-F); repeated-measures one-way ANOVA with Dunnett correction (J), or unpaired t test (K-M). pDC = plasmacytoid dendritic cell

ELISA in (M) and one repeat of pDC depletion performed by Nicholas Provine.

We then sought to determine how type I IFN augments ChAdOx1-induced innate-like lymphocyte activation, focusing first on CD69 which was a sensitive marker of activation. To test the kinetics and sensitivity, we stimulated PBMC with type I IFN (IFN-α2, IFN-β) and measured activation at 6h and 24h. To determine whether activation was unique to type I IFN, IFN-γ and type III IFNs (IFNλ3, IFNλ4) were used as comparators (**Fig3.12**). At baseline MAIT cells have the highest CD69 expression by GMFI among T-cells (**Fig3.12 A B**). Stimulation of PBMC with IFN-α induced CD69 in all T-cells, and CD161+ NK cells, with innate-like lymphocytes exhibiting higher expression than conventional T cells (**Fig3.12 C**). MAIT cells, CD161+ NK cells, and Vδ2+ γδ T cells showed similar sensitivity to IFN-α, with Vδ2- γδ T were less IFN-responsive than Vδ2+ γδ T cells despite high baseline activation (**Fig3.12 D**), consistent with the previous patterns for ChAdOx1-induced CD69 induction and the known enhanced cytokine responsiveness of Vδ2+ γδ T cells [199, 382]. MAIT cell activation was an exquisite marker of IFN-α, with almost all expressing CD69 in response to IFN-α2 (**Fig3.12 C**). Activation was rapid, observed as early as 6h, and also observed with IFN-β but not IFN-γ or IFN-λ (**Fig3.12 E-G**). Although IFN-β and IFN-α showed similar potency at lower concentrations, IFN-β induced CD69 plateaued around 100 U/ml in contrast to IFN-α which continues to robustly induce CD69 in all T cells (**Fig3.12 E, F**).

Figure 3.12 | Type I and not type II/ II IFNs robustly induce early CD69 in innate-like lymphocytes.

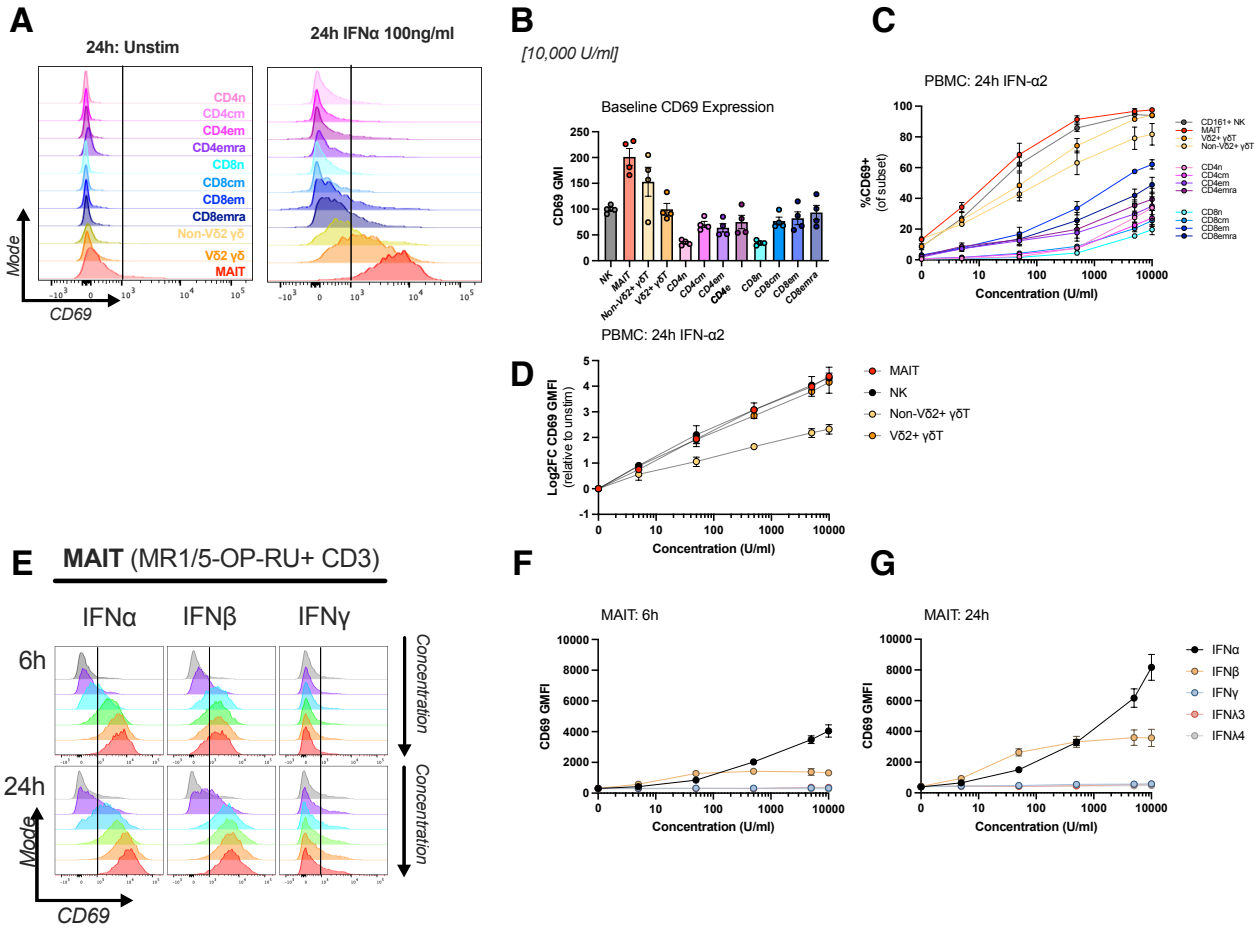

Fig3.12 | Type I and not type II/ II IFNs robustly induce early CD69 in innate-like lymphocytes.
Fresh PBMCs were stimulated with increasing concentrations of IFN-α2, IFN-β, IFN-γ, IFN-λ3, or IFN-λ4, and expression of CD69 measured at baseline, 6h and 24h after stimulation on T cells comparing to CD161+CD3- NK cells (n=4).
(A) Representative plots of CD69 expression at baseline and 24h after IFN-α2 stimulation in PBMC.
(B) CD69 expression (GMFI) prior to activation.
(C) Fraction of cells expressing CD69 24h after increasing concentrations of IFN-α2.
(D) Log2 fold change in CD69 expression compared to unstimulated controls in MAIT cells, CD161+ NK cells, Vδ2 and non-Vδ2+ γδ T cells 24h after IFNα2 stimulation.
(E) Representative plots gated on MAIT cells (MR1//5-OP/RU+) of CD69 expression 6h (top) and 24h (bottom) after stimulation with increasing concentrations of IFNα-2, IFN-β, and IFN-γ.
Symbols indicate individual donors. Mean ±SEM shown.
Tn = naïve; Tcm = central memory; Tem = effector memory; Temra = RA+ effector memory.

As MAIT cells are the most sensitive to type I IFN, with MAIT cell IFN-γ possessing antiviral immune functions in vitro [306], and in vivo[224], we next sought to understand how type I IFN augments their IFN-γ production. We first tested the capacity of IFN-α to induce MAIT cell activation in PBMC alone or in combination with IL-18 (**Fig3.13 A**). Although IFN-α stimulation of PBMC robustly induced expression of CD69 (89±2%) and GzmB (35±5%), only modest IFN-γ was detectable in the absence of additional cytokines after 24h (5.7±1.5%) (**Fig3.13 A B**). IL-18, important for ChAdOx1-induced MAIT activation, does not induce robust IFN-γ alone (**Fig3.13 B**), similar to IL-12 [306]. Combination of IFN-α with IL-18 however was sufficient to mirror potent ChAdOx1-induced MAIT cell IFN-γ (36±5%; **Fig3.13 A, B**). Taken together with observations that blocking type I IFN, IL-18, and IL-12 inhibited ChAdOx1-induced IFN-γ, combinations of cytokines were clearly required. The incomplete inhibition of IFN-γ with either B18R or pDC depletion also supported the notion that type I IFN was not the sole cytokine responsible for induction of early IFN-γ.

To test whether type I IFN can directly activate MAIT cells in the absence of APCs, we stimulated MACS-enriched CD8+ cells (purity >95%) and measured activation after 24h (**Fig3.13 C, D**). IFN-α again induced dose-dependent CD69 expression, as in PBMC, with modest induction of GzmB expression (**Fig3.13 E**). No IFN-γ was detectable however, suggesting that the modest type I IFN induced MAIT cell IFN-γ in PBMC was a consequence of additional indirect IFNAR signalling on non-MAIT cells.

We next tested whether IFN-α could induce MAIT cell IFN-γ in the absence of APCs in combination with another ChAdOx1-induced cytokine such as IL-18. In the absence of APC, neither IFN-α alone or in combination with IL-18 could induce robust IFN-γ in MAIT cells at 24h (**Fig3.13 F G**). Similar reduction in MAIT IFN-γ in the absence of APC was observed for other combinations with type I IFN, but not IL-12 and IL-18 (**Fig3.13 H**).

Figure 3.13 | Type I induced MAIT cell IFN-γ at 24h requires accessory cells found in PBMC.

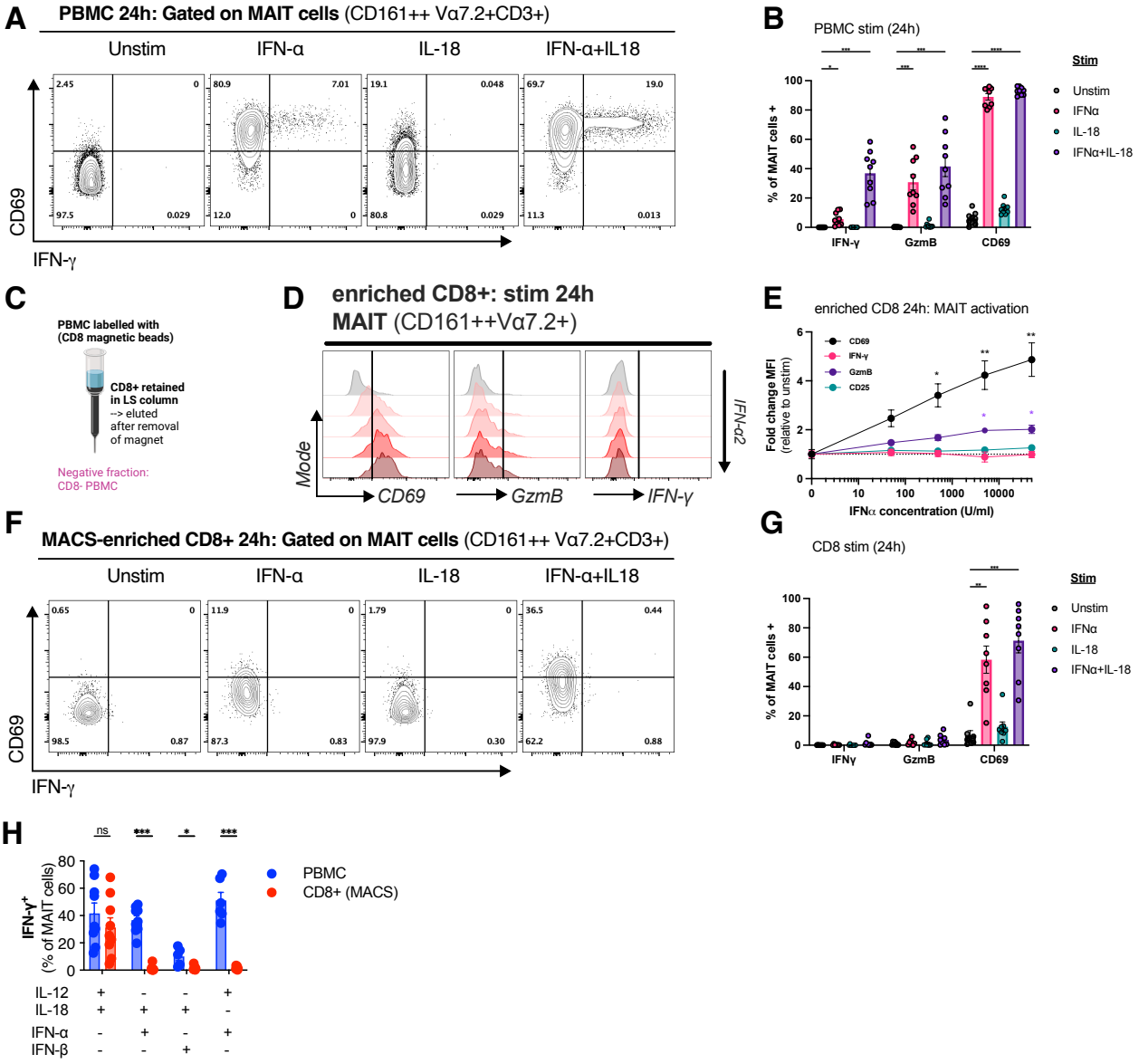

Fig3.13 | Type I induced MAIT cell IFN-γ at 24h requires accessory cells found in PBMC.
MAIT cell (CD161++ Vα7.2+) activation was assessed 24h after cytokine stimulation of cryopreserved PBMC (**A-B; H**), or MACS enriched CD8+ cells (**C-H**) with individual cytokines or combinations at the following concentrations: IFN-α2 (50ng/ml; 5000U/ml), IL-18 (50ng/ml), IL-12 (50ng/ml).
(A-B) PBMCs were stimulated with combinations of cytokines, and MAIT CD69, GzmB, and IFN-γ measured (n=8).
(A) Representative plots gated on MAIT cells.
(B) MAIT cell expression of IFN-γ, GzmB, and CD69.
(C) Schematic for MACS enrichment.
(D, E) MACS enriched CD8+ cells were stimulated with increasing IFNα concentrations and MAIT cell expression of CD69, IFN-γ, GzmB, CD25 measured after 24h (n=3).
(D) Representative histograms gated on MAIT cells.
(E) Fold change in expression (GMFI) of markers compared to unstimulated controls.

(F,G) MACS enriched CD8+ cells were stimulated with combinations of cytokines, and MAIT activation measured.
(F) Representative plots gates on MAIT cells.
(G) MAIT cell expression of IFN-γ, GzmB, and CD69 after cytokine stimulation.

(H) PBMC or enriched CD8 were stimulated with combinations of cytokines and MAIT cell IFN-γ measured at 24h (n=6-8). Symbols indicate individual donors. Mean ±SEM shown.
*p < 0.05; **p < 0.01; ***p < 0.001; ****p < 0.0001; ns, not significant. Statistical significance was determined using using two-way ANOVA with Dunnett's multiple comparison's test (B, E, G); paired t tests (H).

Given that type IFN can directly stimulate very early IFN-γ production from NK cells though non-canonical STAT4 signalling[318], we next assessed whether IFN-γ could be induced at 6h in response (**Fig3.14**). Surprisingly at 6h, unlike 24h, IFN-α in combination with IL-18 induced modest IFN-γ from MAIT cells stimulated in the absence of APC (5.4±1.1%, p <0.05; **Fig3.14 B**). In contrast stimulation with IL-12, a canonical inducer of STAT4 in combination with IL-18 only induced potent APC-independent IFN-γ from MAIT cells at 24h but not at 6h (26.3±6% 24h; 0.4±0.1% 6h; **Fig3.14 B**). Both cytokine combinations were potent MAIT-cell IFN-γ inducers in PBMCs (**Fig3.14 B**). Therefore, type I IFN-dependent MAIT cell IFN-γ at 24h but not 6h required the presence of accessory cells found in PBMC. IL-12 cytokine combinations were potent in enriched CD8 at 24h, therefore APC-derived factors were only specifically required to maintain roust type I IFN-dependent MAIT activation beyond 6h.

Figure 3.14 | Type I interferon induced MAIT cell IFN-γ at 6h in the absence of accessory cells.

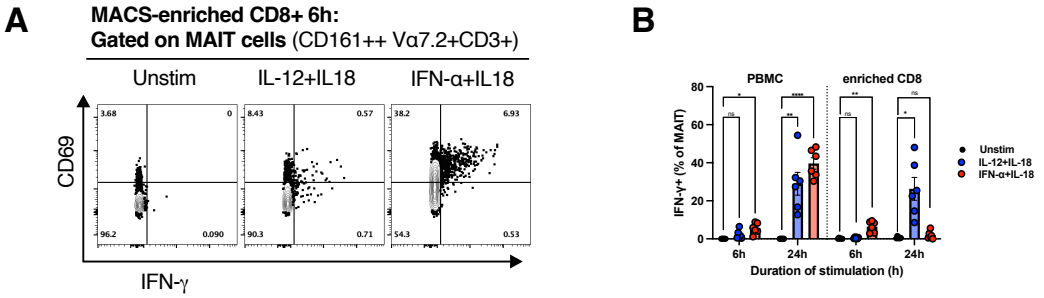

Fig3.14 | Type I interferon induced MAIT cell IFN-γ at 6h in the absence of accessory cells.
MAIT cell (CD161++ Vα7.2+) activation (IFNγ) was assessed 6h or 24h after cytokine stimulation of cryopreserved PBMC or MACS enriched CD8+ cells with IFN-α2 + IL-18, or IL-12 and IL-18 (all 50ng/ml).
(A) Representative plots gated on MAIT cells 6h after cytokine stimulation of enriched CD8.
(B) MAIT cell expression of IFN-γ measured 6h and 24h after stimulation of PBMC or enriched CD8 with IL-12+IL18 (blue) or IFNα+IL18 (red).
Symbols indicate individual donors (n=6, pooled 3 across 3 separate experiments). Mean ±SEM shown.
*p < 0.05; **p < 0.01; ***p < 0.001; ****p < 0.0001; ns, not significant. Statistical significance was determine using two-way ANOVA with Dunnett's multiple comparison's test.

3.3.5 APC-derived factor is sufficient to sustain type I IFN-induced MAIT cell IFN-γ

We then explored which specific cell types produce factors able to support IFN-dependent MAIT-activation. We found that addition of monocytes to enriched CD8+ cells augment MAIT activation in response to IFN-α and IL-18 (**Appendix SF3.4**, *data Nicholas Provine*). Conditioned supernatant from autologous enriched monocytes treated with IFN-α for 24h also phenocopies the addition of monocytes - meaning a cell derived factor is sufficient to promote MAIT activation (**Appendix SF3.4**, *data Nicholas Provine*).

For further experiments, we explored the hypothesis that any PBMC-derived factors must be produced very early to sustain MAIT activation at 24h. Therefore, we stimulated enriched CD8+ T cells with cytokines in combination with supernatant from monocytes treated for only 4h with IFN-α, or rested as controls (**Fig3.15 A**). Surprisingly, CD14+ cell IFN-α treatment was not essential, and supernatants from CD14+ cells rested for 4h was sufficient to induce potent MAIT cell IFN-γ in response to IFN-α and IL-18 stimulation (**Fig3.15 B**). In the absence of cell culture supernatant (R10), MAIT cells did not induce significant IFN-γ at 24h in response to IFN-α+IL-18 (3.2±0.7%, $p > 0.05$; **Fig3.15 B**), but responded robustly to IL-12+IL-18 (42.2±11%, **Fig3.15 C**). The addition of supernatants from CD14+ monocytes rested for 4h had no impact on MAIT cell IFN-γ in response to IL-12+IL-18 (42±10%; **Fig3.15 C**), but did induce substantial IFN-γ from MAIT cells in response to IFN-α+IL-18 (30.6±6.7%; **Fig3.15 B**). Therefore, soluble mediators derived rapidly from CD14+ selected cells are sufficient to sustain IFN-α+IL-18 induced MAIT cell IFN-γ in the absence of APCs.

To confirm cell specificity, accounting for the impact of cell number and MACS-depletion, supernatants from rested PBMC (without MACS-depletion), and CD8+ MACS-enriched cells were compared to that of CD14+ cells (100,000 each) rested for 4h. Only CD14+

selected cells or PBMC supernatant, but not CD8+ cell supernatant could induce APC-independent MAIT cell IFN-γ in response to IFN-α and IL-18 (CD8 supernatant, 2.9±1.3; CD14+ supernatant 54.2±7.5%; PBMC supernatant 56±0.6%; **Fig3.15 D**). Again, cell supernatants had no impact on IL-12+IL-18 stimulation (**Fig3.15 E**), again implying APC-derived factors are specifically required for type I IFN-dependent MAIT cell activation.

Figure 3.15 | A monocyte derived factor is specifically required for IFN-α-dependent MAIT cell activation in the absence of APC at 24h.

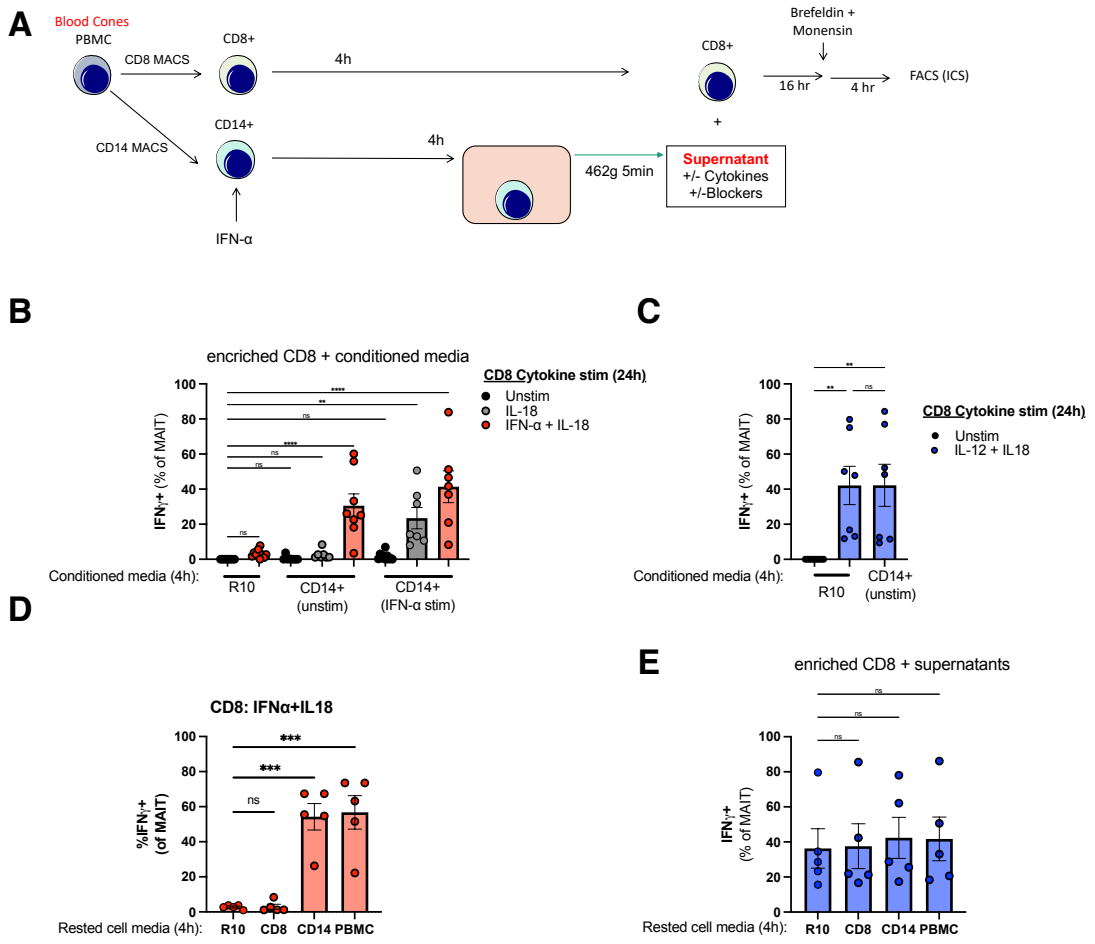

Fig3.15 | A monocyte derived factor is specifically required for IFNα-dependent MAIT cell activation in the absence of APC at 24h.
(A) Experimental schematic. Cryopreserved PBMC were MACS-enriched for CD14+ and CD8+ cells, or untreated. Conditioned media was generated using enriched CD14+, CD8+, or whole PBMC which were either untreated or stimulated with IFNα2 (50ng/ml), prior to incubation for 4h. Cell supernatants (or control incubated R10) were then added to autologous CD8+ cells incubated simultaneously for 4h. MAIT cell activation (CD69, IFN-γ, GzmB) was measured after 24h of stimulation with either IL-18 (grey, 50ng/ml), IFN-α+IL18 (red, 50ng/ml each), IL-12+IL-18 (blue, 50ng/ml each), or unstimulated control.
(B, C) MAIT IFNγ expression 24h after stimulation of enriched CD8 with conditioned CD14+ media in addition to IL-18, or IFNα+IL-18 (**B**), or IL-12+IL18 (**C**). (n=8-10 donors, pooled across experiments)

(D, E) Enriched CD8+ cells were stimulated with IFNα+IL-18 in addition to supernatants of rested CD8+, CD14+ cell or PBMC. MAIT cell IFNγ expression 24h after stimulation of enriched CD8 with rested cell-type specific media in addition to IFNα+IL-18 (**D**), or IL-12+IL18 (**E**). (n=5 donors)

Symbols indicate individual donors. Mean ±SEM shown.
*p < 0.05; **p < 0.01; ***p < 0.001; ****p < 0.0001; ns, not significant. Statistical significance was determine using ordinary one-way ANOVA with Dunnett's (B), or Tukey's (C) multiple comparison's test, or repeated measures one-way ANOVA with Dunnett's multiple comparison's test (D, E).

To identify factors induced by CD14+ monocytes necessary for type I IFN-dependent innate-like lymphocyte activation we next sought to understand the impact of type I IFN on monocytes in vitro with the hypothesis that indirect effects of type I IFN on monocytes during an antiviral response would be crucial secondary signals to bridging innate-like lymphocytes.

Having observed a reduction in monocyte frequency in response to ChAdOx1-GFP in vitro (data not shown), we tested whether stimulation of PBMC with type I IFN alters innate cell frequency. IFN-α reduced the frequency of total live cells in PBMC (**Fig3.16 A**), with a reduction in CD14+ cells as a fraction (**Fig3.16 B**). Among classical and intermediate monocytes, there was a dose-dependent reduction in surface CD14 expression within each subset in response to IFN-α (**Fig3.16 D, E**). Conversely HLA-DR expression peaked at 10ng/ml but was reduced at supra-physiological concentrations (**Fig3.16 F**). Type I IFN can induce MHC class I and class II expression, therefore the reduction in GMFI at high concentrations may be the consequence of increased cell death or shedding of MHC molecules. The reduction in expression was likely not entirely down regulation - as similar results for CD14 and HLA-DR were observed after intracellular staining (data not shown), which supports prior observations of CD14 shedding in response to viral infections with concordant increase in soluble CD14[319]. Both total CD14 and CD123 expression were reduced in PBMC because of type I IFN stimulation (representative plots, **Fig3.16 G, H**).

Figure 3.16 | Type I interferon alters the composition of PBMC, with a reduction in CD14+ cells.

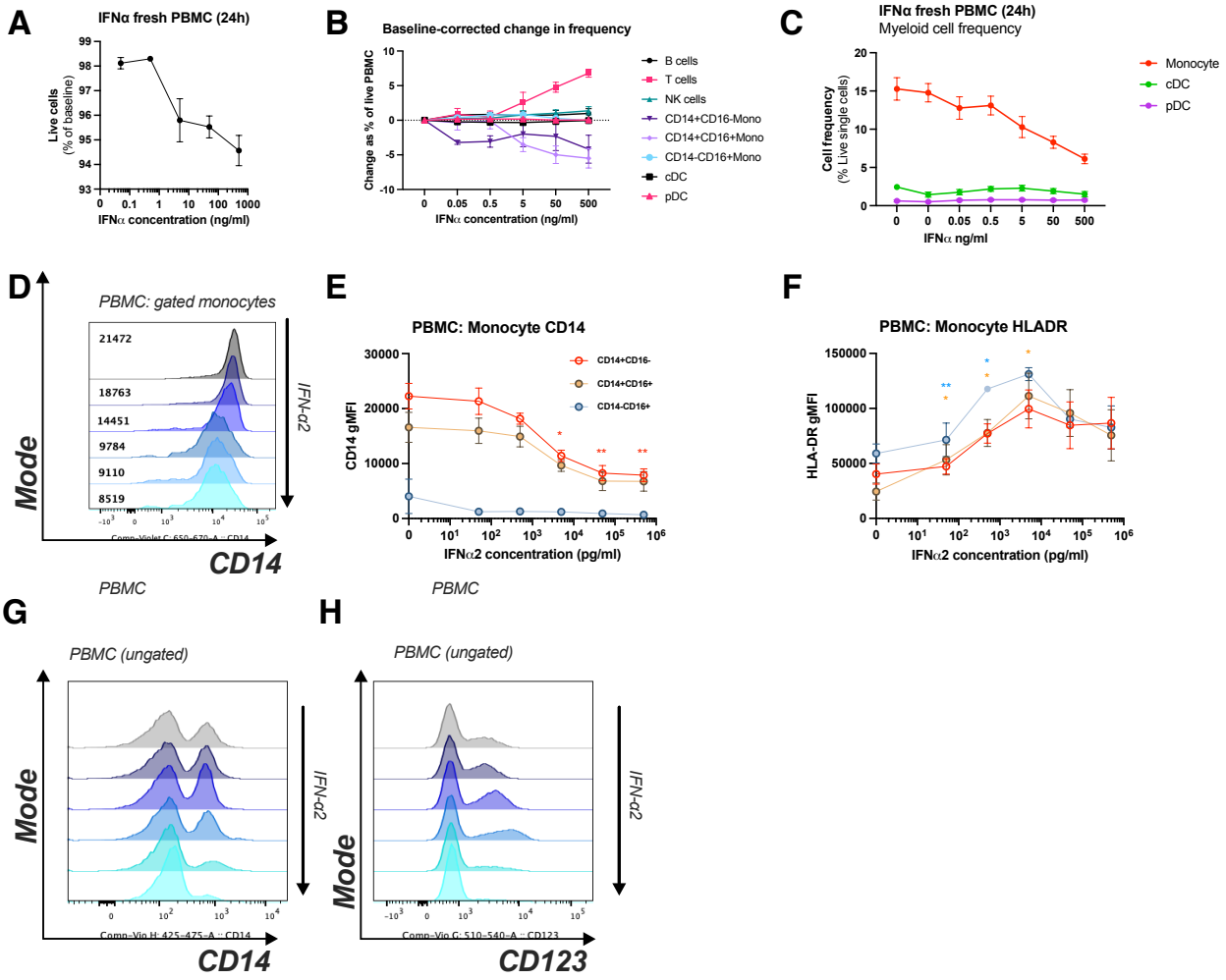

Fig3.16 | Type I interferon alters the composition of PBMC, with a reduction in CD14+ cells.
Fresh PBMC were phenotyped at baseline and 24h after stimulation with increasing concentrations of IFN-α2.
(A) Frequency of live cells after 24h
(B) Change of immune cell frequency as a fraction of total PBMC at 24h compared to baseline.
(C) Frequency of myeloid cells (CD3/19/56-, HLADR+) as percentage of PBMC.
(D) Representative histogram of CD14 expression on monocytes after IFNα titration.
(E, F) Expression of CD14 (E), and HLA-DR (F), on monocyte subsets at 24h after IFNα titration.
(G, H) Representative histograms of CD14 (G) and CD123 (H) expression in PBMC 24h after IFNα titration.

Symbols indicate individual donors. Mean ± SEM is shown. Data were acquired from (n=5) donors, from two independent experiments.
*p < 0.05; **p < 0.01; ***p < 0.001; ****p < 0.0001; ns, not significant
Statistical significance was determined using two-way ANOVA with Dunnett's multiple comparison's test (E,F)

We next assessed the impact of IFN-α on MAC-enriched CD14+ monocytes. As monocyte function can be altered after freeze-thaw, fresh and cryopreserved PBMC were compared (**Fig3.17**). Similar to results from fresh unfractionated PBMC, IFN-α2 induced dose dependent cell death (**Fig3.17 B**), and loss of CD14 expression (**Fig3.17 C**). A similar peak in HLA-DR expression was observed after IFN-α titration, with reduction thereafter (**Fig3.17 D**).

Figure 3.17 | Type I interferon induces cell death and reduced CD14 expression in enriched monocytes.

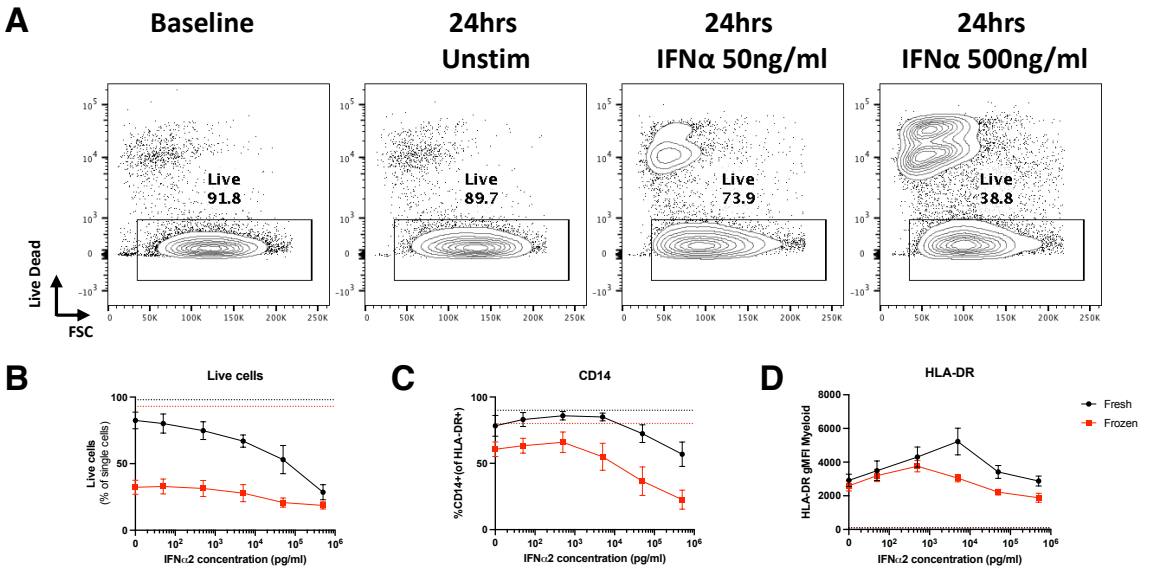

Fig3.17 | Type I interferon induces cell death and reduced CD14 expression in enriched monocytes.
CD14+ monocytes were MACS enriched from fresh or thawed PBMCs and phenotyped at baseline and after 24h stimulation with increasing concentrations of IFNα.
(A) Representative FACS plots of live cells as a fraction of total single cells measured at baseline and 24h after stimulation of fresh CD14 positive cells.
(B) The percentage of live cells as a fraction of total single cells after IFNα stimulation.
(C) The percentage of CD14+ cells as a fraction of total HLA-DR+ cells after IFNα treatment.
(D) HLA-DR expression (GMFI) in live myeloid cells IFNα treatment.
Symbols indicate individual donors. Mean ± SEM is shown. Data were acquired from (n=4) donors, from separate experiments.
*p < 0.05; **p < 0.01; ***p < 0.001; ****p < 0.0001; ns, not significant
Dotted lines represent mean baseline live cell frequency (B), or CD14 expression (C) for fresh (black) or frozen (red) cells.

In addition to surface activation markers, we next assessed whether IFN-α could stimulate relevant monocyte cytokine production for innate-like lymphocyte activation. We stimulated CD14+ cells with IFN-α, using both fresh and cryopreserved monocytes, and measured concentrations of cytokines in supernatants at 24h (**Fig3.18 A, B)**. TNF was clearly the dominant cytokine secreted by fresh enriched CD14+ cells in response to IFN-α (**Fig3.18 C**). There was no difference depending on the freeze-thaw status of PBMC used (**Fig3.18 D**). Other cytokines induced included IL-1β (**Fig3.18 E**), GM-CSF (**Fig3.18 F**), IL-6 (**Fig3.18 G**), IL-10 (**Fig3.18 H**), IL-12p70 (**Fig3.18 I**), and IL-23 (**Fig3.18 J**).

It is difficult to be certain however if these cytokines are released in response to type I IFN alone, or if combination with weak CD14 triggering from magnetic-bead enrichment contributes. Potent LPS induced IL-12p70 and IL-23 secretion from human monocytes is due to synergy between TLR4 and type I IFN signalling[320].

We therefore finally confirmed that TNF could be produced after type I IFN stimulation of untouched fresh PBMC by flow cytometry, comparing with IFN-γ (**Fig3.19**). Both IFN-α and IFN-γ induce TNF from whole PBMC at 8h but not 24h (**Fig3.19 A, B**); IFN-α was more potent, with 14.2±3.2% of SSC-hi monocytes producing TNF at 8h (**Fig3.19 C, D**), compared to more modest production in response to IFN-γ (2.5±0.6%; **Fig3.19 D**).

Therefore, type I IFN induces substantial TNF production from monocytes at early time points which could act as a secondary signal to innate-like lymphocytes for activation in response to viruses and ChAdOx1.

Figure 3.18 | Type I interferon induces cytokines, in particular TNF, from enriched monocytes

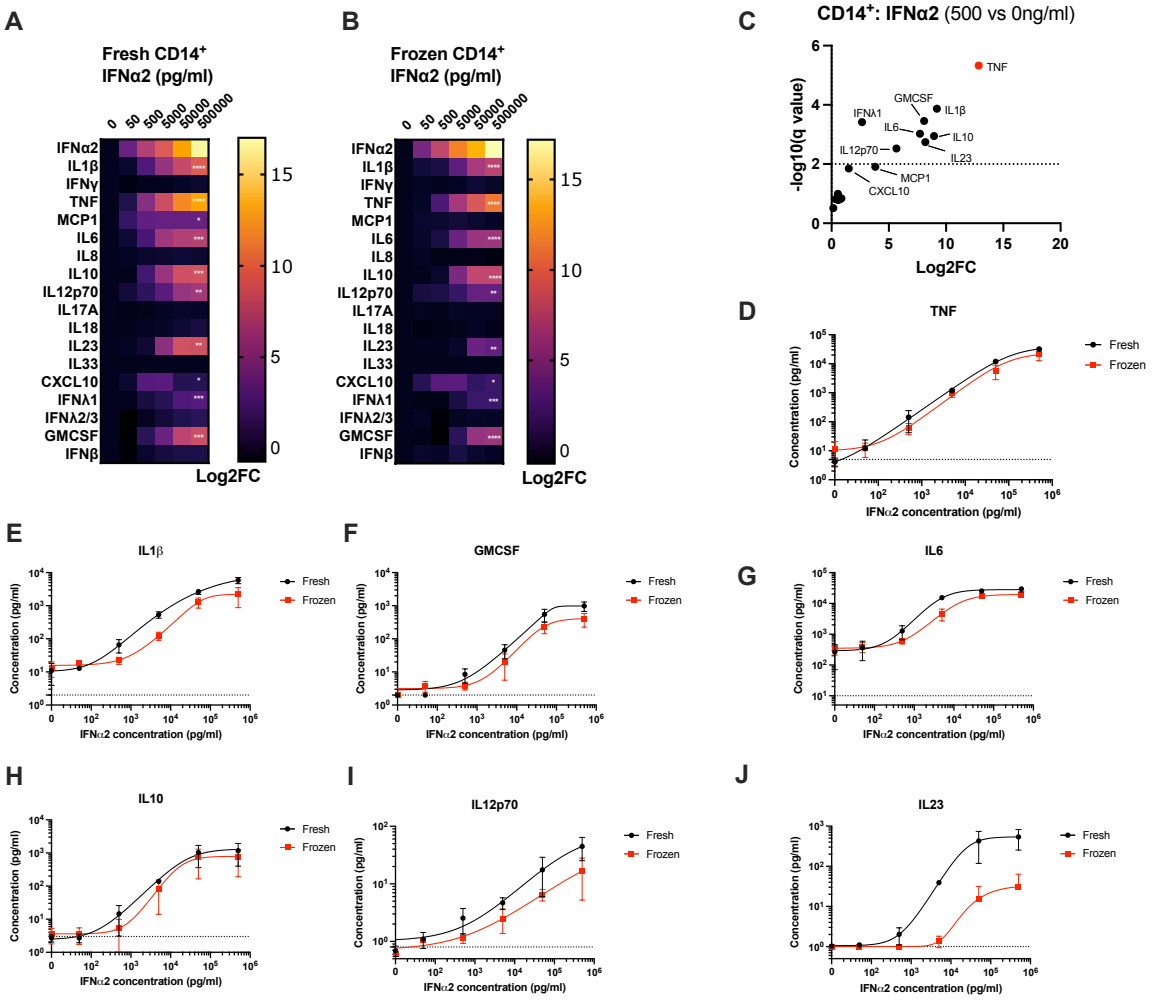

Fig3.18 | Type I interferon induces cytokines, in particular TNF, from enriched monocytes .
CD14+ monocytes were MACS enriched from fresh or thawed PBMCs and stimulated with increasing concentrations of IFNα. Supernatants after 24h were assays for cytokines indicated.
(A, B) Heat map of median log2 fold change in secreted cytokines relative to unstimulated controls from CD14+ monocytes enriched from fresh (A), or frozen (B), PBMCs and stimulated with increasing IFNα (n=4, same donors used after cryopreservation).
(C) Volcano plot of log2 fold change in secreted cytokines in response to 500ng/ml IFN-α.
(D-J) Titration curves with non-linear regression comparing indicated secreted cytokines in supernatants. Data were acquired from (n=4) donors, from separate experiments.
*p < 0.05; **p < 0.01; ***p < 0.001; ****p < 0.0001; ns, not significant
Dotted lines limit of detection.
Statistical significance was determined using multiple unpaired t-tests of log2 transformed cytokine concentrations, with Benjamini, Krieger, & Yekutieli correction for multiple comparisons (A-C).

Figure 3.19 | Interferons induce TNF at early timepoints only in PBMC from monocytes.

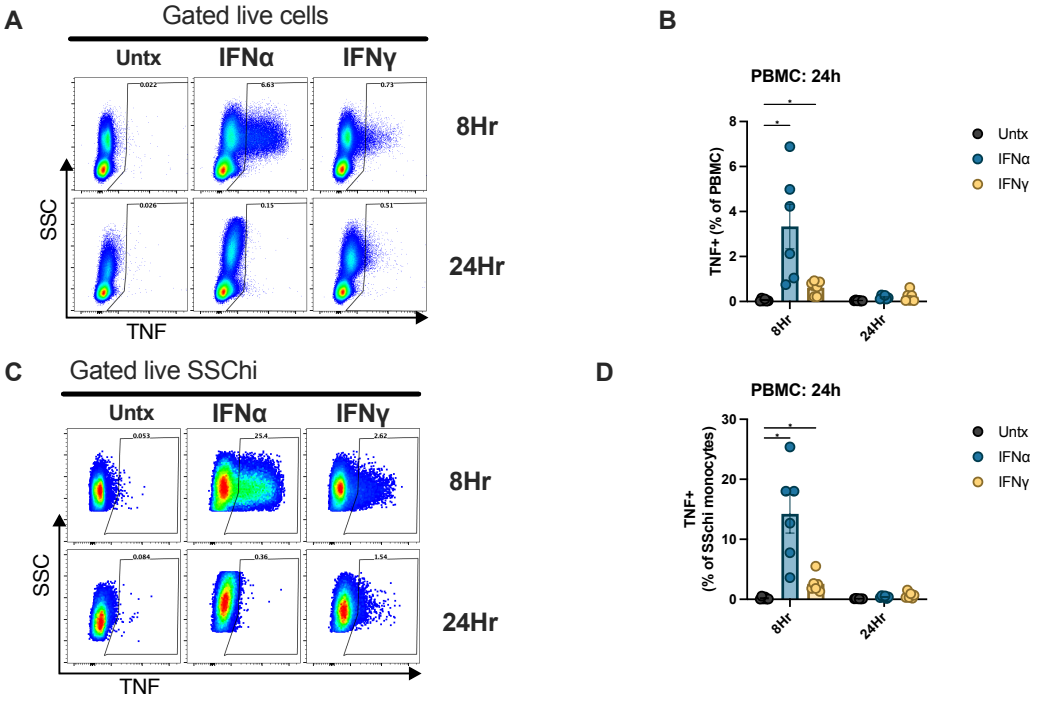

Fig3.19 | Interferons induce TNF at early timepoints only in PBMC from monocytes.
Fresh PBMC were stimulated with IFN-α2 or IFN-γ (50ng/ml) for 8h or 24h, and TNF measured in PBMC by flow cytometry. Monocytes were defined as CD3/CD161/CD19-, SSChi).
(A, B) Representative plots gated on live PBMC (A), and summary TNF expression in response to IFNα and IFNγ at 8h and 24h.
(C,D) Representative plots gated on SSChi monocytes (C), and summary TNF expression in response to IFNα and IFNγ at 8h and 24h (D).
Data were acquired from (n=6) donors, from two separate experiments.
***p < 0.05; **p < 0.01; ***p < 0.001; ****p < 0.0001; ns, not significant
Mean±SEM shown.
Statistical significance was determined using two-way ANOVA with Dunnett's multiple comparison's test (B,D).

3.3.6 TNF augments type I IFN-dependent MAIT cell IFN-γ

Given the significant induction of TNF by monocytes in response to IFN-α, we explored the hypothesis that TNF is an intermediary signal able to directly augment type I IFN mediated MAIT activation.

TNF signals though TNFR1 (CD120a) and TNFR2 (CD120b) [321]. All cells express TNFR1, and MAIT cells have been shown to express both TNFR1 and TNFR2, with TNFR2 upregulated after E.coli induced MAIT cell activation[283]. Furthermore, TNF blockade reduces MAIT cell activation in response to antibody opsonised E.coli [322].

We first confirmed that MAIT cells do express both TNFR1 and TNFR2, thus had the capacity to directly receive TNF signalling in response to ChAdOx1 (**Fig3.20 A, B**). At rest, human MAIT cells and CD161+ T cells express slightly higher TNFR2 than conventional CD161- T cells; this is significantly less than Tregs (**Fig3.20 B,C**), with 50% of CD25hiFoxp3+CD4+ human T cells known to express TNFR2[323]. We asked whether antiviral cytokines could induce MAIT cell TNFR2 expression in PBMC, using E.coli as a positive control given published data (**Fig3.20 D, E**)[283]. At 24h ~40% of MAIT cells express TNFR2 in response to E coli (**Fig3.20 E**). IFN-α stimulation of PBMC alone however also was an equally potent inducer of MAIT TNFR2 expression in untouched PBMC (**Fig3.20 E**). Comparing a range of stimuli, including predominantly TCR and cytokine mediated activation, all induced upregulation of TNFR2 (**Fig3.20 F**). The highest TNFR2 expression at 24h was with cytokine combinations; IFN-α+IL-18 induced TNFR2 expression in ~80% of MAIT cells after 24h (**Fig3.20 F, G**). The fraction of cells expressing TNFR2 subsided by 72h, although ~50% still expressed TNFR2 across stimuli implying that once activated MAIT cells retain TNF responsiveness which may regulate their effector functions (**Fig3.20 H**).

In response to antiviral cytokines IFN-α+IL-18, the majority of MAIT cells expressed TNFR2, contributing to the total TNFR2+ population in PBMC (**Fig3.20 I-K**). In the absence of stimulation over 95% of TNFR2 positive cells were monocytes, with Treg the dominant TNFR2+ lymphocytes. However, after IFN-α+IL-18 stimulation ~4% of lymphocytes were TNF responsive and expressed TNFR2; most of these were NK cells, MAIT cells and CD161+ T cells (**Fig3.20 K**). However, IFN-α induced MAIT cell TNFR2 expression in PBMC could be an indirect consequence of APC-dependent processes (**Fig3.20 E**). We therefore tested whether IFN-α stimulation of enriched CD8+ cells could directly induce TNFR expression in MAIT cells. Combination with IL-12 was also tested given this was an IFN-dependent cytokine in CD14+ monocytes, with combinations of cytokines again required to induce TNFR2 expression in MAIT cells directly (**Fig3.20 L**).

These data suggest that MAIT cells during an in vivo antiviral response would be poised to respond to TNF.

Figure 3.20 | MAIT cells express TNFR2, which is potently up-regulated by antiviral cytokines.

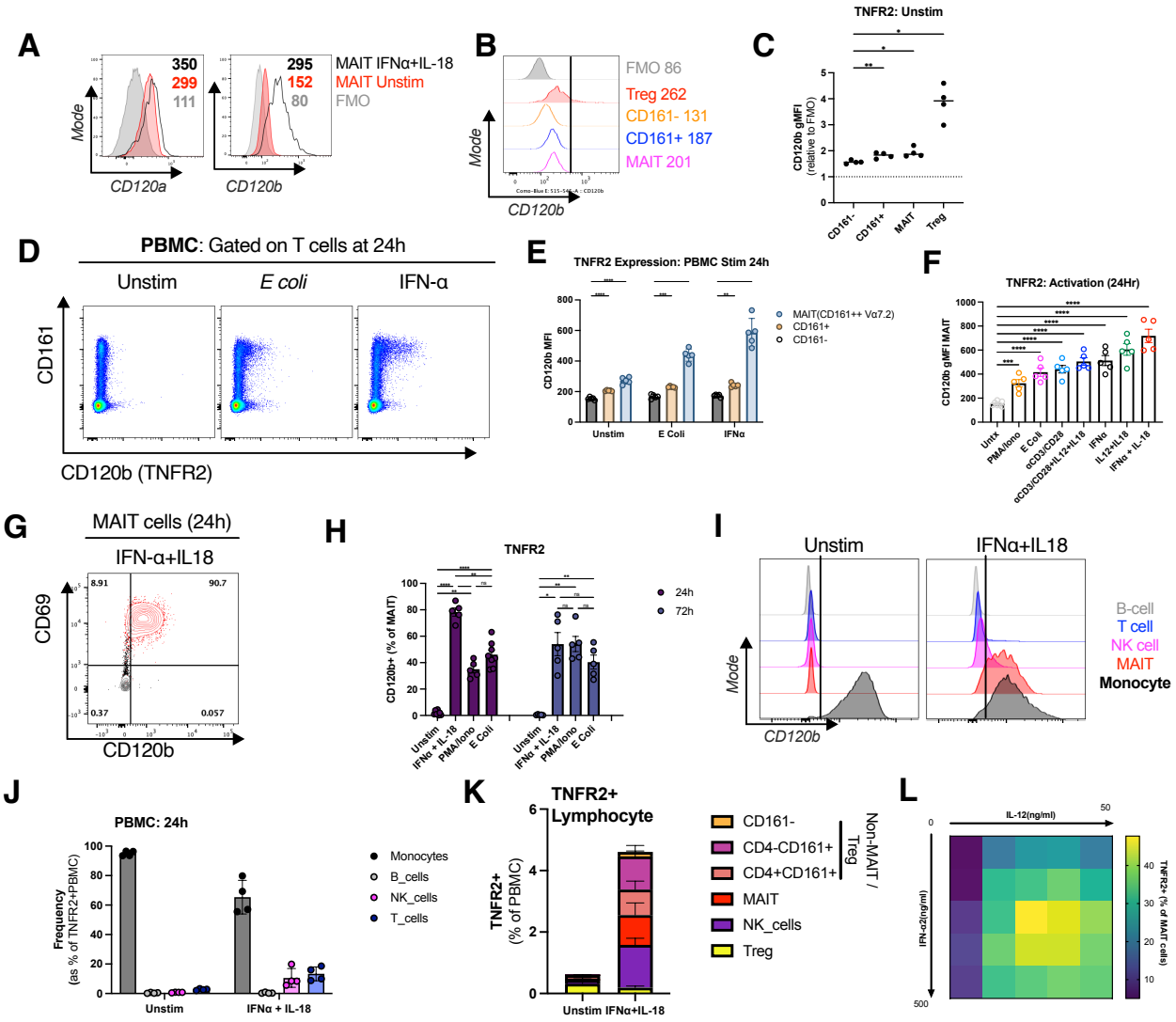

Fig3.20 | MAIT cells express TNFR2, which is potently up-regulated by antiviral cytokines.
Fresh PBMC were either stained at baseline, or after stimulation with cytokines (50ng/ml each), fixed E.coli (25BpC), or TCR-mediated activation using plate bound αCD3 (2.5µg/ml) and soluble αCD28 (1µg/ml), or PMA(20ng/ml)/ ionomycin(1µM). Expression of TNFR1 (A), and TNFR2 (A-K), was assessed on: MAIT cells (CD161++Vα7.2+ T cells), conventional T cells, including Treg (CD4+CD25+CD127-), B cells (CD19+), NK cells (CD3/19-, CD56+ lymphocytes), and monocytes (lin-/CD14+).
(A) Representative histograms for expression of CD120a (TNFR1) and CD120b (TNFR2) on unstimulated and activated MAIT cells compared to FMO.
(B) Representative histograms for expression of TNFR2 on T cell populations (with GMFI indicated).
(C) Expression of CD120b for Treg, CD161-, CD161+ and MAIT cells as fold change in GMFI relative to cell specific FMO.
(D, E) Representative plot gated on T cells, and summary MAIT TNFR2 expression **(E)** 24h after stimulation with E coli or IFN-α.
(F) Summary expression of CD120b on MAIT cells 24h after stimulation with cytokines indicated.
(G) Representative plot of CD120b expression gated on MAIT cells 24h after IFNα+IL-18 stimulation.
(H) Summary CD120b expression on MAIT cells 24h and 72h after stimulation with IFNα+IL-18, PMA/ionomycin, or E.coli.
(I) Summary of CD120b expression on cell types after IFNα+IL-18 stimulation.
(J) Frequency of each immune cell type among total TNFR2+ cells 24hr after IFNα+IL-18 stimulation.
(K) Frequency of live cells which are TNFR2+ non-lymphocytes, with specific subtypes outlined.
(L) Enriched CD8+ cells with stimulated with various increasing concentrations of IFNα+IL-12, measuring CD120b on MAIT cells after 24h. Heatmap showing mean CD120b expression. Data were acquired from n=4 (A-C; J-K), n=5 (D-E, H) or n=2 (L) donors pooled from at least 2 separate experiments.*p < 0.05; **p < 0.01; ***p < 0.001; ****p < 0.0001; ns, not significant. Mean±SEM shown. Statistical significance was determined using repeated measures one-way ANOVA with Dunnett's multiple comparison's test (C, F); two-way ANOVA with Dunnett's (E), or Tukey's multiple comparison's test (H).

As MAIT cells could theoretically respond to TNF through TNFR expression, we next sought to address whether APC-derived TNF has any impact on cytokine induced MAIT cell activation using clinical monoclonal inhibitors of TNF signalling[324]: Adalimumab (full human IgG1, ADA) and Etanercept (TNFR2–Fc fusion protein, ETN). IFN-containing cytokine combinations (IFN-α+IL-18, IFN-α+IL-12) are APC, and thus potentially TNF-dependent. These were compared to IL-12+IL-18 stimulation which robustly activates MAIT cells in enriched CD8. Pre-treatment with Adalimumab or Etanercept, but not control Vedolizumab (human anti-integrin α4β7 monoclonal), reduced the capacity for IFN-α containing cytokine combinations to trigger MAIT cell IFN-γ at 24h; IFN-γ production in response to IFN-α in combination with IL-18 or IL-12 was reduced over 3-fold (39±3% vs 10±2% (ADA), IFN-α+IL-18; 51±6% to 15±3%(ADA), IFN-α+IL-12; **Fig3.21 A, B**), compared to more modest reduction of IL-12+IL-18 activation (29±6% vs 19±5%; **Fig3.21 A, B**). Triggering of IFN-γ was specifically inhibited, with GzmB (**Fig3.21 C**) and CD69 (**Fig3.21 D**), not significantly reduced by anti-TNF. Similar reduction of triggering in Vδ2+ T cell (**Fig3.21 E**) and CD161+NK cell was also observed (**Fig3.21 F**), although the impact of TNF blockade was more modest in NK cells.

Next we assessed whether TNF inhibition had any impact on IFN-γ at very early time points (6h), which was APC independent in response to type I IFN combinations (**Fig3.21 E**). Both IFN-α+IL-18, and IFN-α+IL-12 stimulation of PBMC induced MAIT cell IFN-γ at 6h, which was not inhibited with TNF blockade (**Fig3.21 I, J**). The magnitude of IFN-γ at 6h did not increase at 24h in response to IFN-α+IL-18 (**Fig3.21 K**), suggesting that although the very earliest IFN-γ produced from MAIT cells is APC and TNF independent, TNF signalling is required to amplify and sustain responses in PBMC.

The lack of impact of TNF blockade on early (6h) MAIT cell responses after cytokine stimulation of enriched CD8 T cells further supported the conclusion that early cytokine induced activation was TNF-independent (**Fig3.21 L-M**). No statistically significant change

in late (24h) IL-12+IL-18 induced IFN-γ was observed with TNF inhibition, although a trend to reduction was observed in high responders (24.6±6.8% vs 15.6±4.2%; p = 0.065, **Fig3.21 P**). Given the modest inhibition of IL-12+IL-18 dependent stimulation in PBMC (**Fig3.21 B**), it is possible that TNF from both CD8 T-cell and non-CD8+ T-cells could play some role in cytokine induced MAIT activation more broadly.

Figure 3.21 | Anti-TNF inhibits late but not early IFN-dependent MAIT cell activation in unfractionated PBMC.

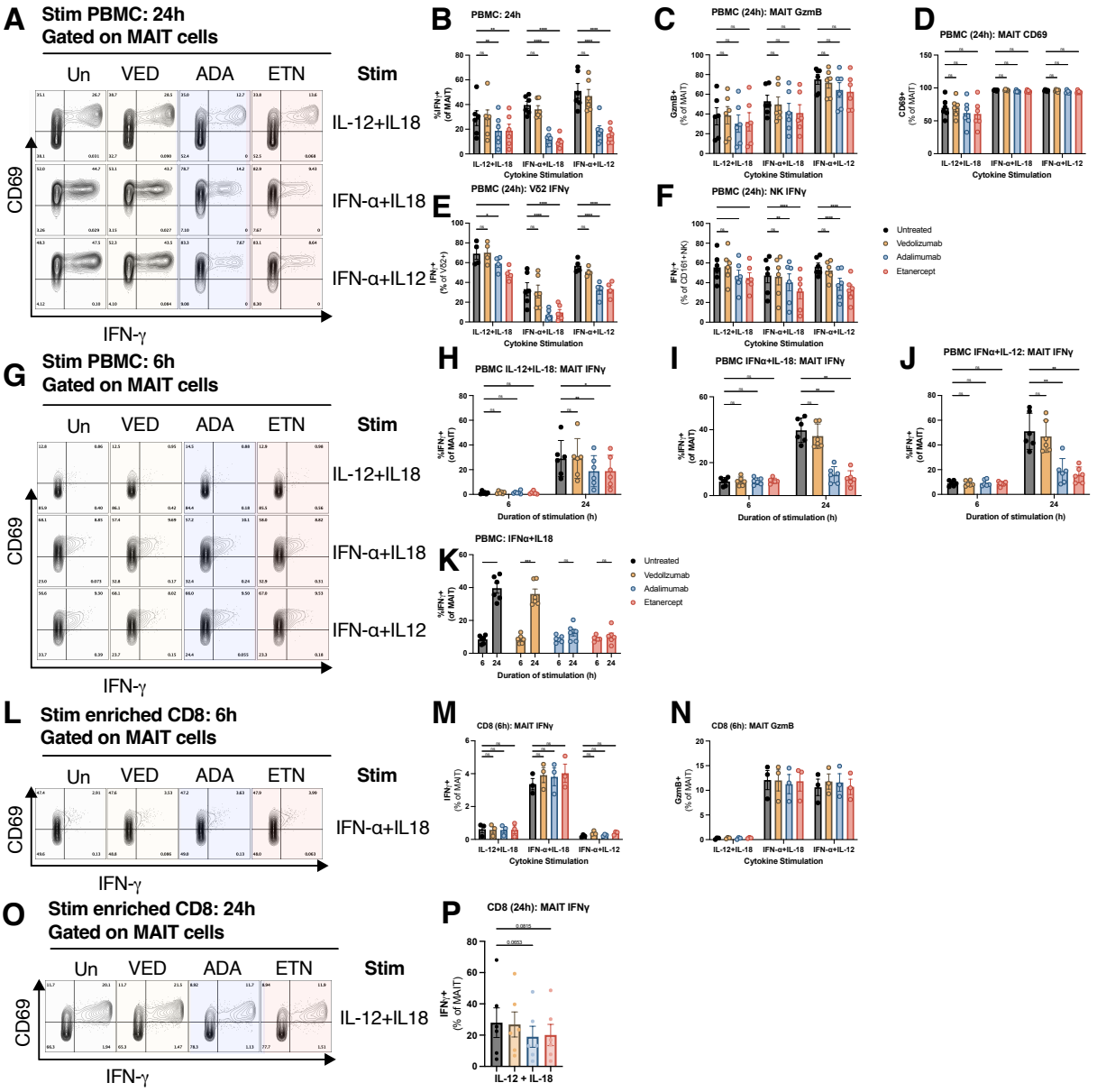

Fig3.21| Anti-TNF inhibits late but not early IFN-dependent MAIT cell activation in unfractionated PBMC.
Cryopreserved human PBMC (**A-K**), or MACS-enriched CD8+ cells (**L-P**) were stimulated with either IL12+IL18 (50ng/ml), IFNα+IL18 (50ng/ml) or IFNα+IL12 (50ng/ml). Adalimumab (anti-TNF antibody; 10μg/ml), Etanercept (TNFR2-Fc fusion protein, 10μg/ml) or Vedolizumab (anti-α4β7 integrin, 10μg/ml) were added prior to cytokines. Activation (CD69, GzmB, IFNγ) was measured on MAIT cells (CD161++Vα7.2+), Vδ2+ T cells (E), or CD161+CD56+ NK cells (F) at 24hr (A-K, O-P), or 6h (H-N).
(A-D) Representative flow plot gated on MAIT cells(A), and summary IFNγ (B), GzmB (C), and CD69 (D) expression after PBMC stimulation with cytokines and inhibitors for 24h.
(E,F) IFNγ expression on Vδ2+ (E), and CD161+NK cells (F) after PBMC stimulation with cytokines and inhibitors for 24h.
(G) Representative flow plot gated on MAIT cells 6h after stimulation of PBMC.
(H-K) IFNγ expression on MAIT cells at 6h and 24h after stimulation with IL-12+IL-18 (H), IFNα+IL-18 (I, K), or IFNα+IL-12.
(L-N) Representative flow plot gated on MAIT cells (L), and summary IFNγ (M), GzmB (N), expression after CD8 stimulation with cytokines and inhibitors for 6h.
(O,P) Representative flow plot gated on MAIT cells(O), and summary IFNγ (P) expression after CD8 stimulation with IL-12+IL-18 and inhibitors for 24h.
Symbols indicate individual donors with summary mean ± SEM shown. *p < 0.05; **p < 0.01; ***p < 0.001; ****p < 0.0001; ns, not significant. Data were acquired from (n=4-6) donors in 2 experiments.
Statistical differences were calculated using two-way ANOVA with Dunnett's multiple comparison's test (B-N), or repeated measures one way ANOVA with Dunnett's correction (P).

To test whether TNF from non-type I IFN-dependent sources could augment MAIT cell IFN-γ, we tested whether TNF blockade could reduce TCR-induced MAIT activation, comparing IFN-α+IL-18, E.coli and PMA/ionomycin triggering (**Fig3.22**). Fresh human PBMC were used to assess if previous findings for IFN-α and IL-18 were generalisable, with Adalimumab and Etanercept again particularly inhibiting MAIT cell IFN-γ in response to IFN-cytokine triggering (~3-fold, **Fig3.22 B, C**). E coli induced MAIT cell IFN-γ was also inhibited, with no impact on PMA/ionomycin triggering (**Fig3.22 B**). E coli induced TLR4 signalling can trigger type I IFN [320], and inhibition of type I IFN signalling modestly reduces MAIT cell activation response to E coli[325]. Therefore, MAIT cell triggering dependent on IFN-α also requires TNF signalling, which can be produced early as an indirect consequence of monocyte IFN-triggering (**Fig3.19**).

The experiments so far showed that inhibition of TNF can reduce MAIT-cell IFN-γ in response to antiviral cytokines. To determine if TNF could augment MAIT cell responses in PBMC, we tested the impact of recombinant TNF, which has a very short half-life (30min). We therefore also tested a monoclonal TNFR2 agonist antibody[326], given that TNFR2 was upregulated to prime responsiveness after in vitro IFN-α stimulation. Although neither TNF nor TNFR2 agonist induce MAIT cell activation alone, the combination of TNFR2 agonist with IFN-α augments IFN-γ at 24h by ~3-fold (6.9%; 18.4%; **Fig3.23 A, B**); no change in GzmB (**Fig3.23 C**) or CD69 expression was observed (**Fig3.23 D**). The impact on IFN-α and IL-18 triggering was similar, with TNF-specific augmentation not observed in the absence of type I IFN triggering (**Fig3.23 B**). Agonism of TNFR1, or antagonism of TNFR2 using commercially available inhibitors had no significant impact on MAIT cell IFN-γ (**Fig3.23 E**). Furthermore, TNFR2 agonism did not alter very early (6h) responses (**Fig3.23 F**).

Figure 3.22 | Anti-TNF inhibits IFN-α and E.coli induced MAIT cell activation in fresh PBMC.

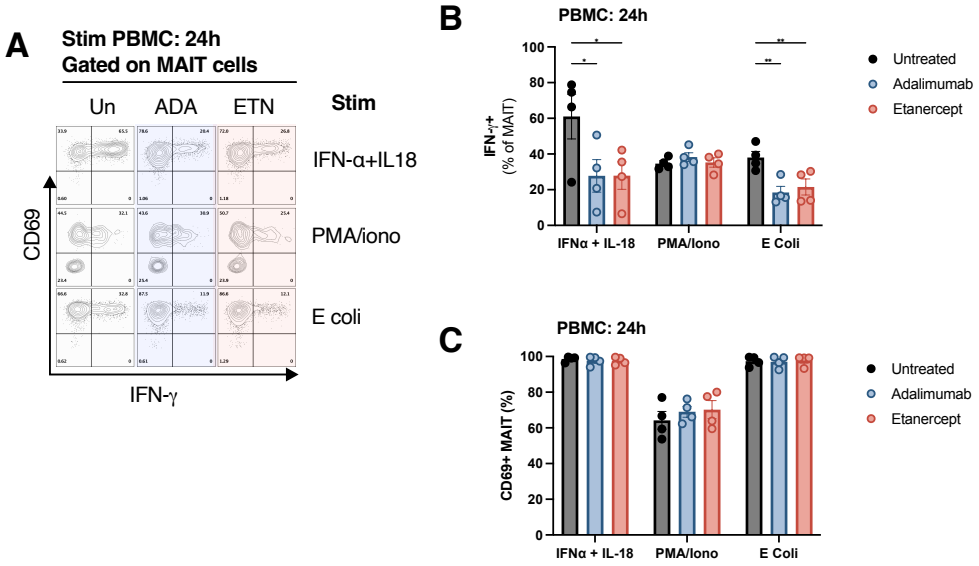

Fig3.22| Anti-TNF inhibits IFNα and E.coli induced MAIT cell activation in fresh PBMC.
Fresh human PBMC (**A-C**) were stimulated with either IFNα+IL18 (50ng/ml) or E coli (25BpC). Adalimumab (anti-TNF antibody; 10µg/ml) or Etanercept (TNFR2-Fc fusion protein, 10µg/ml) were added prior to cytokines. Activation (CD69, GzmB, IFNγ) was measured on MAIT cells (CD161++Vα7.2+).
(A-C) Representative flow plot gated on MAIT cells(A), and summary MAIT cell IFNγ (B), and CD69 (C) expression after PBMC stimulation with inhibitors for 24h.

Symbols indicate individual donors with summary mean ± SEM shown.
*p < 0.05; **p < 0.01; ***p < 0.001; ****p < 0.0001; ns, not significant.
Data were acquired from (n=4) donors.
Statistical differences were calculated using two-way ANOVA with Dunnett's multiple comparison's test (B-C).

Figure 3.23 | TNFR2 agonism increases type I IFN-dependent MAIT IFN-γ in PBMC at 24h.

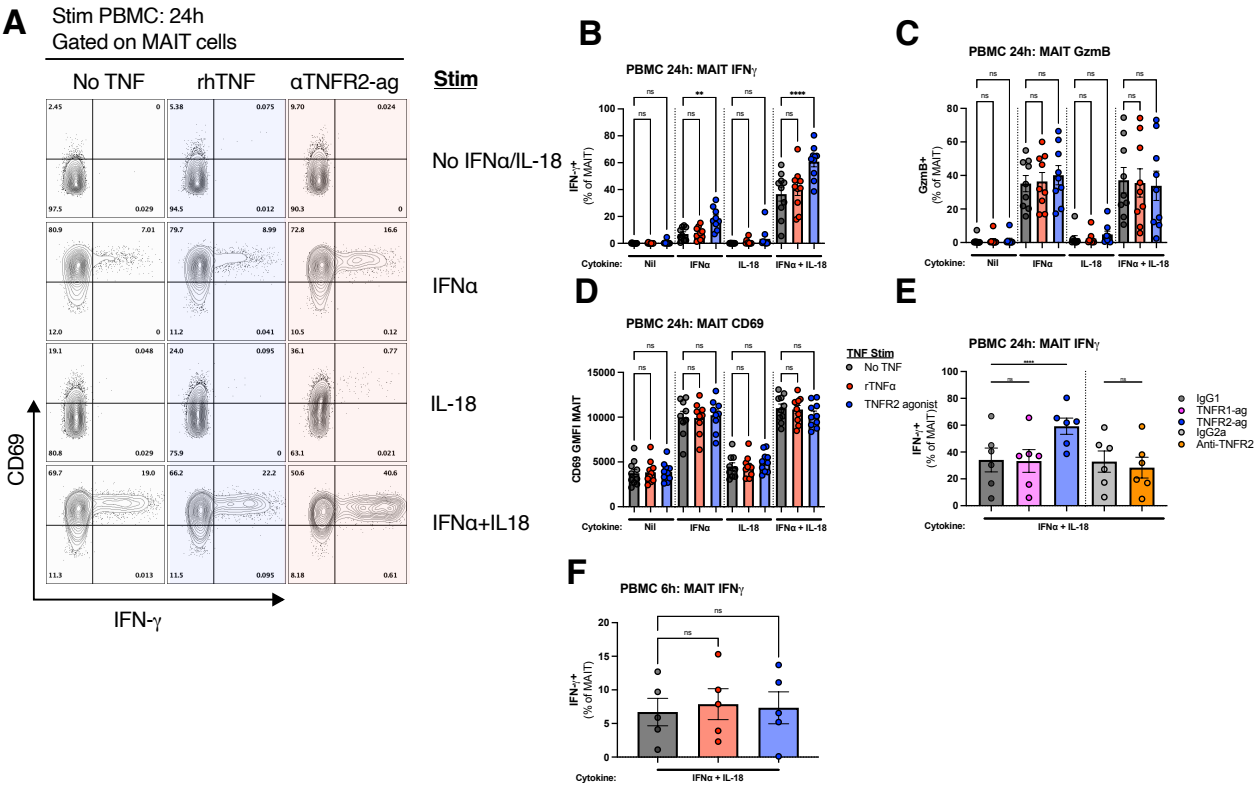

Fig3.23| TNFR2 agonism increases type I IFN-dependent MAIT IFNγ in PBMC at 24h.
Cryopreserved human PBMC were stimulated with cytokines indicated (50ng/ml) for 24h (A-E), or 6h (F), with or without modulators of TNF signalling in the form of: recombinant human TNF (red, 50ng/ml), TNFR2 agonist (clone MR2-1, 2.5µg/ml, blue), TNFR1 agonist (clone MR1-2, 2.5µg/ml), or TNFR2-antagonist(2.5µg/ml). MAIT cell IFNγ, GzmB, and CD69 expression was measured.
(A-D) Representative flow plot gated on MAIT cells (A) and summary MAIT cell IFNγ (B), GzmB (C), and CD69 24h after cytokine stimulation with or without TNF or TNFR2. (n=10 donors)
(E) MAIT cell IFNγ expression 24h after cytokine treatment with or without additional TNFR1 agonist, TNFR2 agonist, or TNFR2 antagonist. (n=6)
(F) MAIT cell IFNγ expression 6h after cytokine stimulation with or without additional TNFR2 agonist.

Symbols indicate individual donors with summary mean ± SEM shown. (n=5)
*p < 0.05; **p < 0.01; ***p < 0.001; ****p < 0.0001; ns, not significant.
Statistical differences were calculated using repeated measures one-way ANOVA with Dunnett's multiple comparison's test (B-F).

To determine if TNF could **directly** trigger MAIT cells to augment IFN-γ production CD8+ cells were MACS-enriched and stimulated with cytokines in the presence or absence of recombinant TNF or a TNFR2 agonist (**Fig3.24 A, B**). The addition of rhTNF, and in particular a TNFR2 agonist, increased MAIT cell IFN-γ production 24h after combined stimulation with both IFN-α and IL-18 only (**Fig3.24 B**). Direct TNF triggering had no impact on MAIT GzmB production (**Fig3.24 C**), with very modest CD69 upregulation (**Fig3.24 D**). Unusually, TNF-dependent MAIT triggering was more potent at higher cell densities, perhaps implying that other CD8 T-cell derived factors could contribute (**Fig3.24 E, F)**. Like results in PBMC, TNF agonism only directly triggered increased IFN-γ at later (24h) time points (**Fig3.24 G, H**).

Therefore, TNF signalling can support APC-independent MAIT cell IFN-γ production in response to antiviral cytokines.

We next asked whether direct TNF signalling to MAIT cells was responsible for the increased triggering observed with monocyte supernatant (**Fig3.15**). IFN-α conditioned monocytes could produce TNF very early (**Fig3.19**), and MACS enrichment has been shown to induce TNF and IL-6 as early as 5h, both from the CD14+ selection process and column filtration[327]. Monocyte-supernatant after 4h IFN-α pre-treatment was added to enriched CD8 T cells at the time of cytokine stimulation in presence or absence of either modulators of TNF signalling (recombinant TNF, TNFR2 agonist, Adalimumab), or type I IFN (B18R) to assess whether type I IFN induced TNF is sufficient to trigger MAIT cell IFN-γ (**Fig3.24**).

Figure 3.24 | TNFR2 agonism increases type I IFN-dependent MAIT cell IFN-γ in enriched CD8 at 24h.

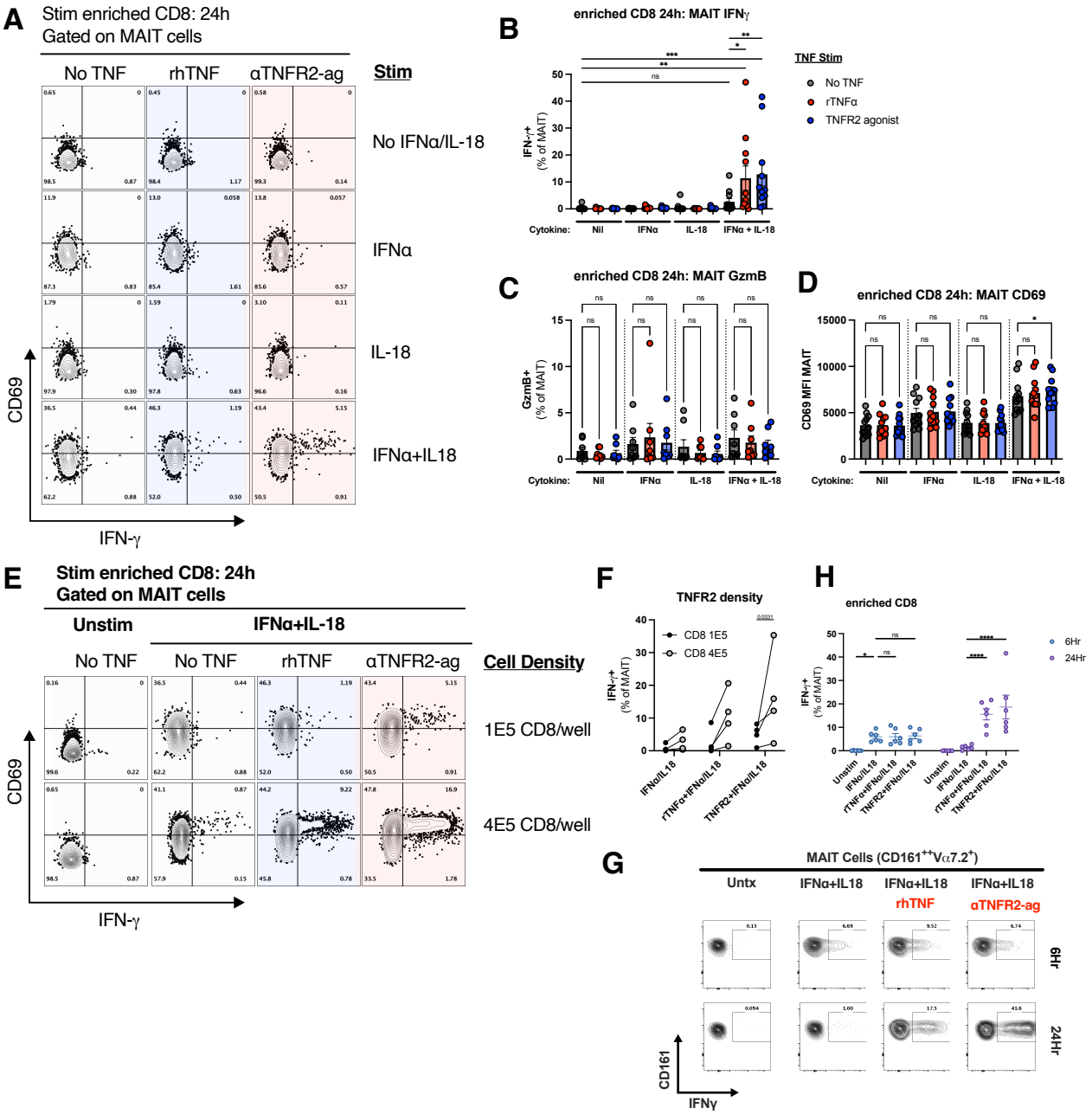

Fig3.24| TNFR2 agonism increases type I IFN-dependent MAIT cell IFNγ in enriched CD8 at 24h.
CD8+ cells were MACS-enriched from cryopreserved human PBMC and stimulated with cytokines indicated at (50ng/ml) for 24h (A-E), or 6h (G), with or without modulators of TNF signalling in the form of: recombinant human TNF (red, 50ng/ml), TNFR2 agonist (clone MR2-1, 2.5µg/ml, blue). CD8 cells were plated at 100,000 per well (A-G), or 400,000/well (E, F).
(A-D) Representative flow plot gated on MAIT cells (A), and summary MAIT cell IFNγ (B), GzmB (C), and CD69 24h after cytokine stimulation with or without TNF or TNFR2. (n=10 donors)
(E,F) Representative flow plots, and summary MAIT IFNγ at 24h (F) in response to cytokine stimulation of low (1E5/well) or high (4E5/well) CD8 T cell density. (n=4)
(G, H) Representative plots (G), and summary MAIT cell IFNγ expression (H) 6h after cytokine stimulation with or without additional TNFR2 agonism. (n=6)

Symbols indicate individual donors with summary mean ± SEM shown.
*p < 0.05; **p < 0.01; ***p < 0.001; ****p < 0.0001; ns, not significant.
Statistical differences were calculated using repeated measures one-way ANOVA with Sidak's multiple comparison's test (B-D); two-way ANOVA (F,G).

Pre-treatment of CD8+ cells with Adalimumab potently inhibited, while TNFR2 agonist augmented MAIT cell IFN-γ (**Fig3.25 B, C**) and CD69 (**Fig3.25 E**) in response to IFN-α-conditioned monocyte supernatant; Adalimumab in particular reduced IFN-γ expression 8-fold (43±8% to 5±2%). Recombinant TNF had no impact, although repeated dosing was not attempted to circumvent potential issues with short half-life. Consistent with previous data, GzmB expression was not altered by TNF signalling (**Fig3.25 D**).

Importantly, B18R also inhibited IL-18 dependent MAIT IFN-γ production in response to IFN-α-conditioned monocyte supernatant (**Fig3.25 B, C**), confirming that direct IFN-α signalling is non-redundant in MAIT cell IFN-γ production.

Finally to test the specificity of TNF to IFN-dependent MAIT activation, enriched CD8+ cells were treated with either Adalimumab and Etanercept prior to stimulation with IL-18 in combination with either IFN-α, or IL-12 (**Fig3.25 F, G**). As previously shown, monocyte supernatant only augments IFN-α-dependent activation, and anti-TNF potently inhibits this (**Fig3.25 F**). Anti-TNF did not have a robust impact on IL-12 induced MAIT activation (**Fig3.25 G**)- suggesting that MAIT cell capacity for IFN-γ is not globally impaired in the presence of TNF inhibitors. More importantly, these data collectively suggest that in the absence of APC, TNF is required for robust MAIT cell IFN-γ production in response to antiviral cytokine combinations - particularly type I IFN - we previously found to be induced by ChAdOx1.

Figure 3.25 | TNF signalling is required for APC-independent MAIT cell IFN-γ in response to monocyte supernatant.

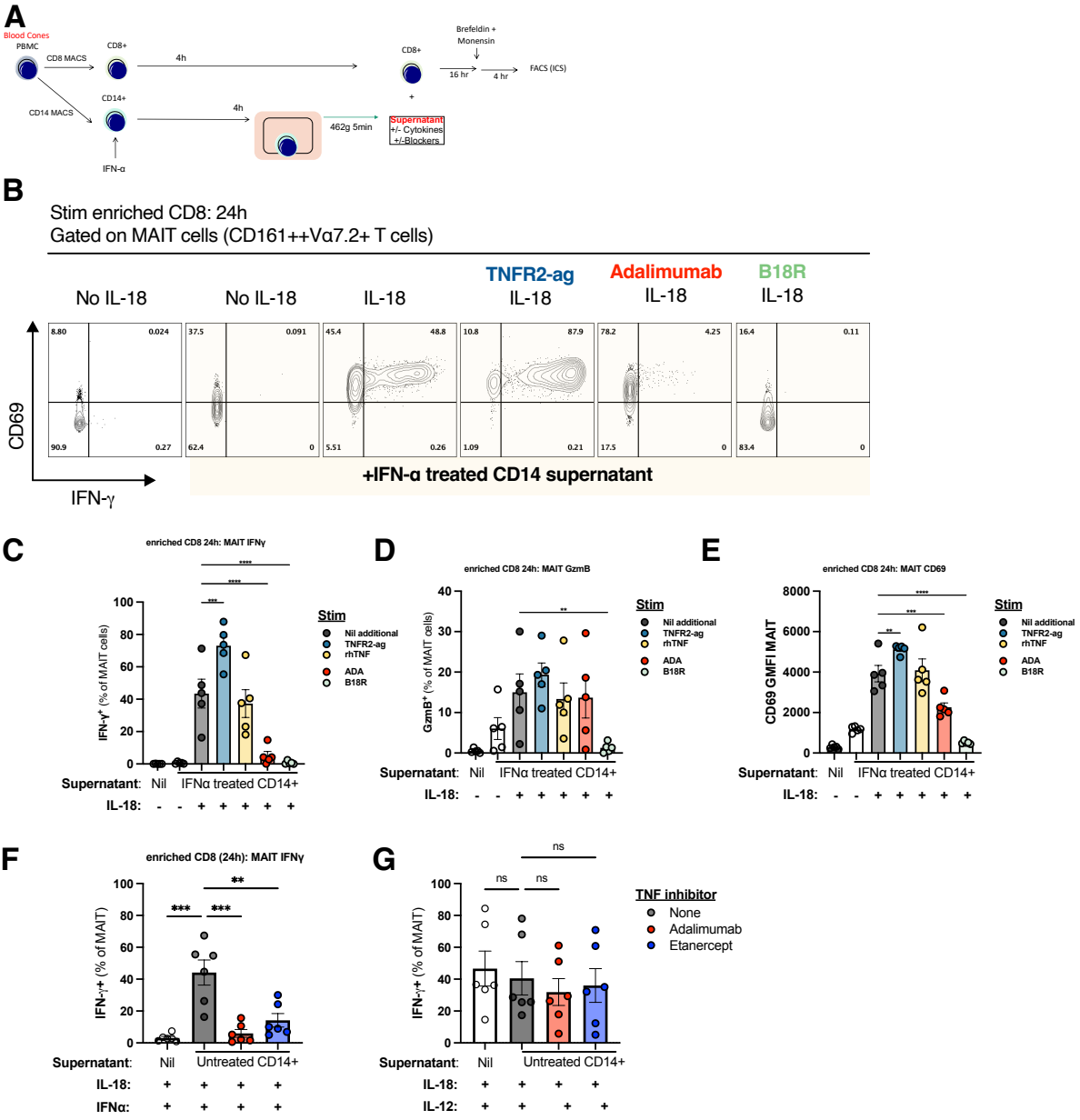

Fig3.25| TNF signalling is required for APC-independent MAIT cell IFNγ in response to monocyte supernatant.
Thawed PBMCs were enriched simultaneously for both CD8+ and CD14+ cells using MACS magnetic bead enrichment. CD8+ cells were rested (CO2 incubator, 4h). CD14+ cells (100,000 cells) were either stimulated with IFNα for 4h (50ng/ml; B-E), or untreated (F, G) in 200µl, after which supernatant was transferred to previously enriched autologous enriched CD8+ cells that were subsequently stimulated with cytokines (50ng/ml) in combination with modulators of TNF or type I IFN signalling; Adalimumab (10µg/ml), Etanercept (10µg/ml), B18R (10µg/ml), recombinant TNF (50ng/ml), and TNFR2 agonist (2.5µg/ml) were used. MAIT cell (CD161++Va7.2+ T cell) IFNγ (B, F-G), GzmB (C), CD69 (D) expression was measured 24h after stimulation.
(A) Schematic of experiment.
(B-E) Representative flow plots (B), and summary of MAIT IFNγ (B), GzmB (C), or CD69 (D) after stimulation of enriched CD8 with IFNα treated monocyte supernatant.
(F,G) Summary of MAIT IFNγ after stimulation of enriched CD8 with untreated monocyte supernatant in addition to IL-18 and IFNα (D), or IL-12 (G).
Symbols indicate individual donors. Mean ± SEM is shown.
*p < 0.05; **p < 0.01; ***p < 0.001; ****p < 0.0001; ns, not significant.
Statistical differences were calculated using repeated measures one-way ANOVA with Dunnett's multiple comparison's test (C-G).

3.3.7 TNF is necessary for ChAdOx1-induced early IFN-γ

I have already shown that TNF is secreted in response to ChAdOx1-GFP in vitro (**Fig3.5 F**; median 430 pg/ml), and that this correlates modestly with total IFN-γ at 24h (**Fig3.6 E**). We therefore tested the hypothesis that TNF is required for robust innate-like lymphocyte IFN-γ production in response to ChAdOx1.

TNF blockade with Adalimumab potently reduced total IFN-γ+ cells in PBMC, predominantly through near total inhibition of the major IFN-γ innate-like lymphocytes (**Fig3.26 A**). Focussing on unconventional sources, both Adalimumab and Etanercept but not Vedolizumab almost completely inhibit MAIT cell (**Fig3.26 B, C**), Vδ2+ γδ T cell (**Fig3.26 D**), and NK cell IFN-γ production in response to ChAdOx1-GFP (**Fig3.26 E**). MAIT cell (**Fig3.26 F**), and Vδ2 cell GzmB was also reduced (**Fig3.26 G**), albeit less appreciable for Vδ2+ γδ T cells which unlike MAIT cells express cytotoxic granules in the absence of activation[328]. Although CD69 upregulation was reduced by anti-TNF, inhibition was less than for IFN-γ (**Fig3.26 H-K**). Most MAIT (**Fig3.26 H**), and Vδ2+ (**Fig3.26 I**) cells still upregulate CD69 in the presence of anti-TNF, suggesting that other signals important for CD69 induction are not inhibited by TNF.

To further determine if a specific TNF receptor signalling pathway was important, we used the addition of agonists or antagonists of TNFR1 or TNFR2. Addition of a TNFR2 agonist, bypassing any impact of soluble TNF neutralisation, was sufficient to reverse the inhibitory effect of Adalimumab on MAIT cell IFN-γ (**Fig3.26 L**). Although blockade of TNFR1 and TNFR2 with commercial mouse anti-human antibodies (10μg/ml each) had a modest inhibitory effect (**Fig3.26 M**), neither antibody alone nor in combination matched the potency of clinical grade Adalimumab.

Anti-TNF monoclonal antibodies are powerful yet incompletely understood in terms of their mechanism of action. In addition to direct neutralisation of both soluble and membrane

bound TNF, other properties have emerged[324]. Direct binding to transmembrane TNF can induce apoptosis, complement or antibody dependent cytotoxicity, some through reverse signalling. Reagent specific effects include Adalimumab-induced Treg expansion via TNFR2 agonism, and Etanercept-specific binding to lymphotoxin alpha. Lastly the human Fc-domain of monoclonals bound to cell surface transmembrane TNF can trigger Fc-R dependent functions in myeloid cells.

Given the partial inhibition with mouse anti-human antibodies, we asked whether reverse or human FcR-dependent signalling in response to Adalimumab-bound membrane TNF was responsible for the remarkable potency observed. To test this, we used Certolizumab-pegol, a clinical PEGylated Fab' fragment of humanised monoclonal anti-TNF[324]. Both Certolizumab and Adalimumab were however equally potent inhibitors of MAIT cell IFN-γ (**Fig3.26 N**), and total ChAdOx1-induced IFN-γ in supernatants (**Fig3.26 O**), suggesting that TNF-TNFR signalling is crucial for ChAdOx1-induced early IFN-γ, rather than TNF neutralization-independent effector mechanisms from anti-TNF engagement with target cells.

Figure 3.26 | TNF blockade and TNFR signalling is crucial for ChAdOx1 induced innate-like lymphocyte activation in vitro.

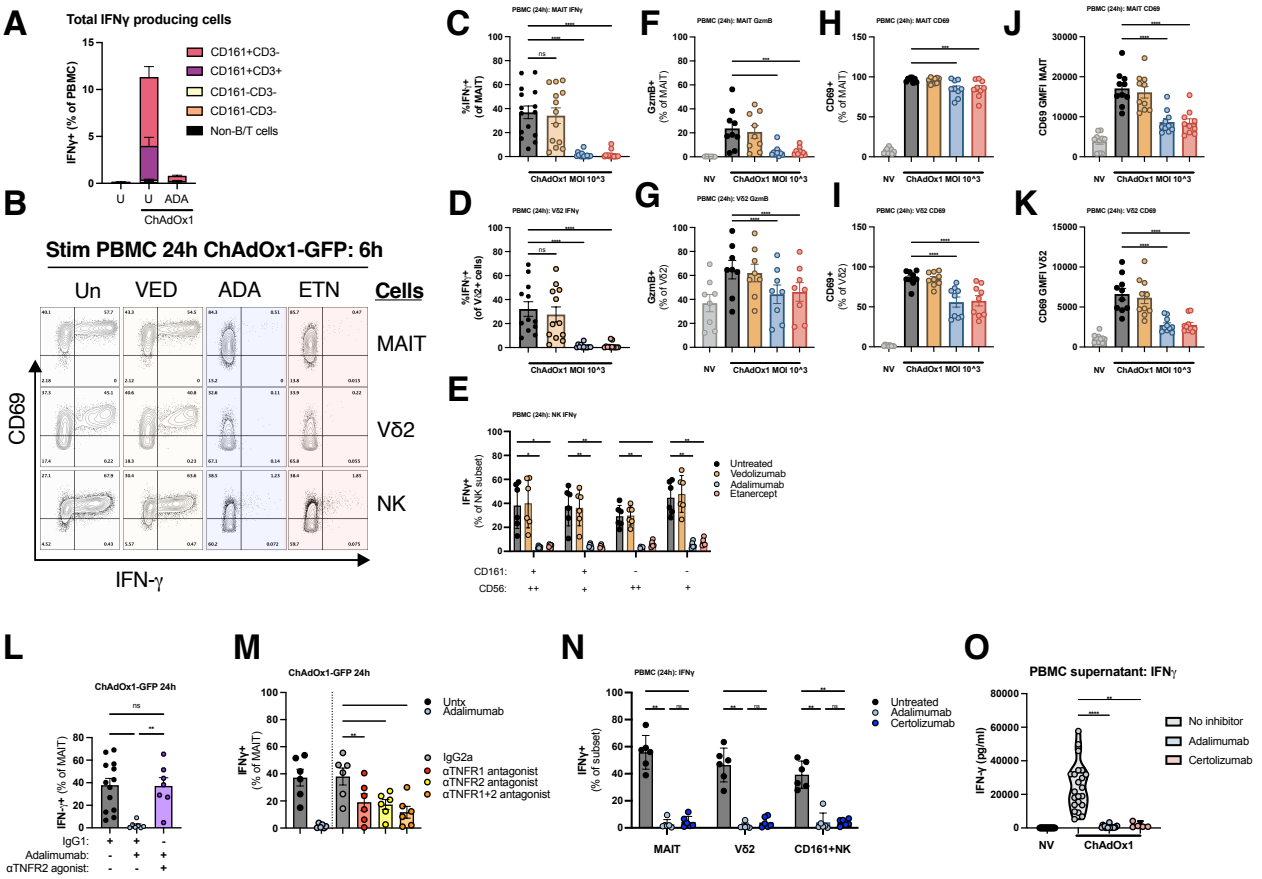

Fig3.26| TNF blockade and TNFR signalling is crucial for ChAdOx1 induced innate-like lymphocyte activation in vitro.

Fresh PBMCs were stimulated with ChAdOx1-GFP (MOI 10^3vp) in the presence or absence of TNF agonists or antagonists. Activation (IFNγ, CD69, GzmB) of MAIT cell (CD161++Va7.2+ T cell), Vδ2+ γδ T cell, and CD161+NK cell (CD56+, non-B/T lymphocytes) was measured after 24h. TNF antagonists added immediately prior to treatment were: Adalimumab (10μg/ml), Etanercept (10μg/ml), Certolizumab (10μg/ml), anti-TNFR1 (10μg/ml), or anti-TNFR2 (10μg/ml). TNF agonists added were αTNFR2 agonist (2.5μg/ml). Control antibodies were Vedolizumab (10μg/ml), or isotype controls.

(A) Total IFNγ positive cells in PBMC after ChAdOx1-GFP treatment with or without Adalimumab (ADA).

(B) Representative flow plots of MAIT, Vδ2 and CD161+NK cell IFNγ.

(C-E) Expression IFNγ (C-E), GzmB (F, G), CD69 (H-K) in MAIT cells (C,F,H,J), Vδ2 (D,G,I,K), and NK cells (E) 24h after ChAdOx1 in the presence of TNF inhibitors.

(L-N) MAIT cell IFNγ after ChAdOx1-GFP in the presence of Adalimumab or with TNFR2 agonist (L), antagonists of TNFR1 and TNFR2 (M), Certolizumab (N).

(O) Total IFNγ in supernatants 24h after ChAdOx1-GFP in the presence of Adalimumab or Certolizumab, or untreated. (samples pooled from across 3 experiments)

Symbols indicate individual donors. Mean ± SEM is shown.

*p < 0.05; **p < 0.01; ***p < 0.001; ****p < 0.0001; ns, not significant.

Statistical differences were calculated using repeated measures one-way ANOVA with Dunnett's multiple comparison's test (C-N), or Kruskal Wallis test (O).

3.3.8 Exosome inhibitors reduce TNF-dependent MAIT cell activation

MAIT cells preferentially express and up regulate TNFR2 (**Fig3.20**), and we found a TNFR2 agonist capable of augmenting APC-independent MAIT activation. TNFR2 preferentially binds membrane TNF [329], yet supernatant transfer experiments suggest a soluble TNF-dependent factor triggers MAIT cells. An analogous report suggested that NK cells are also activated in a TNF-dependent manner - with dendritic-cell exosomes capable of directly activating NK cells in a TNF-dependent manner via both TNFR1 and TNFR2 [330]. Exosomes can also transfer IFN-α-dependent signals from APC[331], thus may represent an important soluble mediator of innate-like lymphocyte activation during both vaccination and antiviral responses.

We therefore hypothesised that exosome-derived membrane TNF could be an important activator of MAIT cell antiviral responses. To test whether exosome biogenesis could contribute to ChAdOx1-induced MAIT activation we used a non-competitive neutral sphingomyelinase-2 (nSMase2) inhibitor, GW4869, which reduces multi-vesicular body formation [331,332]. ChAdOx1-induced MAIT cell IFN-γ in PBMC was abolished in the presence of 10μM GW4869 with no impact on transduction (**Fig3.27 A, B**). GW4869 also reduces IL-18-induced MAIT cell activation in combination with IFN-α but not IL-12 (**Fig3.27 B**). E coli induced IFN-γ - again partially dependent on both type I IFN and TNF - was also inhibited.

We then tested the impact of pre-treatment with exosome biogenesis inhibitors on the capacity for conditioned monocyte supernatant to stimulate MAIT activation. Both GW4869 (**Fig3.27 C**) and Spiroepoxide (**Fig3.27 E**), inhibited MAIT cell IFN-γ suggesting that nSMase2 is important in IFN-α-dependent MAIT cell activation. There was no impact on IL-12+IL-18 induced MAIT activation, confirming that nSMase2 inhibition doesn't generically inhibit IFN-γ production.

Differential centrifugation and ultracentrifugation are used to fractionate cells from extracellular vesicles, including apoptotic bodies, multi-vesicular bodies, and exosomes [333]. The centrifugation speeds used to isolate the supernatant from IFN-α-treated monocytes was found to also alter MAIT cell activation - but unfortunately this work was not continued after the pandemic. These data do however show an impact of nSMase-2 inhibition on the generation of stimulatory factor(s) specifically important for TNF-dependent MAIT activation.

Figure 3.27 | Neutral-sphingomyelinase inhibitors reduce ChAdOx1 and IFN-dependent MAIT cell activation.

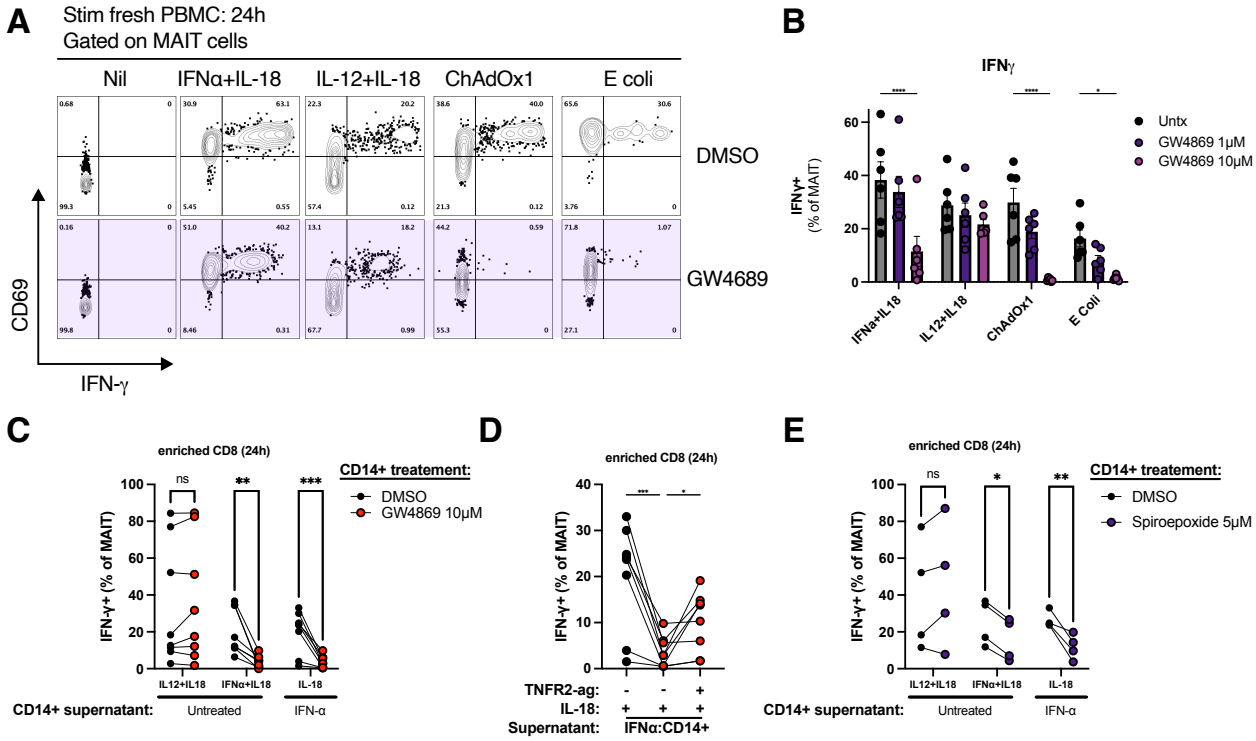

Fig3.27| Neutral-sphingomyelinase inhibitors reduce ChAdOx1 and IFN-dependent MAIT cell activation.

(A, B) Unfractionated fresh PBMCs were stimulated for 24h with the indicated cytokines (50 ng/ml), ChAdOx1 (MOI 10^3 vp), E.coli (25BpC), GW4869 (1μM, 10μM) or DMSO control were added immediately prior to stimulation, and activation of MAIT cells (CD161++ Vα7.2+ T cells) was measured after 24h. Representative flow plot (A), and summary MAIT cell IFNγ (B). (n=6, across 2 experiments)

(C-E) Thawed MACS-enriched CD14+ monocytes were stimulated for 4h with or without IFNα (50ng/ml) in addition to neutral sphingomyelinase inhibition with GW4869 (10μM; C, D), or Spiro-epox (5μM; E). Supernatants were subsequently transferred to autologous MACS-enriched CD8+ cells with or without the indicated additional cytokines, all at 50ng/ml, or TNFR-agonist antibody (TNFR2, 2.5μg/ml). Activation of MAIT cells (CD161++Va7.2+ T cells) was measured at 24h. (n=8 donors, C,D; n=4 donors, E)

Symbols indicate individual donors with summary mean ± SEM.
*, p<0.05; **, p<0.01; ***, p<0.001; ****, p<0.0001.
Statistical differences were calculated using repeated measures two way ANOVA with Sidak correction (B,C, E) or paired t tests (D).
BpC = bacteria per cell.

3.4 Discussion

The work in this chapter demonstrates that innate-like lymphocytes - exemplified by MAIT cells - are potently activated by ChAdOx1 in vitro to produce substantial IFN-γ within 24h. Innate-like lymphocyte activation depends on AdV transduction and activation of innate cells, in particular pDC, which in turn produce necessary IFN-α. Although innate-like lymphocytes are poised and sensitive to respond to type I IFN, which is sufficient to induce rapid CD69 expression, additional control from APC-derived signals is required for sustained IFN-γ production important for antiviral protection[224].

Surprisingly, we found that TNF, a cytokine with an extremely short half-life, is produced rapidly by monocytes in response to antiviral IFN and provides some of this fine control. Combination with inflammasome-derived IL-18 is required to fully activate MAIT cells, however, suggesting a mechanism to further control and limit prolonged and potentially pathogenic activation.

A highly relevant aspect of these results emerged from subsequent experiments by Nicholas Provine & Claire Hutchings, who found that MR1-deficient mice - which lack MAIT cells - have significantly impaired antigen-specific CD8+ T cell responses across multiple ChAdOx1 vaccines, including the recently licensed ChAdOx1-S[334]. The magnitude of impaired adaptive immunity in the absence of MAIT cells varied depending on the specific transgene, but because MAIT cells are 100-fold rarer in mice, they are likely to play a much greater role as vaccine adjuvants in humans.

The precise mechanism and specificity to vaccine induced adaptive responses is unclear and requires further exploration. Would MAIT cell activation observed after ChAdOx1 also augment anti-viral responses induced by non-viral vector vaccines? Identifying key MAIT cell effector functions induced in response to ChAdOx1 may provide insight to manipulable

pathways for optimisation of vaccine-antigen induced adaptive immune responses more generally. MAIT cell derived cytokines have been shown to promote B-cell class switching in vitro[335], and provide B cell help [242]. Therefore, it is important to investigate the role of MAIT cell activation in antigen-specific humoral immune responses in vivo.

3.4.1 Type I IFN-induced MAIT cell activation: sensitive but controlled

The data in this chapter contribute to a growing body of literature on type I IFN-mediated activation of MAIT cells [225,306,336–339]. We found that MAIT cells and other innate-like lymphocytes were highly sensitive to cues generated during the course of an antiviral response. Initially described as responding to influenza, hepatitis C and dengue [224,306,340], MAIT cells have been found to respond to an increasingly diverse range of viruses [341], extending most recently to SARS-CoV-2[225,342,343].

Cytokine responsiveness to IL-12 and IL-18 has been linked with CD161 expression [200], which is partially explained by increased IL-12R and IL-18R expression in CD161+ cells. We do not however have a clear mechanistic explanation for the increased sensitivity of innate-like lymphocytes to type I IFN. In vitro, MAIT cells and innate-like lymphocytes have higher baseline CD69 expression, which is upregulated rapidly in response to type I IFN but not other IFNs.

The mechanism behind the high baseline CD69 expression in MAIT cells is not understood, including why prominent expressed is only observed in a fraction of otherwise transcriptionally homogenous cells. It is possible that these cells have recently been triggered by their TCR, which has been shown to sensitise MAIT cells to type I IFN-dependent activation[325]. Another possible explanation is that MAIT cells may recirculate out of tissues[344], where they would clearly encounter abundant microbial ligands and cytokines at barrier surfaces. This could account for the reduction in CD69 expression among fresh

PBMCs after resting in R10 for 24h, with loss of in vivo signals driving MAIT cell baseline CD69. Basal endogenous type I IFN from the microbiome is normally clinically undetectable, but important for immune system priming[345]. Therefore, MAIT cells may represent exquisite sensors of endogenous IFN signalling. Several studies have shown that MAIT cell phenotypic markers, such as circulating frequency and CD69 expression, are sensitive biomarkers of dysregulated type I IFN signalling and are associated with disease severity in SARS-CoV-2 infection[225,342,343,346]. Hence, harnessing the enhanced type I IFN-sensitivity of innate-like lymphocytes like MAIT cells could have novel diagnostic applications..

Innate-like lymphocytes also shared sensitivity to type I IFN induced IFN-γ. IL-12 normally signals via STAT4[347]. Type I IFN can also signal, through non-canonical pathways, via STAT4 - which is important in early type I IFN induced responses in NK cells and CD8+ memory T cells[255,348]. High basal STAT4 expression has been observed in NK cells, ILC1 [349], Vδ2+ [350], and more recently MAIT cells[337]. In the case of NK cells STAT4 association with the IFNAR is an important mechanism behind early non-canonical type I IFN induced IFN-γ[255]. It would be interesting to further explore if preferential STAT4 activation is a shared mechanism across innate-like lymphocytes. In particular, comparison between the different IFN-responsive γδ T cells populations may be instructive. Given the increasing use of biologics targeting the JAK-STAT pathway, it would also be important to explore the impact these have on type I IFN induced IFN-γ in innate-like lymphocytes, which may be distinct from the impact on conventional T cells.

The data suggests some redundancy as MAIT cells, iNKT cells, Vδ2+ T cells and CD161+ NK cells all show similar responsiveness to type I IFN. Although we only focussed on IFN-γ, it is possible that each subset contributes distinct effector functions to the early ChAdOx1-induced immune response, particularly in tissues where they are capable of integrating unique TCR signals.

3.4.2 Control of antiviral inflammation and TNF

Integration would also appear to be a key mechanism by which IFN-dependent innate-like lymphocyte activation is controlled. The importance of IL-18, which is produced through inflammasome-dependent cell death, suggests that IFN-dependent innate-like lymphocyte activation is controlled by the state of neighbouring cells. One might imagine that control provided by different cell types found in tissues may alter ChAdOx1-induced early immune responses.

We have extended the concept of inflammatory control, identifying TNF as another signal necessary for type I IFN but not IL-12 mediated MAIT cell activation. Soluble TNF has a short half-life, therefore signalling would presumably cease soon after triggers are removed; supporting this we found that in untouched PBMC stimulated with IFN-α, TNF was only detected after 8hr but not 24h. Abundant IFN-α was also detected after IFN-α stimulation of enriched CD14+ monocytes, although some of this may be enhanced due to artefacts from the enrichment process.

It is not fully understood how TNF is involved in sustaining type I IFN-induced IFN-γ production. There are previous reports of interactions between TNF and type I IFN, such as TNF induction of autocrine type I IFN in human macrophages [351]. Both type I IFN and TNF are required for induction of intermediate genes such as CXCL10 in the context of macrophage Ad5 transduction, with anti-TNF reducing CXCL10 production (dependent on both STAT1 and NF-kB signalling). TNF can also activate an IRF1-dependent autocrine loop to sustain STAT1-dependent type I IFN-response genes. As early (STAT4-dependent) IFN-γ production by innate-like lymphocytes is TNF dependent, it could be informative to assess whether TNF uniquely maintains accessibility in these cells to sustain type I IFN-mediated IFN-γ.

The profound impact of anti-TNF in inhibiting early immune responses to ChAdOx1 has immediate clinical implications. ChAdOx1-S has been rolled out and administered globally, with a significant number of patients with IBD and rheumatological conditions on therapy. Chapter 5 will explore this further impact.

The source of TNF could also be relevant for the regulation of innate-like lymphocyte activation. We found that TNFR2 agonism was potent in augmenting IFN-dependent MAIT activation - therefore cell types upregulating membrane TNF (or inhibitors of surface TNF release) could provide more longer lasting control. Our data, using nSmase2 inhibitors, suggests that membrane-bound TNF derived from extracellular vesicles may also be involved in regulating the activation of innate-like lymphocytes. Further experiments are required to exclude off target effects, such as mitochondrial apoptosis [352], and release of apoptotic extracellular vesicles [353].

Finally, T cells are able to produce TNF so one might imagine that during the course of immune responses T cell-derived TNF may regulate innate-like lymphocyte function.

3.4.3 ChAdOx1 innate sensing: type I IFN and pDC

The dominant type I IFN response to ChAdOx1 aligns with published data for other AdV. This has recently been extended to include a ChAd: ChAd155[354,355]. In mice, ChAd immunisation resulted in two temporally distinct peaks in IFN and ISG induced chemokines in tissues. NK and NKT cells migrated to tissues, and one might speculate based on in vitro data that these contribute to the amplification of secondary peaks in innate cytokines. In that particular study NK cells comprised half of the cells in the draining LN two days after immunisation in mice (which lack appreciable MAIT cells); one might expect a more prominent role for MAIT cells in human draining LN.

The transduction of pDC was crucial for ChAdOx1 induced innate-like lymphocyte activation but questions remain as to how these cells are transduced. One would expect similar kinetics to monocytes, yet pDC transduction is delayed. Additionally, specific TLR triggers for pDC-derived type I IFN merit exploration. Lymphoid organs have high frequencies of pDC, in part regulated by type I IFN [356], adding impetus to future studies looking at the orchestration of innate-like lymphocyte responses in draining LN.

All the data presented however only addressed the response to an effective AdV prime as all human blood was from participants naïve to ChAdOx1. Booster vaccination in the presence of anti-vector immunity may alter both innate sensing and innate-like lymphocyte responses. Given that IFNs can regulate AdV transgene expression, this is an important area to understand early responses after homologous prime-boost with AdV.

3.4.4 Limitations

One limitation in the applicability of these results is that they were all carried out in PBMC, which may not reflect the immune cell types in tissues where AdV immune responses are primed. Even in the context of intravenously administered AdV, we are missing the potential impact of granulocytes in PBMC which could alter the magnitude of early innate responses. In tissues, resident APC have distinct innate sensing properties which may again alter the mechanisms of innate-like lymphocyte activation in response to AdV. Mucosal delivery of AdV for example is hindered due to rapid degradation of particles by tissue resident alveolar macrophages [357]. There tissue resident cells are also the dominant contributors to early innate cytokines but have differing capacity for IFN and inflammasome activation. It will be important to explore the translation of these mechanisms to more physiological settings.

Another limitation were the suboptimal markers for sub-setting innate-like lymphocytes. NK cell functionality is inferred from their dominance as CD161+CD3- lymphocytes. Although

Vδ2+ γδ T cells were analysed as a bulk population, expression of CD26 in particular discriminates those with a more MAIT-like phenotype which could be more informative for cytokine responsiveness[199].

3.5 Conclusion and summary

In summary, CD161+ cells, and in particular MAIT cells, are crucial in augmenting early IFN-γ in response to ChAdOx1. Type I IFN - directly linked to innate antiviral sensing - is necessary for maximal type II IFN production during the course of an immune response. Given the role of IFN-γ in optimal adaptive immunity - by promoting antigen processing and presentation - this data directly links innate and adaptive immunity with CD161+ cells as an important bridge.

The **key findings** from this chapter are:

1. Early IFN-γ in response to ChAdOx1 is mostly produced by innate-like lymphocytes, including MAIT cells, Vδ2+ γδ T and NK cells after cytokines mediated (TCR-independent) activation.
2. MAIT cells and Vδ2+ γδ T cells share sensitivity to type I IFN.
3. Monocytes are transduced early and can rapidly produce TNF in response to type I IFN, in addition to IL-18, which are both important for downstream effector responses.
4. Plasmacytoid dendritic cells are transduced after monocytes by ChAdOx1, activated and produce IFN-α.
5. IFN-α can both directly and indirectly promote MAIT cell activation - the later though induction of monocyte-derived TNF.

4 Human early immune responses to SARS-CoV-2 vaccines

4.1 Introduction

The SARS-CoV-2 pandemic resulted in the fastest expansion of vaccine armamentarium in history, with previously unlicensed platforms using mRNA and adenovirus viral vector technology successfully reaching most of the world's population [301]. Most (70%) people have received at least one dose of vaccine designed to induce adaptive immunity against native SARS-CoV-2 spike protein. An array of vaccines using different approaches were developed[301], but most of the 12 billion doses administered by summer 2022 have been nucleoside-modified mRNA vaccines or AdV. The majority of first doses globally were either BNT162b2 (Pfizer/BioNTech, mRNA), mRNA-1273 (Moderna, mRNA), ChAdOx1-S (Oxford -AstraZeneca; chimpanzee-derived AdV), or Ad26.COV2-S (Janssen, rare AdV serotype 26)(**https://ourworldindata.org/**).

We now have unprecedented swathes of data comparing safety, reactogenicity and spike-specific adaptive immune responses after homologous prime-boost immunisation in humans using AdV and mRNA vaccines. Both vaccine platforms provide protection against disease by generating spike-specific antibodies and T cell responses[298,358–361], with large observational and cohort data confirming differences in the quality and durability of adaptive responses based on the exact vaccine regimen used, including boosting intervals [362–365]. Both platforms induce systemic reactogenicity with unique profiles[299,365–369]: RNA vaccine-induced reactogenicity and rare propensity for myocarditis are enhanced at boost[370], whereas AdV vaccines induce more profound flu-like symptoms post-prime, rarely associated with thrombotic complications such as vaccine-induced thrombotic thrombocytopenia (VITT) [371,372]. Epidemiological data show associations with toxicity, such as age and an inverse sex bias for myocarditis and VITT, but only tentative mechanisms have been proposed [373].

The heterogeneity of human immune responses hinders mechanistic studies. Longitudinal cohorts are necessary to understand how variable responses are generated towards the same vaccine, beginning at the earliest immune encounters through to the induction of durable adaptive immunity. Future studies will be further complicated by additional variables, including differences in booster regimens, variant peptide-targets, and an accumulation of asymptomatic SARS-CoV-2 exposure in the general population. Arguably the specificity and quality of first encounters with antigen are the most important, contributing to the divergence in secondary humoral and cellular responses to that antigen among the population[147,374,375]. Therefore, appreciating differences in how original spike-specific responses were generated by these different vaccines longitudinally after primary prime-boost schedules would be most informative in the mechanistic interpretation of vaccine immunogenicity.

Great care was taken to optimise the very first encounters RNA and AdV vaccines have with the immune system before spike antigen production. LNP are optimised to deliver mRNA intracellularly, with nucleoside-modified mRNA base pairs evading cytosolic RNA-sensors which reduce translation[138,376]. Even earlier immune responses could negatively impact AdV immunogenicity; hyper-variable surface hexon proteins are targets for specific and cross-reactive early adaptive immune responses, which together with early antiviral interferon could reduce transduction and transgene durability respectively[303,377,378]The most widely used AdV were therefore selected to avoid the potential negative implications of pre-existing anti-vector immunity, using either chimpanzees-derived (ChAdOx1) or rare human serotypes (Ad26).

Optimised spike antigen production alone is insufficient with early innate responses further shaped by adjuvants required to prime adaptive immunity [379]. As has been described in earlier chapters, dsDNA-based AdV are self-adjuvants, triggering innate antiviral sensors and serotype-dependent downstream responses in human PBMC [334]. Intriguingly, although

nucleoside-modification in mRNA vaccines aims to evade antiviral sensors, an acute inflammatory immune response is nevertheless present. Early trials of BNT162b2 confirmed elevated CRP and lymphopenia one day after prime[145,359]. RNA LNP has some adjuvant capacity[137], and reactogenicity after mRNA prime is dose dependent [368,380].The specific protein structure can also shape early responses to mRNA vaccines. BNT162b1 showed promise in trials, but BNT162b2 was pursued due to lower reactogenicity [380,381]; although both had identical LNP, they differed in the SARS-CoV-2 mRNA sequence induced. Therefore, differences in the delivery vehicle, nucleic-acid message, and transgene (antigen) presentation all contribute to how the immune system responds so differently to these vaccine platforms.

We have recently demonstrated that the earliest innate effector responses to ChAdOx1 are first sensed by cytokine responsive innate-like lymphocytes, including MAIT cells and Vδ2+ γδ T cells [334,382], which in turn amplify early mediators such as IFN-γ important for priming adaptive immunity. Type I IFN-dependent MAIT cell activation, which also induces potent IFN-γ, was required for optimal transgene-specific adaptive CD8+T cell responses to ChAdOx1 vectors in mice[334]. It is unclear if such type I IFN-mediated activation would occur after mRNA vaccines, given that nucleoside modification reduces type I IFN secretion [138,139]. Nevertheless, as the most exquisitely sensitive cells in blood to innate cytokines, we hypothesised that innate-like lymphocytes would also be activated in response to the mRNA vaccine BNT162b2. Given their abundance in a range of tissues, presence in lymph nodes[383,384], and capacity for rapid effector functions, MAIT cells and other innate-like lymphocytes could serve as universal intermediate amplifiers of early tissue innate and adaptive responses. MAIT cells in particular can tune their effector functions based on their mode of activation, so understanding if and how they are triggered would be informative for vaccine design.

4.2 Aims

The primary aim of this chapter was to characterise and understand human early immune responses to novel SARS-CoV-2 vaccines, with a focus on the initial encounter (prime) and subsequent re-encounter (boost) with homologous prime-boost regimens. The regimens evaluated were those used in the UK, BNT162b2 and ChAdOx1-S. For BNT162b2, we compared different dosing interval lengths, which were subsequently shown to impact adaptive immune responses [363]. Building on findings from Chapter3, the aim was to confirm innate-like lymphocyte activation in response to ChAdOx1-S in vivo, compare it to BNT162b2, and assess the impact of re-encounter (homologous boost) on early responses in both cases.

AIMS

(1) To identify shared and unique features of ex vivo early immune responses to SARS-CoV-2 vaccines, with a focus on the contribution of innate-like lymphocytes.

(2) To explore mechanisms by which innate-like lymphocytes are activated post-prime and boost with different vaccines.

(3) To assess the relationships between early and adaptive immune responses.

In addition to the above, mechanistic in vitro work will be conducted to:

(4) Characterise the early immune response to SARS-CoV-2 spike vaccines.

(5) Characterise the function of any early IFN-γ response to SARS-CoV-2 vaccines.

Data shown in this chapter are from experiments performed by me unless explicitly stated. Some samples from patients I recruited and stored were used for publications mentioned on page 9-10,

4.3 Chapter specific materials and methods

4.3.1 Study design, and sample collection

A prospective observational cohort of healthcare workers (HCW) recruited at Oxford University Hospitals NHS Foundation Trust were simultaneously enrolled in the OPTIC Study, a sub study amendment to the Oxford Translational Gastrointestinal Unit GI Biobank Study (REC 16/YH/0247) on 8th June 2020 (**Fig4.1**). The sources of referral were staff-based SARS-CoV-2 screening, official email communications, or word of mouth, and written informed consent was obtained from all participants.

Figure 4.1 | Schematic of healthcare worker study.

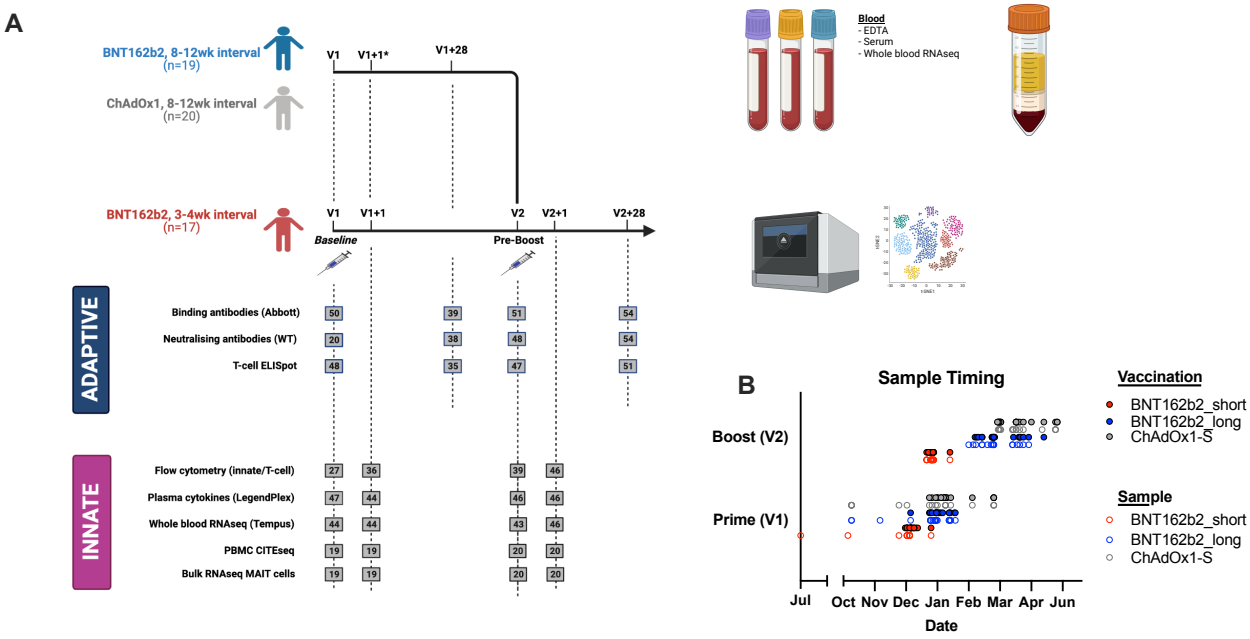

Fig4.1 | Schematic of healthcare worker study.
(A) Summary of longitudinal sample collection from healthcare workers vaccinated with ChAdOx1-S (n=20), or BNT162b2 (n=36), on either short interval (n=17), or long interval boosting regimens (n=19), with timepoints and relevant innate and adaptive immune assays highlighted.

Pre-vaccine timepoints were preprime (V1), and pre boost (V2). Post-vaccine timepoints were day 1 post-prime (V1+1), or day 1 post-boost (V2+1).

Early immune profiling was performed with flow cytometry (innate cells, conventional and unconventional T-cells), plasma multiplex cytokines, whole blood RNA sequencing, and single-cell CITE-seq.

SARS-CoV-2 adaptive immune profiling included S-binding antibodies, live-virus neutralisation titres, and T-cell IFNγ ELISpot assays.

(B) Summary timeline for sample collection.

Eligibility criteria included all adults over 18 years of age working in the healthcare setting, including allied healthcare professionals, hospital laboratory staff and medical students. Vaccination dates ranged from 9th December 2020 to 18th March 2021 (prime), and 2nd January-28th May 2021 (boost).[Table 4.1]

Table 4.1 | HCW cohort characteristics.

		Vaccine Regimen			
Characteristic	Overall, N = 56[1]	BNT162b2-Short, N = 17[1]	BNT162b2 - Long, N = 19[1]	ChAdOx1-S, N = 20[1]	p-value
Dosing interval, *days*	66 (28- 77)	21 (21- 25)	70 (62- 78)	76 (70- 79)	<0.001[2]
Infection, *baseline spike ab detectable*	12 (21%)	4 (24%)	4 (21%)	4 (20%)	>0.99[3]
Age, *years*	35 (30- 43)	37 (35- 44)	33 (31- 38)	28 (22- 46)	0.031[2]
Sex, *female*	36 (64%)	8 (47%)	13 (68%)	15 (75%)	0.19[4]
BMI	23.4 (20.3- 26.0)	23.5 (20.4- 25.8)	24.5 (21.9- 27.3)	23.1 (20.3- 25.6)	0.63[2]
Unknown	18	3	7	8	
Smoking					0.38[3]
Never Smoked	52 (93%)	15 (88%)	17 (89%)	20 (100%)	
Past Smoker	4 (7.1%)	2 (12%)	2 (11%)	0 (0%)	
Ethnicity					0.81[3]
East Asian	5 (8.9%)	2 (12%)	2 (11%)	1 (5.0%)	
Other	3 (5.4%)	2 (12%)	1 (5.3%)	0 (0%)	
South Asian	3 (5.4%)	1 (5.9%)	1 (5.3%)	1 (5.0%)	
White	45 (80%)	12 (71%)	15 (79%)	18 (90%)	

[1]Median (IQR, 25%- 75%); n (%)
[2]Kruskal-Wallis rank sum test
[3]Fisher's exact test
[4]Pearson's Chi-squared test

Blood sampling dates for the entire cohort ranged from 10th July 2020 (pre-vaccine baselines), to 28th June 2021 (day 28 after boost). Samples were collected prior to prime (V1), and boost (V2), with further sampling one day after prime (V1+1), and one day post-boost (V2+1). Most samples for pre-prime and pre-boost and innate timepoints were within 1 day of vaccination date (Table 4.2) (median V1 sample 1 day pre-prime, IQR 0, 3; median V2 sample 1 day pre-boost, IQR 0, 2). Additional samples for measurement of SARS-CoV-

2-specific adaptive responses were 4 weeks post-prime (V1+28; median 28 days, IQR 26, 31.5 days), and post-boost (V2+28; median 30 days, IQR 27, 32).

Participants were sampled after receiving either two doses of BNT162b2 mRNA vaccine (30µg, intramuscular injection in 300µL), or ChAdOx1-S (at least 2.5x10^8 infectious units in 500µL). Clinical information regarding vaccination dates, age (at the time of first vaccination), sex and ethnicity were documented. Prior SARS-CoV-2 history was also recorded, including PCR positivity, symptoms, and previous serology to detect SARS-CoV-2 nucleocapsid or spike protein.

Phlebotomy samples included: EDTA blood, for PBMC and plasma isolation within 4h; serum in serum-separating tubes (SST, Becton Dickinson); and whole blood in Tempus tubes (Life Technologies), which were promptly frozen at -20˚C for subsequent RNA extraction.

Table 4.2 | HCW cohort: summary of interval between sampling and vaccination.

	Overall N = 56	**BNT162b2-Short** N = 17	**BNT162b2 – Long** N = 19	**ChAdOx1-S** N = 20
Prime: interval of sample to vaccine, days *median, [IQR], (range)*	1 [0-2] (0-154)	1 [0.5-9.5] (0-154)	1 [0-4] (1-98)	0 [0-41.5] (0-107)
Boost: interval of sample to vaccine, days *median, [IQR], (range)*	1 [0-2] (0-11)	0 [0-1] (0-3)	1 [0-1.75] (0-11)	0.5 [0-2] (0-6)

4.3.2 Isolation of PBMCs, plasma and serum

PBMC were isolated as previously described in Chapter 2 for vaccination samples, with no dilution of blood prior to layering to allow plasma collection. An aliquot of cells was stained fresh for immune phenotyping panels, with the remainder aliquoted at 10^6 PBMC per vial in freezing media (90% FCS, 10% DMSO), frozen in “Mr Frosties” to -80˚C, prior to transfer

for long term storage in liquid nitrogen (-180˚C). Thawing of vials was as described for vaccine samples, with the addition of 2µl Benzonase (≥ 25 U/µl; Sigma-Aldrich).

4.3.3 Whole blood total RNA extraction and RNA-seq

Whole blood (~3ml) from healthy volunteers was collected in Tempus tubes (Life Technologies), mixed vigorously to homogenise blood in guanidine hydrochloride solution (6ml), and frozen within 2 hours at -20˚C prior to subsequent RNA extraction in batches following manufacturer's protocols.

RNA extraction performed by Nicholas Provine, Lucy Garner or myself. Briefly, Tempus tubes were thawed, after which contents were diluted with 1x PBS in a 50ml conical, vortexed for 30s and then centrifuged at 3000g for 30min (4˚C) to pellet RNA. The supernatant was removed, RNA pellet resuspended and transferred to purification filters to purify and elute RNA using a micro centrifuge. RNA was quantified and stored at -20˚C.

RNA libraries were prepared by Lucy Garner, and Total RNA-seq performed by Oxford Genomics Centre.

4.3.4 Focus Reduction Neutralization Assay (FRNT)

The capacity of serum antibodies to neutralise wild type Victoria strain SARS-CoV-2 were **all performed by Dr Wanwisa Dejnirattisai,** as published[385]. Focus Reduction Neutralisation Test (FRNT) was measured as the reduction of infected foci compare to negative controls without serum, with the percent focus reduction calculated as IC50 and described here as FRNT50.

4.3.5 IFN-γ T cell ELISpot assays

IFN-γ ELISpot data shown here were all performed by either **Sandra Adele, Eloise Philipps, or Tom Malone** using the PITCH ELISpot Standard Operating Procedure[363,386].

4.3.6 Antibody assays Abbott

Binding antibodies against SARS-CoV-2 spike (S) and nucleocapsid (N) proteins were all measured using Abbott SARS-CoV-2 immunoglobulin G (IgG) by **Tim James and Stuart Cox (Oxford University Hospitals).** This chemiluminescent microparticle immunoassay (CMIA) provides both quantitative and qualitative measures of SARS-CoV-2 binding antibodies. For anti-N IgG, the limit of detection was classified as ≥1.40 arbitrary units (au)- with titres between 0.50-1.39au deemed equivocal. For analysis, values below 0.5 were assigned half the LLOQ (0.25).

4.3.7 Spike-specific T cell ICS

To stimulate spike-specific T cells in human PBMC, 10^6 PBMC were stimulated for 20h with overlapping peptide pools to SARS-CoV-2 spike protein (S1+S2 pools with 15 amino acids overlapping by 10, 1µg/ml each). DMSO (1%v/v) treatment was used as a negative control. Brefeldin A and Monensin were added for the final 4h stimulation, then cells were stained as previously described. Conventional CD4+ and CD8+ T cells were defined as γδ-TCR-, non-MAIT (CD161hiVα7.2+) T lymphocytes. Spike-specific responses were background subtracted from DMSO. All incubations were at 37˚C in 5%CO_2.

4.3.8 Spike protein detection in supernatants

Human SARS-CoV-2 RBD ELISA Kit (Invitrogen, Cat#EH492RB), a commercially available sandwich ELISA, was used to quantify spike protein in cell culture supernatants according to manufacturer's instructions. Supernatants were centrifuged to remove debris, diluted 1:2 and plated in duplicate with standards onto a plate pre-coated with anti-RBD capture antibodies. Plates were incubated for 2.5h, then washed three times, and incubated with biotinylated detection antibodies for 1h. Plates were washed again three times, then incubated with streptavidin-HRP solution for 45min. After a further three washes, plates

were incubated with TMB substrate for 30min light protected. Finally stop solution was added and well absorbance measured immediately at 450nm and 630nm (reference filter), with the optimal density (OD) at 630nm subtracted from the OD at 450nm. All incubations were performed at room temperature with gentle shaking. Data were collected using a FLUOstar OPTIMA plate reader (BMG LABTECH). Curve fitting was performed with a four-parameter algorithm using background subtracted absorbance.

4.3.9 Quantification and statistical analysis

Sample sizes were not predetermined by statistical methods but similar to reported publications[334,387]. Randomisation was not performed in the cohort selection, with no blinding for either data collection or analysis.

Statistical analysis was performed in GraphPad PRISM (v9) or R (v.4.0.2), using all available data with no outlier removal. Two-tailed p values were calculated in all cases, with $P<0.05$ deemed significant, and $P<0.1$ considered a trend with exact values reported. Non-parametric tests were used unless the data was normally distributed based on the Shapiro's normality test. Spearman's R correlation coefficient was used for all descriptive correlations.

For analysis of vaccinated human volunteers, a non-parametric paired Wilcoxon rank-sum test was used. For analysis of in vitro stimulations, unpaired t-tests were used for comparison of two groups. A repeated-measures one-way ANOVA with Dunnett correction for multiple comparisons was used, or a mixed-effects model with Dunnett correction for multiple comparisons was used if there were different numbers of data points in each group. For analysis of SARS-CoV-2 spike protein-specific T cell responses, background subtraction of cytokine production from DMSO-treated wells were performed.

4.4 Results

4.4.1 Study design and cohort characteristics

To explore the role of early immune responses to SARS-CoV-2 vaccines, a sub-study was created as part of the observational national PITCH cohort (**Fig4.1 A**). We recruited healthy healthcare workers (HCW) at Oxford University Hospitals before their immunisation as part of the UK SARS-CoV-2 vaccination schedule. Recruitment began in December 2020 with HCW initially receiving BNT162b2. After MHRA approval, some HCW were recruited who received ChAdOx1-S (AZD1222) before this was curtailed in younger age groups due to concerns around VITT [372,388]. During the course of our study the UK vaccine schedule was altered on recommendation of the Joint Committee on Vaccination and Immunisation (JCVI), with BNT162b2 dosing intervals extended up to 12 weeks, so only the earliest recruited participants received the originally licensed schedule (short 3-4-week interval).

A subset of 56 HCW had samples taken from at least one early time point after prime or boost vaccination (**Fig4.1 A**). Volunteers either had homologous BNT162b2 with short interval boosting (BNT_short, n= 17; median, 21 days; IQR, 21–24; range, 17-30), long interval boosting (BNT_long, n = 19; median, 70 days; IQR, 62-78; range, 42-120) or long interval ChAdOx1-S boosting (ChAdOx1, n = 20; median, 76 days; IQR, 70-79; range, 60-98) (**Table 4.1**; **Fig4.1 B**).

The majority (~80%) of participants were SARS-CoV-2 naïve at baseline with undetectable anti-spike IgG binding antibodies. In those where this was not available, nucleocapsid (N) antibodies and/ or confirmed PCR positive infection was used to define previous infection. All HCW with confirmed infection (SARS-CoV-2 PCR positive) also had detectable anti—spike binding Ab pre-vaccination.

There were more female HCW (64%) in line with the normal NHS workforce, with no statistically significant difference in sex distribution between cohorts. The median age was

35 (IQR, 30-43; range 21-65), slightly lower among the ChAdOx1-S sub-cohort (median, 28 years; IQR, 22-46; range, 21-59; **Table 4.1**) due to a higher proportion of medical students who were ineligible for the early BNT162b2 rollout. Most participants self-reported as white (80%), and were never smokers (93%), with median BMI 23.4 (IQR 20.3- 26.0).

Our aim was to longitudinally profile early immune responses at high resolution. Samples were collected at baseline, one day post-prime, pre-boost, and one day post-boost for profiling of early immune responses, together with conventional adaptive time points. Samples included whole blood in EDTA, Tempus RNA, and serum SST tubes. EDTA blood was processed to collect plasma and PBMC. Serum was either freshly analysed for SARS-CoV-2 specific binding antibodies, or frozen for subsequent quantification of binding and neutralising antibodies. Aliquots of fresh PBMCs were used to phenotype innate and T cell activation (**Fig4.1 A;** 10^6 cells per panel). Freeze-thawed cells were used for assays of spike-specific T cell responses, in addition to single-cell RNAseq.

4.4.2 Differential immune activation post-prime and boost

We have previously shown that early MAIT cell activation functionally regulates ChAdOx1-induced CD8+ T cell responses[334]. Upregulation of CD69 expression on MAIT cells and Vδ2+ γδT cells is also a sensitive marker of type I IFN[54], and correlates with adaptive responses after vaccination and infection. We therefore longitudinally profiled early cellular response to SARS-CoV-2 vaccines, focusing on activation of these innate-like lymphocytes in addition to innate immune cells. MAIT cells (MR1-5OPRU/ tetramer+, Vα7.2-TCR+), Vδ2+ and non-Vδ2 γδ T cells, iNKT cells (Vα24-Jα18 TCR+) were assessed, in parallel to naïve (CCR7+CD45RA+), central memory (CCR7+, CD45RA-), effector memory (CCR7-CD45RA-) and terminally differentiated effector memory (CCR7-CD45RA+) conventional T cells (**Appendix SF4.1 A-C**). CD161+CD3- lymphocytes were also assessed and are referred to from hereon in as CD161+NK cells.

Similar to previous in vitro data, MAIT cells express the highest levels of CD69 one day after both primary and secondary (boost) vaccination in vivo (**Fig4.2 A-F**). MAIT cell CD69 expression is lower after BNT162b2 prime (11±2%; **Fig4.2 B**) compared to ChAdOx1-S prime (54±7%, **Fig4.2 C**), with both vaccines inducing comparable MAIT cell activation at boost (ChAdOx1-S, 29±5%; BNT162b2, 21±3%; **Fig4.2 B C**). Although MAIT cells are activated after every vaccine encounter, the pattern of activation is dichotomous between modalities; MAIT cell activation is enhanced at boost compared to prime after BNT162b2 (**Fig4.2 D**), whereas activation after ChAdOx1-S prime is enhanced compared to subsequent boost (**Fig4.2 E**). This mirror pattern between prime and boost was also seen for other innate-like lymphocytes, including Vδ2+ γδT cells, iNKT cells, and CD161+NK cells (**Fig4.2 F-H**). Vaccine-induced Vδ2+ γδT cell CD69 expression was always lower than MAIT cells, similar to our previous work[334,382], particularly after BNT162b2 (**Fig4.2 G-H**); MAIT cells and iNKT were distinctly more sensitive to BNT162b2 induced activation than Vδ2+ γδ T cells, NK cells and conventional CD8 Temra (**Fig4.2 I, J**). CD69 expression prior to each vaccination dose was consistently highest for MAIT and iNKT cells, and did not change from prime to boost for either vaccine, arguing against long lymphocyte changes **(Fig4.2 K, L)**.

For a subset of volunteers we tracked responses daily and confirmed that peak MAIT cell, Vδ2+ T cell, iNKT, and NK cell CD69 expression was 24-48h after vaccination (**Fig4.3 A-C**). Overall CD69 expression on innate-like lymphocytes, in particular MAIT cells, was a sensitive readout of the unique pattern of early vaccine responses.

Figure 4.2 | Innate-like lymphocytes show dynamic dichotomous CD69 expression in response to BNT162b2 and ChAdOx1-S.

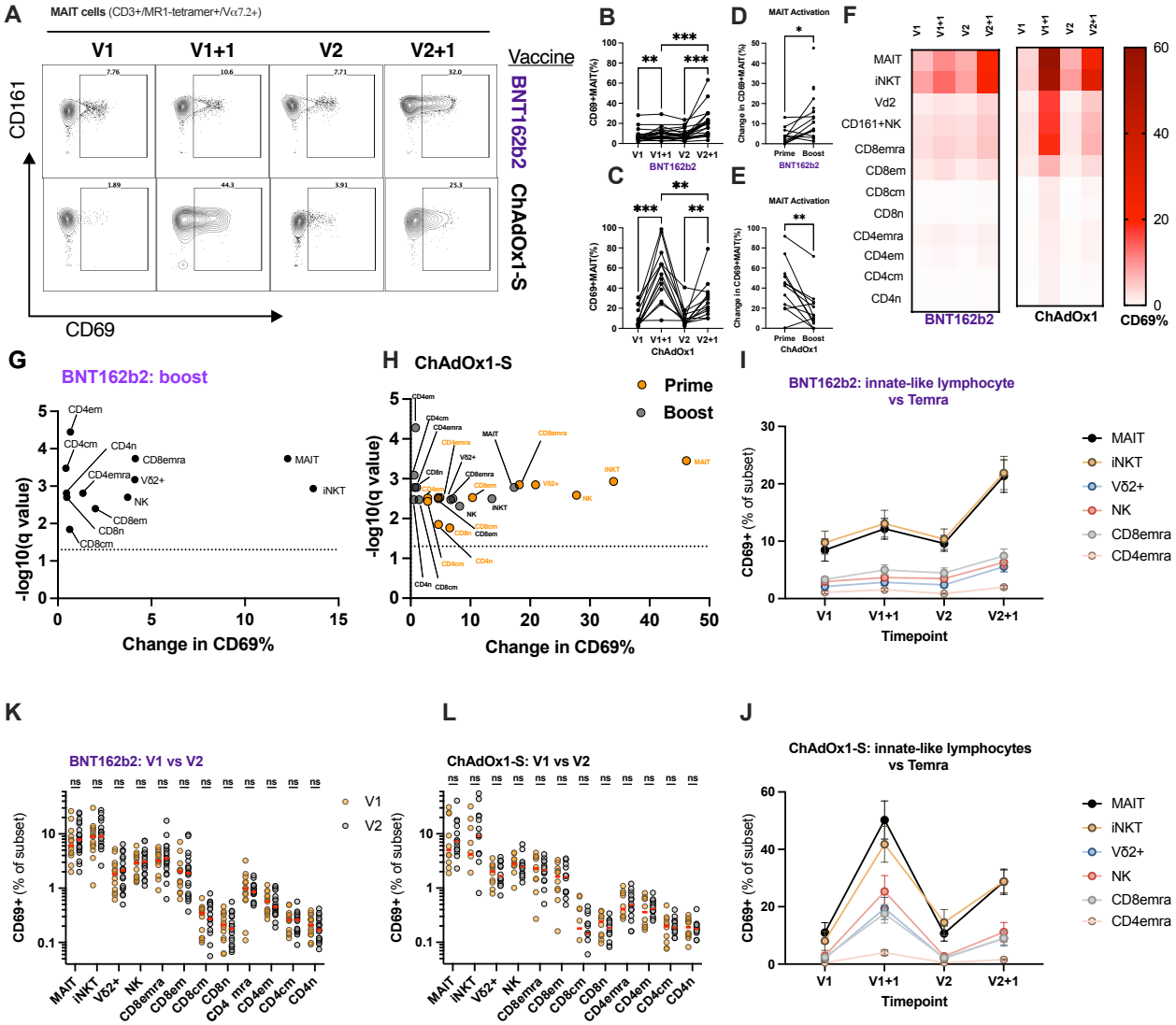

Fig4.2 | Innate-like lymphocytes show dynamic dichotomous CD69 expression in response to BNT162b2 and ChAdOx1-S.
(A) Representative plots gated on MAIT cells (MR1/5-OP-RU tetramer+) showing CD69 expression from a HCW receiving BNT162b2 (purple, top panel) or ChAdOx1-S (bottom panel).
(B, C) Summary of changes in MAIT cell CD69 expression after BNT162b2 **(B)**, or ChAdOx1-S **(C)**.
(D, E) Change in MAIT cell CD69 expression between prime (V1-V+1) and boost (V2-V2+1) for BNT162b2 **(D)**, or ChAdOx1-S **(E)**.
(F) Summary heatmaps of median CD69% expression in cell subsets at key timepoints after BNT162b2 (left) or ChAdOx1-S (right).
(G, H) Volcano plots of change in CD69 expression as a percent of each subset after BNT162b2 boost (V2-V2+1; **G**), or after ChAdOx1-S prime and boost (**H**).
(I, J) Summary of changes in CD69 expression in the indicated T cell populations after BNT162b2 **(I)**, or ChAdOx1-S **(J)**.
(K, L) Summary of CD69 expression at baseline or pre-boost in BNT162b2 **(K)**, or ChAdOx1-S cohort **(L)**.

Symbols indicate individual donors. Mean ± SEM is shown.
*p < 0.05; **p < 0.01; ***p < 0.001; ****p < 0.0001; ns, not significant.
Statistical significance was determined using: mixed-effects ANOVA Šídák's multiple comparisons test (B, C); Wilxocon test (D, E); multiple paired t-tests with Benjamini, Krieger, & Yekutieli correction for multiple comparisons (FDR <0.05; G-H).

Figure 4.3 | Kinetics of innate-like lymphocyte CD69 expression in response to BNT162b2 and ChAdOx1-S peaks between 24-48h after immunisation in vivo.

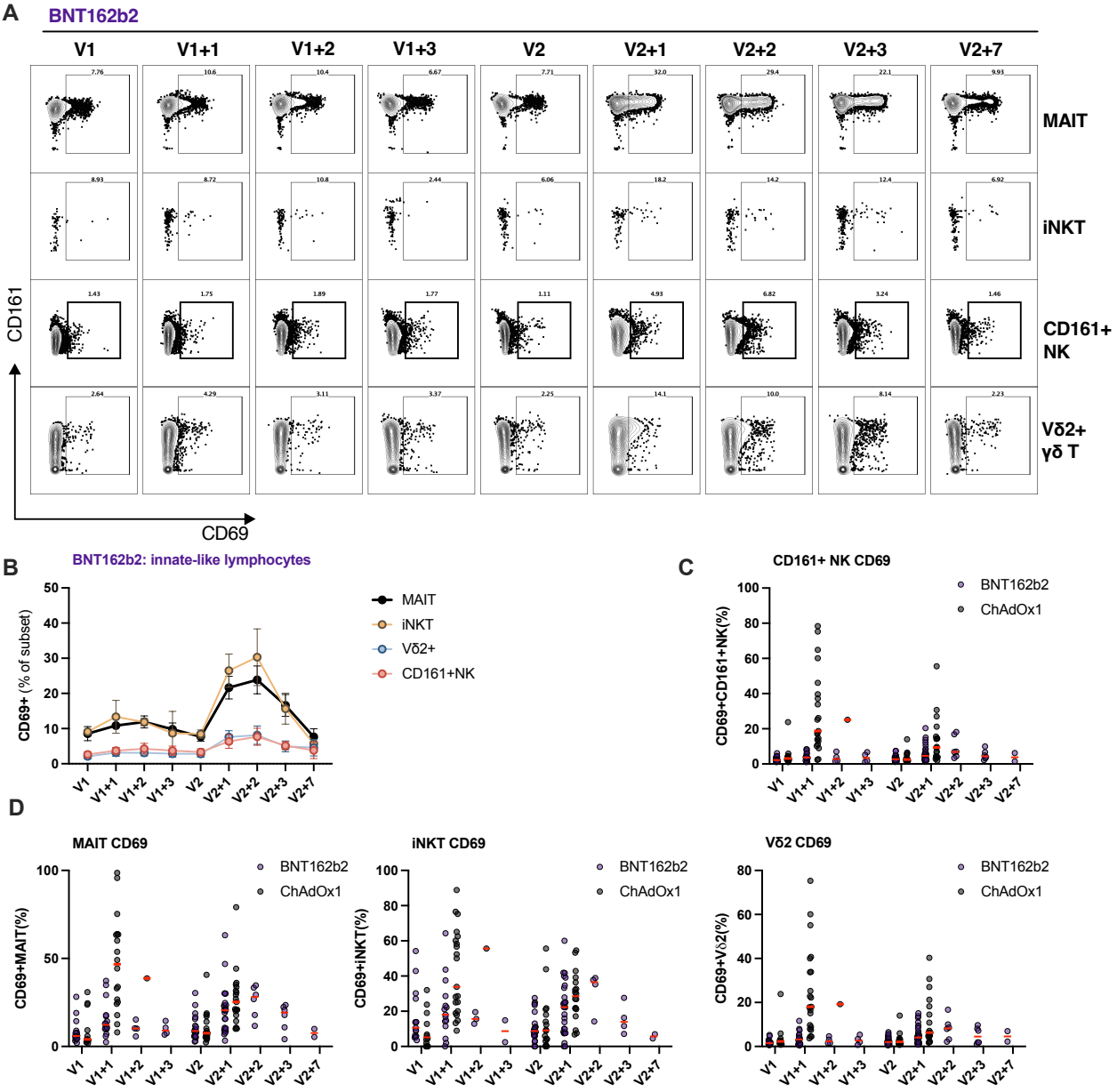

Fig4.3 | Kinetics of innate-like lymphocyte CD69 expression in response to BNT162b2 and ChAdOx1-S peaks between 24-48h after immunisation in vivo.
(A) Representative plots from a single healthcare worker receiving BNT162b2 showing CD69 expression longitudinally on MAIT cells (MR1/5-OP-RU tetramer+); iNKT cells (CD3+ Vα24-Jα18), CD161+NK cells (CD3-, CD161+ lymphocytes), and Vδ2+ γδ T cells.

(B) Summary of longitudinal CD69 expression on innate-like lymphocytes from donors followed intensively (n=6).

(C, D) Summary of CD69 across timepoints for CD161+NK cells (C) and innate-like T cells for both BNT162b2 (purple), or ChAdOx1-S (grey).

Changes in cell frequency also mirrored patterns of vaccine-induced activation (**Fig4.4)**. Lymphopenia, particularly a reduction in circulating MAIT cell frequency, is ubiquitous in numerous inflammatory and infectious states[177,183,389]. For each vaccine, MAIT cell frequency both as a fraction of T-cells (not shown) or live PBMC (**Fig4.4 A-E; I)** was predominantly reduced after ChAdOx1-S prime, and BNT162b2 boost (**Fig4.4 A-E**). The proportion of CD8+MAIT cells was also reduced by vaccination (not shown). Although we did not measure absolute counts, other studies have confirmed absolute lymphopenia after BNT162b2 vaccination[145], suggesting that absolute MAIT cell frequency would also be reduced either due to tissue migration, cell death, or a combination.

Conversely, the frequency of intermediate (CD14+CD16+) monocytes in particular was proportionally increased after prime and boost (**Fig4.4 A-B; F-H**). BNT162b2 increased intermediate monocyte frequency one day after prime, with enhanced monocytosis after boost peaking at 48h (**Fig4.4 G**). This delayed peak could identify monocytosis as a downstream response to the very earliest immune effectors, which include cytokines.

Intriguingly, when comparing non-acute timepoints, the frequency of monocytes was elevated 8-10wk after priming with ChAdOx1-S but not BNT162b2 (**Appendix SF4.2 A-D;** ChAdOx1-S, 13.7±1.8% (V1), 18.1±2.2% (V2); BNT162b2_long, 14.5±1.7% (V1), 15.6±1.8% (V2)). Monocytes also expressed higher HLA-DR (*data not shown*). Conversely, as a fraction of live PBMC, frequencies of pDC (**Appendix SF4.2 E**) and B cells (**Appendix SF4.2 F**) were increased 8-10wk after BNT162b2 prime. Although not a true reflection of cell count, both vaccines could induce long term changes in immune cell populations.

Figure 4.4 | BNT162b2 and ChAdOx1 display inverse patterns of changes in the frequency of MAIT cells, monocytes, and the activation of conventional T cells.

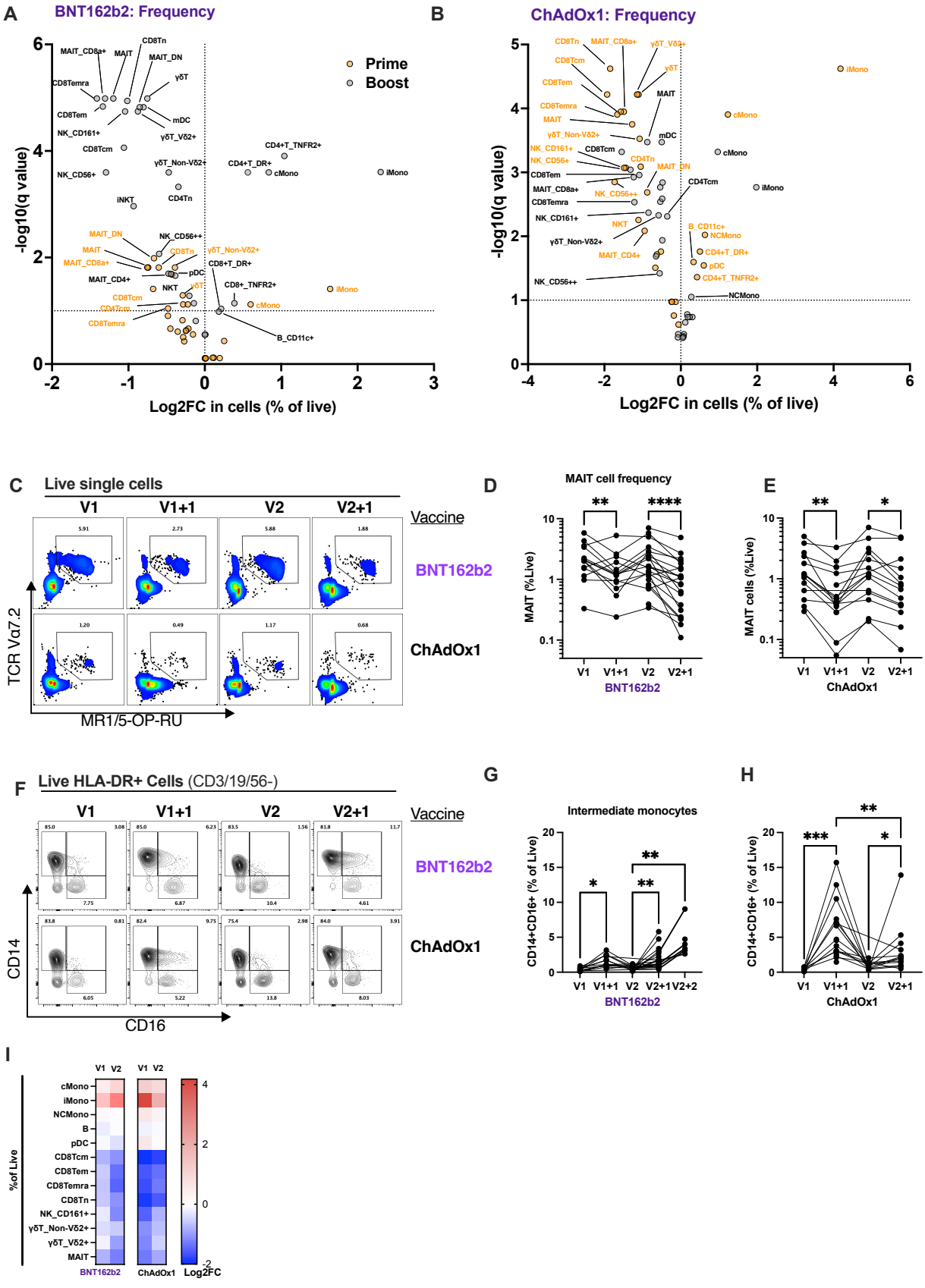

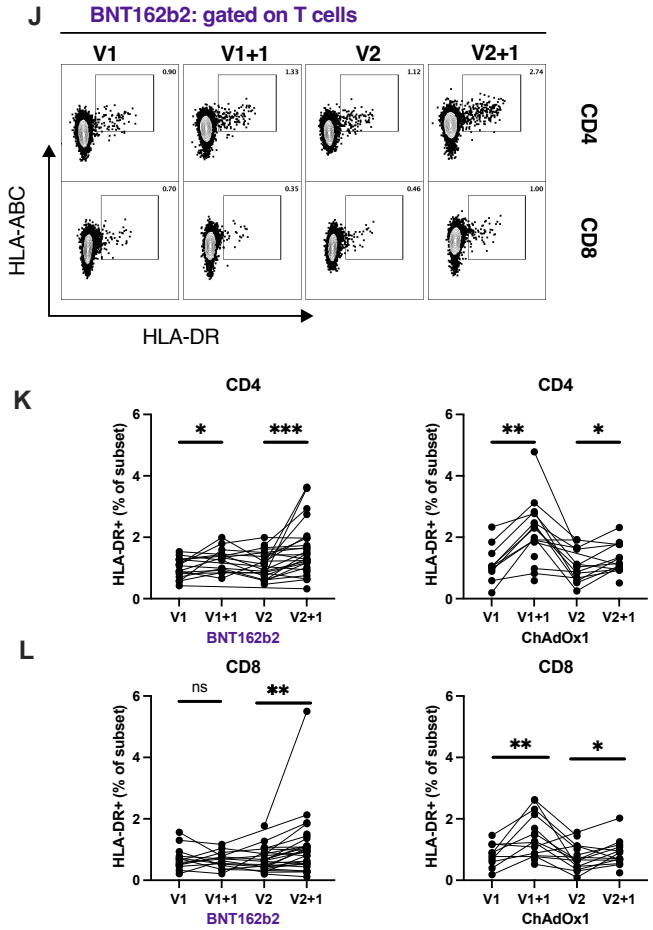

Fig4.4 | BNT162b2 and ChAdOx1 display inverse patterns of changes in the frequency of MAIT cells, monocytes, and the activation of conventional T cells.
(A,B) Volcano plots of log2 fold change in cell frequency as a fraction of live PBMC after BNT162b2 (**A**), or ChAdOx1 (**B**), showing the change at prime (yellow), or boost (grey). Dotted line FDR >0.1.
(C) Representative plots gated on live PBMC showing the frequency of MAIT cells (MR1/5-OP-RU tetramer+ TCR Vα7.2+) in a HCW receiving BNT162b2 (purple, top panel) or ChAdOx1-S (bottom panel).
(D, E) Summary of changes in MAIT cell frequency as a % of live cells in response to BNT162b2 (**D**) or ChAdOx1 (**E**).
(F) Representative plots gated on myeloid cells (CD3/19/56-, HLA-DR+), showing the frequency of monocytes in a HCW receiving BNT162b2 (purple, top panel) or ChAdOx1-S (bottom panel).
(G, H) Summary of changes in intermediate monocyte (CD14+CD16+) frequency after BNT162b2 (**G**) or ChAdOx1 (**H**).
(I) Heatmap of the median log2 fold change in cell frequency (as a % of live PBMC) after prime and boost with BNT162b2 (left panel), or ChAdOx1 (right panel).
(J) Representative plots gated on T cells in a HCW receiving BNT162b2, showing CD4 (top panel), and CD8 (bottom) HLA-DR.
(K,L) Summary of changes in HLA-DR expression in CD4 (**K**), and CD8 (**L**) T cells in response to BNT162b2 and ChAdOx1.
Symbols indicate individual donors (D, E; G, H; K, L) with lines connecting data points from the same donor. Mean ± SEM is shown. *p < 0.05; **p < 0.01; ***p < 0.001; ****p < 0.0001; ns, not significant.
Statistical significance was determined using: mixed-effects ANOVA Šídák's multiple comparisons test (D, E; G, H; K, L); multiple paired t tests with Benjamini, Krieger, & Yekutieli correction for multiple comparisons (FDR <0.1; A, B).
pDC = plasmacytoid dendritic cell; cMono = classical monocyte (CD14+CD16-); iMono = intermediate monocyte (CD14+CD16+); ncMono = non-classical monocyte (CD14-CD16+). Tn = naïve; Tcm = central memory; Tem = effector memory; Temra = RA+ effector memory.

Next, we analysed the expression of other cytokine-inducible markers which may be relevant for vaccine responses. These markers included MHC-I and MHC-II, which are upregulated by type I and type II IFN [87], and TNFR2 (as discussed in **Chapter3**).

Both vaccines induced MHC-I and MHC-II expression on innate cells (not shown), CD4+ and CD8+ T cells (**Fig4.4 J**). HLA-DR up-regulation on CD8+ T cells was observed only after BNT162b2 boost (**Fig4.4 L**), whereas both prime and boost induced HLA-DR expression on CD4+ T cells (**Fig4.4 K**). Notably, some of the activated CD4+ T cells observed after prime may be cross-reactive memory CD4+ T-cells, as previously reported [390]. Overall, these findings suggest that the vaccines induce a vaccine-specific degree and pattern of early cellular inflammation.

4.4.3 Interferons dominate early SARS-CoV-2 vaccine-induced responses

To investigate the activation of CD161+ cells, which are capable of cytokine-responsiveness, we measured plasma cytokine levels before and after homologous prime-boost vaccination to determine the key drivers of CD69 expression in particular.

We found that ChAdOx1-S elicited a higher inflammatory cytokine response than BNT162b2 after prime, with increased levels of IFN-γ, IL-6, MCP-1, and IL-10 induced by both vaccines (**Fig4.5 A**); plasma IFN-γ increased 13-fold relative to baseline one day after ChAdOx1-S prime, compared to only a 4-fold after BNT162b2 prime (**Fig4.5 E**). Uniquely, only ChAdOx1-S prime induced quantifiable IFN-α2 (2.6-fold increase; **Fig4.5 C**), which we have shown to be a potent inducer of CD69 expression on innate-like lymphocytes. Furthermore, there was evidence of unique inflammasome activation after ChAdOx1-S, with detectable plasma levels of IL-18 (**Fig4.5 D**), and IL-1β (**Fig4.5 G**).

Conversely, the cytokine induction after boost was higher in response to BNT162b compared to ChAdOx1-S (**Fig4.5 B**). The highest induction was observed for IFN-γ (mean 14-fold increase; **Fig4.5 B, E**), and IL-6 (mean 5-fold increase; **Fig4.5 B**), peaking at day one (**Fig4.5 F**). In contrast, ChAdOx1-S was less inflammatory post-boost, with inflammasome-derived IL-1β and IL-18 no longer significantly induced (**Fig4.5 D, G, I**).

When comparing prime and boost for each vaccine, an inverse pattern of cytokine induction was observed, with maximal IFN-γ and IL-6 after ChAdOx1-S prime and BNT162b2 boost (**Fig4.5 H-J**). MAIT cell CD69 expression, a highly sensitive marker for type I IFN in innate-like lymphocytes (**Fig3.12**), followed this same pattern (**Fig4.2**), in the absence of detectable IFN-α after BNT162b2.

To investigate if biologically active type I IFN was induced after BNT162b2 vaccination to account for this activation, which can be undetectable by standard ELISAs [391], we performed whole blood bulk RNA sequencing (**Fig4.5 K,** *data analysis by Lucy Garner*). Our analysis revealed an ISG signature dominated the early whole blood transcriptome after BNT162b2 vaccination (**Fig4.5 L, M;** *data analysis by Lucy Garner*; *ChAdOx1 data not shown*), both type I and type II IFN signalling enriched transcriptionally (**Fig4.5 M**). However, only IFN-γ and TNF signalling pathways were enriched when comparing primary and secondary vaccine responses (**Fig4.5 N**), in agreement with the boost-specific plasma cytokine enhancement. Although we did not detect any differences in TNF, a larger cohort study reported an increase in TNF one day after boosting with BNT162b2 on a short interval regimen[452].

Figure 4.5 | BNT162b2 and ChAdOx1-S induce an inverse pattern of interferon responses, with unique inflammasome induced cytokines after ChAdOx1-S prime.

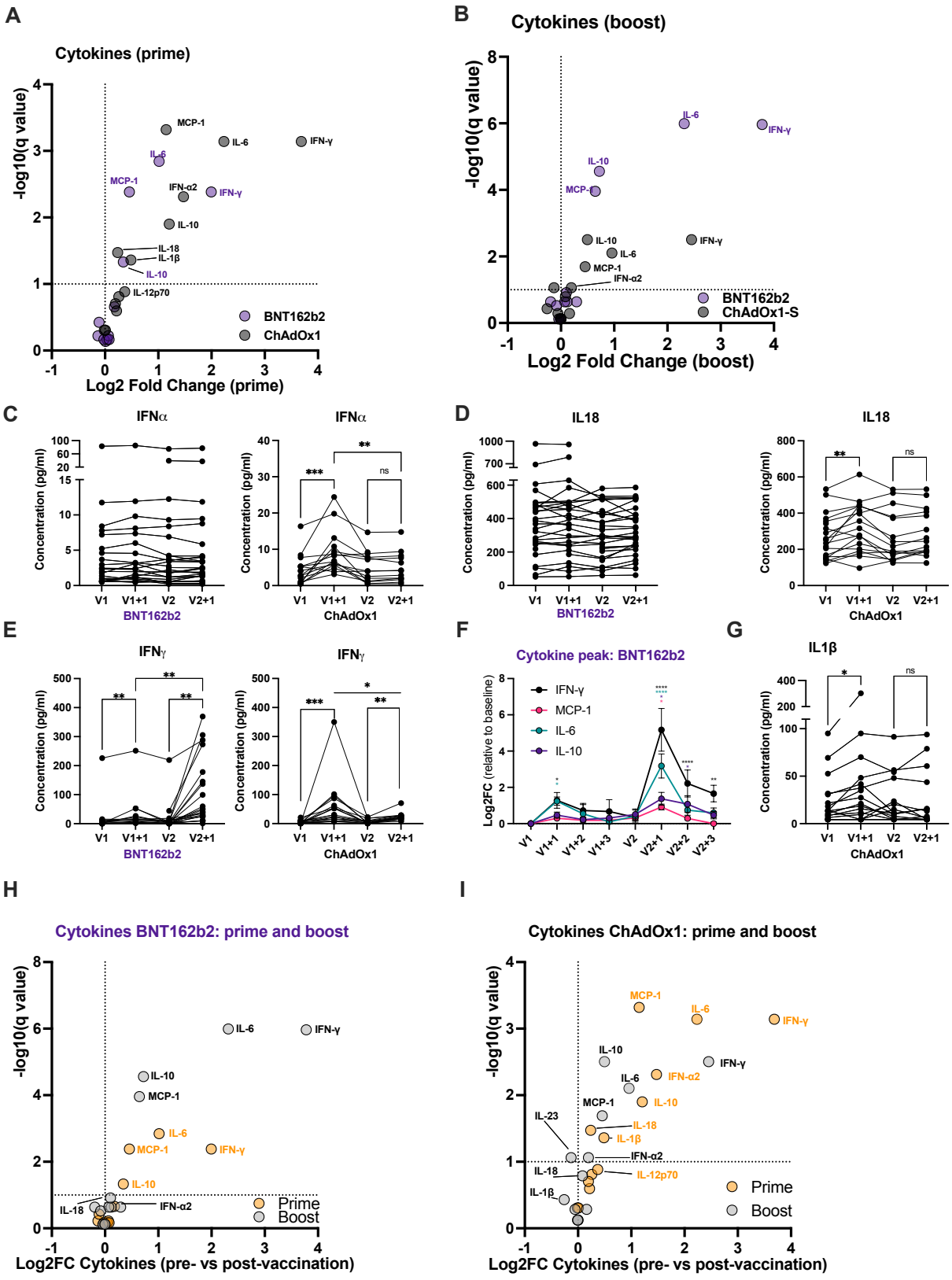

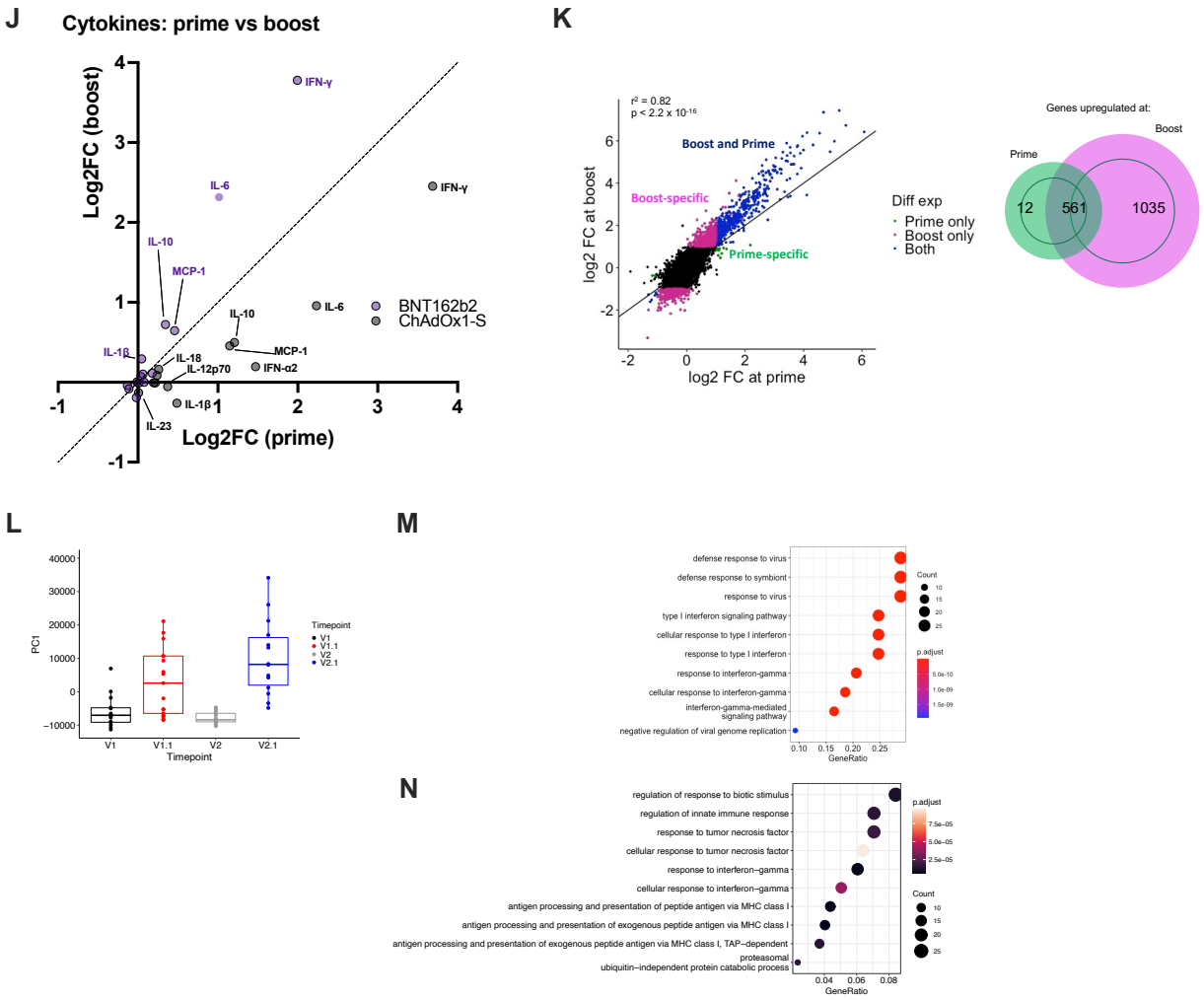

Fig4.5 | BNT162b2 and ChAdOx1-S induce an inverse pattern of interferon responses, with unique inflammasome induced cytokines after ChAdOx1-S prime.
(A, B) Volcano plots showing log2 fold change in cytokines on day 1 after prime (**A**), or boost (**B**) with BNT162b2 or ChAdOx1-S. Dotted line represents FDR >0.1.
(C, D, E) Plasma concentrations of IFN-α (**C**), IL-18 (**D**), and IFN-γ (**E**) from HCW vaccinated with BNT162b2 and ChAdOx1-S at specified timepoints.
(F) Log2 fold change in plasma IFN-γ, MCP-1, IL-6, and IL-10 logitudinally in n=5 healthcare workers followed from baseline.
(G) Plasma concentrations of IL1-β from HCW vaccinated with ChAdOx1-S at specified timepoints.
(H, I) Volcano plots of log2 fold change in cytokines on day 1 after prime and boost with BNT162b2 (**H**), and ChAdOx1-S (**I**). Dotted line represents FDR >0.1.
(J) Summary of the mean log2 fold change in plasma cytokines post-prime (V1-V1+1), and post-boost (V2-V2+1) for both BNT162b2 and ChAdOx1-S.

(K-L) Whole blood total RNAseq. (**K**) Differential gene expression induced by vaccination. (**L**) Boxplot of PC scores along PC1 by timepoint for BNT162b2, and (**M**) GO pathway analysis for PC1.
(N) GO pathway enrichment analysis of the differentially expressed genes between BNT162b2 boost and BNT162b2 prime (short interval only).
Symbols indicate individual donors (C-E; G) with lines connecting data points from the same donor. Mean ± SEM is shown. *p < 0.05; **p < 0.01; ***p < 0.001; ****p < 0.0001; ns, not significant.
Statistical significance was determined using: mixed-effects ANOVA with Šídák's (C-E; G) and Dunnett's test for multiple comparisons (F); multiple paired t-test of log2 cytokine concentrations with Benjamini, Krieger, & Yekutieli correction for multiple comparisons (FDR <0.1; A, B; H, J).
Data K-N generated by Lucy Garner.

Therefore, the innate-like lymphocyte activation, cytokine induction, and transcriptional signatures all converged on type I and type II IFNs as the main constituents of early vaccine responses. While IFN-α2 was only measurable after ChAdOx1-S prime, both vaccines elicited substantial IFN-γ after homologous prime-boost, with the magnitude and pattern unique to the vaccine platform and modality.

4.4.4 Immune correlates of early ChAdOx1-S vaccine response

Previously, we have proposed that early plasma IFN-γ and MAIT-cell activation may be important in predicting subsequent ChAdOx1-induced antigen-specific T-cell ELISpot responses[334]. Therefore, we conducted correlation analysis to identify other potential correlates of these measures in the early ChAdOx1-S immune response that may be relevant in predicting subsequent adaptive immunity **(Fig4.6 A**). We focussed in particular on baseline parameters of innate-like lymphocytes which could predict early IFN-γ after ChAdOx1-S prime, as prior work indicates that these cells are primary drivers of IFN-γ production.

Female sex was the strongest predictor of early IFN-γ in response to ChAdOx1-S, with females showing higher levels of both IFN-γ **(Fig4.6 B**), and IFN-α2 **(Fig4.6 C**), one day after prime with ChAdOx1-S, but not with BNT162b2 **(Fig4.6 B**). Since our cohort consisted mostly of females under 40, we also explored the impact of age as a co-correlate and found that increasing age was inversely associated with early IFN-γ production in response to ChAdOx1-S in females only ($r = -0.57$, $p = 0.034$; **(Fig4.6 D**). Furthermore, we observed additional weak associations with early IFN-γ, including the baseline frequency of CD56++ NK cells ($r = 0.66$, $p = 0.015$; **(Fig4.6 E**), and other innate-like lymphocyte frequencies that contribute to ChAdOx1-induced IFN-γ in vitro (**Chapter3**).

Figure 4.6 | Early IFN-γ after ChAdOx1-S is highest in young females.

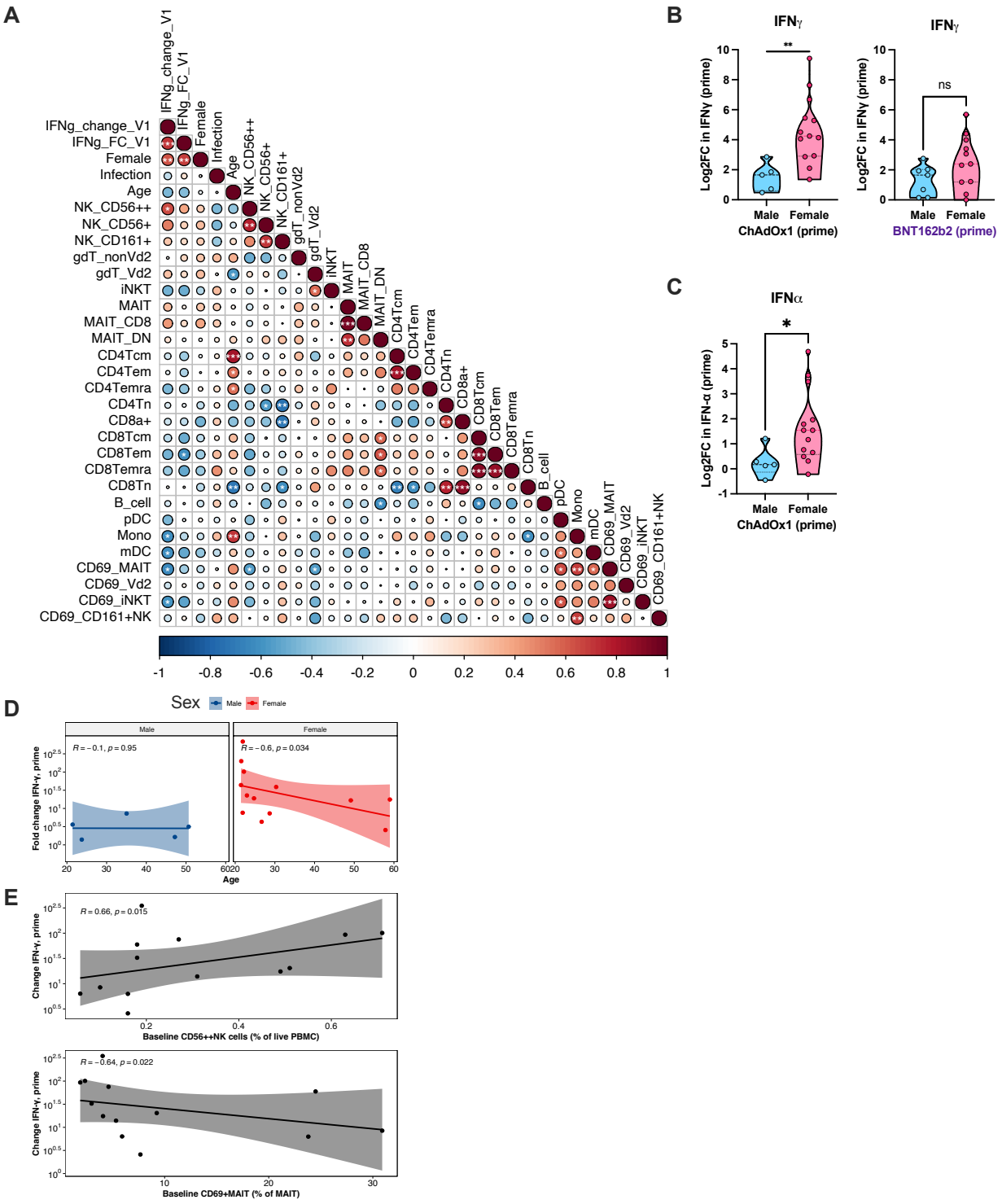

Fig4.6 | Early IFN-γ after ChAdOx1-S is highest in young females.
(A) Multi-parametric correlation matrix plot of baseline immune and demographic characteristics that correlate with early IFN-γ after ChAdOx1-S. Circle size and colour intensity represent Spearman's correlation co-efficients.
(B, C) Violin plots of Log2 fold change in plasma IFN-γ(**B**), and IFN-α(**C**), on day 1 after ChAdOx1-S or BNT162b2 vaccination in males and females.
(D, E) Spearman's correlations of the fold change in plasma IFN-γ post prime (**D**), or absolute change (**E**, pg/ml), on day 1 after ChAdOx1-S prime. Pre-vaccine age (**D**), and frequency of CD56++ NK cells or CD69+ MAIT cells (**E**) are shown.

Symbols indicate individual donors (B-E). *p < 0.05; **p < 0.01; ***p < 0.001; ****p < 0.0001; ns, not significant. Statistical significance was determined using Spearman's correlation (A, D, E) or Mann-Whitney U-test (B-C).

To investigate the cytokines that could have triggered the activation of innate-like lymphocytes and their potential role in reduced responses at boost, we examined plasma cytokine correlates of early ChAdOx1-S induced IFN-γ **(Fig4.7 A**). We found that vaccine-induced IFN-α, capable of activating innate-like lymphocytes independently of TCR, correlated strongly with early IFN-γ produced post prime ($r = 0.7$, $p < 0.0073$; **Fig4.7 B**), along with the level of activation for MAIT cells ($r = 0.59$, $p = 0.049$), Vδ2+ γδ T cells ($r = 0.79$, $p = 0.0036$), and NK cells ($r = 0.59$, $p = 0.049$; **Fig4.7 C**). The decrease in IFN-γ production after ChAdOx1-S boost coincided with lower levels of IFN-α (**Fig4.5 C**), and IL-18 (**Fig4.5 D**), which are crucial for effective innate-like lymphocyte activation. This supports our previous in vitro model that suggests type I IFN-mediated innate-like lymphocyte activation as the main driver of early ChAdOx1-S induced IFN-γ. Moreover, the decline in the frequency of circulating innate-like lymphocytes noted during early responses (**Fig4.4 B, E**) also correlated with global IFN-γ production (Vδ2+, $r = -0.79$, $p = 0.098$; **Fig4.7 D**), indicating that IFN-mediated signalling may be a shared mechanism accounting for lymphopenia during antiviral responses.

Figure 4.7 | Early IFN-γ after ChAdOx1-S correlates with changes in IFN-α, innate-like lymphocyte activation and lymphopenia one day after immunisation.

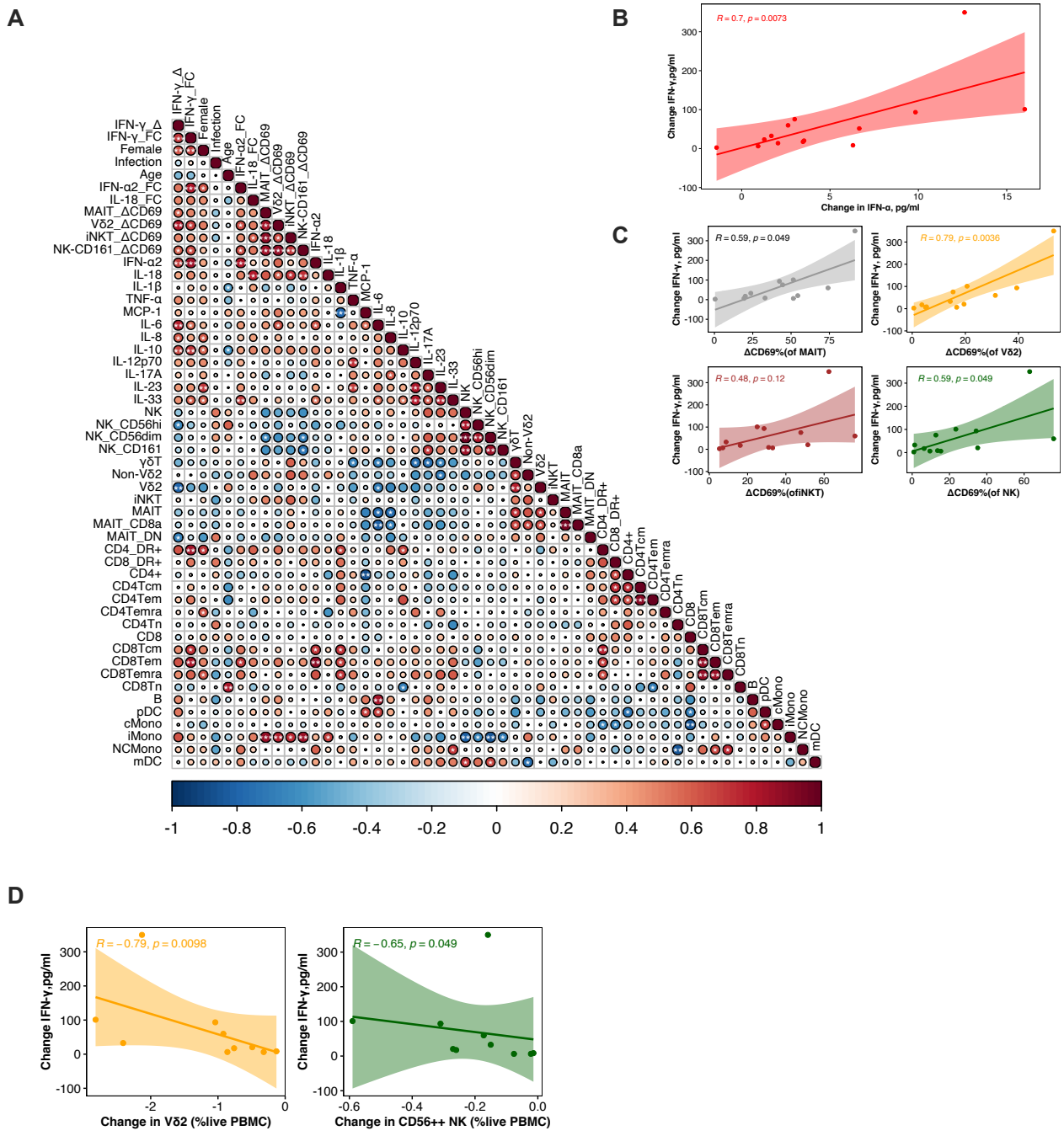

Fig4.7 | Early IFN-γ after ChAdOx1-S correlates with changes in IFN-α, innate-like lymphocyte activation and lymphopenia one day after immunisation.
(A) Multi-parametric correlation matrix plot of change in immune parameters (between baseline and day 1) focussing on correlates of early IFN-γ after ChAdOx1-S. Circle size and colour intensity represent Spearman's correlation co-efficients.
(B) Spearman's correlation of the change in plasma IFN-α and IFN-γ post prime.
(C) Spearman's correlation of the change in CD69 expression in MAIT cells (grey), Vδ2+ cells (yellow), iNKT (brown), or NK cells (green) pre and post prime with the subsequent change in IFN-γ.
(D) Spearman's correlation of the change in frequency of Vδ2+ (yellow) or CD56++NK cells (green) (both as a fraction of live cells) with the subsequent change in IFN-γ.

Symbols indicate individual donors (B-E).
*p < 0.05; **p < 0.01; ***p < 0.001; ****p < 0.0001; ns, not significant.
Statistical significance was determined using Spearman's correlation (A-D).

4.4.5 Immune correlates of early BNT162b2 vaccine response

We next aimed to identify the source of early IFN-γ after BNT162b2, as neither IL-18 nor type I IFN, which are important for innate-like lymphocyte activation, were induced robustly. Given that early IFN-γ production was highest after BNT162b2 boost, we analysed the change in concentration of cytokines, frequencies of immune cells, and activation of innate-like lymphocytes to identify potential drivers of boost-specific augmentation (**Fig4.8 A**).

Multiparameter matrix correlation analysis revealed that changes in IL-6 ($r = 0.72$, $p < 2E-5$; **Fig4.8 B**), and MCP-1 ($r = 0.57$, $p = 0.0026$; **Fig4.8 B**), were the most significant co-correlates of early IFN-γ. The activation of innate-like lymphocytes, including MAIT cells ($r = 0.59$, $p = 0.0018$), Vδ2+ γδ T cells ($r = 0.53$, $p = 0.0084$), and CD161+ NK cells ($r = 0.68$, $p = 4e-4$), also correlated with plasma IFN-γ post-boost (**Fig4.8 C**). The degree of lymphopenia in MAIT cells and Vδ2+ γδ T cells correlated with total IFN-γ production (DN MAIT, $r = -0.45$, $p < 0.035$; Vδ2+, $r = -0.69$, $p < 0.001$; **Fig4.8 D, E**), and their activation, similar to observations in the context of other antiviral responses[225,343]. These results imply that BNT162b2-induced early antiviral inflammatory cytokines may drive both activation and reduced circulating frequencies of innate-like lymphocyte

Figure 4.8 | Early IFN-γ after BNT162b2 boost correlates with innate-like lymphocyte activation and degree of lymphopenia one day after immunisation.

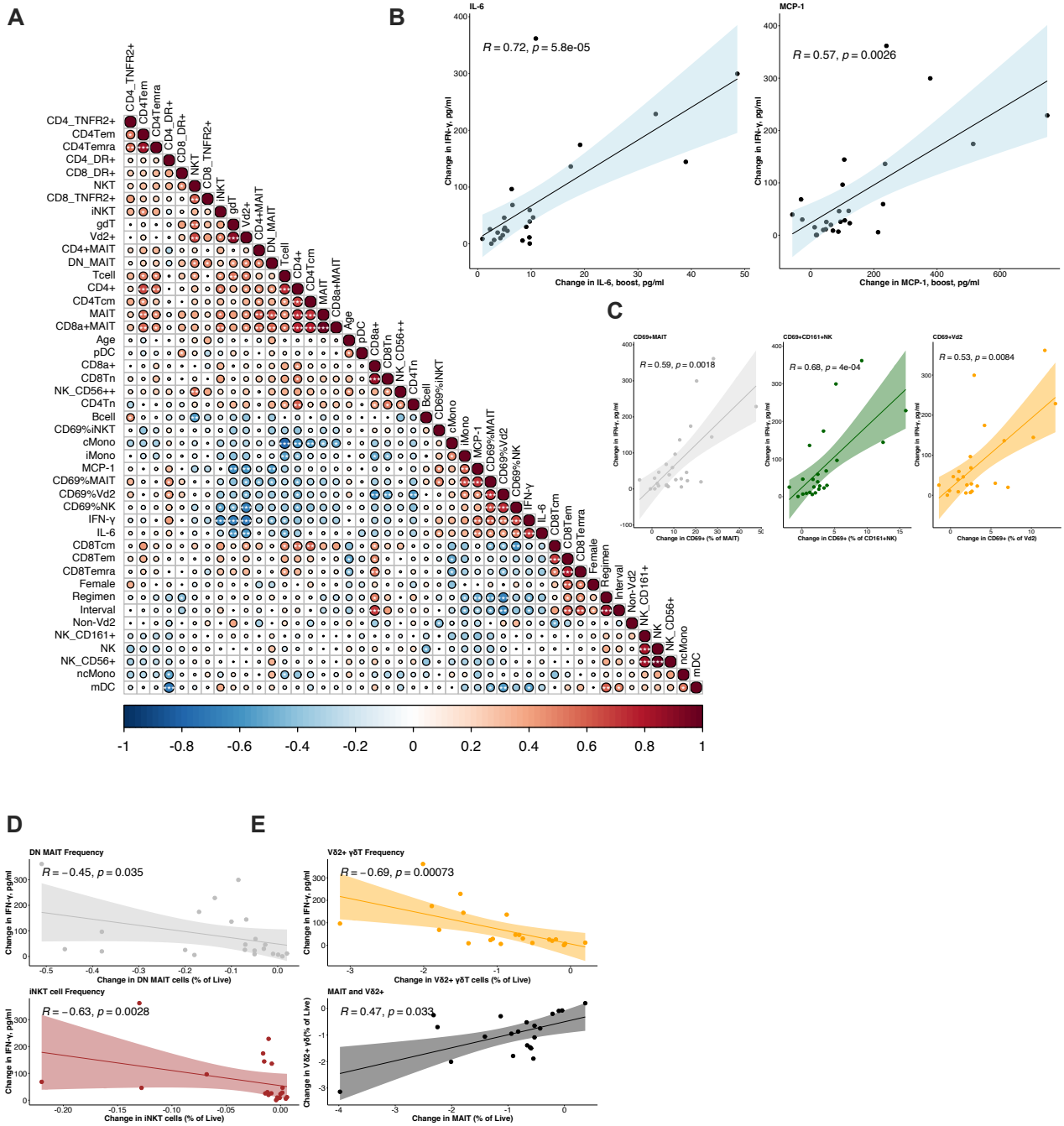

Fig4.8 | Early IFN-γ after BNT162b2 boost correlates with innate-like lymphocyte activation and degree of lymphopenia one day after immunisation.

(A) Multi-parametric matrix correlation plot of change in immune parameters between pre-boost (V2) and day 1 post boost (V2+1), focussing on correlates of early IFN-γ. Circle size and colour intensity represent Spearman's correlation co-efficients. Variables are ordered by hierarchical clustering.

(B) Spearman's correlation of the change in plasma IL-6, MCP-1, and IFN-γ post-boost.

(C) Spearman's correlation of the change in CD69 expression in MAIT cells (grey), Vδ2+ cells (yellow), or CD161+NK cells (green) pre and post boost with the subsequent change in IFN-γ.

(D) Change in frequency of double negative MAIT cells (grey), Vδ2+ γδ T cells (yellow) as a fraction of live cells correlated with early change in plasma IFN-γ.

(E) Correlation of the degree of change in frequency of double negative (DN) MAIT cells, iNKT cells, and Vδ2+ γδ T cells as a fraction of live cells between V2 and V2+1.

Symbols indicate individual donors. *p < 0.05; **p < 0.01; ***p < 0.001; ****p < 0.0001; ns, not significant.

Statistical significance was determined using Spearman's correlation (A-E).

MAIT cells (MR1/5-OP-RU tetramer+); iNKT cells (CD3+ Vα24-Jα18+), CD161+NK cells (CD3-, CD161+ lymphocytes), and Vδ2+ γδ T cells.

Interestingly, the boosting interval between prime and boost was inversely associated with the magnitude of early IFN-γ at the time of boost (r = -0.49, p = 0.01; **Fig4.8 A; Fig4.9 A**). HCW on shorter dosing intervals had higher levels of IFN-γ (**Fig4.9 B**), IL-6 (**Fig4.9 C**), and MCP-1 (**Fig4.9 D**), as well as increased innate-like lymphocyte activation after boosting (**Fig4.9 E, F**), compared to HCW boosted with longer dosing intervals. This suggested that the time since primary vaccination influenced the expected early responses after subsequent homologous boost.

Figure 4.9| BNT162b2 boost induced IFN-γ and innate-like T cell activation higher after shorter boosting intervals.

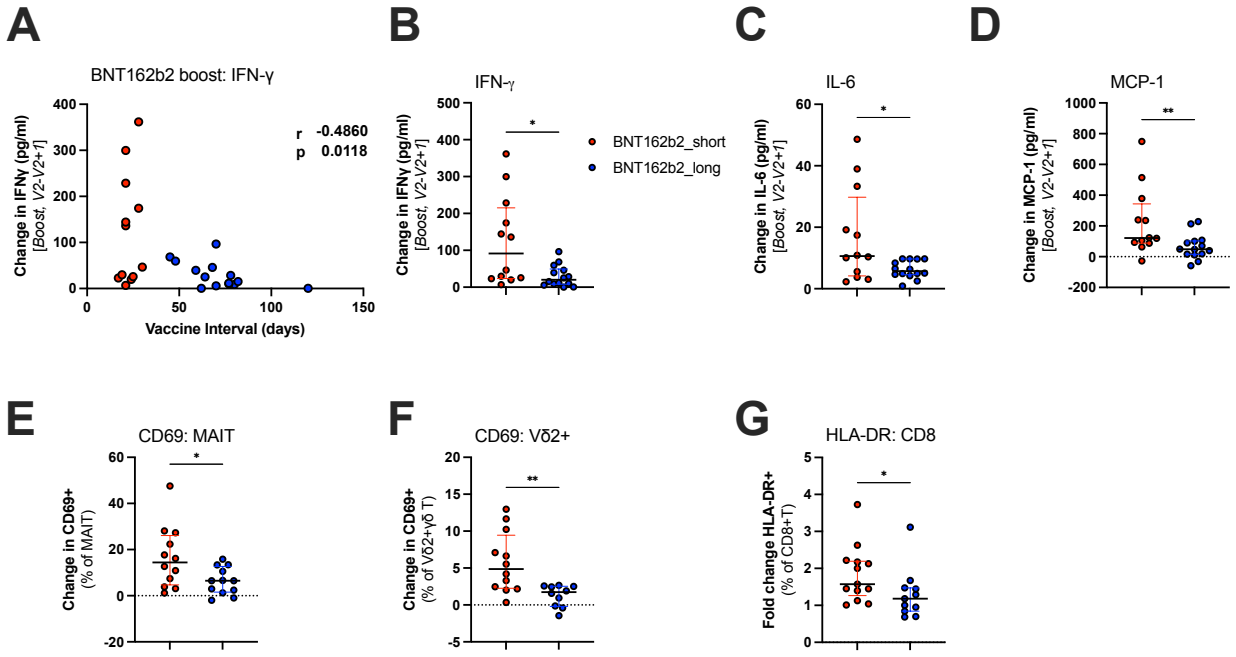

Fig4.9 | BNT162b2 boost induced IFN-γ and innate-like T cell activation higher after shorter boosting intervals.
(A) Correlation of plasma IFN-γ induced post-boost (change between pre-V2 and V2+1) with vaccine interval.
(B-D) Change in plasma cytokines and chemokines one day after BNT162b2 boost in those boosted with short (<4wk, red), or long interval (>4wk, blue). Plasma IFN-γ (**B**), IL-6 (**C**), and MCP-1 (**D**) shown.
(E-G) Change in cellular activation as a fraction of cells one day after BNT162b2 boost in those boosted with short (<4wk, red), or long interval (>4wk, blue). CD69 expression on MAIT cells (**E**), and Vδ2+ γδ T cells (**F**); and HLA-DR expression on CD8+ T cells (**G**) shown.
All donors were naïve to SARS-CoV-2 prior to vaccination. Symbols indicate individual donors.
*p < 0.05; **p < 0.01; ***p < 0.001; ****p < 0.0001; ns, not significant.
Statistical significance was determined using Spearman's correlation (A), or Mann-Whitney unpaired tests (B-G). *MAIT cells (MR1/5-OP-RU tetramer+).*

We hypothesised that differences in adaptive immune parameters at the time of boosting on the long interval (~10wk post-prime) might underpin observed differences in early responses. A large multi-centre study, which included many of the patients in this smaller cohort, showed a clear decline in anti-spike IgG, anti-RBD IgG, and neutralising antibodies between 3 week and 10 weeks after prime in naïve participants (2.6, 2.78, and 3.3-fold reduction respectively)[363]. In our sub cohort, we also observed a reduction in antibodies between 3 and 10wks post-prime (**Fig4.10 A**), with higher anti-spike-binding antibodies in donors on the shorter boosting interval at the time of boost (**Fig4.10 B**). Antibodies in all donors boosted on the extended dosing interval waned from 4wk post-prime (V1+28) to pre-boost timepoints (**Fig4.10 C)**. These data are consistent with all other published cohorts demonstrating a peak at 3wk and subsequent waning of BNT162b2-induced binding and neutralising antibodies, as well as antibody-mediated effector functions such as antibody-dependent cell-mediated cytotoxicity (ADCC)[392].

Waning was not observed in the larger PITCH cohort for BNT162b2 induced spike-specific T-cell IFN-γ ELISpot between 4 weeks and 10weeks post-prime (Payne et al.[363], reanalysed; **Appendix SF4.3**). However, studies measuring spike-specific responses by flow cytometry have found waning of activation-induced marker positive (AIM+), IFN-γ+ and IL-2+ spike-specific CD4+ T cells between 3 weeks and 10 weeks post-prime [393]. In our smaller sub cohort, although total specific IFN-γ+ T-cells by ELISpot were not appreciably different between regimens at the time of boost, S2-specific T-cell IFN-γ responses were lower at boost in donors with extended interval boosting (median 35 vs 5.8 SFU/ million PBMCs; p = 0.0164) (**Fig4.10 D-H**). Longitudinal pairwise analysis of donors (**Fig4.10 G-H**), including those in the larger PITCH cohort (**Appendix SF4.3**), did not reveal convincing waning in T-cell IFN-γ ELISpot responses between V1+28 and V2 timepoints in those boosted with longer intervals. Therefore, we can only conclude that humoral SARS-CoV-2 specific immune responses robustly waned and were of appreciably different magnitude at the time of boost in those boosted with longer intervals.

Figure 4.10 | Comparison of spike-specific adaptive immunity at the time of boost in healthcare workers boosted with longer boosting intervals.

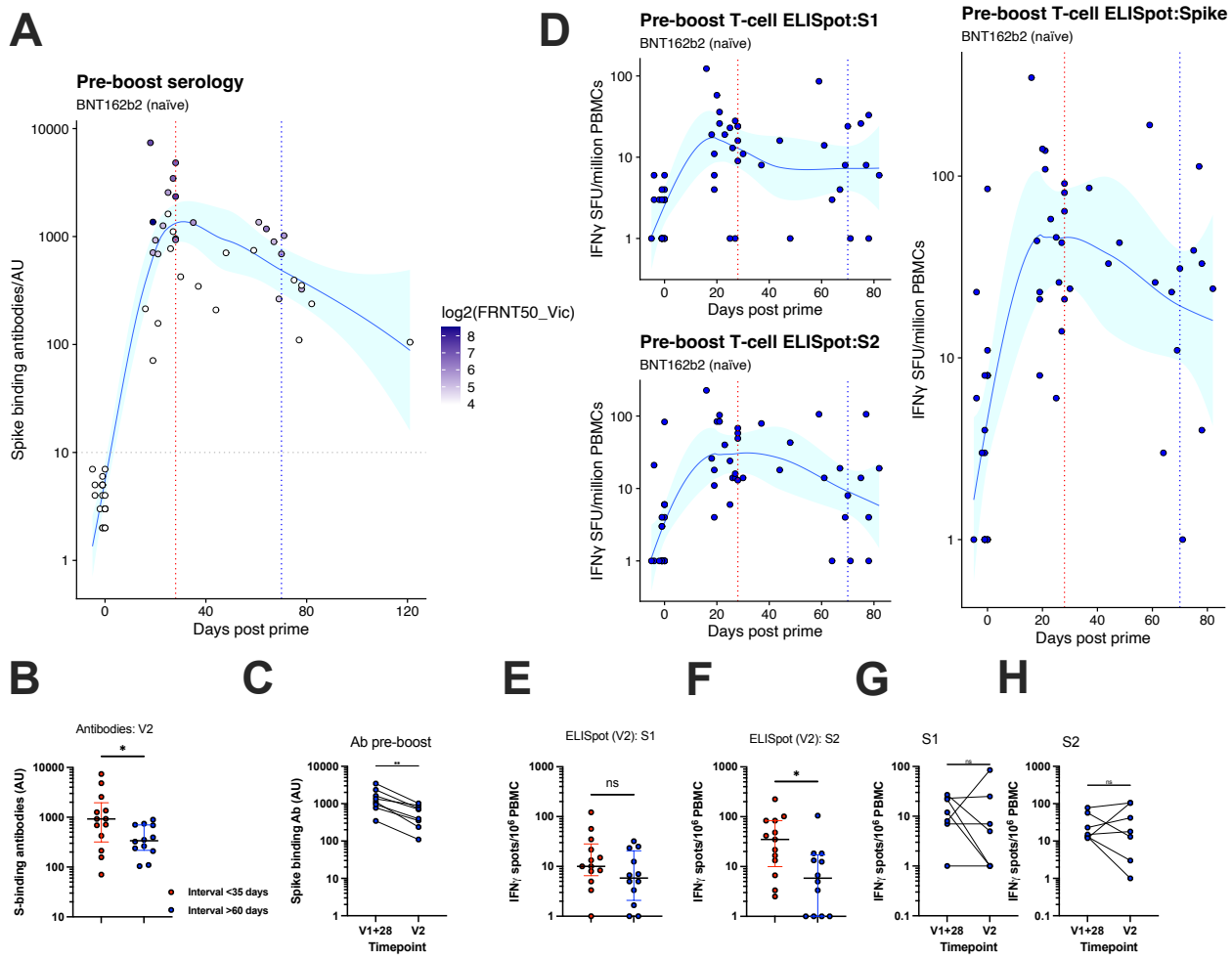

Fig4.10 | Comparison of spike-specific adaptive immunity at the time of boost in healthcare workers boosted with longer boosting intervals.
(A) Concentration of SARS-CoV-2 spike-binding antibodies at indicated days post-prime. Dotted red lines indicate average time at boost with short interval (4wk) or long interval (10wk) boosting. Intensity of fill corresponds to log2 neutralising antibody titre to live Victoria isolate of SARS-CoV-2 (SARS-CoV-2 Victoria; FRNT50_Vic). (open circles below limit of detection).

(B) SARS-CoV-2 spike-specific IgG binding antibody titres at the time of boost (V2) in HCW boosted <35 days post-prime (red, short) compared to those with extended interval boosting (blue, long).

(C) SARS-CoV-2 spike-specific IgG binding antibody titres at 28d post-prime (V1+28) and at the time of boost (V2) in donors on the extended interval regiment. Lines connect individual donors across time.

(D) IFN-γ ELISpot responses to SARS-CoV-2 spike (Victoria), individual or pooled S1 and S2 peptides (Spike, S1+S2) at specified time points after BNT162b2 prime. Dotted red lines indicate average time at boost on short interval (4wk) or long interval (10wk) regimens. Data in spot-forming units per million PBMC (SFU/million PBMC).

(E, F) IFN-γ ELISpot responses to SARS-CoV-2 S1 (**E**), S2 (**F**) peptide at the time of boost (V2) in HCW boosted at <35 days post-prime (red, short) compared to those with extended interval boosting (blue, long). Data in spot-forming units per million PBMC (SFU/million).

(G, H) IFN-γ ELISpot responses to S1 (**G**), S2 (**H**) peptide at 4wk after prime (V1+28), and the time of boost (V2) in HCW boosted on extended interval boosting. Lines connect individual donors across time. Data in spot-forming units per million PBMC (SFU/million).

All donors were naïve to SARS-CoV-2 prior to vaccination. Symbols indicate individual donors.
*p < 0.05; **p < 0.01; ***p < 0.001; ****p < 0.0001; ns, not significant.
Statistical significance was determined using Mann-Whitney unpaired tests (B, E, F), or Wilcoxon matched paired signed rank test (C, G, H).

We next explored whether there was any association between spike-specific adaptive responses at the time of boost and the subsequent magnitude of immune activation, focussing on innate-like lymphocytes and IFN-γ induction (**Fig4.11 A**). We found that adaptive immune measures at boost co-correlated with early IFN-γ, innate-like lymphocyte activation, and increased intermediate monocyte frequency (**Fig4.11 A**). The magnitude of early plasma IFN-γ after boost positively correlated with both the binding antibodies ($r = 0.47$, $p = 0.021$; **Fig4.11 B**), and spike-specific IFN-γ T cell ELISpot at the time of boost ($r = 0.47$, $p = 0.018$; **Fig4.11 C**). The degree of MAIT cell activation, as judged by the change in CD69 expression, was also higher in individuals with increased T-cell ELISpot responses at boost ($r = 0.53$, $p = 0.0065$; **Fig4.11 D**). In addition, the increased monocyte frequency, which is possibly a direct result of increased plasma IFN-γ [387], co-correlated with the magnitude of SARS-CoV-2 spike-specific T cell responses at boost ($r = 0.47$, $p = 0.028$; **Fig4.11 E**).

In summary, our findings indicate that adaptive immune parameters at the time of boost directly correlated with the magnitude of subsequent plasma IFN-γ after 24h, as well as other measures of early immune activation. These results suggest that adaptive immunity may influence the magnitude of early IFN-γ induced at boost, which is consistent with our earlier observations that plasma IFN-γ is specifically augmented post-boost with BNT162b2.

Figure 4.11 | Early post-boost IFN-γ and innate-like lymphocyte activation correlates with spike-specific adaptive immune responses prior to boost.

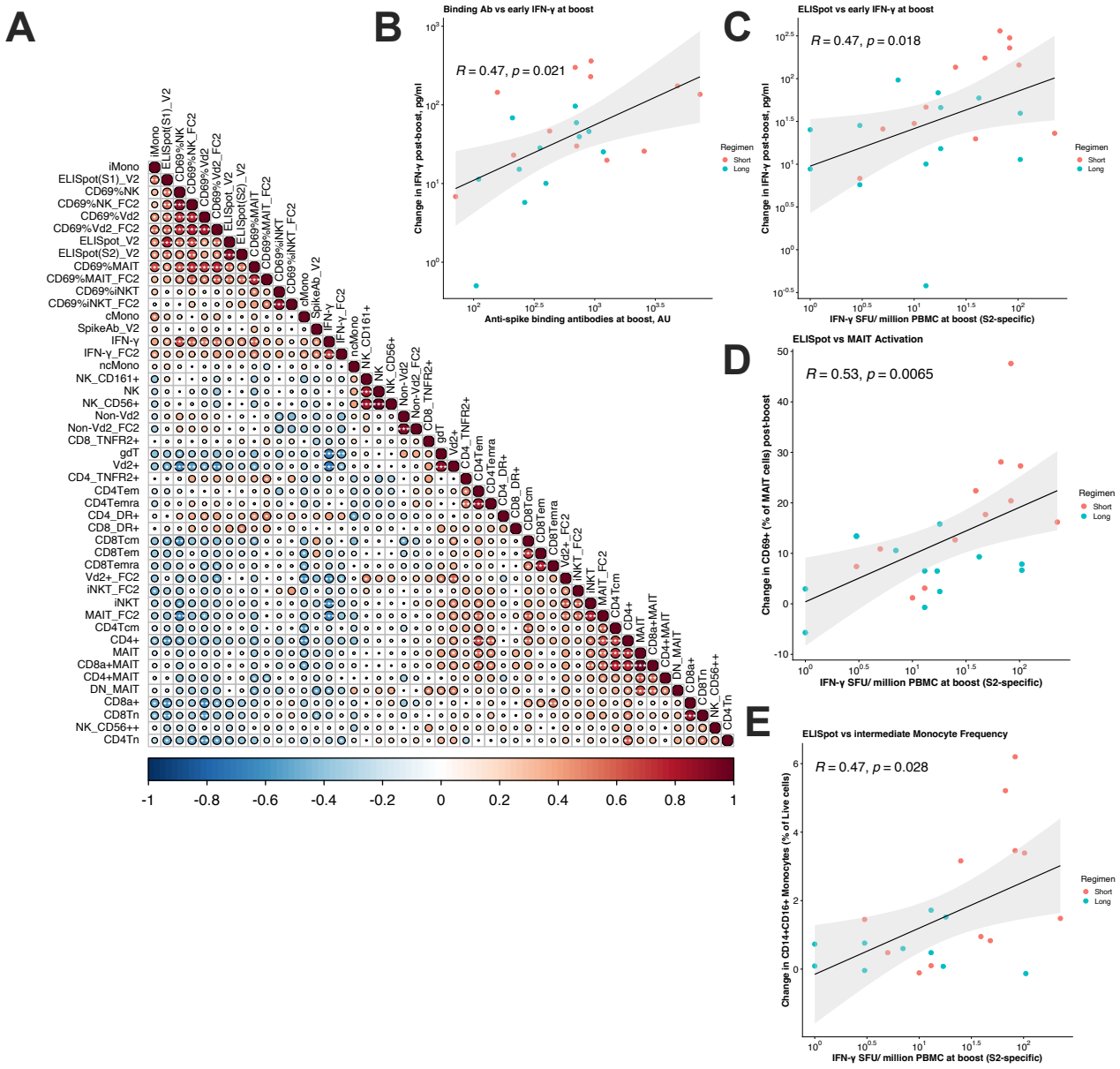

Fig4.11 | Early post-boost IFN-γ and innate-like lymphocyte activation correlates with spike-specific adaptive immune responses prior to boost.

(A) Multi-parametric matrix correlation plot of change in immune parameters between pre-boost (V2) and day 1 post boost (V2+1), focussing on correlates of early IFN-γ induced (V2+1, compared to V2) with adaptive immune measures at the time of boost (V2). Adaptive measures include SARS-CoV-2 IFN-γ ELISpot (spot-forming units per million PBMCs, SFU/10^6) and binding antibodies (arbitrary units, AU). Spearman's correlation co-efficients are shown as circle size and colour intensity. Variables are ordered by hierarchical clustering.

(B, C) Spearman's correlation of the change in plasma IFN-γ at boost (V2 to V2+1) with spike-binding antibodies (**B**), or T-cell IFN-γ ELISpot (S2-specific, **B**) at boost. Symbols indicate individual donors and colour indicates the regimen boosting interval (red, short; blue, long).

(D, E) Spearman's correlation of the change in CD69+MAIT cells (**D**), or CD14+CD16+ monocyte frequency (**E**, fraction of live PBMC) between V2 and V2+1 with the magnitude of T-cell IFN-γ ELISpot at boost (SFU/10^6 PBMC).

(B-E) Symbols indicate individual donors and colour indicates the regimen boosting interval (red, short; blue, long).
All donors were naïve to SARS-CoV-2 prior to vaccination.
*p < 0.05; **p < 0.01; ***p < 0.001; ****p < 0.0001; ns, not significant. Statistical significance was determined using Spearman's correlation (A-E).
ELISpot(S1)_V2 = S1-specific IFN-γ ELISpot at boost; ELISpot(S2)_V2 = S2-specific IFN-γ ELISpot at boost; ELISpot_V2 = pooled S1 and S2-specific ELISpot responses; SpikeAb_V2= anti-spike binding IgG at boost.

To further test the notion that adaptive immunity at the time of second spike-antigen exposure could drive early IFN-γ in response to BNT162b2, we compared early IFN-γ post-prime in those with or without serological evidence of prior infection, for whom primary immunisation was a second spike antigen exposure (**Fig4.12**). The median change in plasma IFN-γ after prime was more than five-fold higher in those with detectable spike-binding antibodies at baseline (median change in IFN-γ 54.5 pg/ml if spike-positive at baseline, compared to 7.5 pg/ml if spike-negative; p = 0.017; **Fig4.12 A**). No difference in IFN-γ was observed based on infection status after ChAdOx1-S prime (**Fig4.12 B**), or BNT162b2 boost (**Fig4.12 C**). Taken together these data would suggest that immune memory of spike antigen exposure may uniquely regulate early responses to mRNA vaccines but not AdV.

Figure 4.12 | Prior infection is specifically associated with increased early IFN-γ and immune activation after BNT162b2 prime.

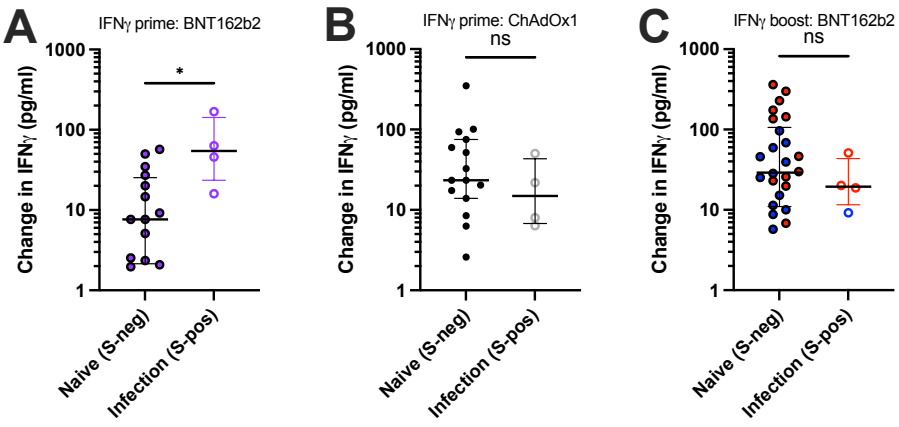

Fig4.12 | Prior infection is specifically associated with increased early IFN-γ and immune activation after BNT162b2 prime.
(A, B) Plasma IFN-γ induced 1 day after prime with BNT162b2 (**A**), or ChAdOx1-S (**B**), in those with or without evidence of prior infection (positive anti-spike binding antibodies at baseline).
(C) Plasma IFN-γ induced 1 day after boost with BNT162b2 (**C**) in those with or without evidence of prior infection. Symbols indicate individual donors. Color indicates boosting interval (red, short; blue, long).

*p < 0.05; **p < 0.01; ***p < 0.001; ****p < 0.0001; ns, not significant.
Statistical significance was determined using Mann-Whitney U test.

4.4.6 SARS-CoV-2 vaccines produce spike protein, activate innate immune cells, and induce IFNs in vitro

To understand how SARS-CoV-2 vaccines might induce interferons and initiate early immune responses, we tested the capacity of licensed vaccines to transfect and activate immune cells in vitro. Further measures of vaccine function included cytokine secretion in supernatants, and activation of spike-specific conventional T-cells (**Fig4.13**).

To determine whether SARS-CoV-2 vaccines were functional in vitro, remnant vaccines were titrated onto PBMCs to measure innate cell activation and spike production (**Fig4.13**); quantification of spike was either using ELISA, measuring total secreted RBD protein, or flow cytometry to detect cells expressing SARS-CoV-2 S1 spike protein (**Fig4.13 A**).

All three licensed SARS-CoV-2 vaccines induced RBD secretion in vitro at 24h (**Fig4.13 B**). The magnitude was nearly 17 times higher after mRNA-1273 (10μg/ml) compared to BNT162b2 (10μg/ml) (median RBD 211pg/ml, mRNA-1273; 12.9 pg/ml, BNT162b2; **Fig4.13 B**). RNA vaccine-induced antigen secretion was much slower compared to ChAdOx1-S over a 48h period; most ChAdOx1-S induced RBD was produced within 24h, with minimal increase thereafter (mean 79.8%; **Fig4.13 C D**), consistent with the known rapid kinetics of AdV CMV promoter-induced transgene expression [394]. RNA vaccines, BNT162b2 and mRNA-1273, shared much slower kinetics for antigen secretion which predominantly occurred between 24h and 48h (mean 73.1% and 67.3% respectively; **Fig4.13 C, D**).

Figure 4.13 | SARS-CoV-2 vaccines secrete spike RBD protein in PBMC in vitro.

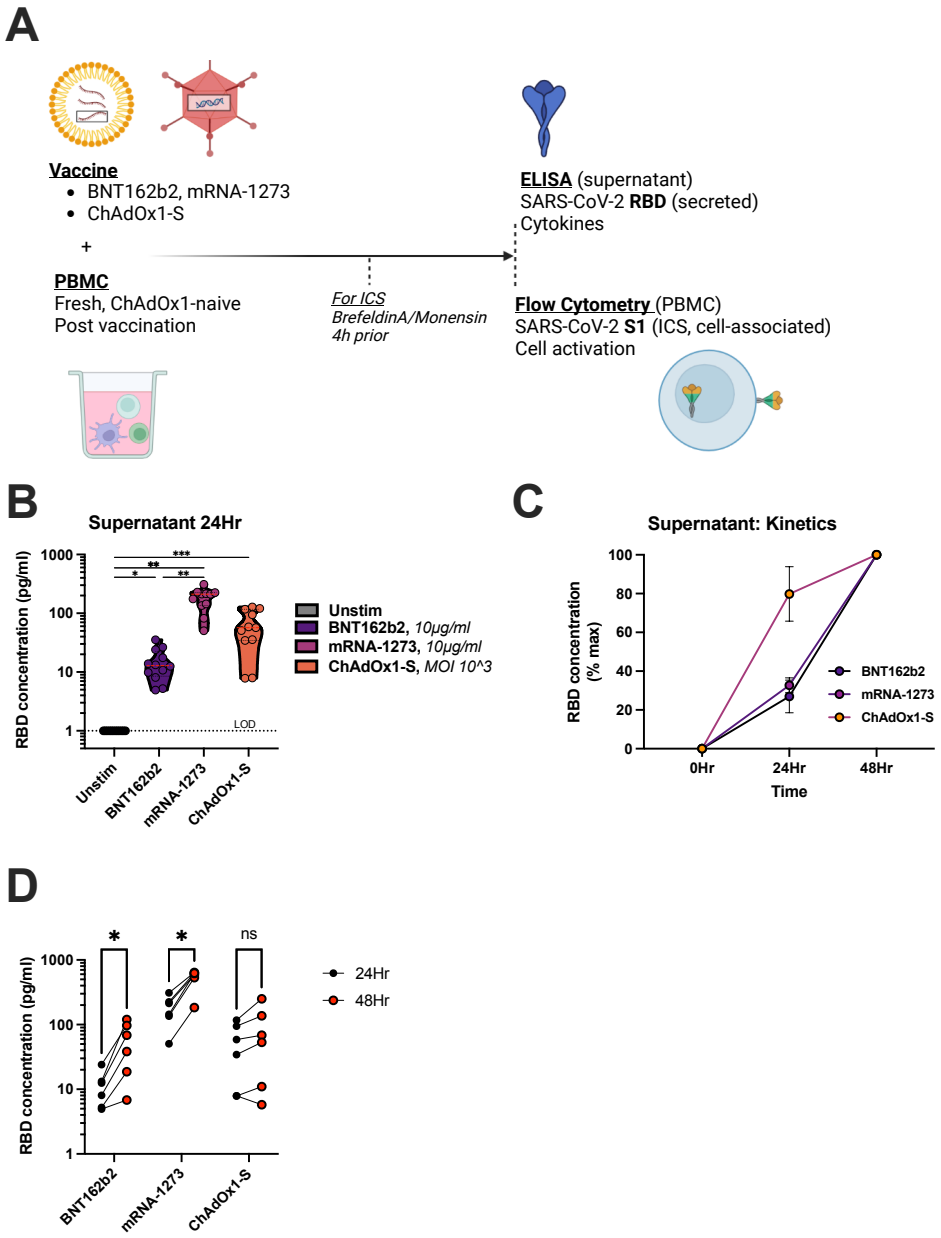

Fig4.13 | SARS-CoV-2 vaccines secrete spike RBD protein in PBMC in vitro.
Fresh PBMCs (10^6 cell in 200µl) from ChAdOx1 and SARS-CoV-2 infection naïve donors (post-BNT162b2 vaccination) were stimulated with ChAdOx1-S (MOI 10^3; 10^9vp/ml), BNT162b2 (10µg/ml), or mRNA-1273 (10µg/ml). Secreted RBD protein was measured in supernatants - or cell-associated S1 protein measured by flow cytometry (see Fig4.14).

(A) Schematic of experimental protocol for measuring secreted and cellular SARS-CoV-2 spike.
(B) Concentration of secreted SARS-CoV-2 RBD protein at 24h. Symbols indicate individual donors. Line at median (red).
(C) Concentration of SARS-CoV-2 RBD protein as a % of maximum measured over a 48h period. Mean±SEM shown.
(D) Concentration of SARS-CoV-2 RBD protein after 24h and 48h with indicated vaccines. Symbols indicate individual donors.

*p < 0.05; **p < 0.01; ***p < 0.001; ****p < 0.0001; ns, not significant.
Statistical significance was determined using non-parametric Kruskal-Wallis test (B), and paired Wilcoxon tests (D).

We next analysed which cells were transfected in vitro to produce spike protein (**Fig4.14**). No spike protein was detectable with BNT162b2 (**Fig4.14 D**). This was confirmed using surface and intracellular staining, different time points (8h, 24h, 48h), and both fresh and freeze thawed vaccine material (data not shown). Both mRNA-1273 and ChAdOx1-S induced SARS-CoV-2 S1 protein on monocytes after 24h (**Fig4.14 A-C, E-I**). ChAdOx1-GFP did not induce spike protein (data not shown). ChAdOx1-S also induced spike expression in 10% of pDC (**Fig4.15 C, F**), which was higher after permeabilisation (intracellular staining) compared to surface staining protocols (**Fig4.14 H**). No pDC spike expression was detectable in response to mRNA-1273 after 24h (**Fig4.14 E, G**), nor at very early (8h) or later (48h) timepoints (**Fig4.15 A, C**). Uniquely, ChAdOx1-S induced very rapid (8h) monocyte spike production (**Fig4.15 D**); total live S1+ cells were highest 8h after ChAdOx1-S stimulation (**Fig4.15 E, G**), and 48h after mRNA-1273 (**Fig4.15 F, H**), again highlighting the different kinetics of antigen production for the vaccines.

Figure 4.14 | ChAdOx1-S and mRNA-1273 express SARS-CoV-2 S1 protein in vitro - with pDC expression unique to ChAdOx1-S.

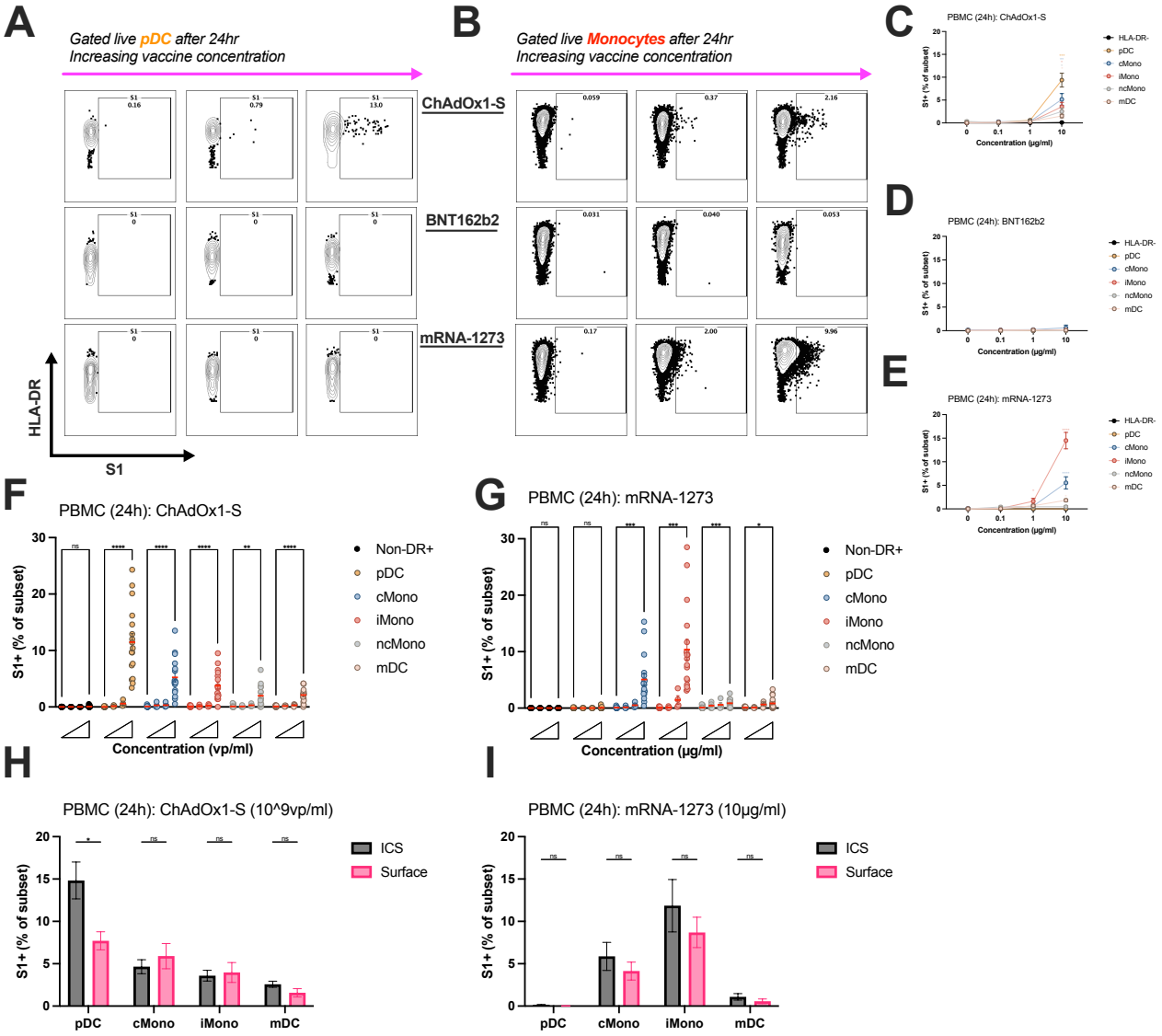

Fig4.14 | ChAdOx1-S and mRNA-1273 express SARS-CoV-2 S1 protein in vitro - with pDC expression unique to ChAdOx1-S.
Fresh PBMCs from ChAdOx1 naïve donors were stimulated with increasing concentrations of ChAdOx1-S (10^7-10^9vp/ml), BNT162b2 (0.1-10µg/ml), or mRNA-1273 (0.1-10µg/ml). Expression of SARS-CoV-2 S1 protein was measured by flow cytometry after intracellular (A-I), or surface staining (H,I). Cell subsets included: non-myeloid and myeloid cells (CD3-/CD19-/CD56-, HLA-DR+), focussing on classical (cMono; CD14+CD16-), intermediate (iMono, CD14+CD16+), and non-classical monocytes (ncMono, CD14-CD16+), in addition to conventional myeloid DC (mDC, CD14-CD16-, CD11c+), and plasmacytoid DC (pDC, CD123+, CD11c-).

(A, B) Representative flow plots of S1 expression on pDC (A), or monocytes (B), 24h after stimulation
(C-E) Summary of S1 expression as a fraction of indicated subsets with increasing concentrations of ChAdOx1-S (C), BNT162b2 (D), or mRNA-1273 (E) after 24h.
(F,G) S1 expression as a fraction of indicated subsets with increasing concentrations of ChAdOx1-S (F), or mRNA-1273 **(G)** after 24h.
(H,I) S1 expression as a fraction of indicated subsets after stimulation with ChAdOx1-S (H, 10^9 vp/ml), or mRNA-1273 (I, 10µg/ml) and staining with surface (red), or intracellular (black) staining at 24h.
Symbols indicate individual donors. Mean±SEM are shown.
*p < 0.05; **p < 0.01; ***p < 0.001; ****p < 0.0001; ns, not significant.
Statistical significance was determined using two-way ANOVA with Dunnett's multiple comparisons test (C-G), or unpaired t tests (H, I).

Mono (monocytes), cMono (classical monocytes, CD14+CD16-), iMono (intermediate monocytes, CD14+CD16+), ncMono (non-classical monocytes, CD14-CD16+); pDC (plasmacytoid dendritic cells); mDC (conventional myeloid dendritic cells)

Figure 4.15 | ChAdOx1-S and mRNA-1273 kinetics of SARS-CoV-2 S1 protein differ - with very early expression in monocytes after ChAdOx1-S, followed by later expression in pDC.

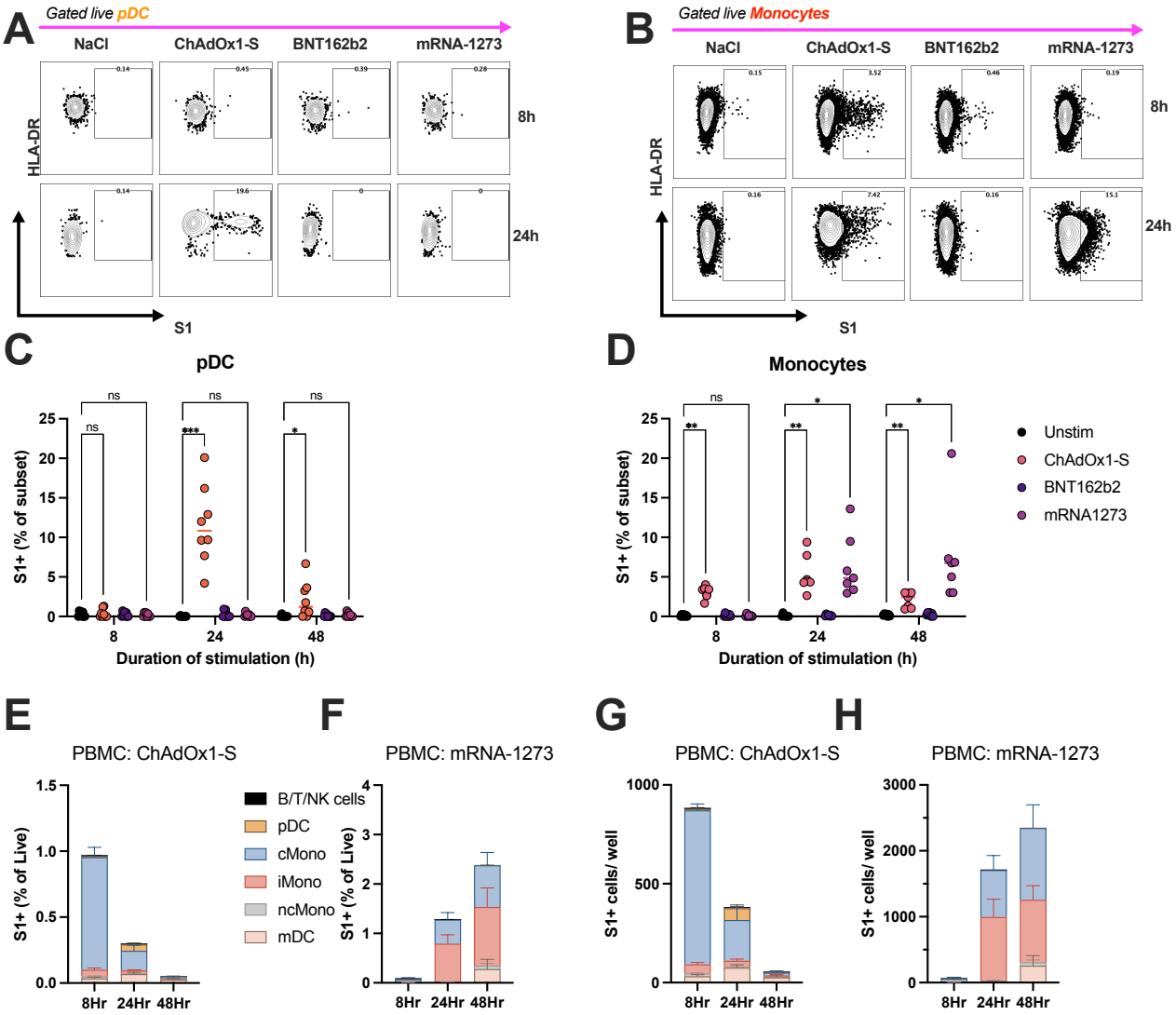

Fig4.15 | ChAdOx1-S and mRNA-1273 kinetics of SARS-CoV-2 S1 protein differ - with very early expression in monocytes after ChAdOx1-S, followed by later expression in pDC.
Fresh PBMCs from ChAdOx1 naïve donors were stimulated with ChAdOx1-S (10^9vp/ml), BNT162b2 (10µg/ml), or mRNA-1273 (10µg/ml). Expression of SARS-CoV-2 S1 protein was measured by flow cytometry after intracellular staining at 8h, 24h, or 48h. Cell subsets included: non-myeloid and myeloid cells (CD3-/CD19-/CD56-, HLA-DR+), focussing on classical (cMono; CD14+CD16-), intermediate (iMono, CD14+CD16+), and non-classical monocytes (ncMono, CD14-CD16+), in addition to conventional myeloid DC (mDC, CD14-CD16-, CD11c+), and plasmacytoid DC (pDC, CD123+, CD11c-).

(A, B) Representative flow plots of S1 expression on pDC (A), or monocytes (B), 8h and 24h after stimulation.
(C-D) Summary of S1 expression as a fraction of pDC(C), or monocytes (D) at 8h, 24h or 48h after stimulation.
(E, F) S1 expressing cells as a fraction of total live PBMCs at 8h, 24h, and 48h after stimulation with ChAdOx1-S (E), or mRNA-1273 (F).
(G, H) S1 expressing cells after stimulation of one millions PBMCs for 8h, 24h, and 48h with ChAdOx1-S (G), or mRNA-1273 (H).
Symbols indicate individual donors. Mean±SEM are shown.
*p < 0.05; **p < 0.01; ***p < 0.001; ****p < 0.0001; ns, not significant.
Statistical significance was determined using two-way ANOVA with Dunnett's multiple comparisons test (C, D).

Mono (monocytes), cMono (classical monocytes, CD14+CD16-), iMono (intermediate monocytes, CD14+CD16+), ncMono (non-classical monocytes, CD14-CD16+); pDC (plasmacytoid dendritic cells); mDC (conventional myeloid dendritic cells)

Given that only ChAdOx1-S transduced pDC, we asked whether this accounted for differences in plasma IFN-α in vivo. We confirmed that ChAdOx1-S, similar to ChAdOx1-GFP, induced appreciable IFN-α2 in pDC by flow cytometry (**Fig4.16 A, B**). No IFN-α was detectable in other cell populations in response to ChAdOx1-S, or any cell population in response to BNT162b2 or mRNA-1273 (**Fig4.16 C**). A higher fraction of S1-negative pDC expressed IFN-α+ in response to ChAdOx1-S compared to S1+pDC (**Fig4.16 D, E**); most IFN-α+ pDC were S1-negative (**Fig4.16 E, F**), albeit with relatively lower HLA-DR expression (**Fig4.16 G**). RNA vaccine insert expression may not be necessary for type I IFN-production, although it remains possible that a high proportion of more activated IFN-α+S1+pDC undergo cell-death. Sensing of ChAdOx1 vector protein, but not vaccine-derived spike protein, was sufficient to induce pDC-derived IFN-α2 as both ChAdOx1-GFP and ChAdOx1-S, but not mRNA spike vaccines induced pDC IFN-α2 in vitro (**Fig4.16 H**).

Figure 4.16 | Plasmacytoid dendritic cells produce IFN-α in response to ChAdOx1-S but not mRNA vaccines in vitro.

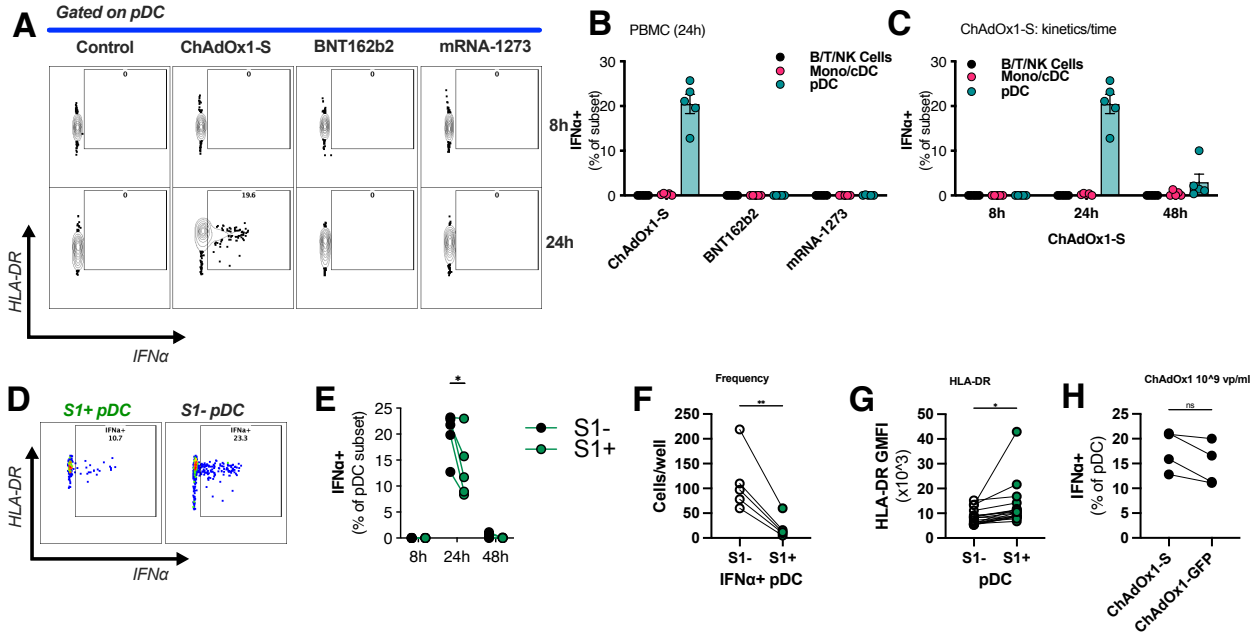

Fig4.16 | Plasmacytoid dendritic cells produce IFNα in response to ChAdOx1-S but not mRNA vaccines in vitro.
Fresh ChAdOx1-naive PBMCs were stimulated with ChAdOx1-S (10^9 vp/ml), BNT162b2 (10μg/ml), or mRNA-1273 (10μg/ml) and I α2 production in PBMC populations measured at 8h, 24h, or 48h.
(A) Representative plots of pDC IFNα2 expression after 24h.
(B) IFN-α2 expression in PBMC populations at 8h, 24h, and 48h after ChAdOx1-S (10^9 vp/ml),
(C) IFN-α2 expression in PBMC populations 24h after ChAdOx1-S (10^9 vp/ml), BNT162b2 (10μg/ml), or mRNA-1273 (10μg/ml).
(D, E) Representative plots (D), and summary IFN-α2 expression (E), in S1+ and S1- pDC.
(F) Number of IFN-α2+ pDC which are S1+ and S1- 24h after stimulation of 1 million PBMC with ChAdOx1-S .
(G) HLA-DR expression (GMFI) in S1+ and S1- pDC.
(H) IFN-α2 expression in pDC 24h after stimulation with 10^9 vp/ml ChAdOx1-S or ChAdOx1-GFP. Connecting lines indicate values from the same donor in the same experiment.
Symbols indicate individual donors. Mean ±SEM shown (B,C). *p < 0.05; **p < 0.01; ***p < 0.001; ****p < 0.0001; ns, not significant. Statistical significance was determined using using paired t test (E-G).

Vaccines and vaccine-derived interferons can induce classical MHC and co-stimulatory molecule expression important for antigen presentation and priming of adaptive immunity. We therefore compared the potential for SARS-CoV-2 vaccines to prime adaptive immunity by measuring APC MHC-I (HLA-ABC), MHC-II (HLA-DR), and CD80 expression (**Fig4.17**).

All licensed SARS-CoV-2 vaccines tested were potent inducers of monocyte CD80 expression with variable magnitude and kinetics (**Fig4.17 A-E**). CD80 up-regulation was earlier and more robust after ChAdOx1-S stimulation (**Fig4.17 C**), but only detectable 48h after mRNA vaccine stimulation in vitro (**Fig4.17 D, E)**. Similar to S1 protein, pDC CD80 expression was only robustly observed after ChAdOx1-S stimulation (**Fig4.17 C-E**).

HLA-DR induction was similar, with more rapid induction following ChAdOx1-S compared to mRNA vaccines (**Fig4.17 H, J**). ChAdOx1-S also potently up-regulated MHC-I (HLA-ABC) expression (**Fig4.17 G, I**). Therefore, although mRNA vaccines can induce innate immune activation, spike antigen presentation and co-stimulation to prime adaptive immune cells, the magnitude and kinetics is reduced and slower compared to ChAdOx1-S. The degree of innate activation was independent of the quantity of spike protein production, given that mRNA-1273 consistently induced higher RBD secretion in vitro.

Figure 4.17 | SARS-CoV-2 vaccines induce distinct patterns and kinetics of MHC-I, MHC-II and CD80 expression in antigen presenting cells.

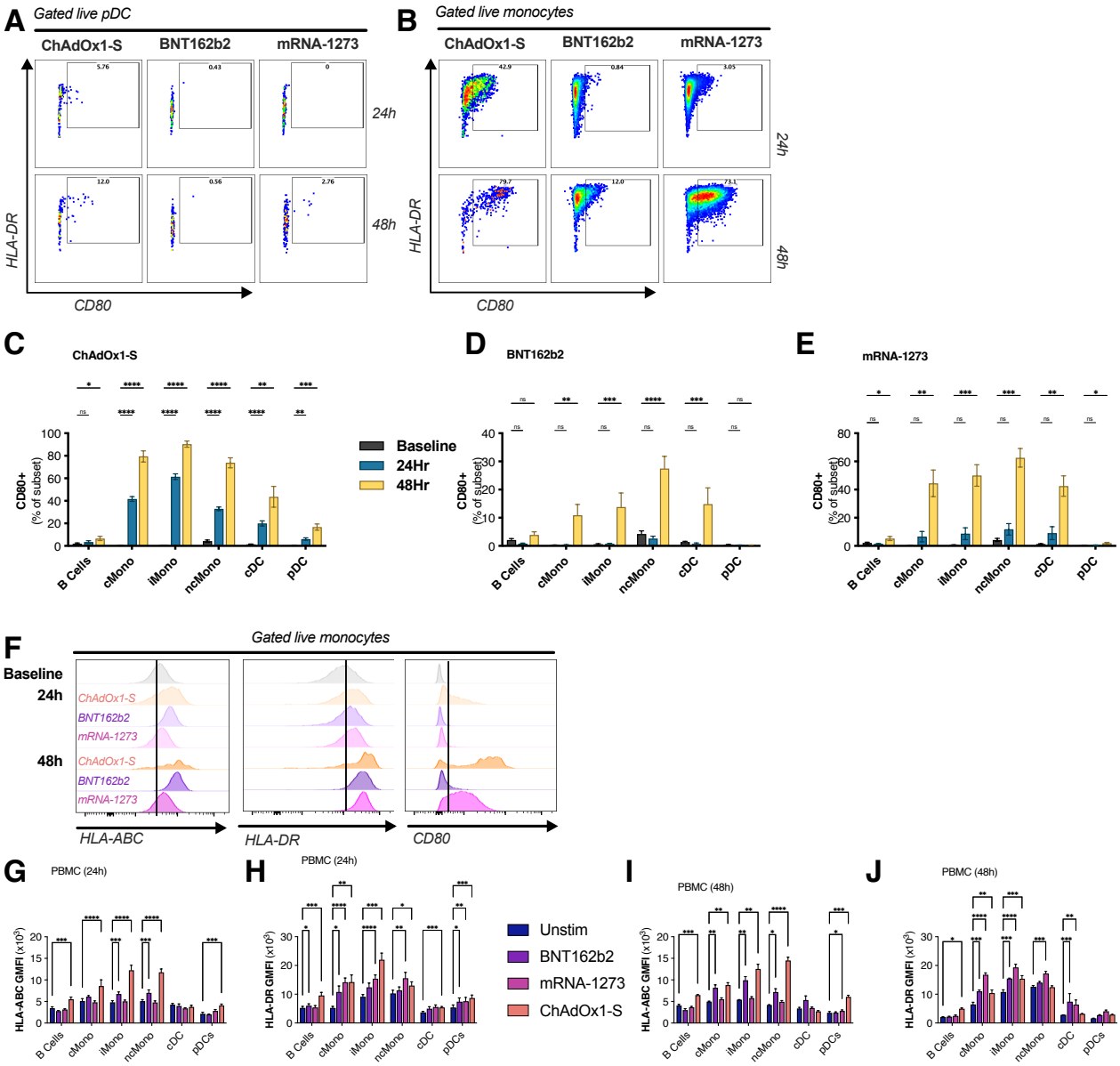

Fig4.17 | SARS-CoV-2 vaccines induce distinct patterns and kinetics of MHC-I, MHC-II and CD80 expression in antigen presenting cells.
Fresh PBMCs were stimulated with ChAdOx1-S (10^9 vp/ml), BNT162b2 (10µg/ml), or mRNA-1273 (10µg/ml) for 24h or 48h. Surface expression of activation markers (HLA-ABC, HLA-DR, CD80) was measured on major PBMC immune populations (data not shown for T cell and NK cells).
(A, B) Representative plots of HLA-DR and CD80 expression, gated on live pDC cells (A), and monocytes (B), 24h and 48h after stimulation with ChAdOx1-S, BNT162b2, and mRNA-1273.
(C-E) Expression of CD80 on PBMC populations at baseline, 24h and 48h after stimulation with ChAdOx1-S (C), BNT162b2 (D), and mRNA-1273 (E). (n=8)
(F) Representative histograms gated on monocytes with expression of HLA-ABC, HLA-DR, and CD80 on at baseline, 24h and 48h after ChAdOx1-S, BNT162b2, and mRNA-1273.
(G-J) Expression (GMFI) of HLA-ABC (G, I), and HLA-DR (H, J) on PBMC populations 24h (G, H) and 48h (I, J) after stimulation with ChAdOx1-S, BNT162b2, or mRNA-1273.
Mean ± SEM shown. *p < 0.05; **p < 0.01; ***p < 0.001; ****p < 0.0001; ns, not significant. Statistical significance was determined using two-way ANOVA with Dunnett's multiple comparison's test (C-E, G-J)
Mono (monocytes), cMono (classical monocytes, CD14+CD16-), iMono (intermediate monocytes, CD14+CD16+), ncMono (non-classical monocytes, CD14-CD16+); pDC (plasmacytoid dendritic cells); mDC (conventional myeloid dendritic cells). GMFI = geometric mean.

As a further assessment of vaccine functionality, we tested the capacity of SARS-CoV-2 vaccine transfected PBMC to secrete cytokines in cell culture supernatants after 24h. Titration of BNT162b2 induced low IFN-γ and IFN-α secretion from PBMC (**Fig4.18 A-C**; IFN-γ, BNT162b2 7.0 pg/ml vs control 3.6 pg/ml). A GMP manufactured self-amplifying RNA SARS-CoV-2 vaccine, LNP-nCoVsaRNA, was also tested (Imperial, Robin Shattock & Paul McKay). Titration of LNP-nCoVsaRNA (hereafter saRNA) induced appreciable IFN-α compared to control (median 2400-fold increase; **Fig4.18 D-F**). Comparing mRNA vaccines, although all were capable of IFN-γ (**Fig4.18 G**) and IFN-α (**Fig4.18 H**) induction in vitro, the magnitude of both IFNs was much lower in response to nucleoside-modified BNT162b2 and mRNA-1273 (**Fig4.18 H**). The most potent IFN-α2 inducers were ChAdOx1 vectors, ChAdOx1-GFP and ChAdOx1-S, together with saRNA (median 13000-, 10000-, and 2500-fold increase respectively). ChAdOx1 constructs were also the most potent inducers of IFN-γ in vitro (median 11000- and 6000-fold increase respectively; **Fig4.18 G**), with some appreciable IFN-γ induced following saRNA stimulation (19-fold induction; **Fig4.18 G**).

We hypothesised that low total IFN-γ after BNT162b2 was the result of reduced innate-like lymphocyte activation in vitro, given their numeric abundance and contribution to PBMC IFN-γ production. As MAIT cell are the most sensitive to type I IFNs and could produce IFN-γ in combination with other cytokines (**Chapter3**), we focused on mRNA vaccine-induced MAIT cell activation (CD69, IFN-γ).

Figure 4.18 | RNA vaccine induced interferons: comparison of self-amplifying and nucleoside-modified vaccines in vitro.

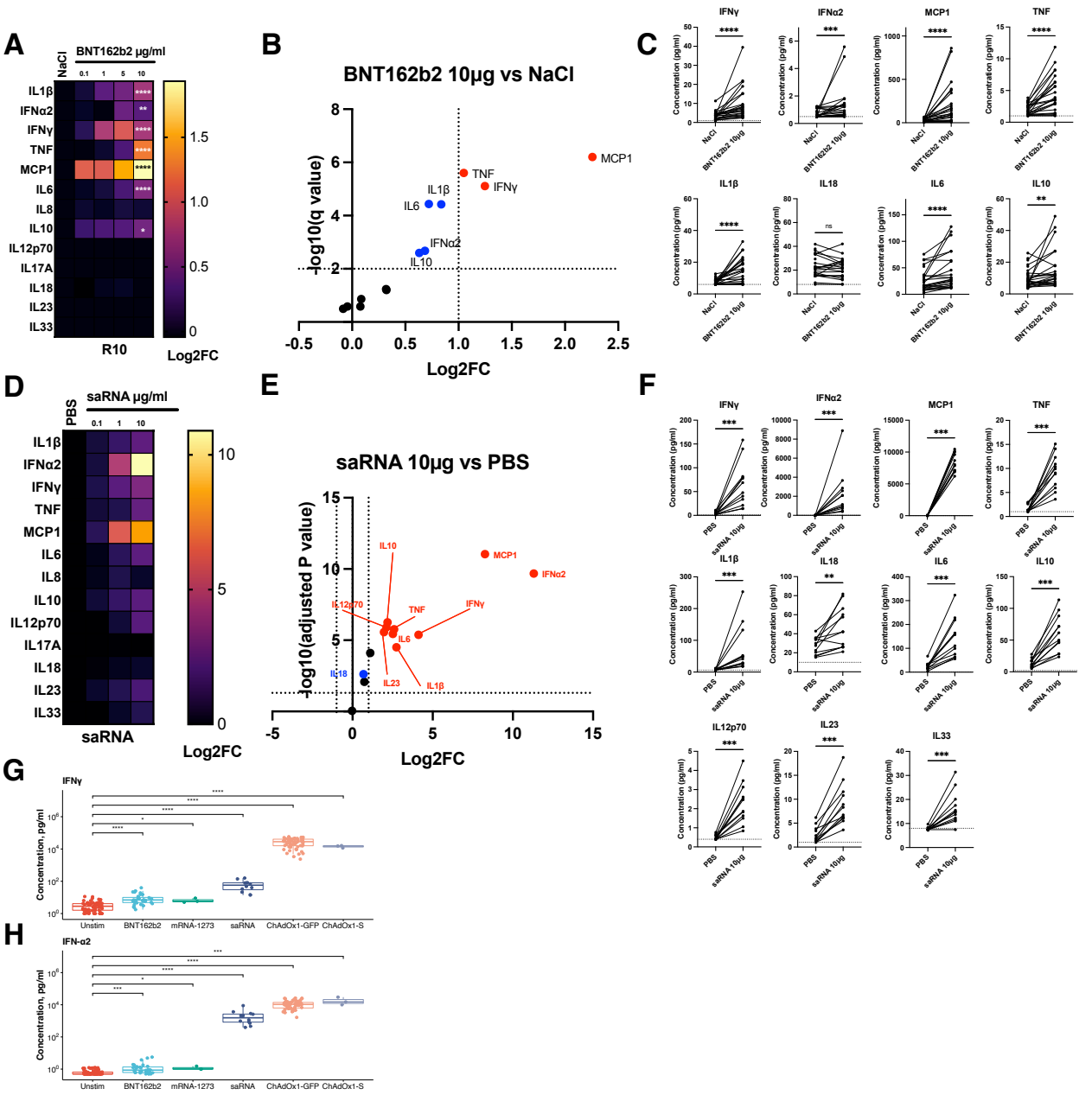

Fig4.18 | RNA vaccine induced interferons: comparison of self-amplifying and nucleoside-modified vaccines in vitro.

Fresh PBMCs were stimulated with BNT162b2 (titration to 10µg/ml), or LNP-nCoVsaRNA (titration to 10µg/ml) for 24h. Secreted cytokines in supernatants were assays for the indicated cytokines and compared to unstimulated controls.
(A) Heatmap of log2 fold change in secreted cytokines in response to BNT162b2 (relative to controls).
(B) Volcano plot of cytokines induced in response to BNT162b2 (10µg/ml) compared to diluent control (sodium chloride). Coloured based on the magnitude of induction (red, > 1 log2FC; blue, <1 log2FC).
(C) Individual cytokines in response to BNT162b2 (10µg/ml) or NaCl (control).
(D) Heatmap of log2 fold change in secreted cytokines in response to LNP-nCoVsaRNA (relative to controls).
(E) Volcano plot of cytokines induced in response to LNP-nCoVsaRNA (10µg/ml) compared to diluent control (PBS). Coloured based on the magnitude of induction (red, > 1 log2FC; blue, <1 log2FC).
(F) Individual cytokines in response to LNP-nCoVsaRNA (10µg/ml) or PBS (control).
(G, H) Concentration of IFN-γ **(G)**, and IFN-α2 **(H)** 24h after stimulation of PBMC with BNT162b2 (10µg/ml), mRNA-1273 (10µg/ml), LNP-nCoVsaRNA (10*µ*g/ml), ChAdOx1-GFP (10^9 vp/ml), or ChAdOx1-S (10^9 vp/ml).
*p < 0.05; **p < 0.01; ***p < 0.001; ****p < 0.0001; ns, not significant. Statistical significance was determined using multiple paired t tests of log2 cytokine concentrations (B, E, G, H), or paired non-parametric Wilcoxon test (C, F).

BNT162b2 induced very modest MAIT cell CD69 expression (**Fig4.19 B**), in contrast to non-nucleoside-modified saRNA which induced robust titratable CD69 expression on MAIT cells (**Fig4.19 C**), and other innate-like lymphocytes (data not shown). Modest MAIT cell TNF secretion was also induced in response to saRNA but not BNT162b2 in vitro (mean saRNA 0.7±0.3%; control 0.10±0.02%; ChAdOx1-GFP 2.9±0.6%; **Fig4.19 F**). Neither mRNA vaccine induced appreciable IFN-γ from MAIT cells or other innate-like lymphocytes at 24h in vitro (**Fig4.19 G-J**), which in the case of saRNA implied that vaccine-derived type I IFN is insufficient and supplementary signals are necessary for potent innate-like lymphocyte IFN-γ production. Modest saRNA induced TNF and IL-18 (**Fig4.18**), both crucial for type I IFN-induced innate-like lymphocyte IFN-γ (**Chapter3**), could be the missing supplementary signals required.

Altogether, mRNA vaccines irrespective of nucleoside-modification could induce IFN-α and IFN-γ in vitro, although IFN-α was particularly reduced with nucleoside-modified vaccines. IFN-γ induction in response to RNA vaccines was orders of magnitude lower than AdV, potentially because mRNA vaccines do not induce important cytokines necessary for potent activation of innate-like lymphocytes.

Figure 4.19 | SARS-CoV-2 mRNA vaccines induce CD69 not potent innate-like lymphocyte IFN-γ or TNF secretion in vitro.

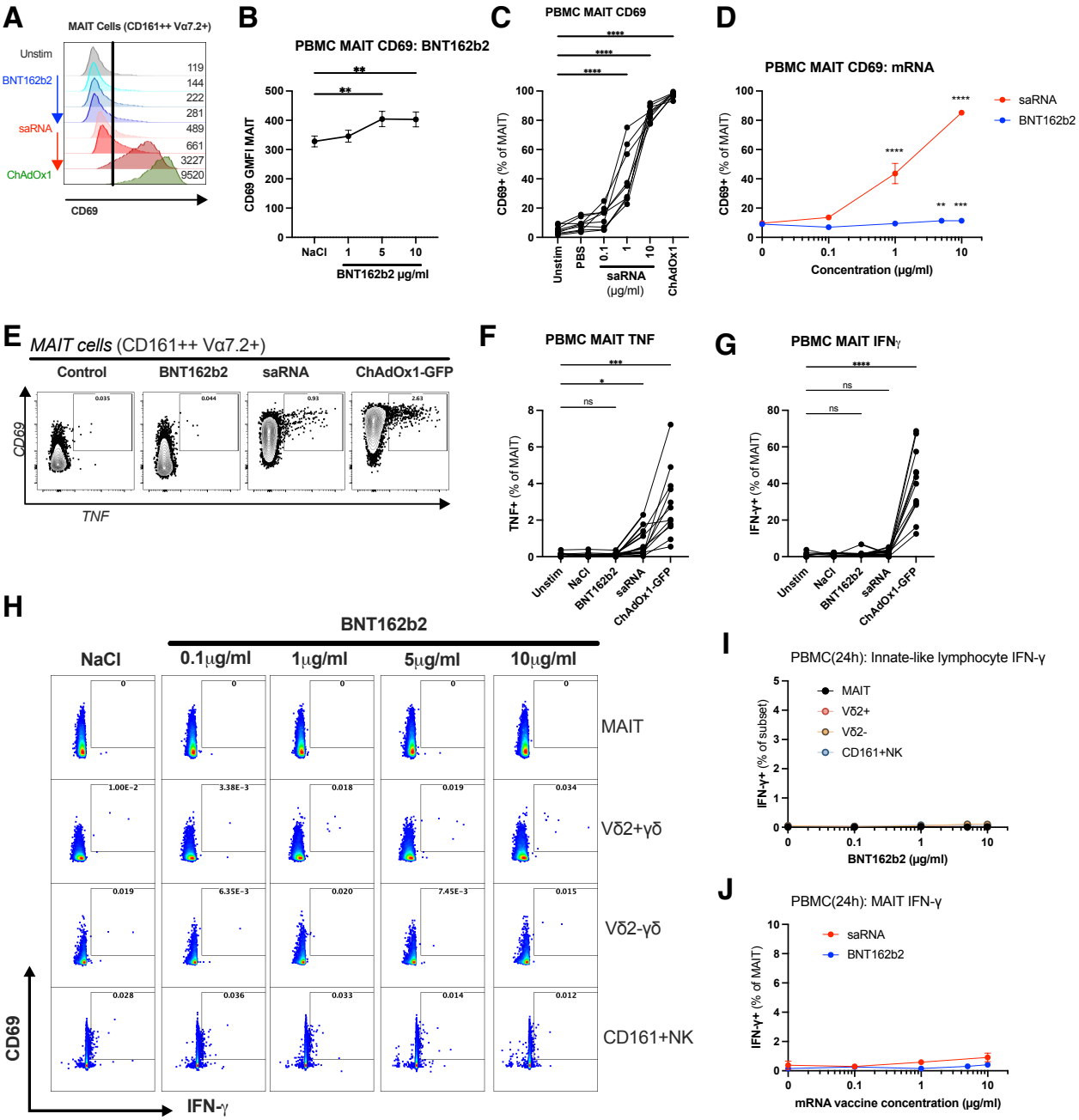

Fig4.19 | SARS-CoV-2 mRNA vaccines induce CD69 not potent innate-like lymphocyte IFN-γ or TNF secretion in vitro.

Fresh PBMCs from ChAdOx1 naïve donors were stimulated with BNT162b2 (titration to 10µg/ml), or LNP-nCoVsaRNA (saRNA, titration to 10µg/ml) for 24h. Activation of MAIT cell (CD161++Vα7.2+CD3+), Vδ2+ and Vδ2- γδ T cell, and CD161+NK cell (CD161+CD3- lymphocytes) was measured after 24h. ChAdOx1-GFP (10^9 vp/ml) was used as a positive control.

(A) Representative MAIT cell CD69 after stimulation with BNT162b2, saRNA (0.1, 1, 10μg/ml), or ChAdOx1-GFP.

(B) MAIT cell CD69 expression (GMFI) after BNT162b2 titration

(C) MAIT cell CD69 expression (% positive) after saRNA titration, compared to positive control ChAdOx1-GFP.

(D) MAIT cell CD69 expression (% positive) after saRNA or BNT162b2 titration.

(E, F, G) Representative plots gated on MAIT cells **(E)**, and summary MAIT cell TNF **(F)**, and IFN-γ expression **(G),** after stimulation with BNT162b2 10µg/ml, or saRNA 10µg/ml, or ChAdOx1-GFP.

(H) Representative plots **(H),** and summary data **(I)** for IFN-γ expression in MAIT cells, Vδ2+γδ, Vδ2-γδ, and CD161+NK cells after stimulation with increasing concentrations of BNT162b2.

(J) MAIT cell IFN-γ expression after titration with BNT162b2 or saRNA 10µg/ml.

*p < 0.05; **p < 0.01; ***p < 0.001; ****p < 0.0001; ns, not significant. Statistical significance was determined using repeated measures one-way ANOVA with Dunnett's test for multiple comparisons (B-D, F, J).

4.4.7 Adaptive immune cells produce IFN-γ in response to SARS-CoV-2 vaccines in vitro

To determine the source of early IFN-γ after BNT162b2, PBMC were stimulated with increasing concentrations of BNT162b2 and all CD69+IFN-γ+ cells assessed after 24h (gating **Appendix SF4.4**). BNT162b2 induced IFN-γ in conventional T-cells in a dose dependent manner (**Fig4.20 A, B**), but only in donors with prior exposure to SARS-CoV-2 spike protein through vaccination, confirming spike-specificity (**Fig4.20 C**); PBMCs from donors naïve to SARS-CoV-2 (through infection or vaccination) did not induce IFN-γ above NaCl control. After background subtraction, the fraction of IFN-γ+CD4+ T cells amongst PBMC (as counts per million, cpm) was much less variable than IFN-γ+CD8+ T cells (median (IQR): CD4, 46 cpm (31-88); CD8, 75 cpm (3-260); **Fig4.20 D**). No appreciable IFN-γ was detectable above background from sources other than conventional T cells (**Fig4.20 E**). CD69+IFN-γ+ conventional T could co-secrete TNF and GzmB (**Fig4.20 F, G**), with almost all CD69+IFN-γ+ CD8+ T cells cytotoxic, expressing GzmB (**Fig4.20 F, G**).

Figure 4.20 | Conventional but not unconventional T cells produce IFN-γ after BNT162b2 stimulation in vitro.

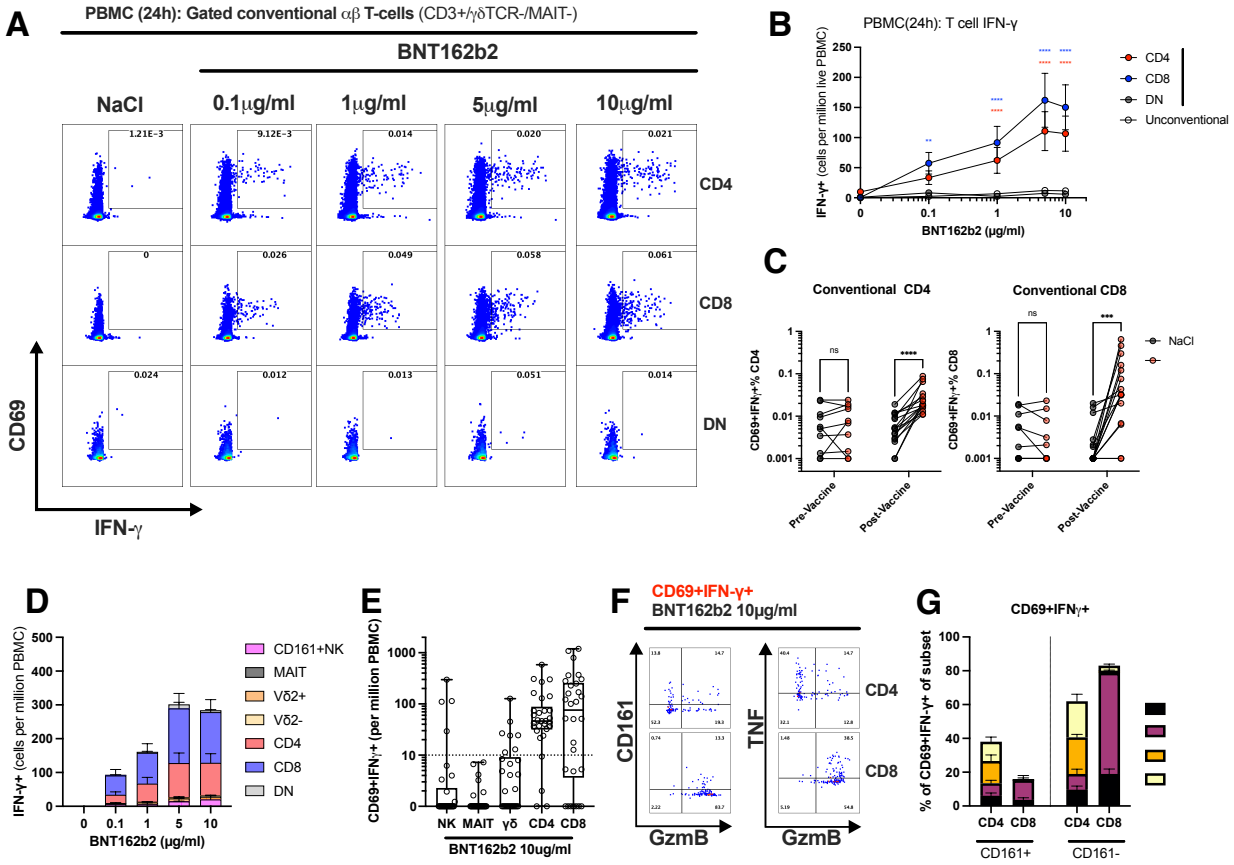

Fig4.20 | Conventional but not unconventional T cells produce IFN-γ after BNT162b2 stimulation in vitro . Fresh PBMCs from ChAdOx1 and SARS-CoV-2 infection naïve donors were stimulated with BNT162b2 (titration to 10μg/ml) for 24h. Activation of MAIT cells (CD161++Vα7.2+CD3+), Vδ2+ and Vδ2- γδ T cells, and non-MAIT/ γδ T cell conventional CD4+, CD8+, and double negative (DN) T cells was measured.

(A) Representative plots of CD69+IFN-γ+ CD4+, CD8+, and DN conventional T-cells 24h after titration with BNT162b2 (or control sodium chloride) at indicated concentrations.
(B) Frequency of IFN-γ secreting conventional (CD4+, CD8+, DN) and unconventional T cells (MAIT cells, γδ T cells) after BNT162b2 titration. (All donors post-vaccine)
(C) IFN-γ expression in conventional CD4+ and CD8+ T cells in response to BNT162b2 (red) or vehicle control (sodium chloride) in donors naïve to SARS-CoV-2 spike protein (uninfected, pre-vaccine), or whom had received at least one dose of BNT162b2 (post-vaccine).
(D) Frequency of IFNγ-secreting cells (background subtracted, cpm live PBMC) after BNT162b2 titration.
(E) Frequency of IFN-γ-secreting cells (background subtracted, cpm live PBMC) in response to BNT162b2 (10μg/ml)
(F) Representative plots of CD69+IFN-γ+ CD4 and CD8 conventional T-cells after BNT162b2 (10μg/ml), showing CD161, TNF, and GzmB expression.
(G) Summary CD161, TNF, and GzmB expression among CD69+IFN-γ+ conventional CD4+ and CD8+ T cells.

Mean ± SEM shown (B, D, G), or box-whisker plots with median, IQR, and range.
*p < 0.05; **p < 0.01; ***p < 0.001; ****p < 0.0001; ns, not significant.
Statistical significance was determined using repeated measures two-way ANOVA with Dunnett's test for multiple comparisons (B), or non-parametric Wilcoxon test (C).
Cpm = cells per million; DN = double negative; GzmB = granzyme B; IQR = interquartile range

We next assessed the capacity of mRNA-1273 to activate innate-like and conventional T-cells in vitro (**Fig4.21**). Compared to control, both BNT162b2 and mRNA-1273 (10μg/ml each) induced IFN-γ 24h after PBMC stimulation in vitro (**Fig4.21 A**). Uniquely, mRNA-1273 also induced modest NK cell IFN-γ in some donors, together with an increased frequency of IFN-γ+CD4+ T cells (**Fig4.21 A, B**). At the same concentration of vaccine, mRNA-1273 also induced higher innate-like lymphocyte CD69 expression (**Fig4.21 C**).

The pattern and magnitude of IFN-γ production in response to SARS-CoV-2 mRNA vaccines was distinct from AdV, ChAdOx1-S or ChAdOx1-GFP, which induced higher innate-like lymphocyte IFN-γ (**Fig4.21 D**). Comparing both AdV at the same multiplicity of infection (MOI 10^3; 10^9 vp/ml), ChAdOx1-GFP induced marginally higher IFN-γ but not CD69 compared to ChAdOx1-S (**Fig4.21 E, F**). As innate-like lymphocyte C69 expression is a sensitive marker of type I IFN, this might imply that other cytokines are responsible for differences in early innate-like lymphocyte IFN-γ. Differences in manufacturing and precise AdV titres are important variables to control for before making a conclusion, but it is plausible that spike-specific adaptive immunity could dampen early IFN-γ in response to ChAdOx1-S but not ChAdOx1-GFP.

Figure 4.21 | Differences in conventional and unconventional IFN-γ responsive cells to SARS-CoV-2 vaccines in vitro.

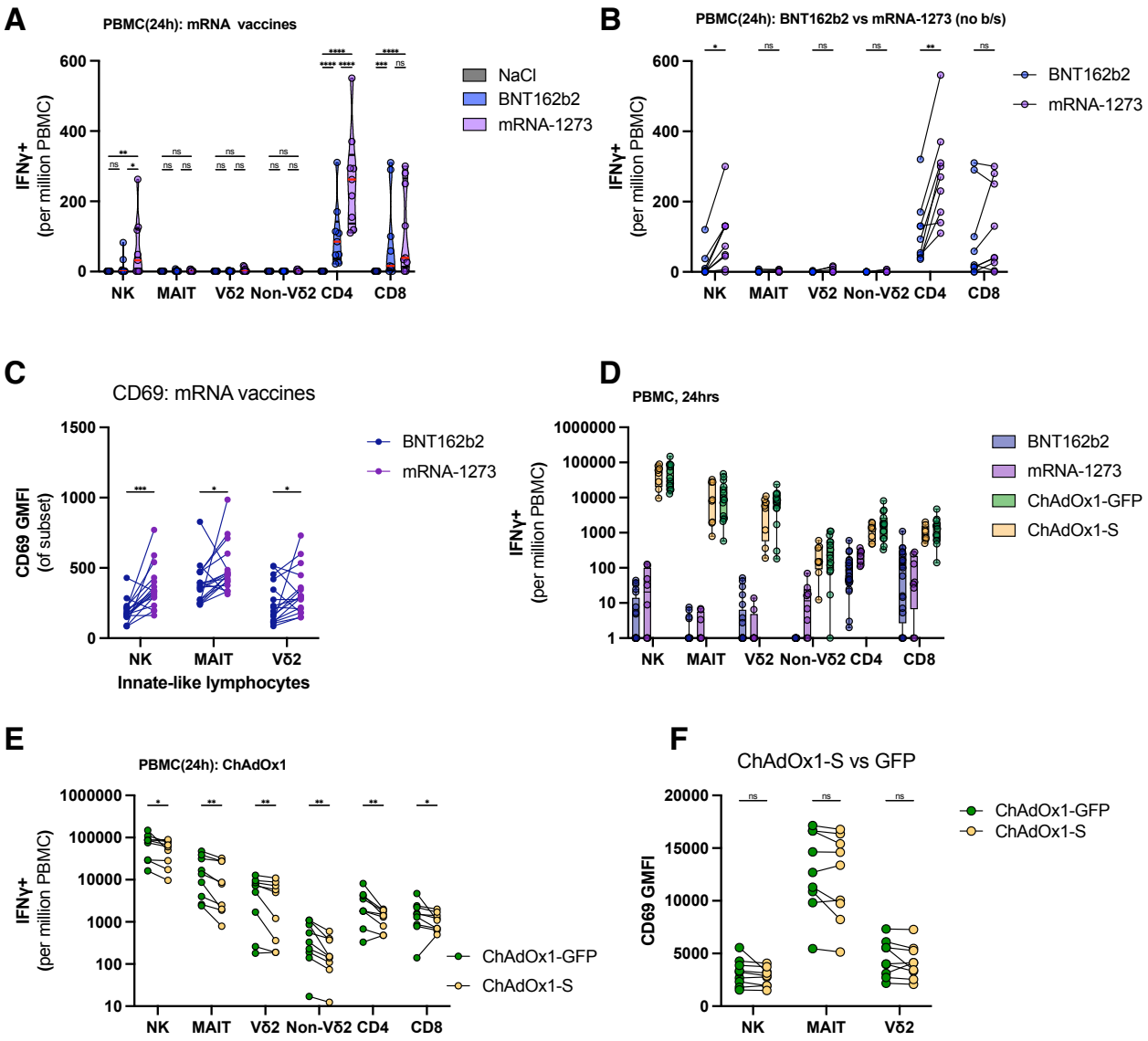

Fig4.21 | Differences in conventional and unconventional IFN-γ responsive cells to SARS-CoV-2 vaccines in vitro. Fresh PBMCs from SARS-CoV-2 vaccinated individuals were stimulated with BNT162b2 (10μg/ml), mRNA-1273 (10μg/ml), ChAdOx1-S (10^3vp/ml), ChAdOx1-GFP (10^9 vp/ml) or control. Activation of MAIT cells (CD161++Vα7.2+CD3+), Vδ2+ and Vδ2- γδ T cells, NK cells (CD161+CD3- lymphocytes) and non-MAIT/ γδ T cell conventional CD4+ and CD8+ T cells was measured after 24h.

(A, B) Violin plots **(A)**, or paired values **(B)** for IFN-γ+ cells (cpm live PBMC) in response to BNT162b2 or mRNA-1273.
(C) CD69 expression (GMFI) on NK cells, MAIT cells and Vδ2+ γδ T cells in response to BNT162b2 or mRNA-1273.
(D) Total IFN-γ+ cells (cpm live PBMC) in response to BNT162b2, mRNA-1273, ChAdOx1-S, or ChAdOx1-GFP.
(E, F) Total IFN-γ+ cells **(E)**, or CD69 expression **(F)** in response to ChAdOx1-S or ChAdOx1-GFP.

Violin plots with median (red; A), or box-whisker plots with median, IQR, and range (D). Responses in the same donor connected with paired lines.
*p < 0.05; **p < 0.01; ***p < 0.001; ****p < 0.0001; ns, not significant. Statistical significance was determined using repeated measures two-way ANOVA with Tukey's test for multiple comparisons (B), non-parametric Mann-Whitney (B, E, F), or t-tests (C). *Cpm = cells per million; IQR = interquartile range*

Conventional T cell responses to RNA vaccines should require transcription and translation of spike protein, which would be absent at the very earliest time points. We therefore examined the very earliest IFN-γ producing cells in PBMC, comparing SARS-CoV-2 vaccines with spike peptide pools (pooled S1 and S2, 1μg/ml) capable of activating conventional T cells in the absence of protein synthesis (**Fig4.22**). After 8h in vitro stimulation spike peptide pools induce IFN-γ production from both CD4 and CD8 T cells (**Fig4.22 A**). Similar to ChAdOx1-GFP (**Chapter3**), ChAdOx1-S induced IFN-γ+ cells at 8h in ChAdOx1 naïve donors which were predominantly CD4+(**Fig4.22 B, C**), therefore likely anti-vector (hexon) cross-reactive T-cells. In contrast robust IFN-γ production was not observed at 8h in response to either BNT162b2 or mRNA-1273 (**Fig4.22 B, C**).

Similar to ChAdOx1-GFP (Chapter 3), the dominant IFN-γ producing cells after ChAdOx1-S were innate-like lymphocytes (**Fig4.22 E, F**). Surprisingly, these cells also made up the dominant IFN-γ producing cells to spike peptide stimulation in vitro at 24h (**Fig4.22 E, F**), in contrast to mRNA vaccines (**Fig4.22 G, H**). As spike-peptide innate-like responses were not observed after 8h (**Fig4.22 H**), secondary bystander activation after TCR triggering of conventional T cells was likely. The high total IFN-γ in response to spike peptide in vitro would similarly require contribution from abundant innate-like lymphocytes (**Appendix SF4.5**).

Taken together conventional T-cells are important sources of IFN-γ in response to spike-protein, with high concentrations in peptide pools capable of subsequently activating innate-like lymphocytes which may be of relevance to SARS-CoV-2 vaccine responses in vivo.

Figure 4.22 | Very early IFN-γ production is absent after mRNA vaccine stimulation, and dominated by CD4+ conventional T cells after ChAdOx1-S and spike-peptide stimulation.

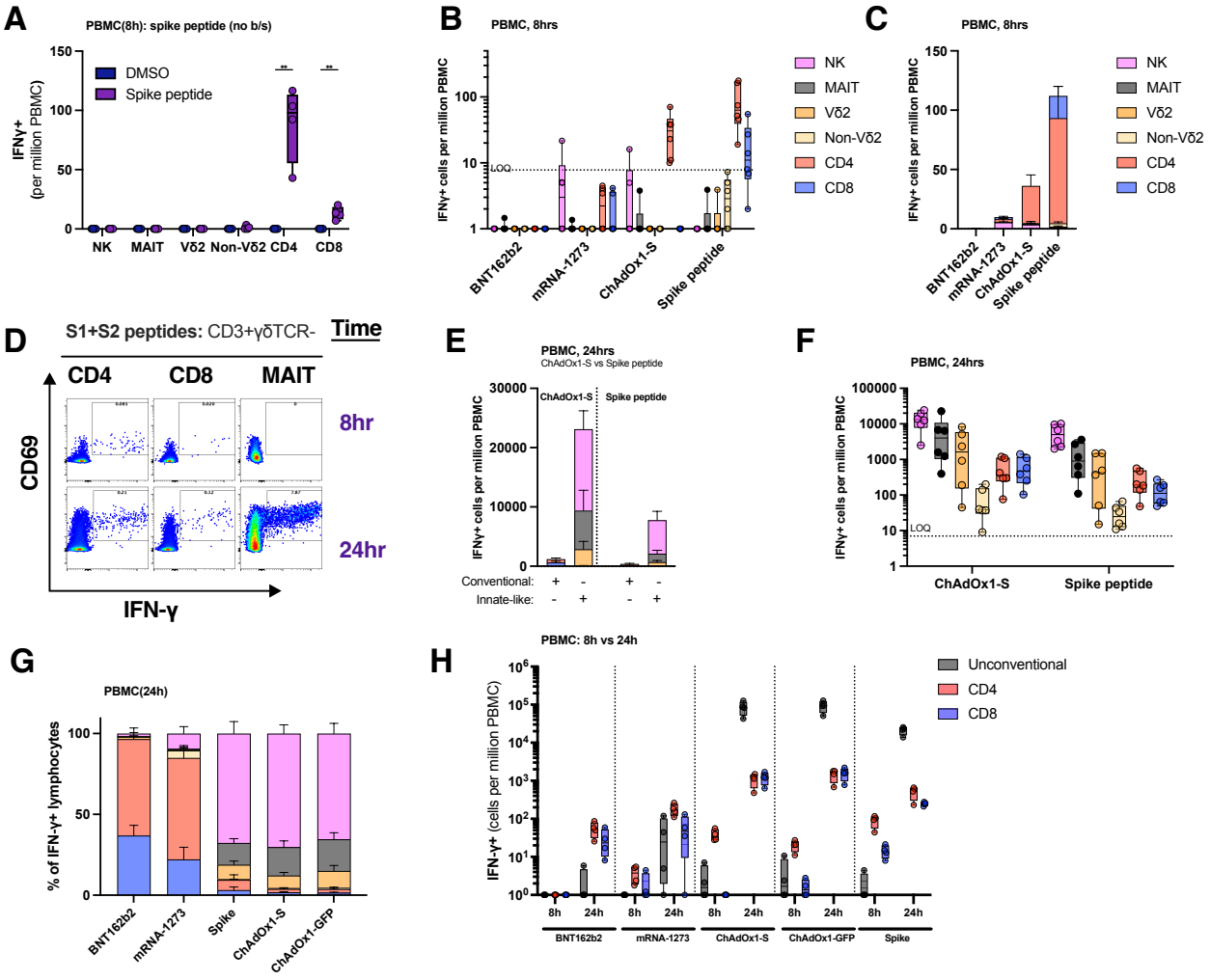

Fig4.22 | Very early IFN-γ production is absent after mRNA vaccine stimulation, and dominated by CD4+ conventional T cells after ChAdOx1-S and spike-peptide stimulation.
Fresh PBMCs from vaccinated individuals were stimulated with BNT162b2 (10μg/ml), mRNA-1273 (10μg/ml), ChAdOx1-S (10^9vp/ml), or pooled S1 and S2 peptides (1μg/ml total) for 8h (A-C; G) or 24h (D-G). Activation of NK cells (CD161+CD3- lymphocytes), MAIT cells (CD161++Vα7.2+CD3+), Vδ2+ and Vδ2- γδ T cells, and non-MAIT/ γδ T cell conventional CD4+ and CD8+ T cells was measured. Background subtraction (B-G) was performed using control stimulated wells, sodium chloride (mRNA vaccines), or DMSO (spike peptide pools). Limit of quantitation (LOQ) shown as dotted line.
(A) Frequency of IFNγ-secreting cells (cpm live PBMC) in response to spike peptide pools or DMSO.
(B) Frequency of IFNγ-secreting cells (background subtracted, cpm live PBMC) with different vaccines at 8h.
(C) Summary of total IFNγ-secreting cells (background subtracted, cpm live PBMC) of each major cell subset in response to vaccines at 8h.
(D) Representative plot of IFN-γ expression amongst conventional CD4, CD8, and MAIT cells 8h and 24h after spike peptide pool stimulation.
(E, F) Box plots **(D)** and summary (**E**, mean ±SEM) of IFNγ-secreting cells (background subtracted, cpm live PBMC) with ChAdOx1-S and spike peptide pools in vitro.
(G) Percentage of total IFN-γ+ lymphocytes which are cell subsets indicated after stimulation with SARS-CoV-2 spike-vaccines, spike-peptide, or ChAdOx1-GFP in vitro.
(H) Frequency of IFNγ-secreting cells (background subtracted, cpm live PBMC) with SARS-CoV-2 spike-vaccines, ChAdOx1-GFP, or spike peptide pools at 8h and 24h.
Box plots with median, IQR, and range (A, B, E, G), or mean±SEM (C, F) are shown.
Statistical significance was determined using unpaired t tests (A).
*p < 0.05; **p < 0.01; ***p < 0.001; ****p < 0.0001; ns, not significant.
Cpm = cells per million; IQR = interquartile range

4.4.8 Innate-like lymphocytes amplify early IFN-γ in an IFN-γR-dependent manner

Thus far, our in vitro data did not entirely recapitulate vaccine-induced responses in vivo. Plasma IFN-γ 24h after boost with BNT162b2 or ChAdOx1-S were of similar magnitude and correlated with innate-like lymphocyte activation in vivo. However, only ChAdOx1-S induced substantial IFN-γ and MAIT cell activation in vitro. BNT162b2 was only capable of inducing IFN-γ from rare antigen-specific conventional T cells in vitro at 24h (**Fig4.21**). Given substantial plasma IFN-γ and CD161+ innate-like lymphocyte activation in vivo, we explored the possibility that missing endogenous factors were necessary in vitro to recapitulate potent IFN-γ production.

Given the positive correlation of serum antibodies at the time of boost with subsequent ex-vivo IFN-γ (**Fig4.11**), the capacity for serum to promote MAIT cell activation in response to BNT162b2 was tested using pre-pandemic and autologous human serum, comparing to FCS control (**Fig4.23**).

Titration of human serum but not FCS increased MAIT cell CD69 in response to BNT162b2 (**Fig4.23 A**), but not NaCl control (**Fig4.23 B**). Supplementary human serum induced IFN-γ secretion from MAIT cells, γδ T cells and CD161+ non-B/T lymphocytes (NK cells) such that the majority of IFN-γ+ cells were not conventional T cells 24h after BNT162b2 stimulation (**Fig4.23 C, D**), with similar serum-dependent augmentation observed after mRNA-1273 (**Fig4.23 E**). Accordingly, the total IFN-γ secreted in response to both vaccines was substantially increased by autologous serum (100-fold, BNT162b2; 300-fold, mRNA-1273; **Fig4.23 F, G**). Pre-pandemic and autologous serum did not significantly differ in vaccine-induced cytokine secretion (**Appendix SF4.6**), suggesting enhancement of responses was predominantly due to serum factors other than spike-specific antibodies.

Figure 4.23 | Autologous serum increases mRNA vaccine-induced IFN-γ in vitro.

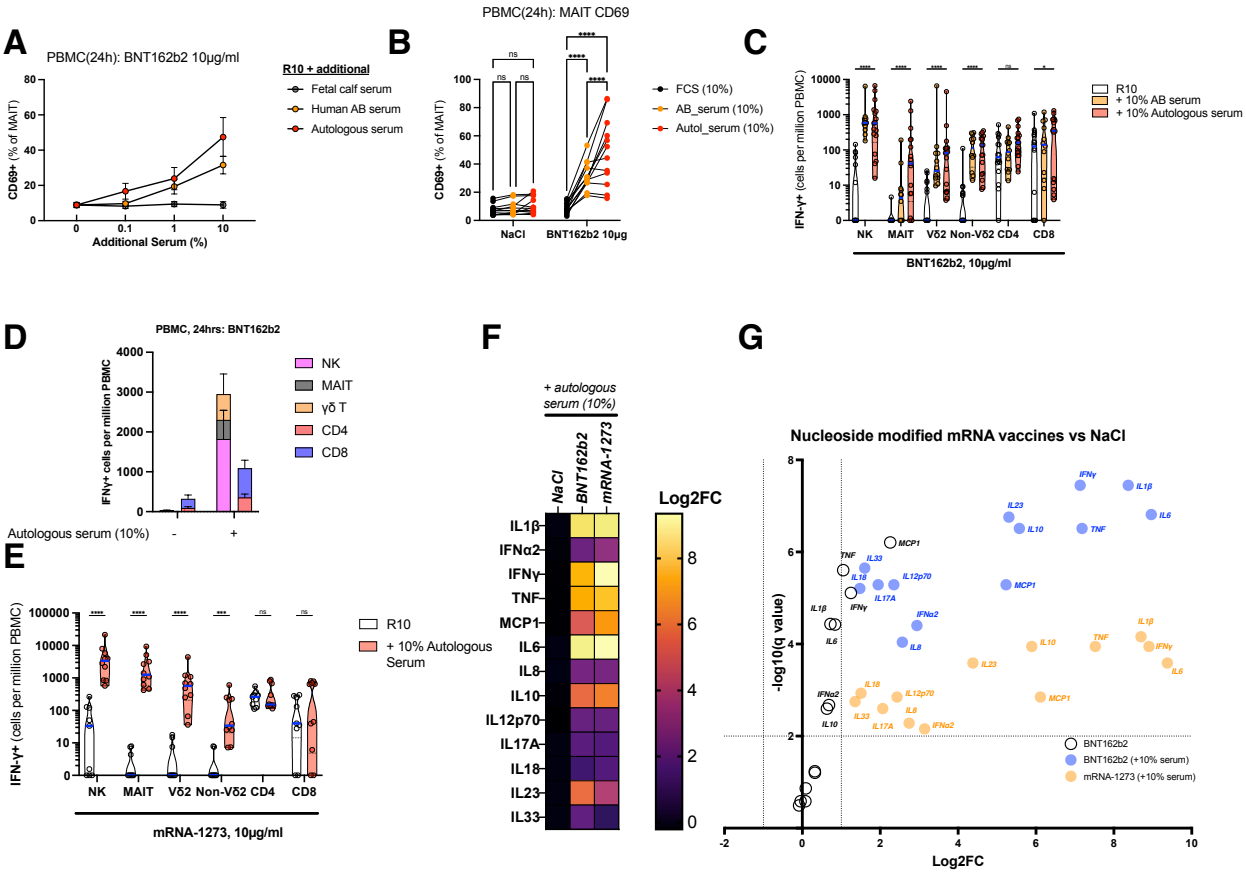

Fig4.23 | Autologous serum increases mRNA vaccine-induced IFN-γ in vitro.
Fresh PBMCs from vaccinated individuals were stimulated with BNT162b2 (10µg/ml; A-D; F, G), or mRNA-1273 (10µg/ml; E-G) for 24h in R10 media with either additional fetal calf serum (FCS, 0.1-1%, A-B); pre-pandemic pooled human AB serum (0.1-10%, A-C, E), or autologous human serum (0.1-10%, A-G). Activation of NK cells (CD161+CD3- lymphocytes), MAIT cells (CD161++Vα7.2+CD3+), Vδ2+ and Vδ2- γδ T cells, and non-MAIT/ γδ T cell conventional CD4+ and CD8+ T cells was measured. Background subtraction was performed using control stimulated wells, sodium chloride (C, D). Concentrations of total cytokines was measured in supernatants at 24h (F, G).

(A) Frequency of CD69+MAIT cells after stimulation with BNT162b2 (10µg/ml), in R10 with additional FCS, pooled pre-pandemic human AB serum, or autologous serum (0.1%, 1%, 10%).
(B) Frequency of CD69+MAIT cells after stimulation with BNT162b2 (10µg/ml), or control sodium chloride (NaCl), in R10 with additional FCS, pooled pre-pandemic human AB serum, or autologous serum (10%).
(C) Total IFN-γ-secreting cells (background subtracted, counts per million live PBMC) which are each cell subset in response to BNT162b2 (10µg/ml) in the presence of R10, or R10 with additional autologous human serum (10%).
(D) Summary IFN-γ-secreting cells (background subtracted, counts per million live PBMC) which are each cell subset in response to BNT162b2 (10µg/ml) in the presence of R10, or R10 with additional autologous human serum (10%).
(E) Total IFN-γ-secreting cells (background subtracted, counts per million live PBMC) which are each cell subset in response to mRNA-1273 (10µg/ml) in the presence of R10, or R10 with additional autologous human serum (10%).
(F) Heatmap of log2 fold change in total cytokinines after stimulation of PBMC in R10+autologous serum with BNT162b2 (10µg/ml), or mRNA-1273 (10µg/ml), compared to control NaCl.
(G) Volcano plot of change in log2 transformed cytokine concentrations after stimulation of PBMC with BNT162b2 (10µg/ml; in R10 with or without 10% serum), or mRNA-1273 (10µg/ml, with 10% serum). Comparisons with control NaCl in matched serum.

Mean ± SEM (A, D), median (C, E; blue line) shown. Statistical significance was determined using repeated measures two-way ANOVA with Dunnett's test for multiple comparisons (B), mixed-effects two-way ANOVA with Dunnett's test (C), or multiple paired t-tests of log2 transformed values with (F). *p < 0.05; **p < 0.01; ***p < 0.001; ****p < 0.0001; ns, not significant.

The magnitude of IFN-γ and TNF secretion in response to SARS-CoV-2 mRNA vaccines in the presence of human serum was similar to ChAdOx1-GFP, a potent inducer of innate-like lymphocyte activation (**Fig4.24 A**). Although mRNA vaccines were capable of significant IFN-γ induction and activation of CD161+ innate-like lymphocytes, the mechanisms for were unclear. IL-18, a potent innate-like lymphocyte IFN-γ inducer was not induced by BNT162b2 in vivo. Similarly in vitro, RNA vaccines stimulated in human serum did not potently induce activators of innate-like lymphocytes, such as IFN-α, IL-18, IL-12p70, or IL-23 (**Fig4.24 B-D**), suggesting another potentially relevant trigger.

Figure 4.24 | Patterns of cytokine secretion in response to vaccines in vitro.

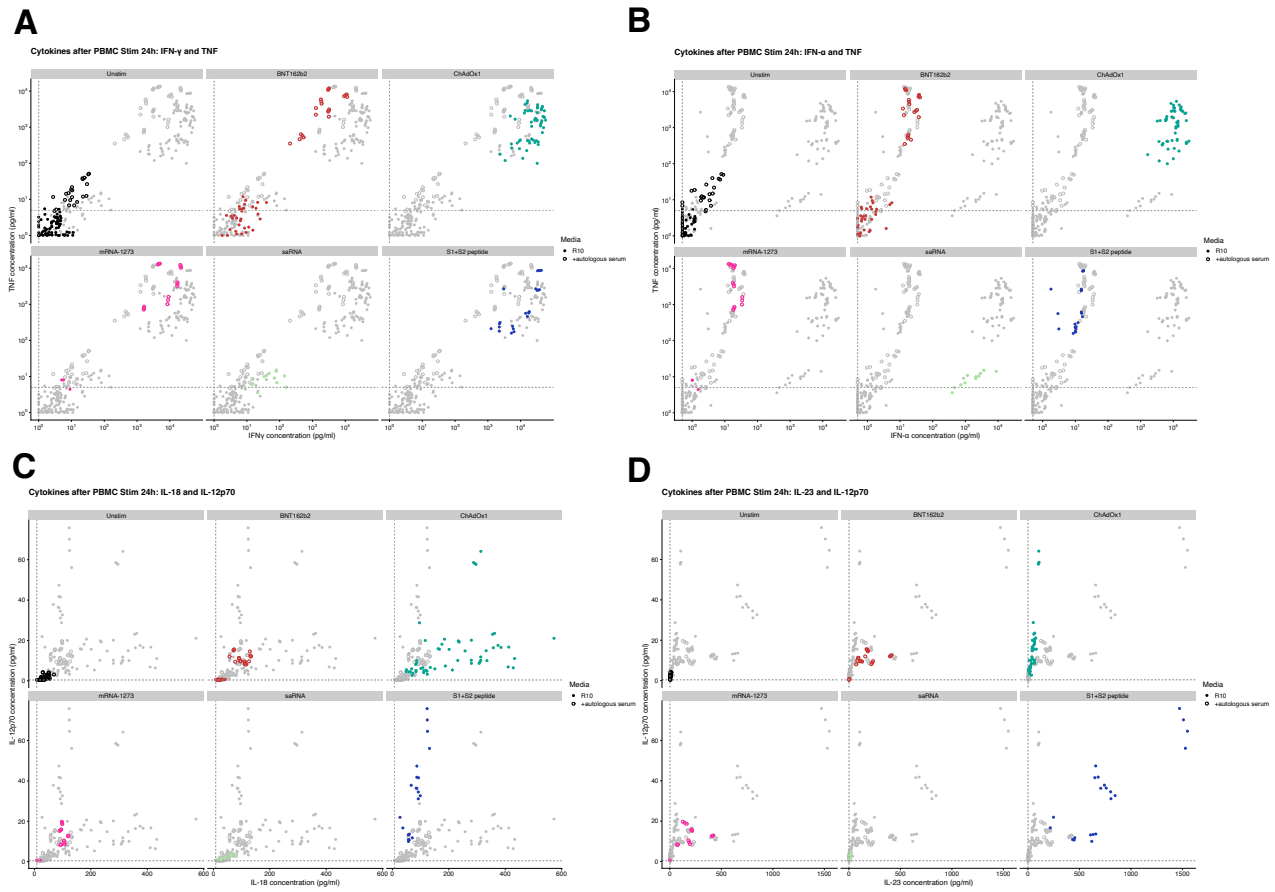

Fig4.24 | Patterns of cytokine secretion in response to vaccines in vitro.
Fresh PBMCs from vaccinated individuals were stimulated with BNT162b2 (10μg/ml), mRNA-1273 (10μg/ml), ChAdOx1-GFP (10^9vp/ml), or pooled S1 and S2 peptides (1μg/ml total) for 24h. PBMCs were either stimulated in R10 media (filled circles), or in R10 supplemented with 10% autologous serum (open circles). Cytokines were then measured in supernatants at 24h (pg/ml).

(A) Total IFN-γ and TNF secretion; **(B)** Total IFN-α and TNF secretion; **(C)** Total IL-18 and IL-12p70 secretion; **(D)** Total IL-23 and IL-12p70 secretion.

Intriguingly, in addition to IL-12R and IL-18R expression, CD161+ cells shar high expression of IFN-γR1 (CD119)[200]. Given that innate-like lymphocyte IFN-γ production in response to spike-peptide pools at 24h followed very early conventional T cell IFN-γ (**Fig4.22**), we hypothesised this conventional T cell IFN-γ could trigger - and therefore amplify - total IFN-γ through activation of CD119 expressing innate-like lymphocytes.

We first tested the impact of IFN-γ inhibition - using an IFN-γ blocking antibody - prior to characterisation of MAIT cell responses to a range of stimuli previously tested in Chapter3 (**Fig4.25**). Surprisingly, IFN-γ blockade (1μg/ml, clone#25718) prior to ChAdOx1 stimulation in particular modestly reduced both MAIT cell and NK cell IFN-γ production at 24h (MAIT cell IFN-γ+: 27±4%, IgG1; 19±4%, anti-IFN-γ; **Fig4.25 A**). Further increase in anti-IFN-γ concentration (10μg/ml) did not increase inhibition (data not shown), however blockade of IFN-γR1 (10μg/ml, clone#92101) was more potent in reducing ChAdOx1-GFP induced IFN-γ (**Fig4.25 B, C**), while also increasing GFP expression in a similar manner to type I IFN blockade (**Fig4.25 D**).

To determine whether innate-like lymphocytes could respond to T-cell derived IFN-γ in the absence of IL-18 or IL-12, neither of which were appreciably induced in vivo or vitro in response to mRNA vaccines, we stimulated PBMC with combinations including IFN-α and TNFR2 agonist. These combinations were used as both IFN-α and TNF were potently induced in response mRNA vaccines at the transcriptional level in vivo, and TNF was induced in vitro in response to both mRNA vaccine and spike-peptide stimulation, partially derived from TCR-triggered T-cells. We had also shown previously that IFN-γ could induce early monocyte TNF production (**Fig3.19**; **Appendix SF4.7**).

IFN-γ treatment augmented innate-like lymphocyte IFN-γ production 24h after PBMC type I IFN stimulation, which was further augmented with additional TNFR2 agonism (**Fig4.25 E**). Granzyme B expression was also increased by IFN-γ treatment (**Fig4.25 F**). Although

IFN-γ did not trigger innate-like lymphocyte activation in the absence of other cytokines (**Fig3.12**), combination with other signals during the course of an antiviral and vaccine response could augment innate-like lymphocyte activation and IFN-γ production.

To test whether T-cell IFN-γR1 signalling had a direct functional role in T-cell derived IFN-γ in the absence of other signals, we used a supernatant transfer model (used in Chapter3). We compared TNF-dependent (IFN-α+IL-18) and independent (IL-12+IL-18) triggering of MAIT cells after stimulation of enriched CD8+ cells with cytokines in the presence of supernatant from enriched CD14+ monocytes (**Fig4.25 G-I**). Blockade of IFN-γ prior to triggering of enriched CD8+ T cells with cytokine supplemented monocyte supernatants reduced MAIT cell IFN-γ two fold after IFN-α+IL-18 stimulation (48.6±6.1%, 24.1±8.1%; **Fig4.25 H**). MAIT cell stimulation with IL-12+IL-18 was unaffected by both TNF or IFN-γ blockade (**Fig4.25 I)**. As IFN-γ in this system could only be produced by enriched CD8 T cells, these data would suggest that T-cell derived IFN-γ could amplify type I IFN-dependent IFN-γ production from other T-cells in the presence of TNF.

Figure 4.25 | MAIT cell IFN-γR signalling can modulate MAIT cell IFN-γ production in response to type I IFN and TNF mediated activation.

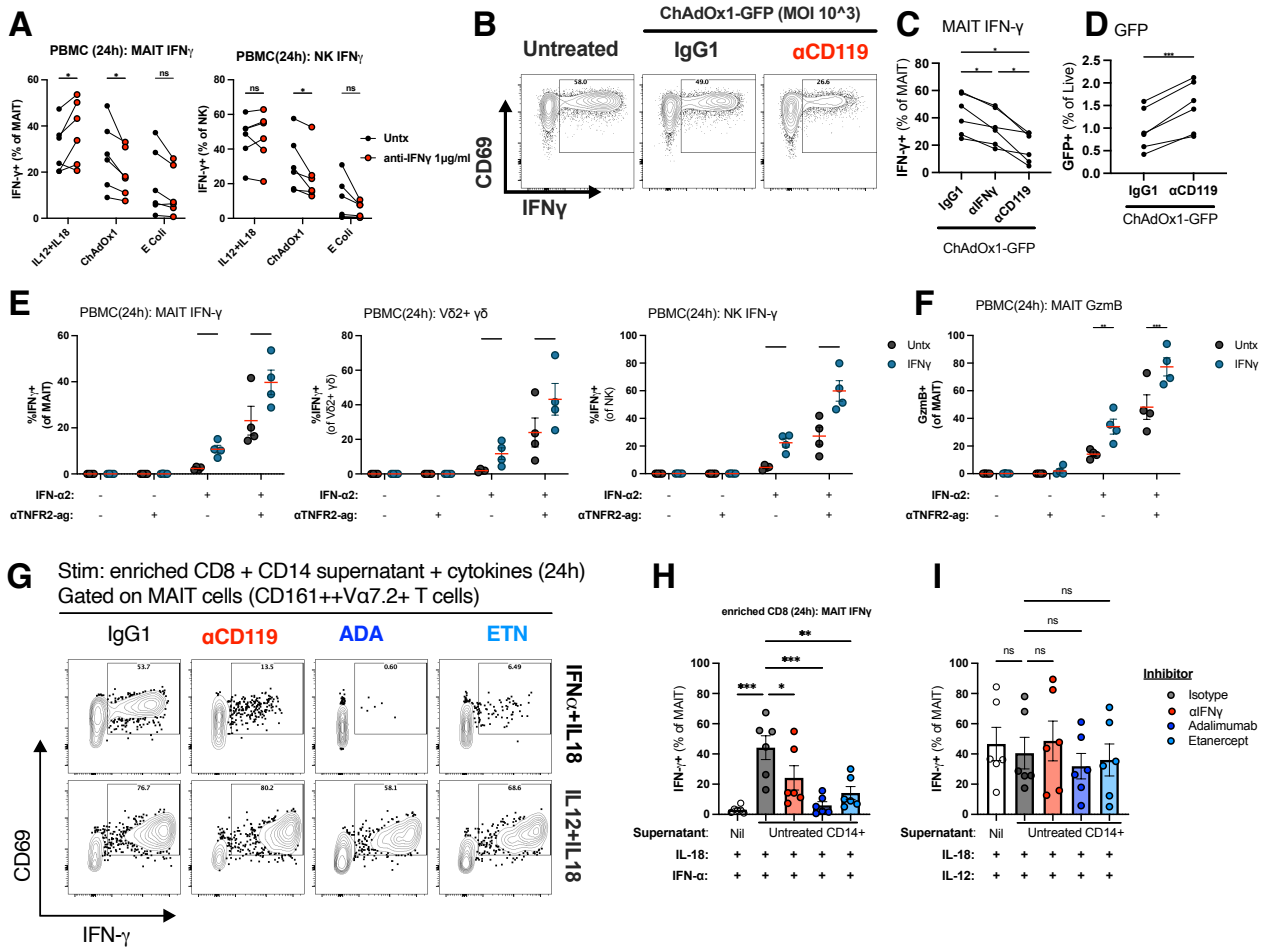

Fig4.25 | MAIT cell IFN-γR signalling can modulate MAIT cell IFN-γ production in response to type I IFN and TNF mediated activation.

(A-D) Fresh PBMCs were stimulated with IL-12+IL-18 (50ng/ml), ChAdOx1-GFP (10^9vp/ml), or Ecoli (25BpC) for 24h in the presence or absence of IFN-γ blockade (1μg/ml, #25718), or IFN-γR1 blockade (αCD119, 10μg/ml, clone # 92101). MAIT cell (CD161++Vα7.2+) or NK cell (CD161+CD3- lymphocytes) activation (CD69, IFN-γ) was measured after 24h.

(A) MAIT cell and NK cell IFN-γ production in response to stimuli in the presence or absence of anti-IFN-γ antibodies.

(B) Representative plots of MAIT cell IFN-γ in response to ChAdOx1-GFP with or without αnti-CD119 antibodies.

(C, D) MAIT cell IFN-γ **(C)**, and PBMC GFP expression (**D**), after stimulation of PBMC with ChAdOx1-GFP in the presence of anti-IFN-γ or anti-CD119 blocking antibodies.

(E, F) PBMC were stimulated with IFN-α (50ng/ml) and/or anti-TNFR2 agonist (2.5μg/ml, clone MR2-1) in the presence or absence of additional IFN-γ (50ng/ml). MAIT cell, Vδ2+ γδ T cell, or CD161+NK cell IFN-γ **(E)**, or GzmB **(F)** were measured.

(G-I) MACS enriched CD8+ T cells were stimulated with supernatants from autologous CD14+ monocytes (rested for 4hrs) and cytokines (IFN-α + IL-18; or IL12 + IL-18; all 50ng/ml). Blocking antibodies were added immediately prior to stimulation: αIFN-γ (1μg/ml), adalimumab (10μg/ml), etanercept (10μg/ml). Representative plots of MAIT cell IFN-γ **(G)**, and summary data after stimulation with IFN-α + IL-18 **(H)**, or IL-12 + IL-18 **(I)**.

Mean ± SEM shown. Statistical significance was determined using repeated measures two-way ANOVA with Sidak correction for multiple comparisons (A, E, F), repeated measures one-way ANOVA with Dunnett's multiple comparisons test (C, H, I), or paired t test (D). *p < 0.05; **p < 0.01; ***p < 0.001; ****p < 0.0001; ns, not significant. IQR = interquartile range

Next, we tested the capacity for IFN-γ to augment vaccine induced innate-like lymphocyte activation (**Fig4.26**). PBMC were treated with IFN-γ immediately prior to stimulation with SARS-CoV-2 vaccines, or spike peptide. Supplemental IFN-γ increased MAIT cell IFN-γ - either as a fraction of MAIT cells or total live PBMC - in response to spike peptide (**Fig4.26 A, C, G**), mRNA-1273 (**Fig4.26 B, D, H**), or BNT162b2 (**Fig4.26 E, I**), but not ChAdOx1-S (**Fig4.26 F, J**). The total fraction of live PBMC producing IFN-γ was also increased in the presence of additional IFN-γ after stimulation with spike peptide (**Fig4.26 K**), and mRNA vaccines (**Fig4.26 L, M**), but not ChAdOx1-S (**Fig4.26 N**). No induction of innate-like lymphocyte IFN-γ was observed in the absence of vaccine or spike petide stimulation (data not shown). Therefore, supplemental IFN-γ could augment innate-like lymphocyte activation and IFN-γ production in response to SARS-CoV-2 vaccines in the absence of potent IL-18 and IFN-α responsible for ChAdOx1-induced IFN-γ.

Figure 4.26 | IFN-γ increases total IFN-γ in response to spike peptide and SARS-CoV-2 mRNA vaccines through augmented innate-like lymphocyte activation.

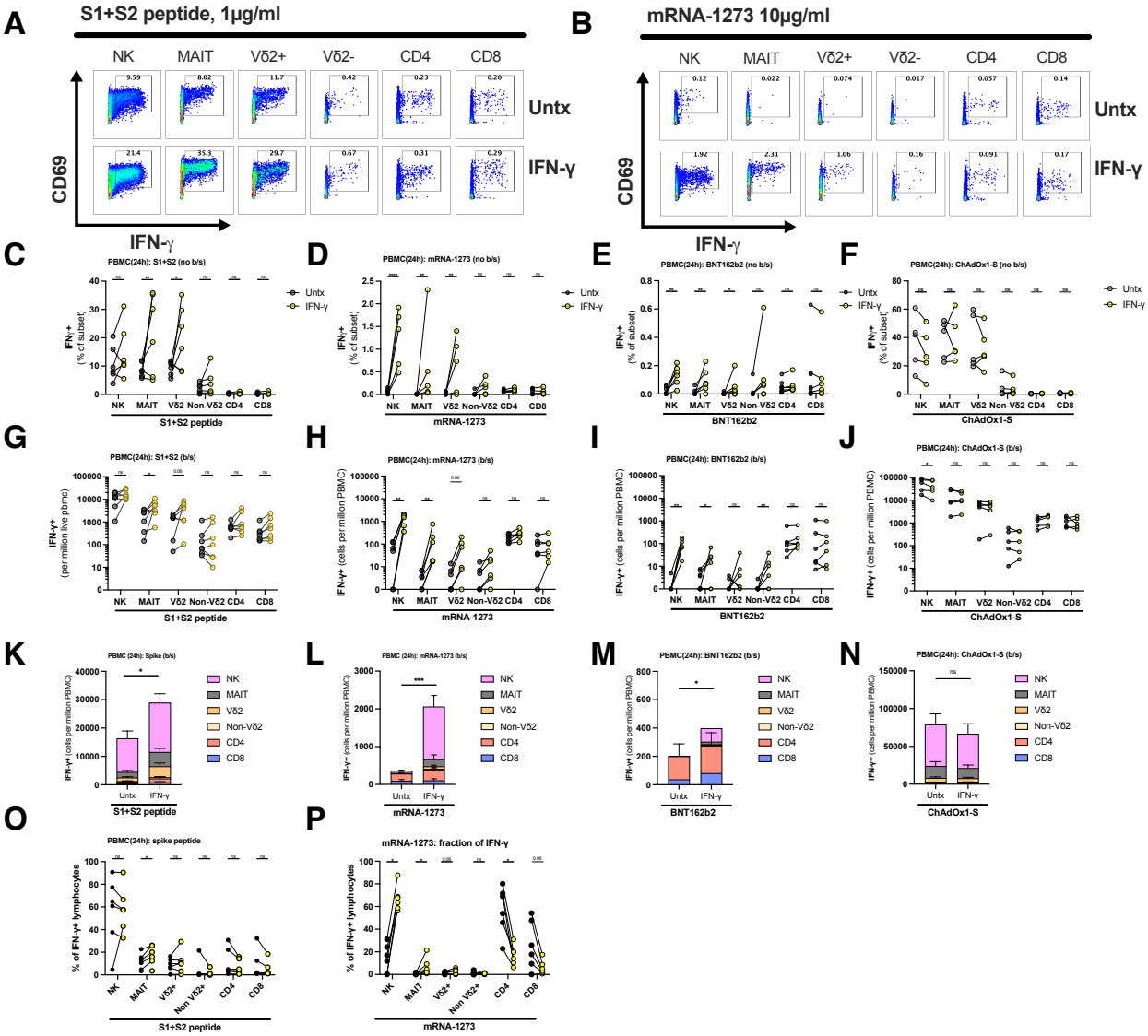

Fig4.26 | IFN-γ increases total IFN-γ in response to spike peptide and SARS-CoV-2 mRNA vaccines through augmented innate-like lymphocyte activation.

Fresh PBMCs from vaccinated individuals either untreated or treated with IFN-γ (50ng/ml) prior to stimulation with: BNT162b2 (10µg/ml; E, I, M), mRNA-1273 (10µg/ml; B, D, H, L, P), ChAdOx1-S (10^9 vp/ml; F, J, N), or pooled S1 and S2 peptides (1µg/ml total; A, C, G, K, O) (all in R10). Activation of NK cells (CD161+CD3- lymphocytes), MAIT cells (CD161+ +Vα7.2+CD3+), Vδ2+ and Vδ2- γδ T cells, and non-MAIT/ γδ T cell conventional CD4+ and CD8+ T cells was measured after 24h. IFN-γ production was either assessed as the % of each subset positive for IFN-γ (C-F), or the fraction of live PBMC (IFN-γ+ cells, cpm live PBMC). Background subtraction was performed using control stimulated wells, sodium chloride (H-J; L-N), or DMSO (G, K). Connected points indicate the same donor.

(A, B) Representative plots of CD69 and IFN-γ expression on NK, MAIT cells, Vδ2+ and Vδ2- γδ T cells, conventional CD4 and CD8 T cells in response to spike peptide pools (A), or mRNA-1273 (B), with/ without prior IFN-γ.

(C-F) IFN-γ production (as a fraction of each subset) in response to spike peptide (C), mRNA-1273 (D), BNT162b2 (E), or ChAdOx1-S (F) with (black) or without (yellow) additional IFN-γ treatment.

(G-J) IFN-γ+ cells (cpm live PBMC) in response to spike peptide (G), mRNA-1273 (H), BNT162b2 (I), or ChAdOx1-S (J) with (black) or without (yellow) additional IFN-γ treatment. Background subtraction performed.

(K-N) Summary IFN-γ+ cells (cpm live PBMC) in response to spike peptide (K), mRNA-1273 (L), BNT162b2 (M), or ChAdOx1-S (N) with or without additional IFN-γ treatment. Background subtraction performed. Mean±SEM shown.

(O, P) Fraction of IFN-γ+ lymphocytes (cpm live PBMC) which are each subset in response to spike peptide (O), or mRNA-1273 (P), with or without additional IFN-γ treatment.

Statistical significance was determined using repeated measures two-way ANOVA with Sidak correction for multiple comparisons (C-F), Mann-Whitney U test (G-N). *p < 0.05; **p < 0.01; ***p < 0.001; ****p < 0.0001; ns, not significant.

Cpm = counts per million.

Finally, we tested the impact of blocking IFN-γR1 signalling on innate-like lymphocyte responses to SARS-CoV-2 spike vaccines or spike-protein in vitro (**Fig4.27**). Given that minimal IFN-γ is induced by mRNA vaccines, we tested in vitro responses in the presence of 10% autologous serum. Addition of anti-CD119 blocking antibody (IFN-γR1; clone#92101) prior to stimulation of PBMC with spike peptide inhibited innate-like lymphocyte CD69 and IFN-γ expression relative to isotype control (**Fig4.27A, B, D**), with no impact on conventional T cells (**Fig4.27 H**). IFN-γR1 blockade also modestly reduced MAIT cell IFN-γ in response to ChAdOx1-GFP (**Fig4.27A, C, E**) and mRNA-1273 (**Fig4.27 G**). The frequency of total IFN-γ+ cells in response to BNT162b2, mRNA-1273, or spike peptide was CD119-dependent (**Fig4.27 J, K**), predominantly due to a reduction of total IFN-γ+ innate-like lymphocytes (**Fig4.27 L-N**). The impact was more specific for IFN-γ, with MAIT cell GzmB not reduced in response to SARS-CoV-2 vaccines (**Fig4.27 O, P**). Furthermore, although inhibition of TNF signalling with both Adalimumab and Certolizumab robustly inhibited ChAdOx1-GFP induced innate-like lymphocyte IFN-γ, only Certolizumab inhibited spike peptide mediated IFN-γ production (**Fig4.27 B-E**).

Figure 4.27| IFN-γR1 (CD119) blockade reduces innate-like lymphocyte activation and total IFN-γ in response to spike peptide and SARS-CoV-2 mRNA vaccines.

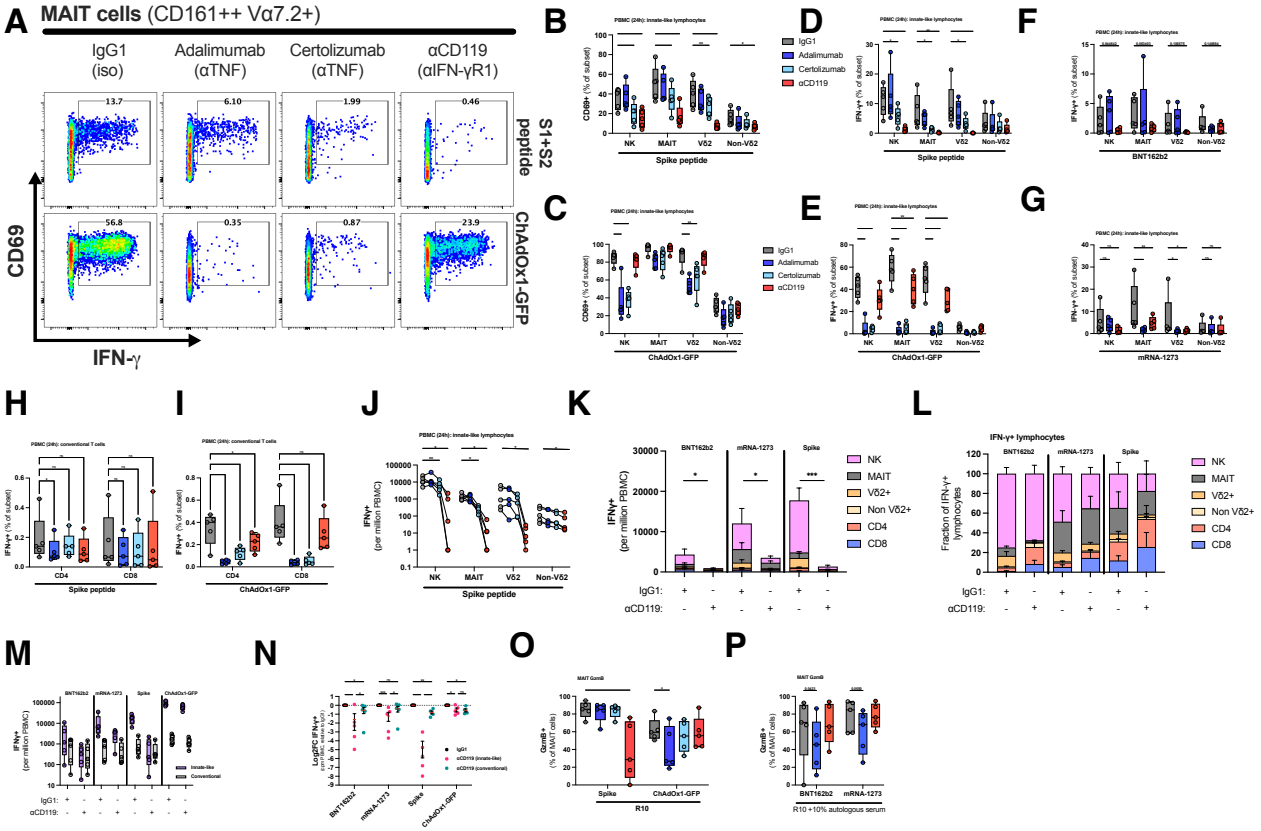

Fig4.27 | IFN-γR1 (CD119) blockade reduces innate-like lymphocyte activation and total IFN-γ in response to spike peptide and SARS-CoV-2 mRNA vaccines .

Fresh PBMCs from vaccinated individuals either untreated or treated with isotype controls (IgG1, 10μg/ml) or inhibitors of CD119 (IFN-γR1; 10μg/ml), or TNF (Adalimumab 10μg/ml, ADA; Certolizumab 10μg/ml, CERT), prior to stimulation with vaccines. Stimulations in R10: pooled S1 and S2 peptides (1μg/ml total; B, D, I, J-O), or ChAdOx1-GFP (10^9vp/ml; C, E, H, K-O). Stimulations in R10 with 10% autologous serum: BNT162b2 (10μg/ml; F, K-N; P) and mRNA-1273 (10μg/ml; G; K-N; P). Activation of NK cells (CD161+CD3- lymphocytes), MAIT cells (CD161++Vα7.2+CD3+), Vδ2+ and Vδ2- γδ T cells, and non-MAIT/ γδ T cell conventional CD4+ and CD8+ T cells was measured after 24h.

(A) Representative plots of MAIT cell CD69 and IFN-γ in response to spike peptide pools (top), or ChAdOx1-GFP (bottom), with or without blocking antibodies (Adalimumab, Certolizumab, or anti-CD119).

(B, C) CD69 expression in NK cells, MAIT cells, Vδ2+ and Vδ2- γδ T cells in response to spike peptide pools (B), or ChAdOx1-GFP (C).

(D-G) IFN-γ expression in NK cells, MAIT cells, Vδ2+ and Vδ2- γδ T cells in response to spike peptide pools (D), ChAdOx1-GFP (E), BNT162b2 (F), or mRNA-1273 (G).

(H, I) IFN-γ expression in CD4+ and CD8+ T cells in response to spike peptide pools (H), or ChAdOx1-GFP (I).

(J) IFN-γ+ cells (cpm live PBMC) which are innate-like lymphocytes in response to spike peptide with or without blocking antibodies (Adalimumab, dark blue; Certolizumab, light blue; or anti-CD119, red).

(K, L) IFN-γ+ cells (cpm live PBMC, K), and frequency which are the indicated cell types (L), in response to spike peptide, BNT162b2, or mRNA-1273 after isotype control (IgG1), or anti-CD119 blocking antibody pre-treatment.

(M) IFN-γ+ cells (cpm live PBMC) which are conventional T cells or innate-like lymphocyte lymphocytes in response to BNT162b2, mRNA-1273, spike peptide, or ChAdOx1-GFP after isotype control (IgG1), or anti-CD119 blocking antibody pre-treatment.

(N) Log2 fold change in IFN-γ+ cells which are innate-like lymphocytes or conventional T cells in response to BNT162b2, mRNA-1273, spike peptide, or ChAdOx1-GFP in the presence or absence of anti-CD119 blocking antibody. Values relative to IFN-γ+ cells (cpm) for each subset after IgG1 pre-treatment.

(O, P) MAIT cell GzmB after stimulation in R10 (O; spike peptide pools or ChAdOx1-GFP), or R10 with human serum (P; BNT162b2 or mRNA-1273), with or without prior anti-CD119 blocking antibody.

Connected points indicate the same donor. Box plots with median, IQR, and range (B-I; M; O, P), or mean±SEM (K, L, N) are shown. Statistical significance was determined using repeated measures two-wa ANOVA with Dunnett's correction for multiple comparisons (B-E; G-J; N-P), or paired t-test (F, K). *p < 0.05; **p < 0.01; ***p < 0.001; ****p < 0.0001; ns, not significant.Cpm = count per million; GzmB = granzyme B.

We confirmed that total secreted IFN-γ in response to spike peptide and mRNA vaccines was reduced after anti-CD119 blockade (**Fig4.28**), together with unique inhibition of TNF secretion. Total IFN-γ in response to ChAdOx1-GFP was only modestly reduced after prior CD119 blockade. Taken together, IFN-γ signalling was required in vitro for maximal IFN-γ and innate-like lymphocyte activation in response to spike protein, either derived from peptide pools or RNA vaccines.

Figure 4.28 | IFN-γR1 (CD119) blockade reduces total IFN-γ in response to spike peptide and SARS-CoV-2 mRNA vaccines.

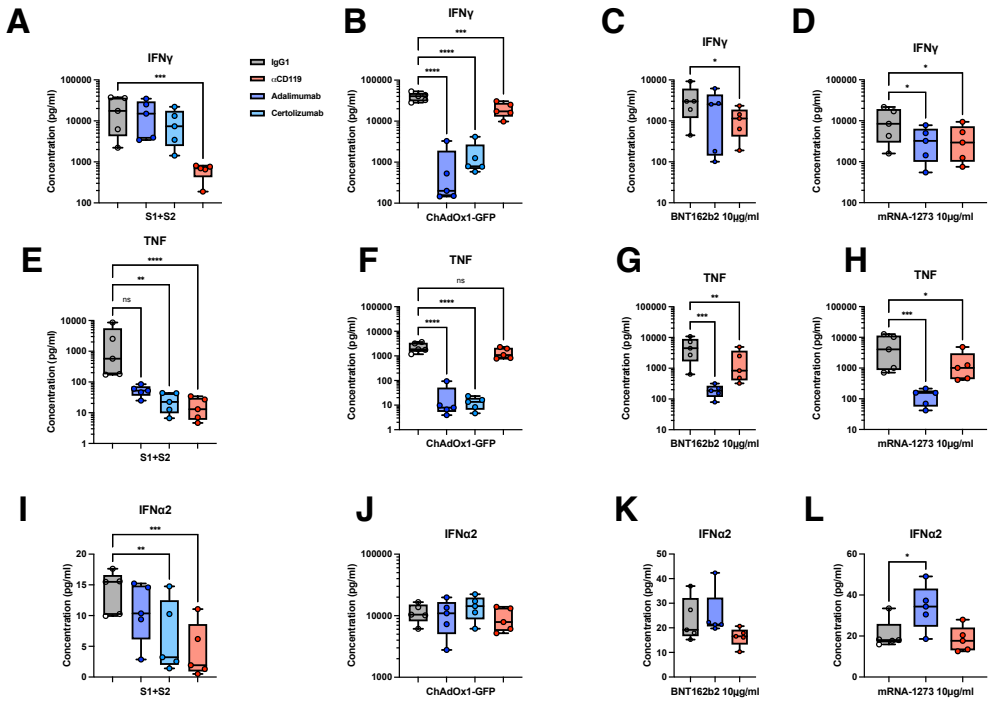

Fig4.28 | IFN-γR1 (CD119) blockade reduces total IFN-γ in response to spike peptide and SARS-CoV-2 mRNA vaccines .
Fresh PBMCs from vaccinated individuals either untreated or treated with isotype controls (IgG1, 10μg/ml) or inhibitors of CD119 (IFN-γR1; 10μg/ml), or TNF (Adalimumab 10μg/ml, ADA; Certolizumab 10μg/ml, CERT), prior to stimulation with vaccines. Pooled S1 and S2 peptides (1μg/ml total; A, E, I), or ChAdOx1-GFP (10^9vp/ml; B, F, J) stimulations were in R10. BNT162b2 (10μg/ml; C, G, K) and mRNA-1273 (10μg/ml; D, H, L) stimulations were in R10 with 10% autologous human serum. Total concentrations of IFN-γ (A-D), TNF (E-H), or IFN-α2 (I-L) were measured in supernatants after 24h.
(A-D) Concentration of IFN-γ in response to spike peptide pools (A), ChAdOx1-GFP (B), BNT162b2 (C), or mRNA-1273 (D), with or without prior treatment with Adalimumab, Certolizumab, or anti-CD119 antibodies.
(E-H) Concentration of TNF in response to spike peptide pools (E), ChAdOx1-GFP (F), BNT162b2 (G), or mRNA-1273 (H), with or without prior treatment with Adalimumab, Certolizumab, or anti-CD119 antibodies.
(I-L) Concentration of IFN-α2 in response to spike peptide pools (I), ChAdOx1-GFP (J), BNT162b2 (K), or mRNA-1273 (L), with or without prior treatment with Adalimumab, Certolizumab, or anti-CD119 antibodies.
Box plots with median, IQR, and range (A-L) are shown. Statistical significance was determined using repeated measures one-way ANOVA with Sidak's test for multiple comparisons. *p < 0.05; **p < 0.01; ***p < 0.001; ****p < 0.0001; ns, not significant.

4.4.9 MHC-dependent MAIT cell activation

We next aimed to identify the source of IFN-γ required for the activation of innate-like lymphocytes. We had found that TCR-triggered conventional antigen specific T cells were the earliest IFN-γ+ cells in vitro. However, in the absence of human serum, BNT162b2 did not induce appreciable IFN-γ+ conventional T cells at 8hr, with no appreciable IFN-γ+ innate-like lymphocytes at 24h (**Fig4.22 H**). In response to mRNA-1273, we observed modest NK IFN-γ production and greater IFN-γ+CD4. Spike peptide pools induced higher conventional T cell IFN-γ at 8hr, and innate-like lymphocyte IFN-γ at 24h. Therefore, we hypothesised that conventional spike-specific T-cells were capable of activating innate-like lymphocytes via IFN-γR signalling.

To support this observation, we found that the frequency of IFN-γ+ CD8+ T cells in response to spike peptide pools in vitro correlated with MAIT cell IFN-γ ($r = 0.93$, $p = 6e\text{-}7$; **Fig4.29 A**), which was more robust compared to ChAdOx1-GFP triggering capable of MAIT cell activation ($r = 0.44$, $p = 0.027$; **Fig4.29 A, B**). We also observed that RNA vaccine-induced innate-like lymphocyte responses in the presence of human serum correlated with CD8+ conventional T-cell IFN-γ, supporting their role as initiators of innate-like lymphocyte activation.

Figure 4.29 | Conventional T cell correlates of vaccine-induced innate-like lymphocyte IFN-γ in vitro.

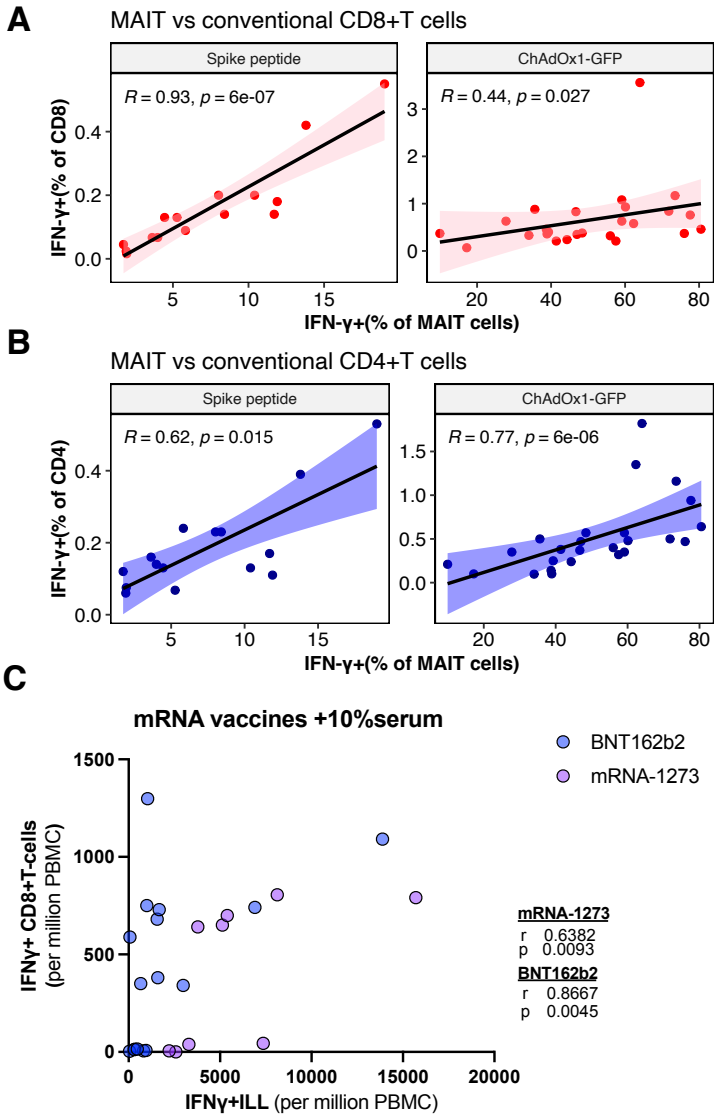

Fig4.29 | Conventional T cell correlates of vaccine-induced innate-like lymphocyte IFN-γ in vitro.
Fresh PBMCs from vaccinated individuals were stimulated with pooled S1 and S2 peptides (Spike peptide, 1µg/ml total; A, B), ChAdOx1-GFP (10^9vp/ml; A, B) in R10 media, or BNT162b2 (10µg/ml; C) and mRNA-1273 (10µg/ml; C) in R10 with 10% autologous human serum. Activation of NK cells (CD161+CD3- lymphocytes), MAIT cells (CD161++Vα7.2+CD3+), Vδ2+ and Vδ2- γδ T cells, and non-MAIT/ γδ T cell conventional CD4+ and CD8+ T cells was measured after 24h.

(A, B) Spearman's correlation of IFN-γ+ MAIT cell activation and the frequency of IFN-γ+ conventional CD8+ (A), and CD4+ T cells (B) in response to spike peptide pools or ChAdOx1-GFP.

(C) Spearman's correlation of the frequency of IFN-γ+ innate-like lymphocytes (NK cells, MAIT cells, γδ T cells) with the frequency of IFN-γ+ conventional CD8 in response to BNT162b2 or mRNA-1273. IFN-γ+ cell frequency expressed as a counts per million live PBMC.

Symbols indicate individual donors. *p < 0.05; **p < 0.01; ***p < 0.001; ****p < 0.0001; ns, not significant. Statistical significance was determined using Spearman's correlation (A-C).

To further assess the impact of conventional T cells in innate-like lymphocyte activation we inhibited classical MHC and measured innate-like lymphocyte activation in response to spike peptide or vaccines. An inhibitor of non-classical MHC-I like molecule, MR1, was used as a control (**Fig4.30**).

Blockade of both MHCI (W6/32, 10µg/ml) and MHCII (Tü39, 10µg/ml) inhibited MAIT cell CD69 and IFN-γ expression in response to spike peptide pools (**Fig4.30 A, B**). Similar inhibition was observed with BNT162b2 and mRNA-1273 induced innate-like lymphocyte activation in vitro (**Fig4.30 C, D**). The total concentration of IFN-γ secreted after 24h in response to peptide stimulation was reduced significantly by blockade of classical MHC (median 18000 pg/ml, IgG2a; 2900 pg/ml, MHC-I; 120 pg/ml, MHC-II; 290 pg/ml, MHCI+II; **Fig4.30 E**). Similarly secretion of IFN-γ (**Fig4.30 F, G**), TNF (**Fig4.30 H-J**), but not IFN-α2 (**Fig4.30 K-M**) was reduced in response to BNT162b2 and mRNA-1273 with MHC blockade. These data were also supported by experiments using live 229E CoV - with MHC blockade again reducing conventional CD8+ T cell IFN-γ and MAIT CD69 expression (data not shown).

Intriguingly, ChAdOx1-GFP induced MAIT cell CD69 and IFN-γ were also partially inhibited by classical MHC-blockade (**Appendix SF4.8 A, B**), with MHCII blockade in particular reducing IFN-γ, TNF and IFN-α2 (**Appendix SF4.8 C-E**). As pDC are the dominant IFN-α2 producers in vitro, the impact of MHC blockade on pDC phenotype and IFN-α2 secretion was assessed. MHCII blockade almost totally depleted live pDCs after ChAdOx1-GFP stimulation (**Appendix SF4.9**). Although the Tü39 antibody has been used extensively in the literature to block class-II presentation, some reports indicate an increase in homotypic clustering and sensitivity of mature DC to apoptosis [395]. It is unclear why class-II blockade specifically reduces live pDCs after ChAdOx1 stimulation, and further experiments would be needed to determine the importance of conventional T cells and classical MHC to SARS-CoV-2 spike induced IFN-γ.

Figure 4.30 | Classical MHC mediated innate-like lymphocyte IFN-γ in vitro in response to SARS-CoV-2 spike protein and vaccines.

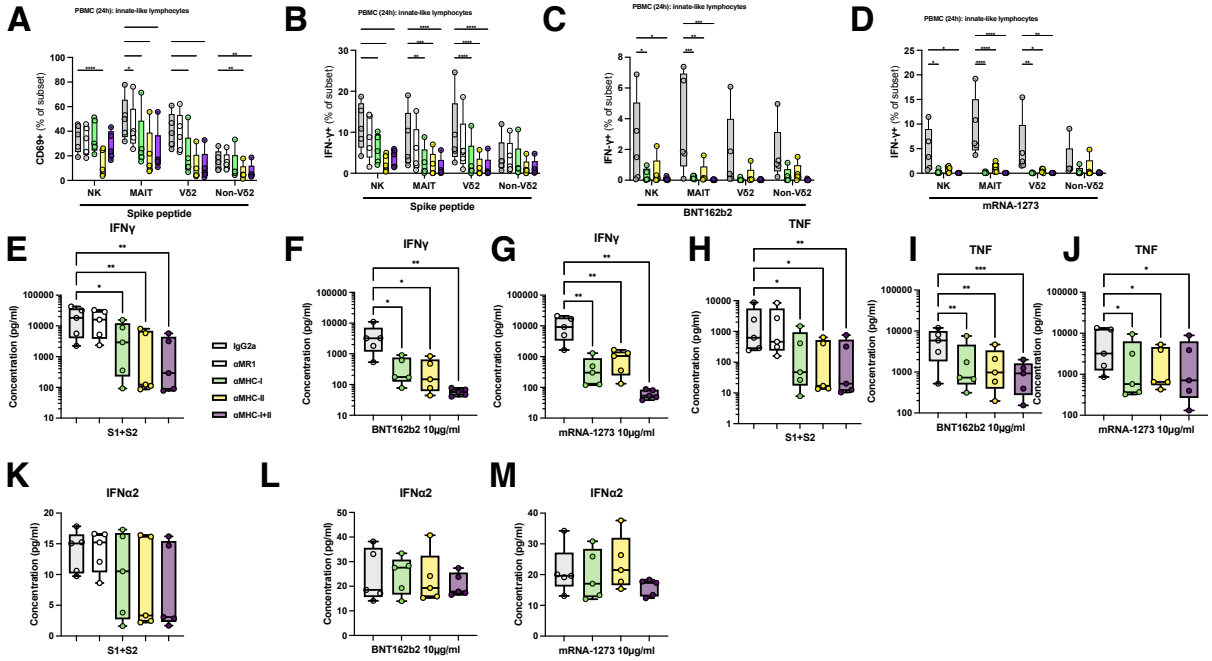

Fig4.30 | Classical MHC mediated innate-like lymphocyte IFN-γ in vitro in response to SARS-CoV-2 spike protein and vaccines.
Fresh PBMCs from vaccinated individuals were stimulated with: pooled S1 and S2 peptides (Spike peptide, 1µg/ml total; A, B, E, H, :) in R10 media; or BNT162b2 (10µg/ml; C, F, I, M) and mRNA-1273 (10µg/ml; D, G, J, N) in R10 with 10% autologous human serum. Inhibitors of MHC-I (clone W6/32, 10µg/ml), MHC-II (Tü39, 10µg/ml), combined MHC-I and MHC-II, MR1 (clone 26.2, 10µg/ml), or isotype control IgG2a (10µg/ml) were added prior to stimulation. Activation of NK cells (CD161+CD3- lymphocytes), MAIT cells (CD161++Vα7.2+CD3+), Vδ2+ and Vδ2- γδ T cells, and non-MAIT/ γδ T cell conventional CD4+ and CD8+ T cells was measured after 24h (A-D). Total concentrations of IFN-γ (E-G), TNF (H-J), or IFN-α2 (L-N) were measured in supernatants after 24h.

(A) Expression of CD69 in NK cells, MAIT cells, Vδ2+ and Vδ2- γδ T cells in response to spike peptide pools.
(B-D) Expression of IFN-γ in NK cells, MAIT cells, Vδ2+ and Vδ2- γδ T cells in response to spike peptide pools (B), BNT162b2 (C), or mRNA-1273 (D), with or without prior treatment with anti-MHC-I, anti-MHC-II, or anti-MR1 antibodies.

(E-G) Concentration of IFN-γ in response to spike peptide pools (E), BNT162b2 (F), or mRNA-1273 (G), with or without prior treatment with anti-MHC-I, anti-MHC-II, or anti-MR1 antibodies.
(H-J) Concentration of TNF in response to spike peptide pools (H), BNT162b2 (I), or mRNA-1273 (J), with or without prior treatment with anti-MHC-I, anti-MHC-II, or anti-MR1 antibodies.
(K-L) Concentration of IFN-α2 in response to spike peptide pools (K), BNT162b2 (L), or mRNA-1273 (M), with or without prior treatment with anti-MHC-I, anti-MHC-II, or anti-MR1 antibodies.

Box plots with median, IQR, and range are shown. Statistical significance was determined using two-way ANOVA with Dunnett's multiple comparison's test (A-D), repeated measures one-way ANOVA with Sidak's test for multiple comparisons (E-L). *p < 0.05; **p < 0.01; ***p < 0.001; ****p < 0.0001; ns, not significant.

4.4.10 Functions of IFN-γ in vitro

Early IFN-γ was prominent 24h after SARS-CoV-2 vaccination in vivo, produced by innate-like lymphocytes, and reduced with extended dosing intervals. Given the impact of dosing intervals on adaptive immunity[363], we asked whether early IFN-γ had a functional role in vaccine efficacy. Both type I and type II IFN driven downstream pathways - as part of the antiviral response - can inhibit key effectors of transcription and translation important for virus lifecycles. As AdV transgene translation is inhibited by IFN-γ in vivo in mice[396,397], we asked if IFN-γ could also inhibit mRNA vaccine induced spike production by pre-treating PBMC with IFN-γ (or IFN-α control) then measuring vaccine induced cellular and secreted SARS-CoV-2 spike protein at 24h (**Fig4.31**).

IFN-α2 treatment reduced cell associated spike protein in response to both mRNA-1273 and ChAdOx1-S at 24h (**Fig4.31 A-G**). IFN-γ pre-treatment was less potent but also reduced total mRNA-1273 induced cell-associated S1 after 24h (**Fig4.31 D**), particularly on monocytes (**Fig4.31 B, D, F**). Total secreted SARS-CoV-2 RBD protein was however increased in response to mRNA vaccines after IFN-γ treatment (**Fig4.31 H-J**). This would suggest that IFNs did not inhibit total mRNA translation but could influence how the adaptive immune system detects mRNA products by regulating the cellular association of transcribed spike protein.

Figure 4.31 | IFN-γ reduces cell-associated SARS-CoV-2 S1 protein but increases secreted SARS-CoV-2 RBD in response to mRNA vaccines.

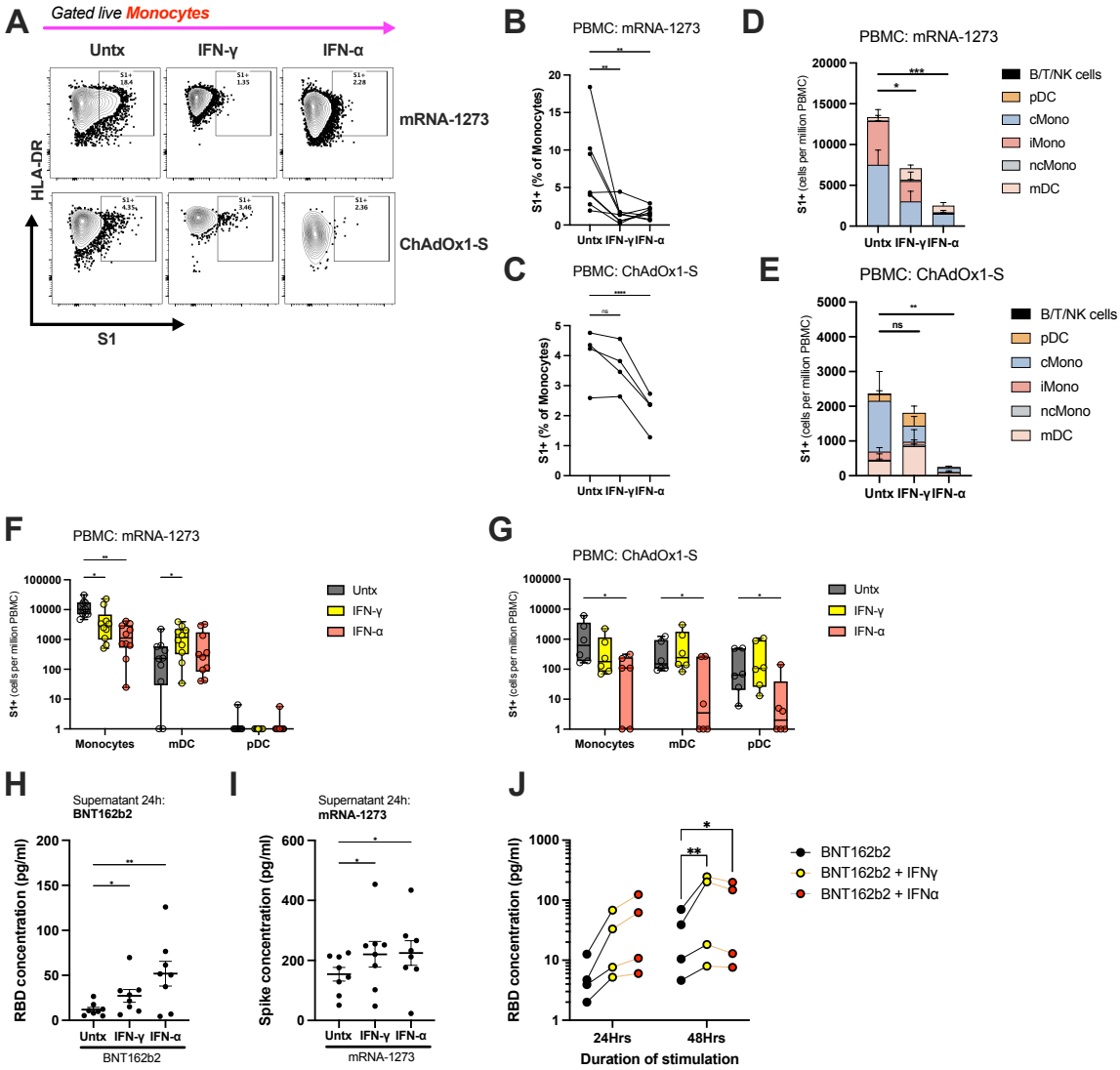

Fig4.31 | IFN-γ reduces cell-associated SARS-CoV-2 S1 protein but increases secreted SARS-CoV-2 RBD in response to mRNA vaccines.
Fresh PBMCs from SARS-CoV-2 vaccinated, ChAdOx1 naïve donors were stimulated with ChAdOx1-S (10^9vp/ml), BNT162b2 (10µg/ml), or mRNA-1273 (10µg/ml). Prior to stimulation, cells were either untreated (Untx), or treated with IFN-α (50ng/ml), or IFN-γ (50ng/ml). Expression of SARS-CoV-2 S1 protein was measured by flow cytometry after intracellular staining at 24h. Cell subsets included: non-myeloid and myeloid cells (CD3-/CD19-/CD56-, HLA-DR+), focussing on classical (cMono; CD14+CD16-), intermediate (iMono, CD14+CD16+), and non-classical monocytes (ncMono, CD14-CD16+), in addition to conventional myeloid DC (mDC, CD14-CD16-, CD11c+), and plasmacytoid DC (pDC, CD123+, CD11c-).
(A) Representative flow plots of S1 expression on monocytes after mRNA-1273 (top) or ChAdOx1-S (bottom) stimulation, with or without prior IFN-α or IFN-γ pretreatment.
(B, C) S1 expression as a fraction of monocytes 24h after stimulation with mRNA-1273 **(B)**, or ChAdOx1-S **(C)** with or without IFN-γ or IFN-α pre-treatment.
(D, E) S1 expressing cells (cpm live PBMCs) 24h after stimulation with mRNA-1273 **(D)**, or ChAdOx1-S **(E)** with or without IFN-γ or IFN-α treatment. Mean±SEM for individual cell types shown.
(F, G) Summary of S1 expressing monocytes, mDC, or pDC (cpm live PBMCs) 24h after stimulation with mRNA-1273 **(F)**, or ChAdOx1-S **(G)** with or without IFN-γ or IFN-α treatment.
(H, I) Secreted RBD protein 24h after stimulation with BNT162b2 **(H)**, or mRNA-1273 **(I)** with or without IFN-γ or IFN-α treatment.
(J) Secreted RBD protein 24h or 48h after stimulation with BNT162b2 with or without IFN-γ or IFN-α treatment.
Symbols indicate individual donors. Mean±SEM are shown. *p < 0.05; **p < 0.01; ***p < 0.001; ****p < 0.0001; ns, not significant. Statistical significance was determined using two-way ANOVA with Holm's multiple comparisons test (C-G; J), non-parametric Friedman test with Dunn's multiple comparison's test (H, I).
Cpm = count per million

4.4.11 Early immune correlates of adaptive responses to vaccines

Finally, we sought to identify early immune markers that correlate with antibody and T-cell responses after immunisation, as these are critical for durable protection and vaccine efficacy (**Fig4.32 A**).

For HCW who received ChAdOx1-S, we observed a positive correlation between the induction of CD69 in innate-like lymphocytes and SARS-CoV-2 specific T-cell IFN-γ as measured by ELISpot at the time of subsequent boost (MAIT cells, r = 0.62, p = 0.035, **Fig4.32 B;** NK cells, r = 0.63, p = 0.032, Fig4.32 **C**). However, there was no significant correlation between changes in innate-like lymphocytes post-prime and SARS-CoV-2 specific antibody responses (**Fig4.32 D-E**).

We also assessed early immune correlates of SARS-CoV-2 spike-specific adaptive immune responses after BNT162b2 vaccination. We found that both the magnitude of plasma IFN-γ induced 24h post-boost, and its co-correlate of MAIT cell activation (CD69 expression), were anti-correlated with changes in spike-specific humoral immune responses in particular (**Fig4.33 A**). Higher early post-boost IFN-γ was associated with lower anti-spike binding antibody titres 28 days post-boost (r -0.67, p < 0.001; **Fig4.33 B**). In agreement with previously published data [363], we also found that extended interval boosting was positively correlated with improved humoral immune responses, as well as lower early innate-like lymphocyte activation and IFN-γ production (**Fig4.33 A**).

Figure 4.32 | Early MAIT cell activation after ChAdOx1-S prime correlates with subsequent spike-specific T-cell responses.

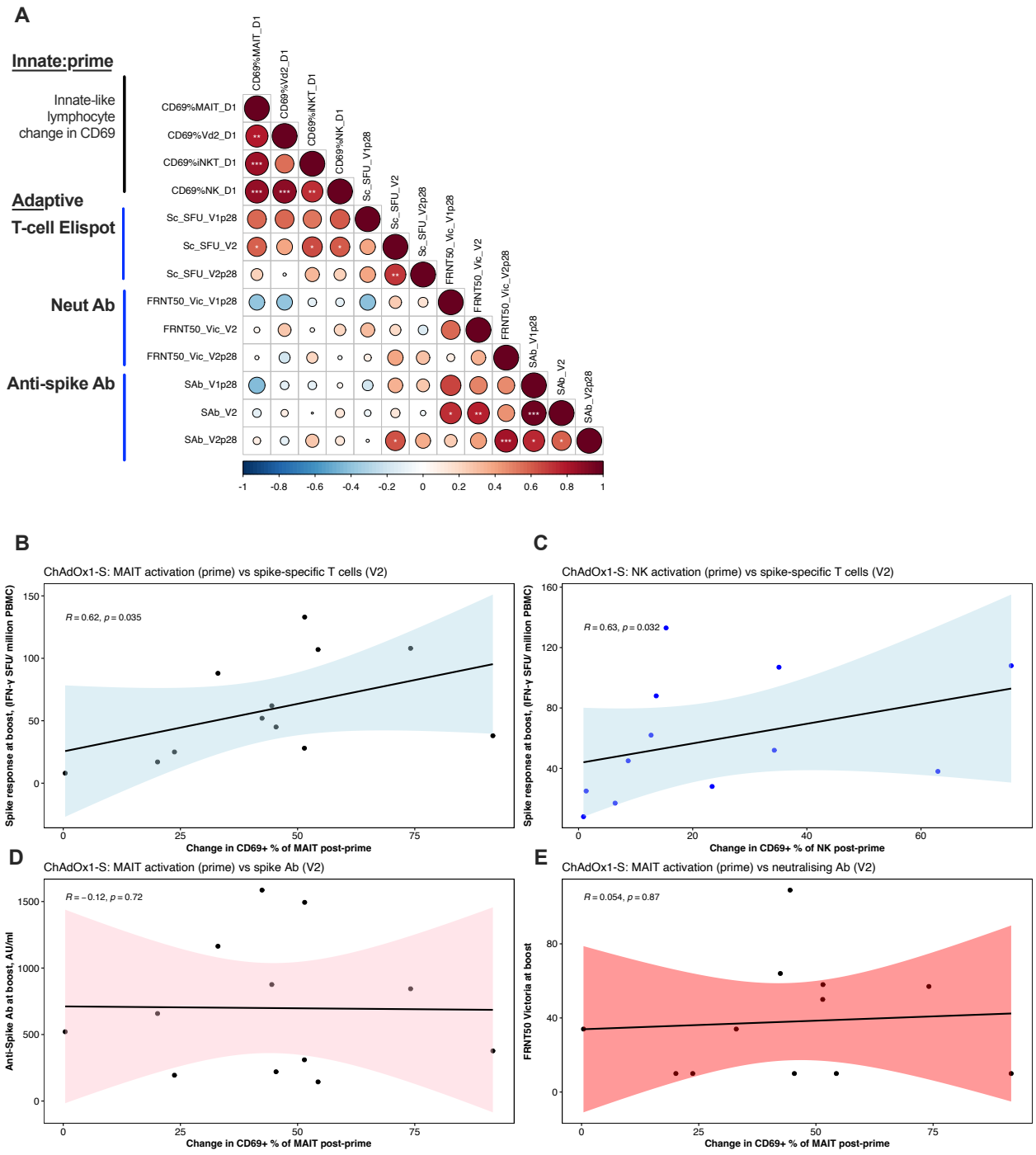

Fig4.32 | Early MAIT cell activation after ChAdOx1-S prime correlates with subsequent spike-specific T-cell responses.

(A) Multi-parametric matrix correlation plot of change in innate-like lymphocyte CD69 expression (between baseline and day 1 post-prime) focussing on subsequent measures of spike-specific adaptive immunity. Spearman's correlation coefficients are shown as circle size and colour intensity.

(B, C) Spearman's correlation of the change in CD69 expression in MAIT cells (B), and NK cells (C) post prime with spike-specific T-cell ELISpot responses induced after 8 weeks (ie., pre-boost).

(D, E) Spearman's correlation of the change in CD69 expression in MAIT cells post-prime with anti-spike antibodies (D), and neutralising antibodies (E) induced after 8 weeks (ie., pre-boost).

Symbols indicate individual donors (B-E).
*p < 0.05; **p < 0.01; ***p < 0.001; ****p < 0.0001; ns, not significant.
Statistical significance was determined using Spearman's correlation (A-E).
SFU = spot forming units

Figure 4.33 | Early IFN-γ after BNT162b2 anti-correlates with spike-specific antibody responses post boost.

A

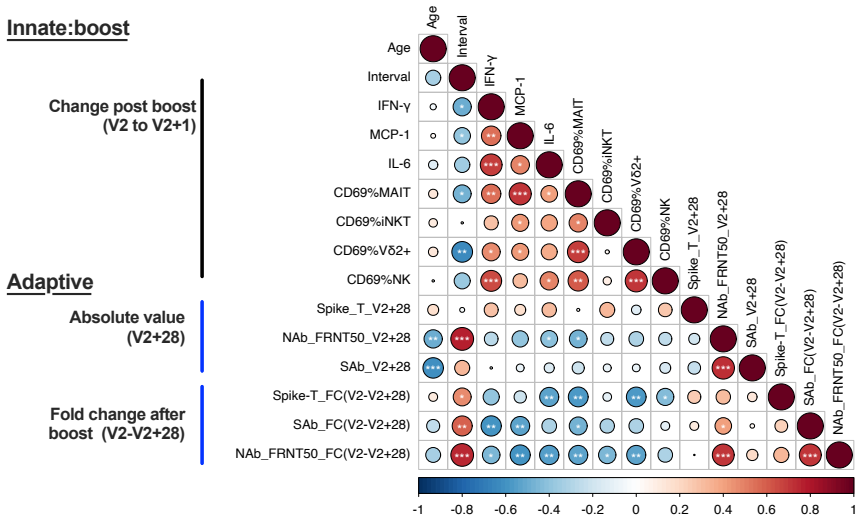

B

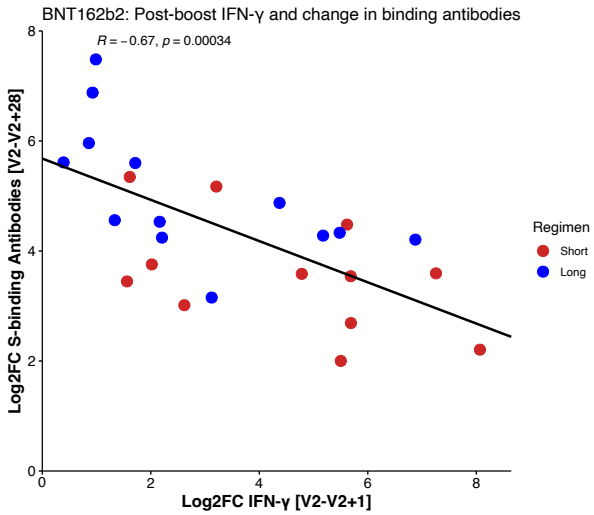

Fig4.33 | Early IFN-γ after BNT162b2 anti-correlates with spike-specific antibody responses post boost.
(A) Multi-parametric matrix correlation plot of change in plasma cytokines (IFN-γ, IL-6, MCP-1) and innate-like lymphocyte CD69 expression (immediatley prior and one day post-boost) focussing on subsequent measures of spike-specific adaptive immunity at four weeks post-boost, or the fold change in these measures from that measured at boost. Age and boosting interval duration (days) were also incorporated in analyses. Spearman's correlation co-efficients are shown as circle size and colour intensity.
(B) Spearman's correlation of the log2 fold change in plasma IFN-γ after BNT162b2 boost with the fold change in anti-spike binding antibodies from boost to four weeks post-boost. Symbols indicate individual donors receiving short (red) or long (blue) boosting intervals are indicated.

*p < 0.05; **p < 0.01; ***p < 0.001; ****p < 0.0001; ns, not significant.
Statistical significance was determined using Spearman's correlation (A, B).
FRNT50 = fractional reduction in neutralisation titres; *NAb = neutralising antibodies; SAb = anti-spike binding antibodies (AU/ml); Spike-T = T-cell IFN-γ ELISpot in SFU (spot forming units) per million PBMC. [V2-V2+28] = change from V2 to V2+28; [V2-V2+1] = change from V2 to V2+1.*

4.5 Discussion

In this Chapter we found that the immune response to SARS-CoV-2 vaccines diverged at the very earliest time points, expanding our understanding of their distinct immunogenicity. We showed that prime-boost early immune responses to AdV and mRNA vaccines followed an inverse pattern, best exemplified by IFN-γ induction and innate-like lymphocyte activation, with implications for understanding reactogenicity and initiation of effective adaptive immunity.

High ChAdOx1-S induced IFN-γ after prime is driven by type I IFN mediated innate-like lymphocyte activation[177] (**Chapter3**), with comparatively dampened early IFN-γ after homologous ChAdOx1-S boost. In contrast BNT162b2-induced early immune responses were enhanced at boost compared to prime; increased innate-like lymphocyte activation post-boost followed spike-specific conventional T cells in vitro and was dependent on IFN-γR1 signalling, implicating a feed-forward loop to amplify early antigen-specific effector functions using more numerically abundant innate-like lymphocytes. In support of this model, mRNA boost after a prolonged interval is associated with waning memory of the initial prime and reduced innate-like lymphocyte activation and early IFN-γ. These findings may explain differences in reactogenicity and immunogenicity with extended dosing intervals [363,392].

Ultimately both vaccine modalities share the capacity to induce high early IFN-γ through co-option of innate-like lymphocytes, but differences in *how* these innate-like lymphocytes are activated shapes the pattern of activation for subsequent boosters which will be important considerations in managing repeated dosing schedules.

4.5.1 Early post-prime vaccine responses are dominated by innate immunity and type I IFN

The distinct early responses to priming with AdV and mRNA vaccines were mirrored by differences in innate antiviral sensing and type I IFN induction. Both vaccines induced a type I IFN transcriptional signature following prime and boost, but only ChAdOx1-S, which was able to transduce pDC in vitro, induced detectable plasma IFN-α as measured by ELISA. However, both BNT162b2 and mRNA-1273 induced modest IFN-α2 in vitro, and this was augmented in the presence of human serum. While BNT162b2-induced plasma IFN-α has been detected using a more sensitive digital SIMOA assay that can detect biologically relevant low-level IFN-α in other immune responses[387,391], the ISG signature observed after BNT162b2 vaccination in both humans [387] and mice [398] could also arise from IFNAR signalling triggered by other subtypes of type I IFN.

Nevertheless, mRNA-induced type I IFN is muted with nucleoside modification[139,399], with uridine to pseudo-uridine modification reducing mRNA affinity for innate TLR sensors[138,400]; in mice identical LNP-mRNA constructs with uridine modification induce considerably lower serum IFN-α2 6h after immunisation[398]. In vitro we found that nucleoside-modified vaccines induced much lower IFN-α compared to non-nucleoside-modified saRNA constructs, although differences in the LNP and kinetics of early antigen production were not controlled for.

Intriguingly, type I IFN is actually necessary for BNT162b2-induced cellular responses[398]. BNT162b2 priming of naïve spike-specific CD8+ T cells is significantly reduced in *Ifnar*$^{-/-}$ mice[398], which we have also replicated (data not shown). In vitro, IFN-α pre-treatment did not reduce mRNA vaccine-derived spike protein, potentially because nucleoside modification renders mRNA resistant to ISG-mediated inhibition[138,376]. Similar to ribosomal RNA, nucleoside-modified mRNA binds with low affinity to PKR and may be less sensitive

to ISG-driven inhibition of translation[376]. Therefore nucleoside-modified RNA vaccines both induce type I IFN - through reduced TLR-binding - and are less sensitive to IFN-mediated antiviral inhibition through reduced binding to inhibitors of translation.

The cell types responsible for mRNA-vaccine induced type I remain unclear. Unlike ChAdOx1-S, neither BNT162b2 or mRNA-1273 induced pDC spike protein or IFN-α expression *in vitro*. However in vivo, one study has detected pDC spike protein in mice immunised with remnant BNT162b2[398]. Unusually pDC nucleic acid sensors (TLR3, 7, 9) played no role in type I IFN-mediated spike-specific CD8+ T cell priming. Instead MDA5, a universally expressed cytosolic dsRNA sensor[401], was crucial for priming antigen-specific cellular immunity[398]. The cell types involved and whether MDA5 triggering is a direct result of mRNA vaccine sensing, or an indirect result of sensing other nucleic acids released from tissue damage is important for future investigation.

The importance of type I IFN for vaccine induced immunogenicity is also an important area for further work, and relevant to understanding differences in immunogenicity and toxicity. Across numerous studies AdV, which induce potent anti-viral host responses, generate superior spike-specific cellular responses after a single dose compared to RNA vaccines [300,360]. From our data, ChAdOx1-S induced plasma IFN-α post-prime was higher than BNT162b2, and correlated with spike-specific IFN-γ ELISpot titres after 28 days. Our transcriptional type I IFN signature after BNT162b2 prime replicates another study, which also showed this ISG signature correlates with spike-specific CD8+ T cell responses at 4 weeks[387]. The kinetics of early interferon induction in response to vaccines may also be relevant when comparing vaccines; for example, yellow-fever vaccine IFN-inhibitory proteins delay peak ISG expression post-prime[402].

Early post-prime IFN-responses also varied based on sex and age. Women had higher ChAdOx1 induced plasma IFN-α and IFN-γ after 24h. Conversely age anti-correlated with

the magnitude of ChAdOx1-S induced IFN-γ. Our ongoing work is exploring the impact of host variables on transcriptional signatures, with similar studies of early influenza vaccine responses showing a reduction in interferon and innate transcriptional gene signatures with increasing age[402]. Our observations after ChAdOx1-S prime also align with the odds of early systemic adverse effects which are 1.95-fold higher in females, and fall by 35% for every 10-year increase in age in adults [403]. A mechanistic link between female sex and immune responses, including those to vaccinations, is an emerging area for further exploration[404,405].

Intriguingly, young females are also most at risk of life-threatening VITT (vaccine-induced thrombotic thrombocytopenia) after AdV prime with both ChAdOx1 and Ad26[388,406]. Type I IFN therapy, either with IFN-α[407,408] or IFN-β[409], has been associated with thrombotic thrombocytopenia syndromes, including the development of anti-platelet antibodies[407], as well as the induction of autoantibodies generally[410–412]. Understanding predictors and downstream effectors of an exaggerated early IFN response could therefore reveal key drivers of vaccine-induced complications.

IFN-γ was one such downstream effector of type I IFN induced post-prime, potentially relevant to reactogenicity and immunogenicity with both vaccines. We have previously shown that ChAdOx1-S induced IFN-γ is dependent on type I IFN and innate-like lymphocyte activation[334]. BNT162b2 induced more modest plasma IFN-γ by comparison. In mice, serum IFN-γ was observed after immunisation of wild type but not *Ifnar*$^{-/-}$ mice with higher doses of BNT162b2 intramuscularly, suggesting a type I IFN and dose dependent mechanism for IFN-γ induction[398]; in this study the majority of IFN-γ+ cells at 24h post-prime were NK cells, which have the capacity for type I IFN dependent IFN-γ production through non-canonical STAT4 signalling [254,413]. Other cytokines induced after BNT162b2 prime in mice, such as IL-2 and IL-15, could also contribute to innate-like lymphocyte activation[306,414–416].

Although BNT162b2 LNP induces inflammasome activation[417], inflammasome activation is not required for immunogenicity in mice[398], and IL-18 has not been detected after vaccination in mice [398] or humans[387], concordant with our data. As IL-18 is a potent inducer of innate-like lymphocyte IFN-γ, this likely drives the much more striking IFN-γ induction after ChAdOx1-S prime compared to BNT162b2. This further support the concept that cell-death derived signals are important adjuvants[141].

In summary, type I and II IFN are core early components of AdV and mRNA vaccines responses, with increased type I IFN in combination with other cytokines after ChAdOx1-S driving innate-like lymphocyte activation and higher IFN-γ.

4.5.2 Early boost responses are regulated by immune memory

Another key finding was that immune memory of past antigen exposure may regulate early immune responses to homologous prime-boost vaccination in different directions; prior priming diminished subsequent ChAdOx1-S boost responses, whereas BNT162b2 responses were enhanced.

ChAdOx1

The cytokines profile induced by **ChAdOx1-S** changed between prime and boost, with inflammasome-derived cytokines IL-18 and IL-1β no longer being significantly induced after boost, potentially contributing to the observed reduction in innate-like lymphocyte activation and IFN-γ. The mechanism remains unclear, but it is known that effector memory CD4+ T cells can inhibit NLRP3 inflammasome activation in an antigen-dependent manner[418]. If such regulation were to occur with ChAdOx1-S, AdV-hexon rather spike-specific (transgene) memory responses are more likely to regulate inflammasome activation. Firstly, levels of inflammasome-derived cytokines were similar after ChAdOx1-S prime in previously infected HCW for whom primary ChAd vaccination was a second spike-antigen

encounter. Additionally, studies examining reactogenicity as a proxy for early immune responses found that ChAdOx1-S boost resulted in lower systemic adverse events when the original prime was also ChAdOx1-S, rather than BNT162b2[369]. BNT162b2 prime induces anti-spike immunity without anti-vector immunity and is linked to greater reactogenicity following heterologous ChAdOx1-S boost. These data suggest that transgene-specific responses in the absence of anti-vector immunity may enhance innate responses to the initial ChAdOx1 exposure.

Both humoral and cellular anti-vector immunity can shape innate and adaptive responses to AdV. For example, pre-existing Ad5-specific CD4+ T cells correlate with reduced transgene-specific responses to Ad5 vaccination in humans[124]. Humoral anti-vector immunity is more likely to account for reduced IFN-α post-boost, presuming this is triggered by cytoplasmic nucleic acid sensors in the short window between transduction and nuclear translocation pre-transcription; neutralising anti-vector antibodies would reduce transduction and the effective dose of translocating AdV. This model would explain the increased ChAdOx1-S reactogenicity after boosting with an extended interval [365], as waning memory of the original AdV exposure would increase the effective AdV dose and ensuing innate response.

Alternative explanations could include innate immune epigenetic changes which change the way cells respond to a ChAdOx1-S encounter at boost [26]. ChAdOx1-S induced changes in the circulating frequency and activation of monocytes which lasted at least 2 months after prime, and may therefore influence subsequent cytokine production on secondary vaccination. Additionally, other non-specific exposures could epigenetically manipulate ChAdOx1-S responses at boost, similar to the postulated mechanism through which BCG vaccination protects against SARS-CoV-2 infection [28]. Against this hypothesis, epigenetic reprogramming normally enhances rather than reduces secondary innate responses as is the case with our data[28]. Further work will be needed to tease out the components of

immune memory responsible for the reduced innate and innate-like immune cell activation after AdV boost, including the contribution of cross-reactive humoral and cellular immunity given obvious implications for future AdV based vaccination choices.

BNT162b2

In contrast to ChAdOx1-S, early responses after homologous BNT162b2 boost, including IFN-γ, were found to be enhanced compared to prime, and these responses waned with extended immunisation intervals. This suggests that priming-induced memory potentiates secondary vaccine responses. The evidence supporting this hypothesis is two-fold. Firstly, infected HCW for whom priming was a second spike antigen encounter, induced greater plasma IFN-γ after BNT162b2 prime compared to SARS-CoV-2 naïve individuals. This finding argues against solely LNP-dependent augmentation and was replicated contemporaneously[419]. Secondly, spike-specific adaptive immune responses correlated both in vivo and in vitro with the magnitude of early BNT162b2-induced IFN-γ. In vitro, innate-like lymphocyte IFN-γ in response to BNT162b2 and spike-peptide pools correlated with the frequency of IFN-γ+ conventional T cells and was inhibited by blocking classical MHC. In vivo, boost-induced IFN-γ and innate-like lymphocyte activation were reduced with extended dosing intervals and correlated with measures of spike-specific adaptive immunity at the time of boost. These data suggest that waning SARS-CoV-2 specific adaptive immunity, rather than non-specific trained immunity, is responsible for our observations, as trained immunity is generally maintained for longer periods after vaccination [28,30]. Reactogenicity data from the COMCOV trial further supports these observations as longer intervals after BNT162b2 prime are associated with reduced systemic reactogenicity at boost[365]. Finally, in vivo data in mice shows that enhancement of BNT162b2-induced IFN-γ at boost is abolished by prior depletion of CD4+ and CD8+ T cells, but not NK cells[398], further implicating adaptive immunity in these early responses.

As an extension, it would be important to determine the relevance of cross-reactive T cells to other in the potentiation of vaccine responses. Pre-existing T cells to spike-protein from other coronaviruses are found in the population[420–423], and may account for modest innate-like lymphocyte activation post-prime. Further studies should determine *if* and *how* activation of these cross-reactive T-cells impacts downstream effectors like innate-like lymphocytes, particularly since baseline SARS-CoV-2 cross-reactive CD4+ T cells correlate with enhanced mRNA vaccine-induced immune responses[390,424].

4.5.3 IFN-γ as a regulator of innate and adaptive immunity

Unexpectedly innate-like lymphocytes were the major source of IFN-γ in response to mRNA vaccines *in vitro*, but only responded to mRNA vaccines and spike-peptide in the presence of spike-specific conventional T cells. Early innate-like lymphocyte IFN-γ was inhibited with antibodies against classical MHC and IFN-γR1, supporting a model whereby very early IFN-γ from antigen-specific cells is amplified by more abundant innate-like lymphocytes expressing IFN-γR1 (CD119). In tissues at the site vaccination other cells, such as Trm and an expanded repertoire of innate-like lymphocytes, could also sense and amplify effector circuits.

Early T-cell derived IFN-γ as an initiator of innate-like lymphocyte mediated amplification has been described historically. In mice, specific iNKT-activation by αGal-Cer accelerates activation of other immune cells[259,425,426]. NK cell activation (CD69, IFN-γ) was observed as early as 90min after α-GalCer injection in wild type mice but not RAG or CD1-deficient animals, or those pre-treated with anti-IFN-γ blocking antibodies, suggesting that iNKT-derived IFN-γ can also drive IFN-γ from NK cells[425].

Similarly, Petley et al., found that 5-OPRU activation of enriched MAIT cells produces IFN-γ very quickly (<8hr) and can activate NK cells in an IFN-γ-dependent, APC-independent

manner[427]. Stimulation of enriched Vα7.2+ cells with 5-OPR-U induced NK-cell IFN-γ and TNF in co-cultures, which was not observed after 5-OP-RU stimulation of NK cells alone. TCR triggered MAIT cell co-cultured with macrophages did not induce macrophage IFN-γ, potentially implicating innate-like lymphocyte specific crosstalk. Functionally IFN-γ blockade prior to 5-OP-RU stimulation in mice abolished the NK-mediated protective anti-tumour effects of 5-OP-RU[427]. These data would imply that very early IFN-γ from TCR triggered MAIT cells can trans activate NK cells, with important implications for host protection.

Conventional antigen specific memory T cells can also trans-activate NK and NKT cells in mice early after secondary Listeria immunisation[258]; functionally accelerated NK and NKT cell activation results in increased recruitment, activation and potentiation of innate effectors, which implies that cells capable of sensing and producing IFN-γ, such as innate-like lymphocytes, collectively amplify very early protective immune responses.

How T-cell derived IFN-γ can activate other innate-like lymphocytes and potentially IFN-γR+ conventional T-cells would be an interesting area for future study. CD8+ T-cells can exchange IFN-γ in homotypic clusters, with IFN-γ secretion polarised and targeted at T-T synapses to drive target cell differentiation[428]. Preliminary data suggests that increased cell density in enriched CD8+ T cell co-cultures augments MAIT cell IFN-γ in response to IFN-γ inducing cytokines (IFN-α, IL-18, TNFR2 agonist), with both ICAM-1 and LFA-1 blockade capable of reducing this MAIT cell derived IFN-γ (*data not shown*). The difference in effector functions from innate-like lymphocytes activated via T-cell derived signals, as opposed to APC-derived (cytokine) signals, would be important future work.

In addition to innate-like lymphocytes, the ***consequences of early IFN-γ for innate and adaptive immune responses*** merits exploration, particularly as mRNA vaccine induced IFN-γ was increased with shorter boosting intervals known to generate differential adaptive

immune responses[363,365,392]; shorter priming intervals are associated with reduced humoral immunogenicity but overall increased T-cell responses for both BNT162b2 [363,365,392], and ChAdOx1-S vaccines[365].

Both human and murine data suggest an important role for early BNT162b2 induced IFN-γ in *innate* immune cell activation. Both in our study and another study looking at early responses after short interval boosting[387], increased early IFN-γ correlates with increased myeloid cell activation and intermediate monocyte frequency. In vitro IFN-γ can induce inflammatory gene expression in enriched CD14+ monocytes[387], in addition to early TNF which in combination with type I IFN could activate innate-like lymphocyte IFN-γ production. In mice, IFN-γR blockade prior to BNT162b2 boost reduces innate immune activation[398], suggesting that the reduced IFN-γ at boost with extended intervals is directly responsible for the diminished peripheral monocytosis and innate activation observed in HCW.

RNA-LNP vaccines were optimised for delivery to lymphoid tissue-resident CD11c+ APC[139]. In addition to regulation of APC MHC expression[429,430], IFN-γ can regulate transgene production and retention with other vaccines[431]. In vitro, we found PBMC IFN-γ pre-treatment increased RBD secretion but reduced cell-associated S1 protein in response to mRNA vaccines, BNT162b2 and mRNA-1273. SARS-CoV-2 spike protein persists for weeks in human LN GCs after mRNA vaccination [147], so early IFN-γ could regulate GC and antibody maturation. Additionally, secreted spike protein could circulate associated with exosomes[432]. Bansal et al., recently found that RBD-decorated exosomes are capable of eliciting mucosal and systemic adaptive immune responses in animals[433], so vaccine-derived IFN-γ could further shape adaptive immunity through exosome secretion and antigen cross-presentation[434], important for CD8+ T cell responses to BNT162b2 in mice[398]. It would be important to confirm whether IFN-γ can also modulate antigen secretion from tissue APCs and stromal cells - the primary depot of persistent ChAdOx1-induced transgenes [435] - as the spatiotemporal regulation of transgene products may be a more

universal means through which vaccine-derived innate and innate-like responses shape adaptive immunity.

Give the heterogeneity and small sample size, we couldn't clearly define a functional role for early IFN-γ in vaccine-induced adaptive immunity. IFN-γ does however have a prominent role in the early initiation of humoral and cellular immunity more broadly, so may contribute differential immunogenicity between regimens. By example early IFN-γ is crucial to developing and maintaining Th1 polarised CD4+ T cells during viral infections[264], in addition to enhancing CD8+ T cell proliferation, cytokine secretion and cytotoxicity[90,436–438]. The impact of early IFN-γ on antibody responses is inconclusive. In severe malaria infection, high early IFN-γ inhibits Tfh development with a reduction in GC and antibody secreting plasma cells reversed by IFN-γ and TNF blockade[439]. Conversely early innate-like lymphocyte derived IFN-γ after influenza vaccination promotes the recruitment of IL-6+ dendritic cells to synergistically promote potent anti-influenza B cell responses [309].

Evidence for the importance of IFN-γ in mRNA vaccination is sparse in human cohorts and complicated by confounders. For example, a reduction in BNT162b2 humoral responses in patients on JAK-STAT inhibitors is confounded by the underlying diseases and derangement of IFN-γ independent signalling pathways [440]. To our knowledge, the only patient with IFNGR1 deficiency reported in the literature had adequate humoral responses 14 days after mRNA boost[441]. Ultimately as mRNA vaccines and AdV both induce IFN-γ, studies exploring the contribution of early vaccine-derived cytokines merit further investigation as a means to optimise individual responses.

4.5.4 Relevance of findings to vaccinology

Reactogenicity and toxicity

Our data provides a mechanistic explanation for vaccine specific differences in reactogenicity and toxicity. The observed pattern of early immune responses after BNT162b2 track with systemic reactogenicity in numerous studies showing boost-enhancement after BNT162b2[367] or mRNA-1273 [366], which is reduced with longer priming intervals[365]. Similarly systemic reactogenicity after mRNA vaccination is greater in those with previous infection[442]. Although we were unable to correlate innate immune activation with symptoms, a recent study found that systemic reactogenicity to BNT162b2 correlated with IL-6, IFN-γ and IFN-γ related chemokines, CXCL10 and CCL2 (MCP-1)[443].

These data also provide insight into serious systemic toxicity after vaccination. ChAdOx1-S prime induced greater immunological and transcriptional antiviral responses compared to BNT162b2, driven by higher type I IFN, which was more pronounced in younger females. Reactogenicity after ChAdOx1-S prime is also greater in younger individuals and females [123], with the risk of severe cerebral venous sinus thrombosis also highest in females of reproductive age and falling with age[444], following a similar pattern to the magnitude of IFN responses in our cohort.

In contrast, vaccine induced myocarditis is most common after boost with mRNA vaccines in men [445,446], specifically higher after mRNA-1273 compared to BNT162b2, and reduced with longer boosting intervals [447]. Vaccine-induced IFN-γ could therefore be causally linked; IFN-γ can induce myocyte atrophy [448] and necrosis in transgenic mice over-expressing IFN-γ, which suffer from phenomena similar to chronic viral myocarditis [449].

Alternatively, the higher incidence of the myocarditis in response to mRNA-1273 could be due to higher secreted plasma spike protein, which may be relevant effector response of

IFN-γ. Spike protein is detectable in serum after intramuscular mRNA vaccination and can travel to distant tissues, in contrast to ChAdOx1 induced transgene products which remain in local tissues. It is unclear what impact antigen-specific responses have on circulating and distant spike-protein. In a future with necessary regular boosters, understanding rules driving potentially harmful responses to different vaccines is critical.

Adaptive immunity

Prior studies have shown that baseline immune parameters can predict the response to vaccination[450]. A recent study found that MAIT cell characteristics, which remained stable between baseline and pre-boost timepoints, were associated with spike-specific responses. Boulois et al., found MAIT cell frequency to positively correlate with BNT162b2-induced AIM+ CD4+ T cell and anti-spike antibody responses[451]; conversely MAIT cell CD69 expression negatively correlated with these measures of adaptive immunity. Mechanistically tonic MAIT cell activation might result in desensitisation to further activation, with differences in the abundance and sensitivity potentially resulting in differential amplification of early vaccine-derived cues important for adaptive immunity.

We also observed associations between early immune responses and antigen-specific humoral and cellular immunity in response to vaccination. Similar observations exist after yellow fever (YF-17D) vaccination in humans, where early type I IFN correlates with subsequent YFV-specific antibody and CD8+ T cell responses [151]. We found that early IFN responses after ChAdOx1-S prime - and surrogate measures including MAIT cell activation and lymphopenia - correlated with the frequency of IFN-γ+ T cells by ELISpot after 1 month, a finding previously demonstrated for a ChAdOx1-MenB vaccine[334]. Similar correlations have been observed after BNT162b2 prime, whereby early type I IFN signatures correlate with antigen specific CD8+ T cells responses. Environmental factors such as the microbiome, which alter baseline 'tonic' and induced IFN signalling, could therefore prove significant contributors to the heterogeneity of human vaccine responses[141].

We also observed an inverse correlation between the magnitude of IFN-γ induced after BNT162b2 boost with the fold change in spike-specific antibody responses. Another study found a positive correlation between the magnitude of post-boost IFN-γ with absolute antibody titres three weeks after boost in HCW exclusively vaccinated with short interval boosting[452] - a correlation we also see albeit not reaching statistical significance when analysing only those boosted after shorter intervals. As adaptive immunity immediately prior to boost correlates with IFN-γ subsequently induced by the boost, final antibody titres would also positively correlate with IFN-γ at boost even if mechanistically IFN-γ played no role in humoral responses. Further mechanistic studies are required using animal models to determine the causal nature of any relationships between early IFN-γ and mRNA vaccine induced immunogenicity.

Assays to measure antigen-specific T cells

An intriguing implication of IFN-γ mediated augmentation of early IFN-γ by innate-like lymphocytes is in the interpretation of assays to detect antigen-specific T cells without the use of peptide-MHC tetramers. Assays gauging the frequency of antigen-specific T-cells after prolonged (>16h) peptide stimulation - particularly in the presence of human serum - may have falsely elevated frequencies due to erroneous inclusion of IFN-γ activated CD8+ MAIT cells. Secondary activation of MAIT cells has previously been observed in response to BCG-vaccination, which can both trigger MR1-restricted T cells via their TCR and cytokines[227]. Spike peptide pools would only be expected to trigger conventional MHC-restricted T cells, yet we found that innate-like lymphocytes made up a significant fraction of spike-responsive cells in vaccinated donors. This is supported by observations in the literature. Firstly, the frequency of 'spike-specific' CD69+IFN-γ+ CD8+ T cells is significantly lower with shorter 6-8h peptide stimulation [453,454] compared to overnight stimulation[360]. Furthermore, after 12h spike-peptide stimulation single cell sequencing identifies TCRs from NK cells, MAIT cells, γδ T cells and iNKT cells amongst AIM+ cells[455]. We also have

similar unpublished data showing that MAIT TCR sequences make up a sizeable portion of 4-1BB+CD40L+ sorted T cells after peptide stimulation (Nicholas Provine).

These data would suggest that ELISpot, AIM and ICS all could non-specifically identify unconventional T-cells activated through IFN-γR1 signalling, and that in addition to shortened stimulation, CD119 blockade could more accurately identify antigen-specific T cells in studies of vaccine responses.

Vaccination schedules

Understanding rules that govern early immune interactions with different vaccines could support decision making on vaccination schedules, including dosing and intervals. For example, lower dose AdV prime should induce lower anti-vector immunity which would further wane with time, greatly enhancing the effective dose at boost in those with extended dosing intervals. Mice primed with low-dose (1000-fold reduced) Ad5-S prime has superior boosting after four weeks compared to mice immunised with standard prime doses [456]. It is also conceivable that lower dose priming would generate reduced spike-transgene specific CTL responses, thereby increasing the durability of the antigen depot.

Measures of adaptive immunity prior to boost with BNT162b2 could also be manipulated to induce greater type I IFN and IFN-γ. Vaccine-induced type I IFN correlates with spike-specific CD8+ T cell and would be expected after short intervals BNT162b2 boosting, or ChAdOx1-S prime. Resultant vaccine-induced IFN-γ would reduce cell-associated spike protein at the expense of secreted spike protein, potentially influencing the composition of adaptive responses. Given that short interval BNT162b2 boosting is associated with reduced humoral immunity and slightly superior cellular immunity to SARS-CoV-2 spike, mRNA vaccine induced IFNs may provide an underpinning mechanistic explanation.

4.5.5 Limitations

As mentioned, our study is limited by the modest sample size and exclusive sampling of peripheral blood from predominantly young healthy individuals. Generalisability to responses in older individuals would require further studies, ideally including tissues as the site of initiation of immune responses, together with clinical data on protective efficacy against the development of SARS-CoV-2. Additionally, we may have under-estimated individuals with prior infection, such that some high prime responses were in fact anamnestic responses following asymptomatic mild SARS-CoV-2 infection.

For studies of mechanism, we were unable to gauge the contribution of mRNA LNP to inflammatory responses - which could further be impacted by vaccine impurities or responses to polyethylene-glycol found in both BNT162b2 and mRNA-1273. Additionally anamnestic responses to SARS-CoV-2 can exist in the absence of serological evidence for prior infection, further complicating interpretation.

4.6 Conclusion and Summary

In conclusion, ChAdOx1 and BNT162b2 induced distinct early immune profiles through different mechanisms. Prior antigen exposure, the delivery vehicle, and nucleic-acid encoded antigen all regulated innate-like lymphocyte activation which then amplified early immune responses through an IFN-γ dependent mechanism. Innate-like lymphocyte contribution to AdV and mRNA-vaccine responses depended on upstream cell types, which included both innate and adaptive cells on antigen re-encounter. Understanding how early type I and type II IFN-mediated effector responses could be amplified and altered by changing boosting intervals provides a framework for understanding variable vaccine efficacy and toxicity. Deeper understanding requires knowledge of tissues and draining lymph nodes where most early responses occur in vivo, with the role of age, sex, and the microbiome all interesting avenues for further studies.

Summary of results

The **key findings** from this chapter are:

1. Early immune responses are dichotomous between mRNA and viral vector SARS-CoV-2 vaccines, with post-prime and post-boost dominant responses after homologous ChAdOx1-nCoV-19 and BNT162b2 vaccination respectively.
2. IFN-γ is the dominant cytokine induced by both vaccines and is derived from activated innate-like lymphocytes through different mechanisms.
3. Early IFN-γ after homologous ChAdOx1-S prime is derived from cytokine-mediated innate-like lymphocyte activation, and reduced at boost due to reduced early innate activation.
4. Enhanced IFN-γ after homologous BNT162b2 boost is associated with adaptive immune measures at the time of boost, and therefore diminished with extended dosing intervals.
5. Activation of innate-like lymphocytes follows spike-specific adaptive immune responses, with amplification of IFN-γ through an IFN-γR1 dependent mechanism.

Figure 4.34 Summary of potential causes and consequences of BNT162b2 induced IFN-γ.

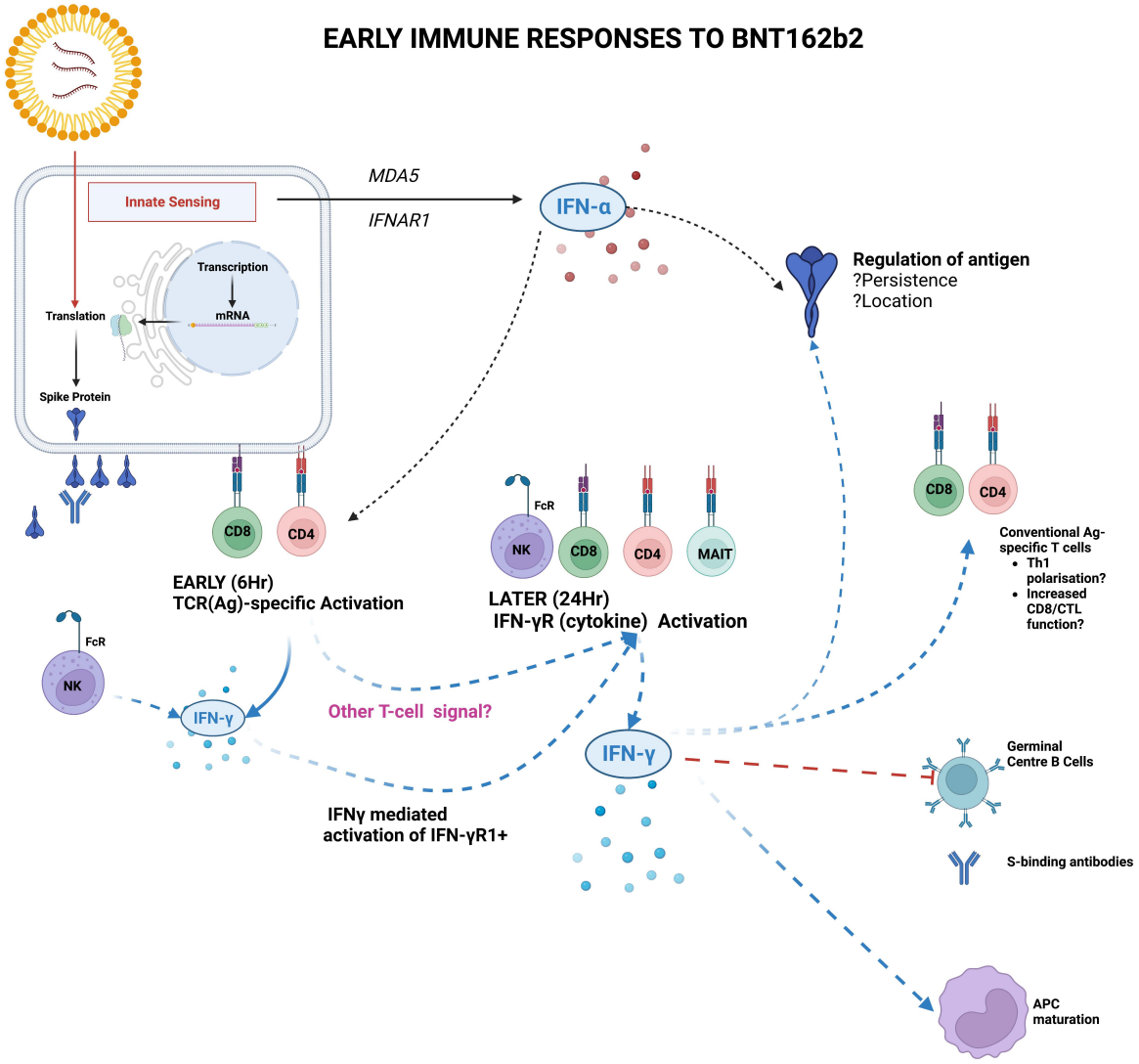

5 Anti-TNF and human early immune responses to ChAdOx1-S

5.1 Introduction

In the previous two Chapters, I have shown novel mechanisms by which early antiviral immune responses can be induced in healthy individuals, with an important role for MAIT cells and other innate-like lymphocytes. Early MAIT cell activation and IFN-γ production are driven by cytokines, including type I IFN and TNF, and correlate with antigen-specific T cell responses after ChAdOx1-prime. Furthermore, *Mr1*$^{-/-}$ mice which lack MAIT cells have reduced antigen-specific CD8+ T cell responses to ChAdOx1 vaccination, suggesting that MAIT cell activation is functionally relevant[334].

However, all human data so far has only included healthy individuals. We now have a mass of data to show reduced SARS-CoV-2 vaccine-induced immune responses in immunocompromised patients [457,458], as well as those with autoimmune disease on immunotherapy, in particular biologic immuno-modulatory therapy. The latter are relevant as biologics often target cytokines vital for innate-like lymphocyte activation. For example, inhibitors of interferon signalling, such as the JAK-inhibitor tofacitinib, reduce pneumococcal but not influenza-specific vaccine responses[459].

Of relevance to mechanisms described in Chapter3, patients receiving inhibitors of TNF signalling have altered vaccine-induced immunity. Inflammatory Bowel Disease (IBD) patients with moderate or severe disease are often treated with monoclonal antibodies targeting either integrin α4β7 (Vedolizumab, humanized monoclonal) and TNF (Infliximab, Adalimumab), or small molecule inhibitors of the JAK-STAT pathway (e.g., Tofacitinib). Infliximab has been associated with reduced vaccine immunogenicity to pneumococcal [460],

influenza [461,462], hepatitis A[463], and hepatitis B vaccination[464]. Vedolizumab is more gut-selective and does not impact hepatitis B vaccine immunogenicity[465].

Since the pandemic, it has become clear that patients receiving therapies targeting TNF and IFN signalling in particular have reduced SARS-CoV-2 vaccine induced immune responses. The CLARITY-IBD study was the first to show that SARS-CoV-2 specific antibody responses after a single dose of BNT162b2 or ChAdOx1-S were reduced in patients on anti-TNF (Infliximab, Adalimumab, or Etanercept) and Tofacitinib therapy compared to those on Vedolizumab or Ustekinumab[466–472]. Importantly a more rapid decay in SARS-CoV-2 spike binding antibodies correlates with increased PCR-confirmed breakthrough infections in those receiving Infliximab rather than Vedolizumab[472], speculatively implicating TNF signalling directly for durable protective vaccine responses.

We have just shown that early IFN and TNF regulate bridging innate-like populations upstream of adaptive immune responses[334]. Intriguingly, biologic therapy has been identified as a negative correlate of early reactogenicity after vaccination in multi-variable analyses [473], in particular TNF inhibitors.[474]. As innate-like lymphocytes are activated early after SARS-CoV-2 vaccination and are TNF-responsive, their response to vaccination could underpin some of these clinical observations.

Characteristics of innate-like lymphocytes - including their frequency, activation and cytokine production could all be relevant to early vaccine responses. A reduced peripheral blood MAIT cell frequency has been shown for both Crohn's disease (CD) and Ulcerative Colitis (UC) compared to healthy controls, in conjunction with accumulation in inflamed tissues [475,476]. The frequency of Vδ2+ γδ T cells normally co-correlates with that of MAIT cells [249,477], but in Crohn's disease increased frequencies of γδ T cells have been described[478], which correlate with disease activity[479]. This may be due to differences in therapy, as initiation of Infliximab therapy induces clonal expansion of Vδ2+ γδ T cells in

Crohn's disease in vivo, particularly in young males[480], with both Infliximab and Adalimumab capable of inducing γδ T cell proliferation in vitro. A similar increase in Vδ2+ γδ T cells has been observed in Infliximab treated patients with Ankylosing Spondylitis[481], suggesting a disease-independent effect. It is unclear if anti-TNF has any impact on MAIT cell frequency in vivo. Therefore, although MAIT cells and Vδ2+ γδ T are the major T cell sources of IFN-γ in response to ChAdOx1-S in particular, the relative contribution may be altered by anti-TNF therapy.

The propensity for activation of innate-like lymphocytes may also vary depending on diseases and therapies. Peripheral MAIT cells are more activated in IBD, with increased expression of CD69, which correlates with disease activity and serum IL-18 concentrations[475]. An increased type I IFN signature is also observed in IBD[482,483], which could contribute to increased MAIT cell CD69 expression. However functional responses of peripheral MAIT cells do not necessarily correlate with the degree of activation: MAIT cells in UC have increased propensity for IL-17 production [475], whereas IFN-γ production is reduced in CD[476]. The impact of TNF is unknown, as are the effect disease and cytokine modulation can have on anti-viral and vaccine induced early immune responses.

HYPOTHESIS

Based on our findings in the previous Chapters, in particular the importance of type I IFN and TNF to innate-like lymphocyte IFN-γ in response to ChAdOx1, we hypothesised that IBD patients receiving anti-TNF therapy would exhibit reduced early innate-like lymphocyte activation and IFN-γ after ChAdOx1-S immunisation which may underpin dysregulated adaptive immune responses to vaccination.

5.2 Aims

The overarching aim of this chapter was to therefore describe in detail the longitudinal early immune response to ChAdOx1-S in patients receiving anti-TNF, focusing on the post-prime response. To do this the work was performed in close collaboration with members of Oxford trial team for OCTAVE (Observational patient Cohort study of T-cells Antibodies and Vaccine efficacy in SARS-Cov-2), a prospective observational trial of patients with gastro-intestinal disease - in particular IBD - which were treated with both Vedolizumab and anti-TNF therapy prior to ChAdOx1 prime.

KEY QUESTIONS:

1. Do IBD patients on anti-TNF have altered baseline innate and innate-like lymphocyte phenotypes which could impact on early responses generated?
2. What are the early (day one) immune responses of innate-like lymphocytes in particular after ChAdOx1-S prime in IBD patients on anti-TNF?

Although additional questions include the relevance to adaptive immunity, I am only focussing data for early responses which were generated and analysed by me.

The **primary aims** of this chapter were therefore to:

1. Characterise baseline innate and innate-like cell populations in IBD patients receiving TNF and non-TNF targeting therapies, using other patients with gastrointestinal disease and healthy HCW as controls.
2. Characterise the early immune response to ChAdOx1-S prime in IBD patients receiving anti-TNF, focusing on innate-like lymphocyte activation and cytokines which can induce IFN-γ.
3. Expand on the mechanisms for any observations above *in vitro*.

5.3 Chapter specific materials and methods

The methods described in this Chapter have been described elsewhere, in particular Flow Cytometry and Legendplex quantification of cytokines in plasma and cell culture supernantants. Specific changes are outlined below. Although I also contributed to RNA extraction for bulk RNA sequencing, this data has not been analysed thus not included in this Chapter.

5.3.1 OCTAVE Trial - design, and sample collection

The OCTAVE Trial was a multi-centre prospective cohort trial designed to assess immune responses to SARS-CoV-2 vaccination (ISRCTN 12821688). The key aims of the trial were to determine differences in the immune response generated in patients with a multitude of diseases, in addition to the impact of the unique immunomodulatory therapies used. Although a collaboration with numerous sites, the data described in this thesis is from a sub-group recruited at Oxford University Hospitals NHS Foundation Trust receiving ChAdOx1-S alone and undergoing deep immune phenotyping at baseline.

Eligibility criteria included: adults aged over 18 years with a diagnosis of gastrointestinal disease, including predominantly those with IBD (Ulcerative colitis, Crohn's) or liver disease (cirrhosis, transplant recipients, autoimmune liver disease) on immunosuppression (**Table 5.1, Table 5.2**). IBD patients were stratified based on those treated with anti-TNF (Infliximab, Adalimumab) or non-TNF based IBD therapies, including immunomodulators such as Vedolizumab, Ustekinumab, and Tocilizumab. Recruitment into the trial was performed by the Oxford OCTAVE Team (led by Professor Ellie Barnes). All participants signed an informed consent form prior to enrolment and sampling. Healthy control samples were all from the sub-study described in Chapter4, part of UK PITCH (Protective Immunity from T cells in Healthcare workers).

Table 5.1 | OCTAVE study – baseline phenotype cohort characteristics.

	Overall, N= 103[1]	HCW, N= 20[1]	CD, N= 36[1]	UC, N= 40[1]	Liver, N = 7[1]	p-value
Prior Infection *(detectable baseline anti-spike antibodies)*	8 (7.8%)	4 (20%)	0 (0%)	4 (10%)	0 (0%)	0.040[2]
Age, *years*	36 (26- 47)	28 (22- 46)	34 (24- 42)	38 (31- 48)	54 (42- 58)	0.008[3]
Sex, *female*	42 (41%)	15 (75%)	11 (31%)	14 (35%)	2 (29%)	0.007[2]
Biologic	44 (43%)	0 (0%)	27 (75%)	17 (42%)	0 (0%)	<0.001[2]
Anti-TNF	44 (43%)	0 (0%)	27 (75%)	17 (42%)	0 (0%)	<0.001[2]
Adalimumab (TNF)	15 (15%)	0 (0%)	11 (31%)	4 (10%)	0 (0%)	0.007[2]
Infliximab (TNF)	29 (28%)	0 (0%)	16 (44%)	13 (32%)	0 (0%)	<0.001[2]
Vedolizumab (ITG)	28 (27%)	0 (0%)	7 (19%)	21 (52%)	0 (0%)	<0.001[2]
Tofacitinib (JAK-STAT)	1 (1.0%)	0 (0%)	0 (0%)	1 (2.5%)	0 (0%)	>0.99[2]
Prednisolone	2 (1.9%)	0 (0%)	0 (0%)	0 (0%)	2 (29%)	0.004[2]
Anti-metabolite	13 (13%)	0 (0%)	7 (19%)	5 (12%)	1 (14%)	0.17[2]
Azathioprine	6 (5.8%)	0 (0%)	4 (11%)	1 (2.5%)	1 (14%)	0.18[2]
Methotrexate	4 (3.9%)	0 (0%)	2 (5.6%)	2 (5.0%)	0 (0%)	0.76[2]
6-Mercaptopurine	3 (2.9%)	0 (0%)	1 (2.8%)	2 (5.0%)	0 (0%)	0.84[2]

1, n (%), Median (25%- 75%); 2, Fisher's exact test; 3, Kruskal-Wallis rank

Table 5.2 | OCTAVE study - baseline phenotype of IBD cohort.

Characteristic	**Overall, N = 76[1]**	**CD, N = 36[1]**	**UC, N = 40[1]**	**p-**value
Prior Infection *(detectable baseline anti-spike antibodies)*	4 (5.3%)	0 (0%)	4 (10%)	0.12[2]
Age*, years*	36 (26- 44)	34 (24- 42)	38 (31- 48)	0.076[3]
Sex*, Female*	25 (33%)	11 (31%)	14 (35%)	0.68[4]
Biologic				
Anti-TNF (TNF)	44 (58%)	27 (75%)	17 (42%)	0.007[2]
Adalimumab (TNF)	15 (20%)	11 (31%)	4 (10%)	0.025[4]
Infliximab (TNF)	29 (38%)	16 (44%)	13 (32%)	0.28[4]
Vedolizumab (ITG)	28 (37%)	7 (19%)	21 (52%)	0.003[4]
Tofacitinib	1 (1.3%)	0 (0%)	1 (2.5%)	>0.99[2]
Antimetabolite	12 (16%)	7 (19%)	5 (12%)	0.41[4]
Azathioprine	5 (6.6%)	4 (11%)	1 (2.5%)	0.18[2]
Methotrexate	4 (5.3%)	2 (5.6%)	2 (5.0%)	>0.99[2]
6-Mercaptopurine	3 (3.9%)	1 (2.8%)	2 (5.0%)	>0.99[2]

Samples were collected prior to prime (V1), and boost (V2), with further sampling one day after prime (V1+1) in a subset (**Table 5.3**). All samples pre-prime and pre-boost were collected immediately prior to immunisation. Additional samples for measurement of SARS-CoV-2-specific adaptive responses were 4 weeks post-boost (V2+28).

Table 5.3 | OCTAVE study – day one cohort characteristics.

	Overall, N = 30[1]	CD, N = 12[1]	UC, N = 18[1]	p-value
Prior Infection *(detectable baseline anti-spike antibodies)*	4 (13%)	0 (0%)	4 (22%)	0.13[2]
Age*, years*	40 (31- 47)	34 (25- 43)	41 (37- 49)	0.086[3]
Sex*, Female*	9 (30%)	1 (8.3%)	8 (44%)	0.049[2]
Biologics				
Anti-TNF	18 (60%)	11 (92%)	7 (39%)	0.007[2]
Adalimumab	5 (17%)	5 (42%)	0 (0%)	0.006[2]
Infliximab	13 (43%)	6 (50%)	7 (39%)	0.55[4]
Vedolizumab	10 (33%)	1 (8.3%)	9 (50%)	0.024[2]
Tofacitinib	1 (3.3%)	0 (0%)	1 (5.6%)	>0.99[2]
Anti-metabolites	5 (17%)	3 (25%)	2 (11%)	0.36[2]
Azathioprine	3 (10%)	3 (25%)	0 (0%)	0.054[2]
Methotrexate	1 (3.3%)	0 (0%)	1 (5.6%)	>0.99[2]
6-Mercaptopurine	1 (3.3%)	0 (0%)	1 (5.6%)	>0.99[2]

1, n (%), Median (IQR 25%- 75%); 2,Fisher's exact test; 3, Wilcoxon rank sum test; 4,Pearson's Chi-squared test

All participants received homologous ChAdOx1-S prime-boost, with prime dates all in March 2021. A subset returned for repeat sampling one day after prime. Clinical information regarding vaccination dates, age (at the time of first vaccination), sex and ethnicity were documented. Prior SARS-CoV-2 history was also recorded, including PCR positivity, symptoms, and previous serology to detect SARS-CoV-2 nucleocapsid or spike proteins. IBD subtypes, disease activity and specific therapies were recorded for all patients.

Phlebotomy samples included: EDTA blood, for PBMC and plasma isolation within 4h; serum in serum-separating tubes (SST, Becton Dickinson); and whole blood in Tempus tubes (Life Technologies), which were promptly frozen at -20˚C for subsequent RNA extraction.

5.3.2 Isolation of PBMCs, plasma and serum

PBMC were isolated as previously described in Chapter 2 for vaccination samples, with no dilution of blood prior to layering to allow plasma collection.

Sample isolation was all carried out by me, together with Nicholas Provine, Sophie Irwin, and Georgina Meacham.

I subsequently stained an aliquot of fresh cells for immune phenotyping panels, with the remainder aliquoted at 10^6 PBMC per vial in freezing media (90% FCS, 10% DMSO), frozen in “Mr Frosties” to -80C, prior to transfer for long term storage in liquid nitrogen (-180˚C). Thawing of vials was again as described for vaccine samples, with the addition of 2µl Benzonase (≥ 25 U/µl; Sigma-Aldrich).

Data described in this thesis is restricted only to flow cytometry and plasma cytokine data collected at baseline and one day after prime, all generated and analysed by me.

5.4 Results

5.4.1 Characteristics of OCTAVE study cohort

To study the impact of TNF on early immune responses to ChAdOx1-S, a sub-study was created as part of the National OCTAVE Clinical Trial (**Fig5.1**). Patients were recruited immediately prior to their primary ChAdOx1-S immunisation schedule over four weeks in March 2021. Given our previous findings, our primary aim was to compare the baseline and early (day one) immune responses in patients on anti-TNF (Adalimumab, Infliximab) with those receiving anti-integrin therapy (Vedolizumab), matching where possible for disease severity with patients (all either mild or moderate disease). Healthy controls were used from Chapter4 to discern treatment and disease specific differences.

The characteristics of the cohorts are summarised (**Table 5.1, Table 5.2, Table 5.3**).

Baseline phenotyping cohort: a total of 103 patients and controls were recruited, including 77 with IBD and 7 with Liver disease for which baseline immune subsets analysed, including innate like lymphocyte activation (**Table 5.1**). Patients had subsequent homologous boosting, with samples banked prior to boost and four weeks after boost (**Fig5.1**). The boosting interval was between 8 and 10 weeks.

The majority of IBD participants were SARS-CoV-2 naïve at baseline with undetectable anti-spike IgG binding antibodies. All participants with confirmed infection (SARS-CoV-2 PCR positive) also had detectable anti-spike binding Ab pre-vaccination. The sex distribution was unequal when comparing healthy controls and the IBD cohorts, with more women in the heathy control cohort (HCW, 75%; CD, 31%; UC, 35%). The median age was similar for CD and UC cohorts, but older for the liver cohort (HCW, 28; CD, 34; UC, 38; Liver, 54 median years).

Figure 5.1 | Schematic of OCTAVE study.

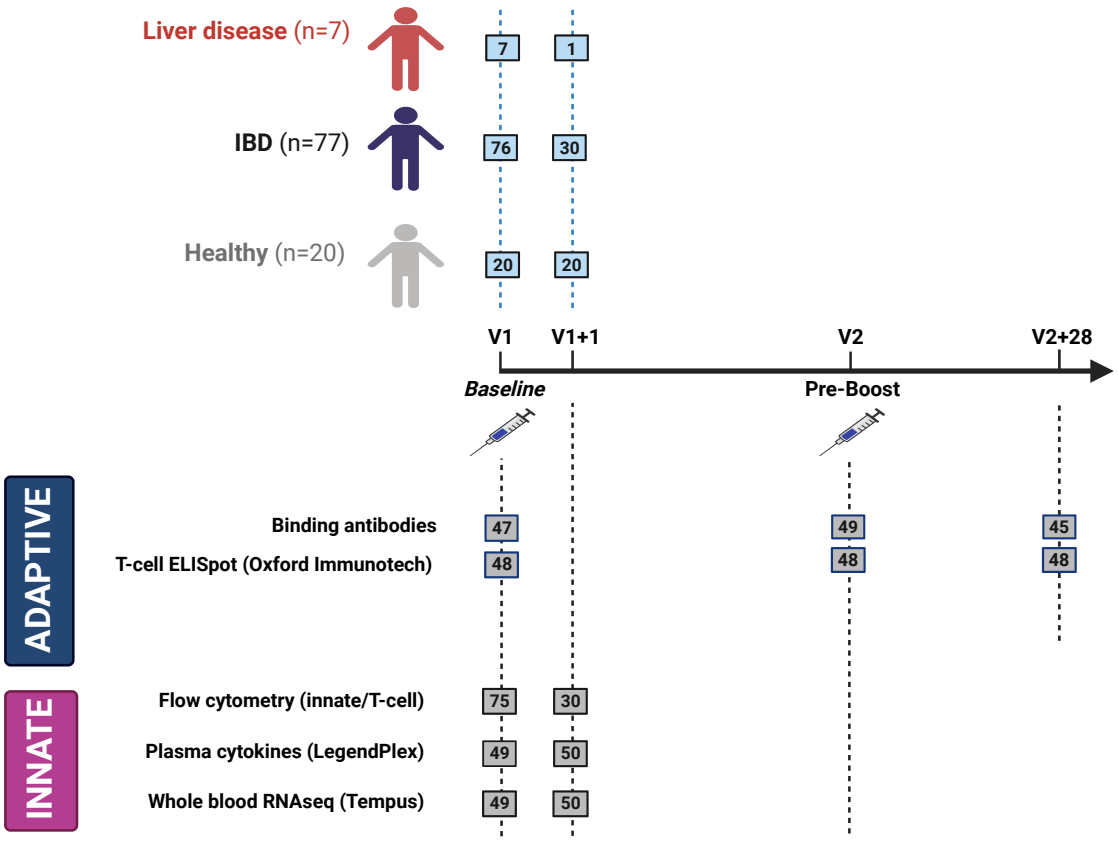

Fig5.1 | Schematic of OCTAVE study.
Summary of longitudinal samples collection from healthcare workers vaccinated with ChAdOx1-S (n=20), or patients with IBD (n=76), or Liver disease (n=7), with timepoints and the relevant innate and adaptive immune assays highlighted.

Pre-vaccine timepoints were preprime (V1), and pre boost (V2). Post-vaccine timepoint was day 1 post-prime (V1+1).

Early immune profiling was performed with: flow cytometry (innate cell, conventional and unconventional T-cells), plasma multiplex cytokines, whole blood RNA sequencing.

SARS-CoV-2 adaptive immune profiling performed included: S-binding antibodies, live-virus neutralisation titres and T-cell IFNγ ELISpots.

Day one cohort: our aim was to profile early immune responses at high resolution in those with anti-TNF. We therefore focused on a sub-cohort of 30 IBD patients at baseline and one day post-prime, together with conventional adaptive time points (**Table 5.3**). Samples included whole blood in EDTA, Tempus RNA, and serum SST tubes. EDTA blood was processed to collect plasma and PBMC. Serum was frozen for subsequent quantification of binding and neutralising antibodies. Aliquots of fresh PBMCs were used to phenotype innate and T cell activation (10^6 cells per panel). Freeze-thawed cells were used for assays of spike-specific T cell responses.

The IBD cohort at day one had a sex bias (44% female UC, $p < 0.049$). Although of similar age, more UC patients were on Vedolizumab compared to CD (50% UC, 8.3% CD). Conversely only CD patients received Adalimumab.

5.4.2 Baseline immune profile of patients with IBD on immunomodulatory therapy

Given the importance of innate-like lymphocytes in the early response to ChAdOx1, we focussed on the unconventional T-cell response to ChAdOx1-S in patients with and without anti-TNF therapy. Patients were matched as closely as possible for disease severity and age, with cirrhosis patients included as a comparator disease.

As has been previously demonstrated, MAIT cell frequency in blood is reduced in patients with IBD and Cirrhosis compared to healthy controls (**Fig5.2 A**). Although the reduction as a fraction of all live cells was only significant in Crohn's disease (**Fig5.2 B**), the total frequency of MAIT cells as a fraction of T cells was reduced for both UC and Crohn's (**Fig5.2 F**); MAIT cells comprised median 2.4% of T cells in healthy controls, compared to 1.2% and 0.65% in UC and Crohn's disease patients respectively. The frequency of iNKT cells was reduced in liver disease but not IBD compared to healthy controls (**Fig5.2 C, G**).

Figure 5.2 | IBD patients have reduced frequencies of MAIT cells compared to healthy controls pre-vaccination.

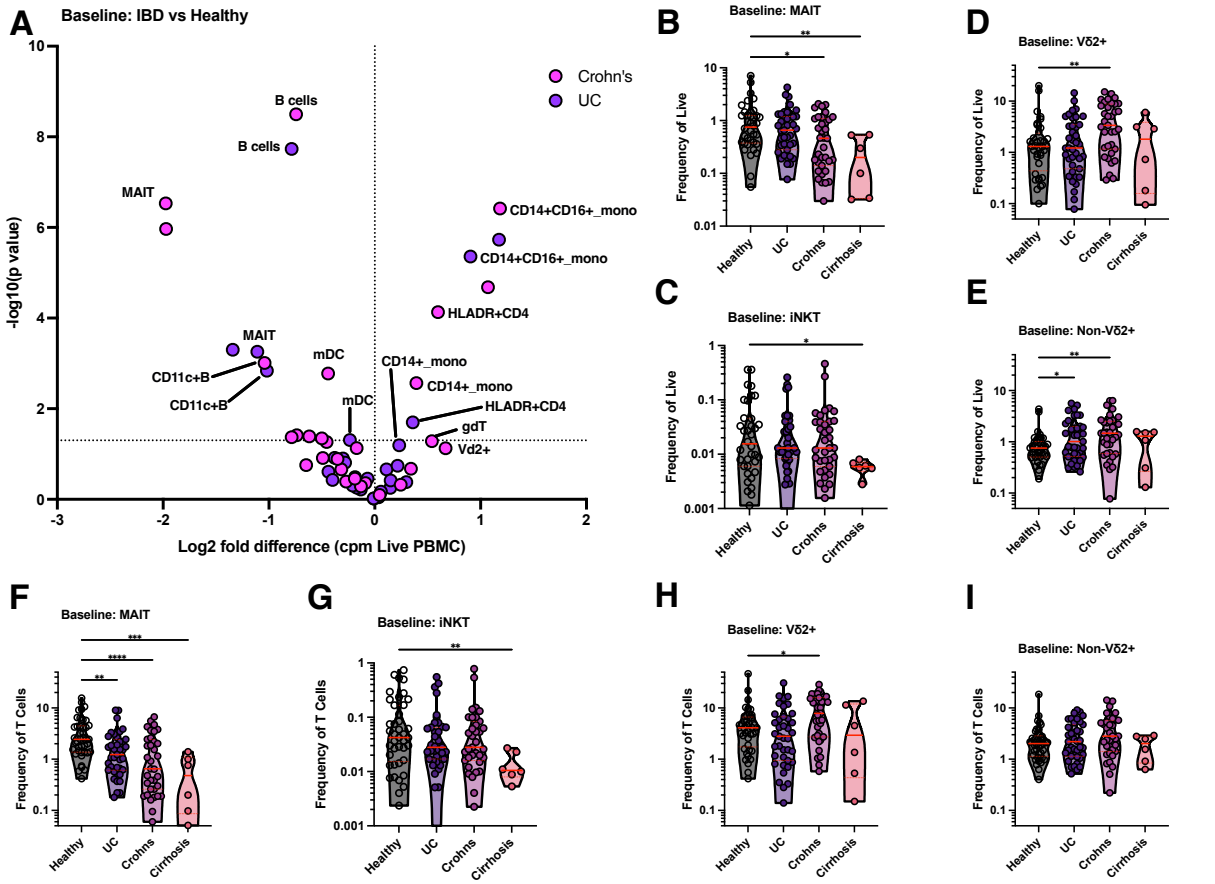

Fig5.2 | IBD patients have reduced frequencies of MAIT cells compared to healthy controls pre-vaccination.
(A) Volcano plots of log2 fold difference in live PBMC for patients with Ulcerative colitis (purple), or Crohns disease (pink), compared to healthy controls.
(B-D) Frequency of MAIT cells (B), iNK T cells (C), Vδ2+ γδT(D), and Non-Vδ2+ γδT cells (E) as a fraction of live PBMC.
(F-I) Frequency of MAIT cells (G), iNK T cells (G), Vδ2+ γδT(H), and Non-Vδ2+ γδT cells (I) as a fraction of live T-cells.
Symbols indicate individual donors.
$p < 0.05$; $^{**}p < 0.01$; $^{***}p < 0.001$; $^{****}p < 0.0001$; ns, not significant.
Statistical significance was determined using multiple paired t-tests of log2 transformed values, with Benjamini, Krieger, & Yekutieli correction for multiple comparisons (A); and unpaired non-parametric Kruskal-Wallis test (B-I).

As has previously been reported[480], Crohn's disease patients had a higher frequency of Vδ2+ γδ T cells compared to healthy controls (**Fig5.2 D, H)**, both as a fraction of total live cells and total T cells; Vδ2+ T cells comprised median 4.1% of T cells in healthy controls but 7.8% of T cells in Crohn's disease patients. Specifically comparing the frequency of cell types in PBMC in patients receiving anti-TNF or Vedolizumab, Vδ2+ cells were increased in IBD patients receiving anti-TNF irrespective of disease (**Fig5.3 A**). For both UC and CD, patients on anti-TNF therapy had increased Vδ2+ but not non-Vδ2+ γδ T cells as a fraction of all T cells (**Fig5.3 B, E**). MAIT cell and iNKT cell frequencies were not altered at baseline in patients receiving anti-TNF (**Fig5.3 C, D, F, G**). Therefore, the baseline innate-like lymphocyte compartment was altered by both disease and therapy, potentially with implications for early responses generated.

Figure 5.3 | IBD patients on anti-TNF have increased frequencies of Vδ2+ γδ T cells pre-vaccination.

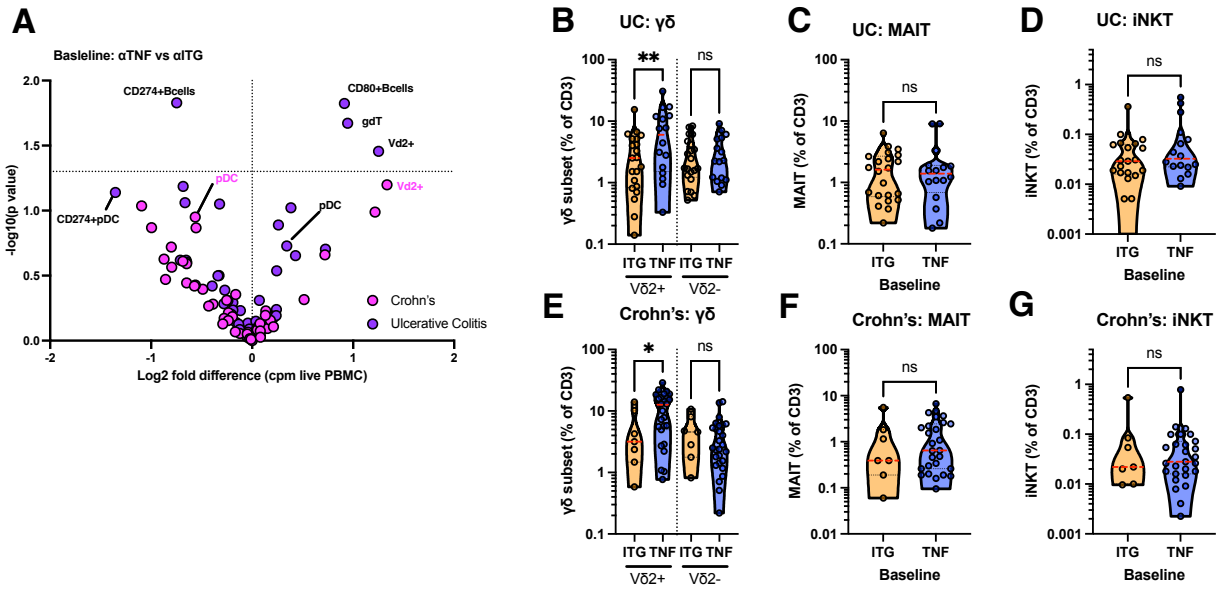

Fig5.3 | IBD patients on anti-TNF have increased frequencies of Vδ2+ γδ T cells pre-vaccination.
(A) Volcano plots of baseline frequency of cells amongst PBMC comparing patients on anti-TNF (Adalimumab, Infliximab) with those on anti-integrin (Vedolizumab) therapy. Ulcerative colitis (purple), or Crohns disease (pink), comparing those **(B-D)** Baseline frequency of γδ T cells (B), MAIT cells (C), or iNKT cells (D) as a fraction of T cells in patients with UC. **(E-G)** Baseline frequency of γδ T cells (E), MAIT cells (F), or iNKT cells (G) as a fraction of T cells in patients with UC. Symbols indicate individual donors.
$p < 0.05$; $^{**}p < 0.01$; $^{***}p < 0.001$; $^{****}p < 0.0001$; ns, not significant.
Statistical significance was determined using multiple paired t-tests of log2 transformed counts per million cells (A); ordinary one-way ANOVA with Šídák's multiple comparisons test (B, E), and unpaired Mann-Whitney non-parametric test (C,D; F, G).

5.4.3 Early immune responses in IBD patients on immunomodulatory therapy

We next asked whether the early activation of innate-like lymphocyte after ChAdOx1-S prime was reduced by anti-TNF. CD69 was upregulated in IBD patients in a similar manner to healthy controls one day after ChAdOx1-S prime (**Fig5.4 A**).MAIT cells, iNKT and Vδ2+ cells all expressed higher CD69 24h after vaccination (**Fig5.4 B**). Although the degree of activation (change in fraction expressing CD69) was reduced in IBD patients compared to HCW (**Fig5.4 B**), there was no difference between UC and Crohn's disease patients (**Fig5.4 C**), or in IBD patients stratified on therapy (**Fig5.4 D**). This would suggest that although IBD patients more generally have a reduced MAIT cell CD69 compared to healthy controls, there is no difference in those receiving inhibitors of TNF compared to integrins. Of note, Crohn's Disease patients in particular had higher baseline MAIT cell CD69 expression (**Fig5.4 E**), which correlated with their age (**Fig5.4 F**), therefore interpretation of changes in MAIT activation become difficult.

As the impact of anti-TNF in vitro was predominantly in the reduction of innate-like lymphocyte IFN-γ, we next measured plasma concentrations of cytokines pre and post ChAdOx1-S in patients to assess whether early anti-viral cytokines are altered by disease or therapies (**Fig5.5**). Similar cytokines were induced in IBD patients irrespective of inhibitors compared to HCW one day after ChAdOx1-S prime (**Fig5.5 A**), with IFN-γ (**Fig5.5 A, B**), IL-6 (**Fig5.5 A, D**), and IFN-α (**Fig5.5 A, F**) induced in all. Early after ChAdOx1-S, IBD patients on anti-TNF had a lower induction of IFN-γ (**Fig5.5 C**) and IL-6 (**Fig5.5 E**), but not IFN-α (**Fig5.5 G**). These data would suggest that anti-TNF has a differential impact on specific cytokines induced in response to ChAdOx1-S prime

Figure 5.4 | Innate-like lymphocytes are activated after ChAdOx1-S in IBD patients.

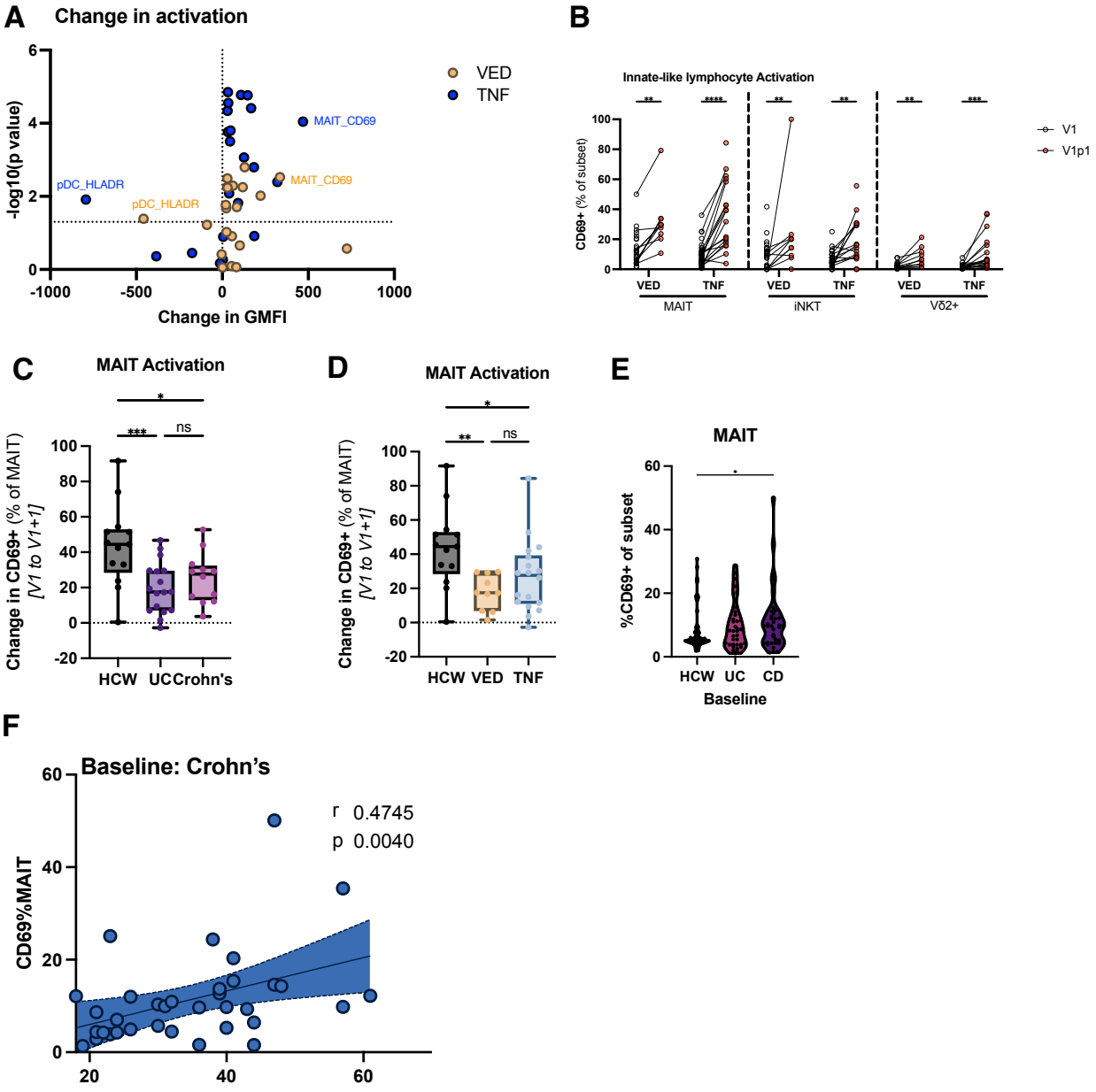

Fig5.4 | Innate-like lymphocytes are activated after ChAdOx1-S in IBD patients.
(A) Volcano plots of change in expression of markers in PBMC pre-and post-prime with ChAdOx1-S for IBD patients receiving Vedolizumab (VED, orange) or anti-TNF (TNF, Adalimumab, Infliximab; blue). MAIT cell CD69 and plasmacytoid DC HLA-DR expression are highlighted.
(B) Frequency of innate-like lymphocytes expressing CD69 pre- (V1) and post- (V1p1) ChAdOx1-S vaccination in patients receiving Vedolizumab or anti-TNF.
(**C**) Change in CD69 expression amongst MAIT cells one day after vaccination in healthy healthcare workers (HCW), or patients with Ulcerative colitis (UC) or Crohn's disease.
(**D**) Change in CD69 expression amongst MAIT cells one day after vaccination in healthy healthcare workers (HCW), or IBD patients receiving Vedolizumab or anti-TNF.
(E) Baseline CD69 expression among HCW, CD, and UC patients.
(F) Spearman's correlation of age and baseline CD69% of MAIT cells in patients with Crohn's Disease.

Symbols indicate individual donors.
$p < 0.05$; $^{**}p < 0.01$; $^{***}p < 0.001$; $^{****}p < 0.0001$; ns, not significant.
Statistical significance was determined using multiple paired t-tests (A, B) or one-way ANOVA (C, D, E).

Figure 5.5 | IBD patients on anti-TNF have reduced induction of IFN-γ and IL-6 one day after ChAdOx1-S prime.

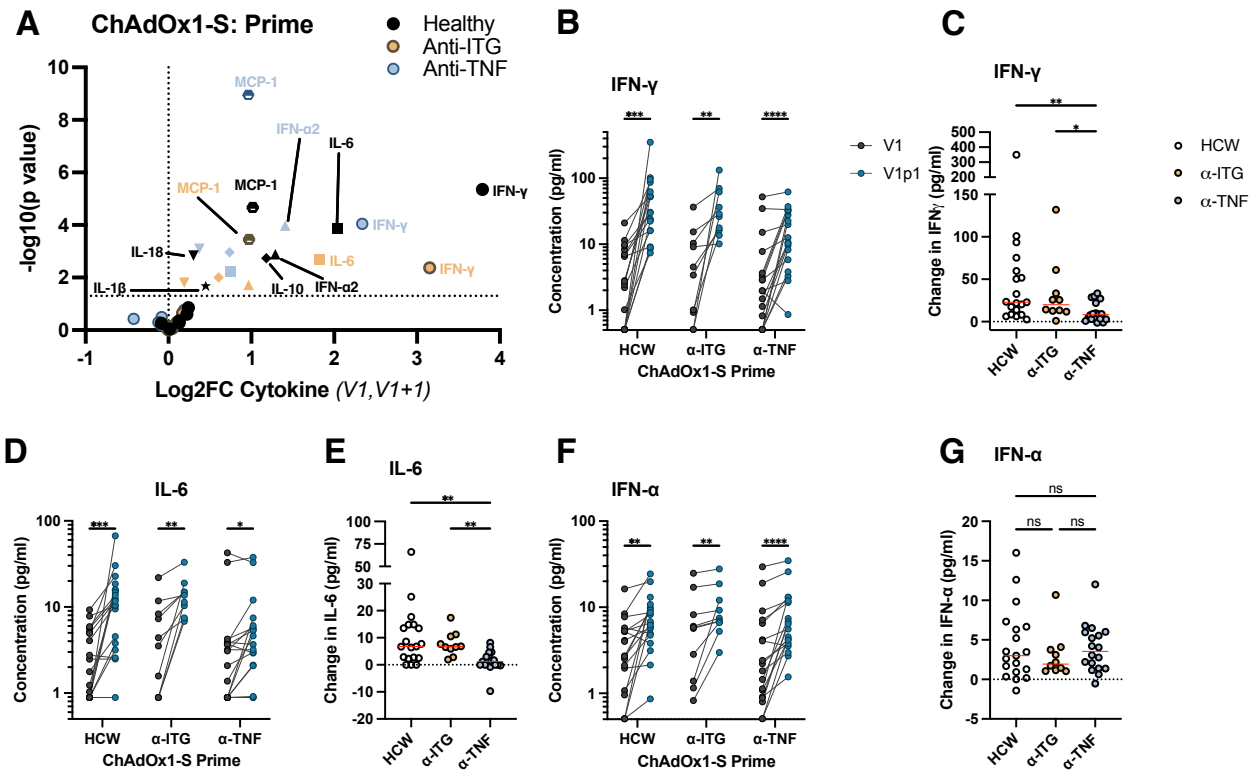

Fig5.5 | IBD patients on anti-TNF have reduced induction of IFN-γ and IL-6 one day after ChAdOx1-S prime.
(A) Volcano plot of log2 fold change in plasma cytokine concentration pre- and post (24h) ChAdOx1-S prime in healthy healthcare workers (HCW), IBD patients on anti-integrin therapy (α-ITG, Vedolizumab), or IBD patients on anti-TNF therapy (Adalimumab, Infliximab).
(B-C) Plasma IFN-γ concentration (B) and change in concentration (C) between baseline (V1) and day 1 post-prime (V1+1).
(D-E) Plasma IL-6 concentration (D) and change in concentration (E) between baseline (V1) and day 1 post-prime (V1+1).
(F-G) Plasma IFN-α concentration (F) and change in concentration (G) between baseline (V1) and day 1 post-prime (V1+1).
Symbols indicate individual donors.
$p < 0.05$; $^{**}p < 0.01$; $^{***}p < 0.001$; $^{****}p < 0.0001$; ns, not significant.
Statistical significance was determined using multiple paired t-tests of log2 transformed counts per million cells (A); multiple non-parametric Wilcoxon tests (B, D, F), and non-parametric Kruskal Wallis test (C, E, G).

5.4.4 Anti-TNF increases pDC-derived type I IFN, but reduces monocyte-derived inflammasome-dependent cytokines in vitro

We have previously shown that TNF is crucial for total IFN-γ in response to ChAdOx1 in vitro, partly through direct effects on innate-like lymphocytes. To determine whether TNF-dependent cytokines could indirectly regulate innate-like lymphocyte IFN-γ through alteration of other cytokines, we measured a range of cytokines 24h after stimulation of PBMC with ChAdOx1-GFP with or without inhibitors of TNF (Adalimumab, 10μg/ml; Certolizumab, 10μg/ml).

Both Adalimumab and Certolizumab reduced TNF as expected in response to ChAdOx1-GFP (**Fig5.6 A**), in addition to IFN-γ and most other inflammatory cytokines. Compared to Vedolizumab control, Adalimumab appreciably reduced MCP-1 (mean log2FC 3.3), IL-6 (mean log2FC 3.0) and IL-12p70 (mean log2FC 3.0). ChAdOx1-induced inflammasome-derived cytokines were also all reduced by TNF blockade: IL-1β (mean log2FC 5.5), IL-18 (mean log2FC 1.9), and IL-33 (**Fig5.6 B-D**). Intriguingly, IFN-α was not significantly reduced in the presence of TNF inhibitors (**Fig5.6 E**), in agreement with in vivo data. As both IL-12p70 and IL-18 are necessary for type I IFN dependent IFN-γ production in response to ChAdOx1, these data suggest that inhibition of TNF signalling may also indirectly inhibit innate-like lymphocyte activation in PBMC by reducing the cytokines required for activation.

Figure 5.6 | Anti-TNF reduces ChAdOx1-GFP induced inflammasome-derived cytokines but not IFN-α.

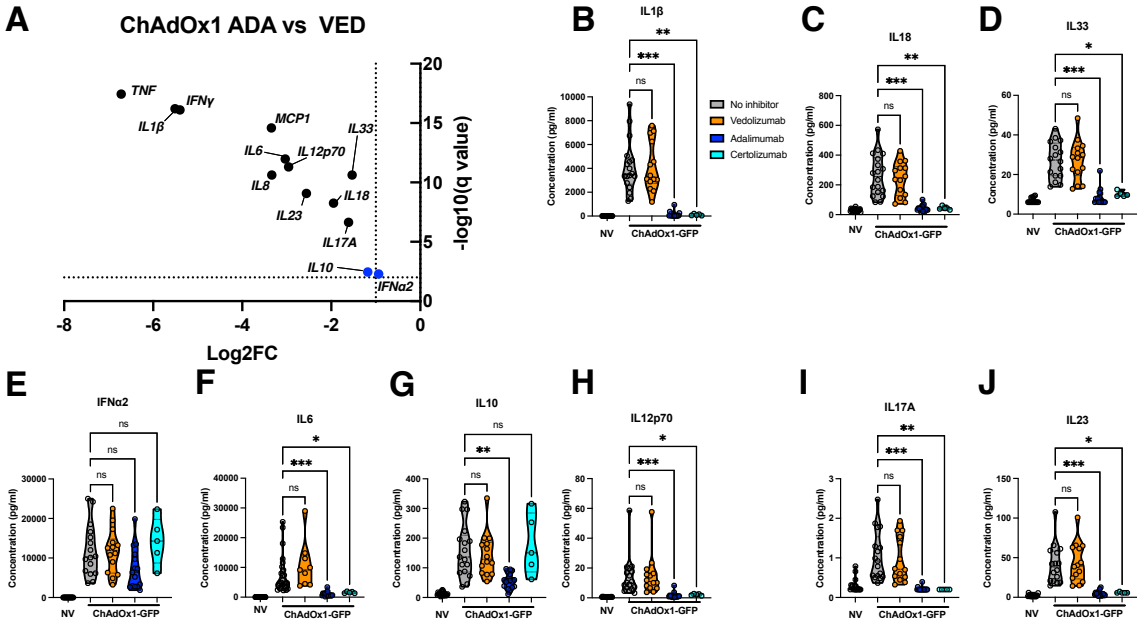

Fig5.6 | Anti-TNF reduces ChAdOx1-GFP induced inflammasome-derived cytokines but not IFN-α.
Fresh PBMCs were stimulated with ChAdOx1-GFP (MOI 10^3 vp) in the presence of Vedolizumab (VED, 10μg/ml), Adalimumab (ADA, 10μg/ml), or Certolizumab (CERT, 10μg/ml), and cell culture supernatants were assayed for inflammatory cytokines at 24h.
(A) Volcano plots of log2FC in cytokines induced by ChAdOx1-GFP in the presence of ADA compared to VED.
(B-D) Total concentration of inflammasome-derived cytokines IL1β (B), IL-18 (C), and IL-33 (D) in supernatants 24h after ChAdOx1-GFP in the presence of ADA or CERT. (samples pooled from across 3 experiments).
(E-J) Total concentration of cytokines IFN-α (E), IL-6 (F), IL-10 (G), IL-12p70 (H), IL-17A (I), and IL-23 (J) in supernatants 24h after ChAdOx1-GFP in the presence of ADA or CERT.
Symbols indicate individual donors. $p < 0.05$; $^{**}p < 0.01$; $^{***}p < 0.001$; $^{****}p < 0.0001$; ns, not significant. Statistical significance was determined using multiple paired t-tests of log2 transformed values, with Benjamini, Krieger, & Yekutieli correction for multiple comparisons (A); and unpaired non-parametric Kruskal-Wallis test (B-J).

TNF accelerates pDC maturation, from predominant type I IFN producers to increase antigen-presenting functionality [484]. One might hypothesise that anti-TNF would delay or prevent pDC maturation, thereby sustaining ChAdOx1-induced IFN-α production. As expected, we found that Adalimumab pre-treatment increased pDC IFN-α (**Fig5.7 B),** and TNF (**Fig5.7 C**) expression 24h after ChAdOx1-GFP stimulation. Potentially as a consequence of increased type I IFN, pDC GFP expression was reduced (**Fig5.7 D**), with most live IFN-α+pDC GFP-negative in the absence of TNF signalling (**Fig5.7 E**). Consistent with delayed maturation, ChAdOx1-GFP induced pDC HLA-DR expression was also reduced with TNF blockade (**Fig5.7 G**).

Taken together, these data suggested that anti-TNF augmented ChAdOx1-induced type I IFN production, with functional consequences including reduced AdV transduction and HLA-DR expression. Furthermore, as innate-like lymphocyte CD69 expression is directly induced by type I IFN alone in the absence of other signals, this could explain why ChAdOx1 -S induced CD69 expression in IBD patients was not impacted by anti-TNF.

Figure 5.7 | Anti-TNF increases pDC IFN-α and TNF production but reduces GFP transduction and activation in response to ChAdOx1-GFP in vitro.

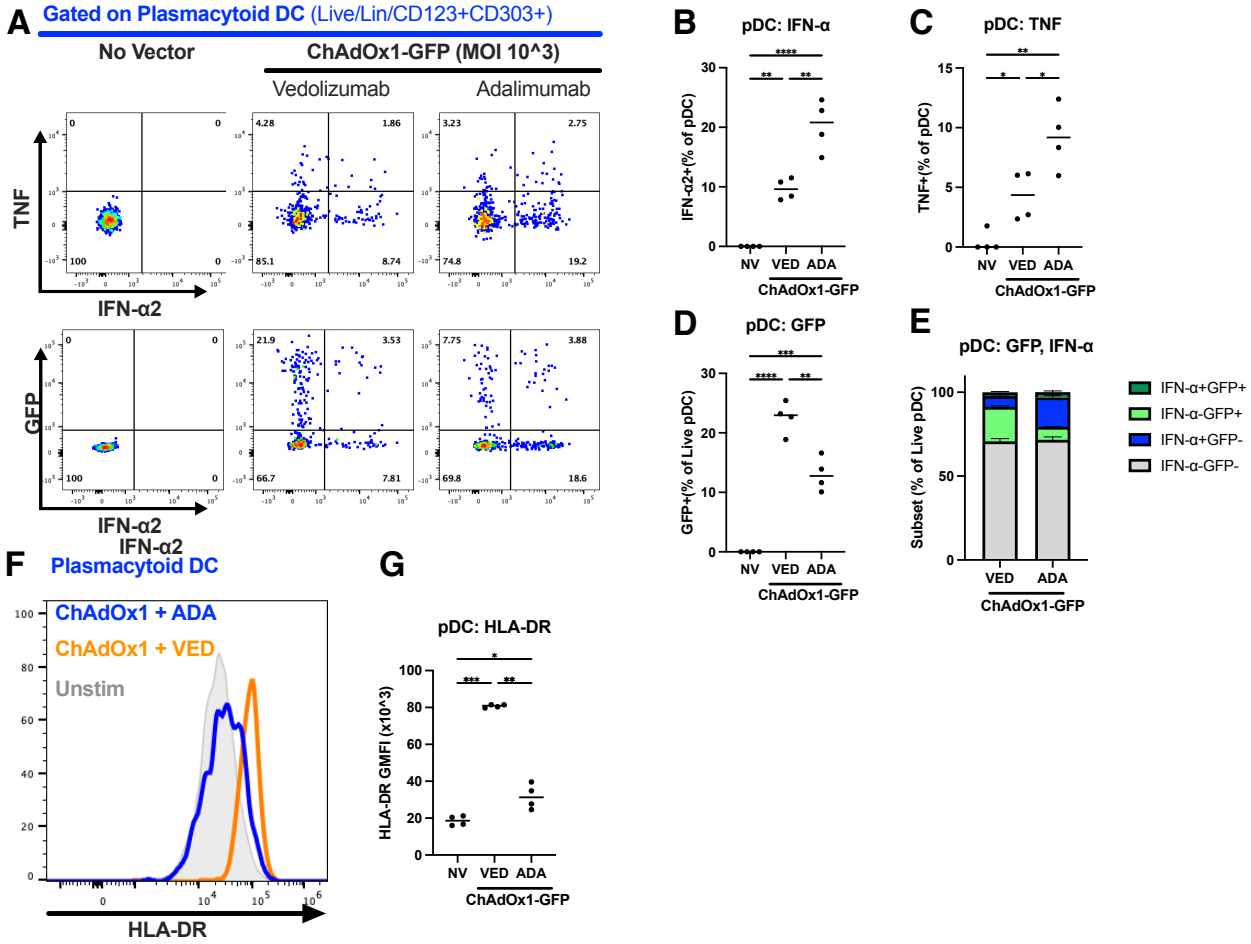

Fig5.7 | Anti-TNF increases pDC IFN-α and TNF production but reduces GFP transduction and activation in response to ChAdOx1-GFP in vitro.
Fresh PBMCs were stimulated with ChAdOx1-GFP (MOI 10^3 vp) in the presence of Vedolizumab (VED, 10μg/ml), Adalimumab (ADA, 10μg/ml), or unstimulated (no vector, NV). Activation and cytokine production was measured in plasmacytoid dendritic cells after 24h.
(A) Representative plots of pDC IFN-α, TNF and GFP expression.
(B-D) Summary expression of IFN-α (B), TNF (C), GFP (D) on live plasmacytoid dendritic cells.
(E) Fraction of live pDC which express IFN-α and GFP after ChAdOx1-GFP stimulation with VED or ADA.
(F) Representative histogram of pDC HLA-DR expression 24h after ChAdOx1-GFP stimulation in the presence of VED (orange) or ADA (blue).
(G) Summary of pDC HLA-DR expression.
Symbols indicate individual donors. $p < 0.05$; **$p < 0.01$; ***$p < 0.001$; ****$p < 0.0001$; ns, not significant.
Statistical significance was determined using repeated measures one-way ANOVA with Tukey's multiple comparison's test.

We have previously shown that in vitro ChAdOx1-GFP induced monocyte death, caspase activation (data not shown), together with IL-18 and IL-1β production implicating inflammasome activation. TNF is required to prime the inflammasome, and concordantly we found ADA pre-treatment reduced inflammasome-derived IL-18 (**Fig5.8 A**) and IL-1β (**Fig5.8 B**), reduced caspase activation (data not shown), and increased monocyte survival 24h after ChAdOx1-GFP stimulation (**Fig5.8 D**). The total frequency of live GFP+ cells was however decreased (**Fig5.8 E**), perhaps implicating TNF in the preferential cell-death of transduced cells.

We have previously shown that anti-TNF reduces ChAdOx1-GFP induced IFN-γ through direct inhibition of innate-like lymphocyte activation (Chapter3). This data suggests indirect inhibition of innate-like lymphocyte responses could also occur through reduced inflammasome activation. This was supported by the observation that supplemental IL-18 was sufficient to overcome anti-TNF mediated inhibition of MAIT cell IFN-γ production in response to ChAdOx1-GFP (**Fig5.8 G**).

Figure 5.8 | Anti-TNF reduces inflammasome-derived cytokines and monocyte cell death in response to ChAdOx1-GFP.

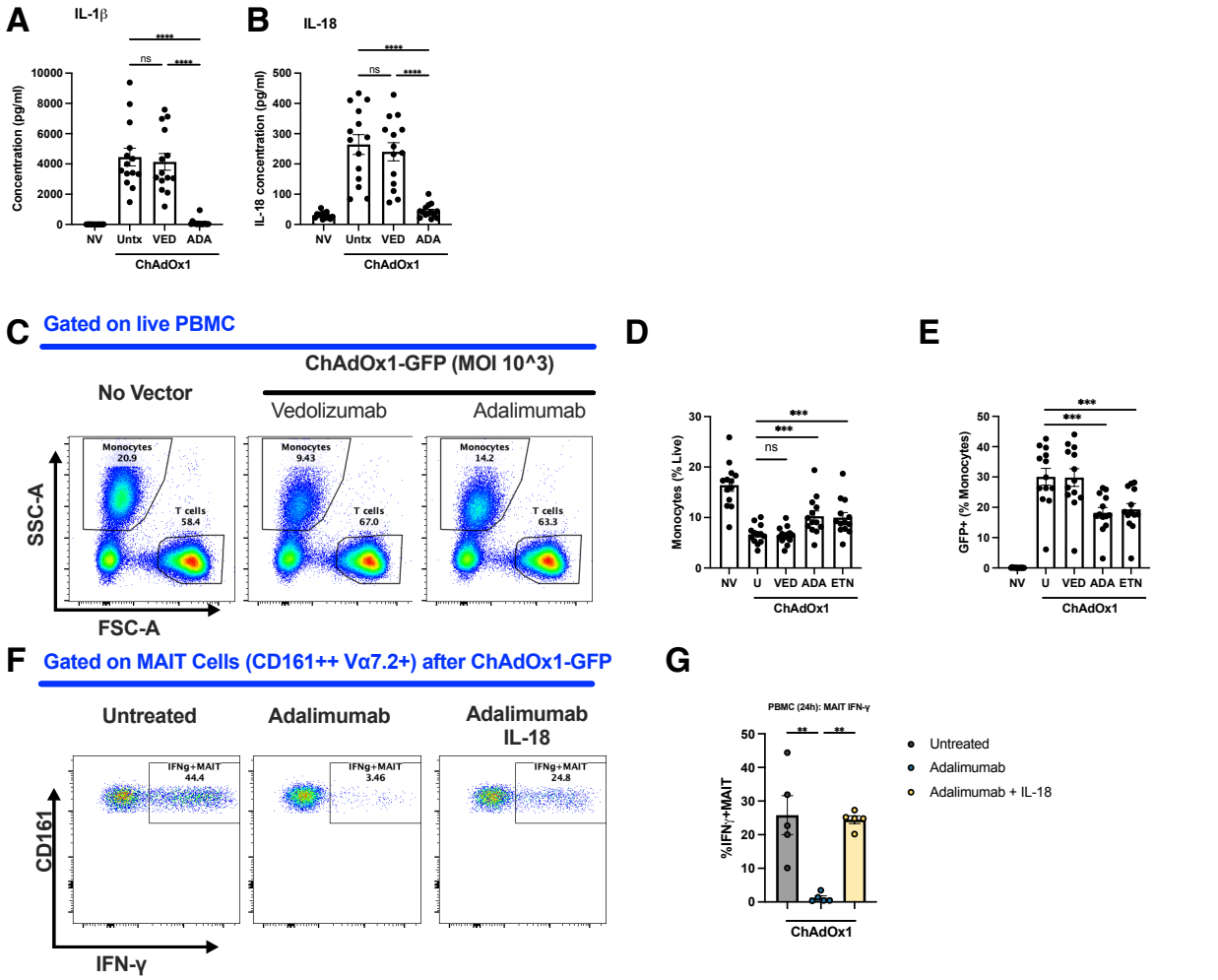

Fig5.8 | Anti-TNF reduces inflammasome-derived cytokines and monocyte cell death in response to ChAdOx1-GFP.

Fresh PBMCs were stimulated with ChAdOx1-GFP (MOI 10^3 vp) in the presence of Vedolizumab (VED, 10µg/ml), Adalimumab (ADA, 10µg/ml), Etanercept (ETN, 10µg/ml), or unstimulated (no vector, NV). GFP expression was measured in live monocytes (SSChi).

(A,B) Concentration of IL1β (D) and IL-18 (E) after ChAdOx1-GFP stimulation in vitro.

(C) Representative plots of live cells after PBMC stimulation with ChAdOx1-GFP in the presence of inhibitors.

(D, E) Frequency of live monocytes (D), and monocyte GFP expression (E).

(**F, G)** Representative plots (F) and summary MAIT cell IFN-γ expression (G) 24h after PBMC stimulation with ChAdOx1-GFP in the presence of ADA with and without additional IL-18 (50ng/ml).

Symbols indicate individual donors. $p < 0.05$; $^{**}p < 0.01$; $^{***}p < 0.001$; $^{****}p < 0.0001$; ns, not significant.

Statistical significance was determined using repeated measures one-way ANOVA with Tukey's multiple comparison's test.

5.5 Discussion

The work in this chapter demonstrates that innate-like lymphocyte frequencies are altered in IBD, with reduced MAIT cells but increased Vδ2+ γδ T cells in those on anti-TNF therapy. All innate-like lymphocytes are activated to express CD69 after ChAdOx1-S in both healthy controls and IBD patients irrespective of immuno-modulatory therapy. The magnitude of vaccine-induced plasma IFN-γ after 24h was lower in patients receiving anti-TNF therapy, concordant with prior in vitro data, with no difference in type I IFN induction or change in CD69 expression. In vitro, anti-TNF increased the frequency of IFN-α producing pDC in response to ChAdOx1-S at 24h which would therefore sustain CD69 expression. In contrast, inflammasome-derived cytokines are reduced by anti-TNF, with increased numbers of live monocytes surviving after ChAdOx1-GFP in vitro. These data would suggest that the TNF differentially regulates innate-like lymphocyte functions in response to ChAdOx1.

The impact of TNF on innate-like lymphocyte responses to AdV merits further exploration, including the relevance to vaccine induced adaptive immunity. Maintained type I IFN and CD69 expression could suggest that these cells are still able to migrate to tissues. Indirect TNF-dependent cell-death and IL-18 production may further reduce IFN-γ production. The range and spectrum of innate-like lymphocyte functions altered is an interesting area for further work. Furthermore, the impact of TNF on mRNA vaccines induced innate-like lymphocyte responses would need to be explored given the scale of use.

5.5.1 Anti-TNF and baseline innate-like lymphocyte frequency

Reassuringly we find a reduced frequency of peripheral blood MAIT cells in IBD patients, similar to previous studies, and shared with other inflammatory diseases[183,475,476]. We were additionally able to compare the baseline frequency in patients with and without anti-TNF therapy, with no difference in MAIT cells but a robust increase in frequency of Vδ2+ γδ T cells in both UC and CD patients on anti-TNF. This extends previous published data in CD[480], Ankylosing Spondylitis [481], and Psoriasis[485], and suggests that therapies can alter the composition of the innate-like lymphocyte compartment.

The mechanisms for increased Vδ2+ γδ T cell frequency are unclear. One study found that anti-TNF agents (Infliximab, Etanercept or Adalimumab) promoted proliferation of IL-2 supplemented human γδ T cells after 5 days in vitro[480]. Conversely another study found that TNFR2 antagonism in particular reduces IPP/IL-2 induced Vδ2+ γδ T cell proliferation in PBMCs after 10 days [486]. Given the shared cytokine responsiveness of MAIT cells, Vδ2+ and iNKT cells - including expression of TNFR - TCR signals likely drive the specificity of differences observed in vivo. Without assessing the impact of anti-TNF on healthy controls in vivo it is difficult to discern whether TCR-signals from Vδ2+ T cell ligands are only restricted to patients with disease, or if anti-TNF therapy drives increased production of such ligands. For example, infections including tuberculous and non-tuberculous mycobacteria can produce phosphoantigens and are more common in anti-TNF treated patients.

Although numbers were too small to assess - in previous studies anti-TNF induced Vδ2+ γδ T cell expansion has been most prominent in young men, who are also at increased risk of hepatosplenic lymphoma in response to anti-TNF therapy. One might therefore imagine that understanding the mechanisms of expansion could help understand these rare complications of therapy.

5.5.2 Anti-TNF reduces early ChAdOx1-S induced IFN-γ but not IFN-α

Comparing early immune responses to ChAdOx1-S prime in IBD patients on anti-TNF compared to those on Vedolizumab we observe reduced plasma IFN-γ, as predicted from in vitro models (Chapter3). Although innate-like lymphocytes are activated in all patients, thus potentially a source of early IFN-γ, we didn't see a reduction in innate-like lymphocyte activation in patients on anti-TNF, so could not conclude a direct link between innate-like lymphocyte TNFR expression and early IFN-γ. This may be as activation was measured by CD69, a marker most sensitive to type I IFN. Given that ChAdOx1-S induced type I IFN induction was preserved irrespective of anti-TNF therapy in vivo, future studies would need to phenotype innate-like lymphocytes using surface markers more reflective of IFN-γ production in humans, or assess the impact of TNF blockade in mouse models of vaccination.

Anti-TNF did not reduce PBMC ChAdOx1-GFP induced IFN-α in vitro - with increased pDC IFN-α observed at 24h. This is compatible with other data from TLR-stimulated pDC in which TNF is required to promote pDC maturation into enhanced antigen presenting cells capable of T cell activation; this function comes at the expense of IFN-α production, as TNF downregulates IRF7 pathway expression[484], while facilitating upregulation of antigen processing and presentation pathways. Reassuringly we also observed a reduction in pDC HLA-DR expression in Adalimumab pre-treated PBMC after ChAdOx1 stimulation. Other markers were tested, including CD80 and CD86 (data not shown), with similar trends in vitro.

The cross-regulation of TNF and type I IFN has clear relevance to innate-like lymphocyte functions during antiviral responses. Although TNF-treated pDC down-regulate many ISGs (SOCS, IRF7, IFITM3, OAS1), others are upregulated, including BST2 and IRF3. A divergent effect is also seen on receptors for IFN: IFNAR1 and IFNAR2 expression are

reduced, whereas IFNGR1 and IFNGR2 expression are increased, suggesting that TNF may change the balance of type I and type II effector functions in pDC [484]. One clear relevance may be in rare anti-TNF associated adverse events associated with an IFN-signature in blood, such as lupus-like reactions[487] and paradoxical psoriasis, which is associated with reduced pDC maturation and prolonged IFN-α production[488].

Prolonged IFN-α production would have profound effects on innate-like lymphocytes and may alter their homeostatic functions. In addition to maintaining CD69 expression, TNF promotes monocyte cell-death and inflammasome-derived cytokine IL-18 production, potentially as a result of reduced pyrin expression and caspase-1 activation[489], which would represent an indirect mechanism through which anti-TNF blocks cytokine-mediated innate-like lymphocyte activation. One might ask whether other cell-death modulators could play similar roles in ChAdOx1-induced early innate-like lymphocyte activation and immunogenicity? Both type I IFN and IFN-γ can promote different inflammatory forms of cell death, particularly in combination with TNF [490], adding yet another layer of complexity in the regulation of responses.

5.5.3 Relevance of findings to vaccinology and immunology

These data could provide a greater understanding for immunological determinants of optimal adaptive immunity more broadly. Baseline human immune determinants predict vaccine immunogenicity to Yellow-Fever. The innate-like lymphocyte compartment is highly variable among healthy humans, and this also applies in disease. As baseline enrichment of innate-like lymphocyte genes has been shown to correlate with reactogenicity, it would be important to assess if these are changed in patients on anti-TNF which clearly changes the composition of various innate-like lymphocytes and their responsiveness. For example, NK-associated genes correlate with moderately severe fatigue after mRNA vaccination -

and one might expect this to be reduced in patients on anti-TNF if driven by IFN-γ related cytokine circuits.

The reduction in early IFN-γ after SARS-CoV-2 prime in patients on anti-TNF may be relevant to differences in adaptive immunity. Multiple studies have shown that irrespective of vaccine modality, patients with IBD on anti-TNF have lower SARS-CoV-2 specific antibodies. The CLARITY study found that after both BNT162b2 and ChAdOx1-S vaccination, mean anti-spike IgG levels are significantly lower in Infliximab treated patients compared to those receiving Vedolizumab (6 U/ml vs 29 U/ml), which on multivariate analysis was further reduced by age and smoking status[467]. Conversely an increase in spike-specific T cell responses has been observed in response to mRNA vaccination in patients with IBD on anti-TNF [491]. These effects could be through direct effects of TNF on adaptive immune cells - potentially regulating B cell maturation[492], T cell expansion [493], or T-cell help[494]. We are currently analysing longitudinal cellular and transcriptional data at baseline and early timepoints, with the aim of correlating with subsequent adaptive parameters to understand the predominant cell types impacted by anti-TNF.

Our data also provides a mechanistic framework for understanding adverse effects of anti-TNF therapy. Anti-TNF induced expansion of Vδ2+ γδ T cells may have implications for anti-TNF induced hepatosplenic T cell lymphoma (HSTCL), a γδ T cell origin tumour[495,496]. Anti-TNF also augments pDC type I IFN production, which we can further characterise at greater resolution using transcriptional data pre- and post- vaccination in whole blood. These and other studies should ideally also be powered to explore the role of sex in adverse events. Future studies should explore mechanisms for γδ T cell expansion, including confirming any sex bias, to expand our knowledge of potentially harmful consequences of anti-TNF therapy.

5.5.4 Limitations

Our study on humans is significantly limited by the small sample sizes of volunteers returning for day one sampling, which makes it difficult to perform multivariable analysis considering various factors such as disease, treatments, age, and sex that shape early immune responses. Additionally, peripheral blood sampling and in vitro studies of PBMC may not accurately reflect the local early immune response to vaccination. Future studies should incorporate models that assess responses in lymphoid organs and mucosal tissues, especially in the case of novel vaccination routes.

Furthermore, our data is limited to intensive sampling around the first dose, and we need to explore other mechanisms by which TNF may regulate early responses, particularly after boost. Our previous findings have shown long-terms changes in the myeloid compartment after ChAdOx1-S prime, resulting in reduced early cytokine induction after homologous boost. It is important to assess whether TNF plays a role in mRNA vaccine-induced responses, potentially comparing it to inhibitors of IFN-pathways that reduce IFN-γ induced innate-like lymphocyte activation.

Finally, we are in the process of compiling relevant data, so cannot comment on any associations of early immune responses with the development of SARS-CoV-2-specific adaptive immunity. These studies may lead to more mechanistic investigations on innate-like lymphocytes and their contribution to vaccine-induced antiviral responses.

5.6 Conclusions and summary

In conclusion, differences in the early immune response in patients on anti-TNF may be important determinants of distinct immunogenicity to ChAdOx1-S. Innate-like lymphocytes are sensitive to direct and indirect cytokine mediated modulation in the absence of TNF in vivo and in vitro, and understanding these could provide important insights into vaccine-induced reactogenicity and immunogenicity.

Key findings

The **key findings** from this chapter are:

1. Baseline immune profiles in IBD patients are distinct in those receiving anti-TNF therapy, with higher frequencies of Vδ2+ γδ T cells in particular compared to healthy controls and IBD patients on Vedolizumab therapy.
2. Early IFN-γ after ChAdOx1-S prime is lower in IBD patients on anti-TNF therapy compared to healthy controls and IBD patients on Vedolizumab therapy.
3. Type I IFN production and innate-like lymphocyte CD69 expression are not reduced in patients receiving anti-TNF therapy compared to those on Vedolizumab therapy.
4. TNF also indirectly modulates ChAdOx1 induced innate-like lymphocyte activation by differentially regulating IFN-α and IL-18 important for triggering. Anti-TNF reduces pDC maturation and monocyte inflammasome activation, concordantly promoting pDC-derived IFN-and reducing monocyte-derived IL-18 and cell-death.

6 Work during COVID-19 pandemic

6.1 List of work published as part of a COVID-19 response team

During the COVID-19 pandemic, I was seconded back to the NHS working in Infectious Diseases, contributing to Oxford University Hospitals Staff Testing Group – then after returning helped process patient samples as part of the Oxford Immunology Network Covid-19 Response T Cell Consortium, and PITCH Consortium.

Oxford University Hospitals Staff Testing Group

- Lumley SF, O'Donnell D, Stoesser NE, et al. Antibody Status and Incidence of SARS-CoV-2 Infection in Health Care Workers. N Engl J Med. 2021;384(6):533-540.

Oxford Immunology Network Covid-19 Response T Cell Consortium

- Peng Y, Mentzer AJ, Liu G, et al. Broad and strong memory CD4+ and CD8+ T cells induced by SARS-CoV-2 in UK convalescent individuals following COVID-19. Nat Immunol. 2020;21(11):1336-1345.
- Ogbe A, Kronsteiner B, Skelly DT, et al. T cell assays differentiate clinical and subclinical SARS-CoV-2 infections from cross-reactive antiviral responses. Nat Commun. 2021;12(1):2055.

PITCH Consortium

- Angyal A, Longet S, Moore SC, et al. T-cell and antibody responses to first BNT162b2 vaccine dose in previously infected and SARS-CoV-2-naive UK health-care workers: a multicentre prospective cohort study. Lancet Microbe. 2022;3(1):e21-e31.

6.2 List of papers published

Eyre DW, Lumley SF, O'Donnell D, Campbell M, Sims E, Lawson E, Warren F, James T, Cox S, Howarth A, Doherty G, Hatch SB, Kavanagh J, Chau KK, Fowler PW, Swann J, Volk D, Yang-Turner F, Stoesser N, Matthews PC, Dudareva M, Davies T, Shaw RH, Peto L, Downs LO, Vogt A, **Amini A**, Young BC, Drennan PG, Mentzer AJ, Skelly DT, Karpe F, Neville MJ, Andersson M, Brent AJ, Jones N, Martins Ferreira L, Christott T, Marsden BD, Hoosdally S, Cornall R, Crook DW, Stuart DI, Screaton G; Oxford University Hospitals Staff Testing Group, Peto TE, Holthof B, O'Donnell AM, Ebner D, Conlon CP, Jeffery K, Walker TM. Differential occupational risks to healthcare workers from SARS-CoV-2 observed during a prospective observational study. Elife. 2020 Aug 21;9:e60675.

- Youngs J*, Provine NM*, Lim N*, Sharpe HR+, **Amini A+,** Chen YL+, Luo J, Edmans MD, Zacharopoulou P, Chen W, Sampson O, Paton R, Hurt WJ, Duncan DA, McNaughton AL, Miao VN, Leaver S, Wyncoll DLA, Ball J, Hopkins P, Skelly DT, Barnes E, Dunachie S, Ogg G, Lambe T, Pavord I, Shalek AK, Thompson CP, Xue L, Macallan DC, Goulder P, Klenerman P, Bicanic T. Identification of immune correlates of fatal outcomes in critically ill COVID-19 patients. PLoS Pathog. 2021 Sep 16;17(9):e1009804. (co-second author)

7 Conclusions

In this thesis I have shown how early human immune responses to nucleic acid vaccines are generated, and shown that MAIT cells together with other CD161+innate-like lymphocytes can sense cytokine cues from both AdV and mRNA vaccines to generate amplified IFN-γ responses. I have also proposed means through which non-heritable factors could regulate these early responses, namely (adaptive) immune memory, diseases and their therapies, and tissue environmental factors.

7.1 MAIT cells and interferons

CD161+ innate-like lymphocytes as exquisite type I interferon sensors

One of my key findings has been to show that innate-like lymphocytes, and in particular MAIT cell CD69 expression, are sensitive early markers of vaccine-mediated interferon responses, expanding on similar observations in virus infection more broadly[306]. In other work not included in the thesis we showed that MAIT cell CD69 expression is also a very sensitive marker of severe disease in SARS-CoV-2[342], where a similar pattern emerges in terms of reduced circulating MAIT cell frequency as seen after vaccination. A picture therefore emerges where MAIT cells and functionally similar CD161+ cell innate-like lymphocytes are tuned to type I IFN, with the full consequences of such activation still to be explored.

In the case of MAIT cells, baseline CD69 expression negatively correlates with BNT162b2 induced spike-specific antibody and AIM+ CD4+ T cells [451]. I also found that in the case of IBD, MAIT cell CD69 expression was elevated in patients with IBD and increased with age, therefore a potential marker of immune dysregulation. As CD69 acts downstream of type I IFN signalling[54], MAIT cell CD69 expression could act as very sensitive marker of the variability in basal IFN in humans[574].

Functionally, a ‘tonic IFN signature’ is thought to derive from the microbiome and induces a poised basal state in APCs[345]; MAIT cell sensitivity may therefore derive from their fundamental (direct and indirect) responsiveness to a dysregulated microbiome[575], which is thought to underlie some of the differences in vaccine-responsiveness across human cohorts[576].

Acutely after ChAdOx1 vaccination, type I IFN dependent MAIT cell activation was a key determinant of their effector functions, in particular IFN-γ, both in vitro and in vivo in healthy HCW and IBD patients. The data I present, as well as other data we have published[334], show early MAIT cell activation and IFN-γ to correlate with subsequent ChAdOx1 vaccine-induced antigen specific T-cell responses. Therefore, MAIT cell IFN-responsiveness is not only a marker of immune homeostasis in health, but may have functional consequences.

Innate-like lymphocyte IFN-γ: adjuvants or culprits?

In addition to universal type I IFN sensitivity, I show that innate-like lymphocyte IFN-γ production is a universal early response to nucleic acid vaccines in vivo and vitro. Type I IFN and IFN-γ dependent IFN-γ production are behind the early IFN-γ induced in response to DNA (AdV) and mRNA vaccines respectively, with contrasting regulation in the presence of prior immunisation. Prior immunisation promoted augmented RNA vaccine innate-like lymphocyte IFN-γ, whereas prior AdV immunisation inhibited early responses at boost. Mechanistically this was likely due to transgene-specific (BNT162b2) or vector-specific (ChAdOx1-S) adaptive immunity, and may underpin some of the differences in the immune response to various vaccine regimens [363].

Early innate-like lymphocyte IFN-γ could cultivate a prompt host response by promoting APC and maturation and antigen presentation to adaptive immune cells[258,577]. A number of studies have now shown that characteristics of the innate-like lymphocyte compartment

correlate with subsequent adaptive immune measures, which may align with their role as vaccine adjuvants[451,578].

The pattern of innate-like lymphocyte activation mirrored the pattern of vaccine-induced inflammatory cytokines, including IFN-γ, and reactogenicity after prime and boost for both vaccines (**Fig8.1**). It is unclear to what extent innate-like lymphocyte activation and reactogenicity are causally linked – but potentially harmful downstream effects of dysregulated innate-like lymphocyte IFN-γ:IFN-γ R1 mediated feed-forward loops are possible. By analogy, lethal cytokine release syndromes (CRS) accompany infusion of antibody or cellular therapies, including CAR-T cell therapy, and are associated with rapid increases in plasma IFN-γ in animals, which correlate with disease severity. Clinically IFN-γ inhibition with Emapalumab was found to be even more effective than a range of other more conventional targets for refractory CAR-T cell mediated CRS, switching off aberrant macrophage activation without compromising conventional CAR-T efficacy[579]. If innate-like cells are key intermediates, one might expect that that IFN-γR1 may be more effective than IFN-γ blockade in reducing adverse effects of innate-like lymphocyte IFN-γ. Aberrant tissue IFN-γ[580], including MAIT cell activation[581], has also been reported after checkpoint inhibitor therapy – implying that the pathogenic potential of innate-like lymphocyte IFN-γ and IFN-γ dependent activation may be a critical determinant of the adverse responses more broadly.

7.2 TNF regulates innate-like lymphocytes

Another key component of the thesis has been the concept that TNF is an important regulator of innate-like lymphocytes – both directly and indirectly. I show Vδ2+ γδ T cells are uniquely expanded in homeostasis in IBD patients receiving anti-TNF, altering the innate-like lymphocyte compartment composition. Both in vitro and in vivo, TNF was critical for ChAdOx1-induced IFN-γ. In vitro, MAIT cells and other innate-like lymphocyte were

poised for TNF responsiveness by type I IFN, with both cytokines crucial for their capacity to produce IFN-γ.

In vitro, TNF and type I IFN formed a regulatory circuit through multiple accessory cells. Type I IFN was crucial for monocyte TNF production, and innate-like lymphocyte TNF responsiveness. TNF however promoted pDC maturation –therefore reducing type I IFN production – which would provide feedback inhibition guarding against excessive inflammation. An intriguing question remains as to the relevance of T-cell compared to APC derived TNF in these feedback circuits? Early (1.5hr) LPS-induced TNF is 10-fold lower in Jα18−/− mice (which lack iNKT), compared to wild-type mice, despite similar total concentrations of IL-12 and IL-18, potentially suggesting that innate-like lymphocyte could also contribute to TNF-IFN feedback circuits.

7.3 Redundant and unique features of innate-like lymphocytes

Across multiple studies, I found that all CD161+ innate-like lymphocytes in blood were capable of cytokine-induced IFN-γ production in response to vaccines. An important question that arises is whether there are cell type specific functions, or if these cell populations display a degree of redundancy? CD161+ T cells all have similar cytokine receptor expression, and thus mechanisms of activation, which result in similar patterns of effector functions in response to TCR-independent triggering in vitro and in vivo,

In the case of unconventional T cells, many have complementary functions and may even compete for a finite niche shaped by the early microbiome; *Tcrδ* -deficient animals have increased tissue-resident iNKT and MAIT cell populations [582], *Cd1d*-deficient animals have increased splenic and thymic MAIT cells [187], while GF mice have increased iNKT cells [583]. A competing or compensatory interaction is also supported by the massive expansion of Vδ2+ T cells in a patient with a homozygous point mutation in MR1 and MAIT cell [584].

Further supporting the presence of complementary functions, human blood MAIT cell and iNKT cell frequencies positively correlate [585,586]. Additional work is needed to clarify the relationship between innate-like T cells, and whether this varies depending on antigen availability, age and disease.

Despite similarities, some unique features emerge for innate-like lymphocyte populations. MAIT cells and iNKT cells in vitro and in vivo universally express CD161+ and have higher CD69 expression at baseline (compared to Vδ2+ γδ T cells or NK cells), and show a greater degree of CD69 induction after BNT162b2 vaccination in vivo. In HCW, Vδ2+ γδ T cell activation was much weaker after BNT162b2 compared to ChAdOx1-S in vivo. This may reflect different sensitivity to type I IFN and IFN-γ, the key drivers of early IFN-γ after BNT162b2 and ChAdOx1-S vaccination respectively.

7.4 Non-heritable regulation of innate-like lymphocyte responses

Immune memory

In Chapter 4, I examine the impact of prior immune responses on innate-like lymphocytes and describe two potential mechanisms. The first mechanism entails a decrease in innate-like lymphocyte activation and IFN-γ production following homologous ChAdOx1-S prime-boost. This is likely because neutralising anti-vector immunity hinders AdV transduction, reducing the necessary production of type I IFN and IL-18 required for the rapid induction of IFN-γ. Further work is necessary to confirm this hypothesis.

The second mechanism is characterised by boost-specific enhancement after BNT162b2. Early IFN-γ and activation of innate-like lymphocytes correlated with spike-specific adaptive immunity at boost, and I demonstrate in vitro that classical MHC antigen-presentation, conventional antigen-specific T cell IFN-γ , and IFN-γR1 signalling are important drivers.

This supports a model in which adaptive immunity moderates innate-like and innate immunity.

Figure 7.1 | Model for immune memory and differential regulation of vaccine-induced IFN-γ.

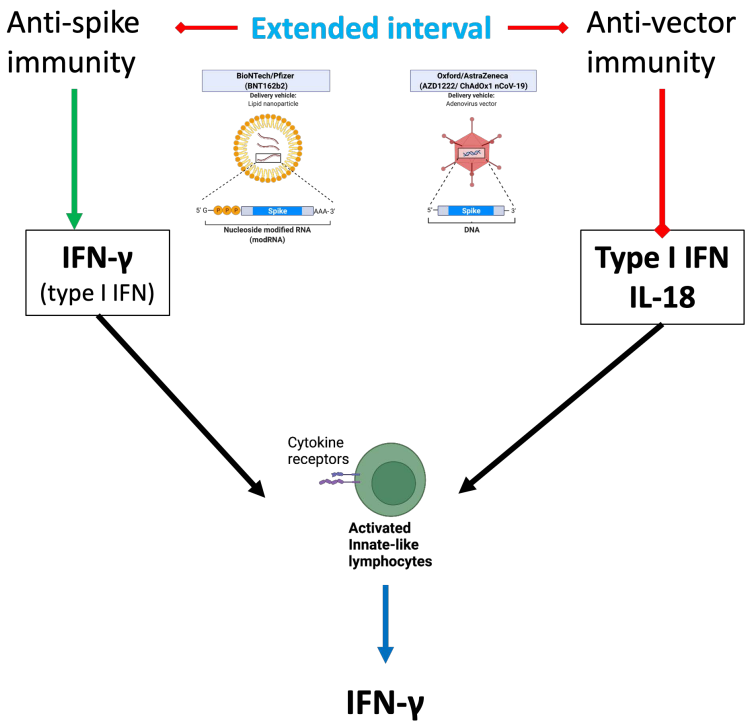

An alternative explanation is that epigenetic changes result in trained innate (or innate-like) immune memory that amplifies and accelerates immune responses upon subsequent exposure, a phenomenon observed with other vaccines[587]. Some data supports this hypothesis, particularly given persistent changes in the myeloid compartment 8 weeks after ChAdOx1-S prime. Although no lasting differences in innate-like lymphocyte phenotypic markers were observed, vaccine-induced inflammatory cytokines could drive changes in chromatin accessibility in these cells in a similar manner to trained immunity reported in NK cells; cytokines produced in response to BCG vaccination, human or murine CMV infection, such as IL-12, IL-15 and IL-18, lead to increased cytokine responsiveness of NK cells upon subsequent stimulation [29,588,589], including heterologous challenges such as malaria infection[590]. There is currently no data on epigenetic changes to MAIT cells and iNKT cells

after infections and vaccines, but plausible parallels may exist with NK cells, where enhanced responsiveness following CMV infection is associated with changes in DNA methylation patterns of the transcription factor PLZF[591].

Tissue environment

Despite accounting for differences in age, sex, and vaccine regimen, we still observe significant variation in immune responses in our study cohort, which has also been consistently seen in other human vaccine studies [576]. The microbiome appears to be a contributor to this variability [576], and is particularly relevant to innate-like T cell populations. The microbiome varies widely amongst individuals with similar genetic backgrounds, making it a crucial environmental factor driving human immune variation. Moreover, microbial diversity decreases with age, which may be linked to decreased immune responses to viruses and vaccines [576].

Preliminary in vitro work (Appendix Chapter) suggests that both sodium and bicarbonate can regulate MAIT cell effector functions. Sodium bicarbonate ($NaHCO_3$) is an established drug used to treat acidosis caused by renal failure, and could potentially enhance MAIT cell and effector memory T cell function in conditions of metabolic stress. A recent study in patients with relapsed acute myeloid leukaemia after stem-cell transplant found that $NaHCO_3$ treatment improved CD8+ T cell function by alleviating lactic acid-induced intracellular acidosis, which reduces glycolytic function and IFN-γ production [592]. The potential effects of $NaHCO_3$ treatment on SLC4A10-dependent pathways and other sodium-bicarbonate co-transporters (NBC), each with possibly unique functional properties, requires further exploration.

7.5 Future directions

MAIT cells and type I IFN

MAIT cells are abundant in humans and highly sensitive to ubiquitous type I IFN and IFN-γ, therefore further work should explore the full range of downstream effector functions which could be generated in response to vaccines and viruses, particularly in tissues. The impact of clinical modulators of the IFN-pathway could provide further insight. Although inherited type I IFN deficiency does not impact on humoral immune responses to mRNA vaccines [593], acquired anti-IFN autoantibodies increase in prevalence with age, and are linked to severe virus infections[594], which may in part occur through effects on MAIT cell activation. Type I IFN also influences tissue homeostasis and function of γδ T cells, therefore analogous implications need to be explored for MAIT cells [595].

The full role of TNF in type I IFN induced IFN-γ needs to be defined, including direct and other indirect mechanisms for potentiation of MAIT cell function; one example is ISG15, a 15kDa IFN-induced protein released from human lymphocytes and monocytes which can act as an immunomodulatory cytokine[596], including historical impact on NK and NKT cell IFN-γ.

Unpublished data from SARS-CoV-2 human challenge studies shows that MAIT cell CD69 is a sensitive marker of both controlled and perhaps persistent sequalae of infection, correlating with local type I IFN responses (*Sarah Teichmann, conference presentation*). It is entirely unclear ***why*** MAIT cells are so much more sensitive to type I IFN and the full range of protective (and pathogenic) IFN-mediated effector functions. As MAIT cells potentially recirculate, it is possible they are tuned by memory of tissues – or tissue specific cytokines, as a pre-adaptation to even more rapid effector functions. One could test the epigenetic signature of MAIT cells, in particular CD69+ and CD69- MAIT cells, comparing

across tissues. Experiments exploring MAIT cell epigenetic changes would be even more informative in disease, where patients have higher baseline CD69 expression.

Leading on from increased CD69 expression, a reduction in MAIT frequency is almost always observed concomitantly with increased peripheral activation in blood. Again, MAIT cell activation and lymphopenia were sensitive hallmarks of COVID-19. We still do not know how much of this is cell death compared to migration; given the importance of CD69 in tissue residency, one might expect a combination.

MAIT cells and IFN-γ

The precise mechanisms controlling IFN-γ dependent innate-like lymphocyte activation are important to pursue. Does it matter ***which*** cell types are communicating? Does conventional T cell TCR specificity impact on innate-like lymphocyte activation? Most adults will have reactive or cross-reactive T cells to common pathogens, which may therefore have an effect on subsequent homologous and heterologous responses. Comparative studies in younger age groups with an expanded naïve T cell compartment would be informative.

Could some of these mechanisms explain (auto-)inflammation with aging? The effector T-cell compartment, especially in tissues, expands, and changes over the course of life which is also associated with delayed kinetics of type I IFN production. If IFN-γR1 dependent signalling extends to other CD161+ effector memory cells, excess antigen from ineffective early type I IFN mediated control could pre-dispose to excess IFN-γR dependent IFN-γ, through both excessive antigen-specific T cell activation, and perhaps excess IFN-γ dependent antigen secretion.

A separate question is ***how*** cells communicate via IFN-γ:IFN-γR signalling? CD8+ T-cells can exchange IFN-γ in homotypic clusters, with IFN-γ secretion polarised and targeted at T-T synapses to drive target cell differentiation[428]. Preliminary data suggests that increased

cell density in enriched CD8+ T cell co-cultures augments MAIT cell IFN-γ in response to IFN-γ inducing cytokines (IFN-α, IL-18, TNFR2 agonist), with both ICAM-1 and LFA-1 blockade capable of reducing this MAIT cell derived IFN-γ (data not shown).

Finally, there remains a question as to ***what*** innate-like lymphocyte effector functions are induced from IFN-γ signalling, and whether they more closely align to APC-derived (cytokine) signals, or T-cell derived (TCR) signals? Cytokine and TCR activated MAIT cells diverge transcriptionally[282]. We have bulk and single-cell RNA-seq data for MAIT cells after ChAdOx1 and BNT162b-mediated activation, which may help to further distinguish the range and magnitude of effector functions in response to these different modes of activation.

Figure 7.2 | Hypothesis for reciprocal control of innate, adaptive, and tissue immunity.

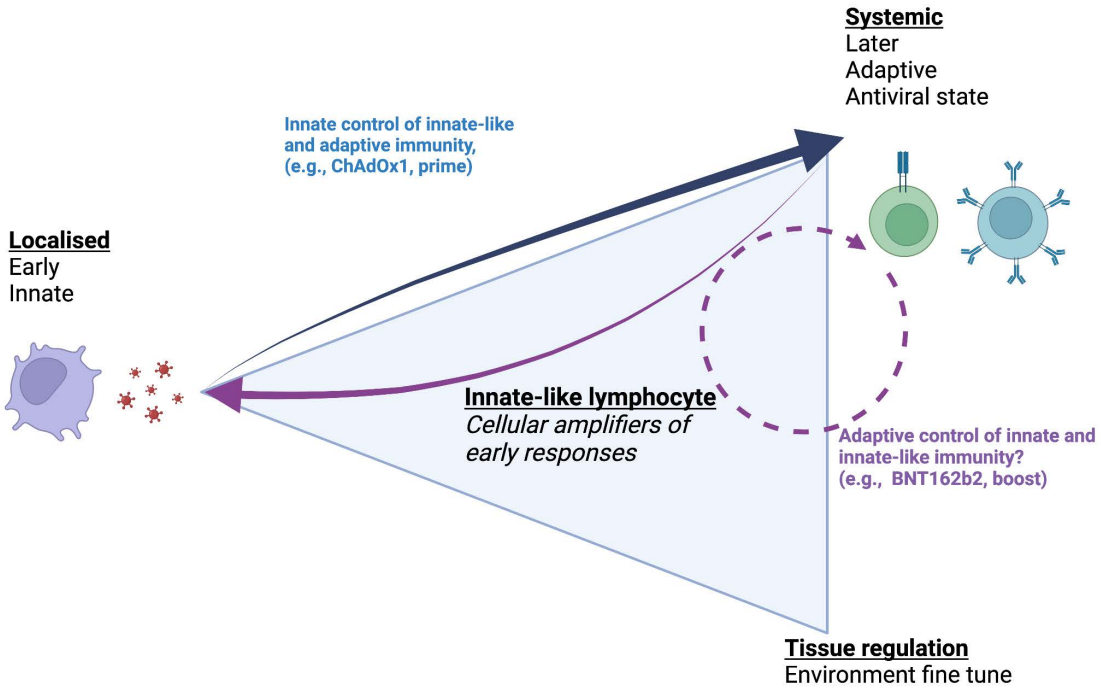

8 References

1. Iwasaki, A. & Medzhitov, R. Control of adaptive immunity by the innate immune system. Nat Immunol 16, 343–353 (2015).
2. Janeway, C. A. Approaching the Asymptote? Evolution and Revolution in Immunology. Cold Spring Harb Sym 54, 1–13 (1989).
3. Lemaitre, B., Nicolas, E., Michaut, L., Reichhart, J.-M. & Hoffmann, J. A. The Dorsoventral Regulatory Gene Cassette spätzle/Toll/cactus Controls the Potent Antifungal Response in Drosophila Adults. Cell 86, 973–983 (1996).
4. Medzhitov, R., Preston-Hurlburt, P. & Janeway, C. A. A human homologue of the Drosophila Toll protein signals activation of adaptive immunity. Nature 388, 394–397 (1997).
5. Poltorak, A. et al. Defective LPS Signaling in C3H/HeJ and C57BL/10ScCr Mice: Mutations in Tlr4 Gene. Science 282, 2085–2088 (1998).
6. Medzhitov, R. Toll-like receptors and innate immunity. Nat Rev Immunol 1, 135–145 (2001).
7. Hemmi, H. et al. A Toll-like receptor recognizes bacterial DNA. Nature 408, 740–745 (2000).
8. Ishii, S., Kihara, Y. & Shimizu, T. Identification of T Cell Death-associated Gene 8 (TDAG8) as a Novel Acid Sensing G-protein-coupled Receptor. J Biol Chem 280, 9083–9087 (2005).
9. Stetson, D. B. & Medzhitov, R. Antiviral defense: interferons and beyond. J Exp Med 203, 1837–1841 (2006).
10. Wu, J. & Chen, Z. J. Innate Immune Sensing and Signaling of Cytosolic Nucleic Acids. Immunology 32, 461–488 (2014).
11. Takaoka, A. et al. DAI (DLM-1/ZBP1) is a cytosolic DNA sensor and an activator of innate immune response. Nature 448, 501–505 (2007).
12. Ishikawa, H. & Barber, G. N. STING is an endoplasmic reticulum adaptor that facilitates innate immune signalling. Nature 455, 674–678 (2008).
13. Ishikawa, H., Ma, Z. & Barber, G. N. STING regulates intracellular DNA-mediated, type I interferon-dependent innate immunity. Nature 461, 788–792 (2009).
14. Hornung, V. et al. AIM2 recognizes cytosolic dsDNA and forms a caspase-1-activating inflammasome with ASC. Nature 458, 514–518 (2009).
15. Hornung, V. et al. 5'-Triphosphate RNA Is the Ligand for RIG-I. Science 314, 994–997 (2006).
16. Pulendran, B., Arunachalam, P. S. & O'Hagan, D. T. Emerging concepts in the science of vaccine adjuvants. Nat Rev Drug Discov 20, 1–22 (2021).
17. Chovatiya, R. & Medzhitov, R. Stress, inflammation, and defense of homeostasis. Mol Cell 54, 281–288 (2014).
18. Liston, A. & Masters, S. L. Homeostasis-altering molecular processes as mechanisms of inflammasome activation. Nat Rev Immunol 17, 208–214 (2017).
19. Lamkanfi, M. & Dixit, V. M. Inflammasomes: guardians of cytosolic sanctity. Immunol Rev 227, 95–105 (2009).
20. Martinon, F., Mayor, A. & Tschopp, J. The Inflammasomes: Guardians of the Body. Annu Rev Immunol 27, 229–265 (2009).
21. Franchi, L., Eigenbrod, T., Muñoz-Planillo, R. & Núñez, G. The inflammasome: a caspase-1-activation platform that regulates immune responses and disease pathogenesis. Nat Immunol 10, 241–247 (2009).
22. Kärre, K., Ljunggren, H. G., Piontek, G. & Kiessling, R. Selective rejection of H-2-deficient lymphoma variants suggests alternative immune defence strategy. Nature 319, 675–678 (1986).
23. Jost, S. & Altfeld, M. Control of Human Viral Infections by Natural Killer Cells. Immunology 31, 163–194 (2013).

24. Swanson, C. L. et al. Type I IFN enhances follicular B cell contribution to the T cell–independent antibody response. J Exp Med 207, 1485–1500 (2010).
25. Domeier, P. P. et al. B-Cell-Intrinsic Type 1 Interferon Signaling Is Crucial for Loss of Tolerance and the Development of Autoreactive B Cells. Cell Reports 24, 406–418 (2018).
26. Zhang, B. et al. Prevention and cure of rotavirus infection via TLR5/NLRC4–mediated production of IL-22 and IL-18. Science 346, 861–865 (2014).
27. Netea, M. G. et al. Trained immunity: A program of innate immune memory in health and disease. Science 352, aaf1098 (2016).
28. Netea, M. G. et al. Defining trained immunity and its role in health and disease. Nat Rev Immunol 20, 375–388 (2020).
29. Kleinnijenhuis, J. et al. BCG-induced trained immunity in NK cells: Role for non-specific protection to infection. Clin Immunol 155, 213-219 (2014).
30. Nankabirwa, V. et al. Child survival and BCG vaccination: a community based prospective cohort study in Uganda. BMC Public Health 15, 175 (2015).
31. Kong, L. et al. Single-cell transcriptomic profiles reveal changes associated with BCG-induced trained immunity and protective effects in circulating monocytes. Cell Reports 37, 110028 (2021).
32. Bree, L. C. J. et al. The impact of sex hormones on BCG-induced trained immunity. J Leukocyte Biol 104, 573–578 (2018).
33. Angelidou, A. et al. Human Newborn Monocytes Demonstrate Distinct BCG-Induced Primary and Trained Innate Cytokine Production and Metabolic Activation In Vitro. Front Immunol 12, 674334 (2021).
34. Bree, L. C. J. de et al. Circadian rhythm influences induction of trained immunity by BCG vaccination. J Clin Invest 130, 5603–5617 (2020).
35. Isaacs, A. & Lindenmann, J. Virus interference. I. The interferon. Proc R Soc Lond B Biol Sci 147, 258–267 (1957).
36. McNab, F., Mayer-Barber, K., Sher, A., Wack, A. & O'Garra, A. Type I interferons in infectious disease. Nat Rev Immunol 15, 87–103 (2015).
37. Mesev, E. V., LeDesma, R. A. & Ploss, A. Decoding type I and III interferon signalling during viral infection. Nat Microbiol 4, 914–924 (2019).
38. Fung, K. Y. et al. Interferon-ε protects the female reproductive tract from viral and bacterial infection. Science 339, 1088–1092 (2013).
39. Honda, K., Takaoka, A. & Taniguchi, T. Type I Interferon Gene Induction by the Interferon Regulatory Factor Family of Transcription Factors. Immunity 25, 349–360 (2006).
40. Colonna, M., Trinchieri, G. & Liu, Y.-J. Plasmacytoid dendritic cells in immunity. Nat Immunol 5, 1219–1226 (2004).
41. Swiecki, M. & Colonna, M. The multifaceted biology of plasmacytoid dendritic cells. Nat Rev Immunol 15, 471–485 (2015).
42. Jaks, E., Gavutis, M., Uzé, G., Martal, J. & Piehler, J. Differential Receptor Subunit Affinities of Type I Interferons Govern Differential Signal Activation. J Mol Biol 366, 525–539 (2007).
43. Platanias, L. C. Mechanisms of type-I- and type-II-interferon-mediated signalling. Nat Rev Immunol 5, 375–386 (2005).
44. Schoggins, J. W. & Rice, C. M. Interferon-stimulated genes and their antiviral effector functions. Curr Opin Virol 1, 519–525 (2011).
45. Teijaro, J. R. Type I interferons in viral control and immune regulation. Curr Opin Virol 16, 31–40 (2016).
46. Bailey, C. C., Zhong, G., Huang, I.-C. & Farzan, M. IFITM-Family Proteins: The Cell's First Line of Antiviral Defense. Annu Rev Virol 1, 261–283 (2014).
47. Felix, J. & Savvides, S. N. Mechanisms of immunomodulation by mammalian and viral decoy receptors: insights from structures. Nat Rev Immunol 17, 112–129 (2017).

48. Santini, S. M. et al. The Natural Alliance Between Type I Interferon and Dendritic Cells and Its Role in Linking Innate and Adaptive Immunity. J Interferon Cytokine Res 22, 1071–1080 (2002).
49. Simmons, D. P. et al. Type I IFN Drives a Distinctive Dendritic Cell Maturation Phenotype That Allows Continued Class II MHC Synthesis and Antigen Processing. J Immunol 188, 3116–3126 (2012).
50. Montoya, M. et al. Type I interferons produced by dendritic cells promote their phenotypic and functional activation. Blood 99, 3263–3271 (2002).
51. Zuniga, E. I., McGavern, D. B., Pruneda-Paz, J. L., Teng, C. & Oldstone, M. B. A. Bone marrow plasmacytoid dendritic cells can differentiate into myeloid dendritic cells upon virus infection. Nat Immunol 5, 1227–1234 (2004).
52. Kolumam, G. A., Thomas, S., Thompson, L. J., Sprent, J. & Murali-Krishna, K. Type I interferons act directly on CD8 T cells to allow clonal expansion and memory formation in response to viral infection. J Exp Med 202, 637–650 (2005).
53. Curtsinger, J. M., Lins, D. C., Johnson, C. M. & Mescher, M. F. Signal 3 tolerant CD8 T cells degranulate in response to antigen but lack granzyme B to mediate cytolysis. J Immunol 175, 4392–4399 (2005).
54. Shiow, L. R. et al. CD69 acts downstream of interferon-alpha/beta to inhibit S1P1 and lymphocyte egress from lymphoid organs. Nature 440, 540–544 (2006).
55. Kreins, A. Y. et al. Human TYK2 deficiency: Mycobacterial and viral infections without hyper-IgE syndrome. J Exp Med 212, 1641–1662 (2015).
56. Dupuis, S. et al. Impaired response to interferon-α/β and lethal viral disease in human STAT1 deficiency. Nat Genet. 33, 388–391 (2003).
57. Moens, L. et al. A novel kindred with inherited STAT2 deficiency and severe viral illness. J Allergy Clin Immun 139, 1995-1997.e9 (2017).
58. Ciancanelli, M. J. et al. Infectious disease. Life-threatening influenza and impaired interferon amplification in human IRF7 deficiency. Science 348, 448–453 (2015).
59. Hernandez, N. et al. Life-threatening influenza pneumonitis in a child with inherited IRF9 deficiency. J Exp Med 215, 2567–2585 (2018).
60. Duncan, C. J. A. & Hambleton, S. Varicella zoster virus immunity: A primer. J Infect 71, S47–S53 (2015).
61. Hernandez, N. et al. Inherited IFNAR1 deficiency in otherwise healthy patients with adverse reaction to measles and yellow fever live vaccines. J Exp Med 216, 2057–2070 (2019).
62. Hambleton, S. et al. STAT2 deficiency and susceptibility to viral illness in humans. Proceedings of the National Academy of Sciences 110, 3053–3058 (2013).
63. Kalliolias, G. D. & Ivashkiv, L. B. TNF biology, pathogenic mechanisms and emerging therapeutic strategies. Nat Rev Rheumatol 12, 49–62 (2016).
64. Chan, A. H. & Schroder, K. Inflammasome signaling and regulation of interleukin-1 family cytokines. J Exp Med 217, e20190314 (2019).
65. Schroder, K. & Tschopp, J. The Inflammasomes. Cell 140, 821–832 (2010).
66. Kaplanski, G. Interleukin-18: Biological properties and role in disease pathogenesis. Immunol Rev 281, 138–153 (2017).
67. Wheelock, E. F. Interferon-Like Virus-Inhibitor Induced in Human Leukocytes by Phytohemagglutinin. Science 149, 310–311 (1965).
68. Derynck, R., Leung, D. W., Gray, P. W. & Goeddel, D. V. Human Interferon γ is encoded by a single class of mRNA. Nucleic Acids Res 10, 3605–3615 (1982).
69. Rinderknecht, E., O'Connor, B. H. & Rodriguez, H. Natural human interferon-gamma. Complete amino acid sequence and determination of sites of glycosylation. J Biol Chem 259, 6790–6797 (1984).
70. Ealick, S. E. et al. Three-Dimensional Structure of Recombinant Human Interferon-γ. Science 252, 698–702 (1991).
71. Farrar, M. A. & Schreiber, R. D. The Molecular Cell Biology of Interferon-gamma and its Receptor. Annu Rev Immunol 11, 571–611 (1993).

72. Valente, G. et al. Distribution of interferon-γ receptor in human tissues. Eur J Immunol 22, 2403–2412 (1992).
73. Weerd, N. A. de et al. Structural basis of a unique interferon-β signaling axis mediated via the receptor IFNAR1. Nat Immunol 14, 901–907 (2013).
74. Ihle, J. N. STATs: Signal Transducers and Activators of Transcription. Cell 84, 331–334 (1996).
75. Chistiakov, D. A., Myasoedova, V. A., Revin, V. V., Orekhov, A. N. & Bobryshev, Y. V. The impact of interferon-regulatory factors to macrophage differentiation and polarization into M1 and M2. Immunobiology 223, 101–111 (2018).
76. Kim, T. K. & Maniatis, T. Regulation of Interferon-γ-Activated STAT1 by the Ubiquitin-Proteasome Pathway. Science 273, 1717–1719 (1996).
77. Sad, S., Marcotte, R. & Mosmann, T. R. Cytokine-induced differentiation of precursor mouse CD8+ T cells into cytotoxic CD8+ T cells secreting Th1 or Th2 cytokines. Immunity 2, 271–279 (1995).
78. Schoenborn, J. R. & Wilson, C. B. Regulation of Interferon-γ During Innate and Adaptive Immune Responses. Adv Immunol 96, 41–101 (2007).
79. Dalton, D. K. et al. Multiple Defects of Immune Cell Function in Mice with Disrupted Interferon-γ Genes. Science 259, 1739–1742 (1993).
80. Huang, S. et al. Immune Response in Mice that Lack the Interferon-γ Receptor. Science 259, 1742–1745 (1993).
81. Wang, Z. E., Reiner, S. L., Zheng, S., Dalton, D. K. & Locksley, R. M. CD4+ effector cells default to the Th2 pathway in interferon gamma-deficient mice infected with Leishmania major. J Exp Medicine 179, 1367–1371 (1994).
82. Alcaïs, A., Abel, L. & Casanova, J.-L. Human genetics of infectious diseases: between proof of principle and paradigm. J Clin Invest 119, 2506–2514 (2009).
83. Hambleton, S. et al. IRF8 Mutations and Human Dendritic-Cell Immunodeficiency. N Engl J Med 365, 127–138 (2011).
84. Nuara, A. A. et al. Structure and mechanism of IFN-γ antagonism by an orthopoxvirus IFN-γ-binding protein. Proc Natl Acad Sci U S A, 1861–1866 (2008).
85. Müller, U. et al. Functional role of type I and type II interferons in antiviral defense. Science 264, 1918–1921 (1994).
86. Graham, M. B. et al. Response to influenza infection in mice with a targeted disruption in the interferon gamma gene. J Exp Medicine 178, 1725–1732 (1993).
87. Boehm, U., Klamp, T., Groot, M. & Howard, J. C. Cellular responses to interferon-gamma. Annu Rev Immunol 15, 749–795 (1997).
88. Su, X. et al. Interferon-γ regulates cellular metabolism and mRNA translation to potentiate macrophage activation. Nat Immunol 16, 838–849 (2015).
89. Afkarian, M. et al. T-bet is a STAT1-induced regulator of IL-12R expression in naïve CD4+ T cells. Nat Immunol 3, 549–557 (2002).
90. Whitmire, J. K., Tan, J. T. & Whitton, J. L. Interferon-γ acts directly on CD8+ T cells to increase their abundance during virus infection. J Exp Medicine 201, 1053–1059 (2005).
91. Lee, Y. et al. Induction and molecular signature of pathogenic TH17 cells. Nat Immunol 13, 991–999 (2012).
92. Yu, D., Walker, L. S. K., Liu, Z., Linterman, M. A. & Li, Z. Targeting TFH cells in human diseases and vaccination: rationale and practice. Nat Immunol 23, 1157–1168 (2022).
93. Fang, D. et al. Transient T-bet expression functionally specifies a distinct T follicular helper subset. J Exp Med 215, 2705–2714 (2018).
94. Sidman, C. L., Marshall, J. D., Shultz, L. D., Gray, P. W. & Johnson, H. M. γ-Interferon is one of several direct B cell-maturing lymphokines. Nature 309, 801–804 (1984).
95. Defrance, T., Aubry, J. P., Vanbervliet, B. & Banchereau, J. Human interferon-gamma acts as a B cell growth factor in the anti-IgM antibody co-stimulatory assay but has no direct B cell differentiation activity. J Immunol 137, 3861–7 (1986).

96. Leibson, H. J., Gefter, M., Zlotnik, A., Marrack, P. & Kappler, J. W. Role of γ-interferon in antibody-producing responses. Nature 309, 799–801 (1984).
97. Jackson, S. W. et al. B cell IFN-γ receptor signaling promotes autoimmune germinal centers via cell-intrinsic induction of BCL-6. J Exp Medicine 213, 733–750 (2016).
98. Peng, S. L., Szabo, S. J. & Glimcher, L. H. T-bet regulates IgG class switching and pathogenic autoantibody production. Proc Natl Acad Sci U S A 99, 5545–5550 (2002).
99. Pollard, A. J. & Bijker, E. M. A guide to vaccinology: from basic principles to new developments. Nat Rev Immunol 21, 83–100 (2021).
100. Moss, B., Smith, G. L., Gerin, J. L. & Purcell, R. H. Live recombinant vaccinia virus protects chimpanzees against hepatitis B. Nature 311, 67–69 (1984).
101. Alonso-Padilla, J. et al. Development of Novel Adenoviral Vectors to Overcome Challenges Observed With HAdV-5-based Constructs. Mol Ther 24, 6–16 (2016).
102. Crystal, R. G. et al. Administration of an adenovirus containing the human CFTR cDNA to the respiratory tract of individuals with cystic fibrosis. Nat Genet 8, 42–51 (1994).
103. Lemarchand, P. et al. Adenovirus-mediated transfer of a recombinant human alpha 1-antitrypsin cDNA to human endothelial cells. Proc Natl Acad Sci U S A 89, 6482–6486 (1992).
104. Iacobelli-Martinez, M. & Nemerow, G. R. Preferential Activation of Toll-Like Receptor Nine by CD46-Utilizing Adenoviruses. J Virol 81, 1305–1312 (2007).
105. Sallusto, F., Lanzavecchia, A., Araki, K. & Ahmed, R. From Vaccines to Memory and Back. Immunity 33, 451–463 (2010).
106. Quinn, K. M. et al. Antigen expression determines adenoviral vaccine potency independent of IFN and STING signaling. J Clin Invest 125, 1129–1146 (2015).
107. Rhee, E. G. et al. Multiple Innate Immune Pathways Contribute to the Immunogenicity of Recombinant Adenovirus Vaccine Vectors. J Virol 85, 315–323 (2011).
108. Zhu, J., Huang, X. & Yang, Y. Innate immune response to adenoviral vectors is mediated by both Toll-like receptor-dependent and -independent pathways. J Virol 81, 3170–3180 (2007).
109. Atasheva, S. & Shayakhmetov, D. M. Adenovirus sensing by the immune system. Curr Opin Virol 21, 109–113 (2016).
110. Appledorn, D. M. et al. Adenovirus Vector-Induced Innate Inflammatory Mediators, MAPK Signaling, As Well As Adaptive Immune Responses Are Dependent upon Both TLR2 and TLR9 In Vivo. J Immunol 181, 2134–2144 (2008).
111. Appledorn, D. M., Patial, S., Godbehere, S., Parameswaran, N. & Amalfitano, A. TRIF, and TRIF-Interacting TLRs Differentially Modulate Several Adenovirus Vector-Induced Immune Responses. J Innate Immun 1, 376–388 (2009).
112. Lindsay, R. W. B. et al. CD8+ T Cell Responses following Replication-Defective Adenovirus Serotype 5 Immunization Are Dependent on CD11c+ Dendritic Cells but Show Redundancy in Their Requirement of TLR and Nucleotide-Binding Oligomerization Domain-Like Receptor Signaling. J Immunol 185, 1513–1521 (2010).
113. Lam, E., Stein, S. & Falck-Pedersen, E. Adenovirus Detection by the cGAS/STING/TBK1 DNA Sensing Cascade. J Virol 88, 974–981 (2014).
114. Anghelina, D., Lam, E. & Falck-Pedersen, E. Diminished Innate Antiviral Response to Adenovirus Vectors in cGAS/STING-Deficient Mice Minimally Impacts Adaptive Immunity. J Virol 90, 5915–5927 (2016).
115. Burdette, D. L. et al. STING is a direct innate immune sensor of cyclic di-GMP. Nature 478, 515–518 (2011).
116. Muruve, D. A. et al. The inflammasome recognizes cytosolic microbial and host DNA and triggers an innate immune response. Nature 452, 103–107 (2008).

117. Paolo, N. C. D. et al. Virus Binding to a Plasma Membrane Receptor Triggers Interleukin-1α-Mediated Proinflammatory Macrophage Response In Vivo. Immunity 31, 110–121 (2009).
118. Barouch, D. H., Letvin, N. L. & Seder, R. A. The role of cytokine DNAs as vaccine adjuvants for optimizing cellular immune responses. Immunol Rev 202, 266–274 (2004).
119. Zhu, N. et al. A Novel Coronavirus from Patients with Pneumonia in China, 2019. New Engl J Med 382, 727–733 (2020).
120. Li, H.-B. et al. m6A mRNA methylation controls T cell homeostasis by targeting the IL-7/STAT5/SOCS pathways. Nature 548, 338–342 (2017).
121. Barouch, D. H. et al. International seroepidemiology of adenovirus serotypes 5, 26, 35, and 48 in pediatric and adult populations. Vaccine 29, 5203–5209 (2011).
122. Baden, L. R. et al. First-in-Human Evaluation of the Safety and Immunogenicity of a Recombinant Adenovirus Serotype 26 HIV-1 Env Vaccine (IPCAVD 001). J Infect Dis 207, 240–247 (2013).
123. Ramasamy, M. N. et al. Safety and immunogenicity of ChAdOx1 nCoV-19 vaccine administered in a prime-boost regimen in young and old adults (COV002): a single-blind, randomised, controlled, phase 2/3 trial. Lancet 396, 1979–1993 (2020).
124. Frahm, N. et al. Human adenovirus-specific T cells modulate HIV-specific T cell responses to an Ad5-vectored HIV-1 vaccine. J Clin Invest 122, 359–367 (2012).
125. Loré, K. et al. Myeloid and plasmacytoid dendritic cells are susceptible to recombinant adenovirus vectors and stimulate polyfunctional memory T cell responses. J Immunol 179, 1721–1729 (2007).
126. Hensley, S. E. et al. Type I interferon inhibits antibody responses induced by a chimpanzee adenovirus vector. Mol Ther 15, 393–403 (2007).
127. Dicks, M. D. J. et al. Differential immunogenicity between HAdV-5 and chimpanzee adenovirus vector ChAdOx1 is independent of fiber and penton RGD loop sequences in mice. Sci Rep 5, 1881 (2015).
128. Tatsis, N. et al. Adenoviral vectors persist in vivo and maintain activated CD8+ T cells: implications for their use as vaccines. Blood 110, 1916–1923 (2007).
129. Finn, J. D. et al. Persistence of Transgene Expression Influences CD8 + T-Cell Expansion and Maintenance following Immunization with Recombinant Adenovirus. J Virol 83, 12027–12036 (2009).
130. Johnson, M. J. et al. Type I IFN Induced by Adenovirus Serotypes 28 and 35 Has Multiple Effects on T Cell Immunogenicity. J Immunol 188, 6109–6118 (2012).
131. Vitelli, A. et al. Chimpanzee adenoviral vectors as vaccines – challenges to move the technology into the fast lane. Expert Rev Vaccines 16, 1241–1252 (2017).
132. Welsh, R. M., Bahl, K., Marshall, H. D. & Urban, S. L. Type 1 interferons and antiviral CD8 T-cell responses. PLoS Pathog 8, e1002352 (2012).
133. Palacio, N. et al. Early type I IFN blockade improves the efficacy of viral vaccines. J Exp Med 217, 3050 (2020).
134. Pardi, N., Hogan, M. J., Porter, F. W. & Weissman, D. mRNA vaccines - a new era in vaccinology. Nat Rev Drug Discov 17, 261–279 (2018).
135. Blakney, A. K. et al. Innate Inhibiting Proteins Enhance Expression and Immunogenicity of Self-Amplifying RNA. Mol Ther 29, 1174–1185 (2021).
136. McKay, P. F. et al. Self-amplifying RNA SARS-CoV-2 lipid nanoparticle vaccine candidate induces high neutralizing antibody titers in mice. Nat Commun 11, 3523–7 (2020).
137. Verbeke, R., Hogan, M. J., Loré, K. & Pardi, N. Innate immune mechanisms of mRNA vaccines. Immunity 55, 1993–2005 (2022).
138. Karikó, K., Buckstein, M., Ni, H. & Weissman, D. Suppression of RNA Recognition by Toll-like Receptors: The Impact of Nucleoside Modification and the Evolutionary Origin of RNA. Immunity 23, 165–175 (2005).

139. Krienke, C. et al. A noninflammatory mRNA vaccine for treatment of experimental autoimmune encephalomyelitis. Science 371, 145–153 (2021).
140. Diebold, S. S., Kaisho, T., Hemmi, H., Akira, S. & Sousa, C. R. e. Innate Antiviral Responses by Means of TLR7-Mediated Recognition of Single-Stranded RNA. Science 303, 1529–1531 (2004).
141. Pulendran, B. & Davis, M. M. The science and medicine of human immunology. Science 369, (2020).
142. Swaminathan, G. et al. A novel lipid nanoparticle adjuvant significantly enhances B cell and T cell responses to sub-unit vaccine antigens. Vaccine 34, 110–119 (2016).
143. Alameh, M.-G. et al. Lipid nanoparticles enhance the efficacy of mRNA and protein subunit vaccines by inducing robust T follicular helper cell and humoral responses. Immunity 54, 2877-2892.e7 (2021).
144. Pardi, N. et al. Nucleoside-modified mRNA vaccines induce potent T follicular helper and germinal center B cell responses. J Exp Med 215, 1571–1588 (2018).
145. Sahin, U. et al. BNT162b2 vaccine induces neutralizing antibodies and poly-specific T cells in humans. Nature 595, 572–577 (2021).
146. Trougakos, I. P. et al. Adverse effects of COVID-19 mRNA vaccines: The Spike hypothesis. Trends Mol Med 28, 542–554 (2022).
147. Röltgen, K. et al. Immune imprinting, breadth of variant recognition, and germinal center response in human SARS-CoV-2 infection and vaccination. Cell 185, 1025-1040.e14 (2022).
148. Lindgren, G. et al. Induction of Robust B Cell Responses after Influenza mRNA Vaccination Is Accompanied by Circulating Hemagglutinin-Specific ICOS+ PD-1+ CXCR3+ T Follicular Helper Cells. Front Immunol 8, 1539 (2017).
149. Liang, F. et al. Vaccine priming is restricted to draining lymph nodes and controlled by adjuvant-mediated antigen uptake. Sci Transl Med 9, (2017).
150. Corbett, K. S. et al. SARS-CoV-2 mRNA vaccine design enabled by prototype pathogen preparedness. Nature 586, 567–571 (2020).
151. Gaucher, D. et al. Yellow fever vaccine induces integrated multilineage and polyfunctional immune responses. J Exp Medicine 205, 3119–3131 (2008).
152. Pulendran, B., Li, S. & Nakaya, H. I. Systems Vaccinology. Immunity 33, 516–529 (2010).
153. Pulendran, B. & Ahmed, R. Immunological mechanisms of vaccination. Nat Immunol 12, 509–517 (2011).
154. Kaer, L. V., Postoak, J. L., Song, W. & Wu, L. Innate and Innate-like Effector Lymphocytes in Health and Disease. J Immunol 209, 199–207 (2022).
155. Wencker, M. et al. Innate-like T cells straddle innate and adaptive immunity by altering antigen-receptor responsiveness. Nat Immunol 15, 80–87 (2014).
156. Fan, X. & Rudensky, A. Y. Hallmarks of Tissue-Resident Lymphocytes. Cell 164, 1198–1211 (2016).
157. Vivier, E. et al. Innate Lymphoid Cells: 10 Years On. Cell 174, 1054–1066 (2018).
158. Herberman, R. B., Nunn, M. E., Holden, H. T. & Lavrin, D. H. Natural cytotoxic reactivity of mouse lymphoid cells against syngeneic and allogeneic tumors. II. Characterization of effector cells. Int J Cancer 16, 230–239 (1975).
159. Cella, M. et al. A human natural killer cell subset provides an innate source of IL-22 for mucosal immunity. Nature 457, 722–725 (2009).
160. Lanier, L. L., Cwirla, S., Federspiel, N. & Phillips, J. H. Human natural killer cells isolated from peripheral blood do not rearrange T cell antigen receptor beta chain genes. J Exp Medicine 163, 209–214 (1986).
161. Godfrey, D. I., Uldrich, A. P., McCluskey, J., Rossjohn, J. & Moody, D. B. The burgeoning family of unconventional T cells. Nat Immunol 16, 1114–1123 (2015).
162. Lee, S., Channappanavar, R. & Kanneganti, T.-D. Coronaviruses: Innate Immunity, Inflammasome Activation, Inflammatory Cell Death, and Cytokines. Trends Immunol 41, 1083–1099 (2020).

163. Salou, M. & Lantz, O. A TCR-Dependent Tissue Repair Potential of MAIT Cells. Trends Immunol 40, 975-977 (2019).
164. Provine, N. M. et al. Unique and Common Features of Innate-Like Human Vδ2+ γδT Cells and Mucosal-Associated Invariant T Cells. Front Immunol 9, 756 (2018).
165. Budd, R. C. et al. Developmentally regulated expression of T cell receptor beta chain variable domains in immature thymocytes. J Exp Medicine 166, 577–582 (1987).
166. Ceredig, R., Allan, J. E., Tabi, Z., Lynch, F. & Doherty, P. C. Phenotypic analysis of the inflammatory exudate in murine lymphocytic choriomeningitis. J Exp Medicine 165, 1539–1551 (1987).
167. Sykes, M. Unusual T cell populations in adult murine bone marrow. Prevalence of CD3+CD4-CD8- and alpha beta TCR+NK1.1+ cells. J Immunol 145, 3209–15 (1990).
168. Exley, M., Garcia, J., Balk, S. P. & Porcelli, S. Requirements for CD1d Recognition by Human Invariant Vα24+ CD4−CD8− T Cells. J Exp Medicine 186, 109–120 (1997).
169. Godfrey, D. I., MacDonald, H. R., Kronenberg, M., Smyth, M. J. & Kaer, L. V. NKT cells: what's in a name? Nat Rev Immunol 4, 231–237 (2004).
170. Lantz, O. & Bendelac, A. An invariant T cell receptor alpha chain is used by a unique subset of major histocompatibility complex class I-specific CD4+ and CD4-8- T cells in mice and humans. J Exp Medicine 180, 1097–1106 (1994).
171. Porcelli, S., Yockey, C. E., Brenner, M. B. & Balk, S. P. Analysis of T cell antigen receptor (TCR) expression by human peripheral blood CD4-8- alpha/beta T cells demonstrates preferential use of several V beta genes and an invariant TCR alpha chain. J Exp Med 178, 1–16 (1993).
172. Bendelac, A. Positive selection of mouse NK1+ T cells by CD1-expressing cortical thymocytes. J Exp Med 182, 2091–2096 (1995).
173. Kawano, T. et al. CD1d-Restricted and TCR-Mediated Activation of Vα14 NKT Cells by Glycosylceramides. Science 278, 1626–1629 (1997).
174. Pellicci, D. G. et al. A Natural Killer T (NKT) Cell Developmental Pathway Involving a Thymus-dependent NK1.1−CD4+ CD1d-dependent Precursor Stage. J Exp Medicine 195, 835–844 (2002).
175. Treiner, E. et al. Selection of evolutionarily conserved mucosal-associated invariant T cells by MR1. Nature 422, 164–169 (2003).
176. Dusseaux, M. et al. Human MAIT cells are xenobiotic-resistant, tissue-targeted, CD161hi IL-17–secreting T cells. Blood 117, 1250–1259 (2011).
177. Provine, N. M. & Klenerman, P. MAIT Cells in Health and Disease. Annu Rev Immunol 38, 1–26 (2020).
178. Tilloy, F. et al. An invariant T cell receptor alpha chain defines a novel TAP-independent major histocompatibility complex class Ib-restricted alpha/beta T cell subpopulation in mammals. J Exp Med 189, 1907–1921 (1999).
179. Reantragoon, R. et al. Antigen-loaded MR1 tetramers define T cell receptor heterogeneity in mucosal-associated invariant T cells. J Exp Med 210, 2305–2320 (2013).
180. Bourhis, L. L. et al. Antimicrobial activity of mucosal-associated invariant T cells. Nat Immunol 11, 701–708 (2010).
181. Gold, M. C. et al. Human mucosal associated invariant T cells detect bacterially infected cells. PLoS Biol 8, e1000407 (2010).
182. Kjer-Nielsen, L. et al. MR1 presents microbial vitamin B metabolites to MAIT cells. Nature 491, 717–723 (2012).
183. Godfrey, D. I., Koay, H. F., McCluskey, J. & Gherardin, N. A. The biology and functional importance of MAIT cells. Nat Immunol 20, 1110–1128 (2019).
184. Boudinot, P. et al. Restricting nonclassical MHC genes coevolve with TRAV genes used by innate-like T cells in mammals. Proc Natl Acad Sci U S A 113, E2983-92 (2016).

185. Corbett, A. J., Awad, W., Wang, H. & Chen, Z. Antigen Recognition by MR1-Reactive T Cells; MAIT Cells, Metabolites, and Remaining Mysteries. Front Immunol 11, 1961 (2020).
186. Garner, L. C., Klenerman, P. & Provine, N. M. Insights Into Mucosal-Associated Invariant T Cell Biology From Studies of Invariant Natural Killer T Cells. Front Immunol 9, 1478 (2018).
187. Koay, H. F. et al. A three-stage intrathymic development pathway for the mucosal-associated invariant T cell lineage. Nat Immunol 17, 1300–1311 (2016).
188. Novak, J., Dobrovolny, J., Novakova, L. & Kozak, T. The Decrease in Number and Change in Phenotype of Mucosal-Associated Invariant T cells in the Elderly and Differences in Men and Women of Reproductive Age. Scand J Immunol 80, 271–275 (2014).
189. Dias, J., Leeansyah, E. & Sandberg, J. K. Multiple layers of heterogeneity and subset diversity in human MAIT cell responses to distinct microorganisms and to innate cytokines. Proc Natl Acad Sci U S A 114, E5434–E5443 (2017).
190. Rahimpour, A. et al. Identification of phenotypically and functionally heterogeneous mouse mucosal-associated invariant T cells using MR1 tetramers. J Exp Med 212, 1095–1108 (2015).
191. Leeansyah, E. et al. Arming of MAIT Cell Cytolytic Antimicrobial Activity Is Induced by IL-7 and Defective in HIV-1 Infection. PLoS Pathog 11, e1005072 (2015).
192. Saito, H. et al. A third rearranged and expressed gene in a clone of cytotoxic T lymphocytes. Nature 312, 36–40 (1984).
193. Hayday, A. C. et al. Structure, organization, and somatic rearrangement of T cell gamma genes. Cell 40, 259–269 (1985).
194. Chien, Y., Meyer, C. & Bonneville, M. γδ T Cells: First Line of Defense and Beyond. Immunology 32, 121–155 (2014).
195. McMurray, J. L. et al. Transcriptional profiling of human Vδ1 T cells reveals a pathogen-driven adaptive differentiation program. Cell Reports 39, 110858 (2022).
196. Jensen, K. D. C. et al. Thymic Selection Determines γδ T Cell Effector Fate: Antigen-Naive Cells Make Interleukin-17 and Antigen-Experienced Cells Make Interferon γ. Immunity 29, 90–100 (2008).
197. Uldrich, A. P., Rigau, M. & Godfrey, D. I. Immune recognition of phosphoantigen-butyrophilin molecular complexes by γδ T cells. Immunol Rev 298, 74–83 (2020).
198. Shen, Y. et al. Adaptive Immune Response of Vγ2Vδ2+ T Cells During Mycobacterial Infections. Science 295, 2255–2258 (2002).
199. Wragg, K. M. et al. High CD26 and Low CD94 Expression Identifies an IL-23 Responsive Vδ2+ T Cell Subset with a MAIT Cell-like Transcriptional Profile. Cell Reports 31, 107773 (2020).
200. Fergusson, J. R. et al. CD161 Defines a Transcriptional and Functional Phenotype across Distinct Human T Cell Lineages. Cell Reports 9, 1075–1088 (2014).
201. Ussher, J. E. et al. CD161++CD8+ T cells, including the MAIT cell subset, are specifically activated by IL-12+IL-18 in a TCR-independent manner. Eur J Immunol 44, 195–203 (2014).
202. Savage, A. K. et al. The Transcription Factor PLZF Directs the Effector Program of the NKT Cell Lineage. Immunity 29, 391–403 (2008).
203. Brigl, M., Bry, L., Kent, S. C., Gumperz, J. E. & Brenner, M. B. Mechanism of CD1d-restricted natural killer T cell activation during microbial infection. Nat Immunol 4, 1230–1237 (2003).
204. Cesano, A., Visonneau, S., Clark, S. C. & Santoli, D. Cellular and molecular mechanisms of activation of MHC nonrestricted cytotoxic cells by IL-12. J Immunol 151, 2943–57 (1993).
205. Cohavy, O., Shih, D. Q., Doherty, T. M., Ware, C. F. & Targan, S. R. CD161 defines effector T cells that express light and respond to TL1A-DR3 signaling. European J Microbiol Immunol 1, 70–79 (2011).

206. Kurioka, A. et al. CD161 Defines a Functionally Distinct Subset of Pro-Inflammatory Natural Killer Cells. Front Immunol 9, 486 (2018).
207. Yokoyama, W. M. & Seaman, W. E. The Ly-49 and NKR-P1 Gene Families Encoding Lectin-Like Receptors on Natural Killer Cells: The NK Gene Complex. Annu Rev Immunol 11, 613–635 (1993).
208. Lanier, L. L., Chang, C. & Phillips, J. H. Human NKR-P1A. A disulfide-linked homodimer of the C-type lectin superfamily expressed by a subset of NK and T lymphocytes. J Immunol 153, 2417–2428 (1994).
209. Takahashi, T., Dejbakhsh-Jones, S. & Strober, S. Expression of CD161 (NKR-P1A) Defines Subsets of Human CD4 and CD8 T Cells with Different Functional Activities. J Immunol 176, 211–216 (2006).
210. Aldemir, H. et al. Cutting edge: lectin-like transcript 1 is a ligand for the CD161 receptor. J Immunol 175, 7791–7795 (2005).
211. Rosen, D. B. et al. Cutting edge: lectin-like transcript-1 is a ligand for the inhibitory human NKR-P1A receptor. J Immunol 175, 7796–7799 (2005).
212. Germain, C. et al. Induction of lectin-like transcript 1 (LLT1) protein cell surface expression by pathogens and interferon-γ contributes to modulate immune responses. J Biol Chem 286, 37964–37975 (2011).
213. Bourhis, L. L. et al. MAIT cells detect and efficiently lyse bacterially-infected epithelial cells. PLoS Pathog 9, e1003681 (2013).
214. Rosen, D. B. et al. Functional Consequences of Interactions between Human NKR-P1A and Its Ligand LLT1 Expressed on Activated Dendritic Cells and B Cells. J Immunol 180, 6508–6517 (2008).
215. Exley, M., Porcelli, S., Furman, M., Garcia, J. & Balk, S. CD161 (NKR-P1A) Costimulation of CD1d-dependent Activation of Human T Cells Expressing Invariant Vα24JαQ T Cell Receptor α Chains. J Exp Medicine 188, 867–876 (1998).
216. Maggi, L. et al. CD161 is a marker of all human IL-17-producing T-cell subsets and is induced by RORC. Eur J Immunol 40, 2174–2181 (2010).
217. Battistini, L. et al. Phenotypic and cytokine analysis of human peripheral blood gamma delta T cells expressing NK cell receptors. J Immunol 159, 3723–3730 (1997).
218. Bukowski, J. F., Warner, J. F., Dennert, G. & Welsh, R. M. Adoptive transfer studies demonstrating the antiviral effect of natural killer cells in vivo. J Exp Medicine 161, 40–52 (1985).
219. Lanier, L. L. NK CELL RECEPTORS. Annu Rev Immunol 16, 359–393 (1998).
220. Ahlenstiel, G. et al. Natural Killer Cells Are Polarized Toward Cytotoxicity in Chronic Hepatitis C in an Interferon-Alfa–Dependent Manner. Gastroenterology 138, 325-335.e2 (2010).
221. Ho, L. et al. Activation of invariant NKT cells enhances the innate immune response and improves the disease course in influenza A virus infection. Eur J Immunol 38, 1913–1922 (2008).
222. Santo, C. D. et al. Invariant NKT cells reduce the immunosuppressive activity of influenza A virus–induced myeloid-derived suppressor cells in mice and humans. J Clin Invest 118, 4036–4048 (2008).
223. Lee, Y. K., Menezes, J. S., Umesaki, Y. & Mazmanian, S. K. Proinflammatory T-cell responses to gut microbiota promote experimental autoimmune encephalomyelitis. Proc Natl Acad Sci U S A 108, 4615–4622 (2011).
224. Wilgenburg, B. van et al. MAIT cells contribute to protection against lethal influenza infection in vivo. Nat Commun 9, 4706 (2018).
225. Flament, H. et al. Outcome of SARS-CoV-2 infection is linked to MAIT cell activation and cytotoxicity. Nat Immunol 22, 322–335 (2021).
226. Jouan, Y. et al. Phenotypical and functional alteration of unconventional T cells in severe COVID-19 patients. J Exp Med 217, 467 (2020).

227. Suliman, S. et al. MR1-Independent Activation of Human Mucosal-Associated Invariant T Cells by Mycobacteria. J Immunol 203, 2917–2927 (2019).
228. Darrah, P. A. et al. Prevention of tuberculosis in macaques after intravenous BCG immunization. Nature 577, 95–102 (2020).
229. Fehniger, T. A. et al. CD56bright natural killer cells are present in human lymph nodes and are activated by T cell-derived IL-2: a potential new link between adaptive and innate immunity. Blood 101, 3052–3057 (2003).
230. Goodier, M. R. et al. Sustained Immune Complex-Mediated Reduction in CD16 Expression after Vaccination Regulates NK Cell Function. Front Immunol 7, 384 (2016).
231. Nielsen, C. M. et al. Impaired NK Cell Responses to Pertussis and H1N1 Influenza Vaccine Antigens in Human Cytomegalovirus-Infected Individuals. J Immunol 194, 4657–4667 (2015).
232. Cerundolo, V., Silk, J. D., Masri, S. H. & Salio, M. Harnessing invariant NKT cells in vaccination strategies. Nat Rev Immunol 9, 28–38 (2009).
233. Hermans, I. F. et al. NKT Cells Enhance CD4+ and CD8+ T Cell Responses to Soluble Antigen In Vivo through Direct Interaction with Dendritic Cells. J Immunol 171, 5140–5147 (2003).
234. Inoue, A. et al. TGFα shedding assay: an accurate and versatile method for detecting GPCR activation. Nat Methods 9, 1021–1029 (2012).
235. Salio, M. et al. Activation of Human Mucosal-Associated Invariant T Cells Induces CD40L-Dependent Maturation of Monocyte-Derived and Primary Dendritic Cells. J Immunol 199, 2631–2638 (2017).
236. Ge, M. Q. et al. NK Cells Regulate CD8+ T Cell Priming and Dendritic Cell Migration during Influenza A Infection by IFN-γ and Perforin-Dependent Mechanisms. J Immunol 189, 2099–2109 (2012).
237. Geiben-Lynn, R., Greenland, J. R., Frimpong-Boateng, K. & Letvin, N. L. Non-classical Natural Killer T Cells Modulate Plasmid DNA Vaccine Antigen Expression and Vaccine-elicited Immune Responses by MCP-1 Secretion after Interaction with a β2-Microglobulin-independent CD1d*. J Biol Chem 284, 33800–33806 (2009).
238. Murayama, G. et al. A Critical Role for Mucosal-Associated Invariant T Cells as Regulators and Therapeutic Targets in Systemic Lupus Erythematosus. Front Immunol 10, 2681 (2019).
239. Rahman, M. A. et al. Mucosal-associated invariant T (MAIT) cells provide B-cell help in vaccinated and subsequently SIV-infected Rhesus Macaques. Sci Rep 10, 10060–17 (2020).
240. Tonti, E. et al. NKT-cell help to B lymphocytes can occur independently of cognate interaction. Blood 113, 370–376 (2009).
241. Rezende, R. M. et al. γδ T cells control humoral immune response by inducing T follicular helper cell differentiation. Nat Commun 9, 3151 (2018).
242. Jensen, O. et al. A subset of follicular helper-like MAIT cells can provide B cell help and support antibody production in the mucosa. Sci Immunol 7, eabe8931 (2022).
243. King, I. L. et al. Invariant natural killer T cells direct B cell responses to cognate lipid antigen in an IL-21-dependent manner. Nat Immunol 13, 44–50 (2011).
244. Chang, P.-P. et al. Identification of Bcl-6-dependent follicular helper NKT cells that provide cognate help for B cell responses. Nat Immunol 13, 35–43 (2012).
245. Leadbetter, E. A. et al. NK T cells provide lipid antigen-specific cognate help for B cells. Proc Natl Acad Sci U S A 105, 8339–8344 (2008).
246. Scanlon, S. T. et al. Airborne lipid antigens mobilize resident intravascular NKT cells to induce allergic airway inflammation. J Exp Med 208, 2113–2124 (2011).
247. Caccamo, N. et al. CXCR5 Identifies a Subset of Vγ9Vδ2 T Cells which Secrete IL-4 and IL-10 and Help B Cells for Antibody Production. J Immunol 177, 5290–5295 (2006).

248. Bansal, R. R., Mackay, C. R., Moser, B. & Eberl, M. IL-21 enhances the potential of human γδ T cells to provide B-cell help. Eur J Immunol 42, 110–119 (2012).
249. Gutierrez-Arcelus, M. et al. Lymphocyte innateness defined by transcriptional states reflects a balance between proliferation and effector functions. Nat Commun 10, 687 (2019).
250. Zhu, Y. et al. Lowering glycosphingolipid levels in CD4+ T cells attenuates T cell receptor signaling, cytokine production, and differentiation to the Th17 lineage. J Biol Chem 286, 14787–14794 (2011).
251. Yang, R. et al. Human T-bet Governs Innate and Innate-like Adaptive IFN-γ Immunity against Mycobacteria. Cell 183, 1826-1847.e31 (2020).
252. Trinchieri, G. Interleukin-12: A Proinflammatory Cytokine with Immunoregulatory Functions that Bridge Innate Resistance and Antigen-Specific Adaptive Immunity. Annu Rev Immunol 13, 251–276 (1995).
253. Kannan, Y. et al. IκBζ augments IL-12– and IL-18–mediated IFN-γ production in human NK cells. Blood 117, 2855–2863 (2011).
254. Suarez-Ramirez, J. E., Tarrio, M. L., Kim, K., Demers, D. A. & Biron, C. A. CD8 T cells in innate immune responses: using STAT4-dependent but antigen-independent pathways to gamma interferon during viral infection. MBio 5, e01978-14 (2014).
255. Matikainen, S. et al. IFN-α and IL-18 synergistically enhance IFN-γ production in human NK cells: differential regulation of Stat4 activation and IFN-γ gene expression by IFN-α and IL-12. Eur J Immunol 31, 2236–2245 (2001).
256. Maldonado, R. A., Irvine, D. J., Schreiber, R. & Glimcher, L. H. A role for the immunological synapse in lineage commitment of CD4 lymphocytes. Nature 431, 527–532 (2004).
257. Nakanishi, Y., Lu, B., Gerard, C. & Iwasaki, A. CD8+ T lymphocyte mobilization to virus-infected tissue requires CD4+ T-cell help. Nature 462, 510–513 (2009).
258. Soudja, S. M. et al. Memory-T-Cell-Derived Interferon-γ Instructs Potent Innate Cell Activation for Protective Immunity. Immunity 40, 974–988 (2014).
259. Eberl, G. & MacDonald, H. R. Selective induction of NK cell proliferation and cytotoxicity by activated NKT cells. Eur J Immunol 30, 985–992 (2000).
260. Eberl, G., Brawand, P. & MacDonald, H. R. Selective Bystander Proliferation of Memory CD4+ and CD8+ T Cells Upon NK T or T Cell Activation. J Immunol 165, 4305–4311 (2000).
261. Panitch, H. S., Hirsch, R. L., Schindler, J. & Johnson, K. P. Treatment of multiple sclerosis with gamma interferon Exacerbations associated with activation of the immune system. Neurology 37, 1097–1097 (1987).
262. Playfair, J. H. & Souza, J. B. D. Recombinant gamma interferon is a potent adjuvant for a malaria vaccine in mice. Clin Exp Immunol 67, 5–10 (1987).
263. Schijns, V. E. C. J., Weining, K. C., Nuijten, P., Rijke, E. O. & Staeheli, P. Immunoadjuvant activities of E. coli- and plasmid-expressed recombinant chicken IFN-α/β, IFN-γ and IL-1β in 1-day- and 3-week-old chickens. Vaccine 18, 2147–2154 (2000).
264. Schroder, K., Hertzog, P. J., Ravasi, T. & Hume, D. A. Interferon-γ: an overview of signals, mechanisms and functions. J Leukocyte Biol 75, 163–189 (2004).
265. Shtrichman, R. & Samuel, C. E. The role of gamma interferon in antimicrobial immunity. Curr Opin Microbiol 4, 251–259 (2001).
266. Biron, C. A. Interferons α and β as Immune Regulators—A New Look. Immunity 14, 661–664 (2001).
267. Gebhardt, T. et al. Memory T cells in nonlymphoid tissue that provide enhanced local immunity during infection with herpes simplex virus. Nat Immunol 10, 524–530 (2009).
268. Simoni, Y. et al. Human Innate Lymphoid Cell Subsets Possess Tissue-Type Based Heterogeneity in Phenotype and Frequency. Immunity 46, 148–161 (2017).

269. Veldhoen, M. Interleukin 17 is a chief orchestrator of immunity. Nat Immunol 18, 612–621 (2017).
270. Cua, D. J. & Tato, C. M. Innate IL-17-producing cells: The sentinels of the immune system. Nat Rev Immunol 10, 479–489 (2010).
271. Tang, X.-Z. et al. IL-7 licenses activation of human liver intrasinusoidal mucosal-associated invariant T cells. J Immunol 190, 3142–3152 (2013).
272. Slichter, C. K. et al. Distinct activation thresholds of human conventional and innate-like memory T cells. JCI Insight 1, e86292 (2016).
273. Schmaler, M. et al. Modulation of bacterial metabolism by the microenvironment controls MAIT cell stimulation. Mucosal Immunology 11, 1060–1070 (2018).
274. Ramsay, G. & Cantrell, D. Environmental and Metabolic Sensors That Control T Cell Biology. Front Immunol 6, 99 (2015).
275. Veldhoen, M. & Brucklacher-Waldert, V. Dietary influences on intestinal immunity. Nat Rev Immunol 12, 696–708 (2012).
276. Quintana, F. J. et al. Control of T(reg) and T(H)17 cell differentiation by the aryl hydrocarbon receptor. Nature 453, 65–71 (2008).
277. Rothhammer, V. & Quintana, F. J. The aryl hydrocarbon receptor: an environmental sensor integrating immune responses in health and disease. Nat Rev Immunol 19, 184–197 (2019).
278. Sobkowiak, M. J. et al. Tissue-resident MAIT cell populations in human oral mucosa exhibit an activated profile and produce IL-17. Eur J Immunol 49, 133–143 (2018).
279. Berkson, J. D. et al. Inflammatory Cytokines Induce Sustained CTLA-4 Cell Surface Expression on Human MAIT Cells. Immunohorizons 4, 14–22 (2020).
280. Booth, J. S. et al. Mucosal-Associated Invariant T Cells in the Human Gastric Mucosa and Blood: Role in Helicobacter pylori Infection. Front Immunol 6, 466 (2015).
281. D'Souza, C., Chen, Z. & Corbett, A. J. Revealing the protective and pathogenic potential of MAIT cells. Molecular Immunology 103, 46–54 (2018).
282. Leng, T. et al. TCR and Inflammatory Signals Tune Human MAIT Cells to Exert Specific Tissue Repair and Effector Functions. Cell Reports 28, 3077-3091.e5 (2019).
283. Cosgrove, C. et al. Early and nonreversible decrease of CD161++/MAIT cells in HIV infection. Blood 121, 951–961 (2013).
284. Leeansyah, E. et al. Activation, exhaustion, and persistent decline of the antimicrobial MR1-restricted MAIT-cell population in chronic HIV-1 infection. Blood 121, 1124–1135 (2013).
285. Leeansyah, E., Loh, L., Nixon, D. F. & Sandberg, J. K. Acquisition of innate-like microbial reactivity in mucosal tissues during human fetal MAIT-cell development. Nat Commun 5, 3143 (2014).
286. Hinks, T. S. C. Mucosal-associated invariant T cells in autoimmunity, immune-mediated diseases and airways disease. Immunology 148, 1–12 (2016).
287. Wong, E. B. et al. TRAV1-2+ CD8+ T-cells including oligoconal expansions of MAIT cells are enriched in the airways in human tuberculosis. Commun Biology 2, 203 (2019).
288. Mvaya, L. et al. Airway CD8+CD161++TCRvα7.2+ T Cell Depletion During Untreated HIV Infection Targets CD103 Expressing Cells. Front Immunol 10, 2003 (2019).
289. Lu, B. et al. IL-17 production by tissue-resident MAIT cells is locally induced in children with pneumonia. Mucosal Immunology 117, 1250 (2020).
290. Teunissen, M. B. M. et al. The IL-17A-producing CD8+ T-cell population in psoriatic lesional skin comprises mucosa-associated invariant T cells and conventional T cells. J Invest Dermatol 134, 2898–2907 (2014).
291. Dias, J. et al. The CD4-CD8- MAIT cell subpopulation is a functionally distinct subset developmentally related to the main CD8+ MAIT cell pool. Proc Natl Acad Sci U S A 5, 201812273-E11522 (2018).

292. Gibbs, A. et al. MAIT cells reside in the female genital mucosa and are biased towards IL-17 and IL-22 production in response to bacterial stimulation. Mucosal Immunol 10, 35–45 (2017).
293. Solders, M. et al. MAIT cells accumulate in placental intervillous space and display a highly cytotoxic phenotype upon bacterial stimulation. Sci Rep 7, 6123 (2017).
294. Iwasaki, A., Foxman, E. F. & Molony, R. D. Early local immune defences in the respiratory tract. Nat Rev Immunol 17, 7–20 (2017).
295. Dicks, M. D. J. et al. A novel chimpanzee adenovirus vector with low human seroprevalence: improved systems for vector derivation and comparative immunogenicity. PLoS One 7, e40385 (2012).
296. Maheshwari, G., Jannat, R., McCormick, L. & Hsu, D. Thermal inactivation of adenovirus type 5. J Virol Methods 118, 141–146 (2004).
297. Rauch, S., Jasny, E., Schmidt, K. E. & Petsch, B. New Vaccine Technologies to Combat Outbreak Situations. Front Immunol 9, 1963 (2018).
298. Folegatti, P. M. et al. Safety and immunogenicity of a candidate Middle East respiratory syndrome coronavirus viral-vectored vaccine: a dose-escalation, open-label, non-randomised, uncontrolled, phase 1 trial. Lancet Infect Dis 20, 816–826 (2020).
299. Voysey, M. et al. Single-dose administration and the influence of the timing of the booster dose on immunogenicity and efficacy of ChAdOx1 nCoV-19 (AZD1222) vaccine: a pooled analysis of four randomised trials. Lancet 397, 881–891 (2021).
300. Alter, G. et al. Immunogenicity of Ad26.COV2.S vaccine against SARS-CoV-2 variants in humans. Nature 596, 268–272 (2021).
301. Krammer, F. SARS-CoV-2 vaccines in development. Nature 586, 516–527 (2020).
302. Sadoff, J. et al. Interim Results of a Phase 1-2a Trial of Ad26.COV2.S Covid-19 Vaccine. N Engl J Med 384, 1824-1835 (2021).
303. Fausther-Bovendo, H. & Kobinger, G. P. Pre-existing immunity against Ad vectors. Hum Vaccin Immunother 10, 2875–2884 (2014).
304. Teigler, J. E., Iampietro, M. J. & Barouch, D. H. Vaccination with adenovirus serotypes 35, 26, and 48 elicits higher levels of innate cytokine responses than adenovirus serotype 5 in rhesus monkeys. J Virol 86, 9590–9598 (2012).
305. Kurioka, A., Klenerman, P. & Willberg, C. B. Innate-like CD8+ T-cells and NK cells: converging functions and phenotypes. Immunology 154, 547–556 (2018).
306. Wilgenburg, B. van et al. MAIT cells are activated during human viral infections. Nat Commun 7, 11653 (2016).
307. Cimini, E. et al. Interferon-α Improves Phosphoantigen-Induced Vγ9Vδ2 T-Cells Interferon-γ Production during Chronic HCV Infection. PLoS One 7, e37014 (2012).
308. Paget, C. et al. Potential Role of Invariant NKT Cells in the Control of Pulmonary Inflammation and CD8+ T Cell Response during Acute Influenza A Virus H3N2 Pneumonia. J Immunol 186, 5590–5602 (2011).
309. Farsakoglu, Y. et al. Influenza Vaccination Induces NK-Cell-Mediated Type-II IFN Response that Regulates Humoral Immunity in an IL-6-Dependent Manner. Cell Reports 26, 2307-2315.e5 (2019).
310. Dokun, A. O. et al. Specific and nonspecific NK cell activation during virus infection. Nat Immunol 2, 951–956 (2001).
311. Lee, H., Jeong, S. & Shin, E.-C. Significance of bystander T cell activation in microbial infection. Nat Immunol 23, 13–22 (2022).
312. Wang, H. et al. IL-23 costimulates antigen-specific MAIT cell activation and enables vaccination against bacterial infection. Sci Immunol 4, eaaw0402 (2019).
313. Wilson, R. P. et al. STAT3 is a critical cell-intrinsic regulator of human unconventional T cell numbers and function. J Exp Med 212, 855–864 (2015).
314. Ziblat, A. et al. Interleukin (IL)-23 Stimulates IFN-γ Secretion by CD56bright Natural Killer Cells and Enhances IL-18-Driven Dendritic Cells Activation. Front Immunol 8, 1959 (2018).

315. Moens, E. et al. IL-23R and TCR signaling drives the generation of neonatal Vγ9Vδ2 T cells expressing high levels of cytotoxic mediators and producing IFN-γ and IL-17. J Leukocyte Biol 89, 743–752 (2011).
316. Symons, J. A., Alcamí, A. & Smith, G. L. Vaccinia virus encodes a soluble type I interferon receptor of novel structure and broad species specificity. Cell 81, 551–560 (1995).
317. Zhang, Z. et al. The helicase DDX41 senses intracellular DNA mediated by the adaptor STING in dendritic cells. Nat Immunol 12, 959–965 (2011).
318. Miyagi, T. et al. High basal STAT4 balanced by STAT1 induction to control type 1 interferon effects in natural killer cells. J Exp Medicine 204, 2383–2396 (2007).
319. Lal, K. G. et al. Dynamic MAIT cell response with progressively enhanced innateness during acute HIV-1 infection. Nat Commun 11, 272–13 (2020).
320. Posseme, C. et al. Early IFNβ secretion determines variable downstream IL-12p70 responses upon TLR4 activation. Cell Reports 39, 110989–110989.
321. Grell, M. et al. The transmembrane form of tumor necrosis factor is the prime activating ligand of the 80 kDa tumor necrosis factor receptor. Cell 83, 793–802 (1995).
322. Bánki, Z. et al. Antibody opsonization enhances MAIT cell responsiveness to bacteria via a TNF-dependent mechanism. Immunol Cell Biol 97, 538–551 (2019).
323. He, X. et al. A TNFR2-Agonist Facilitates High Purity Expansion of Human Low Purity Treg Cells. PLoS One 11, e0156311 (2016).
324. Mitoma, H., Horiuchi, T., Tsukamoto, H. & Ueda, N. Molecular mechanisms of action of anti-TNF-α agents – Comparison among therapeutic TNF-α antagonists. Cytokine 101, 56–63 (2018).
325. Lamichhane, R. et al. TCR- or Cytokine-Activated CD8+ Mucosal-Associated Invariant T Cells Are Rapid Polyfunctional Effectors That Can Coordinate Immune Responses. Cell Reports 28, 3061-3076.e5 (2019).
326. Kawano, S. et al. TNFR2 Signaling Enhances Suppressive Abilities of Human Circulating T Follicular Regulatory Cells. J Immunol 208, 1057-1065 (2022).
327. Nguyen, M.-T., Schellerhoff, L. H., Niemann, S., Schaumburg, F. & Herrmann, M. Quiescence of Human Monocytes after Affinity Purification: A Novel Method Apt for Monocyte Stimulation Assays. Biomolecules 12, 395 (2022).
328. Kurioka, A. et al. MAIT cells are licensed through granzyme exchange to kill bacterially sensitized targets. Mucosal Immunology 8, 429–440 (2015).
329. Grell, M. Tumor necrosis factor (TNF) receptors in cellular signaling of soluble and membrane-expressed TNF. J Inflamm 47, 8–17 (1995).
330. Munich, S., Sobo-Vujanovic, A., Buchser, W. J., Beer-Stolz, D. & Vujanovic, N. L. Dendritic cell exosomes directly kill tumor cells and activate natural killer cells via TNF superfamily ligands. Oncoimmunology 1, 1074–1083 (2012).
331. Li, J. et al. Exosomes mediate the cell-to-cell transmission of IFN-α-induced antiviral activity. Nat Immunol 14, 793–803 (2013).
332. Trajkovic, K. et al. Ceramide triggers budding of exosome vesicles into multivesicular endosomes. Science 319, 1244–1247 (2008).
333. Li, X.-D. et al. Pivotal roles of cGAS-cGAMP signaling in antiviral defense and immune adjuvant effects. Science 341, 1390–1394 (2013).
334. Provine, N. M. et al. MAIT cell activation augments adenovirus vector vaccine immunogenicity. Science 371, 521–526 (2021).
335. Bennett, M. S., Trivedi, S., Iyer, A. S., Hale, J. S. & Leung, D. T. Human mucosal-associated invariant T (MAIT) cells possess capacity for B-cell help. J Leukoc Biol 102, 1261-1269 (2017).
336. Lamichhane, R. et al. Type I interferons are important co-stimulatory signals during T cell receptor mediated human MAIT cell activation. Eur J Immunol 50, 178–191 (2019).

337. Pavlovic, M., Gross, C., Chili, C., Secher, T. & Treiner, E. MAIT Cells Display a Specific Response to Type 1 IFN Underlying the Adjuvant Effect of TLR7/8 Ligands. Front Immunol 11, 2097 (2020).
338. Yang, Q. et al. Suppressive Monocytes Impair MAIT Cells Response via IL-10 in Patients with Severe COVID-19. J Immunol 207, 1848-1856 (2021).
339. Tang, X. et al. Sustained IFN-I stimulation impairs MAIT cell responses to bacteria by inducing IL-10 during chronic HIV-1 infection. Sci Adv 6, eaaz0374 (2020).
340. Loh, L. et al. Human mucosal-associated invariant T cells contribute to antiviral influenza immunity via IL-18-dependent activation. Proc Natl Acad Sci U S A 113, 10133–10138 (2016).
341. Ussher, J. E., Willberg, C. B. & Klenerman, P. MAIT cells and viruses. Immunol Cell Biol 96, 630–641 (2018).
342. Youngs, J. et al. Identification of immune correlates of fatal outcomes in critically ill COVID-19 patients. PLoS Pathog 17, e1009804 (2021).
343. Parrot, T. et al. MAIT cell activation and dynamics associated with COVID-19 disease severity. Sci Immunol 5, eabe1670 (2020).
344. Voillet, V. et al. Human MAIT cells exit peripheral tissues and recirculate via lymph in steady state conditions. JCI Insight 3, e98487 (2018).
345. Schaupp, L. et al. Microbiota-Induced Type I Interferons Instruct a Poised Basal State of Dendritic Cells. Cell 181, 1080-1096.e19 (2020).
346. Ahern, D. J. et al. A blood atlas of COVID-19 defines hallmarks of disease severity and specificity. Cell 185, 916-938.e58 (2022).
347. Nakahira, M. et al. An absolute requirement for STAT4 and a role for IFN-gamma as an amplifying factor in IL-12 induction of the functional IL-18 receptor complex. J Immunol 167, 1306–1312 (2001).
348. Curtsinger, J. M., Valenzuela, J. O., Agarwal, P., Lins, D. & Mescher, M. F. Type I IFNs provide a third signal to CD8 T cells to stimulate clonal expansion and differentiation. J Immunol 174, 4465–4469 (2005).
349. Weizman, O.-E. et al. ILC1 Confer Early Host Protection at Initial Sites of Viral Infection. Cell 171, 795-808.e12 (2017).
350. Lafont, V. et al. Specific signaling pathways triggered by IL-2 in human V gamma 9V delta 2 T cells: an amalgamation of NK and alpha beta T cell signaling. J Immunol 171, 5225–5232 (2003).
351. Yarilina, A., Park-Min, K.-H., Antoniv, T., Hu, X. & Ivashkiv, L. B. TNF activates an IRF1-dependent autocrine loop leading to sustained expression of chemokines and STAT1-dependent type I interferon-response genes. Nat Immunol 9, 378–387 (2008).
352. Chipuk, J. E. et al. Sphingolipid Metabolism Cooperates with BAK and BAX to Promote the Mitochondrial Pathway of Apoptosis. Cell 148, 988–1000 (2012).
353. Park, S. J. et al. Molecular mechanisms of biogenesis of apoptotic exosome-like vesicles and their roles as damage-associated molecular patterns. Proc Natl Acad Sci U S A 115, E11721–E11730 (2018).
354. Collignon, C. et al. Innate Immune Responses to Chimpanzee Adenovirus Vector 155 Vaccination in Mice and Monkeys. Front Immunol 11, 579872 (2020).
355. Sheerin, D., Dold, C., O'Connor, D., Pollard, A. J. & Rollier, C. S. Distinct patterns of whole blood transcriptional responses are induced in mice following immunisation with adenoviral and poxviral vector vaccines encoding the same antigen. BMC Genomics 22, 777 (2021).
356. Gao, Y., Majchrzak-Kita, B., Fish, E. N. & Gommerman, J. L. Dynamic accumulation of plasmacytoid dendritic cells in lymph nodes is regulated by interferon-β. Blood 114, 2623–2631 (2009).
357. Worgall, S., Wolff, G., Falck-Pedersen, E. & Crystal, R. G. Innate Immune Mechanisms Dominate Elimination of Adenoviral Vectors Following In Vivo Administration. Hum Gene Ther 8, 37–44 (1997).

358. Andrews, N. et al. Effectiveness of COVID-19 booster vaccines against COVID-19-related symptoms, hospitalization and death in England. Nat Med 28, 831-837 (2022).
359. Sahin, U. et al. COVID-19 vaccine BNT162b1 elicits human antibody and TH1 T cell responses. Nature 586, 594–599 (2020).
360. Zhang, Z. et al. Humoral and cellular immune memory to four COVID-19 vaccines. Cell 185, 2434-2451.e17 (2022).
361. Wei, J. et al. Antibody responses and correlates of protection in the general population after two doses of the ChAdOx1 or BNT162b2 vaccines. Nat Med 28, 1072-1082 (2022).
362. Tarke, A. et al. SARS-CoV-2 vaccination induces immunological T cell memory able to cross-recognize variants from Alpha to Omicron. Cell 185, 847-859.e11 (2022).
363. Payne, R. P. et al. Immunogenicity of standard and extended dosing intervals of BNT162b2 mRNA vaccine. Cell 184, 5699-5714.e11 (2021).
364. Hall, V. G. et al. Delayed-interval BNT162b2 mRNA COVID-19 vaccination enhances humoral immunity and induces robust T cell responses. Nat Immunol 23, 380-385 (2022).
365. Shaw, R. H. et al. Effect of priming interval on reactogenicity, peak immunological response, and waning after homologous and heterologous COVID-19 vaccine schedules: exploratory analyses of Com-COV, a randomised control trial. Lancet Respir Medicine 10, 1049-1060 (2022).
366. Baden, L. R. et al. Efficacy and Safety of the mRNA-1273 SARS-CoV-2 Vaccine. New Engl J Medicine 384, 403-416 (2020).
367. Polack, F. P. et al. Safety and Efficacy of the BNT162b2 mRNA Covid-19 Vaccine. N Engl J Med 383, 2603–2615 (2020).
368. Walsh, E. E. et al. Safety and Immunogenicity of Two RNA-Based Covid-19 Vaccine Candidates. N Engl J Med 383, 2439–2450 (2020).
369. Shaw, R. H. et al. Heterologous prime-boost COVID-19 vaccination: initial reactogenicity data. Lancet 397, 2043–2046 (2021).
370. Wong, H.-L. et al. Risk of myocarditis and pericarditis after the COVID-19 mRNA vaccination in the USA: a cohort study in claims databases. Lancet 399, 2191–2199 (2022).
371. Greinacher, A. et al. Thrombotic Thrombocytopenia after ChAdOx1 nCov-19 Vaccination. New Engl J Med 384, 2092–2101 (2021).
372. Simpson, C. R. et al. First-dose ChAdOx1 and BNT162b2 COVID-19 vaccines and thrombocytopenic, thromboembolic and hemorrhagic events in Scotland. Nat Med 27, 1290–1297 (2021).
373. Pillay, J. et al. Incidence, risk factors, natural history, and hypothesised mechanisms of myocarditis and pericarditis following covid-19 vaccination: living evidence syntheses and review. BMJ 13, e069445 (2022).
374. Anderson, E. M. et al. SARS-CoV-2 infections elicit higher levels of original antigenic sin antibodies compared with SARS-CoV-2 mRNA vaccinations. Cell Reports 41, 111496 (2022).
375. Lin, C.-Y. et al. Pre-existing humoral immunity to human common cold coronaviruses negatively impacts the protective SARS-CoV-2 antibody response. Cell Host Microbe 30, 83-96.e4 (2022).
376. Anderson, B. R. et al. Incorporation of pseudouridine into mRNA enhances translation by diminishing PKR activation. Nucleic Acids Res 38, 5884–5892 (2010).
377. Hensley, S. E., Giles-Davis, W., McCoy, K. C., Weninger, W. & Ertl, H. C. J. Dendritic cell maturation, but not CD8+ T cell induction, is dependent on type I IFN signaling during vaccination with adenovirus vectors. J Immunol 175, 6032–6041 (2005).
378. Temizoz, B. & Ishii, K. J. Type I and II interferons toward ideal vaccine and immunotherapy. Expert Rev Vaccines 20, 1–18 (2021).

379. Teijaro, J. R. & Farber, D. L. COVID-19 vaccines: modes of immune activation and future challenges. Nat Rev Immunol 21, 195–197 (2021).
380. Mulligan, M. J. et al. Phase I/II study of COVID-19 RNA vaccine BNT162b1 in adults. Nature 586, 589–593 (2020).
381. Vogel, A. B. et al. Immunogenic BNT162b vaccines protect rhesus macaques from SARS-CoV-2. Nature 592, 283-289 (2021).
382. Provine, N. M. et al. Adenovirus vectors activate Vδ2+ γδT cells in a type I interferon-, TNF-, and IL-18-dependent manner. Eur J Immunol 52, 835-837 (2022).
383. Ataide, M. A. et al. Lymphatic migration of unconventional T cells promotes site-specific immunity in distinct lymph nodes. Immunity 55, 1813-1828.e9 (2022).
384. Johnson, D. N. et al. Differential location of NKT and MAIT cells within lymphoid tissue. Sci Rep 12, 4034 (2022).
385. Dejnirattisai, W. et al. SARS-CoV-2 Omicron-B.1.1.529 leads to widespread escape from neutralizing antibody responses. Cell 185, 467-484.e15 (2022).
386. Skelly, D. T. et al. Two doses of SARS-CoV-2 vaccination induce robust immune responses to emerging SARS-CoV-2 variants of concern. Nat Commun 12, 5061 (2021).
387. Arunachalam, P. S. et al. Systems vaccinology of the BNT162b2 mRNA vaccine in humans. Nature 596, 410–416 (2021).
388. Greinacher, A. et al. Insights in ChAdOx1 nCov-19 Vaccine-induced Immune Thrombotic Thrombocytopenia (VITT). Blood 138, 2256–2268 (2021).
389. Toubal, A., Nel, I., Lotersztajn, S. & Lehuen, A. Mucosal-associated invariant T cells and disease. Nat Rev Immunol 178, 1–657 (2019).
390. Loyal, L. et al. Cross-reactive CD4+ T cells enhance SARS-CoV-2 immune responses upon infection and vaccination. Science 374, eabh1823 (2021).
391. Rodero, M. P. & Crow, Y. J. Type I interferon-mediated monogenic autoinflammation: The type I interferonopathies, a conceptual overview. J Exp Med 213, 2527–2538 (2016).
392. Tauzin, A. et al. Strong humoral immune responses against SARS-CoV-2 Spike after BNT162b2 mRNA vaccination with a 16-week interval between doses. Cell Host Microbe 30, 97-109.e5 (2022).
393. Nayrac, M. et al. Temporal associations of B and T cell immunity with robust vaccine responsiveness in a 16-week interval BNT162b2 regimen. Cell Reports 39, 111013–111013 (2022).
394. Schaack, J. et al. Strong foreign promoters contribute to innate inflammatory responses induced by adenovirus transducing vectors. Virology 412, 28–35 (2011).
395. Lokshin, A. E. et al. Differential regulation of maturation and apoptosis of human monocyte-derived dendritic cells mediated by MHC class II. Int Immunol 14, 1027–1037 (2002).
396. Qin, L. et al. Promoter Attenuation in Gene Therapy: Interferon- and Tumor Necrosis Factor- Inhibit Transgene Expression. Hum Gene Ther 8, 2019–2029 (1997).
397. Sung, R. S., Qin, L. & Bromberg, J. S. TNFα and IFNγ Induced by Innate Anti-adenoviral Immune Responses Inhibit Adenovirus-Mediated Transgene Expression. Mol Ther 3, 757–767 (2001).
398. Li, Y. et al. Bacteroides ovatus-mediated CD27− MAIT cell activation is associated with obesity-related T2D progression. Cell Mol Immunol 19, 791-804 (2022).
399. Baiersdörfer, M. et al. A Facile Method for the Removal of dsRNA Contaminant from In Vitro-Transcribed mRNA. Mol Ther Nucleic Acids 15, 26–35 (2019).
400. Karikó, K., Muramatsu, H., Ludwig, J. & Weissman, D. Generating the optimal mRNA for therapy: HPLC purification eliminates immune activation and improves translation of nucleoside-modified, protein-encoding mRNA. Nucleic Acids Res 39, e142–e142 (2011).
401. Rehwinkel, J. & Gack, M. U. RIG-I-like receptors: their regulation and roles in RNA sensing. Nat Rev Immunol 147, 258–15 (2020).

402. Hagan, T. et al. Transcriptional atlas of the human immune response to 13 vaccines reveals a common predictor of vaccine-induced antibody responses. Nat Immunol 23, 1788-1798 (2022).
403. Marchevsky, N. G. et al. An exploratory analysis of the response to ChAdOx1 nCoV-19 (AZD1222) vaccine in males and females. EBioMedicine 81, 104128 (2022).
404. Wilkinson, N. M., Chen, H.-C., Lechner, M. G. & Su, M. A. Sex Differences in Immunity. Annu Rev Immunol 40, 1–20 (2022).
405. Aaby, P. et al. The non-specific and sex-differential effects of vaccines. Nat Rev Immunol 20, 464–470 (2020).
406. Muir, K.-L., Kallam, A., Koepsell, S. A. & Gundabolu, K. Thrombotic Thrombocytopenia after Ad26.COV2.S Vaccination. New Engl J Med 384, 1964–1965 (2021).
407. Li, L. & Sherry, B. IFN-α expression and antiviral effects are subtype and cell type specific in the cardiac response to viral infection. Virology 396, 59–68 (2010).
408. Deutsch, M., Manesis, E. K., Hadziyannis, E., Vassilopoulos, D. & Archimandritis, A. J. Thrombotic thrombocytopenic purpura with fatal outcome in a patient with chronic hepatitis C treated with pegylated interferon-a/2b. Scand J Gastroenterol 42, 408–409 (2007).
409. Malekzadeh, M. M., Alizadeh, R., Aghsaeifard, Z. & Sahraian, M. A. Thrombotic Microangiopathy in Interferon-beta-Treated Multiple Sclerosis Patient. Clin Case Reports 8, 1061–1064 (2020).
410. Rönnblom, L. E., Alm, G. V. & Öberg, K. Autoimmune Phenomena in Patients with Malignant Carcinoid Tumors During Interferon-α Treatment. Acta Oncol 30, 537–540 (2009).
411. Theofilopoulos, A. N., Baccala, R., Beutler, B. & Kono, D. H. Type I Interferons (α/β) in Immunity and Autoimmunity. Annu Rev Immunol 23, 307–335 (2005).
412. Dumoulin, F. L., Leifeld, L., Sauerbruch, T. & Spengler, U. Autoimmunity induced by interferon-α therapy for chronic viral hepatitis. Biomed Pharmacother 53, 242–254 (1999).
413. Nguyen, K. B. et al. Critical role for STAT4 activation by type 1 interferons in the interferon-gamma response to viral infection. Science 297, 2063–2066 (2002).
414. Nguyen, K. B. et al. Coordinated and distinct roles for IFN-alpha beta, IL-12, and IL-15 regulation of NK cell responses to viral infection. J Immunol 169, 4279–4287 (2002).
415. Jiang, J., Cao, Z., Shan, W., Liu, H. & Cheng, X. 4-1BB expression on MAIT cells is associated with enhanced IFN-γ production and depends on IL-2. Cell Immunol 328, 58–69 (2018).
416. Sattler, A., Dang-Heine, C., Reinke, P. & Babel, N. IL-15 dependent induction of IL-18 secretion as a feedback mechanism controlling human MAIT-cell effector functions. Eur J Immunol 45, 2286–2298 (2015).
417. Tahtinen, S. et al. IL-1 and IL-1ra are key regulators of the inflammatory response to RNA vaccines. Nat Immunol 23, 532-542 (2022).
418. Guarda, G. et al. T cells dampen innate immune responses through inhibition of NLRP1 and NLRP3 inflammasomes. Nature 460, 269–273 (2009).
419. Bergamaschi, L. et al. Longitudinal analysis reveals that delayed bystander CD8+ T cell activation and early immune pathology distinguish severe COVID-19 from mild disease. Immunity 54, 1257-1275.e8 (2021).
420. Braun, J. et al. SARS-CoV-2-reactive T cells in healthy donors and patients with COVID-19. Nature 587, 270-274 (2020).
421. Grifoni, A. et al. Targets of T Cell Responses to SARS-CoV-2 Coronavirus in Humans with COVID-19 Disease and Unexposed Individuals. Cell 181, 1489-1501.e15 (2020).
422. Niessl, J., Sekine, T. & Buggert, M. T cell immunity to SARS-CoV-2. Semin Immunol 50, 101422 (2021).

423. Schulien, I. et al. Characterization of pre-existing and induced SARS-CoV-2-specific CD8+ T cells. Nat Med 27, 78–85 (2021).
424. Mateus, J. et al. Selective and cross-reactive SARS-CoV-2 T cell epitopes in unexposed humans. Science 370, 89-94 (2020).
425. Carnaud, C. et al. Cutting edge: Cross-talk between cells of the innate immune system: NKT cells rapidly activate NK cells. J Immunol 163, 4647–50 (1999).
426. Smyth, M. J. et al. Sequential production of interferon-γ by NK1.1+ T cells and natural killer cells is essential for the antimetastatic effect of α-galactosylceramide. Blood 99, 1259–1266 (2002).
427. Petley, E. V. et al. MAIT cells regulate NK cell-mediated tumor immunity. Nat Commun 12, 4746 (2021).
428. Gérard, A. et al. Secondary T cell-T cell synaptic interactions drive the differentiation of protective CD8+ T cells. Nat Immunol 14, 356–363 (2013).
429. Steimle, V., Siegrist, C.-A., Mottet, A., Lisowska-Grospierre, B. & Mach, B. Regulation of MHC Class II Expression by Interferon-γ Mediated by the Transactivator Gene CIITA. Science 265, 106–109 (1994).
430. Farrar, M. A. & Schreiber, R. D. The Molecular Cell Biology of Interferon-gamma and its Receptor. Annu Rev Immunol 11, 571–611 (1993).
431. Jackson, S. S., Schmitz, J. E. & Letvin, N. L. Anti-Gamma Interferon Antibodies Enhance the Immunogenicity of Recombinant Adenovirus Vectors. Clin Vaccine Immunol 18, 1969–1978 (2011).
432. Bansal, S. et al. Cutting Edge: Circulating Exosomes with COVID Spike Protein Are Induced by BNT162b2 (Pfizer–BioNTech) Vaccination prior to Development of Antibodies: A Novel Mechanism for Immune Activation by mRNA Vaccines. J Immunol 207, 2405-2410 (2021).
433. Wang, Z. et al. Exosomes decorated with a recombinant SARS-CoV-2 receptor-binding domain as an inhalable COVID-19 vaccine. Nat Biomed Eng 6, 791–805 (2022).
434. Lindenbergh, M. F. S. & Stoorvogel, W. Antigen Presentation by Extracellular Vesicles from Professional Antigen-Presenting Cells. Annu Rev Immunol 36, 1–25 (2018).
435. Cupovic, J. et al. Adenovirus vector vaccination reprograms pulmonary fibroblastic niches to support protective inflating memory CD8+ T cells. Nat Immunol 22, 1042–1051 (2021).
436. Tough, D. F., Zhang, X. & Sprent, J. An IFN-γ-Dependent Pathway Controls Stimulation of Memory Phenotype CD8+ T Cell Turnover In Vivo by IL-12, IL-18, and IFN-γ. J Immunol 166, 6007–6011 (2001).
437. Bhat, P., Leggatt, G., Waterhouse, N. & Frazer, I. H. Interferon-γ derived from cytotoxic lymphocytes directly enhances their motility and cytotoxicity. Cell Death Dis 8, e2836 (2017).
438. Eberl, M. et al. IL-18 potentiates the adjuvant properties of IL-12 in the induction of a strong Th1 type immune response against a recombinant antigen. Vaccine 18, 2002–2008 (2000).
439. Ryg-Cornejo, V. et al. Severe Malaria Infections Impair Germinal Center Responses by Inhibiting T Follicular Helper Cell Differentiation. Cell Reports 14, 68–81 (2016).
440. Iancovici, L. et al. Rheumatoid arthritis patients treated with Janus kinase inhibitors show reduced humoral immune responses following BNT162b2 vaccination. Rheumatology 61, keab879- (2021).
441. Ponsford, M. J. et al. COVID-19 Vaccine Uptake and Efficacy in a National Immunodeficiency Cohort. J Clin Immunol 42, 728–731 (2022).
442. Kelsen, S. G. et al. SARS-CoV-2 BNT162b2 vaccine–induced humoral response and reactogenicity in individuals with prior COVID-19 disease. JCI Insight 7, e155889 (2022).

443. Takano, T. et al. Distinct immune cell dynamics correlate with the immunogenicity and reactogenicity of SARS-CoV-2 mRNA vaccine. Cell Reports Medicine 3, 100631 (2022).
444. Cari, L., Fiore, P., Alhosseini, M. N., Sava, G. & Nocentini, G. Blood clots and bleeding events following BNT162b2 and ChAdOx1 nCoV-19 vaccine: An analysis of European data. J Autoimmun 122, 102685 (2021).
445. Goddard, K. et al. Incidence of Myocarditis/Pericarditis Following mRNA COVID-19 Vaccination Among Children and Younger Adults in the United States. Ann Intern Med 175, 1169-1771 (2022).
446. Patone, M. et al. Risks of myocarditis, pericarditis, and cardiac arrhythmias associated with COVID-19 vaccination or SARS-CoV-2 infection. Nat Med 28, 410–422 (2021).
447. Weintraub, E. S., Oster, M. E. & Klein, N. P. Myocarditis or Pericarditis Following mRNA COVID-19 Vaccination. Jama Netw Open 5, e2218512 (2022).
448. Cosper, P. F., Harvey, P. A. & Leinwand, L. A. Interferon-γ Causes Cardiac Myocyte Atrophy via Selective Degradation of Myosin Heavy Chain in a Model of Chronic Myocarditis. Am J Pathology 181, 2038–2046 (2012).
449. Reifenberg, K. et al. Interferon-γ Induces Chronic Active Myocarditis and Cardiomyopathy in Transgenic Mice. Am J Pathology 171, 463–472 (2007).
450. Tsang, J. S. et al. Global Analyses of Human Immune Variation Reveal Baseline Predictors of Postvaccination Responses. Cell 157, 499–513 (2014).
451. Boulouis, C. et al. MAIT cell compartment characteristics are associated with the immune response magnitude to the BNT162b2 mRNA anti-SARS-CoV-2 vaccine. Mol Med 28, 54 (2022).
452. Bergamaschi, C. et al. Systemic IL-15, IFN-γ, and IP-10/CXCL10 signature associated with effective immune response to SARS-CoV-2 in BNT162b2 mRNA vaccine recipients. Cell Reports 36, 109504 (2021).
453. Atmar, R. L. et al. Homologous and Heterologous Covid-19 Booster Vaccinations. New Engl J Med 386, 1046–1057 (2022).
454. Collier, A. Y. et al. Differential Kinetics of Immune Responses Elicited by Covid-19 Vaccines. New Engl J Medicine 385, 2010-2012 (2021).
455. Gao, Y. et al. Immunodeficiency syndromes differentially impact the functional spectrum of SARS-CoV-2-specific T cells elicited by mRNA vaccination. Immunity 55, 1732-1746.e5 (2022).
456. Sanchez, S., Palacio, N., Dangi, T., Ciucci, T. & Penaloza-MacMaster, P. Fractionating a COVID-19 Ad5-vectored vaccine improves virus-specific immunity. Sci Immunol 6, eabi8635 (2021).
457. Hagin, D. et al. Immunogenicity of Pfizer-BioNTech COVID-19 vaccine in patients with inborn errors of immunity. J Allergy Clin Immun 148, 739–749 (2021).
458. Galmiche, S. et al. Immunological and clinical efficacy of COVID-19 vaccines in immunocompromised populations: a systematic review. Clin Microbiol Infec 28, 163–177 (2022).
459. Winthrop, K. L. et al. The effect of tofacitinib on pneumococcal and influenza vaccine responses in rheumatoid arthritis. Ann Rheum Dis 75, 687 (2016).
460. Lee, C. K. et al. Patients with Crohn's disease on anti-tumor necrosis factor therapy are at significant risk of inadequate response to the 23-valent pneumococcal polysaccharide vaccine. J Crohn's Colitis 8, 384–391 (2014).
461. Hagihara, Y. et al. Infliximab and/or immunomodulators inhibit immune responses to trivalent influenza vaccination in adults with inflammatory bowel disease. J Crohn's Colitis 8, 223–233 (2014).
462. Mamula, P. et al. Immune Response to Influenza Vaccine in Pediatric Patients With Inflammatory Bowel Disease. Clin Gastroenterol H 5, 851–856 (2007).
463. Park, S.-H. & Rehermann, B. Immune Responses to HCV and Other Hepatitis Viruses. Immunity 40, 13–24 (2014).

464. Pratt, P. K. et al. Antibody Response to Hepatitis B Virus Vaccine is Impaired in Patients With Inflammatory Bowel Disease on Infliximab Therapy. Inflamm Bowel Dis 24, 380–386 (2018).
465. Wyant, T. et al. Vedolizumab affects antibody responses to immunisation selectively in the gastrointestinal tract: randomised controlled trial results. Gut 64, 77 (2015).
466. Kennedy, N. A. et al. Anti-SARS-CoV-2 antibody responses are attenuated in patients with IBD treated with infliximab. Gut 70, 865–875 (2021).
467. Kennedy, N. A. et al. Infliximab is associated with attenuated immunogenicity to BNT162b2 and ChAdOx1 nCoV-19 SARS-CoV-2 vaccines in patients with IBD. Gut 70, 1884–1893 (2021).
468. Chanchlani, N. et al. Adalimumab and infliximab impair SARS-CoV-2 antibody responses: results from a therapeutic drug monitoring study in 11422 biologic-treated patients. J Crohn's Colitis 16, 389-397 (2021).
469. Alexander, J. L. et al. COVID-19 vaccine-induced antibody and T-cell responses in immunosuppressed patients with inflammatory bowel disease after the third vaccine dose (VIP): a multicentre, prospective, case-control study. Lancet Gastroenterology Hepatology 7, 342-352 (2022).
470. Edelman-Klapper, H. et al. Lower Serologic Response to COVID-19 mRNA Vaccine in Patients With Inflammatory Bowel Diseases Treated With Anti-TNFα. Gastroenterology 162, 454–467 (2022).
471. Rabinowitz, K. M. et al. Anti-TNFα Treatment Impairs Long-Term Immune Responses to COVID-19 mRNA Vaccine in Patients with Inflammatory Bowel Diseases. Nato Adv Sci Inst Se 10, 1186 (2022).
472. Lin, S. et al. Antibody decay, T cell immunity and breakthrough infections following two SARS-CoV-2 vaccine doses in inflammatory bowel disease patients treated with infliximab and vedolizumab. Nat Commun 13, 1379 (2022).
473. Botwin, G. J. et al. Adverse Events After SARS-CoV-2 mRNA Vaccination Among Patients With Inflammatory Bowel Disease. Am J Gastroenterology 116, 1746–1751 (2021).
474. Yang, A. C. et al. A human brain vascular atlas reveals diverse mediators of Alzheimer's risk. Nature 603, 885-892 (2022).
475. Haga, K. et al. MAIT cells are activated and accumulated in the inflamed mucosa of ulcerative colitis. J Gastroen Hepatol 31, 965–972 (2016).
476. Serriari, N. -E. et al. Innate mucosal-associated invariant T (MAIT) cells are activated in inflammatory bowel diseases. Clin Exp Immunol 176, 266–274 (2014).
477. Andrlová, H. et al. MAIT and Vδ2 unconventional T cells are supported by a diverse intestinal microbiome and correlate with favorable patient outcome after allogeneic HCT. Sci Transl Med 14, eabj2829 (2022).
478. Söderström, K. et al. Increased frequency of abnormal gamma delta T cells in blood of patients with inflammatory bowel diseases. J Immunol 156, 2331–9 (1996).
479. Giacomelli, R. et al. Increase of circulating γ/δ T lymphocytes in the peripheral blood of patients affected by active inflammatory bowel disease. Clin Exp Immunol 98, 83–88 (1994).
480. Kelsen, J. et al. Infliximab Induces Clonal Expansion of γδ-T Cells in Crohn's Disease: A Predictor of Lymphoma Risk? PLoS One 6, e17890 (2011).
481. Gracey, E., Qaiyum, Z., Kuruvilla, J. & Inman, R. D. Gamma Delta T Cell Subset V Gamma 2+ Expansion Associated with Longterm Infliximab Treatment in a Patient with Ankylosing Spondylitis. J Rheumatology 43, 2079–2082 (2016).
482. Mavragani, C. P. et al. Type I and II Interferon Signatures Can Predict the Response to Anti-TNF Agents in Inflammatory Bowel Disease Patients: Involvement of the Microbiota. Inflamm Bowel Dis 26, 1543–1553 (2020).
483. Andreou, N.-P., Legaki, E. & Gazouli, M. Inflammatory bowel disease pathobiology: the role of the interferon signature. Ann Gastroenterology 33, 125–133 (2020).

484. Psarras, A. et al. TNF-α Regulates Human Plasmacytoid Dendritic Cells by Suppressing IFN-α Production and Enhancing T Cell Activation. J Immunol 206, 785-796 (2021).
485. Kelsen, J., Dige, A., Christensen, M., D'Amore, F. & Iversen, L. Frequency and clonality of peripheral γδ T cells in psoriasis patients receiving anti-tumour necrosis factor-α therapy. Clin Exp Immunol 177, 142–148 (2014).
486. Li, H., Luo, K. & Pauza, C. D. TNF-α Is a Positive Regulatory Factor for Human Vγ2Vδ2 T Cells. J Immunol 181, 7131–7137 (2008).
487. Williams, E. L., Gadola, S. & Edwards, C. J. Anti-TNF-induced lupus. Rheumatology 48, 716–720 (2009).
488. Conrad, C. et al. TNF blockade induces a dysregulated type I interferon response without autoimmunity in paradoxical psoriasis. Nat Commun 9, 25 (2018).
489. Sharma, D., Malik, A., Guy, C., Vogel, P. & Kanneganti, T.-D. TNF/TNFR axis promotes pyrin inflammasome activation and distinctly modulates pyrin inflammasomopathy. J Clin Invest 129, 150–162 (2019).
490. Malireddi, R. K. S. & Kanneganti, T.-D. Role of type I interferons in inflammasome activation, cell death, and disease during microbial infection. Front Cell Infect Mi 3, 77 (2013).
491. Qui, M. et al. Favorable vaccine-induced SARS-CoV-2 specific T cell response profile in patients undergoing immune-modifying therapies. J Clin Invest 132, e159500 (2022).
492. Pasparakis, M., Alexopoulou, L., Episkopou, V. & Kollias, G. Immune and inflammatory responses in TNF alpha-deficient mice: a critical requirement for TNF alpha in the formation of primary B cell follicles, follicular dendritic cell networks and germinal centers, and in the maturation of the humoral immune response. J Exp Medicine 184, 1397–1411 (1996).
493. Suresh, M., Singh, A. & Fischer, C. Role of tumor necrosis factor receptors in regulating CD8 T-cell responses during acute lymphocytic choriomeningitis virus infection. J Virol 79, 202–213 (2005).
494. Salinas, G. F. et al. Anti-TNF treatment blocks the induction of T cell-dependent humoral responses. Ann Rheum Dis 72, 1037 (2013).
495. Miyazaki, K. et al. Gene expression profiling of peripheral T-cell lymphoma including γδ T-cell lymphoma. Blood 113, 1071–1074 (2009).
496. Shale, M., Kanfer, E., Panaccione, R. & Ghosh, S. Hepatosplenic T cell lymphoma in inflammatory bowel disease. Gut 57, 1639 (2008).
497. Belkaid, Y. & Segre, J. A. Dialogue between skin microbiota and immunity. Science 346, 954–959 (2014).
498. Chen, Y. E., Fischbach, M. A. & Belkaid, Y. Skin microbiota-host interactions. Nature 553, 427–436 (2018).
499. Solis, A. G. et al. Mechanosensation of cyclical force by PIEZO1 is essential for innate immunity. Nature 78, 630 (2019).
500. Buck, M. D., O'Sullivan, D. & Pearce, E. L. T cell metabolism drives immunity. J Exp Med 212, 1345–1360 (2015).
501. MacIver, N. J., Michalek, R. D. & Rathmell, J. C. Metabolic Regulation of T Lymphocytes. Immunology 31, 259–283 (2013).
502. Chapman, N. M., Boothby, M. R. & Chi, H. Metabolic coordination of T cell quiescence and activation. Nat Rev Immunol 20, 55–70 (2020).
503. Zinser, M. E. et al. Human MAIT cells show metabolic quiescence with rapid glucose-dependent upregulation of granzyme B upon stimulation. Immunol Cell Biol 96, 666–674 (2018).
504. O'Brien, A. et al. Obesity Reduces mTORC1 Activity in Mucosal-Associated Invariant T Cells, Driving Defective Metabolic and Functional Responses. J Immunol 202, 3404–3411 (2019).

505. Bulitta, B. et al. Proteomic definition of human mucosal-associated invariant T cells determines their unique molecular effector phenotype. Eur J Immunol 48, 1336–1349 (2018).
506. Atarashi, K. et al. ATP drives lamina propria T(H)17 cell differentiation. Nature 455, 808–812 (2008).
507. Hubert, S. et al. Extracellular NAD+ shapes the Foxp3+ regulatory T cell compartment through the ART2-P2X7 pathway. J Exp Med 207, 2561–2568 (2010).
508. Bovens, A. A. et al. Murine iNKT cells are depleted by liver damage via activation of P2RX7. Eur J Immunol 50, 1515–1524 (2020).
509. Belkaid, Y. & Tamoutounour, S. The influence of skin microorganisms on cutaneous immunity. Nat Rev Immunol 16, 353–366 (2016).
510. Naik, S. et al. Compartmentalized control of skin immunity by resident commensals. Science 337, 1115–1119 (2012).
511. Kennedy, E. A., King, K. Y. & Baldridge, M. T. Mouse Microbiota Models: Comparing Germ-Free Mice and Antibiotics Treatment as Tools for Modifying Gut Bacteria. Front Physiol 9, 1534 (2018).
512. Beura, L. K. et al. Normalizing the environment recapitulates adult human immune traits in laboratory mice. Nature 532, 512–516 (2016).
513. Zaid, A. et al. Persistence of skin-resident memory T cells within an epidermal niche. Proc Natl Acad Sci U S A 111, 5307–5312 (2014).
514. Medzhitov, R. Origin and physiological roles of inflammation. Nature 454, 428–435 (2008).
515. Haas, R., Marelli-Berg, F. & Mauro, C. In the eye of the storm: T cell behavior in the inflammatory microenvironment. Am J Clin Exp Immunol 2, 146–55 (2013).
516. Chen, G. et al. Exosomal PD-L1 contributes to immunosuppression and is associated with anti-PD-1 response. Nature 560, 382–386 (2018).
517. Colgan, S. P., Furuta, G. T. & Taylor, C. T. Hypoxia and Innate Immunity: Keeping Up with the HIFsters. Annu Rev Immunol 38, 1–23 (2020).
518. Doedens, A. L. et al. Hypoxia-inducible factors enhance the effector responses of CD8(+) T cells to persistent antigen. Nat Immunol 14, 1173–1182 (2013).
519. Lee, J. S. et al. Interleukin-23-Independent IL-17 Production Regulates Intestinal Epithelial Permeability. Immunity 43, 727–738 (2015).
520. Westendorf, A. M. et al. Hypoxia Enhances Immunosuppression by Inhibiting CD4+ Effector T Cell Function and Promoting Treg Activity. Cell Physiol Biochem 41, 1271–1284 (2017).
521. Dang, E. V. et al. Control of TH17/Treg Balance by Hypoxia-Inducible Factor 1. Cell 146, 772–784 (2011).
522. Shi, L. Z. et al. HIF1alpha-dependent glycolytic pathway orchestrates a metabolic checkpoint for the differentiation of TH17 and Treg cells. J Exp Med 208, 1367–1376 (2011).
523. Pattison, L. A., Callejo, G. & Smith, E. S. J. Evolution of acid nociception: ion channels and receptors for detecting acid. Philos Trans R Soc Lond B Biol Sci 374, 20190291 (2019).
524. Ihara, Y. et al. The G protein-coupled receptor T-cell death-associated gene 8 (TDAG8) facilitates tumor development by serving as an extracellular pH sensor. Proc Natl Acad Sci U S A 107, 17309–17314 (2010).
525. Ciofani, M. et al. A Validated Regulatory Network for Th17 Cell Specification. Cell 151, 289–303 (2012).
526. Gaublomme, J. T. et al. Single-Cell Genomics Unveils Critical Regulators of Th17 Cell Pathogenicity. Cell 163, 1400–1412 (2015).
527. Wirasinha, R. C. et al. GPR65 inhibits experimental autoimmune encephalomyelitis through CD4+ T cell independent mechanisms that include effects on iNKT cells. Immunol Cell Biol 96, 128–136 (2018).

528. Haas, R. et al. Lactate Regulates Metabolic and Pro-inflammatory Circuits in Control of T Cell Migration and Effector Functions. PLoS Biol 13, e1002202 (2015).
529. Pucino, V. et al. Lactate Buildup at the Site of Chronic Inflammation Promotes Disease by Inducing CD4+ T Cell Metabolic Rewiring. Cell Metab 30, 1055-1074.e8 (2019).
530. Pucino, V., Bombardieri, M., Pitzalis, C. & Mauro, C. Lactate at the crossroads of metabolism, inflammation, and autoimmunity. Eur J Immunol 47, 14–21 (2017).
531. Kumar, A. et al. NF-κB Protects NKT Cells from Tumor Necrosis Factor Receptor 1-induced Death. Sci Rep 7, 15594 (2017).
532. Shime, H. et al. Tumor-secreted lactic acid promotes IL-23/IL-17 proinflammatory pathway. J Immunol 180, 7175–7183 (2008).
533. Witkin, S. S., Alvi, S., Bongiovanni, A. M., Linhares, I. M. & Ledger, W. J. Lactic acid stimulates interleukin-23 production by peripheral blood mononuclear cells exposed to bacterial lipopolysaccharide. FEMS Immunol Medical Microbiol 61, 153–158 (2011).
534. Hanson, D. F. Fever and the immune response. The effects of physiological temperatures on primary murine splenic T-cell responses in vitro. J Immunol 151, 436–448 (1993).
535. Smith, J. B., Knowlton, R. P. & Agarwal, S. S. Human lymphocyte responses are enhanced by culture at 40 degrees C. J Immunol 121, 691–694 (1978).
536. Zynda, E. R. et al. A role for the thermal environment in defining co-stimulation requirements for CD4+ T cell activation. Cell Cycle 14, 2340–2354 (2015).
537. Mace, T. A. et al. Differentiation of CD8+ T cells into effector cells is enhanced by physiological range hyperthermia. J Leukoc Biol 90, 951–962 (2011).
538. Wang, X. et al. Artemisinin inhibits the replication of flaviviruses by promoting the type I interferon production. Antivir Res 179, 104810 (2020).
539. Wang, H. et al. MAIT cells protect against pulmonary Legionella longbeachae infection. Nat Commun 9, 3350 (2018).
540. Hassane, M. et al. Interleukin-7 protects against bacterial respiratory infection by promoting IL-17A-producing innate T-cell response. Mucosal Immunology 13, 128–139 (2020).
541. Eil, R. et al. Ionic immune suppression within the tumour microenvironment limits T cell effector function. Nature 537, 539–543 (2016).
542. Kopp, C. et al. 23Na Magnetic Resonance Imaging-Determined Tissue Sodium in Healthy Subjects and Hypertensive Patients. Hypertension 61, 635–640 (2013).
543. Wu, J. et al. Cyclic GMP-AMP is an endogenous second messenger in innate immune signaling by cytosolic DNA. Science 339, 826–830 (2013).
544. Kleinewietfeld, M. et al. Sodium chloride drives autoimmune disease by the induction of pathogenic TH17 cells. Nature 496, 518–522 (2013).
545. Hernandez, A. L. et al. Sodium chloride inhibits the suppressive function of FOXP3+ regulatory T cells. J Clin Invest 125, 4212–4222 (2015).
546. Yang, A. C. et al. Physiological blood-brain transport is impaired with age by a shift in transcytosis. Nature 19, 1584–6 (2020).
547. Matthias, J. et al. Sodium chloride is an ionic checkpoint for human TH2 cells and shapes the atopic skin microenvironment. Sci Transl Med 11, eaau0683 (2019).
548. Ip, W. K. E. & Medzhitov, R. Macrophages monitor tissue osmolarity and induce inflammatory response through NLRP3 and NLRC4 inflammasome activation. Nat Commun 6, 6931 (2015).
549. Yi, B. et al. Effects of dietary salt levels on monocytic cells and immune responses in healthy human subjects: a longitudinal study. Transl Res 166, 103–110 (2015).
550. Casey, J. R., Grinstein, S. & Orlowski, J. Sensors and regulators of intracellular pH. Nat Rev Mol Cell Biol 11, 50–61 (2010).
551. Boron, W. F., Chen, L. & Parker, M. D. Modular structure of sodium-coupled bicarbonate transporters. J Exp Biol 212, 1697–1706 (2009).

552. Wang, C.-Z., Yano, H., Nagashima, K. & Seino, S. The Na+-driven Cl-/HCO3- exchanger. Cloning, tissue distribution, and functional characterization. J Biol Chem 275, 35486–35490 (2000).
553. Giffard, R. G., Lee, Y., Ouyang, Y., Murphy, S. L. & Monyer, H. Two variants of the rat brain sodium-driven chloride bicarbonate exchanger (NCBE): developmental expression and addition of a PDZ motif. Eur J Neurosci 18, 2935–2945 (2003).
554. Damkier, H. H., Aalkjaer, C. & Praetorius, J. Na+-dependent HCO3− Import by the slc4a10 Gene Product Involves Cl− Export. J Biol Chem 27, 26998–27007 (2010).
555. Jacobs, S. et al. Mice with targeted Slc4a10 gene disruption have small brain ventricles and show reduced neuronal excitability. Proc Natl Acad Sci U S A 105, 311–316 (2008).
556. Chen, X. et al. Cutting edge: expression of TNFR2 defines a maximally suppressive subset of mouse CD4+CD25+FoxP3+ T regulatory cells: applicability to tumor-infiltrating T regulatory cells. J Immunol 180, 6467–6471 (2008).
557. Hilgen, G. et al. Lack of the sodium-driven chloride bicarbonate exchanger NCBE impairs visual function in the mouse retina. PLoS One 7, e46155 (2012).
558. Parker, M. D. et al. Characterization of Human SLC4A10 as an Electroneutral Na/HCO3 Cotransporter (NBCn2) with Cl– Self-exchange Activity. J Biol Chem 283, 12777–12788 (2008).
559. Gurnett, C. A. et al. Disruption of Sodium Bicarbonate Transporter SLC4A10 in a Patient With Complex Partial Epilepsy and Mental Retardation. Arch Neurol-chicago 65, 550–553 (2008).
560. Belengeanu, V. et al. A de novo 2.3Mb deletion in 2q24.2q24.3 in a 20-month-old developmentally delayed girl. Gene 539, 168–172 (2014).
561. Krepischi, A. C. V. et al. Two distinct regions in 2q24.2-q24.3 associated with idiopathic epilepsy. Epilepsia 51, 2457–2460 (2010).
562. Böger, C. A. et al. NFAT5 and SLC4A10 Loci Associate with Plasma Osmolality. J Am Soc Nephrol 28, 2311–2321 (2017).
563. Pilling, L. C. et al. Gene expression markers of age-related inflammation in two human cohorts. Exp Gerontol 70, 37–45 (2015).
564. Smeland, O. B. et al. Genetic Overlap Between Schizophrenia and Volumes of Hippocampus, Putamen, and Intracranial Volume Indicates Shared Molecular Genetic Mechanisms. Schizophrenia Bull 44, 854–864 (2017).
565. Pourhaghighi, R. et al. BraInMap Elucidates the Macromolecular Connectivity Landscape of Mammalian Brain. Cell Syst 10, 333-350.e14 (2020).
566. Billerbeck, E. et al. Analysis of CD161 expression on human CD8+ T cells defines a distinct functional subset with tissue-homing properties. Proc Natl Acad Sci U S A 107, 3006–3011 (2010).
567. Huang, H. et al. Select sequencing of clonally expanded CD8+ T cells reveals limits to clonal expansion. Proc Natl Acad Sci U S A 116, 8995–9001 (2019).
568. Elmentaite, R. et al. Cells of the human intestinal tract mapped across space and time. Nature 597, 250–255 (2021).
569. Thomas, J. A., Buchsbaum, R. N., Zimniak, A. & Racker, E. Intracellular pH measurements in Ehrlich ascites tumor cells utilizing spectroscopic probes generated in situ. Biochemistry-us 18, 2210–2218 (1979).
570. Cole, S. et al. Interleukin (IL)-12 and IL-18 Synergize to Promote MAIT Cell IL-17A and IL-17F Production Independently of IL-23 Signaling. Front Immunol 11, 585134 (2020).
571. Hinks, T. S. C. et al. Activation and In Vivo Evolution of the MAIT Cell Transcriptome in Mice and Humans Reveals Tissue Repair Functionality. Cell Reports 28, 3249-3262.e5 (2019).
572. Wu, J. et al. T Cell Factor 1 Suppresses CD103+ Lung Tissue-Resident Memory T Cell Development. Cell Reports 31, 107484 (2020).

573. Müller, D. N., Wilck, N., Haase, S., Kleinewietfeld, M. & Linker, R. A. Sodium in the microenvironment regulates immune responses and tissue homeostasis. Nat Rev Immunol 19, 243–254 (2019).
574. Gough, D. J., Messina, N. L., Clarke, C. J. P., Johnstone, R. W. & Levy, D. E. Constitutive Type I Interferon Modulates Homeostatic Balance through Tonic Signaling. Immunity 36, 166–174 (2012).
575. Domizio, J. D. et al. The commensal skin microbiota triggers type I IFN-dependent innate repair responses in injured skin. Nat Immunol 17, 763–12 (2020).
576. Lynn, D. J., Benson, S. C., Lynn, M. A. & Pulendran, B. Modulation of immune responses to vaccination by the microbiota: implications and potential mechanisms. Nat Rev Immunol 22, 33–46 (2022).
577. Benedetti, F. D., Prencipe, G., Bracaglia, C., Marasco, E. & Grom, A. A. Targeting interferon-γ in hyperinflammation: opportunities and challenges. Nat Rev Rheumatol 17, 678–691 (2021).
578. Cuapio, A. et al. NK cell frequencies, function and correlates to vaccine outcome in BNT162b2 mRNA anti-SARS-CoV-2 vaccinated healthy and immunocompromised individuals. Mol Med 28, 20 (2022).
579. McNerney, K. O., DiNofia, A. M., Teachey, D. T., Grupp, S. A. & Maude, S. L. Potential Role of IFNγ Inhibition in Refractory Cytokine Release Syndrome Associated with CAR T-cell Therapy. Blood Cancer Discov 3, 90–94 (2022).
580. Luoma, A. M. et al. Molecular Pathways of Colon Inflammation Induced by Cancer Immunotherapy. Cell 182, 655-671.e22 (2020).
581. Sasson, S. C. et al. Mucosal-associated invariant T (MAIT) cells are activated in the gastrointestinal tissue of patients with combination ipilimumab and nivolumab therapy-related colitis in a pathology distinct from ulcerative colitis. Clin Exp Immunol 202, 335–352 (2020).
582. Constantinides, M. G. et al. MAIT cells are imprinted by the microbiota in early life and promote tissue repair. Science 366, (2019).
583. Olszak, T. et al. Microbial exposure during early life has persistent effects on natural killer T cell function. Science 336, 489–493 (2012).
584. Howson, L. J. et al. Absence of mucosal-associated invariant T cells in a person with a homozygous point mutation in MR1. Sci Immunol 5, eabc9492 (2020).
585. Gherardin, N. A. et al. Human blood MAIT cell subsets defined using MR1 tetramers. Immunol Cell Biol 96, 507–525 (2018).
586. Youssef, G. B. et al. Ontogeny of human mucosal-associated invariant T cells and related T cell subsets. J Exp Med 215, 459–479 (2018).
587. Wimmers, F. et al. The single-cell epigenomic and transcriptional landscape of immunity to influenza vaccination. Cell 184, 3915-3935.e21 (2021).
588. Sun, J.C. et al. Proinflammatory cytokine signaling required for the generation of natural killer cell memory. J Exp Med 209, 947–954 (2012).
589. Sun, J.C. et al. Adaptive immune features of natural killer cells. Nature 457, 557-561 (2009).
590. Walk, J. et al. Outcomes of controlled human malaria infection after BCG vaccination. Nat Commun 10, 874 (2019).
591. Schlums, H. et al. Cytomegalovirus infection drives adaptive epigenetic diversification of NK cells with altered signaling and effector function. Immunity 42, 443–456 (2015).
592. Uhl, F. M. et al. Metabolic reprogramming of donor T cells enhances graft-versus-leukemia effects in mice and humans. Sci Transl Med 12, eabb8969 (2020).
593. Sokal, A. et al. Human type I IFN deficiency does not impair B cell response to SARS-CoV-2 mRNA vaccination. J Exp Med 220, e20220258 (2022).
594. Zhang, Q. et al. Human genetic and immunological determinants of critical COVID-19 pneumonia. Nature 603, 587–598 (2022).

595. Agerholm, R., Kadekar, D., Rizk, J. & Bekiaris, V. Type I interferon supports γδ T-cell homeostasis and immunity through direct and indirect receptor signaling in mice. Eur J Immunol 51, 3186–3193 (2021).
596. Bogunovic, D. et al. Mycobacterial disease and impaired IFN-γ immunity in humans with inherited ISG15 deficiency. Science 337, 1684–1688 (2012).

9 Appendices

9.1 Supplementary Chapter: Tissue regulation of MAIT cells: sodium, bicarbonate, and SLC4A10

9.1.1 Introduction

In previous Chapters the entire focus has been on early vaccine-induced responses and the contribution of innate-like lymphocytes in peripheral blood. Depending on the delivery route, most early vaccine responses will occur in muscle or mucosal tissues, concentrated around draining lymph nodes. The work in this Chapter preceded the pandemic and has been the most disrupted, with the focus on MAIT cell responses in barrier tissues.

Some of the introduction has been published here, with all text written by me:

- **Amini A**, Pang D, Hackstein CP, Klenerman P. MAIT Cells in Barrier Tissues: Lessons from Immediate Neighbours. Front Immunol. 2020 Nov 30;11:584521.

9.1.1.1 Barrier Tissues

Most pathogens and increasing numbers of vaccines are first sensed in barrier tissues. Mammalian barrier surfaces are diverse physiological, chemical, and cellular niches. The skin is dry, lipid-rich, and acidic, primarily due to epidermal fatty acids, with unique exposures to high-salt content, UV-radiation, and large fluctuations in temperature [497,498]. The digestive system varies along its length, both in terms of physical factors and the unique composition of the microbiome: the oral mucosa is subject to occasional physical trauma from mastication, while the gut has the largest microbial biomass in the body in addition to a nutrient rich environment consisting of bile acids and diet-derived metabolites. Even the lungs are subject to fluctuating mechanical shear stress from ventilation and gravitational posture dependent changes, and also differ in structure and microbial sterility from higher to lower order bronchi and alveoli [499].

Most sites have underlying dense neural networks and varying concentrations of physiological parameters such as oxygen tension, lactate, glucose and amino acids depending on the specific location and inflammatory context; relative hypoxia is physiological in healthy skin hair follicles and the intestinal lumen, and induced in the face of increasing tissue demand during inflammation in all tissues. The inflammatory tissue microenvironment is further dysregulated by the catabolic processes necessary for generating an immune response, through excess nutrient consumption and generation of potentially toxic metabolic by-products. Moreover, these physical and biochemical changes interact with and shape the microbiome, therefore directly and indirectly interacting with resident immune cells, including MAIT cells.

9.1.1.2 Barrier tissue adaptation and sensing

T cell development, differentiation, activation, function, and survival are regulated by the cell intrinsic metabolism of glucose, amino acids, and lipids [500–502]. Nutrient availability differs between T cell compartments: circulating lymphocytes function in secondary lymphoid organs with high glucose and amino acid concentrations, whereas barrier tissues are more restrictive anatomically with variable nutrient composition. Any innate-like lymphocyte in tissues must therefore adapt to these niches for continued survival and proliferation, which may also influence their effector function.

Activated peripheral blood MAIT cells increase glucose uptake as glycolysis is required for their cytotoxicity and IFN-γ production [503,504], and human circulating MAIT cells have reduced mitochondrial activity compared to CD161-CD8+ T cells [503]. Amino acid metabolism is also crucial - peripheral MAIT cells express high levels of the L-type amino acid transporter, SLC7A5, and L-amino acid oxidase [504,505]. Some functions are dependent on OXPHOS, which correlates with TNF and IL-17[504]. So understanding innate-like lymphocyte tissue metabolism could help understand barrier specific effector functions.

Homeostatic perturbations in metabolic or environmental factors are more common at these peripheral barrier sites, as toxic by-products accumulate including oxidative stress from excessive free radicals, and acidosis. Relevant to adjuvant induced cell death, many tissue resident innate-like lymphocytes are enriched for the purinergic receptor, P2RX7, which recognizes extracellular purines (ATP, NAD+) released after cell lysis and has cell type specific effects to limit immunopathology [506–508].

The dialogue between tissue innate-like lymphocytes and barrier tissues also introduces a number of environmental factors which may drive variability in their effector functions, and ultimately explain some aspects of human immune variation. The clearest example is the commensal microbiome which is essential for tissue immunity in homeostasis and shapes the composition and phenotype of innate and adaptive cells [509,510]. Numerous mucosal cell types are perturbed in germ-free (GF) and antibiotic treated mice [511]. Conversely cohousing laboratory mice with wild mice to induce a more diverse microbiome promotes a human adult-like immune composition, with increased tissue innate and differentiated memory CD8+ T cell populations [512].

We have known MAIT cells are also reliant on the microbiome since Treiner et al. discovered that they were absent in the lamina propria of GF mice [175]. It was subsequently found that metabolites from riboflavin-synthesizing commensals, which engage the MAIT cell TCR, are necessary for most stages of MAIT cell intra-thymic development and subsequent peripheral expansion [187].

9.1.1.3 Barrier tissue environment

Within the tissue environment MAIT cells and other innate-like lymphocyte in a shared niche would compete for space and soluble mediators, particularly cytokines, important for survival [513]. Tissue inflammation and infiltration of metabolically active, cytotoxic cells into

this niche can disrupt homeostatic regulation by depleting nutrients (glucose, amino acids) and oxygen, producing waste products such as reaction oxygen species and lactate which contributes to tissue acidosis [514,515]. Resident immune cells are themselves in turn tuned by these non-immune tissue parameters.

Oxygen tension and regulation varies in vivo: blood and primary lymphoid organs have tightly regulated levels, whereas physiological hypoxia is observed in tissues such as the skin and intestine [274,516,517]. Hypoxia regulates immune cells directly by preventing cytosolic degradation of the oxygen sensing transcription factor, hypoxia-inducible factor (HIF1A). T cell upregulation of HIF1A expression is STAT3-dependent and promotes CD8+ T cell effector functions [518], Treg plasticity [519,520], and TH17 differentiation through induction of glycolysis, RORγt expression and Foxp3 proteasomal degradation [521,522].

pH

Although, homeostasis maintains circulating pH around pH 7.4, deviations are seen in tissues. Healthy skin is acidic due to a high free-fatty acid content, and inflammation drives tissue acidosis through glycolytic products [498]. Many immune cells possess mechanisms for proton sensing, including acid-sensing ion channels (ASIC), transient receptor potential (TRP) channels and GPCRs [523]. Amongst T cells, human MAIT cells and other CD161+ T cells share functionality and a conserved transcriptional signature by bulk microarray, which includes enrichment for two candidate GPCR proton sensors, GPR65 and GPR68 [8,200,524]. GPR65 may play an important role in RORγt+ T cells; the Gpr65 promoter has a RORγt binding site [525], and Gpr65 expressing T cells regulate the development of EAE in mice which is driven by type 17 inflammation [526]. Naïve *Gpr65*$^{-/-}$ CD4+ T cells differentiated under TH17 conditions, or memory *Gpr65*$^{-/-}$ CD4+ T cells reactivated with IL-23 produce less IL-17A in vitro, and the adoptive transfer of *Gpr65*$^{-/-}$ CD4+ T cells into *Rag1*$^{-/-}$ recipients prior to EAE induction markedly delays and reduces disease [526].

Another study however found that Gpr65-deficient mice develop exacerbated EAE, which was lost in the absence of iNKT [527]; functionally deficient *Gpr65*$^{gfp/gfp}$ but not *Cd1d*$^{-/-}$ *Gpr65*$^{gfp/gfp}$ mice develop more severe disease compared to wild-type. It is particularly interesting to note that murine Gpr65 expression is important for CD4+ T survival in culture and highest in iNKT, followed by γδT and NK cells, suggesting a homeostatic role for acidic sensing in innate-lymphoid cells. MAIT cells were not assessed in this study, but in humans share similarities with and are a hundred times more common than iNKT [186], thus may represent the most prominent GPR65 expressing cell. Indeed type 17 bronchoalveolar MAIT cells in children with pneumonia are enriched for GPR65 expression so future studies should explore whether acid-sensing can promote MAIT cell mucosal function [289].

Lactate

Increased lactate occurs in conjunction with inflammation-induced acidosis, and may be sensed directly by CD4+ T and CD8+ T cells through SLC5A12 and SLC16A1 transporters respectively, which inhibit T cell migration to potentially promote tissue retention [528–530]. However, in mice, cells with low glycolytic capability, including murine iNKT, show reduced survival under high lactate conditions in vitro [531]. MAIT cells and other IL-23R+ lymphocytes could also be indirectly regulated by lactic acid augmentation of TLR-induced IL-23p19 production [532], which would skew towards type 17 responses in tissues [292,533].

Temperature

Fever is a conserved response to infection and autoinflammatory disease across species. Although core temperature is rigorously regulated, peripheral tissues such as the skin where MAIT cells reside, are prone to deviations [534]. High temperatures have long been known to enhance human lymphocyte proliferation and cytotoxicity in vitro [535], as well as CD8+ T cell differentiation and CD4+ T cell activation through increased membrane fluidity and reduced co-stimulation thresholds [536,537]. In mice, antipyretics (aspirin, ibuprofen) inhibit TH17 differentiation, with high temperatures selectively promoting inflammatory TH17

differentiation and increased lung neutrophil recruitment [538]. Pulmonary MAIT cells and IL-17A producing innate-like T cells clearly protect against bacterial and viral infections in mice, which become pyrexial during the course of a normal immune response [224,539,540]. It is unclear if pharmacological or pathological alteration of this normal febrile response, or significant exposure to cold environments, could modulate the response of tissue MAIT cells.

Electrolyte and osmotic stress

Similar to pH, electrolytes such as sodium, potassium and chloride are normally tightly regulated in blood. Elevated extracellular potassium is however found in necrotic tissues and tumours, which paralyses human cytotoxic T cell responses [541]. It is also appreciated that salt (NaCl) concentration can be enriched in barrier tissues such as the skin, particularly during inflammation [516,542]. High salt diet increases EAE severity in mice due to increased TH17 differentiation from naïve precursors; direct salt-sensing ultimately induces TH17 IL-23R expression [543,544] and inhibits Treg differentiation [545,546].

In humans, high salt in vitro augments both naïve CD4+ TH17 polarization and memory CD8+ T cell IL-17A production in response to TCR-activation in the absence of polarizing cytokines [547]. Interestingly, the skin of patients with atopic dermatitis has higher salt concentrations, and salt promotes both TH2 and TH17 cytokine production and skin-homing CCR8 expression by TCR-activated memory CD4+ T cells, thus potentially linking the environment with pathogenic mucosal T cell responses [547]. Salt also indirectly regulates mucosal T cell function through differential production of polarizing cytokines: osmotic stress increases macrophage IL-1β production and Th17 generation in mice [548]; and humans with a fixed high salt diet have increased plasma IL-23 [549]. As MAIT cells are IL-23+ T-cells in the skin, it would be interesting to determine whether their responses are also skewed in a similar way by the tissue electrolyte composition and if this contributes to disease.

9.1.1.4 SLC4A10

As alluded, extracellular pH (pHe) is under intense homeostatic control, with buffering predominantly controlled by the carbon dioxide (CO_2)-bicarbonate (HCO_3^-) buffering system to maintain a plasma pH ~7.4; CO_2 and HCO_3^- are regulated by the lungs and kidneys respectively, with the balance determining exact pH.

Intracellular pH (pHi) is more acidic than pHe but nevertheless homeostasis is equally crucial for all cells to function, with glycolytic enzymes particularly sensitive to pH-mediated inhibition[550]. Intracellular [H+] can be changed either by net acid-loaders or extruders: the consequences of cellular metabolism are generally acid-generating, so the regulation of pHi is primarily dependent on acid-extrusion, best achieved by HCO_3^- transport via solute carriers (SLC).

Solute carrier 4 (SLC4) genes encode for NBCs that play a crucial role in importing bicarbonate ions and regulating intracellular pH. NBCs are highly conserved throughout evolution and are all membrane HCO_3^- exchangers or co-transporters [551]. In humans, ten SLC4 genes have been identified, of which nine code for functional proteins capable of plasma membrane bicarbonate transport. Amongst these, three are sodium-independent Cl^-/ HCO_3^- exchangers, thus electroneutral. The remaining five NBC transporters are either electrogenic or, in the case of SLC4A10 (also known as NBCn2), electroneutral. SLC4A10 was initially identified as an electroneutral Na-driven Cl^-/ HCO_3^- exchanger (NCBE)[552], but it was later renamed NBCn2 as it was thought to maintain electroneutrality as a (chloride-independent) Na^+/ HCO_3^- co-transporter[553]. However, recent studies have confirmed the original description, and both NCBE and NBCn2 are still used in the literature [554].

Slc4a10 transcripts were initially identified in rodents, where expression was found in the CNS (brain and choroid plexus) [553,555,556], retina[557], and inner ear, indicating a potential role

in neuronal function. Recent studies have also identified SLC4A10 transcripts in the human brain[558], further supporting this hypothesis. In mice, knockout of *Slc4a10* results in reduced ventricular volume and neuronal excitability[555], possibly due to a decreased response to intracellular acidosis and an increased seizure threshold. Furthermore, these mice exhibit early onset hearing loss.

In humans, mutations in SLC4A10 are associated with refractory epilepsy and cognitive impairment[559–561]. Isolated mutations have been reported to cause autism, abnormal gait, and behaviour. Some studies have also suggested a link between SLC4A10 and haematological abnormalities, such as increased MCH and small spleens. At a population level, single nucleotide polymorphisms and expression levels of SLC4A10 have been associated with hypertension, plasma sodium and osmolality[562], aging associated inflammation[563], and hippocampal volume[564]. The importance of SLC4A10. in neuronal function is further evidenced by its putative gene enrichment in synaptic vesicle transmission pathways in the mammalian Brain Map [565]. However, the function of the human protein has only been studied by expression in Xenopus oocytes[558].

Intriguingly, SLC4A10 expression is not limited to neuronal tissues in human tissues. Recent studies have shown it is also present in T-cells, specifically MAIT-cells, which are abundant in human blood. Originally described amongst CD161+CD8+ T cells in the liver[566], further reports have repeatedly confirmed enrichment and exclusive expression of SLC4A10 in human MAIT cells and a related subset of Vδ2+ γδ T in blood[567]. Single-cell RNA-sequencing studies during the SARS-CoV-2 pandemic have further supported this finding, with SLC4A10 regularly used as a marker to define MAIT cell clusters together with TRAV1-2 (TCR Vα7.2) and KLRB1 (CD161) in genomic datasets[568].

However, the function of SLC4A10 in human T-cells remains unknown, including implications for immune responses. This is particularly relevant in the context of skin and

mucosal surfaces, which are promising targets for novel vaccination strategies. These tissues have a more acidic pH than blood, which also determines pHi. In addition, muscle and skin, which are common sites for vaccination, have higher sodium content than blood, potentially implicating sodium and bicarbonate transport in vaccine responses. Understanding the impact of these physiological parameters on SLC4A10 function could provide insights into the mechanisms underlying immune responses and pave the way for novel strategies to enhance vaccination efficacy.

9.1.2 Aims

The work in this Chapter is based on the observations that:

(1) MAIT cells are abundant in blood and tissues, therefore exposed to a more diverse range of physiological perturbations compared to conventional T cells.

(2) SLC4A10, an electroneutral NBC, is highly expressed and serves as a defining transcriptional marker of human MAIT cells.

(3) An alkaline intracellular pH is necessary for optimal glycolysis, a metabolic process required for rapid effector functions.

Based on these observations, the main aims of this chapter are to investigate the role of **sodium** and **bicarbonate** in the function of MAIT cells. Specifically, the chapter aims to explore the hypothesis that the SLC4A10 helps maintain alkaline intracellular pH in MAIT cells, which in turn is important for their metabolism and rapid effector functions.

9.1.3 Chapter specific materials and methods

Methods described below are in addition to or modifications of methods in prior chapters. Gating strategies for identification of MAIT cells after in vitro stim are below (**Appendix SF9.1**).

9.1.3.1 Fluorescence Activated Cell Sorting (FACS)

To sort MAIT cells (MR1-5-OP-RU+) T cells, naïve and effector memory non-MAIT CD8+ T cells from fresh PBMCs a panel was optimised to avoiding emission spectra which would overlap with c-SNARF (**Appendix SF9.2**). Additionally, after sorting MAIT cells in particular are prone to cell-death, which was subverted through optimised sorting media and the addition of an overnight rest step in X-VIVO15 media (*data not shown for comparisons*).

All cell sorting was kindly performed by Helen Ferry. Cells were stained fresh with antibodies at concentrations described previously, with MR1-5-OP-RU tetramer staining at room temperature for 40min as previously described. Cells were then washed twice, and resuspended in a sorting buffer optimised for cell survival. Cell sorting was performed using a BD FACSAria III with a 70 µm nozzle into sorting collection media on ice. Sort purity was consistently > 99%.

9.1.3.2 Solutions for steady state pH measurement

Overnight resting media (sorted cells): XVIVO15 (Lonza)

Solutions for calibration with nigericin: KCl (145mM), MgCl2 (1mM), EGTA (0.5mM), HEPES (10mM), MES (10mM). Final pH was adjusted to required levels with NaOH.

Solutions for pHi measurement in bicarbonate: DMEM (D5030), Glucose (25mM), Glutamine (2mM), FCS (10%). 1x Penicillin/Streptomycin. Bicarbonate (44m) and NaCl (44mM) stock solutions were made, then mixed using these ratios. (**Appendix Table 9.1**)

Appendix Table 9.1 | Bicarbonate solutions

pH	$NaHCO_3$ (44mM)	NaCl (44mM)	Final BC
6.2	0	40	0
6.6	2.5	37.5	2.75
6.9	5	35	5
7.1	10	30	11
7.4	20	20	22
7.7	40	0	44

Solutions for pHi measurement without bicarbonate (HEPES): DMEM (D5030), Glucose (25mM), Glutamine (2mM), FCS (10%). MES (10mM), HEPES (10mM), 1x Penicillin/Streptomycin. NaCl was added to titrate pH.

All solutions were made using a calorimeter, magnetically stirred and at 37˚C.

9.1.3.3 Intracellular pH measurements

Live cell intracellular pH measurement

After overnight resting, sorted cells were incubated for 20min in 1ml X-VIVO media supplemented with 10µg/ml cSNARF1-AM (5-(and-6)-carboxy SNARF-1 acetoxymethyl ester) (C1272, Invitrogen). Cells were then washed twice with their relevant buffered media (bicarbonate or HEPES media at 6 pH points each). To wash 80µl aliquots of cells were added to Eppendorf tubes with 1ml of buffer, then centrifuged at 500g for 5min. After each spin, media was carefully aspirated to avoid disruption of the visible cell pellet.

After the final wash, sorted cells were resuspended in duplicate into Ibidi plates at 75,000 per well with 200µl media. Ibidi plates are 96-well black-walled, with flat coverslip bottoms for optimised imaging. Poly-lysine was used to coat the wells, with brief centrifugation (100g, 5 min) to aid cell attachment.

Cells were imaged at 10x objective using the Cytation_5 plate reader (Biotek) in the presence or absence of 5% CO_2, all at 37˚C. Fluorescence was excited at 555nm excitation and emission measured at 580nm and 640nm. Ratios of fluorescence emission for cSNARF1 (580:640nm) were converted to absolute values for intracellular pH (pHi) using calibration curves determined with the nigericin method.

Nigericin method for pH calibration

To measure intracellular pH, the ratio of c-SNARF emission spectra were calibrated with the Nigericin method[569] (**Appendix Fig9.1**). Nigericin - a carboxylic K+/H+ ionophore - equilibrates intracellular and extracellular pH when cells are resuspended in high K+ buffers, allowing the intracellular fluorescence properties of cSNARF1 to be calculated for known pH values. Cells were therefore suspended in calibration media with nigericin 10μM. Cell volume and nucleus to cytoplasm ratio can influence fluorescence, so calibration curves were created using fresh PBMCs and MACS enriched CD8+ T cells with similar results for both (**Appendix Fig9.1 D**). We therefore used a combined curve of best fit to calculate intracellular pH from known cSNARF1 (580:640nm) fluorescence ratios.

Image analysis

Calculation of cytoplasmic pH was performed by Pawel Swietach using a custom MATLAB script for Image J. Briefly, cells were identified by gate using threshold Hoechst signals. For each identified cell, fluorescence at 580nm and 640nm were averaged and background subtracted prior to calculation of cSNARF1 ratio (580:640nm).

Appendix Figure 9.1 | Calibration of intracellular pH using cSNARF1.

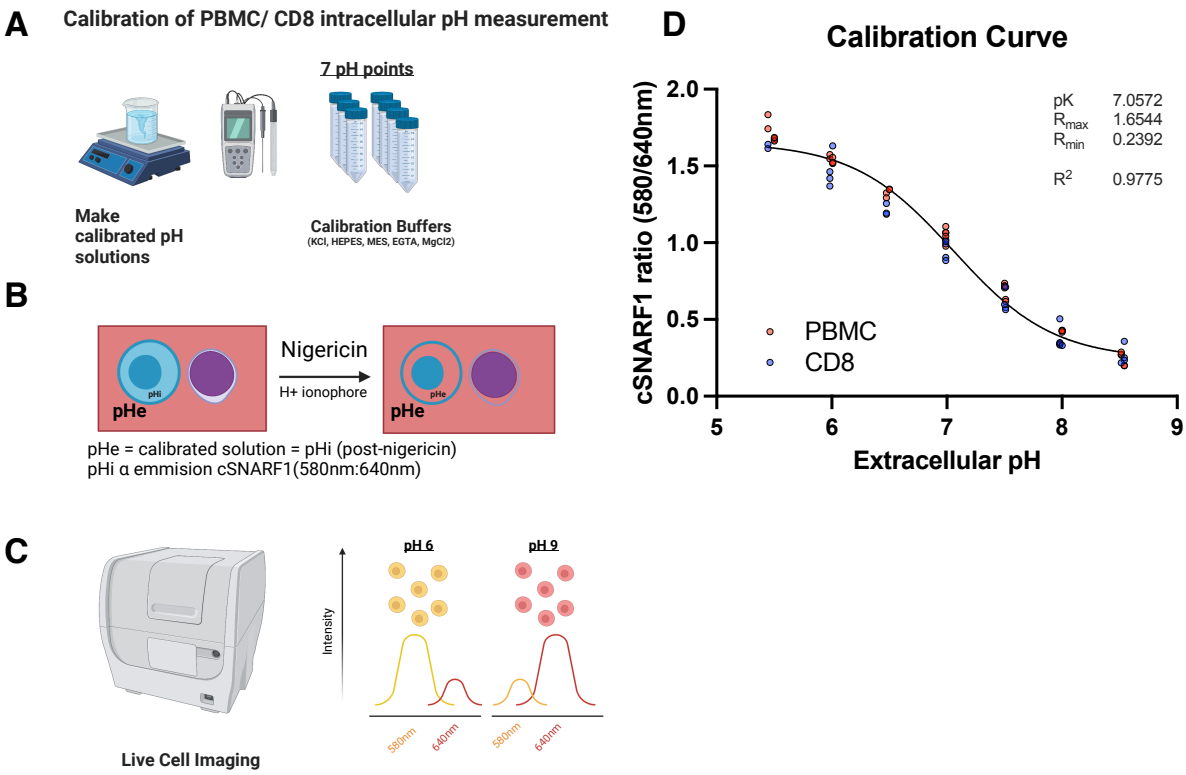

Appendix Figure 9.1 | Calibration of intracellular pH using cSNARF1.
(A-C) Schematic for calibration.
(A) Calibration buffer solutions made at 7 pH points, using non-bicarbonate buffers (pH 5.5-8.5) at 37˚C.
(B) Unfractionated PBMC or MACS enriched CD8+ cells (75,000 cells per well) were added to buffers with known extracellular pH. After the addition of Nigericin (10μM) in a high K+ solution, intracellular pH was allowed to equilibrate for 15 mins.
(C) Live cell imaging was undertaken in the absence of CO2 at 37˚C.
(D) Calibration curve for intracellular pH (pHi) of cSNARF1. Combined PBMC and CD8 values fitted to pH calibration curve with line of best fit (sigmoidal, least squares regression). pK, R_max and R_min shown.
Equation: pH = 7.0572 + log((1.6544-ratio)/(ratio-0.2392))

Mean ± SEM shown from 4 experiments, with at least 40-60 cells measured at each pH point per experiment.

MATLAB analysis to generate raw cSNARF1 ratio from image stacks performed by Pawel Swietach.

9.1.4 Results

9.1.4.1 Sodium chloride skews MAIT activation and prevents cell death

To determine if sodium chloride can alter MAIT cell responses to vaccines within a tissue environment, a model of activation was chosen to reflect signals received in vivo during the course of a tissue response. MAIT cells would be exposed to TCR triggers, from microbial-derived ligands, particularly with barrier perturbation. Innate-cell activation would induce co-stimulatory molecules and cytokine production, including type I IFN and IL-18[306]. To fully appreciate the impact on a range of effector functions, an optimised 72hr PBMC stimulation protocol was used without the use of PMA/ionomycin, which can skew MAIT cell IL-17A and IL-17F production[570].

After 72hr stimulation of PBMC with plate-bound αCD3/CD28 in addition to cytokines (IL-18 ± IFN-α), MAIT cells secrete IFN-γ, IL-17F and IL-17A (**Appendix Fig9.2**). The addition of supplemental extracellular NaCl prior to stimulation with αCD3/CD28+IL-18 without (**Appendix Fig9.2 B)** or with IFN-α (**Appendix Fig9.2 C)** increased IFN-γ production from MAIT cells and other CD161+ T cells in particular, with peak IFN-γ after additional 40mM NaCl. MAIT cell IL-17A but not IL-17F was appreciably increased with supplemental NaCl (**Appendix Fig9.2 B, C, E, F**), resulting in an increased ratio of IL-17A:IL-17F+ MAIT cells (**Appendix Fig9.2 G**), suggesting that extra-cellular NaCl can regulate the type of cytokines induced in response to the same triggers.

Appendix Figure 9.2 | Sodium chloride alters MAIT cell cytokine responses in vitro.

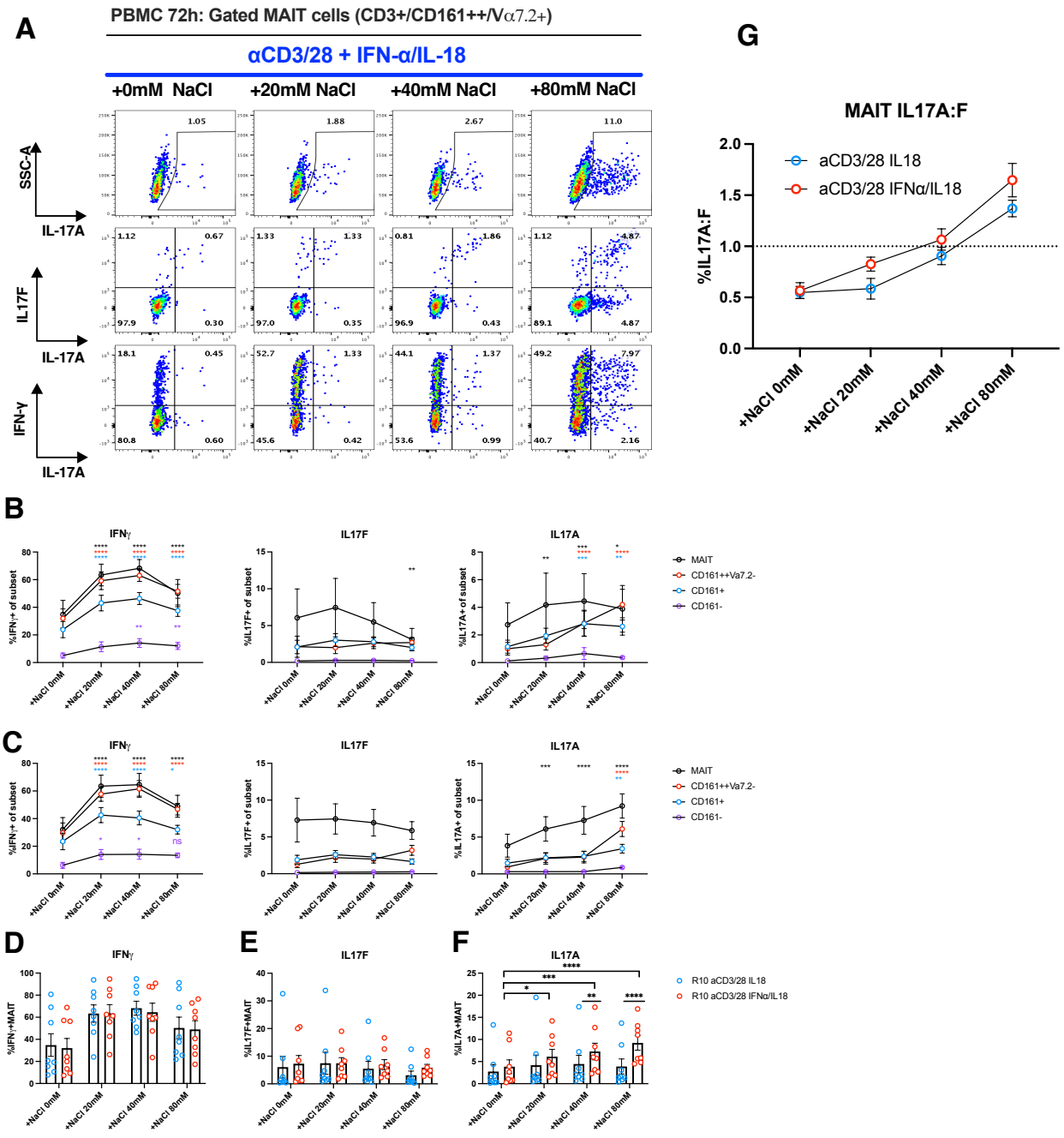

Appendix Fig9.2 | Sodium chloride alters MAIT cell cytokine responses in vitro.
Unfractionated whole PBMC were stimulated for 3 days with plate-bound anti-CD3 (2.5µg/ml) and soluble anti-CD28 (1µg/ml) in the presence of either IL-18 (50ng/ml), or α+IL-18 (50ng/ml). Supplemental NaCl (range up to 80mM final concentration) was added at the beginning of cultures to R10 medium.
(A) Representative FACS plots gated on live MAIT cells (CD161++Va7.2+) measuring IFNγ, IL17A, and IL17F production.
(B,C) Summary data for CD161-, CD161+(intermediate), CD161++Va7.2- and CD161++Va7.2+ (MAIT) cell cytokine production after stimulation of salt supplemented PBMC with anti-CD3/28 and IL-18 (B), or IFNα+IL-18 (C).
(D-F) Summary data for MAIT cell IFN-γ (D), IL17F (E), and IL17A (F) production after 3 days stimulation of whole PBMC with plate bound anti-CD3/28 and IL-18 (blue) or IFNα+IL-18 (red).
(G) Ratio of MAIT cell IL17A:IL17F production.
Symbols indicate individual donors with summary mean ± SEM.
*, p<0.05; **, p<0.01; ***, p<0.001; ****, p<0.0001.
Data were acquired from (n=8) donors in 2 independent experiments.
Statistical differences were calculated using repeated measures two way ANOVA with Sidak correction.

To further understand the mechanisms, we assessed the expression of activation markers with differing kinetics (CD69, CD25). NaCl supplementation prior to stimulation preferentially increased the fraction of CD69+CD25+ cells at 72h (**Appendix Fig9.3 A-B**).

Appendix Figure 9.3 | Sodium chloride alters MAIT cell cytokine responses in vitro after 72hr PBMC stimulation.

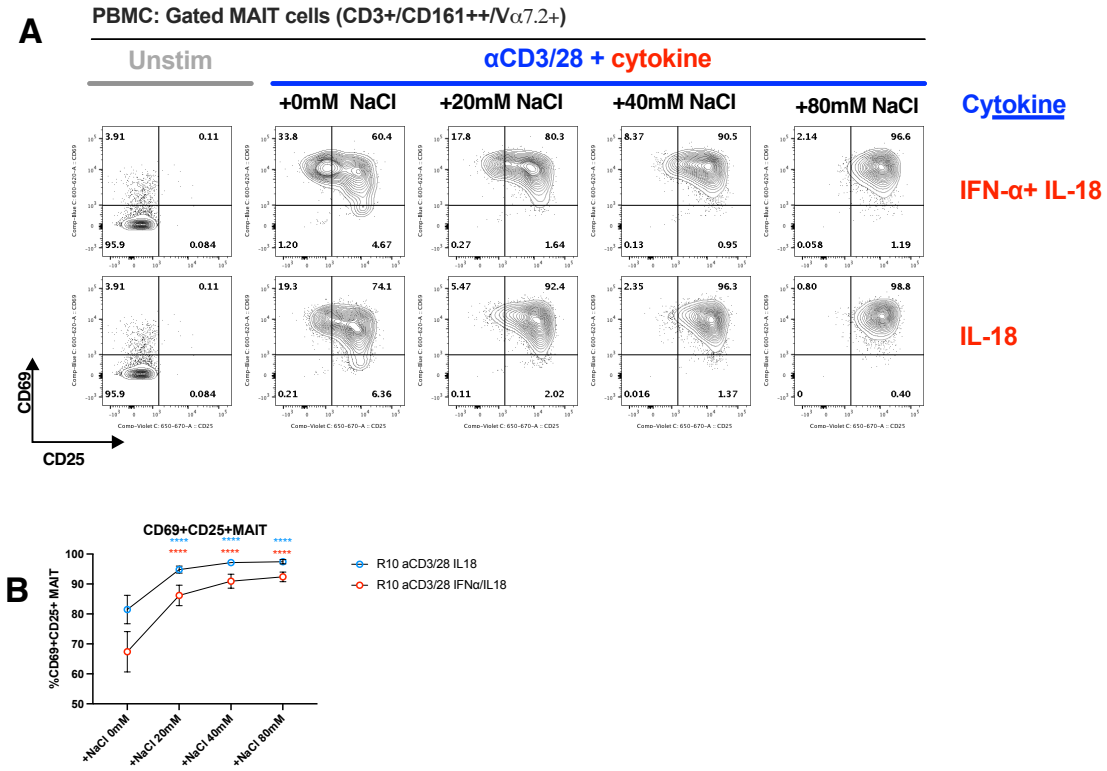

Appendix Fig9.3 | Sodium chloride alters MAIT cell cytokine responses in vitro after 72hr PBMC stimulation.
(A) Representative FACS plots gated on live MAIT cells (CD161++Va7.2+) among unfractionated whole PBMC stimulated for 3 days without (unstim) or with plate-bound anti-CD3(2.5µg/ml)/CD28(1µg/ml) and cytokines (IL-18, 50ng/ml; IFNα+IL-18, 50ng/ml). Supplemental NaCl (range up to 80mM final concentration) added at the beginning of cultures to R10 medium.
(B) Summary data of fraction of MAIT cells in PBMC which are CD69+CD25+ 72h after stimulation. Comparisons with no salt condition.
Mean ±SEM is shown.
*p<0.05; **, p<0.01; ***, p<0.001; ****, p<0.0001
Data were acquired from (n=8) donors in at least 2 independent experiments.
Statistical differences were calculated using repeated measures two way ANOVA with Sidak correction.

Prolonged or potent T-cell activation, particularly TCR in combination with cytokines, can induce MAIT cell death. We found that additional IFN-α was particularly potent at reducing the frequency of live MAIT cells among PBMC in combination with TCR triggering (**Appendix Fig9.4 A-C**). Supplemental NaCl (80mM) prior to stimulation reduced this IFN-α dependent reduction in MAIT cell frequency (**Appendix Fig9.4C**).

Appendix Figure 9.4 | Salt prevents type I IFN induced reduction in MAIT cell frequency.

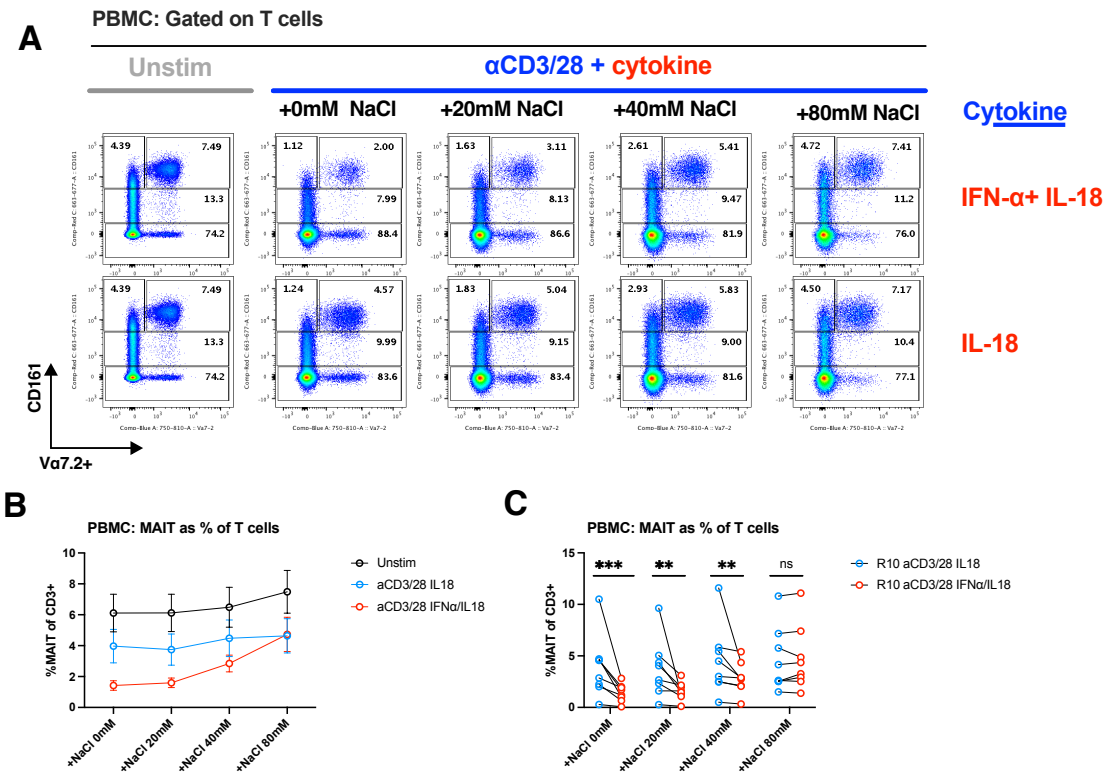

Appendix Fig9.4 | Salt prevents type I IFN induced caspase-activation and MAIT cell death.
(A) Representative FACS plots gated on live CD3+ T cells among unfractionated whole PBMC stimulated for 3 days without (unstim) or with plate-bound anti-CD3(2.5µg/ml)/CD28(1µg/ml) and cytokines (IL-18, 50ng/ml; IFNα+IL-18, 50ng/ml). Supplemental NaCl (range up to 80mM final concentration) added at the beginning of cultures.
(B) Summary data demonstrating percentage of MAIT cells (CD161++Vα7.2+) amongst live CD3+ T cells. Mean ± SEM shown (n=8)
(C) Summary data demonstrating percentage of MAIT cells (CD161++Vα7.2+) amongst live CD3+ T cells. Symbols indicate individual donors.
*, p<0.05; **, p<0.01; ***, p<0.001; ****, p<0.0001.
Data were acquired from (n=8) donors in at least 2 independent experiments.
Statistical differences were calculated using repeated measures two way ANOVA with Sidak correction.

We next asked whether the loss of MAIT cells was due to increased cell death, measuring activated caspases using the FLICA assay. IFN-α augmented MAIT cell FLICA expression among PBMC stimulated with plate-bound αCD3/28, which was reduced by the addition of supplemental NaCl (**Appendix Fig9.5 C**). As IFN-α dependent MAIT cell caspase activation is inhibited by salt, one might expect that in some tissues MAIT cells will be less likely to undergo cell death. For example, during infection the skin and muscle of mice undergo 40mM increase in Na+, which could be relevant during IFN-mediated vaccine responses.

Appendix Figure 9.5 | Salt prevents type I interferon induced caspase activation and cell-death.

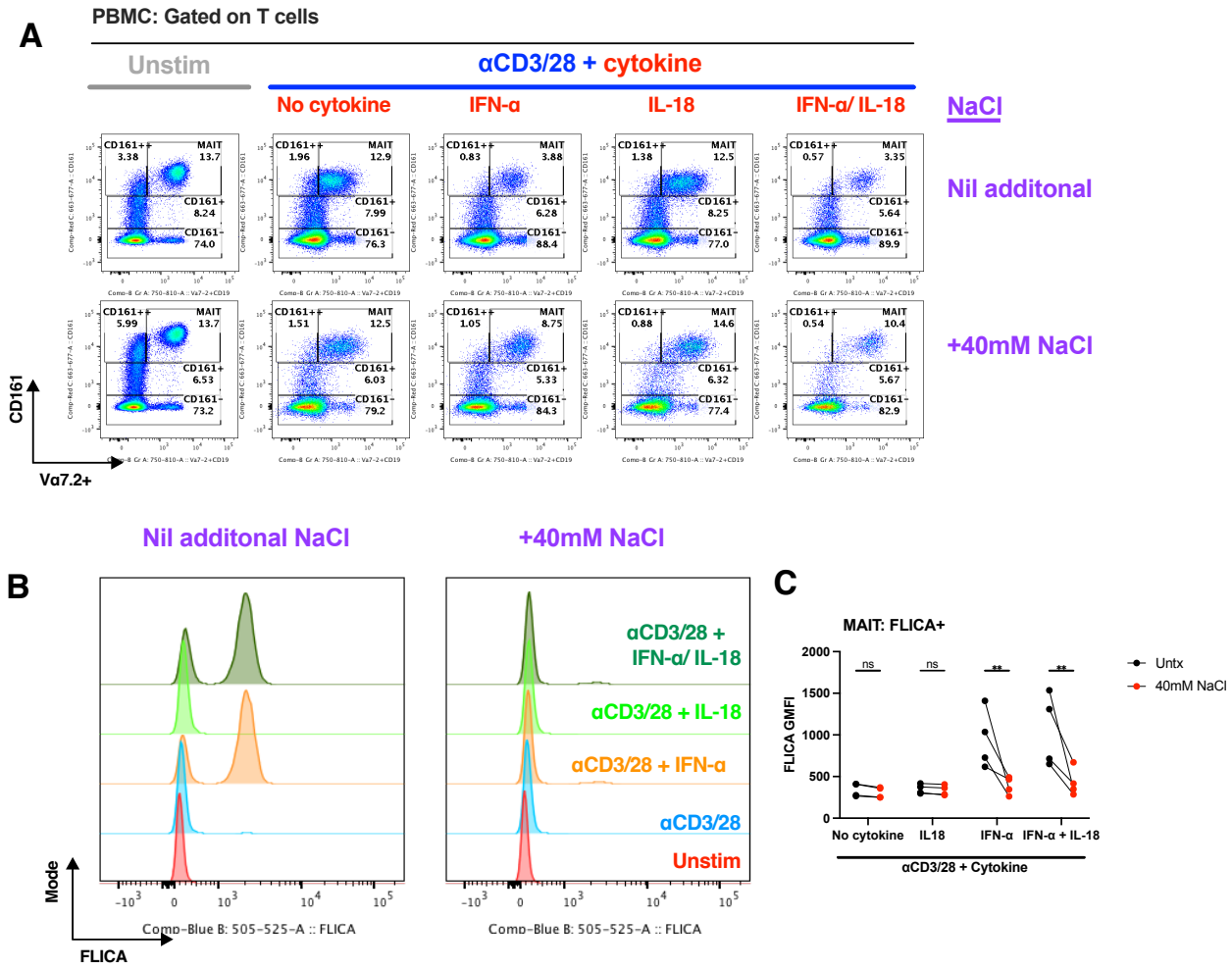

Appendix Figure 9.5 | Salt prevents type I interferon induced caspase activation and cell-death.
(A) Representative plots from a single donor gated on CD3+ T cells among unfractionated whole PBMC stimulated for 3 days without (unstim) or with plate-bound anti-CD3(2.5µg/ml)/CD28(1µg/ml) alone or with additional cytokines (IFNα, 50ng/ml; IL-18, 50ng/ml; IL-18, 50ng/ml; IFNα+IL-18, 50ng/ml). Supplemental NaCl (40mM final concentration) added at the beginning of cultures to R10 medium.
(B, C) Representaive histograms, and summary of MAIT cell expression of FLICA (fluorescent inhibitor of caspase). Symbols indicate individual donors. ns = not significant; *, p<0.05; **, p<0.01
Statistical differences were calculated using repeated measures two way ANOVA with Sidak correction.

9.1.4.2 Bicarbonate and SLC4A10

To measure the impact of **bicarbonate** transport on MAIT cell function, a protocol was optimised with the help of Pawel Swietach (**Appendix Fig9.6**). To measure cytoplasmic pH, we performed live cell imaging using a cell impermeant dye, carboxy-seminaphtharhodafluor (c-SNARF), which can be loaded intracellularly as its cell-permeant ester. SNARF has a pKa around 7.35 at 37˚C, with distinct pH dependent emission spectra on deprotonation in basic conditions, shifting from 580nm (yellow-orange) to 640nm (deep red) fluorescence.

Appendix Figure 9.6 | Method to assess impact of bicarbonate on intracellular pH of sorted human T cell populations.

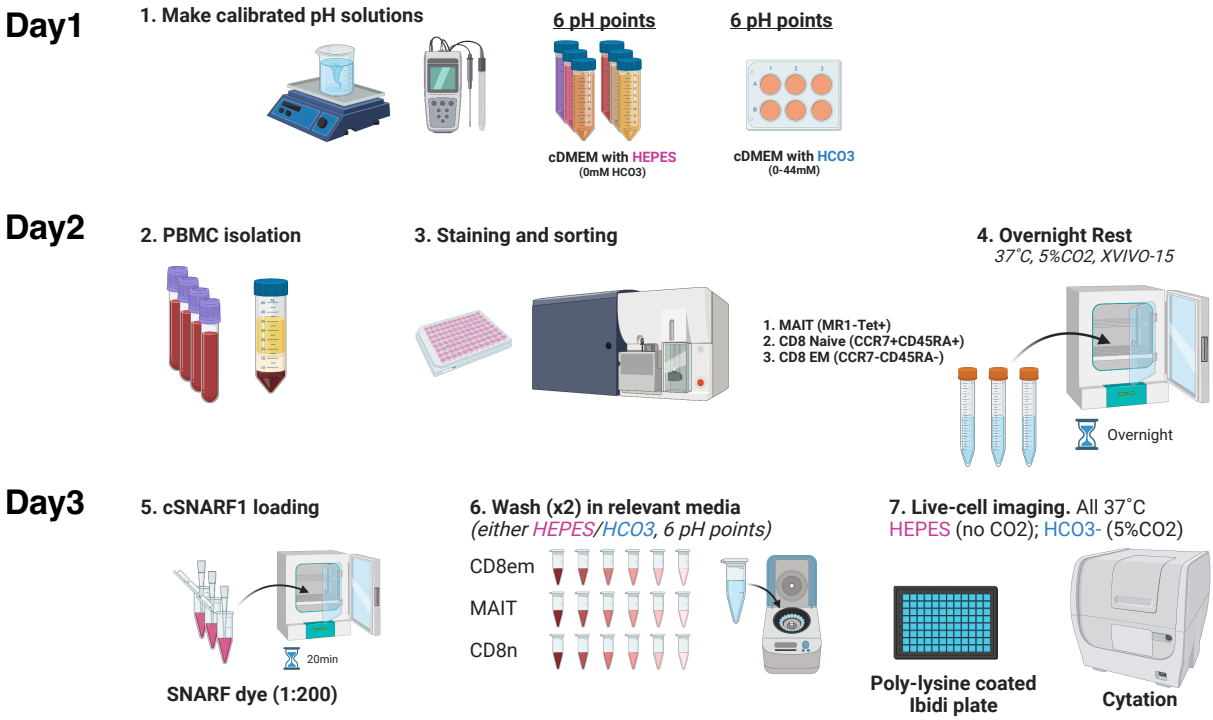

Appendix Figure 9.6 | Method to assess impact of bicarbonate on intracellular pH of sorted human T cell populations.
Schematic of three day protocol.
(Day1) Solutions made with or without bicarbonate (HCO3) at a range of pH points. All measurements performed at 37˚C with magnetic stirring. HCO3 solutions made using pre-calculated recipes, with exact pH measured after a period of equilibration in 5% CO2 incubator. Non-bicarbonate solutions made using HEPES to adjust pH.

(Day2) Isolation of fresh PBMC and staining of T cell populations prior to sorting MAIT cells and non-MAIT CD8+ T cell effector memory and naïve cells. Cells sorted into collection media (PBS, 20% FCS, 20mM HEPES) on ice, then washed and rested overnight in XVIVO15 media (5E5 cells/ml).

(Day3) Rested cells were loaded with cSNARF1 (10µg/ml), aliquoted into 6 eppendorf tubes then washed twice in the relevant solution to remove background unloaded SNARF dye. Cells were then loaded on poly-lysine coated Ibidi plates, allowed to equilibrate to 37˚C and images at 10x objective in the presence (HCO3 solution) or absence of CO2 (HEPES solution).

SLC4A10 is highly conserved between humans, mice, and rats, partially underlying the lack of available quality monoclonal antibodies. I have tested all commercially available polyclonal anti-SLC4A10 antibodies - none of which convincingly stain cells in PBMC (*data not shown*). It was therefore not possible to sort SLC4A10 positive and negative cells to functionally compare populations which differentially express NBCn2. However, there is data to suggest significant differential gene expression between human MAIT cells and naïve CD8 T cells[571], so these cells were sorted as a negative control. Non-MAIT effector memory CD8+ T cells were also included to determine the specificity of bicarbonate-dependence to MAIT cells.

Extracellular pH (pHe) can regulate intracellular pH (pHi). To determine the importance of bicarbonate transport in cytoplasmic acidosis, we first examined the steady-state relationship between pHe and pHi both the presence and absence of CO_2/bicarbonate buffering. HEPES buffered DMEM, calibrated to known pH points was used as a non-bicarbonate buffered control.

In the absence of bicarbonate, pHi for both sorted MAIT cells and non-MAIT CD8Tem, but not naïve CD8 T cells, was independent of pHe (**Appendix Fig9.7 A**). Even at maximal pH tested, pHi was below 7.0 for MAIT cells, which is required for optimal glycolysis. Conversely in the presence of CO_2/HCO_3^-, MAIT and non-MAIT CD8Tem pHi becomes sensitive to pHe (**Appendix Fig9.7 B**). Therefore, bicarbonate transport is required for both MAIT and non-MAIT CD8Tem cells to maintain alkaline cytoplasmic pH above 7.0 required for cellular processes (**Appendix Fig9.7 C**).

Appendix Figure 9.7 | Bicarbonate is necessary to maintain optimum intracellular pH in MAIT cells but not naive CD8 T cells.

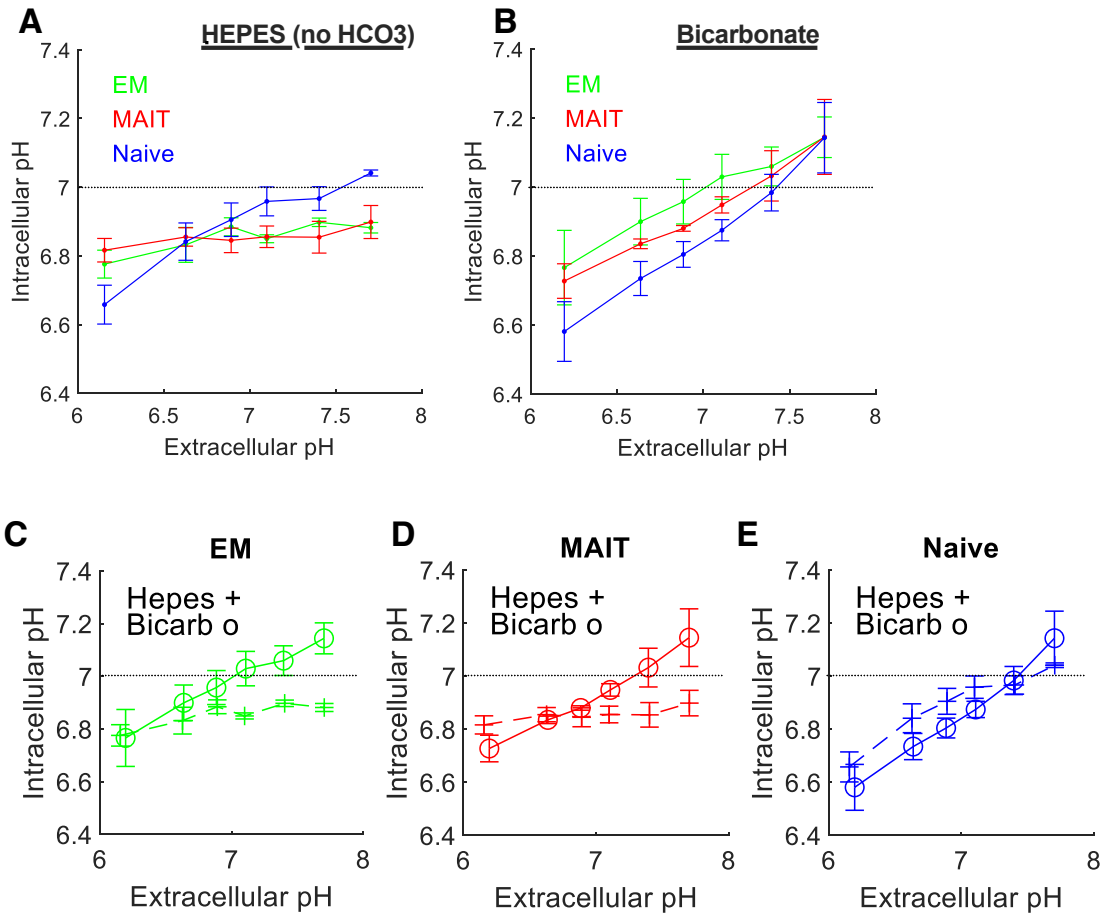

Appendix Figure 9.7 | Bicarbonate is necessary to maintain optimum intracellular pH in MAIT cells but not naive CD8 T cells.
MAIT cell (MAIT), non-MAIT CD8+ effector memory T cell (EM), and CD8+ naïve T cell (naïve) steady state intracellular pH (pHi) were measured as a function of extracellular pH (pHe) in the absence (HEPES) or presence of CO2/HCO3 buffering.
(A) Intracellular pH as a function of extracellular pH in the absence of bicarbonate (HEPES buffered).
(B) Intracellular pH as a function of extracellular pH in the presence of bicarbonate (CO2/HCO3 buffered).
(C-D) Intracellular pH as a function of extracellular pH for CD8+ T EM (C), MAIT (D), and CD8+ Naïve T cells (E) n the presence or absence of bicarbonate.

Data shown as mean±SEM. Fluorescence ratios from at least 100 cells were measured at each pH point in duplicate from 4 donors across 4 experiments, then converted to pHi values calibrations curve best equation.

MATLAB analysis to generate raw cSNARF1 ratio from image stacks performed by Pawel Swietach.

No specific modulators of SLC4A10 have been described. To confirm the functional impact of bicarbonate transport on MAIT cell function, a previously characterised inhibitor of NBC transport was used, S0859. In a single experiment, S0859 (10μM) inhibited the capacity of MAIT cells to alkalinise intracellular pH in the presence of bicarbonate but not HEPES (**Appendix Fig9.8**). Repeat experiments were impacted by the COVID pandemic and departmental closures. If reproducible, S0859 could inhibit MAIT cell bicarbonate transport (putatively SLC4A10) with an effect on immune function. As maintaining intracellular pH is critical for T-cells to sustain glycolysis, there would be many downstream implications[572].

Appendix Figure 9.8 | Bicarbonate channel blocker, S0859, inhibits MAIT cell intracellular pH regulation.

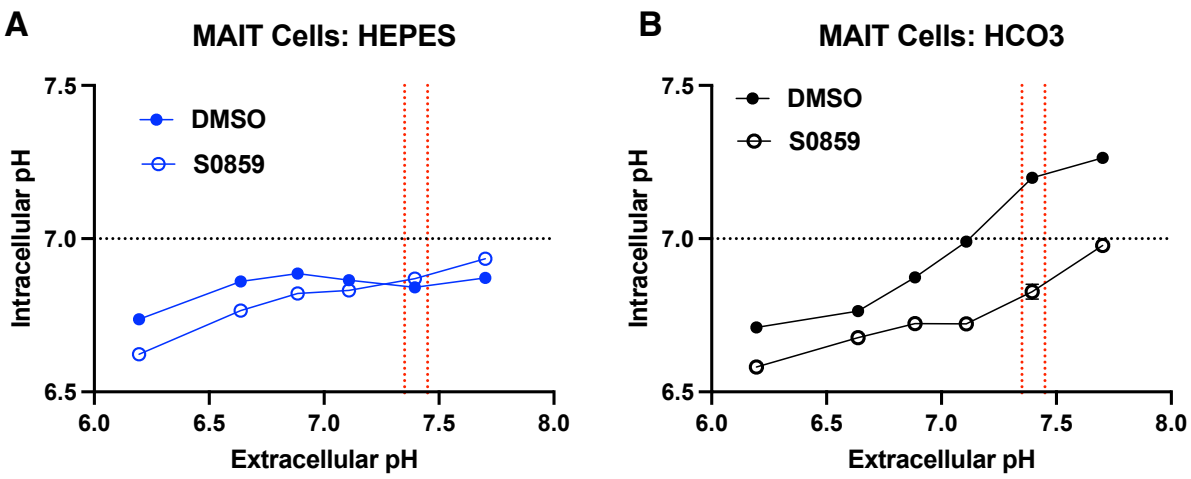

Appendix Figure 6.8 l Bicarbonate channel blocker, S0859, inhibits MAIT cell intracelluar pH regulation. MAIT cell steady state intracellular pH (pHi) were measured as a function of extracellular pH (pHe) in the absence (HEPES) or presence of CO2/HCO3 buffering. S0859 (10μM) (or DMSO control) was added 30min prior to buffering.

(A) MAIT cell intracellular pH as a function of extracellular pH in the absence of bicarbonate (HEPES buffered) with or without S0859.

(B) MAIT cell intracellular pH as a function of extracellular pH in presence of bicarbonate (CO2/HCO3 buffered) with or without S0859.

Summary data (n=1 donor) with fluorescence ratios from at least 300 cells measured at each pH point in duplicate, then converted to pHi values calibrations curve best equation.

Grey dotted lines = intracellular pH 7.0, below which glycolysis shut down.
Red dotted lines = normal range for peripheral blood extracellular pH.

MATLAB analysis to generate raw cSNARF1 ratio from image stacks performed by Pawel Swietach.

Finally, other incomplete ongoing work has been to characterise the impact of S0859 on MAIT cell function. Relevant to the rest of this thesis, MAIT cell activation - including IFN-γ production - in response to ChAdOx1-GFP is reduced in the presence of S0859 (10μM) compared to DMSO control (**Appendix Fig9.9**). Although preliminary this may be a novel way by which environmental factors regulate early antiviral and vaccine induced responses.

Appendix Figure 9.9 | Bicarbonate transport may impact on MAIT cell antiviral responses.

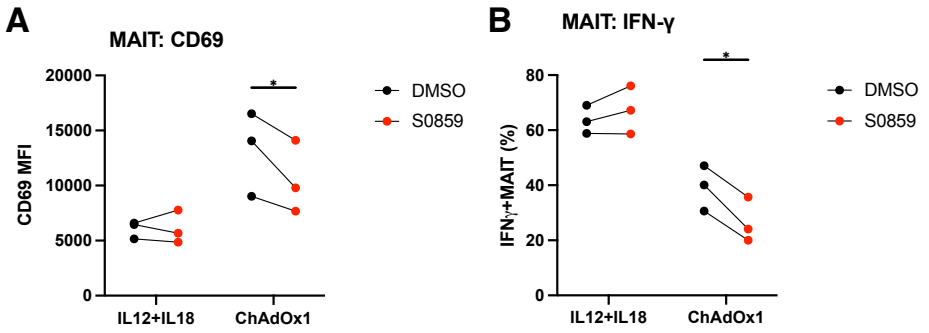

Appendix Figure 6.9 l Bicarbonate transport may impact on MAIT cell antiviral responses.
(A, B) Fresh PBMC were stimulated with either ChAdOx1-GFP (MOI 10^3 vp) or cytokines (IL-12+IL-18, 50ng/ml each) in the presence of either S0859 (10μM) or DMSO control. MAIT cell activation was measured as either CD69 (A), or IFN-γ expression(B) after 24h.
Symbols represent individual donors (n=3, single experiment)
ns = not significant; *p<0.05
Statistical differences were calculated using repeated measures two way ANOVA with Sidak correction.

9.1.5 Discussion

The data in this Chapter is incomplete, and was most affected by the pandemic, but provides some evidence to suggest that MAIT cell effector functions may be influenced by environmental electrolyte composition - namely sodium and bicarbonate - and that this could putatively be due to SLC4A10.

We found that MAIT cells triggered in the presence of supplemental sodium chloride have a skewed effector profile with increased IFN-γ and IL-17A, and reduced caspase-1 dependent cell death, after triggering with TCR and type I IFN in particular. Extracellular

bicarbonate availability was also a limiting factor in MAIT cell intracellular pH regulation - distinct from naïve CD8+ T cells - potentially of functional relevance in their unique effector functions. These studies will be followed up in due course, but a working model is shown (**Appendix Fig9.10**).

Appendix Figure 9.10 |Working Model for the effects of Na and HCO3.

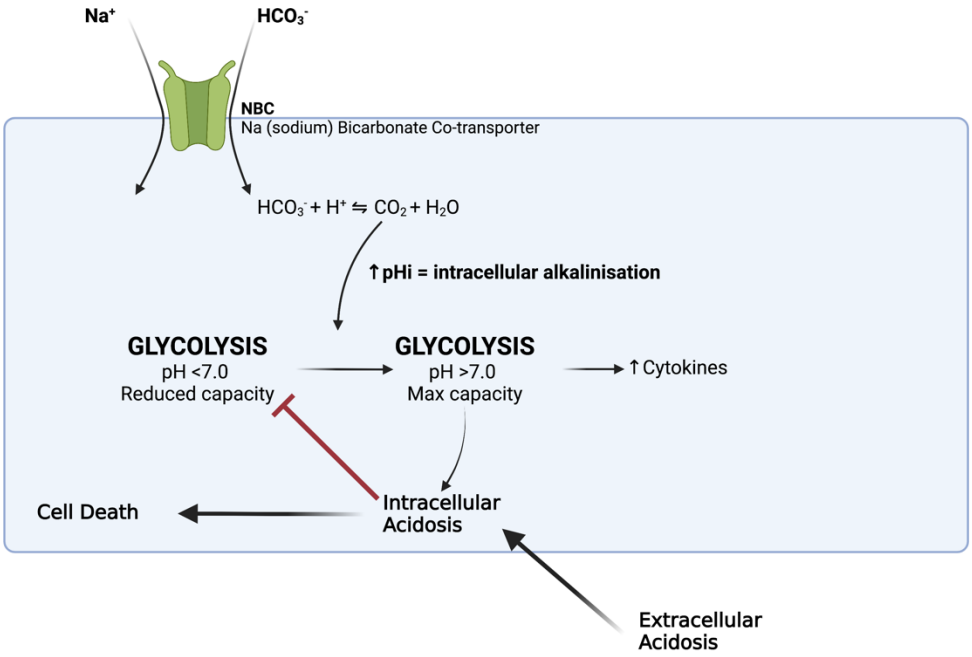

Although we found that NaCl can regulate MAIT cell function, further work is needed to determine the mechanism. These data could support a functional role for extracellular sodium, which by driving SLC4A10-induced HCO3 transport would rapidly alkalinise MAIT pHi during the course of an immune response. This would be particularly beneficial in highly glycolytic states generating a significant [H+] load, or in tissues with increased pHe. Indeed, this could be one explanation for the reduced MAIT cell-death in high salt conditions in response to TCR + IFN-α.

The concept that NaCl can regulate MAIT cells supports emerging data where sodium and osmolality regulate immune cell function, particularly in tissues where levels are often enriched during infection[573]. Macrophages can sense salt and osmolality through NFAT5

and NRCL4 inflammasome to drive differential Th17 function [562]. Humans on a high salt diet have a higher frequency of monocytes producing increased IL-23 and IL-17[549]. Barrier enriched CD4 T cells, including Th17 and Treg, sense increased sodium through the salt-sensitive kinase (SGK1) which promotes RORγT and FOXP3 expression respectively to increase IL-17A and IFN-γ production[543,544]. In addition to SLC4A10, MAIT cells express RORγT, and increase NFAT5 and SGK1 on TCR-activation, thus might sense tissue osmolality or sodium concentration.

The putative function of SLC4A10 in primary human MAIT will be ongoing work in collaboration with Professor Swietach (DPAG). We have found that MAIT-cells, unlike conventional naïve T-cells, are dependent on bicarbonate transport to maintain an alkaline intracellular pH. Although no specific modulators of SLC4A10 have been described, preliminary data suggests that the generic NBC inhibitor (S0859), inhibits MAIT cell bicarbonate transport (putatively SLC4A10) with an effect on immune function.

Limitations and further work

There are number of limitations with this so far preliminary data. Primarily, both for NaCl and the impact of S0859 on MAIT cell cytokine function, alterations in effector functions could be indirect from the impact on APC. This will require use of sorted MAIT cell populations to test.

Additional controls need to be tested. NaCl driven changes could be due to osmolality or chloride, so alternative salts should be tested. S0859 unsurprisingly can have off target effects as a small molecule drug, in this case as an inhibitor of lactate transporters. Further experiments will need to probe the potential alternative effects, in addition to ideally genetic manipulation of SLC4A10 with knock-down experiments.

9.1.6 Conclusions and summary

Key findings

The key findings in this Chapter are:

1. Sodium chloride supplementation (mimicking tissue-associated levels) augments MAIT cell survival and cytokine production in response to T-cell receptor mediation stimulation in PBMC.

2. MAIT cells, unlike naive CD8+ T cells, require bicarbonate transport to maintain alkaline intracellular pH (for cellular function).

9.2 Supplemental figures

Appendix Figure 9.11 SF3.1 | Human MAIT cells are activated by Adenovirus vectors in vitro.

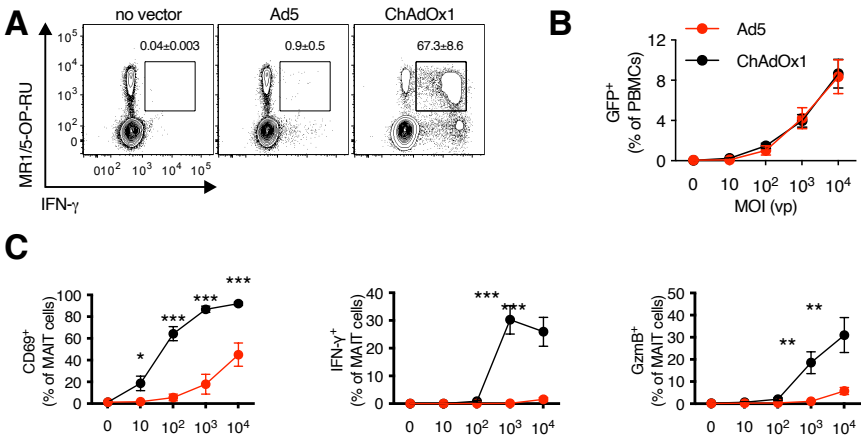

Appendix SF3.1 | Human MAIT cells are activated by Adenovirus vectors in vitro.
Experiments performed by Nicholas Provine {Provine.2021}
Fresh PBMCs were stimulated with ChAdOx1-GFP or Ad5-GFP at increasing multiplicity of infection (MOI). MAIT cell activation was measured (CD69, IFNγ, GzmB) at 24h.
(A) Repesentative plots identifying MAIT cells using MR1/5-OP-RU tetramer.
(B) Summary of GFP expression after stimulation with Ad5-GFP (red) or ChAdOx1-GFP (black).
(C) Summary of MAIT cell activation kinetics for CD69, IFN-γ, and GzmB. Statistical comparisons between vectors.
Symbols indicate individual donors.
*p < 0.05; **p < 0.01; ***p < 0.001; ****p < 0.0001; ns, not significant.
Mean ± SEM is shown.
Statistical significance was determined using a two-way ANOVA with Dunnett's multiple comparison test (B,C).

Appendix Figure 9.12 SF3.2 | Monocyte-derived IL-18 is necessary for potent innate-like lymphocyte induced IFN-γ in response to AdV.

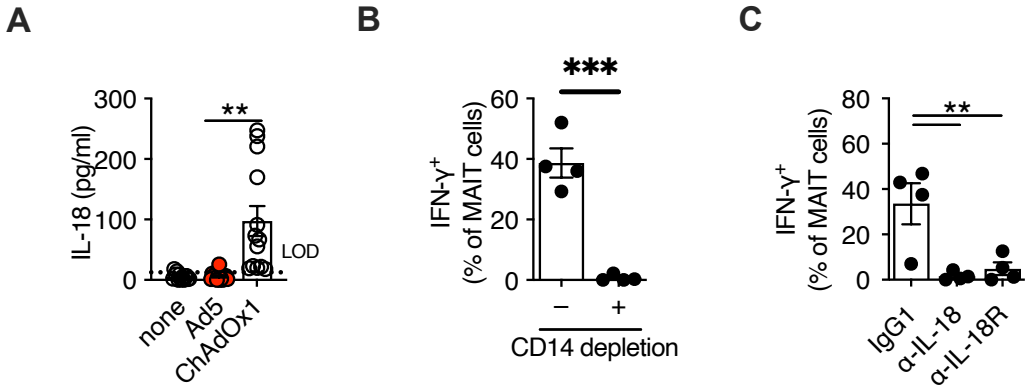

Appendix SF3.2| Monocyte-derived IL-18 is necessary for potent innate-like lymphocyte induced IFNγ in response to AdV.
All data generated by Nick Provine and published *(Provine et al, Science 2021)*

Fresh PBMCs (with or without CD14+ monocyte depletion) were stimulated with ChAdOx1-GFP and Ad5-GFP for 24h. Cytokines IL-18 and TNF was measured in supernatants after 24h.
(A) IL-18 measures in supernatants 24h after unfractionated ChAdOx1-GFP and Ad5-GFP stimulation.
(B) MAIT cell IFN-γ expression after unfractionated or CD14+ deplete PBMC stimualtion.
(C) MAIT cell IFN-γ expression after stimulation of PBMC with ChAdOx1 with or without inhibitors of IL-18, or IL-18R (10µg/ml).

Appendix Figure 9.13 SF3.3 | IL-12, IL-23 and IL-18 blockade reduce MAIT cell IFN-γ in response to ChAdOx1-GFP.

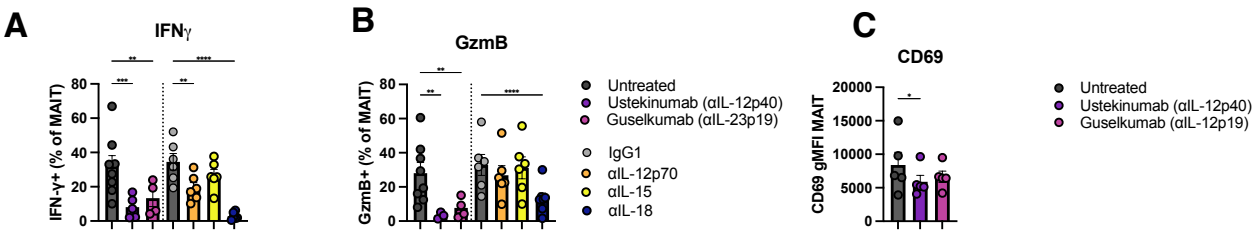

Appendix SF3.3 | IL-12, IL-23 and IL-18 blockade reduce MAIT cell IFN-γ in response to ChAdOx1-GFP.
Fresh PBMCs were treated with 10µg/ml of indicated inhibitory antibodies (or controls) prior to stimulaton with ChAdOx1-GFP (10^3vp) for 24h and MAIT cell activation measured (CD69, IFNγ, GzmB). Inhibitors, all at 10µg/ml, included: αIL-12p70, αIL-12p40 (Ustekinuman), αIL-23p19 (Guselkumab), IL-18, and IL-15 or isotype control (IgG1).

MAIT cell IFN-γ **(A),** GzmB **(B)**, and CD69 **(C)** in response to inhibitors.
Mean ± SEM is shown. Symbols indicate individual donors. Data represent at least 2 independent experiments (n=4-8donors). *p < 0.05; **p < 0.01; ***p < 0.001; ****p < 0.0001; ns, not significant.
Statistical significance was determined using Mixed effects analysis with Sidak's test for multiple comparisons.

Appendix Figure 9.14 SF3.4 | A monocyte-derived factor is required for IFN-dependent MAIT cell IFN-γ.

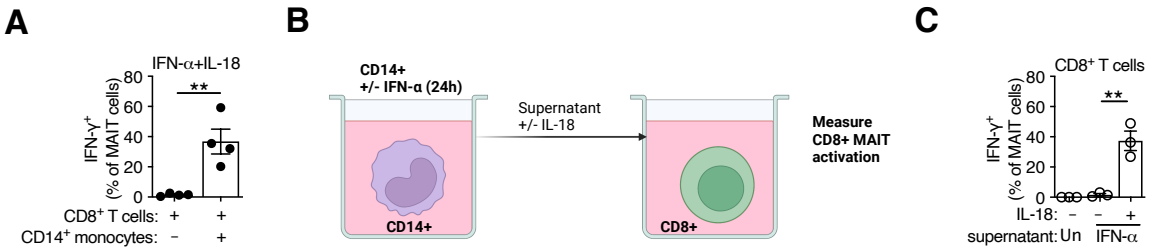

Appendix SF3.4 | A monocyte-derived factor is required for IFN-dependent MAIT cell IFN-γ.
All data generated by Nick Provine and published *(Provine et al, Science 2021)*

(A) MACS-enriched CD8+ T cells with or without autologous MACS-enriched CD14+ cells were stimulated with IFN-α and IL-18 (50ng/ml each). MAIT cell IFN-γ (among CD8+ cells) was measured after 24h.
(B, C) IFN-α treated monocyte supernatant added to MACS-enriched CD8+ cells with additional IL-18. MAIT cell activaton then measured after 24h.
(B) Schematic, and **(C)** Simmary MAIT IFN-γ among CD8+.
Symbols indicate individual donors. Mean ± SEM is shown. *p < 0.05; **p < 0.01; ***p < 0.001; ****p < 0.0001; ns, not significant. Statistical significance was determined using unpaired t-test.

Appendix Figure 9.15 SF4.1 | Gating strategies for cellular phenotyping.

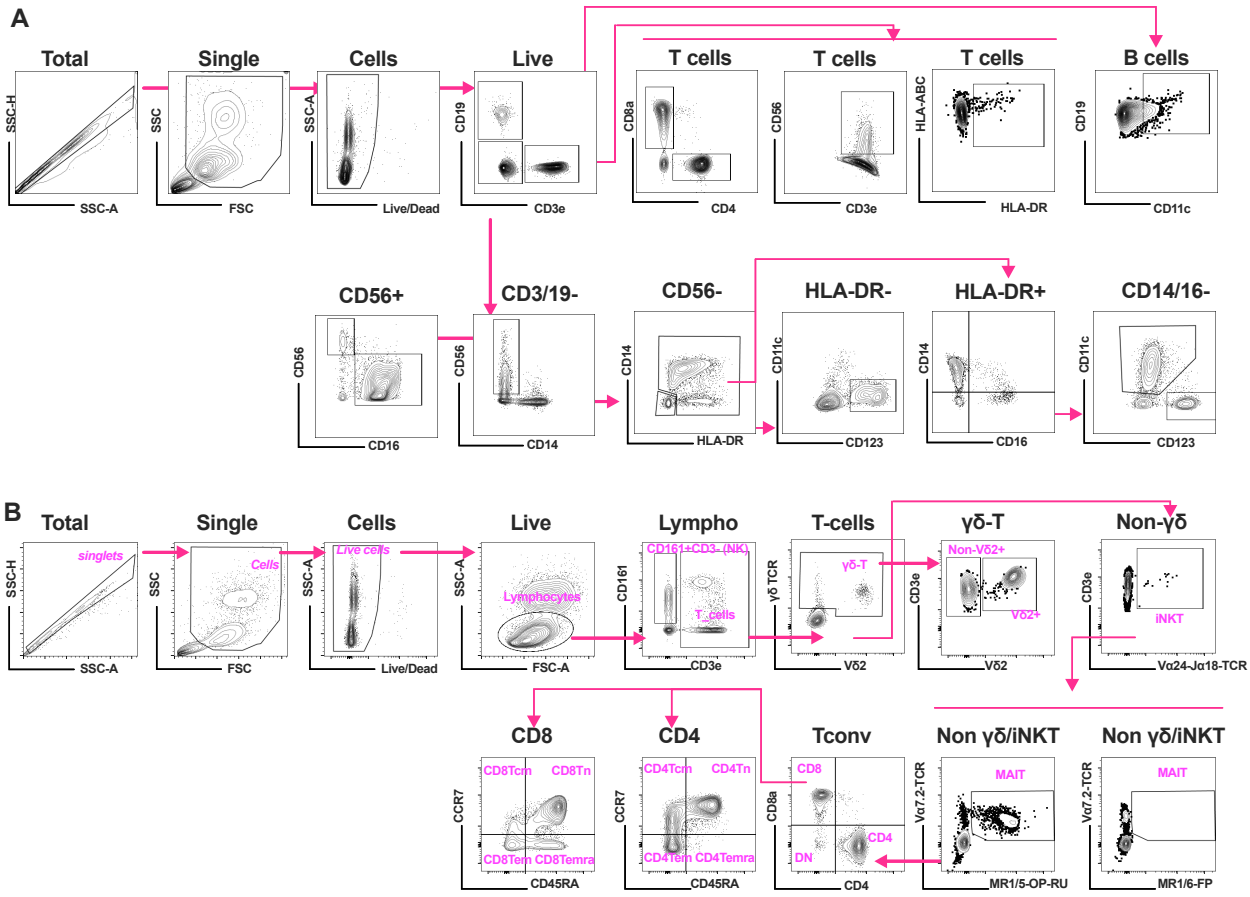

Appendix SF4.1 | Gating strategies for cellular phenotyping.
(A) Representative gating scheme for identification of major innate immune cell subsets in PBMC, including expression of HLA-ABC, HLA-DR, and TNFR2.
(B) Representative gating scheme for identification of major innate lymphocyte populations, including CD161+CD3- (NK cells).
(C) MAIT cells defined as MR1/5-OP-RU+, TCR Vα7.2+ cells, with MR1/6-FP tetramer used for gating.

cMono = classical monocytes (CD14+CD16-); iMono = intermediate monocytes (CD14+CD16+); non-classical monocytes (CD14-CD16-); mDC = conventional myeloid DC; DN = double negative; iNKT = invariant natural-killer T cells; MAIT = Mucosal associated invariant T cells; Tn = naïve T cells; Tcm = central memory T cells; Tem = effector memory T cells; Temra. = RA+ effector memory T cells.

Appendix Figure 9.16 SF4.2 | Persistently increased monocyte frequency 8 weeks after ChAdOx1-S prime.

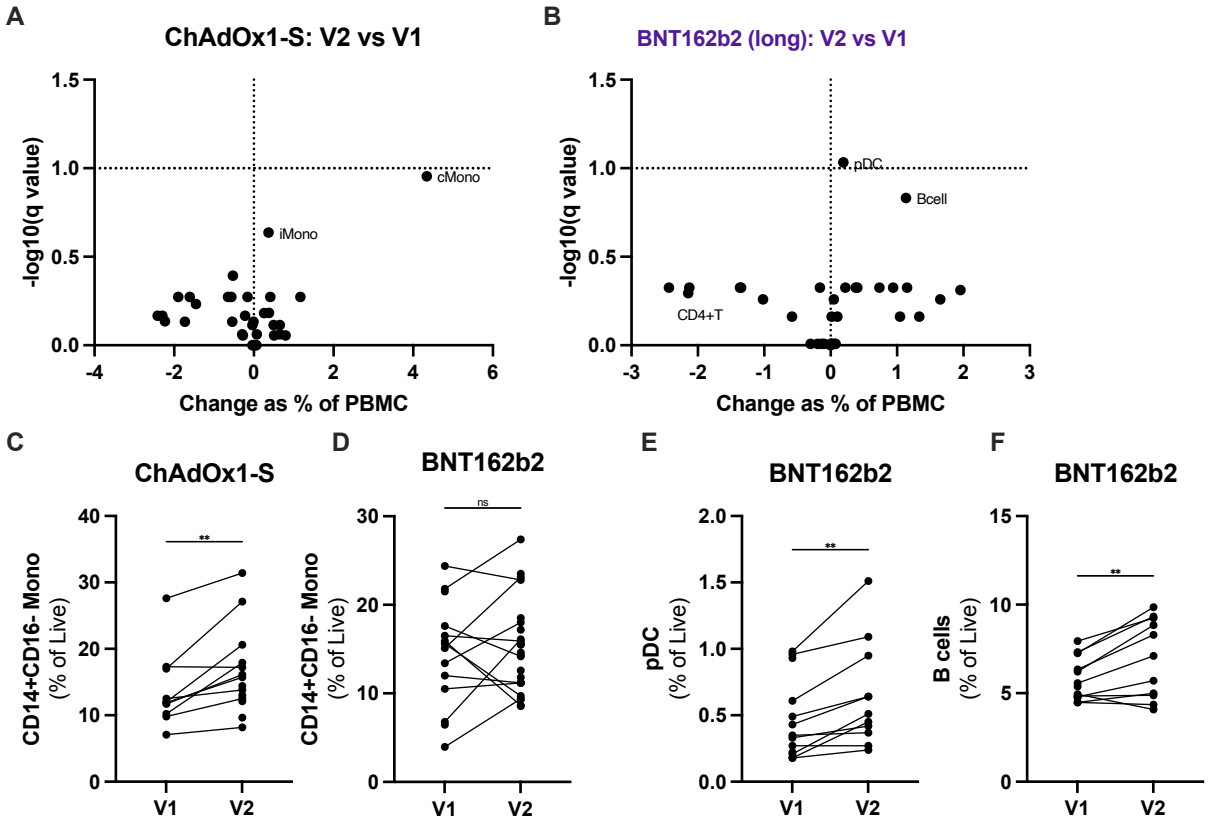

Appendix SF4.2 | Persistently increased monocyte frequency 8 weeks after ChAdOx1-S prime.
(A, B) Volcano plots of change in cell frequency as a fraction of live PBMC after ChAdOx1-S (**A**), or BNT162b2 (**B**), both with extended dosing intervals (>4wk).
(C, D) Frequency of classical CD14+CD16+ monocytes as a frequency of live PBMC pre-prime (V1) and pre-boost (V2) in healthcare workers receiving homologous ChAdOx1-S or BNT162b2 immunisation with extended boosting intervals.

(E, F) Frequency of plasmacytoid dendritic cells (**E**), and B cells (**F**) as a frequency of live PBMC pre-prime (V1) and pre-boost (V2) in healthcare workers receiving homologous BNT162b2 immunisation with extended boosting intervals.

Symbols indicate individual donors (C-E) with lines connecting data points from the same donor.
*p < 0.05; **p < 0.01; ***p < 0.001; ****p < 0.0001; ns, not significant.
Statistical significance was determined using: multiple paired t tests with Benjamini, Krieger, & Yekutieli correction for multiple comparisons (FDR <0.1; A, B), or paired students t tests (C-E).
pDC = plasmacytoid dendritic cell; cMono = classical monocyte (CD14+CD16-).

Appendix Figure 9.17 SF4.3 | Spike-specific T-cell ELISpot after BNT162b2 prime in data reanalysed from Payne et., al.

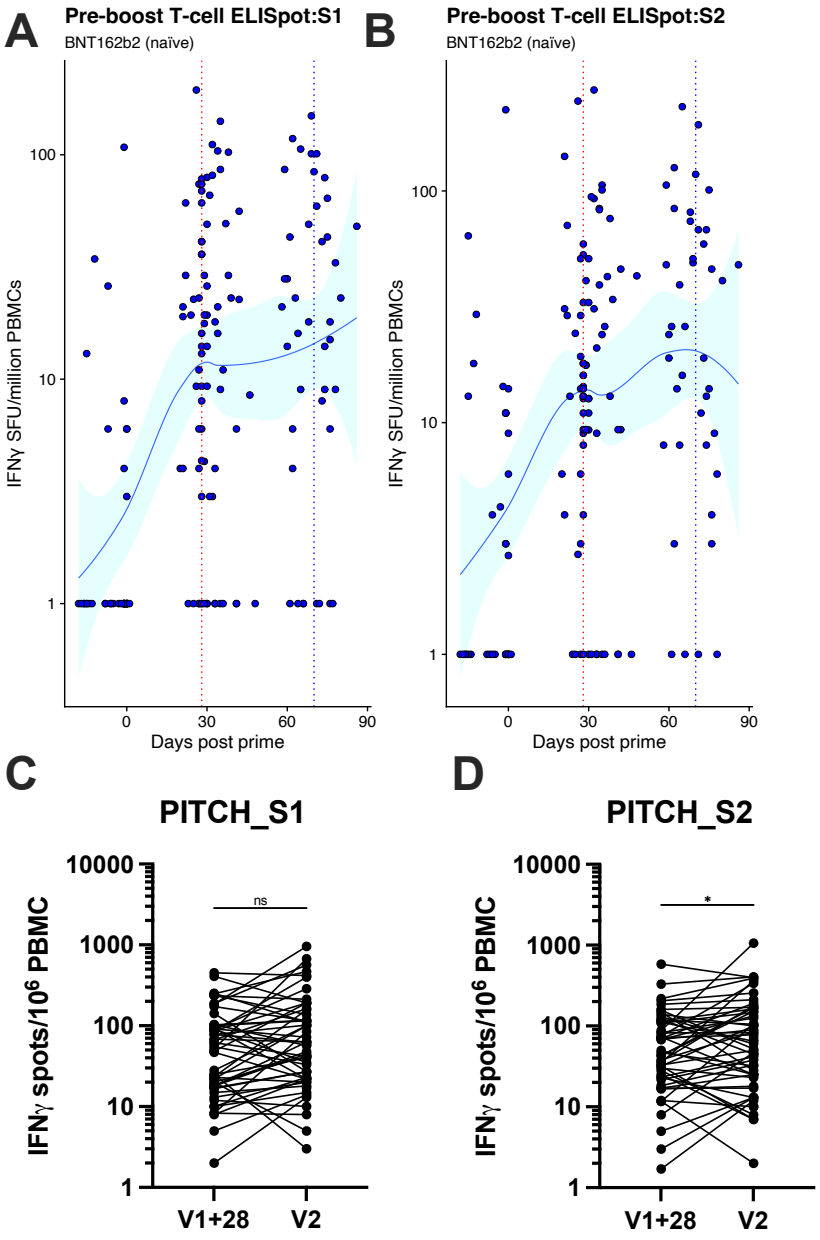

Appendix SF4.3 | Spike-specific T-cell ELISpot after BNT162b2 prime in data reanalysed from Payne et., al.
(A, B) IFN-γ ELISpot responses to SARS-CoV-2 (Victoria) S1 (**A**) or S2 (**B**) peptides at specified time points after BNT162b2 prime. Dotted red lines indicate average time for boosting on short interval (4wk) and long interval (10wk). Data in spot-forming units per million PBMC (SFU/million PBMC).

(C, D) IFN-γ ELISpot responses to SARS-CoV-2 S1 (**C**), or S2 (**D**) peptide at 4wk post-prime (V1+28), and at the time of boost (V2) in HCW boosted on extended interval boosting. Data in spot-forming units per million PBMC (SFU/million). Lines connect individual donors across time.

All donors were naïve to SARS-CoV-2 prior to vaccination. Symbols indicate individual donors.
*p < 0.05; **p < 0.01; ***p < 0.001; ****p < 0.0001; ns, not significant.
Statistical significance was determined using Wilcoxon matched paired signed rank test (C, D).

Appendix Figure 9.18 SF4.4 | Representative gating and plot after BNT162b2 in vitro.

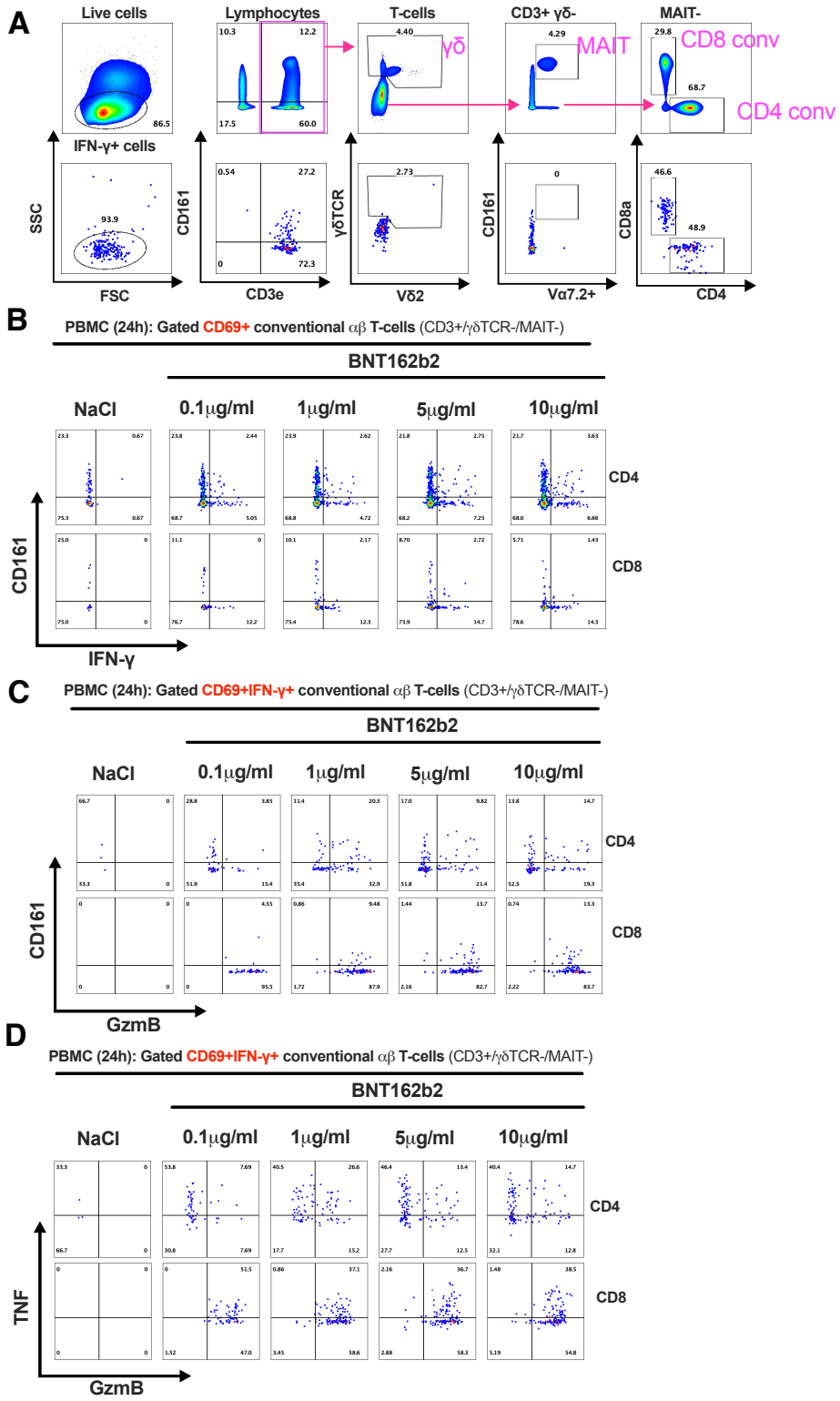

Appendix SF4.4 | Representative gating and plot after BNT162b2 in vitro.
(A) Representative gating of live PBMC, or IFN-γ+ PBMC, to identify T cells (CD3+ lymphocytes), γδ T cells, MAIT cells (CD161++Vα7.2+ non-γδ+), or conventional CD4+ or CD8+ T cells (non-MAIT / γδ TCR+ T cells).
(B) Representative plots of CD161 and IFN-γ expression on CD69+ conventional T cells after BNT162b2.
(C) Representative plots of CD161 and GzmB expression on CD69+IFN-γ+ conventional T cells after BNT162b2.
(D) Representative plots of TNF and GzmB expression on CD69+IFN-γ+ conventional T cells after BNT162b2.

Appendix Figure 9.19 SF4.5 | Cytokines induced by PBMC in response to SARS-CoV-2 vaccines, ChAdOx1-GFP, or spike protein in conventional media (R10).

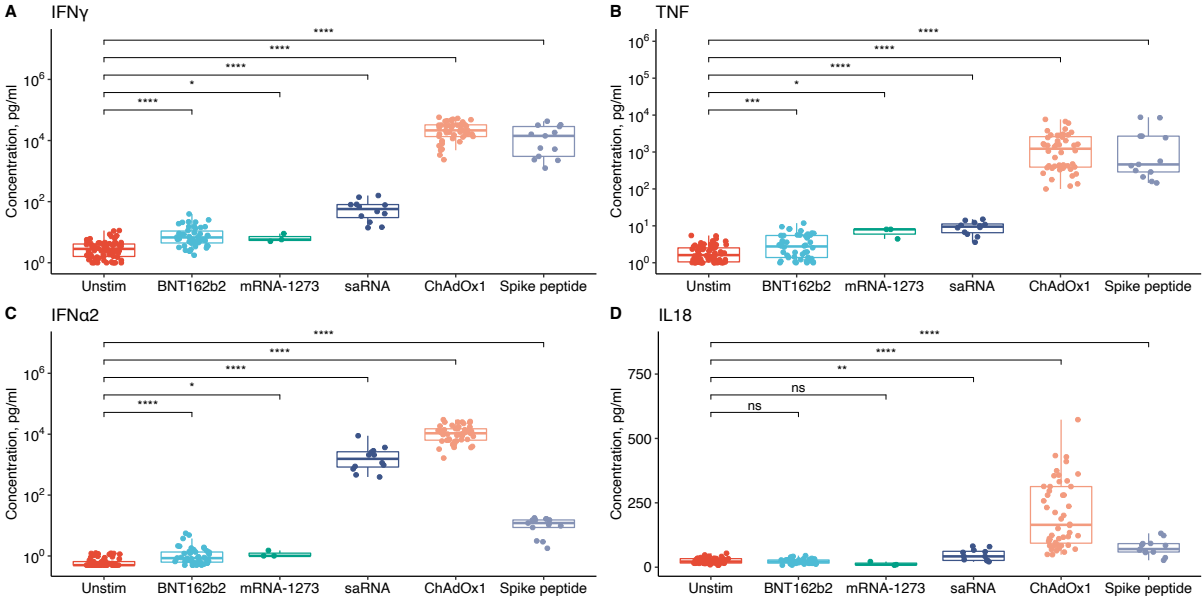

Appendix SF4.5 | Cytokines induced by PBMC in response to SARS-CoV-2 vaccines, ChAdOx1-GFP, or spike protein in conventional media (R10).
Fresh PBMCs from vaccinated individuals were stimulated with BNT162b2 (10µg/ml), mRNA-1273 (10µg/ml), saRNA (10µg/ml), ChAdOx1-GFP (10^9vp/ml), or pooled S1 and S2 peptides (1µg/ml total) for 24h.
Concentrations of IFN-γ **(A)**, TNF **(B)**, IFN-α2 **(C)**, and IL-18 **(D)** were measured.

Box plots show median, IQR (interquartile range), and range.

Appendix Figure 9.20 SF4.6 | BNT162b2 cytokine secretion in the presence of absence of additional human serum

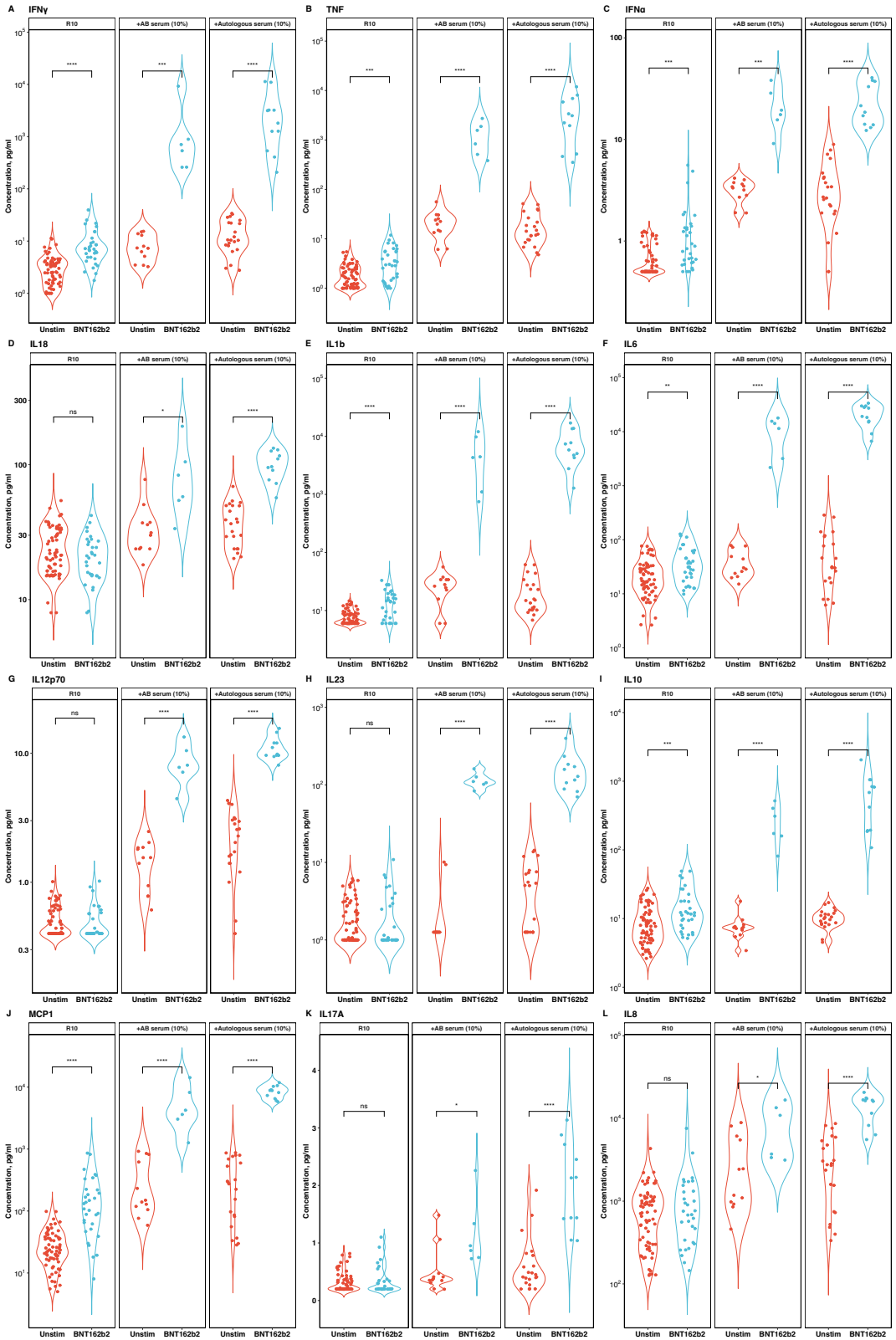

Appendix SF4.6 | BNT162b2 cytokine secretion in the presence of absence of additional human serum
(A-L) Fresh PBMCs from vaccinated individuals were stimulated with BNT162b2 (10µg/ml, blue) for 24h in R10 media with either additional pre-pandemic pooled human AB serum (10%), or autologous human serum (10%). Concentrations of cytokines were measures in cell culture supernatants: IFN-γ **(A),** TNF **(B),** IFN-α **(C),** IL-18 **(D),** IL-1β **(E)**, IL-6 **(F)**, IL-12p70 **(G)**, IL-23 **(H)**, IL-10 **(I)**, MCP-1 **(J)**, IL-17A **(K)**, IL-8 **(L)**. Statistical significance was determined using unpaired t-tests of log transformed values. *p < 0.05; **p < 0.01; ***p < 0.001; ****p < 0.0001; ns, not significant.

Appendix Figure 9.21 SF4.7 | IFN-γ induces monocyte TNF.

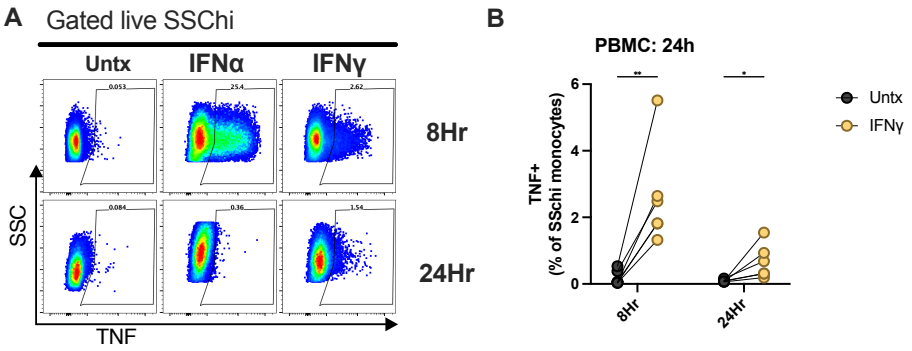

Appendix SF4.7 | IFN-γ induces monocyte TNF.
Fresh PBMC were stimulated with IFN-γ1 (50ng/ml) for 8h or 24h, and TNF secretion measured in monocytes (CD3/CD161/CD19-, SSChi)
(A, B) Representative plots **(A)**, and summary TNF expression **(B)** in monocytes.
Data were acquired from (n=6) donors, from two separate experiments.
*p < 0.05; **p < 0.01; ***p < 0.001; ****p < 0.0001; ns, not significant
Statistical significance was determined using multiple paired t-tests.

Appendix Figure 9.22 SF4.8 | Classical MHC blockade reduces early innate-like lymphocyte IFN-γ in response to ChAdOx1-GFP *in vitro*.

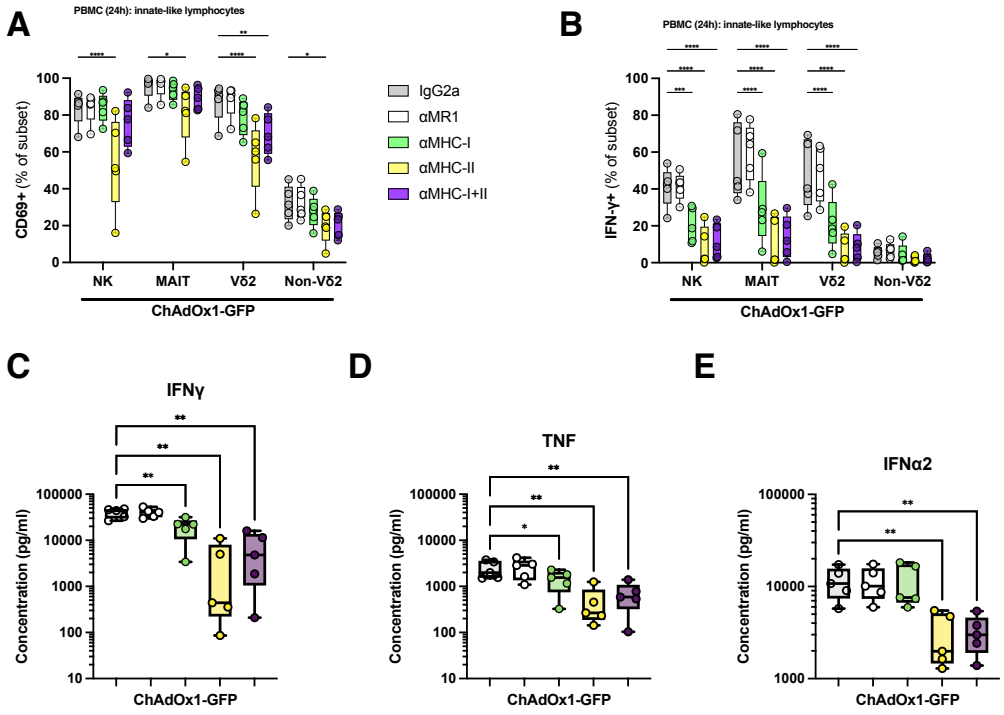

Appendix SF4.8 | Classical MHC blockade reduces early innate-like lymphocyte IFN-γ in response to ChAdOx1-GFP *in vitro*.
Fresh PBMCs from vaccinated individuals were stimulated with ChAdOx1-GFP (10^9 vp/ml) in R10 media. Inhibitors of MHC-I (clone W6/32, 10µg/ml), MHC-II (Tü39, 10µg/ml), combined MHC-I and MHC-II, MR1 (clone 26.2, 10µg/ml), or isotype control IgG2a (10µg/ml) were added prior to stimulation. Activation of NK cells (CD161+CD3- lymphocytes), MAIT cells (CD161++Vα7.2+CD3+), Vδ2+ and Vδ2- γδ T cells, and non-MAIT/ γδ T cell conventional CD4+ and CD8+ T cells was measured after 24h.

(**A, B**) Expression of CD69 (A) and IFN-γ (B) in NK cells, MAIT cells, Vδ2+ and Vδ2- γδ T cells in response to ChAdOx1-GFP.

(C-E) Total concentrations of IFN-γ (C), TNF (D), or IFN-α2 (E) in supernatants after 24h.

Box plots with median, IQR, and range are shown. Statistical significance was determined using two-way ANOVA with Dunnett's multiple comparison's test (A-B), repeated measures one-way ANOVA with Sidak's test for multiple comparisons (C-E). *p < 0.05; **p < 0.01; ***p < 0.001; ****p < 0.0001; ns, not significant.

Appendix Figure 9.23 SF4.9 | Classical MHC blockade reduces early MAIT cell IFN-γ in response to ChAdOx1-GFP *in vitro*.

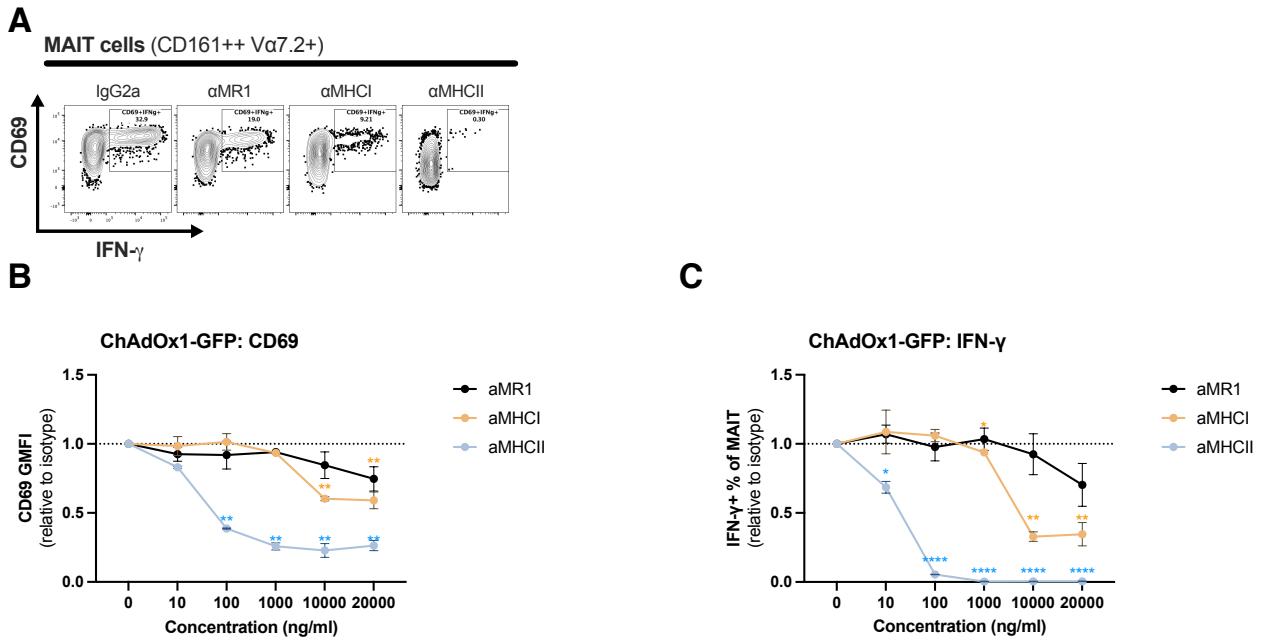

Appendix SF4.9 | Classical MHC blockade reduces early MAIT cell IFN-γ in response to ChAdOx1-GFP *in vitro*.
Fresh PBMCs from vaccinated individuals were stimulated with ChAdOx1-GFP (10^9 vp/ml) in R10 media. Titrations of inhibitors for MHC-I (clone W6/32, up to 10μg/ml), MHC-II (Tü39, up to 10μg/ml), MR1 (clone 26.2, up to 10μg/ml), or isotype control IgG2a (up to 10μg/ml) were added prior to stimulation. Activation of MAIT cells (CD161++Vα7.2+CD3+) was measured after 24h.

(**A**) Representative plots of MAI activation.
(B) Expression of CD69 (GMFI) relative to isotype control.
(**C**) Expression of IFN γ (%+ of MAIT) relative to isotype control.

Mean±SEM shown. Statistical significance was determined using two-way ANOVA with Dunnett's multiple comparison's test (A-B). *p < 0.05; **p < 0.01; ***p < 0.001; ****p < 0.0001; ns, not significant.

Appendix Figure 9.24 SF9.1 | Gating strategy for identification of live single T cells among unfractionated fresh PBMC stimulated with plate bound aCD3/28 and cytokines.

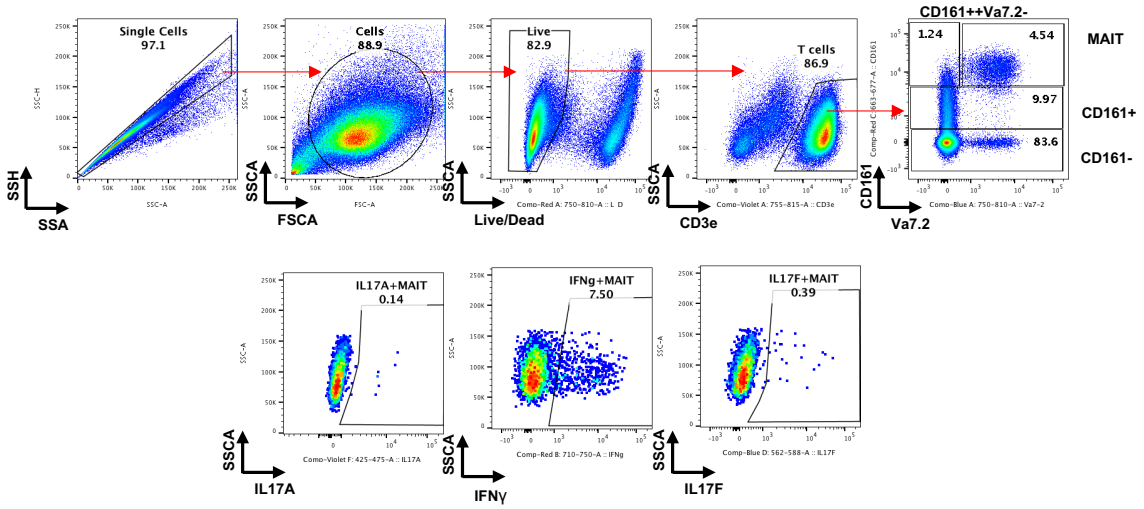

Appendix SF9.1| Gating strategy for identification of live single T cells among unfractionated fresh PBMC stimulated with plate bound aCD3/28 and cytokines.
T cells gated on CD161 and TCR Vα7.2 as: MAIT cells (CD161++Vα7.2+), non-MAIT CD161++ (CD161++Vα7.2-), CD161+ (intermediate), and CD161-

Appendix Figure 9.25 SF9.2 | Identification and sorting of MAIT cells, naïve and effector memory CD8+ T cells.

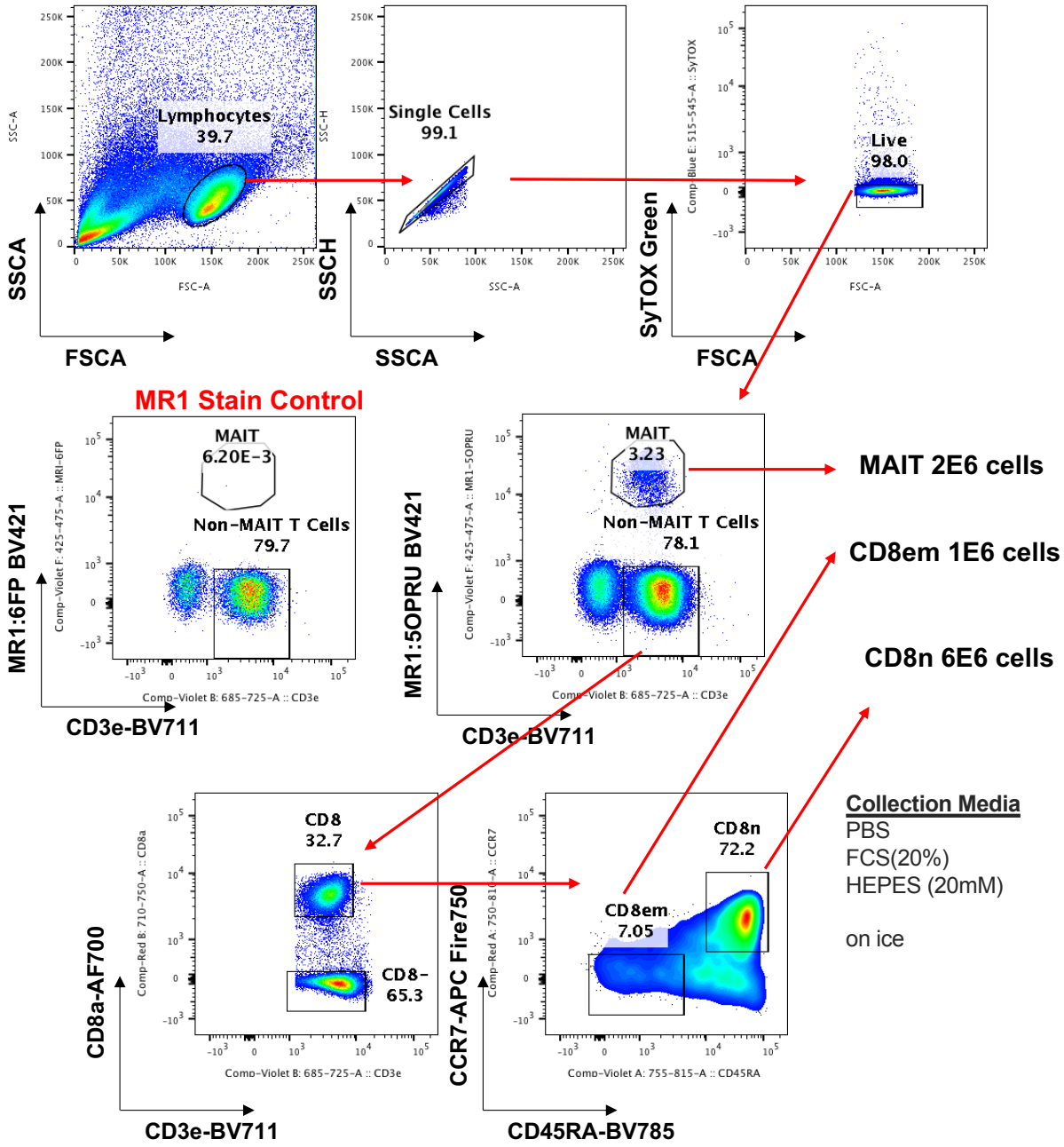

Appendix SF9.2 | Identification and sorting of MAIT cells, naïve and effector memory CD8+ T cells.
Representative gating strategy to identify MAIT cells, and non-MAIT naïve CD8+ (CD8n) and effector memory CD8+ T cells (CD8em) from fresh PBMCs.
Cells were stained with either MR1-5-OP-RU tetramer, or MR1-6-FP tetramer as a negative control.
Cells were sorted into collection media on ice containing PBS, FCS(20%) and HEPES (20mM).
Sorting all kindly performed by Helen Ferry.